Szkoła Doktorska Nauk Ścisłych i Przyrodniczych
Uniwersytetu Łódzkiego

Natalia Gocek-Szczurtek

Udział olejku eterycznego z *Thymus vulgaris* L. w łagodzeniu stresu wywołanego kadmem w komórkach merystemów korzeniowych *Vicia faba* L. var. *minor*

The role of *Thymus vulgaris* L. essential oil in alleviating cadmium-induced stress in root meristem cells of *Vicia faba* L. var. *minor*

Praca doktorska wykonana
pod kierunkiem promotora
dr hab. Justyny T. Polit, prof. UŁ
oraz promotora pomocniczego
dr Anety Żabki
w Katedrze Cytofizjologii
Wydziału Biologii i Ochrony Środowiska
Uniwersytetu Łódzkiego

Łódź 2026

Podziękowania:

Niniejsza rozprawa jest efektem nie tylko pracy własnej, lecz także wsparcia i życzliwości wielu osób, którym pragnę wyrazić głęboką wdzięczność.

- Na szczególne podziękowania zasługuje moja Promotor – Pani dr hab. **Justyna Polit**, prof. UŁ – za zaufanie, cierpliwość oraz życzliwość i wsparcie towarzyszące mi na wszystkich etapach powstawania tej pracy, jak również za nieustanną gotowość dzielenia się wiedzą i doświadczeniem.

- Promotor pomocniczej – Pani dr **Anecie Żabce** – dziękuję za życzliwość, cenne uwagi oraz wsparcie, które towarzyszyło mi na tej drodze.

- Pragnę wyrazić wdzięczność także wszystkim osobom, których wkład przyczynił się do powstania niniejszej pracy, w szczególności **współautorom** publikacji stanowiących jej podstawę.

- **Mojej Rodzinie** dziękuję za obecność, wsparcie i wiarę.
Mężowi – Szymonowi – za spokój, zrozumienie i codzienną siłę.

- Na końcu pragnę wyrazić wdzięczność za Cichą Obecność, która towarzyszyła mi w chwilach zwątpienia, za spokój odnajdywany w trudzie oraz za światło, które nie pozwalało zagubić drogi.

Spis treści

1. Źródła finansowania badań

Dofinansowanie działalności naukowej doktorantów z budżetu Szkoły Doktorskiej Nauk Ścisłych i Przyrodniczych Uniwersytetu Łódzkiego

2. Współpraca

1. Katedra Biologii i Ekologii Roślin, Wydział Biologii, Uniwersytet w Białymstoku
2. Katedra Chemii Analitycznej i Nieorganicznej, Wydział Chemii, Uniwersytet w Białymstoku
3. Katedra Farmakognozji i Botaniki Farmaceutycznej, Wydział Farmaceutyczny, Uniwersytet Medyczny w Lublinie
4. Katedra Technologii Leków i Biochemii, Wydział Chemiczny, Politechnika Gdańska
5. Katedra Agronomii, Wydział Rolnictwa, Ogrodnictwa i Biotechnologii, Uniwersytet Przyrodniczy w Poznaniu

3. Spis publikacji wchodzących w skład rozprawy doktorskiej

1. **Gocek-Szczurtek, N.***; Żabka, A.; Wróblewski, M.; Kukula-Koch, W.; Szczeblewski, P.; Polit, J.T. Thyme Oil Mitigates Cadmium-Induced Oxidative and Genotoxic Stress in *Vicia faba* Root Meristem Cells under *in vitro* Conditions. *Sci Rep* **2025**, 15, 38689, doi:10.1038/s41598-025-22588-w.

2. Żabka, A.*; **Gocek, N.**; Polit, J.T.; Maszewski, J. Epigenetic Modifications Evidenced by Isolation of Proteins on Nascent DNA and Immunofluorescence in Hydroxyurea-Treated Root Meristem Cells of *Vicia faba*. *Planta* **2023**, 258, 95, doi:10.1007/s00425-023-04249-2.

3. **Gocek-Szczurtek, N.**; Żabka, A.; Wróblewski, M.; Polit, J.T.* Stabilization of the MAPK–Epigenetic Signaling Axis Underlies the Protective Effect of Thyme Oil against Cadmium Stress in Root Meristem Cells of *Vicia faba*. *Int. J. Mol. Sci.* **2025**, 27, 208, doi:10.3390/ijms27010208.

4. **Gocek-Szczurtek, N**.; Wróblewski, M.; Żabka, A.; Polit, J.T.* Thyme Oil Alleviates Cadmium Induced Disturbances in Mitotic Activity, Cytoskeletal Organization and H3T3/H3S10 Phosphorylation in *Vicia faba. Int. J. Mol. Sci.* **2026**, 27, 2798, doi:10.3390/ijms27062798.

5. **Gocek-Szczurtek, N.***; Piotrowska-Niczyporuk, A.; Zambrzycka-Szelewa, E.; Ciereszko, I.; Żabka, A.; Wróblewski, M.; Polit, J.T. Thyme Essential Oil Reduces Cadmium Uptake and Toxicity in *Vicia faba* Root Meristem Cells, Involving Stabilization of Cell Ultrastructure and Modulation of Redox Response and Thiol Metabolism. - manuskrypt wysłany do czasopisma *The Plant Journal*

* – autor korespondujący

Sumaryczny współczynnik wpływu (ang. *Impact Factor*, IF) opublikowanych prac wchodzących w skład rozprawy doktorskiej (1-4): **IF = 17,5**

Łączna liczba punktów dla opublikowanych prac wchodzących w skład rozprawy doktorskiej (1-4), według listy czasopism punktowanych Ministerstwa Nauki i Szkolnictwa Wyższego (**MNiSW**): **520 pkt**

IF dla czasopisma ***The Plant Journal*** do którego wysłano pracę nr 5 wynosi **– 5,7;** natomiast **liczba punktów MNiSW** wynosi **140 pkt**.

4. Streszczenie

Wobec narastającego skażenia środowiska metalami ciężkimi, zwłaszcza kadmem (Cd), który w komórkach organizmów żywych nie pełni żadnej funkcji poza toksyczną, celem badań była ocena 24-godzinnego wpływu 175 μM $CdCl_2$ na funkcjonowanie merystemów korzeni zarodkowych *Vicia faba* L. var. *minor* oraz określenie, w jakim stopniu olejek tymiankowy (TO; 0,03%) może chronić komórki przed działaniem Cd. Pierwszą reakcją merystemów była znaczna akumulacja Cd w komórkach, której towarzyszyła nadprodukcja reaktywnych form tlenu (RFT). Pomimo aktywacji mechanizmów antyoksydacyjnych, obejmujących wzrost aktywności enzymów i puli nieenzymatycznych przeciwutleniaczy, a także mechanizmów detoksykacyjnych opartych na metabolizmie tiolowym, odpowiedź ta okazała się niewystarczająca, prowadząc do nasilonej peroksydacji lipidów i uszkodzeń DNA. Zaburzenia te korelowały z dezorganizacją ultrastruktury organelli komórkowych. W rezultacie komórki prawdopodobnie zmagały się z upośledzeniem funkcji barierowej ściany komórkowej, związanym z trudnościami we wzmacnianiu jej fibrylarnymi prekursorami transportowanymi przez pęcherzyki aparatów Golgiego, które były pozbawione tych komponentów, oraz zapewne z niedoborem niezbędnych białek, co odzwierciedlała ograniczona gęstość rybosomów w cytoplazmie. Na poziomie aparatu genetycznego obserwowano zaburzenia przebiegu replikacji i spadek liczby komórek aktywnie syntetyzujących DNA. Towarzyszyła temu aktywacja szlaku MAPK oraz zmiany epigenetyczne, obejmujące wzrost globalnej metylacji DNA i przeprogramowanie kodu histonowego, prowadzące do kondensacji chromatyny i ograniczenia globalnej aktywności transkrypcyjnej. Zaburzenia te, w połączeniu ze spadkiem zawartości głównych regulatorów cyklu komórkowego (CDKA i CycB), blokowały mitozę i silnie obniżały indeks mitotyczny. W komórkach dzielących się, nieprawidłowa fosforylacja histonu H3 i zaburzenia cytoszkieletu, objawiające się pakietowaniem i ograniczoną reorganizacją mikrotubul i filamentów aktynowych, skutkowały dezorganizacją aparatu mitotycznego i hamowaniem progresji mitozy. W konsekwencji dochodziło do zahamowania proliferacji komórek merystematycznych i ograniczenia wzrostu korzeni zarodkowych. Na tym tle szczególnie wyraźnie ujawniało się działanie ochronne olejku tymiankowego (TO), który samodzielnie nie destabilizował struktury ani funkcji komórek merystematycznych. Podany podczas ekspozycji merystemów na $CdCl_2$, nie tylko częściowo ograniczał akumulację Cd w tkankach, ale przede wszystkim skutecznie łagodził jego destrukcyjny wpływ na kolejnych poziomach organizacji komórkowej. Redukcja poziomu RFT w obecności TO oraz silne wzmocnienie aktywności enzymatycznego i nieenzymatycznego systemu antyoksydacyjnego prowadziły do znacznego ograniczenia peroksydacji lipidów i redukcji ilości dwuniciowych pęknięć DNA. Efektem tych skoordynowanych działań było wyraźne ograniczenie zmian ultrastrukturalnych organelli, stymulacja produkcji prekursorów ściany komórkowej w pęcherzykach sekrecyjnych aparatu Golgiego oraz wzmożony transport podjednostek rybosomów do cytoplazmy, związany z tworzeniem wakuol jąderkowych, sprzyjający intensyfikacji translacji, ujawnionej poprzez liczne rybosomy osadzone na retikulum endoplazmatycznym. Na poziomie regulacji jądrowej TO ograniczał aktywację kaskady sygnałowej MAPK oraz zapobiegał zmianom epigenetycznym, utrzymując parametry metylacji DNA i modyfikacji histonów na poziomie zbliżonym do kontroli, co sprzyjało zachowaniu aktywności transkrypcyjnej. Jednocześnie TO stabilizował aparat replikacyjny i mitotyczny, umożliwiając zachowanie sprawnej proliferacji prowadzącej do prawidłowego wzrostu korzeni. W tym kontekście opracowanie i adaptacja metody iPOND do materiału roślinnego otworzyła nowe możliwości przyszłej bezpośredniej analizy białek związanych z nowo syntetyzowanym DNA i weryfikacji mechanizmów ochronnych TO w obrębie widełek replikacyjnych. Reasumując, TO działał wielokierunkowo, stabilizując strukturę i podstawowe procesy komórek merystematycznych oraz skutecznie przerywając kaskadę toksyczności indukowaną przez kadm, potwierdzając tym samym jego potencjał jako naturalnego czynnika wspierającego strategie ochrony roślin przed stresem kadmowym.

5. Abstract

In the context of increasing environmental contamination with heavy metals, particularly cadmium (Cd), which has no biological function in living cells other than toxicity, this study aimed to evaluate the effects of 175 µM $CdCl_2$ after 24 h of exposure on the functioning of root meristems of *Vicia faba* L. var. *minor*, as well as to determine the extent to which thyme essential oil (TO; 0.03%) can protect cells against Cd toxicity. The initial response of the meristems was a substantial accumulation of Cd in the cells, accompanied by an overproduction of reactive oxygen species (ROS). Despite the activation of antioxidant mechanisms, including increased enzymatic activity and elevated levels of non-enzymatic antioxidants, as well as detoxification pathways based on thiol metabolism, this response proved insufficient, leading to enhanced lipid peroxidation and DNA damage. These disturbances were associated with disorganization of the ultrastructure of cellular organelles. Consequently, cells likely experienced impaired barrier function of the cell wall, related to difficulties in its reinforcement by fibrillar precursors transported in Golgi-derived vesicles, which were devoid of these components, as well as a probable deficiency of essential proteins, reflected by a reduced ribosome density in the cytoplasm. At the level of the genetic apparatus, disturbances in DNA replication and a decreased number of cells actively synthesizing DNA were observed. These changes were accompanied by activation of the MAPK signaling pathway and epigenetic alterations, including increased global DNA methylation and reprogramming of the histone code, leading to chromatin condensation and reduced global transcriptional activity. Together with decreased levels of key cell cycle regulators (CDKA and CycB), these disturbances contributed to mitotic arrest and a marked reduction in the mitotic index. In dividing cells, abnormal phosphorylation of histone H3 and cytoskeletal alterations, manifested as bundling and impaired rearrangement of microtubules and actin filaments, resulted in disorganization of the mitotic apparatus and inhibition of mitotic progression. Consequently, proliferation of meristematic cells was suppressed, leading to reduced root growth. Against this background, the protective effect of thyme essential oil (TO) was particularly evident, as TO alone did not destabilize the structure or function of meristematic cells. When applied during Cd exposure, TO not only partially reduced Cd accumulation in tissues but, more importantly, effectively mitigated its detrimental effects at multiple levels of cellular organization. The reduction of ROS levels in the presence of TO, along with a strong enhancement of both enzymatic and non-enzymatic antioxidant systems, led to a significant decrease in lipid peroxidation and double-strand DNA breaks. These coordinated effects resulted in a marked reduction of ultrastructural alterations in organelles, stimulation of cell wall precursor production in Golgi secretory vesicles, and enhanced transport of ribosomal subunits to the cytoplasm, associated with the formation of nucleolar vacuoles, thereby promoting translational activity, as evidenced by abundant ribosomes associated with the endoplasmic reticulum. At the level of nuclear regulation, TO attenuated activation of the MAPK signaling cascade and prevented epigenetic alterations, maintaining DNA methylation and histone modification patterns close to control levels, which supported the preservation of transcriptional activity. At the same time, TO stabilized both the replication and mitotic machinery, enabling sustained cell proliferation and proper root growth. In this context, the development and adaptation of the iPOND method for plant material provides new opportunities for the direct analysis of proteins associated with newly synthesized DNA and for further verification of the protective mechanisms of TO at replication forks. In summary, TO exerts a multifaceted protective effect, stabilizing cellular structure and essential processes in meristematic cells and effectively interrupting the cascade of Cd-induced toxicity, thereby confirming its potential as a natural agent supporting plant tolerance to cadmium stress.

6. Określenie celu badawczego pracy i prezentacja wyników jego realizacji

6.1. Wprowadzenie

Wśród pierwiastków śladowych obecnych w środowisku niewiele wzbudza tak duże zainteresowanie badaczy jak kadm (Cd). Choć pierwiastek ten naturalnie występuje w skorupie ziemskiej, działalność człowieka doprowadziła do jego znacznej akumulacji w wielu ekosystemach, czyniąc z niego jeden z istotnych współczesnych czynników stresu środowiskowego. W związku z tym rośnie znaczenie badań ukierunkowanych zarówno na poznanie mechanizmów jego oddziaływania biologicznego, jak i na opracowanie strategii wspomagających organizmy żywe narażone na jego obecność w środowisku.

6.1.1. Kadm jako czynnik zanieczyszczenia środowiska

Do naturalnych źródeł kadmu należą przede wszystkim procesy wietrzenia skał zawierających minerały cynku, ołowiu i miedzi oraz aktywność wulkaniczna [1–3]. Intensyfikacja działalności antropogenicznej zaburzyła naturalne cykle geochemiczne metali ciężkich, prowadząc do zwiększonej biodostępności kadmu i jego kumulacji w różnych komponentach środowiska [4–7]. Główne źródła emisji antropogenicznych kadmu obejmują procesy metalurgiczne, spalanie paliw kopalnych, produkcję akumulatorów niklowo-kadmowych oraz stosowanie nawozów fosforowych [8,9].

Kadm występuje głównie w postaci kationu Cd^{2+}, który charakteryzuje się wysoką rozpuszczalnością oraz znaczną mobilnością w środowisku wodnym i glebowym [1]. Istotną cechą tego pierwiastka jest także jego wysoka trwałość [10]. Pobierany przez rośliny z roztworu glebowego może gromadzić się w ich tkankach, stanowiąc potencjalne źródło skażenia dla organizmów z wyższych poziomów troficznych [11]. Proces ten prowadzi do biomagnifikacji, czyli stopniowego wzrostu stężenia kadmu w kolejnych ogniwach łańcuchów pokarmowych [12]. W konsekwencji kadm uznawany jest za trwały czynnik stresu środowiskowego, który wymaga podejmowania działań mających na celu ograniczenie jego emisji oraz minimalizację skutków biologicznych.

6.1.2. Toksyczność kadmu dla organizmów żywych

Kadm nie pełni funkcji fizjologicznych u organizmów wyższych, a jego obecność w komórkach ma charakter wyłącznie toksyczny (Ryc. 1). Wysoka mobilność, zdolność do bioakumulacji oraz długi okres półtrwania w tkankach sprawiają, że metal ten może oddziaływać na różne poziomy organizacji biologicznej - od procesów molekularnych i komórkowych po funkcjonowanie całych organizmów i populacji [13,14].

U roślin, stanowiących pierwszy poziom troficzny oraz ważne ogniwo transferu kadmu w łańcuchach pokarmowych, metal ten wywołuje liczne efekty toksyczne [15]. Kadm jest stosunkowo łatwo pobierany z roztworu glebowego przez systemy korzeniowe, a po wniknięciu do komórek indukuje zaburzenia obejmujące m.in. ograniczenie syntezy chlorofilu i uszkodzenia chloroplastów, prowadzące do nieprawidłowości w funkcjonowaniu aparatu

fotosyntetycznego [16,17]. Ponadto kadm może zaburzać funkcjonowanie mitochondrialnego łańcucha transportu elektronów, ograniczać syntezę ATP oraz nasilać wytwarzanie reaktywnych form tlenu (RFT) [17–19]. Konsekwencją tych zmian są zaburzenia fizjologiczne obserwowane na poziomie całej rośliny, takie jak zahamowanie wzrostu i rozwoju, ograniczenie elongacji korzeni, zmniejszenie biomasy, chloroza liści, nekroza oraz przedwczesne obumieranie tkanek zarówno w organach nadziemnych, jak i podziemnych [20–22]. Kadm może również zakłócać gospodarkę wodną roślin poprzez wpływ na funkcjonowanie aparatów szparkowych, a także zaburzać pobieranie i transport składników mineralnych [23–25].

U ludzi i zwierząt nagromadzenie kadmu prowadzi do zaburzeń funkcjonowania narządów, przede wszystkim uszkodzeń nerek, zaburzeń gospodarki mineralnej oraz zmian w układzie kostnym [26–29]. W nerkach kadm kumuluje się głównie w komórkach kanalików proksymalnych, powodując ich uszkodzenie oraz upośledzenie procesów filtracji i reabsorpcji [30]. Dysfunkcja nerek zaburza metabolizm wapnia i witaminy D, przyczyniając się do demineralizacji kości i rozwoju zmian osteomalacyjnych [31]. Jednym z najbardziej znanych przykładów zdrowotnych konsekwencji środowiskowego skażenia kadmem jest choroba Itai-Itai, opisana w Japonii w połowie XX wieku. Schorzenie to wynikało z długotrwałego spożywania żywności zanieczyszczonej kadmem i objawiało się poważnymi uszkodzeniami nerek, silnymi bólami kości oraz ich rozmiękaniem, czyli osteomalacją [32]. Kadm i jego związki zostały zaklasyfikowane przez Międzynarodową Agencję Badań nad Rakiem (IARC, ang. *International Agency for Research on Cancer)* jako substancje rakotwórcze dla ludzi (grupa 1) [33]. Ekspozycja na ten metal ciężki wiąże się ze zwiększonym ryzykiem rozwoju raka płuc, a także nowotworów nerek i prostaty [34]. Kancerogenne właściwości tego pierwiastka przypisuje się jego zdolności do indukowania uszkodzeń DNA, zaburzania mechanizmów naprawy materiału genetycznego, modulowania proliferacji komórkowej oraz hamowania apoptozy [35,36], co sprzyja transformacji nowotworowej i progresji guza [34]. Szczególnie wrażliwymi grupami na działanie kadmu są kobiety w ciąży, niemowlęta oraz dzieci, ze względu na większą podatność organizmu rozwijającego się na czynniki toksyczne. Ekspozycja na kadm w okresie prenatalnym wiąże się z niekorzystnym przebiegiem ciąży, w tym niską masą urodzeniową, przedwczesnym porodem oraz zaburzeniami rozwoju dziecka [37].

Źródeł większości opisanych powyżej zjawisk indukowanych przez kadm można upatrywać w kilku podstawowych mechanizmach molekularnych. Jednym z nich jest wysokie powinowactwo tego metalu do grup siarkowych, azotowych i tlenowych, w szczególności do grup tiolowych (–SH) obecnych w licznych białkach. Interakcje kadmu z tymi grupami prowadzą do zmian konformacyjnych białek strukturalnych i regulatorowych oraz do hamowania aktywności wielu enzymów [38–41]. Istotną rolę odgrywa również zdolność kadmu do wypierania fizjologicznych kationów metali, takich jak Ca^{2+}, Zn^{2+} czy Fe^{2+}, z ich miejsc wiązania w enzymach i białkach strukturalnych, co prowadzi do zaburzeń homeostazy jonowej oraz destabilizacji licznych procesów metabolicznych i szlaków sygnalizacyjnych [42,43,19]. Kolejnym ważnym mechanizmem działania kadmu jest jego zdolność do zaburzania homeostazy redoks komórki. Ekspozycja na ten metal sprzyja nadprodukcji

reaktywnych form tlenu (RFT), takich jak anionorodnik ponadtlenkowy, nadtlenek wodoru czy rodnik hydroksylowy [44]. Nadmiar RFT prowadzi do oksydacyjnych uszkodzeń makrocząsteczek komórkowych, w tym białek, lipidów i kwasów nukleinowych [45]. W szczególności lipidy błonowe są podatne na peroksydację, co skutkuje utratą integralności i płynności błon oraz zaburzeniami funkcjonowania systemów transportowych i enzymów błonowych [46]. Z kolei uszkodzenia DNA obejmują zarówno modyfikacje zasad azotowych, jak i pęknięcia nici, co może prowadzić do zaburzeń regulacji cyklu komórkowego oraz zmian w ekspresji genów [47,48]. Ponadto wykazano, że kadm może hamować aktywność enzymów antyoksydacyjnych oraz zakłócać funkcjonowanie systemów naprawy DNA, co potęguje skutki stresu oksydacyjnego i sprzyja akumulacji uszkodzeń komórkowych [49,50].

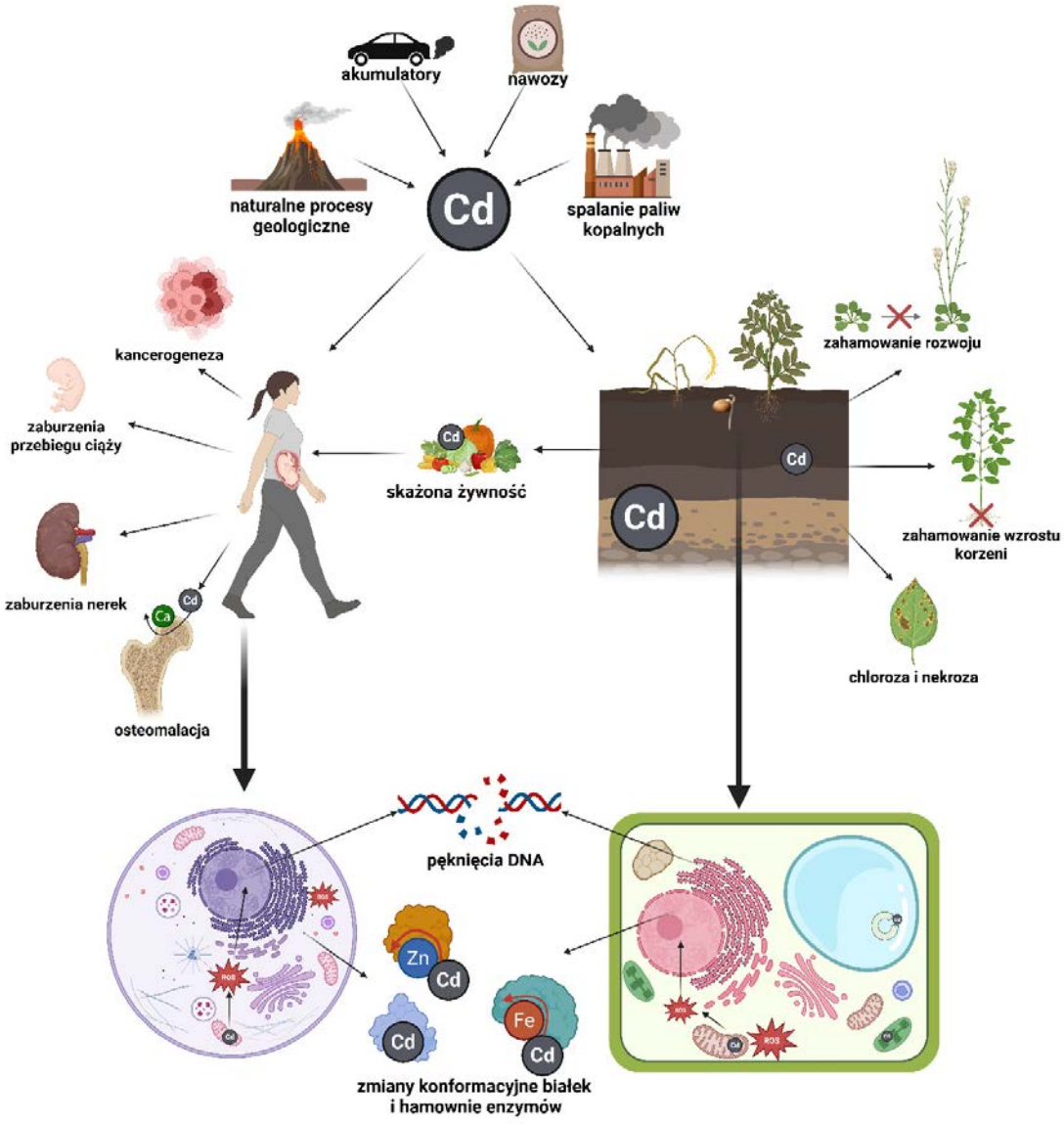

Ryc. 1. Schemat ilustrujący główne źródła kadmu w środowisku oraz najważniejsze mechanizmy molekularne leżące u podstaw jego toksyczności u roślin i ludzi. Uwzględniono zarówno naturalne i antropogeniczne źródła emisji tego metalu, jak i jego akumulację w glebie oraz transfer w łańcuchach troficznych. Schemat przedstawia kluczowe procesy komórkowe zaburzane przez kadm, w tym indukcję stresu oksydacyjnego, uszkodzenia struktur komórkowych i materiału genetycznego oraz zakłócenia funkcjonowania enzymów. Rycina przygotowana z wykorzystaniem BioRender.com.

6.1.3. Strategie ograniczania skażenia kadmem

Kadm może ulegać sorpcji oraz chemicznemu kompleksowaniu z nieorganicznymi i organicznymi ligandami, jednak część tego pierwiastka pozostaje w roztworze glebowym w postaci jonów Cd^{2+}, które stanowią formę najbardziej dostępną dla roślin [4]. Przemiany i transport kadmu w glebie są determinowane przez szereg czynników fizykochemicznych. Do najważniejszych należą odczyn gleby (pH), potencjał redoks, zawartość materii organicznej oraz konkurencja ze strony innych kationów, takich jak Zn^{2+}, Ca^{2+} czy Fe^{2+} [1]. W praktyce rolniczej szczególne znaczenie ma odczyn gleby, gdyż w warunkach obniżonego pH rozpuszczalność i biodostepność kadmu zazwyczaj wzrastają [51]. Zakwaszenie gleby osłabienia bowiem wiązanie Cd w kompleksach sorpcyjnych i zwiększa jego udziału w roztworze glebowym [52], sprzyjając pobieraniu tego metalu przez rośliny. Zjawisko to może być dodatkowo nasilane przez procesy degradacji środowiska, zwłaszcza acydyfikację ekosystemów spowodowaną depozycją zanieczyszczeń atmosferycznych, intensywnym nawożeniem mineralnym czy innymi czynnikami zakwaszającymi [53].

Ze względu na trwałość kadmu w środowisku oraz możliwość jego transferu do łańcuchów pokarmowych, istotnym kierunkiem badań i działań praktycznych jest opracowanie metod ograniczajacych mobilność tego metalu oraz jego negatywny wpływ na organizmy żywe. W praktyce stosuje się różnorodne strategie remediacji gleb skażonych metalami ciężkimi, które można podzielić na metody fizyczne, chemiczne oraz biologiczne [54]. Dobór odpowiedniej strategii zależy m.in. od stopnia skażenia gleby, jej właściwości fizykochemicznych, a także od uwarunkowań ekonomicznych i środowiskowych.

Do najstarszych i najbardziej bezpośrednich metod remediacji należą strategie fizyczne, polegające na usuwaniu zanieczyszczonej warstwy gleby, jej wymianie lub separacji frakcji zawierających metale ciężkie. Choć pozwalają one szybko obniżyć poziom zanieczyszczenia, są kosztowne, energochłonne i silnie ingerują w strukturę ekosystemu glebowego, dlatego stosuje się je głównie na silnie zdegradowanych terenach przemysłowych [55]. Alternatywę stanowią metody chemiczne, których celem jest ograniczenie biodostępności metali ciężkich poprzez modyfikację właściwości chemicznych gleby [56]. W praktyce rolniczej szeroko stosowane jest wapnowanie, prowadzące do podwyższenia pH gleby i zmniejszenia rozpuszczalności kadmu, co zwykle ogranicza jego pobieranie przez rośliny [57,58]. Stosowane są także różnego rodzaju dodatki stabilizujące, takie jak fosforany, biochar, zeolity czy inne materiały sorpcyjne, które mogą immobilizować jony metali poprzez sorpcję powierzchniową, kompleksowanie lub wytrącanie trudno rozpuszczalnych związków [59,60]. Skuteczność tych metod zależy jednak od wielu czynników, w tym właściwości gleby, form chemicznych metalu oraz rodzaju zastosowanego materiału stabilizującego [61].

W ostatnich latach coraz większe zainteresowanie budzą metody biologiczne, uznawane za bardziej przyjazne środowisku i potencjalnie bardziej zrównoważone [62,63]. W zależności od mechanizmu działania wyróżnia się kilka strategii fitoremediacyjnych [64]. Fitoekstrakcja polega na pobieraniu metali z gleby i ich akumulacji w tkankach nadziemnych roślin, co umożliwia stopniowe usuwanie zanieczyszczeń wraz z biomasą [65,66]. Fitostabilizacja

prowadzi natomiast do immobilizacji metali w strefie korzeniowej, ograniczając ich biodostępność w glebie [67]. W przypadku środowisk wodnych lub gleb silnie uwodnionych stosowana jest ryzofiltracja, polegająca na sorpcji i akumulacji metali przez system korzeniowy roślin [62]. Fitodegradacja obejmuje transformację lub rozkład zanieczyszczeń przy udziale enzymów roślinnych, często wspomaganąych przez mikroorganizmy ryzosferowe [68]. Z kolei fitowolatylizacja polega na pobieraniu pierwiastków przez rośliny, ich przekształceniu w formy lotne i uwalnianiu do atmosfery [69]. W przypadku metali ciężkich szczególne znaczenie przypisuje się jednak fitoekstrakcji i fitostabilizacji, które umożliwiają odpowiednio usuwanie metali z gleby lub ograniczanie ich dostępności biologicznej [67,70].

W procesie fitoekstrakcji istotną rolę odgrywają rośliny zdolne do intensywnego pobierania i akumulacji metali w tkankach nadziemnych, określane jako akumulatory lub hiperakumulatory [70]. Do najlepiej poznanych hiperakumulatorów kadmu należą m.in. tobołek alpejski (*Noccaea caerulescens*, syn. *Thlaspi caerulescens*) oraz *Sedum alfredii*, które stanowią modelowe gatunki wykorzystywane w badaniach nad fitoekstrakcją Cd [71–75]. Rośliny te przyczyniają się do stopniowego zmniejszania puli kadmu w glebie poprzez jego pobieranie i akumulację w biomasie. Efektywność fitoekstrakcji w warunkach praktycznych jest jednak często ograniczana przez długi czas trwania procesu, specyficzne uwarunkowania glebowe wpływające na biodostępność Cd oraz cechy biologiczne samych roślin, takie jak tempo wzrostu czy wielkość wytwarzanej biomasy [76]. Dodatkowo w warunkach wysokiego skażenia kadmem może dochodzić do zahamowania wzrostu roślin, co w konsekwencji obniża wydajność procesu remediacji [17]. W odpowiedzi na te ograniczenia coraz większe zainteresowanie budzą strategie zintegrowane, łączące różne podejścia remediacyjne w celu zwiększenia skuteczności. Integracja fitoremediacji z dodatkami glebowymi, takimi jak biochar czy mikroorganizmy ryzosferowe, może prowadzić do efektów synergistycznych obejmujących zarówno zmianę biodostępności metali w glebie, jak i poprawę wzrostu roślin w warunkach stresu wywołanego metalami ciężkimi [77,78].

W związku z tym rośnie zainteresowanie biologicznymi strategiami ograniczania stresu oraz wspierania funkcjonowania organizmów w środowisku skażonym. Szczególną uwagę zwraca poszukiwanie czynników, często pochodzenia naturalnego, zdolnych do modulowania odpowiedzi komórkowych i fizjologicznych na stres wywołany obecnością metali ciężkich [79].

Najważniejsze strategie remediacji gleb skażonych kadmem, wraz z ich mechanizmami działania, zaletami oraz ograniczeniami, zestawiono w Tabeli 1.

Tabela 1. Strategie remediacji gleb skażonych kadmem – mechanizmy działania, przykłady metod oraz ich zalety i ograniczenia.

Kategoria strategii	Przykładowe metody	Mechanizm działania	Zalety	Ograniczenia
Fizyczne	Usuwanie lub wymiana gleby	Mechaniczne usunięcie skażonej warstwy gleby lub separacja frakcji zawierających metale [55]	szybkie obniżenie poziomu zanieczyszczeń	wysokie koszty, silna ingerencja w ekosystem glebowy
Chemiczne	Wapnowanie, stabilizacja chemiczna	Zmiana właściwości chemicznych gleby i immobilizacja Cd poprzez sorpcję, kompleksowanie lub wytrącanie [57,56,58]	stosunkowo szybkie ograniczenie mobilności Cd, łatwe wdrożenie w praktyce	skuteczność zależna od właściwości gleby i warunków środowiskowych
Biologiczne	Fitoremediacja (fitoekstrakcja, fitostabilizacja, ryzofiltracja)	Pobieranie, akumulacja lub immobilizacja Cd przez rośliny [62,63,79]	metoda przyjazna środowisku, możliwość stopniowego oczyszczania gleby	Powolny proces, ograniczenia związane z biomasą roślin i biodostępnością metalu
Zintegrowane	Łączenie metod biologicznych i chemicznych	Wspomaganie fitoremediacji dodatkami glebowymi lub mikroorganizmami ryzosferowymi [77,78]	zwiększona skuteczność i stabilność procesu remediacji	większa złożoność technologiczna i potrzeba optymalizacji warunków

6.1.4. Olejki eteryczne – właściwości chemiczne, aktywność biologiczna i potencjalne zastosowania

Olejki eteryczne stanowią złożoną grupę naturalnych, lotnych metabolitów wtórnych syntetyzowanych przez liczne gatunki roślin wyższych [80]. Gromadzone są w wyspecjalizowanych strukturach wydzielniczych, najczęściej w liściach, kwiatach i młodych pędach, choć mogą występować również w innych organach roślin, w tym w korzeniach, owocach czy nasionach [81]. Olejki eteryczne są wieloskładnikowymi mieszaninami niskocząsteczkowych związków organicznych, w których dominują terpenoidy - przede wszystkim monoterpeny i seskwiterpeny - oraz związki fenylopropanoidowe [82]. Do najczęściej identyfikowanych monoterpenów należą m.in. tymol i γ-terpinen charakterystyczne dla *Thymus vulgaris* [83], karwakrol występujący w olejkach *Origanum vulgare* i *Thymus spp.*[84], a także limonen obecny w olejkach cytrusowych (*Citrus spp.*) [85] oraz linalol charakterytyczny dla lawendy (*Lavandula angustifolia*) [86]. Wśród seskwiterpenów często spotykany jest β-kariofilen obecny m.in. w olejku goździkowym (*Syzygium aromaticum*) [87], a także bisabolol charakterystyczny dla rumianku (*Matricaria chamomilla*) [88]. Do ważnych składników olejków eterycznych należą również fenylopropanoidy, takie jak eugenol obecny w olejku goździkowym (*Syzygium aromaticum*) [89]. Skład jakościowy i ilościowy olejków eterycznych zależy od wielu czynników, w tym gatunku rośliny, chemotypu, warunków środowiskowych, stadium rozwojowego oraz zastosowanej metody ekstrakcji [90].

W wielu przypadkach aktywność biologiczna całych olejków jest silniejsza niż działanie pojedynczych wyizolowanych składników, co wskazuje na występowanie efektów synergistycznych lub addytywnych pomiędzy poszczególnymi komponentami [91,92]. Te lotne metabolity wtórne pełnią w organizmach roślinnych szereg istotnych funkcji, takich jak ochrona przed patogenami oraz roślinożercami, a także udział w komunikacji chemicznej z innymi organizmami [93]. Olejki eteryczne mogą również uczestniczyć w oddziaływaniach allelopatycznych, polegających na uwalnianiu do środowiska związków chemicznych zdolnych do modulowania kiełkowania nasion oraz wzrostu i rozwoju innych roślin, co może wpływać na kształtowanie relacji konkurencyjnych w zbiorowiskach roślinnych [94].

Olejki eteryczne mogą być pozyskiwane z materiału roślinnego różnymi metodami ekstrakcji. Do najczęściej stosowanych technik należą hydrodestylacja oraz destylacja z parą wodną, które są powszechnie wykorzystywane w przemyśle ze względu na stosunkowo wysoką wydajność, prostotę technologiczną oraz korzystne aspekty ekonomiczne [95]. W przypadku surowców cytrusowych stosowane jest również tłoczenie na zimno [96]. W ostatnich latach coraz większe znaczenie zyskują nowoczesne metody ekstrakcji, takie jak ekstrakcja nadkrytycznym dwutlenkiem węgla, ekstrakcja wspomagana ultradźwiękami lub mikrofalami, które pozwalają uzyskać ekstrakty o wysokiej jakości przy jednoczesnym ograniczeniu degradacji związków wrażliwych na wysokie temperatury [97,98].

Szerokie spektrum aktywności biologicznej olejków eterycznych sprawia, że są one intensywnie badane w kontekście wielu zastosowań praktycznych. Jednym z najlepiej udokumentowanych efektów ich działania jest aktywność przeciwdrobnoustrojowa. Liczne badania wykazały, że olejki eteryczne mogą hamować wzrost zarówno bakterii Gram-dodatnich i Gram-ujemnych, jak i wielu patogenów grzybowych [99–104]. Mechanizm ich działania związany jest przede wszystkim z destabilizacją błon komórkowych mikroorganizmów, zwiększeniem ich przepuszczalności oraz zaburzeniem podstawowych procesów metabolicznych [105–107]. Olejki eteryczne wykazują również właściwości przeciwutleniające, wynikające głównie z obecności związków fenolowych zdolnych do neutralizacji reaktywnych form tlenu oraz modulowania aktywności enzymów antyoksydacyjnych [108,109]. Ze względu na te właściwości olejki eteryczne znajdują zastosowanie w wielu sektorach gospodarki. W medycynie wykorzystywane są jako składniki preparatów o działaniu przeciwbakteryjnym, przeciwzapalnym, wykrztuśnym czy rozkurczowym [110–112]. Ponadto są szeroko stosowane w kosmetologii i przemyśle spożywczym, gdzie pełnią funkcję składników zapachowych oraz substancji o działaniu antyoksydacyjnym i przeciwzapalnym, a także analizowany jest ich potencjał jako naturalnych konserwantów ograniczających rozwój drobnoustrojów i hamujących procesy oksydacyjne w produktach spożywczych [113–115].

W ostatnich latach rośnie także zainteresowanie wykorzystaniem olejków eterycznych w rolnictwie. Badania wskazują, że związki te mogą wykazywać aktywność wobec różnych organizmów szkodliwych dla roślin uprawnych, w tym owadów, roztoczy, nicieni oraz patogenów grzybowych [116–120]. Jedną z istotnych zalet olejków eterycznych jako

komponentów biopestycydów jest ich korzystny profil środowiskowy. W porównaniu z konwencjonalnymi pestycydami syntetycznymi charakteryzują się one wysoką biodegradowalnością oraz stosunkowo krótkim czasem półtrwania w środowisku [121,122], co ogranicza ich akumulację w glebie i wodach powierzchniowych. W wielu przypadkach wykazują one także relatywnie niską toksyczność wobec organizmów niedocelowych, w tym pożytecznych gatunków obecnych w agroekosystemach, takich jak zapylacze czy naturalni wrogowie szkodników [123,124]. Rosnące zainteresowanie zastosowaniem olejków eterycznych w ochronie roślin doprowadziło do opracowania szeregu komercyjnych preparatów agrotechnicznych opartych na tych związkach. Przykładem jest preparat EcoSMART® Organic Insecticide (EcoSMART Technologies Inc., USA) zawierający mieszaninę olejków roślinnych, w tym olejek rozmarynowy (*Rosmarinus officinalis*), tymiankowy (*Thymus vulgaris*) oraz goździkowy (*Syzygium aromaticum*), stosowany do zwalczania mszyc, wciornastków i przędziorków [125]. Innym przykładem jest także herbicyd Weed Zap® (JH Biotech Inc., Ventura, CA, USA), którego głównym składnikiem aktywnym jest olejek goździkowy bogaty w eugenol, wykazujący działanie kontaktowe wobec młodych chwastów [126]. Jednym z najlepiej znanych preparatów opartych na olejkach eterycznych w Europie jest fungicyd Timorex Gold® (STK Bio-Ag Technologies, Rehovot, Izrael), którego substancją aktywną jest olejek z drzewa herbacianego (*Melaleuca alternifolia*), wykazujący skuteczność wobec licznych patogenów grzybowych [127].

Pomimo licznych zalet praktyczne zastosowanie olejków eterycznych w rolnictwie wiąże się również z pewnymi ograniczeniami. Do najważniejszych należą wysoka lotność tych związków, zmienność składu chemicznego zależna od chemotypu roślin oraz ograniczona stabilność w warunkach polowych [128]. W związku z tym coraz większą uwagę poświęca się opracowywaniu nowych formulacji, takich jak nanoemulsje, systemy mikrokapsułkowania czy formulacje polimerowe, które mogą zwiększyć stabilność olejków oraz umożliwić kontrolowane uwalnianie substancji aktywnych [129].

Podsumowując, olejki eteryczne stanowią ważną grupę naturalnych związków biologicznie aktywnych o szerokim spektrum działania. Ich właściwości przeciwdrobnoustrojowe, przeciwutleniające oraz owadobójcze sprawiają, że mogą one znaleźć zastosowanie zarówno w medycynie, jak i w strategiach zrównoważonego rolnictwa (Ryc. 2).

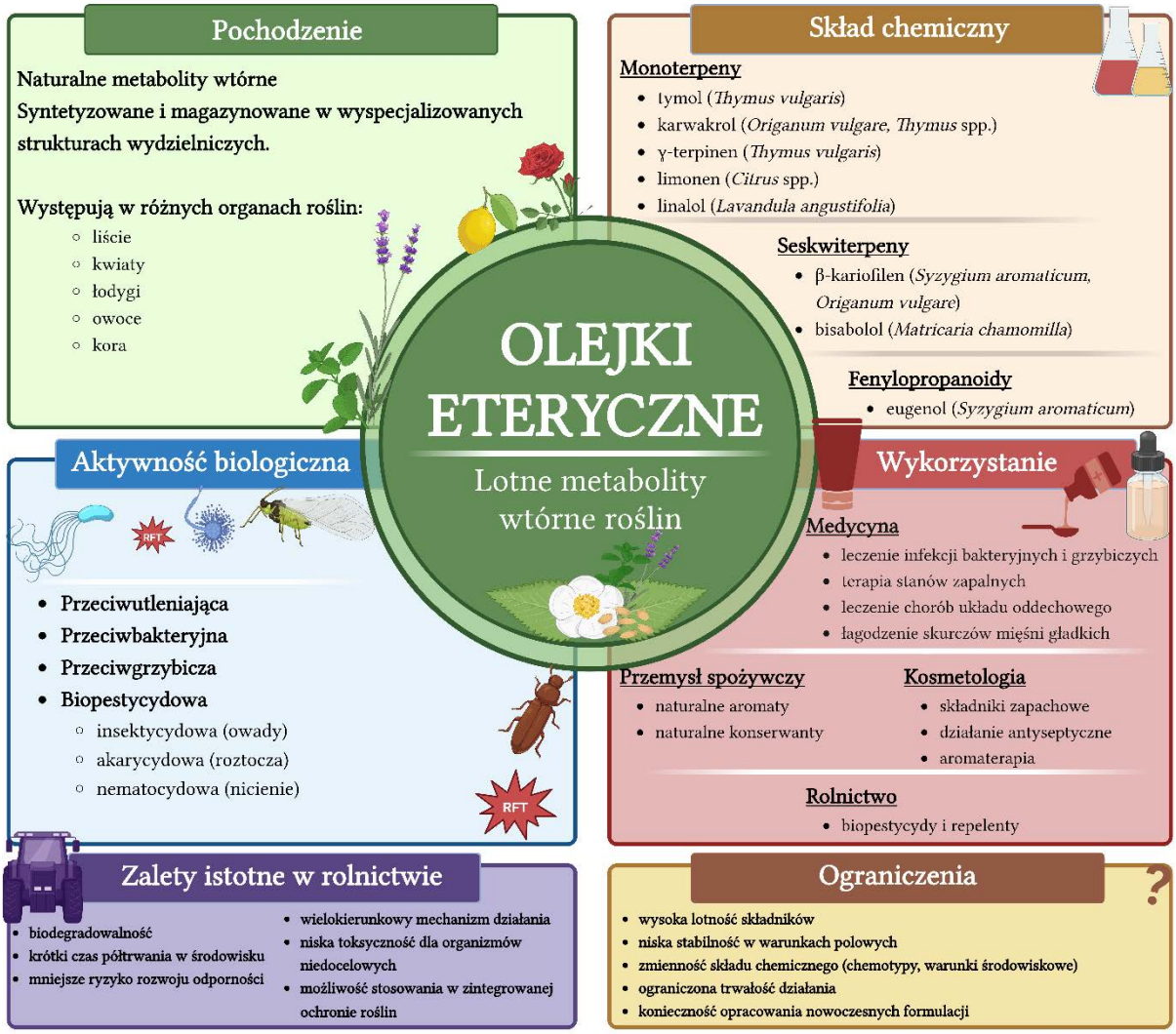

Ryc. 2. Schemat przedstawiający pochodzenie, skład chemiczny, aktywność biologiczną oraz główne kierunki zastosowań olejków eterycznych. Rycina przygotowana z wykorzystaniem BioRender.com.

6.1.5. Olejek tymiankowy – pochodzenie, bioaktywność i wielokierunkowy potencjał aplikacyjny

Wśród licznych olejków eterycznych szczególne zainteresowanie badawcze budzi olejek tymiankowy pozyskiwany z macierzanki zwyczajnej (*Thymus vulgaris* L.), rośliny należącej do rodziny jasnowatych (Lamiaceae) [130]. Chociaż olejek tymiankowy może być pozyskiwany również z innych gatunków rodzaju *Thymus*, takich jak *T. serpyllum* czy *T. zygis*, to właśnie *T. vulgaris* stanowi najczęściej wykorzystywane źródło surowca olejkowego [131]. Gatunek ten pochodzi z regionu śródziemnomorskiego, jednak obecnie jest szeroko uprawiany w wielu regionach świata jako roślina przyprawowa, lecznicza oraz surowiec do produkcji olejku eterycznego [132]. Olejek tymiankowy pozyskiwany jest najczęściej z nadziemnych części rośliny, przede wszystkim z liści i kwitnących pędów [83]. Jego skład chemiczny zależy od chemotypu, jednak najczęściej dominującymi składnikami są tymol, p-cymen, γ-terpinen oraz karwakrol [133,134].

Kompozycje olejku tymiankowego, a także obecne w nim fenolowe monoterpeny, takie jak tymol i karwakrol, wykazują szerokie spektrum aktywności biologicznej. W licznych badaniach potwierdzono jego działanie przeciwbakteryjne wobec *Staphylococcus aureus*, *Listeria monocytogenes*, *Escherichia coli* oraz *Salmonella* spp., przeciwgrzybicze wobec drożdżaków z rodzaju *Candida* (*Candida* spp.) oraz grzybów pleśniowych z rodzaju *Aspergillus* (*Aspergillus* spp.) [135–138]. Wykazano również jego właściwości antyoksydacyjne [139]. Coraz więcej badań wskazuje ponadto na potencjalne właściwości przeciwnowotworowe olejku tymiankowego [140–142]. Warto podkreślić, że olejek tymiankowy znajduje zastosowanie w medycynie tradycyjnej oraz farmakoterapii od wielu stuleci. Preparaty zawierające ekstrakty lub olejek z *Thymus vulgaris* stosowane są przede wszystkim jako środki o działaniu wykrztuśnym i sekretolitycznym, łagodzące objawy kaszlu, bólu gardła oraz stanów zapalnych górnych dróg oddechowych [143,144].

Oprócz właściwości istotnych z punktu widzenia medycyny, olejek tymiankowy wykazuje również znaczącą aktywność biologiczną wobec organizmów uznawanych za szkodniki w rolnictwie. W badaniach wykazano jego działanie owadobójcze wobec m.in. chrząszczy magazynowych oraz roztoczy z rodzaju *Tetranychus* [145–147]. Szerokie spektrum aktywności biologicznej olejku tymiankowego znajduje odzwierciedlenie w jego zastosowaniu w komercyjnych preparatach wykorzystywanych w rolnictwie oraz pszczelarstwie. Przykładem jest biopestycyd Thymox® (Laboratoire M2, Quebec, QC, Kanada), stosowany do zwalczania patogenów roślinnych, takich jak *Botrytis cinere* (sprawca szarej pleśni) oraz *Erwinia amylovora* (czynnik etiologiczny zarazy ogniowej). Olejek tymiankowy stanowi również substancję aktywną preparatu Thymovar® (Andermat BioVet, Grossdietwil, Szwajcaria), a także wchodzi w skład produktu ApiLife Var® (Chemicals Laif SPA, Vigonza, Włochy), w którym występuje w połączeniu z olejkiem eukaliptusowym i kamforą. Preparaty te stosowane są przede wszystkim do zwalczania pasożytniczego roztocza *Varroa destructor* u pszczoły miodnej (*Apis mellifera*).

Interesującym kierunkiem badań jest także potencjalna zdolność olejku tymiankowego do łagodzenia skutków toksycznego działania metali ciężkich. W zwierzęcych modelach eksperymentalnych wykazano, że związki obecne w olejkach z rodzaju *Thymus* mogą ograniczać stres oksydacyjny oraz uszkodzenia tkanek indukowane przez kadm poprzez zwiększenie aktywności enzymów antyoksydacyjnych i zmniejszenie peroksydacji lipidów [148,149].

Podsumowując, olejek tymiankowy, ze względu na dobrze udokumentowaną aktywność biologiczną oraz dostępność surowca roślinnego, stanowi obiecujący obiekt badań nad jego potencjalnym wykorzystaniem w ochronie zarówno organizmów zwierzęcych, jak i roślinnych w zakresie ograniczania skutków stresów środowiskowych (Ryc. 3).

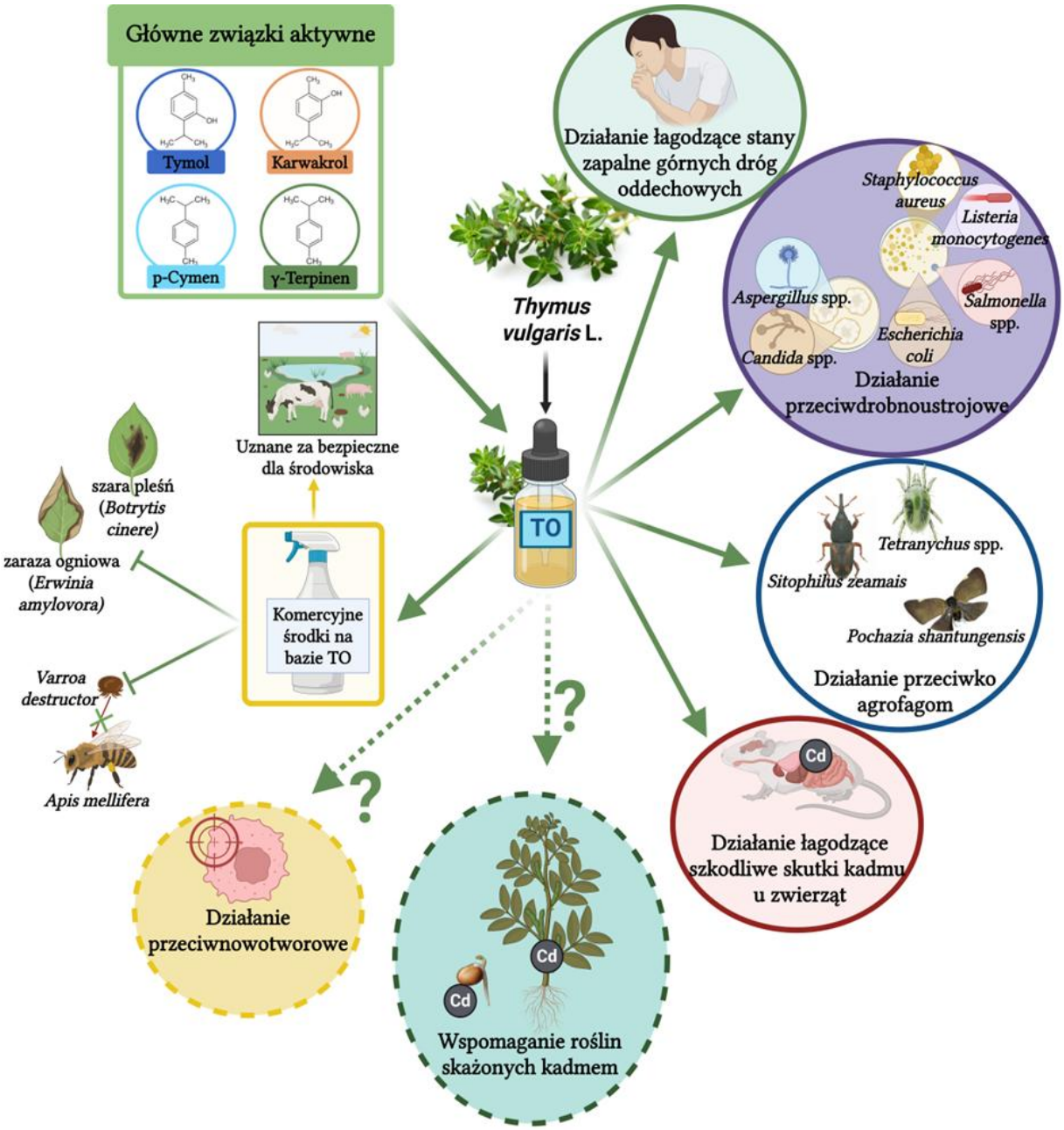

Ryc. 3. Schemat przedstawiający pochodzenie olejku tymiankowego, jego główne składniki aktywne oraz zakres udokumentowanej aktywności biologicznej i zastosowań praktycznych. Uwzględniono źródło surowca olejkowego, przede wszystkim *Thymus vulgaris* L., a także najważniejsze składniki chemiczne olejku, takie jak tymol, karwakrol, p-cymen i γ-terpinen. Schemat ilustruje również udowodnione działania biologiczne olejku tymiankowego oraz przykłady opracowanych komercyjnych preparatów i ich docelowych zastosowań. Strzałki ciągłe oznaczają zależności i mechanizmy potwierdzone w badaniach naukowych, natomiast strzałki przerywane (oznaczone znakami zapytania) wskazują potencjalne, wciąż badane lub hipotetyczne kierunki przyszłych zastosowań olejku tymiankowego. Rycina przygotowana z wykorzystaniem BioRender.com.

6.1.6. Uzasadnienie wyboru tematyki badawczej

Przedstawione zagadnienia wskazują, że mimo licznych badań nad oddziaływaniem kadmu na organizmy żywe oraz rozwijanych strategii ograniczania jego negatywnego wpływu, poszukiwanie nowych czynników mogących wspomagać organizmy w warunkach stresu wywołanego metalami ciężkimi pozostaje aktualnym wyzwaniem badawczym. Biorąc pod uwagę szerokie spektrum właściwości biologicznych olejków eterycznych, ich względne bezpieczeństwo środowiskowe oraz rosnące zainteresowanie ich wykorzystaniem w rolnictwie, m.in. jako naturalnych środków ograniczających rozwój patogenów i szkodników, zasadne wydaje się rozważenie ich potencjalnej roli w łagodzeniu skutków stresu wywołanego obecnością metali ciężkich. W tym kontekście szczególne zainteresowanie budzi olejek tymiankowy, należący do najlepiej poznanych olejków eterycznych, bogaty w biologicznie aktywne związki fenolowe, takie jak tymol i karwakrol. Związki te wykazują silne właściwości przeciwutleniające oraz zdolność do modulowania odpowiedzi organizmów na stres oksydacyjny. Co istotne, olejek tymiankowy jest już wykorzystywany jako składnik komercyjnych preparatów stosowanych w ochronie roślin i pszczelarstwie, a jego stosowanie uznawane jest za względnie bezpieczne dla środowiska. W związku z tym interesującym kierunkiem badań jest ocena, czy olejek tymiankowy może wspomagać rośliny narażone na toksyczne działanie kadmu, którego obecność w środowisku stanowi narastający problem ekologiczny.

6.2. Cel pracy

Analiza wpływu kadmu (175 µM $CdCl_2$) na aparat strukturalny, mechanizmy regulacyjne oraz przebieg procesów związanych z cyklem komórkowym w merystemach korzeni zarodkowych *Vicia faba* L. var. *minor*, a także określenie mechanizmów ochronnych olejku tymiankowego (TO; 0,03%) oraz jego zdolności do neutralizacji toksycznego działania kadmu w komórkach.

Badania zostały podzielone na etapy, z których każdy obejmował cele cząstkowe wsparte hipotezą badawczą.

6.2.1. Praca 1 (Załącznik nr 1)

Cel: Określenie wpływu kadmu jako induktora ROS na integralność genomu, proces replikacji DNA i dynamikę cyklu komórkowego, oraz ocena zdolności TO w zakresie ograniczania wywołanych przez kadm zaburzeń i przywracania stabilności w procesie powielania materiału genetycznego.

Hipoteza badawcza: Stres kadmowy prowadzi do nadprodukcji ROS, co skutkuje indukcją dwuniciowych pęknięć DNA, zaburzeniami replikacji oraz aktywacją punktów kontrolnych cyklu komórkowego, natomiast TO, dzięki swoim właściwościom antyoksydacyjnym, ogranicza akumulację ROS, chroniąc komórki merystematyczne przed stresem genotoksycznym i replikacyjnym indukowanym przez kadm.

Cele etapowe:

1. Analiza składu chemicznego olejku tymiankowego metodą GC-MS w celu powiązania uzyskanych efektów biologicznych z obecnością związków o potencjale antyoksydacyjnym.
2. Ocena poziomu stresu oksydacyjnego na podstawie analizy zawartości nadtlenku wodoru (H_2O_2) oraz anionorodnika ponadtlenkowego ($O_2^{\bullet -}$) w komórkach merystematycznych.
3. Analiza rozkładu komórek w poszczególnych fazach interfazy (G1, S, G2) na podstawie cytofotometrycznych pomiarów zawartości DNA.
4. Ocena przebiegu replikacji DNA z wykorzystaniem markera syntezy DNA (IdU), obejmująca analizę odsetka komórek replikujących oraz dynamiki poszczególnych etapów fazy S.
5. Określenie poziomu uszkodzeń DNA na podstawie immunocytochemicznej detekcji γH2A.X jako markera dwuniciowych pęknięć DNA.

6.2.2. Praca 2 (Załącznik nr 2)

Cel: Opracowanie procedury adaptacji metody izolacji białek związanych z nowo syntetyzowanym DNA (iPOND; *isolation of Proteins On Nascent DNA*) do badań w materiale roślinnym (*Vicia faba* L. var. *minor*).

Hipoteza: Metoda iPOND może zostać skutecznie zaadaptowana do komórek merystematycznych roślin, umożliwiając ocenę wpływu badanych czynników na zmiany składu białek związanych z nowo syntetyzowanym DNA, w tym komponentów replisomu, odzwierciedlających reorganizację chromatyny w obrębie widełek replikacyjnych.

Cele etapowe:

1. Adaptacja i optymalizacja metody iPOND do zastosowania w badaniach materiału roślinnego (korzeni zarodkowych *V. faba*).
2. Walidacja skuteczności metody iPOND poprzez potwierdzenie selektywnej izolacji białek związanych z nowo syntetyzowanym DNA w komórkach kontrolnych oraz komórkach poddanych działaniu czynnika indukującego stres replikacyjny.
3. Ocena przydatności metody iPOND do analizy składu białek związanych z aktywnymi i zahamowanymi widełkami replikacyjnymi oraz jej potencjału w badaniach mechanizmów stresu replikacyjnego w komórkach roślinnych.

6.2.3. Praca 3 (Załącznik nr 3)

Cel: Określenie wpływu kadmu na aktywację jądrowych kinaz sygnałowych (MAPK) oraz związane z tym zmiany epigenetyczne i transkrypcyjne w komórkach merystematycznych, a także ocena zdolności TO do stabilizacji osi sygnałowej MAPK–chromatyna oraz ograniczania skutków stresu wywołanego kadmem na poziomie organizacji chromatyny oraz aktywności transkrypcyjnej.

Hipoteza badawcza: Kadm aktywuje jądrowe kinazy MAPK w komórkach merystematycznych, które pośredniczą w indukcji zmian epigenetycznych, prowadzących do kondensacji chromatyny i represji transkrypcji, natomiast TO wykazuje działanie ochronne poprzez stabilizację osi MAPK–chromatyna i ograniczanie epigenetycznych oraz transkrypcyjnych skutków stresu kadmowego.

Cele etapowe:

1. Analiza aktywności jądrowych kinaz MAPK (MPK3/MPK6), na podstawie liczby, powierzchni i intensywności ognisk immunofluorescencyjnych.
2. Analiza zmian globalnego poziomu metylacji DNA (5-metylocytozyny)
3. Identyfikacja i ilościowa ocena poziomu wybranych modyfikacji epigenetycznych histonów:
    - dimetylacji histonu H3 w pozycji lizyny 4 (H3K4Me2),
    - fosforylacji histonu H3 w pozycji treoniny 45 (H3T45Ph),
    - acetylacji histonu H4 w pozycji lizyny 5 (H4K5Ac),
    - acetylacji histonu H3 w pozycji lizyny 9 (H3K9Ac),
    - acetylacji histonu H3 w pozycji lizyny 56 (H3K56Ac).
4. Ocena aktywności transkrypcyjnej na podstawie analizy inkorporacji 5-etynylo-urydyny (EU) do syntetyzowanego RNA w jądrach i jąderkach komórek merystematycznych.

6.2.4. Praca 4 (Załącznik nr 4)

Cel: Określenie mechanizmów, poprzez które kadm wpływa na regulację i przebieg mitozy w komórkach merystematycznych, oraz ocena potencjału ochronnego TO w zakresie integralności i stabilizacji aparatu podziałowego w warunkach stresu wywołanego kadmem.

Hipoteza badawcza: Kadm zaburza integralność aparatu mitotycznego komórek merystematycznych, poprzez wpływ na regulatory cyklu komórkowego, organizację cytoszkieletu oraz mitotyczne modyfikacje epigenetyczne chromatyny, natomiast TO wykazuje działanie ochronne, stabilizując te procesy i utrzymując aktywność podziałową komórek.

Cele etapowe:

1. Ocena przyrostu korzeni zarodkowych jako wskaźnika ogólnej aktywności proliferacyjnej komórek merystematycznych.
2. Określenie indeksu mitotycznego poprzez wyznaczenie procentowego udziału komórek dzielących się oraz rozkładu komórek w poszczególnych fazach mitozy (profaza, metafaza, anafaza, telofaza), wraz z identyfikacją i charakterystyką zmian w organizacji chromatyny oraz chromosomów mitotycznych.
3. Analiza poziomu białkowych regulatorów przejścia G2/M cyklu komórkowego (CDKA, CycB) oraz ekspresji genu *CycB*, w celu oceny sprawności molekularnych mechanizmów kontroli mitozy.
4. Ocena organizacji i dynamiki elementów cytoszkieletu, obejmująca analizę mikrotubul interfazowych i mitotycznych oraz filamentów aktynowych.
5. Charakterystyka wzorców fosforylacji histonu H3 specyficznych dla fazy M (H3T3Ph, H3S10Ph) jako markerów kondensacji chromatyny i prawidłowej segregacji chromatyd podczas przebiegu mitozy.

6.2.5. Praca 5 (Załącznik nr 5)

Cel: Ocena zawartości kadmu i jego wpływu na homeostazę redoks, mechanizm detoksykacji, organizację ultrastrukturalną komórek merystematycznych oraz skuteczność naprawy uszkodzeń DNA, a także weryfikacja potencjału ochronnego TO w ograniczaniu zmian indukowanych stresem kadmowym.

Hipoteza: Toksyczność kadmu w komórkach merystematycznych wynika z jego akumulacji prowadzącej do zaburzenia równowagi redoks, destabilizacji błon komórkowych, uszkodzeń materiału genetycznego oraz zmian ultrastrukturalnych organelli, a także ograniczenia efektywności mechanizmów detoksykacyjnych i naprawczych natomiast TO, poprzez modulację poziomu akumulowanego kadmu oraz stabilizację środowiska redoks, ogranicza zakres tych zaburzeń.

Cele etapowe:

1. Oznaczenie zawartości kadmu w korzeniach zarodkowych w celu oceny wpływu TO na akumulację badanego metalu ciężkiego.
2. Ocena statusu oksydacyjnego komórek poprzez oznaczenie poziomu nadtlenku wodoru (H_2O_2).
3. Charakterystyka enzymatycznego systemu antyoksydacyjnego, obejmująca oznaczenie aktywności dysmutazy ponadtlenkowej (SOD), katalazy (CAT), peroksydazy askorbinianowej (APX) oraz reduktazy glutationowej (GR).

4. Analiza nieenzymatycznych elementów obrony antyoksydacyjnej, obejmująca oznaczenie poziomu askorbinianu, glutationu (GSH), cysteiny, γ-glutamylocysteiny oraz proliny.
5. Ocena aktywacji metabolizmu tiolowego i mechanizmów chelatacyjnych, poprzez oznaczenie poziomu fitochelatyn (PC2–PC5).
6. Określenie stopnia oksydacyjnego uszkodzenia błon komórkowych na podstawie zawartości malondialdehydu (MDA) jako markera peroksydacji lipidów.
7. Ocena integralności genomu poprzez analizę fragmentacji DNA metodą TUNEL stanowiącą wskaźnik nieefektywnie naprawionych uszkodzeń.
8. Charakterystyka zmian ultrastrukturalnych w komórkach merystematycznych z wykorzystaniem transmisyjnej mikroskopii elektronowej (TEM).

6.3. Metodyka badań

6.3.1. Model badawczy

6.3.1.1. Materiał badawczy

Materiałem badawczym były merystemy korzeni zarodkowych pochodzące z trzydniowych siewek bobiku (*Vicia faba* L. var. *minor*). Gatunek ten jest powszechnie wykorzystywany w badaniach cytologicznych ze względu na wyjątkowo korzystne cechy morfologiczne jąder komórkowych. Komórki merystematyczne bobiku posiadają jądra typu siatkowatego, charakteryzujące się wyraźnie zorganizowaną chromatyną interfazową z dobrze widocznymi obszarami chromatyny skondensowanej, tworzącymi charakterystyczne chromocentra. Struktury te odpowiadają regionom przycentromerowym i telomerowym bogatym w heterochromatynę, a ich rozmieszczenie odzwierciedla polaryzację chromosomów zgodną z modelem Rabla, zakładającym ich uporządkowaną, nieprzypadkową organizację w jądrze interfazowym. Taka architektura jądra umożliwia analizę zmian w organizacji chromatyny interfazowej oraz ocenę zaburzeń jej struktury w mikroskopii świetlnej, fluorescencyjnej i elektronowej. Dodatkowym atutem tego modelu jest niewielka, diploidalna liczba chromosomów ($2n = 12$) o wyraźnej morfologii i dużych rozmiarach, które w trakcie mitozy są łatwe do obserwacji i tworzą czytelne figury podziałowe. Sprzyjają one analizie przebiegu mitozy, ocenie stopnia kondensacji oraz identyfikacji zaburzeń segregacji do jąder potomnych.

Gatunek ten wykazuje również duże znaczenie gospodarcze. Charakteryzuje się wysokim potencjałem plonotwórczym, wytwarzając nasiona o dużej masie i wysokiej zawartości białka, wykorzystywane głównie jako wartościowa pasza dla zwierząt. Ponadto może pełnić funkcję rośliny międzyplonowej, wzbogacając glebę w materię organiczną i azot, co przyczynia się do poprawy jej żyzności. Z tego względu stanowi nie tylko dogodny model badawczy, ale także gatunek istotny z punktu widzenia praktyki rolniczej.

6.3.1.2. Kadm jako związek toksyczny

W badaniach zastosowano Cd w postaci $CdCl_2$ ze względu na jego wysoką rozpuszczalność w wodzie, łatwą dysocjację do biologicznie aktywnych jonów Cd^{2+}, brak tendencji do tworzenia osadów oraz możliwość przygotowania stabilnych roztworów o kontrolowanym stężeniu. Forma ta jest powszechnie wykorzystywana w eksperymentalnych modelach fitotoksyczności, co umożliwia porównywanie uzyskanych wyników z danymi literaturowymi. Stężenie $CdCl_2$ wynoszące 175 µM, dobrane w celu wywołania wyraźnych zmian makroskopowych, w postaci zahamowanego wzrostu korzeni zarodkowych, oraz widocznych pod mikroskopem zaburzeń na poziomie komórkowym, ustalono na podstawie danych literaturowych i wyników wstępnych eksperymentów, w których testowano zakres stężeń od 100 do 200 µM [150–152].

6.3.1.3. Olejek tymiankowy jako bio-protektor

W badaniach zastosowano komercyjnie dostępny olejek eteryczny z macierzanki zwyczajnej (*Thymus vulgaris* L.) w stężeniu 0,03%, dobranym w celu przywrócenia prawidłowego wzrostu korzeni zarodkowych. Stężenie to ustalono na podstawie testów przeprowadzonych w zakresie stężeń 0,01–0,06%. Wybór olejku eterycznego powszechnie określanego olejkiem tymiankowym (TO) wynikał z udokumentowanych właściwości modulujących procesy redoks. Mimo wielowiekowego wykorzystania w tradycyjnej medycynie, kosmetyce i przemyśle spożywczym oraz potwierdzonej aktywności biologicznej w modelach zwierzęcych i systemach *in vitro* [153–156], molekularne mechanizmy działania TO w komórkach roślinnych pozostają nadal słabo poznane. Dodatkowym kryterium wyboru była łatwa dostępność surowca roślinnego, umożliwiająca jego potencjalne szerokie zastosowanie w programach ochrony roślin.

Ze względu na hydrofobowy charakter olejku, w celu zapewnienia jego stabilności, biodostępności oraz równomiernego kontaktu z tkanką roślinną, zastosowano formę zemulgowaną [157–159]. Olejek przygotowano w mieszaninie emulgującej (zawierającej nasycone kwasy tłuszczowe C14–18, nienasycone C16–18 mono- i di-etoksylowane glicerydy oraz etoksylowany olej *Brassica napus*) w proporcji 1:4 (v/v), co odpowiadało końcowemu stężeniu emulgatora 0,0075% (v/v). Skład i proporcje emulsji opracowano na Wydziale Agronomii Uniwersytetu Przyrodniczego w Poznaniu, w oparciu o analizy potwierdzające jej skuteczność i stabilność, zgodnie z protokołem stosowanym w badaniach szklarniowych [160]. Postać niezemulgowana powodowała nierównomierny kontakt TO z korzeniami zarodkowymi oraz większą zmienność wyników, dlatego we wszystkich doświadczeniach stosowano wyłącznie formę zemulgowaną.

6.3.1.4. Hodowla

Trzydniowe siewki *V. faba* o długości korzeni zarodkowych około 2–3 cm inkubowano przez 24 godziny w szczelnie zamkniętych szalkach Petriego. Jako kontrole zastosowano hodowlę w wodzie oraz w roztworze emulgatora w stężeniu użytym do przygotowania olejku. Eksperymentalne warianty obejmowały hodowlę w roztworze chlorku kadmu ($CdCl_2$, 175 µM),

w roztworze emulgowanego olejku tymiankowego (TO, 0,03%) oraz w roztworze $CdCl_2$ uzupełnionym emulgowanym TO.

6.3.2. Metody badawcze

6.3.2.1. Praca 1 (Załącznik 1)

6.3.2.1.1. Analiza składu chemicznego olejku eterycznego

6.3.2.1.1.1. Metoda chromatograficzna i spektroskopowa GC-MS

Analizę składu chemicznego olejku eterycznego przeprowadzono z wykorzystaniem chromatografii gazowej sprzężonej ze spektrometrią mas (GC-MS), które umożliwiają jakościową i półilościową identyfikację jego poszczególnych składników lotnych. Przed analizą próbki olejku rozcieńczano w rozpuszczalniku organicznym, a następnie wprowadzano do układu chromatograficznego, w którym rozdział związków odbywał się na podstawie ich właściwości fizykochemicznych i interakcji z fazą stacjonarną kolumny. Detekcja z wykorzystaniem spektrometrii mas pozwalała na identyfikację komponentów poprzez porównanie uzyskanych widm masowych z bazami danych referencyjnych oraz danymi literaturowymi. Identyfikację związków potwierdzano również na podstawie obliczonych indeksów retencji, wyznaczonych w odniesieniu do homologicznej mieszaniny n-alkanów analizowanej w tych samych warunkach chromatograficznych. Takie podejście umożliwia wiarygodne określenie profilu chemicznego olejku oraz wskazanie dominujących składników odpowiedzialnych za jego aktywność biologiczną.

6.3.2.1.2. Wizualizacja stresu oksydacyjnego w komórkach proliferujących

6.3.2.1.2.1. Detekcja nadtlenku wodoru z użyciem 3,3'-diaminobenzydyny (DAB)

Metoda z wykorzystaniem 3,3'-diaminobenzydyny (DAB) jest stosowana do histochemicznej wizualizacji nadtlenku wodoru (H_2O_2) bezpośrednio w tkankach i umożliwia jego obserwację w preparatach analizowanych w mikroskopie świetlnym. Technika opiera się na reakcji DAB z H_2O_2 katalizowanej przez peroksydazy, prowadzącej do powstania nierozpuszczalnego, brązowego produktu reakcji w miejscach gromadzenia się H_2O_2. Pozwala to na lokalizację tego związku w strukturach komórkowych oraz na jego jakościową lub półilościową ocenę. Intensywność zabarwienia odzwierciedla poziom stresu oksydacyjnego i zazwyczaj pozostaje zgodna z wynikami analiz ilościowych. Metoda ta jest przydatna w identyfikacji komórek doświadczających stresu oksydacyjnego pod wpływem badanych związków oraz może stanowić etap wstępny przed bardziej zaawansowanymi badaniami mechanizmów odpowiedzi komórkowej.

6.3.2.1.2.2. Detekcja anionorodnika ponadtlenkowego barwnikiem NBT

Technika z zastosowaniem błękitu nitrotetrazolowego (NBT) służy do histochemicznej detekcji anionorodnika ponadtlenkowego ($O_2^{-}\bullet$) bezpośrednio w tkankach roślinnych i umożliwia jego obserwację w mikroskopie świetlnym. Metoda opiera się na redukcji NBT przez $O_2^{-}\bullet$ do nierozpuszczalnego, niebieskiego formazanu, który wytrąca się w miejscach wzmożonej generacji tego rodnika. Powstałe wybarwienie pozwala na lokalizację komórek charakteryzujących się podwyższonym poziomem reaktywnych form tlenu, a intensywność

zabarwienia stanowi wskaźnik nasilenia stresu oksydacyjnego. Technika umożliwia zarówno ocenę jakościową, jak i półilościową, a uzyskane obserwacje pozostają zgodne z wynikami analiz ilościowych. Metoda jest użyteczna jako narzędzie wstępnej identyfikacji zmian oksydacyjnych w komórkach poddanych działaniu badanych czynników oraz jako etap poprzedzający bardziej szczegółowe analizy mechanizmów odpowiedzi komórkowej.

6.3.2.1.3. Analiza procentowego rozkładu komórek w interfazie

6.3.2.1.3.1. Cytofotometryczny pomiar zawartości DNA

Metoda opiera się na cytofotometrycznym pomiarze zawartości DNA wybarwionego metodą Feulgena w preparatach mikroskopowych z merystemów korzeniowych, przy wykorzystaniu mikroskopii świetlnej oraz komputerowego systemu do mikrodensytometrii. Metoda umożliwia ilościowe określenie udziału komórek w poszczególnych fazach interfazy (G1, S, G2), a także ocenę zmian w dynamice cyklu komórkowego pod wpływem badanych czynników fitotoksycznych. Analiza rozkładu zawartości DNA pozwala na wnioskowanie o sprawności punktów kontrolnych G1/S i G2/M, występowaniu zaburzeń replikacji oraz ewentualnym przejściu komórek w cykl endoreplikacyjny. Technika ta dostarcza dokładnych danych ilościowych niezbędnych do oceny wpływu stresu na proliferację komórek i regulację przebiegu cyklu komórkowego.

6.3.2.1.4. Analiza procesu replikacji DNA

6.3.2.1.4.1. Immunodetekcja jąder replikujących za pomocą IdU

Identyfikacja jąder replikujących polega na immunofluorescencyjnej detekcji włączania 5-jodo-2′-deoksyurydyny (IdU), analogu tymidyny inkorporowanego do DNA podczas replikacji. Metoda ta umożliwia selektywne znakowanie komórek znajdujących się w fazie S cyklu komórkowego, ponieważ IdU ulega wbudowaniu wyłącznie do nowo syntetyzowanych nici DNA w trakcie jego syntezy. W celu odsłonięcia wbudowanego analogu materiał poddaje się częściowej denaturacji DNA, która umożliwienia jego rozpoznanie przez swoiste przeciwciała. Detekcja immunofluorescencyjna z użyciem przeciwciał skierowanych przeciwko IdU pozwala na wizualizację jąder aktywnie replikujących DNA przy użyciu mikroskopii fluorescencyjnej. Liczba jąder wykazujących sygnał fluorescencyjny, intensywność sygnału oraz wzór jego rozmieszczenia w jądrach, stanowią miarę dynamiki procesu replikacji oraz aktywności proliferacyjnej badanej tkanki pod wpływem badanych czynników stresowych lub fitotoksycznych.

6.3.2.1.5. Analiza uszkodzeń DNA

6.3.2.1.5.1. Immunodetekcja γ-H2AX

Wczesną odpowiedź komórki na podwójne pęknięcia nici DNA można identyfikować za pomocą immunofluorescencyjnego znakowania histonu H2AX ufosforylowanego w pozycji seryny 139 (γ-H2AX). Technika ta umożliwia wizualizację tzw. „ognisk γ-H2AX", które odpowiadają miejscom uszkodzeń DNA oraz inicjowanym w tych rejonach procesom naprawczym. Analiza sygnału pozwala zarówno na ocenę jakościową (rozmieszczenie ognisk w obrębie jąder), jak i ilościową (liczba ognisk na jądro), co daje możliwość oceny stopnia

genotoksyczności wywołanej działaniem czynników fitotoksycznych. Dodatkowo możliwe jest określenie odsetka jąder wykazujących sygnał (indeks znakowania), czyli ustalenie wielkości populacji komórek zawierających uszkodzenia.

6.3.2.2. Praca 2 (Załącznik 2)

6.3.2.2.1. Analiza białek związanych z replikacją

Analizę białek związanych z nowo syntetyzowanym DNA przeprowadza się przy zastosowaniu techniki iPOND (*isolation of Proteins On Nascent DNA*). Metoda ta umożliwia selektywną izolację kompleksów DNA–białko obecnych w obrębie aktywnych widełek replikacyjnych oraz świeżo zreplikowanej chromatyny. Opiera się ona na czasowym znakowaniu nowo syntetyzowanego DNA analogiem nukleozydu EdU (5-etynylo-2′-deoksyurydyną), który ulega wbudowaniu wyłącznie w DNA syntetyzowane podczas inkubacji, a następnie jego oznakowanie biotyną w wyniku specyficznej reakcji chemicznej „click chemistry". Utrwalenie komórek pozwala zachować natywne interakcje między DNA a związanymi z nim białkami, natomiast fragmentacja chromatyny w wyniku sonikacji oraz wykorzystanie powinowactwa biotyny do streptawidyny umożliwiają izolację znakowanych fragmentów DNA wraz z towarzyszącymi im białkami przy użyciu kulek opłaszczonych streptawidyną.

Uzyskany materiał poddaje się analizie immunochemicznej lub proteomicznej, które pozwalają określić skład molekularny kompleksów obecnych na nowo syntetyzowanym DNA w określonym czasie. Zastosowanie tej techniki umożliwia ocenę dynamiki procesów replikacyjnych, identyfikację białek replisomu oraz czynników zaangażowanych w odpowiedź na stres replikacyjny i naprawę DNA, dostarczając informacji o zmianach zachodzących w obrębie aktywnej chromatyny.

6.3.2.2.2. Elektroforeza DNA z żelu agarozowym

Metoda elektroforezy DNA w żelu agarozowym została zastosowana w celu oceny efektywności sonikacji oraz określenia długości uzyskanych fragmentów DNA. Fragmentacja DNA ujawnia się w postaci rozmytej smugi lub szeregu prążków odpowiadających krótszym fragmentom, podczas gdy nienaruszone, wysokocząsteczkowe DNA pozostaje w pobliżu miejsca naniesienia próbki, tworząc wyraźny prążek. Uzyskany profil elektroforetyczny pozwala zweryfikować, czy stopień fragmentacji chromatyny jest odpowiedni do dalszych etapów analizy metodą iPOND.

6.3.2.3. Praca 3 (Załącznik 3)

6.3.2.3.1. Analiza sygnalizacji komórkowej

6.3.2.3.1.1. Immunodetekcja aktywności kinaz MAP

Aktywność kinaz sygnałowych MAPK (MPK3 i MPK6, funkcjonalnych odpowiedników ERK1/2 u zwierząt), zaangażowanych w odpowiedź na stres i regulację cyklu komórkowego, analizowano metodą immunofluorescencyjną. Technika ta pozwala na wizualizację sygnału

bezpośrednio w komórkach, ocenę rozmieszczenia aktywnych kinaz oraz wykazanie translokacji sygnału (lub jej braku) do jądra, co jest istotnym etapem przekazywania informacji do aparatu transkrypcyjnego. Ponadto, metoda ta łącznie z programem komputerowym ImageJ umożliwia uzyskanie danych ilościowych poprzez analizę intensywności fluorescencji oraz liczby i wielkości wyznakowanych ognisk sygnału.

6.3.2.3.2. Analiza modyfikacji epigenetycznych w obrębie chromatyny

6.3.2.3.2.1. Immunodetekcja modyfikacji epigenetycznych DNA

Poziom metylacji DNA oceniano metodą immunofluorescencyjnej detekcji 5-metylocytozyny (5-mC). Technika ta umożliwia bezpośrednią analizę intensywności oraz przestrzennego rozmieszczenia sygnału metylacji w jądrach komórek merystematycznych. Z uwagi na istotną rolę metylacji DNA w epigenetycznej regulacji transkrypcji, jej oznaczenie pozwala określić, czy działanie czynników stresowych lub fitotoksycznych prowadzi do zaburzeń stabilności epigenomu oraz kontroli ekspresji genów. Uzyskane wyniki umożliwiają zarówno ocenę zmian w globalnym poziomie metylacji, jak i oszacowanie ich potencjalnych konsekwencji dla aktywności transkrypcyjnej i funkcjonowania komórek proliferujących.

6.3.2.3.2.2. Immunodetekcja modyfikacji epigenetycznych histonów

Potranslacyjne modyfikacje histonów (H3K4Me2, H3K56Ac, H3T45Ph, H3K9Ac, H4K5Ac) analizowano metodą immunofluorescencyjną umożliwiającą określenie ich rozmieszczenia w jądrach komórek merystematycznych. Badane markery epigenetyczne pozostają w ścisłym związku zarówno z represją transkrypcji i procesami naprawy DNA, jak i z aktywacją genów zaangażowanych w odpowiedź na stres. Jakościowa i ilościowa analiza sygnału przeprowadzona przy użyciu programu ImageJ pozwala ocenić, czy działanie czynników fitotoksycznych prowadzi do zaburzenia równowagi między stanem represji a aktywacją transkrypcji, a tym samym wpływa na regulację ekspresji genów kontrolujących odpowiedź na stres.

6.3.2.3.3. Analiza procesu transkrypcji

6.3.2.3.3.1. Fluorescencyjna detekcja inkorporacji EU

Aktywność transkrypcyjną oceniano na podstawie inkorporacji 5-etynylourydyny (EU) do nowo syntetyzowanego RNA, wizualizowanej z użyciem mikroskopii fluorescencyjnej. Metoda ta umożliwia analizę intensywności oraz przestrzennego rozmieszczenia sygnału, dostarczając informacji o globalnym poziomie transkrypcji w komórkach merystematycznych. Stanowi ona funkcjonalne uzupełnienie analiz epigenetycznych obejmujących metylację DNA i potranslacyjne modyfikacje histonów, pozwalając powiązać obserwowane zmiany w strukturze chromatyny z rzeczywistą aktywnością transkrypcyjną. Umożliwia to określenie wpływu czynników fitotoksycznych na podstawowy mechanizm regulujący ekspresję genów zaangażowanych w proliferację i odpowiedź na stres.

6.3.2.4. Praca 4 (Załącznik 4)

6.3.2.4.1. Analiza przyrostu korzeni

6.3.2.4.1.1. Analiza morfometryczna

Pomiar morfometryczny długości korzeni zarodkowych zastosowano jako wskaźnik wczesnej odpowiedzi wzrostowej siewek na działanie badanych związków.

6.3.2.4.2. Analiza aktywności mitotycznej w merystemach korzeni

6.3.2.4.2.1. Identyfikacja jąder interfazowych i figur mitotycznych

W preparatach merystemów korzeniowych barwionych metodą Feulgena, swoistą dla jądrowego DNA, oceniano aktywność proliferacyjną komórek poprzez wyznaczenie indeksu mitotycznego (MI), określanego jako odsetek komórek pozostających w mitozie względem całkowitej liczby analizowanych komórek. Dodatkowo obliczano indeksy fazowe, odzwierciedlające udział komórek w poszczególnych stadiach mitozy (profaza, metafaza, anafaza, telofaza), co umożliwiało ocenę dynamiki przebiegu podziału. Parametry te pozwalały na ilościową ocenę wpływu badanego czynnika fitotoksycznego na aktywność proliferacyjną oraz prawidłowość przebiegu mitozy w komórkach merystematycznych.

6.3.2.4.3. Analiza molekularnych komponentów MPF (M-phase Promoting Factor)

6.3.2.4.3.1. Immunodetekcja poziomu białka CDKA i CycB

Detekcję poziomu kinazy CDKA przeprowadzono metodą immunofluorescencyjnego znakowania komórek merystematycznych, umożliwiającą półilościową ocenę zawartości białka bezpośrednio w komórkach z wykorzystaniem analizy sygnału w programie ImageJ. Poziom białka CDKA weryfikowano również techniką Western blot, którą zastosowano także do analizy poziomu cykliny B (CycB). Metoda ta, po elektroforetycznym rozdziale całkowitych ekstraktów białkowych z merystemów korzeniowych w żelu poliakrylamidowym i przeniesieniu na membrany PVDF, umożliwia identyfikację badanych białek przy użyciu przeciwciał swoistych wobec CDKA i CycB oraz odpowiedniego przeciwciała wtórnego sprzężonego z markerem detekcyjnym. Ilościową analizę intensywności prążków przeprowadzono na podstawie densytometrii z wykorzystaniem programu GelAnalyzer. CDKA stanowi główną kinazę regulującą przebieg cyklu komórkowego i jest utrzymywana w komórkach na względnie stabilnym poziomie, natomiast CycB wykazuje ekspresję okresową. Obydwa białka wchodzą w skład kompleksu kontrolującego przejście przez punkt kontrolny G2/M. Zmiany ich poziomu mogą wskazywać na zaburzenia regulacji cyklu komórkowego oraz potencjalny wpływ czynnika fitotoksycznego na stabilność i aktywność tego kompleksu.

6.3.2.4.3.2. Ocena ekspresji genu CycB metodą RT-qPCR

Analizę ekspresji genu CycB przeprowadzono metodą ilościowej reakcji łańcuchowej polimerazy z odwrotną transkrypcją (RT-qPCR, *Reverse Transcription-quantitative Polymerase Chain Reaction*). Technika ta umożliwia precyzyjne oznaczenie poziomu transkryptów wybranego genu w komórkach merystematycznych oraz ocenę zmian jego ekspresji w odpowiedzi na działanie czynników stresowych lub fitotoksycznych. RT-qPCR dostarcza danych ilościowych pozwalających na porównanie poziomu ekspresji pomiędzy

próbami oraz identyfikację genów ulegających istotnej regulacji w warunkach eksperymentalnych.

6.3.2.4.4. Analiza struktury cytoszkieletu

6.3.2.4.4.1. Immunodetekcja tubuliny i aktyny

Do analizy struktury i organizacji cytoszkieletu zastosowano metodę immunofluorescencyjną z przeciwciałami swoistymi wobec tubuliny (mikrotubule) oraz aktyny (mikrofilamenty). Technika ta umożliwia wizualizację przestrzennej architektury głównych komponentów cytoszkieletu w komórkach merystematycznych oraz ocenę ich organizacji i zmian strukturalnych. Znakowanie fluorescencyjne pozwala na analizę ciągłości włókien oraz ich reorganizacji, co jest istotne w badaniach nad reakcją komórek roślinnych na działanie czynników stresowych i fitotoksycznych. Mikrotubule i mikrofilamenty pełnią istotną rolę w regulacji podziałów komórkowych, uczestnicząc w tworzeniu wrzeciona kariokinetycznego i cytokinetycznego oraz w procesach transportu wewnątrzkomórkowego. Ocena ich organizacji dostarcza informacji o wpływie stresu na dynamikę cytoszkieletu i proliferację.

6.3.2.4.5. Analiza mitotycznych modyfikacji epigenetycznych

6.3.2.4.5.1. Immunodetekcja fosforylacji histonu H3

Do detekcji modyfikacji epigenetycznych histonu H3 (fosforylacji treoniny 3 - H3T3Ph i seryny 10 - H3S10Ph), związanych z regulacją cyklu komórkowego, zastosowano metodę immunofluorescencyjną. Technika ta umożliwia wizualizację przestrzennego rozmieszczenia badanych modyfikacji bezpośrednio w chromosomach mitotycznych. Analiza poziomu H3T3Ph i H3S10Ph dostarcza informacji zarówno o zmianach strukturalnych chromatyny, jak i o aktywności mechanizmów regulacyjnych cyklu komórkowego, ponieważ modyfikacje te są dynamicznie dodawane i usuwane przez specyficzne kinazy oraz fosfatazy w ściśle kontrolowanych etapach mitozy. Ilościowa ocena sygnału przeprowadzona w programie ImageJ pozwala określić, czy obserwowane zaburzenia podziałów komórkowych wynikają z zakłóceń mechanizmów regulacyjnych mitozy.

6.3.2.5. Praca 5 (Załącznik 5)

6.3.2.5.1. Analiza zawartości kadmu

Zawartość kadmu w tkankach roślinnych oznaczano po uprzedniej mineralizacji materiału, która polega na całkowitym rozkładzie materii organicznej przy użyciu silnych utleniaczy. Proces ten prowadzi do przejścia pierwiastków śladowych, w tym kadmu, do roztworu, umożliwiając ich analizę ilościową. Stężenie kadmu oznaczano metodą atomowej spektrometrii absorpcyjnej z atomizacją w płomieniu (FAAS; *Flame Atomic Absorption Spectrometry*). Technika ta opiera się na pomiarze pochłaniania promieniowania o charakterystycznej długości fali przez wolne atomy badanego pierwiastka w stanie gazowym. Intensywność absorpcji jest proporcjonalna do stężenia kadmu w próbce, co pozwala na jego precyzyjne oznaczenie ilościowe na podstawie krzywej wzorcowej. Zastosowana metoda umożliwia czułe

i wiarygodne określenie poziomu akumulacji kadmu w tkankach roślinnych, stanowiąc podstawę do oceny stopnia jego pobierania i nagromadzenia w badanym materiale biologicznym.

6.3.2.5.2. Analiza stresu oksydacyjnego i systemów antyoksydacyjnych

6.3.2.5.2.1. Spektrofotometryczna ocena zawartości nadtlenku wodoru (H_2O_2)

Oznaczanie poziomu H_2O_2 jest jednym z podstawowych sposobów oceny stresu oksydacyjnego w komórkach roślinnych. Związek ten stanowi względnie trwałą i możliwą do precyzyjnego oznaczenia formę reaktywnych form tlenu, a jego kumulacja odzwierciedla stopień nasilenia procesów oksydacyjnych w tkankach. W porównaniu z wysoce reaktywnymi i krótkotrwałymi ROS, takimi jak anionorodnik ponadtlenkowy (O_2^{-}•) czy rodnik hydroksylowy (•OH), H_2O_2 cechuje się większą stabilnością, co pozwala na jego wiarygodną analizę ilościową. Parametr ten w zestawieniu z innymi wskaźnikami, takimi jak aktywność enzymów antyoksydacyjnych oraz peroksydacja lipidów, umożliwił wnioskowanie o mechanizmach obronnych uruchamianych w odpowiedzi na działanie SEO.

6.3.2.5.2.2. Spektrofotometryczna ocena aktywności enzymów antyoksydacyjnych (SOD, CAT, APX, GR) oraz askorbinianu i proliny

Oznaczenie aktywności wybranych enzymów antyoksydacyjnych, dysmutazy ponadtlenkowej (SOD), katalazy (CAT), peroksydazy askorbinianowej (APX) oraz reduktazy glutationowej (GR), w połączeniu z analizą poziomu askorbinianu i proliny stanowiło podstawę do oceny potencjału komórek roślinnych w zakresie neutralizacji reaktywnych form tlenu oraz utrzymania homeostazy redoks. Uwzględnienie zarówno komponentów enzymatycznych, jak i nieenzymatycznych pozwoliło na kompleksowe ujęcie funkcjonowania systemu antyoksydacyjnego.

6.3.2.5.2.3. Ocena zawartości glutationu, cysteiny, γ-glutamylocysteiny i fitochelatyn z użyciem HPLC

Niskocząsteczkowe antyoksydanty nieenzymatyczne, takie jak glutation, cysteina i γ-glutamylocysteina, stanowią istotne uzupełnienie enzymatycznych systemów ochronnych, wspólnie uczestnicząc w neutralizacji reaktywnych form tlenu, natomiast fitochelatyny odgrywają główną rolę w detoksykacji jonów metali ciężkich poprzez ich chelatowanie. Zastosowanie wysokosprawnej chromatografii cieczowej (HPLC) pozwala na skuteczne rozdzielenie oraz ilościową analizę tych związków w złożonych ekstraktach tkankowych. Technika ta charakteryzuje się dużą czułością i selektywnością, umożliwiającą porównanie profili antyoksydantów nieenzymatycznych oraz związków chelatujących metale, a także monitorowanie ich zmian w odpowiedzi na działanie analizowanych czynników.

6.3.2.5.3. Analiza uszkodzeń wywołanych stresem

6.3.2.5.3.1. Spektrofotometryczna ocena peroksydacji lipidów

Oznaczanie poziomu malonylodialdehydu (MDA) jest powszechnie stosowane jako ilościowa miara peroksydacji lipidów, czyli degradacji nienasyconych kwasów tłuszczowych w błonach komórkowych zachodzącej pod wpływem reaktywnych form tlenu. Związek ten powstaje jako wtórny produkt utleniania lipidów i dlatego może służyć jako wskaźnik stopnia uszkodzeń

struktur błonowych oraz nasilenia stresu oksydacyjnego w tkankach. Analiza MDA uzupełnia informacje dotyczące aktywności enzymów antyoksydacyjnych i poziomu antyoksydantów nieenzymatycznych, umożliwiając ocenę skuteczności systemów ochronnych w zabezpieczaniu błon komórkowych przed skutkami działania czynników generujących stres.

6.3.2.5.3.2. Ocena uszkodzeń DNA Testem TUNEL

Test TUNEL (*Terminal deoxynucleotidyl transferase dUTP Nick End Labeling*) zastosowano w celu kompleksowej oceny stopnia uszkodzeń DNA w merystemach. Metoda ta umożliwia wykrywanie pęknięć nici DNA z wolnymi końcami 3'-OH poprzez enzymatyczne przyłączanie znakowanych nukleotydów, katalizowane przez terminalną transferazę deoksynukleotydową (TdT). Fluorescencyjna detekcja sygnału oraz jego ilościowa analiza z wykorzystaniem programu ImageJ pozwalają na ocenę poziomu degradacji DNA w pojedynczych komórkach. Zastosowanie tej techniki umożliwia określenie zakresu utrzymywania się uszkodzeń genomu pomimo aktywacji mechanizmów naprawczych, których aktywność można pośrednio monitorować poprzez detekcję γ-H2AX, markera wczesnej odpowiedzi komórkowej na uszkodzenia DNA. Metoda ta dostarcza zatem informacji o skali potencjalnie nieodwracalnych zmian w genomie wywołanych przez czynniki stresowe lub fitotoksyczne.

6.3.2.5.3.3. Ocena ultrastruktury komórek z użyciem TEM

Do analizy zmian ultrastrukturalnych w komórkach merystematycznych zastosowano transmisyjną mikroskopię elektronową (*transmission electron microscopy*, TEM). Technika ta pozwala identyfikować, niewykrywalne w mikroskopii świetlnej i fluorescencyjnej, subtelne modyfikacje morfologiczne indukowane przez czynniki stresowe lub związki fitotoksyczne. Uzyskane dane stanowią uzupełnienie analiz biochemicznych i immunocytochemicznych, umożliwiające pełniejszą charakterystykę odpowiedzi komórkowej na działanie stresora.

6.4. Wyniki badań

6.4.1. Praca 1 (Załącznik nr 1)

- **Gocek-Szczurtek, N.***; Żabka, A.; Wróblewski, M.; Kukula-Koch, W.; Szczeblewski, P.; Polit, J.T. Thyme Oil Mitigates Cadmium-Induced Oxidative and Genotoxic Stress in *Vicia faba* Root Meristem Cells under in vitro Conditions. *Sci Rep* **2025**, *15*, 38689, doi:10.1038/s41598-025-22588-w.

W pierwszym etapie badań analizowano wpływ kadmu, jako czynnika prooksydacyjnego i genotoksycznego, na proces replikacji DNA oraz dynamikę przebiegu interfazy w merystemach korzeni zarodkowych, a także oceniano potencjał ochronny TO, znanego z właściwości antyoksydacyjnych, w warunkach stresu indukowanego kadmem.

Wykazano, że ekspozycja komórek na $CdCl_2$ prowadzi do wyraźnej cytoplazmatycznej akumulacji nadtlenku wodoru (H_2O_2) oraz anionorodnika ponadtlenkowego ($O_2^{\bullet-}$). Nadmierna produkcja ROS była związana z zaburzeniami cyklu komórkowego, przejawiającymi się znacznym spadkiem odsetka komórek w fazie S oraz zwiększeniem udziału komórek w fazach G1 i G2, co potwierdzono zarówno metodą cytofotometrycznego pomiaru zawartości DNA, jak i immunofluorescencyjną analizą inkorporacji markera replikacji (IdU). Wyniki te wskazują na aktywację punktów kontrolnych cyklu komórkowego, które w niesprzyjających warunkach hamują inicjację replikacji DNA oraz mitozy. W populacji komórek replikujących znaczna ich część kumulowała się w początkowych etapach fazy S. Świadczyły o tym niewielkie rozmiary jąder, zawartość DNA zbliżona do poziomu charakterystycznego dla fazy G1 oraz obecność nielicznych, rozproszonych sygnałów immunofluorescencyjnych, wskazujących na ograniczoną liczbę aktywnych replikonów. Obniżona intensywność fluorescencji jądrowej, odzwierciedlająca niski poziom inkorporacji IdU, potwierdzała także spowolnienie tempa replikacji niezależnie od etapu fazy S. Zarówno w stadium środkowym, charakteryzującym się bardziej jednorodnym („drobnoziarnistym") znakowaniem, jak i w stadium późnym, z typowym skupiskowym sygnałem odpowiadającym replikacji obszarów heterochromatynowych, obserwowano osłabioną aktywność syntezy DNA. Stwierdzone zaburzenia przebiegu replikacji skłoniły do oceny stanu materiału genetycznego. Detekcja ufosforylowanej postaci histonu H2A.X (γ-H2A.X) wykazała wyraźny wzrost liczby jąder immunopozytywnych, świadczący o nasilonej indukcji dwuniciowych pęknięć DNA oraz aktywacji mechanizmów naprawczych.

Przed zastosowaniem TO w doświadczeniach przeprowadzono analizę jego składu chemicznego metodą GC-MS. Wykazano, że wybrany, komercyjnie dostępny preparat charakteryzuje się wysoką zawartością monoterpenów, w szczególności tymolu, p-cymenu, linalolu, karwakrolu, limonenu i α-pinenu. Związki te należą do substancji o potwierdzonych właściwościach antyoksydacyjnych, dlatego w kolejnym etapie oceniono, czy TO w formie zemulgowanej może ograniczać stres oksydacyjny indukowany przez kadm. Zastosowanie samego emulgatora, umożliwiającego jednorodne rozprowadzenie olejku w medium

hodowlanym, jak również zemulgowanego TO, nie wpływało na poziom H_2O_2 ani $O_2^{\bullet-}$ w komórkach merystematycznych, wartości te pozostawały na poziomie kontrolnym. Nie obserwowano również zaburzeń cyklu komórkowego, zmian w rozkładzie populacji komórek, spowolnienia replikacji ani zwiększenia liczby uszkodzeń DNA. Natomiast dodatek TO do podłoża zawierającego $CdCl_2$ istotnie ograniczał stres oksydacyjny: poziom H_2O_2 obniżył się o około 72%, a akumulacja $O_2^{\bullet-}$ zmniejszyła się o ponad 40% w porównaniu z wariantem traktowanym wyłącznie kadmem. Jednoczesne zastosowanie $CdCl_2$ i TO w znacznym stopniu łagodziło także zaburzenia w proporcji komórek w poszczególnych etapach interfazy, przywracając rozkład zbliżony do kontrolnego, z jedynie niewielkim zwiększeniem udziału komórek w fazie G2. Ponadto zarówno odsetek komórek replikujących, jak i intensywność sygnału IdU oraz dynamika replikacji ulegały wyraźnej poprawie w porównaniu z komórkami eksponowanymi wyłącznie na $CdCl_2$. Dodatek TO prowadził także do około 25% zmniejszenia liczby komórek γH2A.X-dodatnich, potwierdzając zdolność olejku do ograniczania genotoksycznych następstw stresu oksydacyjnego.

Uzyskane wyniki wskazują, że toksyczne działanie kadmu w komórkach merystematycznych odbywa się poprzez kaskadę zdarzeń obejmującą nadprodukcję ROS, wystąpienie uszkodzeń DNA, indukcję stresu replikacyjnego, aktywację punktów kontrolnych cyklu komórkowego oraz uruchomienie mechanizmów naprawczych, czego wyrazem jest obecność ognisk γ-H2A.X. Olejek tymiankowy skutecznie przerywa ten ciąg zdarzeń na wczesnym etapie, ograniczając stres oksydacyjny, zachowując integralności genomu i stabilizując przebieg replikacji, co sprzyja prawidłowej dynamice cyklu komórkowego. Praca dostarcza silnych dowodów na ochronne działanie TO w komórkach merystematycznych w warunkach stresu wywołanego kadmem i stanowi istotne uzupełnienie badań nad mechanizmami tolerancji roślin na działanie kadmu.

6.4.2. Praca 2 (Załącznik nr 2)

- Żabka, A.*; **Gocek, N.**; Polit, J.T.; Maszewski, J. Epigenetic Modifications Evidenced by Isolation of Proteins on Nascent DNA and Immunofluorescence in Hydroxyurea-Treated Root Meristem Cells of *Vicia faba*. *Planta* **2023**, 258, 95, doi:10.1007/s00425-023-04249-2.

Prezentowana praca stanowi część projektu realizowanego w Katedrze Cytofizjologii Wydziału Biologii i Ochrony Środowiska Uniwersytetu Łódzkiego, którego celem jest analiza mechanizmów stresu replikacyjnego oraz epigenetycznej regulacji odpowiedzi komórek roślinnych na czynniki zaburzające syntezę DNA. W niniejszej dysertacji uwzględniono wyłącznie fragment badań bezpośrednio związany z opracowaniem i adaptacją metody iPOND (*isolation of Proteins On Nascent DNA*) do materiału roślinnego, a uzyskane wyniki przedstawiono w artykule w postaci schematu metody (Figura 3), analiz immunoblot oraz analiz fragmentacji DNA (Figura 4).

Adaptacja metody iPOND do komórek merystematycznych *Vicia faba* wymagała optymalizacji podstawowych etapów procedury, w tym warunków znakowania nowo syntetyzowanego DNA analogiem tymidyny (EdU), enzymatycznej degradacji ściany komórkowej, lizy komórek oraz fragmentacji chromatyny. Ocena efektywności fragmentacji chromatyny wykazała dominację fragmentów DNA o długości 2000–4000 pz, co potwierdziło przydatność uzyskanego materiału do dalszych analiz.

W celu walidacji metody zastosowano model stresu replikacyjnego indukowanego hydroksymocznikiem (HU; 3 mM), który stanowi dobrze scharakteryzowany i kontrolowany czynnik blokujący progresję widełek replikacyjnych. Wybór tego modelu podyktowany był koniecznością jednoznacznego potwierdzenia funkcjonalności procedury w warunkach silnie i przewidywalnie hamujących syntezę DNA, bez dodatkowych zmiennych związanych z toksycznością kadmu. Analiza metodą Western blot uzyskanych frakcji DNA-białko, umożliwiła identyfikację zmian w poziomie białek związanych z aktywnymi oraz zahamowanymi widełkami replikacyjnymi, potwierdzając funkcjonalność opracowanej procedury.

Pozostała część publikacji, obejmująca szczegółową charakterystykę odpowiedzi komórek na hydroksymocznik, w tym analizę zaburzeń przebiegu mitozy oraz szerszy kontekst molekularny stresu replikacyjnego, została zrealizowana w ramach badań zespołowych i nie wchodzi bezpośrednio w zakres niniejszej rozprawy, stanowi jednak istotne tło metodologiczne i koncepcyjne dla dalszych badań.

Opracowanie i walidacja metody iPOND w materiale roślinnym otwierają możliwość jej zastosowania w analizie molekularnych mechanizmów działania kadmu oraz czynników ochronnych, takich jak olejek eteryczny pozyskiwany z *Thymus vulgaris* L., w obrębie nowo syntetyzowanego DNA. W kontekście wyników prezentowanych w niniejszej dysertacji, wskazujących na zaburzenia progresji cyklu komórkowego, destabilizację procesu replikacji oraz zmiany epigenetyczne indukowane przez metal ciężki, metoda ta stanowi perspektywiczne narzędzie do bezpośredniej analizy dynamiki modyfikacji histonów i reorganizacji chromatyny w obrębie widełek replikacyjnych w warunkach stresu wywołanego kadmem oraz w obecności czynnika o potencjale ochronnym.

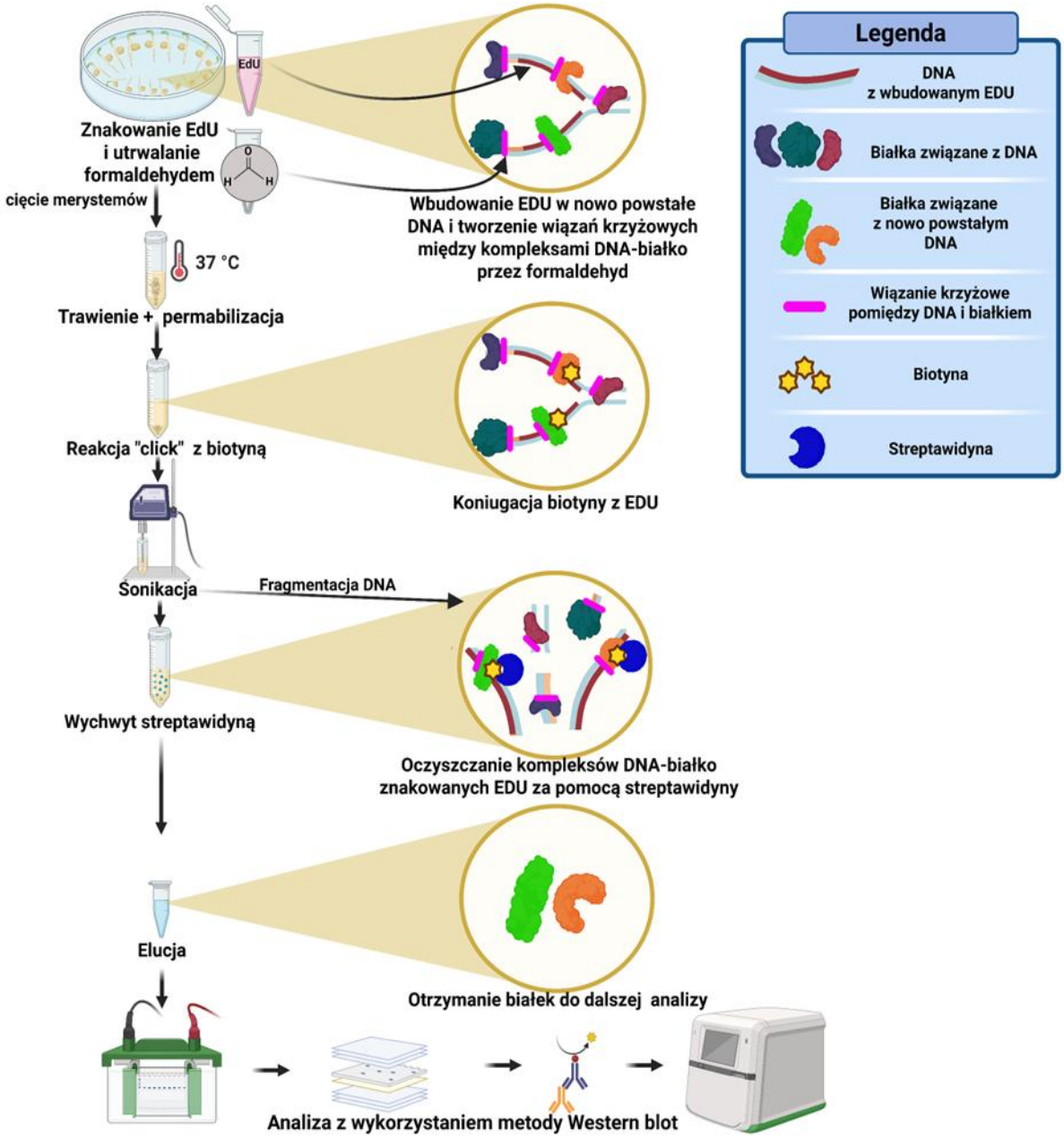

Ryc. 4. Przebieg metody iPOND (isolation of proteins on nascent DNA) umożliwiającej identyfikację białek związanych z nowo syntetyzowanym DNA. Schemat przedstawia równolegle procesy zachodzące w komórce oraz odpowiadające im etapy procedury eksperymentalnej. Rycina przygotowana z wykorzystaniem BioRender.com.

6.4.3. Praca 3 (Załącznik nr 3)

- **Gocek-Szczurtek, N.**; Żabka, A.; Wróblewski, M.; Polit, J.T.* Stabilization of the MAPK–Epigenetic Signaling Axis Underlies the Protective Effect of Thyme Oil against Cadmium Stress in Root Meristem Cells of *Vicia faba*. *IJMS* **2025**, 27, 208, doi:10.3390/ijms27010208.

Ze względu na to, że kadm indukuje stres oksydacyjny pełniący istotną rolę w sygnalizacji komórkowej, a jednocześnie prowadzi do zaburzeń struktury chromatyny interfazowej, obejmujących powstawanie dwuniciowych pęknięć DNA oraz zakłócenia replikacji, wykazane

w poprzednich badaniach, zasadne było zbadanie czy zmiany te wpływają również na regulację procesu transkrypcji oraz ustalenie czy TO wykazuje potencjał ochronny. W niniejszej pracy przeanalizowano aktywację szlaku sygnałowego MAPK, którego podstawowymi elementami są kinazy MPK3 i MPK6. Kinazy te, przekazując sygnał stresowy do jądra komórkowego, mogą inicjować procesy przebudowy chromatyny oraz modulować ekspresję genów, co w konsekwencji prowadzi do zmian globalnej aktywności transkrypcyjnej. Następnie oceniono globalny poziom metylacji DNA oraz wybrane modyfikacje epigenetyczne histonów, pozostające w ścisłym związku ze stanem kondensacji chromatyny, zarówno jej zamykaniem i represją transkrypcji, jak i rozluźnieniem sprzyjającym aktywacji genów odpowiedzi na stres. W celu określenia funkcjonalnych następstw tych zmian przeprowadzono analizę syntezy RNA z wykorzystaniem inkorporacji 5-etynylo-urydyny (EU), umożliwiającą ocenę globalnego poziomu aktywności transkrypcyjnej.

Analizy immunocytochemiczne wykazały, iż ekspozycja na kadm prowadzi do wyraźnej aktywacji jądrowych kinaz MAPK, przejawiającej się niemal dwukrotnym wzrostem liczby ognisk sygnału oraz zwiększeniem ich powierzchni i intensywności fluorescencji. Zmiany te wskazują na rozszerzenie domen chromatynowych objętych aktywną sygnalizacją MAPK i potwierdzają udział tych kinaz we wczesnej odpowiedzi komórkowej na stres wywołany kadmem. Aktywacji MPK3/MPK6 towarzyszył wyraźny wzrost globalnego poziomu metylacji DNA oraz zmiany w profilu epigenetycznych modyfikacji histonowych, sprzyjające kondensacji chromatyny. Odnotowano bowiem spadek poziomu fosforylacji H3T45, która uczestnicząc w rozluźnianiu struktury nukleosomu, znacząco wpływa na lokalną dostępność DNA dla kompleksów transkrypcyjnych, naprawczych i replikacyjnych, oraz obniżenie globalnej acetylacji H4K5, zwykle związanej z otwartą strukturą chromatyny. Ponadto odnotowano spadek poziomu dimetylacji H3K4 (H3K4Me2), markera powiązanego z regionami regulatorowymi genów i utrzymaniem epigenetycznej plastyczności chromatyny.

Jednocześnie mimo ogólnego ograniczenia modyfikacji sprzyjających rozluźnieniu chromatyny zaobserwowano wzrost wybranych znaków epigenetycznych związanych z aktywnością transkrypcyjną. Dotyczyło to zwiększonego poziomu acetylacji H3K9 (H3K9Ac), która występuje w regionach promotorowych genów aktywowanych w odpowiedzi na stres abiotyczny, oraz acetylacji H3K56 (H3K56Ac), uznawanej za marker odpowiedzi na uszkodzenia DNA. Ponadto przy globalnym spadku acetylacji H4K5 stwierdzono jej lokalne wzbogacenie w obszarach organizatorów jąderkowych, co może wskazywać na adaptacyjne utrzymanie transkrypcji rDNA i biosyntezy rybosomów.

W rezultacie odpowiedź epigenetyczna na kadm miała charakter dwutorowy: globalne wyciszenie chromatyny sprzyjało ochronie integralności genomu, natomiast selektywne utrzymanie lub wzrost aktywności w wybranych regionach umożliwiały adaptację komórek do warunków stresowych. Zmiany te znalazły odzwierciedlenie w dynamice transkrypcji, ekspozycja na kadm prowadziła do wyraźnego zahamowania syntezy RNA zarówno w obszarze jądra jak i w jąderkach, wskazując na globalną represję transkrypcyjną.

W kolejnym etapie oceniono, czy TO w formie zemulgowanej może ograniczać zmiany indukowane przez kadm. Zastosowanie samego emulgatora, umożliwiającego jednorodne rozprowadzenie olejku w medium hodowlanym, jak również zemulgowanego TO, nie wpływało na aktywność jądrowych kinaz MPK3/MPK6 w komórkach merystematycznych, wartości te pozostawały na poziomie kontrolnym. Nie stwierdzono również istotnych zmian w zakresie metylacji DNA, analizowanych modyfikacji epigenetycznych histonów ani globalnej aktywności transkrypcyjnej.

Zastosowanie TO równocześnie z kadmem znacząco ograniczało aktywację jądrowych kinaz MAPK, prowadząc do częściowej normalizacji liczby, powierzchni oraz intensywności ognisk sygnału w porównaniu z wariantem traktowanym wyłącznie kadmem. W komórkach traktowanych łącznie kadmem i TO, globalny poziom 5-metylocytozyny pozostawał jedynie nieznacznie podwyższony względem kontroli, co wskazuje na zdolność TO do ograniczania hipermetylacji DNA indukowanej przez kadm oraz utrzymania wyższego potencjału transkrypcyjnego chromatyny. Obecność TO sprzyjała również stabilizacji profilu modyfikacji histonowych. Poziomy H3K4Me2, H3T45Ph, H4K5Ac, H3K9Ac oraz H3K56Ac w większości przypadków pozostawały zbliżone do wartości kontrolnych lub wykazywały jedynie niewielkie odchylenia, co świadczy o zachowaniu epigenetycznej równowagi i ograniczeniu kondensacji chromatyny wywołanej przez kadm. Stabilizacja sygnalizacji jądrowej oraz parametrów epigenetycznych skutkowała utrzymaniem aktywności transkrypcyjnej. Synteza RNA w obszarze jąder i jąderek pozostała na poziomie zbliżonym do kontroli, potwierdzając protekcyjny wpływ TO na funkcjonowanie aparatu transkrypcyjnego roślin.

Zintegrowana analiza tych parametrów dostarcza nowych danych na temat powiazań między sygnalizacją MAPK a regulacją epigenetyczną w warunkach stresu wywołanego kadmem oraz potwierdza zdolność TO do modulowania szlaku odpowiedzi komórkowej na działanie kadmu.

6.4.4. Praca 4 (Załącznik nr 4)

- **Gocek-Szczurtek, N**.; Wróblewski, M.; Żabka, A.; Polit, J.T.* Thyme Oil Alleviates Cadmium Induced Disturbances in Mitotic Activity, Cytoskeletal Organization and H3T3/H3S10 Phosphorylation in *Vicia faba. IJMS* **2026**, 27, 2798, doi:10.3390/ijms27062798.

W związku z tym, że kadm narusza integralność genomu, indukuje zaburzenia replikacji DNA i hamowanie komórek w fazach G1 i G2 oraz inicjuje przebudowę sieci sygnałowych, czemu towarzyszą istotne zmiany epigenetyczne i transkrypcyjne wykazane w poprzednich badaniach, zasadnym stało się określenie, jak konsekwencje tych procesów przekładają się na regulację mitozy w komórkach merystematycznych i określenie czy TO, łagodząc działanie kadmu, chroni również aparat mitotyczny.

Uzyskane wyniki jednoznacznie potwierdzają silny, hamujący wpływ kadmu na wzrost korzeni zarodkowych, które osiągnęły jedynie około 50% długości korzeni kontrolnych. Zmianom tym

towarzyszył blisko 10-krotny spadek indeksu mitotycznego, wskazując na istotne zahamowanie przebiegu cyklu komórkowego. Na poziomie cytologicznym obserwowano wyraźne zaburzenia organizacji i stopnia kondensacji chromatyny, od niejednorodnej struktury jąder interfazowych po nadmiernie skondensowane, miejscami „lepkie" chromosomy mitotyczne wykazujące adhezję regionów telomerowych. Analiza molekularnych regulatorów przejścia G2/M wykazała, że kadm nieznacznie obniżał poziom kinazy CDKA, natomiast wyraźnie redukował zarówno poziom białka CycB, jak i ilość jej transkryptów. Wyniki te wskazują, że oprócz gromadzenia komórek w pierwszym punkcie kontrolnym i spowolnienia replikacji w związku z aktywacją procesu naprawczego, głównym powodem spadku indeksu mitotycznego i blokady wejścia komórek w mitozę jest zaburzenie funkcjonowania kompleksu CDK–CycB, niezbędnego do inicjacji fazy M. Kadm powodował również znaczną dezorganizację cytoszkieletu poprzez nadmierną stabilizację i agregację mikrotubul oraz filamentów aktynowych. Obserwowano zaburzenia sieci mikrotubul korowych, defekty formowania wiązki pre-profazowej, deformacje wrzeciona kariokinetycznego oraz nieprawidłową organizację fragmoplastu, co bezpośrednio wskazuje na destabilizację aparatu mitotycznego. Ponadto, analiza mitotycznych modyfikacji histonu H3 wykazała, że kadm zakłóca również precyzyjną regulację epigenetyczną podziału komórkowego. Utrzymywanie się fosforylacji H3T3 (H3T3Ph) oraz rozproszenie i osłabienie sygnału H3S10Ph w późnych fazach mitozy wskazują na zaburzenia aktywności kinaz i fosfataz kontrolujących dynamiczne zmiany fosforylacji białek towarzyszące kolejnym etapom mitozy.

W kolejnym etapie oceniono, czy zemulgowany TO może ograniczać zmiany indukowane przez kadm. Zastosowanie samego emulgatora, umożliwiającego jednorodne rozprowadzenie olejku w medium hodowlanym, jak również TO, nie wpływało na wzrost korzeni zarodkowych ani na aktywność mitotyczną komórek merystematycznych. Poziom kinazy CDKA oraz cykliny B pozostawał zbliżony do kontroli, a obserwowany niewielki spadek ilości transkryptu *CycB* nie był istotny statystycznie. Organizacja i dynamika cytoszkieletu nie ulegały zaburzeniom, natomiast mitotyczne modyfikacje histonu H3 wykazywały wzorce charakterystyczne dla komórek kontrolnych.

Obecność TO w warunkach stresu wywołanego kadmem pozwoliła na utrzymanie tempa wzrostu korzeni charakterystycznego dla kontroli. Aktywność mitotyczna chociaż nie osiągnęła wartości kontrolnej, była zdecydowanie wyższa i sięgała około 50% kontroli. Poziomy głównych białek regulatorowych kompleksu CDKA-CycB były bliskie kontroli, podobnie jak poziom transkryptu *CycB* był równy kontrolnemu. Jednoczesna aplikacja TO niemal całkowicie chroniła przed defektami cytoszkieletu, podtrzymując prawidłową architekturę mikrotubul i filamentów aktynowych. TO normalizował także dynamikę modyfikacji epigenetycznych mitozy. Wyniki te dowodzą, że TO istotnie ogranicza negatywne skutki stresu kadmowego na poziomie cyklu komórkowego, organizacji chromatyny, cytoszkieletu i regulacji epigenetycznej. Stanowiło to silne uzasadnienie dla dalszych badań nad mechanizmami molekularnymi leżącymi u podstaw jego działania ochronnego. Obecność TO w warunkach stresu wywołanego kadmem umożliwiała utrzymanie tempa wzrostu korzeni zarodkowych zbliżonego do kontroli. Aktywność mitotyczna, choć nie osiągnęła wartości kontrolnych, była

istotnie wyższa niż w wariancie z samym kadmem i stanowiła ponad 50% poziomu kontrolnego. Poziomy głównych białek regulatorowych tworzących kompleks CDKA–CycB pozostawały zbliżone do kontroli, podobnie jak ilość transkryptu *CycB*. Jednoczesna aplikacja TO w znacznym stopniu chroniła także komórki przed defektami cytoszkieletu, podtrzymując prawidłową architekturę mikrotubul i filamentów aktynowych. TO normalizował również dynamikę mitotycznych modyfikacji histonu H3.

Wyniki te wskazują, że TO istotnie ogranicza negatywne skutki stresu kadmowego na poziomie regulacji cyklu komórkowego, organizacji chromatyny, cytoszkieletu oraz mechanizmów epigenetycznych. Stanowi to silne uzasadnienie dla dalszych badań nad molekularnymi podstawami jego działania ochronnego.

6.4.5. Praca 5 (Załącznik nr 5)

- **Gocek-Szczurtek, N.***; Piotrowska-Niczyporuk, A.; Zambrzycka-Szelewa, E.; Ciereszko, I.; Żabka, A.; Wróblewski, M.; Polit, J.T. Thyme Essential Oil Reduces Cadmium Uptake and Toxicity in *Vicia faba* Root Meristem Cells, Involving Stabilization of Cell Ultrastructure and Modulation of Redox Response and Thiol Metabolism. - manuskrypt wysłany do czasopisma *The Plant Journal*

Uwzględniając, że kadm zaburza homeostazę redoks i inicjuje szereg zmian prowadzących do destabilizacji funkcjonowania komórek merystematycznych, przeprowadzono analizę jego zawartości w tkankach oraz kompleksową charakterystykę enzymatycznych i nieenzymatycznych mechanizmów obrony antyoksydacyjnej, aktywności systemów detoksykacyjnych, stopnia uszkodzeń błon komórkowych, efektywności naprawy materiału genetycznego oraz zmian ultrastrukturalnych. Równolegle oceniono, czy TO wpływa na akumulację kadmu i ogranicza skutki stresu oksydacyjnego oraz wynikające z niego zmiany strukturalne.

Ekspozycja komórek merystematycznych na kadm prowadziła do jego istotnej akumulacji w tkance (254,637 µg/g) oraz indukcji mechanizmów detoksykacyjnych, czego potwierdzeniem była obecność fitochelatyn PC2–PC5 – oligomerów bogatych w grupy tiolowe zdolne do wiązania metalu. Wśród nich dominowały frakcje PC2 i PC3. Akumulacji kadmu towarzyszył czterokrotny, w stosunku do kontroli, wzrost poziomu H_2O_2 oraz wyraźna indukcja odpowiedzi antyoksydacyjnej, przejawiająca się zwiększoną aktywnością enzymów (SOD, CAT, APX, GR) i podwyższonym stężeniem nieenzymatycznych komponentów systemu redoks, w tym glutationu, cysteiny, γ-glutamylocysteiny, askorbinianu i proliny. Pomimo aktywacji mechanizmów obronnych obserwowano silne zaburzenia równowagi redoks, potwierdzone również czterokrotnym wzrostem poziomu MDA, wskazującym na intensyfikację peroksydacji lipidów. Towarzyszył temu wysoki odsetek komórek TUNEL-pozytywnych (ok. 37%), co świadczy o nasilonej fragmentacji DNA i nieefektywnej naprawie materiału genetycznego, mimo wcześniejszej aktywacji szlaków naprawczych sygnalizowanych obecnością γ-H2A.X. Analiza ultrastruktury ujawniła natomiast wyraźne

zmiany organizacji komórkowej, obejmujące zaburzenia struktury ściany komórkowej, aparatów Golgiego, plastydów i mitochondriów, obecność ciał mielinowych, redukcję liczby rybosomów, a także silną kondensację chromatyny jądrowej i zmiany w strukturze jąderka, polegające na braku wyraźnego składnika włóknistego i rozluźnieniu składnika ziarnistego.

Zastosowanie zemulgowanego TO nie wpływało istotnie na poziom H_2O_2 w porównaniu z roślinami kontrolnymi. Obserwowano natomiast umiarkowaną indukcję aktywności SOD i CAT przy braku istotnych zmian w aktywności APX i GR, czemu towarzyszył wyraźny wzrost poziomu γ-glutamylocysteiny oraz glutationu. Nie stwierdzono jednocześnie wzrostu poziomu MDA ani zwiększenia odsetka komórek TUNEL-pozytywnych, co wskazuje na brak nasilonej peroksydacji lipidów i fragmentacji DNA. Analiza ultrastruktury nie wykazała daleko idących różnic w organizacji komórek merystematycznych w porównaniu z kontrolą w wyjątkiem silnie rozbudowanej sieci retikulum endoplazmatycznego.

Dodatek TO do podłoża zawierającego $CdCl_2$ istotnie ograniczał akumulację metalu w tkankach, redukując jego zawartość o około 38%. Mimo obniżonego poziomu Cd jego stężenie nadal mieściło się w zakresie uznawanym za biologicznie istotne i potencjalnie toksyczne dla komórek roślinnych. Towarzyszyła temu indukcja syntezy fitochelatyn PC2–PC5, jednak ich poziom był ok. 30% niższy niż w roślinach traktowanych wyłącznie kadmem. Pomimo obecności metalu ciężkiego w tkankach poziom H_2O_2 pozostawał o połowę niższy niż w komórkach eksponowanych wyłącznie na Cd, choć nadal dwukrotnie wyższy niż w kontroli. Równocześnie odnotowano najwyższą aktywność analizowanych enzymów antyoksydacyjnych (SOD, CAT, APX, GR) oraz najwyższe stężenie nieenzymatycznych komponentów systemu redoks, w tym glutationu, cysteiny, γ-glutamylocysteiny i proliny, w porównaniu z pozostałymi wariantami eksperymentalnymi. Ograniczeniu stresu oksydacyjnego towarzyszyło dwukrotne obniżenie poziomu MDA względem roślin eksponowanych wyłącznie na $CdCl_2$. Indeks komórek TUNEL-pozytywnych nie różnił się istotnie od kontroli, co wskazuje na skuteczne ograniczenie fragmentacji DNA. Analiza ultrastruktury potwierdziła ochronny charakter działania TO. W komórkach nie obserwowano zaburzeń typowych dla wariantu z kadmem. Plastydy zawierały ziarna skrobi oraz umiarkowanie rozwinięty system błon wewnętrznych. Mitochondria wykazywały dobrze zachowane wnętrza wypełnione grzebieniami, a ciała mielinowe występowały sporadycznie. Organizacja chromatyny jądrowej była zbliżona do organizacji kontrolnej, natomiast jąderka charakteryzowały się obecnością licznych, dużych wakuol, co może wskazywać na intensywny transport podjednostek rybosomów do cytoplazmy, w której zagęszczenie rybosomów pozostawało porównywalne z kontrolnym.

6.5. Wnioski ogólne

1. Kadm w stężeniu 175 μM indukuje wielopoziomowe zaburzenia struktury i funkcjonowania komórek merystematycznych, obejmujące zakłócenia w sygnalizacji komórkowej, regulacji epigenetycznej oraz procesach odpowiedzialnych za proliferację i wzrost korzeni zarodkowych, prowadząc do ograniczenia rozwoju siewek *Vicia faba* L. var. *minor*.
2. Olejek tymiankowy (TO w stężeniu 0,003%) stosowany samodzielnie nie wpływa negatywnie na analizowane parametry cytologiczne i molekularne oraz wzrost korzeni zarodkowych, potwierdzając bezpieczeństwo jego stosowania podczas wczesnego etapu rozwoju siewek.
3. TO wyraźnie ogranicza skutki stresu indukowanego przez kadm, utrzymując w komórkach merystematycznych bezpieczne środowisko redoks, stabilizując elementy ich struktury oraz mechanizmy sygnalizacyjne i regulatorowe, a także równoważąc modyfikacje epigenetyczne związane z ochroną, dostępnością i powielaniem informacji genetycznej. W efekcie TO zabezpiecza istotne procesy związane z proliferacją, takie jak transkrypcja, replikacja i segregacja materiału genetycznego, potwierdzając jego potencjał jako naturalnego czynnika wspierającego strategie ograniczania negatywnego wpływu metali ciężkich na rośliny.

6.5.1. Praca 1 (Załącznik nr 1)

Wnioski:

1. Ekspozycja komórek merystematycznych na kadm prowadzi do wyraźnej indukcji stresu oksydacyjnego, przejawiającej się istotnym wzrostem poziomu reaktywnych form tlenu (ROS), w tym nadtlenku wodoru oraz anionorodnika ponadtlenkowego, potwierdzając silne właściwości prooksydacyjne tego metalu ciężkiego.
2. Stres oksydacyjny generowany przez kadm skutkuje zwiększeniem liczby dwuniciowych pęknięć DNA, wykrywanych na podstawie obecności ufosforylowanej postaci histonu H2A.X (γH2A.X)
3. Powstawanie dwuniciowych pęknięć DNA prowadzi do indukcji stresu replikacyjnego, ograniczenia liczby komórek replikujących oraz osłabienia dynamiki replikacji, co prawdopodobnie wiąże się z aktywacją mechanizmów naprawczych, potwierdzonych obecnością γH2A.X.
4. Zaburzenia przebiegu replikacji wywołane przez kadm prowadzą prawdopodobnie do aktywacji punktów kontrolnych cyklu komórkowego i gromadzenia komórek w fazach G1 i G2, co manifestuje się wzrostem ich odsetka oraz zakłóceniem proporcji komórek interfazowych w porównaniu z wariantem kontrolnym.
5. TO stosowany samodzielnie nie indukuje pęknięć DNA, nie zaburza przebiegu replikacji ani proporcji komórek w interfazie, co wskazuje na jego neutralność wobec analizowanych parametrów w komórkach merystematycznych.

6. Zastosowanie TO istotnie ogranicza indukowaną kadmem akumulację ROS w komórkach merystematycznych prowadząc do złagodzenia stresu oksydacyjnego.
7. Redukcja stresu oksydacyjnego przez TO sprzyja zachowaniu integralności genomu i ogranicza częstość występowania dwuniciowych pęknięć DNA w komórkach eksponowanych na działanie kadmu.
8. Ograniczenie stresu oksydacyjnego oraz stabilizacja struktury DNA w obecności TO w komórkach eksponowanych na kadm przekładają się na utrzymanie aktywności replikacyjnej, zachowanie wysokiego odsetka komórek syntetyzujących DNA oraz przywrócenie intensywności i tempa replikacji do poziomów zbliżonych do kontroli.
9. Prawidłowy przebieg replikacji w warunkach jednoczesnej ekspozycji na kadm i TO nie prowadzi do aktywacji punktów kontrolnych w fazach G1 i G2, dzięki czemu zachowane zostają właściwe proporcje komórek w interfazie.

6.5.2. Praca 2 (Załącznik nr 2)

Wnioski:

1. Metoda iPOND została skutecznie zaadaptowana i zoptymalizowana do zastosowania w materiale roślinnym, takim jak korzenie zarodkowe *V. faba*, umożliwiając po raz pierwszy izolację i analizę białek związanych z nowo syntetyzowanym DNA w komórkach roślinnych.
2. Przeprowadzona walidacja potwierdziła funkcjonalność opracowanej procedury poprzez selektywną identyfikację komponentów związanych z aktywnymi i zahamowanymi widełkami replikacyjnymi, co dowodzi jej przydatności w badaniach mechanizmów regulacji replikacji DNA.
3. Adaptacja metody iPOND rozszerza dostępny warsztat badawczy w zakresie analizy dynamicznych zmian replisomu i reorganizacji chromatyny w warunkach stresu środowiskowego, stanowiąc narzędzie o potencjale aplikacyjnym w przyszłych badaniach nad molekularnymi mechanizmami odpowiedzi roślin na czynniki stresowe.
4. Opracowana procedura stanowi podstawę do bezpośredniej analizy wpływu czynników toksycznych, takich jak metale ciężkie, w tym kadm, oraz czynników protekcyjnych, takich jak TO, na skład białkowy widełek replikacyjnych w warunkach *in vivo.*

6.5.3. Praca 3 (Załącznik nr 3)

Wnioski:

1. Kadm silnie indukuje szlak sygnalizacyjny MAPK prowadząc do wzrostu aktywności kinaz MPK3/MPK6 w komórkach merystematycznych oraz do zwiększenia liczby i rozszerzenia domen chromatynowych związanych z ich sygnalizacją.

2. Aktywacja MAPK pod wpływem kadmu jest sprzężona z głębokimi zmianami epigenetycznymi, obejmującymi wzrost globalnej metylacji DNA oraz istotne modyfikacje profilu histonów sprzyjające kondensacji chromatyny.
3. Zmiany epigenetyczne indukowane przez kadm wiążą się z wyraźnym obniżeniem globalnej aktywności transkrypcyjnej w komórkach merystematycznych, zarówno w jądrze, jak i w jąderkach.
4. Olejek tymiankowy stosowany samodzielnie nie wpływa istotnie na aktywację szlaku MAPK, stan epigenetyczny chromatyny ani dynamikę transkrypcji, co wskazuje na jego neutralność wobec analizowanych parametrów w komórkach merystematycznych.
5. W warunkach współdziałania z kadmem TO istotnie ogranicza aktywację MAPK indukowaną przez Cd oraz częściowo normalizuje poziom metylacji DNA i profil modyfikacji histonów, redukując zakres epigenetycznej przebudowy chromatyny.
6. Ochronne działanie TO sprzyja zachowaniu prawidłowej organizacji chromatyny oraz utrzymaniu aktywności transkrypcyjnej na poziomie zbliżonym do kontroli mimo obecności czynnika stresowego.
7. Uzyskane wyniki wskazują, że TO działa jako naturalny czynnik bioprotekcyjny, modulujący oś sygnałową łączącą aktywację MAPK z regulacją epigenetyczną i kontrolą transkrypcji w odpowiedzi na stres wywołany kadmem.

6.5.4. Praca 4 (Załącznik nr 4)

Wnioski:

1. Kadm wywiera silne działanie antyproliferacyjne w komórkach merystematycznych *V. faba*, prowadząc do zahamowania wzrostu korzeni w wyniku ograniczenia aktywności mitotycznej i zatrzymania komórek przed wejściem w fazę M.
2. Spadek liczby komórek mitotycznych w merystemach eksponowanych na Cd może wynikać w znacznym stopniu z aktywacji punktów kontrolnych cyklu komórkowego w odpowiedzi na uszkodzenia DNA oraz z towarzyszące im zmiany architektury chromatyny interfazowej ograniczające aktywność transkrypcyjną i obniżające kompetencję komórek do przejścia przez punkt G2/M.
3. Istotną przyczyną blokowania mitozy w warunkach stresu wywołanego kadmem jest ograniczenie aktywności czynnika promującego wejście w mitozę (MPF), wynikające przede wszystkim z wyraźnego obniżenia zawartości CycB, zarówno na poziomie białka jak i transkryptu.
4. Spadek indeksu mitotycznego oraz zaburzenia proporcji komórek w poszczególnych fazach mitozy, w tym redukcja liczby komórek w anafazie i telofazie, mogą być konsekwencją indukowanej przez kadm agregacji i dezorganizacji elementów cytoszkieletu (mikrotubul i filamentów aktynowych), prowadzącej do defektów formowania i dynamiki wiązki pre-profazowej, wrzeciona kariokinetycznego oraz fragmoplastu.

5. Stres wywołany kadmem zakłóca epigenetyczną kontrolę kondensacji i segregacji chromosomów poprzez zaburzenie dynamicznej regulacji mitotycznych modyfikacji histonu H3 (H3T3Ph i H3S10Ph), co może odzwierciedlać brak równowagi pomiędzy aktywnością mitotycznych kinaz (Haspin/Aurora B) i fosfataz (PP1/2A).
6. TO stosowany samodzielnie nie wywołuje istotnych zmian w aktywności mitotycznej, poziomie regulatorów cyklu komórkowego, organizacji cytoszkieletu ani wzorcach mitotycznych modyfikacji histonu H3, co potwierdza jego neutralność wobec analizowanych parametrów w komórkach merystematycznych.
7. Szerokie działanie ochronne TO w warunkach stresu wywołanego kadmem, obejmujące stabilizację regulatorów mitozy, ograniczenie zaburzeń struktury chromatyny oraz przywrócenie prawidłowej organizacji cytoszkieletu i profili mitotycznych modyfikacji histonów sugeruje, że jego efekt realizuje się na nadrzędnym poziomie regulacyjnym, potencjalnie związanym z ograniczeniem stresu oksydacyjnego.
8. Niepełne przywrócenie przez TO indeksu mitotycznego w komórkach eksponowanych na działanie kadmu może wynikać z histerezy CDKA–CycB, zgodnie z którą próg aktywności kompleksu wymagany do inicjacji mitozy jest wyższy niż ten niezbędny do jej podtrzymania. Sugeruje to, że jedynie część komórek osiągnęła poziom aktywności umożliwiający przejście przez punkt kontrolny G2/M.
9. Zachowanie integralności cytoszkieletu w obecności TO ograniczało aktywację punktu kontrolnego wrzeciona (SAC), sprzyjając tym samym utrzymanie właściwych proporcji komórek w kolejnych etapach mitozy.
10. Redukcja poziomu ROS w obecności TO (lub inna droga działania TO) mogły sprzyjać utrzymaniu aktywności fosfataz PP1/PP2A oraz prawidłowej lokalizacji kinazy Aurora B, umożliwiając przywrócenie mitotycznego wzorca fosforylacji H3.
11. TO jako naturalny czynnik ochronny stabilizuje przebieg mitozy w komórkach merystematycznych eksponowanych na kadm, ograniczając jego działanie antyproliferacyjne i częściowo przywracając aktywność podziałową merystemu.

6.5.5. Praca 5 (Załącznik nr 5)

Wnioski:

1. Wysoka zawartość kadmu w komórkach merystematycznych może wiązać się z osłabieniem funkcji bariery ściany komórkowej ograniczającej jego akumulację w obrębie symplastu, wynikającym z zaburzeń w odkładaniu składników ściany. Wskazuje na to obecność pęcherzyków aparatu Golgiego o nieregularnej morfologii, w większości elektronowo jasnych i pozbawionych włóknistej zawartości prekursorów ściany.
2. Toksyczność kadmu w komórkach merystematycznych wynika z zaburzenia równowagi pomiędzy generacją ROS a zdolnością komórki do ich efektywnej neutralizacji, która prowadzi do kaskady uszkodzeń molekularnych i strukturalnych w obrębie organelli cytoplazmatycznych i jądra komórkowego.

3. Indukowana przez kadm aktywacja enzymatycznych i nieenzymatycznych mechanizmów antyoksydacyjnych oraz metabolizmu tiolowego stanowi element odpowiedzi adaptacyjnej, jednak ma ona charakter kompensacyjny i nie prowadzi do pełnego przywrócenia homeostazy redoks w komórce.
4. Synteza fitochelatyn i wzrost puli związków tiolowych wskazuje na aktywację mechanizmów chelatacji i sekwestracji kadmu, jednak nie zapobiega w pełni wtórnym skutkom stresu oksydacyjnego, takim jak peroksydacja lipidów i fragmentacja DNA.
5. Brak równowagi umożliwiającej skuteczne przeciwdziałanie stresowi wywołanemu przez kadm i ROS w komórkach merystematycznych może wynikać z niedoboru niezbędnych białek, będącego konsekwencją zahamowania transkrypcji rRNA i mającego odzwierciedlenie w zaniku składnika włóknistego w jąderkach oraz spadku ilości rybosomów w cytoplazmie.
6. Ochronne działanie TO względem komórek merystematycznych polega zarówno na ograniczeniu akumulacji kadmu w tkankach, jak i na aktywnej modulacji odpowiedzi komórkowej na stres wywołany kadmem.
7. Obecność TO w komórkach merystematycznych eksponowanych na kadm sprzyja wzmożonej syntezie składników ściany komórkowej, widocznych w postaci włóknistych prekursorów wypełniających duże pęcherzyki sekrecyjne aparatu Golgiego.
8. Obecność TO sprzyja skuteczniejszej koordynacji enzymatycznego i nieenzymatycznego systemu antyoksydacyjnego, wzmacniając równowagę pomiędzy generacją ROS a ich neutralizacją i prowadząc do ograniczenia stresu oksydacyjnego oraz stabilizacji środowiska redoks.
9. Wzmocniony system antyoksydacyjny może wynikać z odpowiedniej dostępności enzymów antyoksydacyjnych i znajduje odzwierciedlenie w obserwacjach ultrastrukturalnych. Obecność licznych i dużych wakuol jąderkowych wskazuje na nasilony transport podjednostek rybosomów do cytoplazmy, a ich wzmożona akumulacja na elektronowo ciemnych kanałach retikulum endoplazmatycznego oraz w obrębie otoczki jądrowej świadczy o intensyfikacji procesu translacji, prowadzącej do zwiększonej syntezy białek niezbędnych w warunkach stresu.
10. Redukcja stresu oksydacyjnego przez TO w komórkach eksponowanych na kadm ogranicza wtórne uszkodzenia, stabilizuje błony komórkowe oraz wspiera zachowanie integralności organelli cytoplazmatycznych i genomu.
11. TO zwiększa zdolności adaptacyjne komórek do obecności kadmu, działając jako wielopłaszczyznowy modulator odpowiedzi na stres. Na poziomie biochemicznym integruje ograniczanie akumulacji metalu, utrzymanie homeostazy redoks oraz wspieranie metabolizmu tiolowego, jednocześnie chroniąc integralność błon komórkowych i genomu oraz zachowując architekturę komórkową.

6.6. Bibliografia

1. Kubier, A.; Wilkin, R.T.; Pichler, T. Cadmium in Soils and Groundwater: A Review. *Appl. Geochem.* **2019**, *108*, 104388, doi:10.1016/j.apgeochem.2019.104388.
2. Zhao, Y.; Deng, Q.; Lin, Q.; Zeng, C.; Zhong, C. Cadmium Source Identification in Soils and High-Risk Regions Predicted by Geographical Detector Method. *Environ. Pollut.* **2020**, *263*, 114338, doi:10.1016/j.envpol.2020.114338.
3. Torres, P.; Llopis, A.L.; Melo, C.S.; Rodrigues, A. Environmental Impact of Cadmium in a Volcanic Archipelago: Research Challenges Related to a Natural Pollution Source. *J. Mar. Sci. Eng.* **2023**, *11*, 100, doi:10.3390/jmse11010100.
4. Violante, A.; Cozzolino, V.; Perelomov, L.; Caporale, A.G.; Pigna, M. Mobility and Bioavailability of Heavy Metals and Metalloids in Soil Environments. *J. Soil Sci. Plant Nutr.* **2010**, *10*, 1–25, doi:10.4067/S0718-95162010000100005.
5. Briffa, J.; Sinagra, E.; Blundell, R. Heavy Metal Pollution in the Environment and Their Toxicological Effects on Humans. *Heliyon* **2020**, *6*, e04691, doi:10.1016/j.heliyon.2020.e04691.
6. Ju, Y.; Luo, Z.; Bi, J.; Liu, C.; Liu, X. Transfer of Heavy Metals from Soil to Tea and the Potential Human Health Risk in a Regional High Geochemical Background Area in Southwest China. *Sci. Total Environ.* **2024**, *908*, 168122, doi:10.1016/j.scitotenv.2023.168122.
7. Gavrilaş, S.; Burescu, F.-L.; Chereji, B.-D.; Munteanu, F.-D. The Impact of Anthropogenic Activities on the Catchment's Water Quality Parameters. *Water* **2025**, *17*, 1791, doi:10.3390/w17121791.
8. Yuan, Z.; Luo, T.; Liu, X.; Hua, H.; Zhuang, Y.; Zhang, X.; Zhang, L.; Zhang, Y.; Xu, W.; Ren, J. Tracing Anthropogenic Cadmium Emissions: From Sources to Pollution. *Sci. Total Environ.* **2019**, *676*, 87–96, doi:10.1016/j.scitotenv.2019.04.250.
9. Khan, Z.; Elahi, A.; Bukhari, D.A.; Rehman, A. Cadmium Sources, Toxicity, Resistance and Removal by Microorganisms-a Potential Strategy for Cadmium Eradication. *J. Saudi Chem. Soc.* **2022**, *26*, 101569, doi:10.1016/j.jscs.2022.101569.
10. Edo, G.I.; Samuel, P.O.; Oloni, G.O.; Ezekiel, G.O.; Ikpekoro, V.O.; Obasohan, P.; Ongulu, J.; Otunuya, C.F.; Opiti, A.R.; Ajakaye, R.S.; et al. Environmental Persistence, Bioaccumulation, and Ecotoxicology of Heavy Metals. *Chem. Ecol.* **2024**, *40*, 322–349, doi:10.1080/02757540.2024.2306839.
11. Wang, R.; Sang, P.; Guo, Y.; Jin, P.; Cheng, Y.; Yu, H.; Xie, Y.; Yao, W.; Qian, H. Cadmium in Food: Source, Distribution and Removal. *Food Chem.* **2023**, *405*, 134666, doi:10.1016/j.foodchem.2022.134666.
12. Croteau, M.-N.; Luoma, S.N.; Stewart, A.R. Trophic Transfer of Metals along Freshwater Food Webs: Evidence of Cadmium Biomagnification in Nature. *Limnol. Oceanogr.* **2005**, *50*, 1511–1519, doi:10.4319/lo.2005.50.5.1511.
13. Mezynska, M.; Brzóska, M.M. Environmental Exposure to Cadmium – a Risk for Health of the General Population in Industrialized Countries and Preventive Strategies. *Environ. Sci. Pollut. Res.* **2018**, *25*, 3211–3232, doi:10.1007/s11356-017-0827-z.
14. Wang, M.; Chen, Z.; Song, W.; Hong, D.; Huang, L.; Li, Y. A Review on Cadmium Exposure in the Population and Intervention Strategies against Cadmium Toxicity. *Bull. Environ. Contam. Toxicol.* **2021**, *106*, 65–74, doi:10.1007/s00128-020-03088-1.
15. Khan, M.M.; Fan, Z.-Y.; Wang, X.-M.; Qiu, B.-L. Distribution and Accumulation of Cadmium in Different Trophic Levels Affecting Serangium Japonicum, the Predatory Beetle of Whitefly Bemisia Tabaci, Biologically, Physiologically and Genetically: An Experimental Study. *J. Hazard. Mater.* **2024**, *465*, 133244, doi:10.1016/j.jhazmat.2023.133244.
16. Gallego, S.M.; Pena, L.B.; Barcia, R.A.; Azpilicueta, C.E.; Iannone, M.F.; Rosales, E.P.; Zawoznik, M.S.; Groppa, M.D.; Benavides, M.P. Unravelling Cadmium Toxicity and Tolerance in Plants: Insight into Regulatory Mechanisms. *Environ. Exp. Bot.* **2012**, *83*, 33–46, doi:10.1016/j.envexpbot.2012.04.006.
17. Hu, Y.; He, R.; Mu, X.; Zhou, Y.; Li, X.; Wang, H.; Xing, W.; Liu, D. Cadmium Toxicity in Plants: From Transport to Tolerance Mechanisms. *Plant Signal. Behav.* **2025**, *20*, 2544316, doi:10.1080/15592324.2025.2544316.
18. Bi, Y.; Chen, W.; Zhang, W.; Zhou, Q.; Yun, L.; Xing, D. Production of Reactive Oxygen Species, Impairment of Photosynthetic Function and Dynamic Changes in Mitochondria Are Early Events in Cadmium-Induced Cell Death in *Arabidopsis Thaliana*. *Biol. Cell* **2009**, *101*, 629–643, doi:10.1042/BC20090015.
19. Haider, F.U.; Liqun, C.; Coulter, J.A.; Cheema, S.A.; Wu, J.; Zhang, R.; Wenjun, M.; Farooq, M. Cadmium Toxicity in Plants: Impacts and Remediation Strategies. *Ecotoxicol. Environ. Saf.* **2021**, *211*, 111887, doi:10.1016/j.ecoenv.2020.111887.
20. Molnárová, M.; Fargašová, A. Relationship between Various Physiological and Biochemical Parameters Activated by Cadmium in Sinapis Alba L. and Hordeum Vulgare L. *Ecol. Eng.* **2012**, *49*, 65–72, doi:10.1016/j.ecoleng.2012.08.025.

21. Zhao, H.; Guan, J.; Liang, Q.; Zhang, X.; Hu, H.; Zhang, J. Effects of Cadmium Stress on Growth and Physiological Characteristics of Sassafras Seedlings. *Sci. Rep.* **2021**, *11*, 9913, doi:10.1038/s41598-021-89322-0.
22. Shaari, N.E.M.; Tajudin, M.T.F.M.; Khandaker, M.M.; Majrashi, A.; Alenazi, M.M.; Abdullahi, U.A.; Mohd, K.S. Cadmium Toxicity Symptoms and Uptake Mechanism in Plants: A Review. *Braz. J. Biol.* **2024**, *84*, e252143, doi:10.1590/1519-6984.252143.
23. Jiang, X.J.; Luo, Y.M.; Liu, Q.; Liu, S.L.; Zhao, Q.G. Effects of Cadmium on Nutrient Uptake and Translocation by Indian Mustard. *Environ. Geochem. Health* **2004**, *26*, 319–324, doi:10.1023/B:EGAH.0000039596.15586.b3.
24. Rucińska-Sobkowiak, R. Water Relations in Plants Subjected to Heavy Metal Stresses. *Acta Physiol. Plant.* **2016**, *38*, 257, doi:10.1007/s11738-016-2277-5.
25. Guo, Z.; Gao, Y.; Yuan, X.; Yuan, M.; Huang, L.; Wang, S.; Liu, C.; Duan, C. Effects of Heavy Metals on Stomata in Plants: A Review. *Int. J. Mol. Sci.* **2023**, *24*, 9302, doi:10.3390/ijms24119302.
26. Liu, W.; Dai, N.; Wang, Y.; Xu, C.; Zhao, H.; Xia, P.; Gu, J.; Liu, X.; Bian, J.; Yuan, Y.; et al. Role of Autophagy in Cadmium-Induced Apoptosis of Primary Rat Osteoblasts. *Sci. Rep.* **2016**, *6*, 20404, doi:10.1038/srep20404.
27. Fujiki, K.; Inamura, H.; Sugaya, T.; Matsuoka, M. Blockade of ALK4/5 Signaling Suppresses Cadmium- and Erastin-Induced Cell Death in Renal Proximal Tubular Epithelial Cells via Distinct Signaling Mechanisms. *Cell Death Differ.* **2019**, *26*, 2371–2385, doi:10.1038/s41418-019-0307-8.
28. Ma, Y.; Su, Q.; Yue, C.; Zou, H.; Zhu, J.; Zhao, H.; Song, R.; Liu, Z. The Effect of Oxidative Stress-Induced Autophagy by Cadmium Exposure in Kidney, Liver, and Bone Damage, and Neurotoxicity. *Int. J. Mol. Sci.* **2022**, *23*, 13491, doi:10.3390/ijms232113491.
29. Yang, Y.; Cheng, R.; Liu, J.; Fang, J.; Wang, X.; Cui, Y.; Zhang, P.; Du, B. Linarin Protects against Cadmium-Induced Osteoporosis via Reducing Oxidative Stress and Inflammation and Altering RANK/RANKL/OPG Pathway. *Biol. Trace Elem. Res.* **2022**, *200*, 3688–3700, doi:10.1007/s12011-021-02967-w.
30. Johri, N.; Jacquillet, G.; Unwin, R. Heavy Metal Poisoning: The Effects of Cadmium on the Kidney. *BioMetals* **2010**, *23*, 783–792, doi:10.1007/s10534-010-9328-y.
31. Godt, J.; Scheidig, F.; Grosse-Siestrup, C.; Esche, V.; Brandenburg, P.; Reich, A.; Groneberg, D.A. The Toxicity of Cadmium and Resulting Hazards for Human Health. *J. Occup. Med. Toxicol.* **2006**, *1*, 22–27, doi:10.1186/1745-6673-1-22.
32. Aoshima, K. *Itai-Itai* Disease: Renal Tubular Osteomalacia Induced by Environmental Exposure to Cadmium—Historical Review and Perspectives. *Soil Sci. Plant Nutr.* **2016**, *62*, 319–326, doi:10.1080/00380768.2016.1159116.
33. IARC. Cadmium and Cadmium Compounds. *IARC Monographs on the Evaluation of Carcinogenic Risks to Humans; International Agency for Research on Cancer:* Lyon, France, **2012**; Vol. 100C.
34. Waalkes, M.P. Cadmium Carcinogenesis. *Mutat. Res. Fundam. Mol. Mech. Mutagen.* **2003**, *533*, 107–120, doi:10.1016/j.mrfmmm.2003.07.011.
35. Joseph, P. Mechanisms of Cadmium Carcinogenesis. *Toxicol. Appl. Pharmacol.* **2009**, *238*, 272–279, doi:10.1016/j.taap.2009.01.011.
36. Hartwig, A. Cadmium and Cancer. In: *Cadmium: from toxicity to essentiality*; Sigel, A., Sigel, H., Sigel, R.K., Eds.; Metal Ions in Life Sciences; Springer Netherlands: Dordrecht, 2013; Vol. 11, pp. 491–507 ISBN 978-94-007-5178-1.
37. Ali, W.; Bian, Y.; Zhang, H.; Qazi, I.H.; Zou, H.; Zhu, J.; Liu, Z. Effect of Cadmium Exposure during and after Pregnancy of Females. *Environ. Pollut. Bioavailability* **2023**, *35*, 2181124, doi:10.1080/26395940.2023.2181124.
38. Benavides, M.P.; Gallego, S.M.; Tomaro, M.L. Cadmium Toxicity in Plants. *Braz. J. Plant Physiol.* **2005**, *17*, 21–34, doi:10.1590/S1677-04202005000100003.
39. Nazar, R.; Iqbal, N.; Masood, A.; Khan, M.I.R.; Syeed, S.; Khan, N.A. Cadmium Toxicity in Plants and Role of Mineral Nutrients in Its Alleviation. *Am. J. Plant Sci.* **2012**, *3*, 1476–1489, doi:10.4236/ajps.2012.310178.
40. Zhou, L.; Le Roux, G.; Ducrot, C.; Chédin, S.; Labarre, J.; Riva, M.; Carles, C. Repression of Class I Transcription by Cadmium Is Mediated by the Protein Phosphatase 2A. *Nucleic Acids Res.* **2013**, *41*, 6087–6097, doi:10.1093/nar/gkt335.
41. Davidova, S.; Milushev, V.; Satchanska, G. The Mechanisms of Cadmium Toxicity in Living Organisms. *Toxics* **2024**, *12*, 875, doi:10.3390/toxics12120875.
42. Andresen, E.; Kappel, S.; Stärk, H.-J.; Riegger, U.; Borovec, J.; Mattusch, J.; Heinz, A.; Schmelzer, C.E.H.; Matoušková, Š.; Dickinson, B.; et al. Cadmium Toxicity Investigated at the Physiological and Biophysical Levels under Environmentally Relevant Conditions Using the Aquatic Model Plant *Ceratophyllum Demersum*. *New Phytol.* **2016**, *210*, 1244–1258, doi:10.1111/nph.13840.

43. Rajakumar, S.; Abhishek, A.; Selvam, G.S.; Nachiappan, V. Effect of Cadmium on Essential Metals and Their Impact on Lipid Metabolism in Saccharomyces Cerevisiae. *Cell Stress Chaperones* **2020**, *25*, 19–33, doi:10.1007/s12192-019-01058-z.
44. Cuypers, A.; Plusquin, M.; Remans, T.; Jozefczak, M.; Keunen, E.; Gielen, H.; Opdenakker, K.; Nair, A.R.; Munters, E.; Artois, T.J.; et al. Cadmium Stress: An Oxidative Challenge. *BioMetals* **2010**, *23*, 927–940, doi:10.1007/s10534-010-9329-x.
45. Krishnamurthy, H.K.; Pereira, M.; Rajavelu, I.; Jayaraman, V.; Krishna, K.; Wang, T.; Bei, K.; Rajasekaran, J.J. Oxidative Stress: Fundamentals and Advances in Quantification Techniques. *Front. Chem.* **2024**, *12*, 1470458, doi:10.3389/fchem.2024.1470458.
46. Juan, C.A.; Pérez de la Lastra, J.M.; Plou, F.J.; Pérez-Lebeña, E. The Chemistry of Reactive Oxygen Species (ROS) Revisited: Outlining Their Role in Biological Macromolecules (DNA, Lipids and Proteins) and Induced Pathologies. *Int. J. Mol. Sci.* **2021**, *22*, 4642, doi:10.3390/ijms22094642.
47. Salmon, T.B. Biological Consequences of Oxidative Stress-Induced DNA Damage in Saccharomyces Cerevisiae. *Nucleic Acids Res.* **2004**, *32*, 3712–3723, doi:10.1093/nar/gkh696.
48. Caldecott, K.W. Causes and Consequences of DNA Single-Strand Breaks. *Trends Biochem. Sci.* **2024**, *49*, 68–78, doi:10.1016/j.tibs.2023.11.001.
49. Casalino, E.; Calzaretti, G.; Sblano, C.; Landriscina, C. Molecular Inhibitory Mechanisms of Antioxidant Enzymes in Rat Liver and Kidney by Cadmium. *Toxicology* **2002**, *179*, 37–50, doi:10.1016/S0300-483X(02)00245-7.
50. Hussein, M. A.; Kamalakkannan, A.; Valinezhad, K.; Kannan, J.; Paleati, N.; Saad, R.; Kajdacsy-Balla, A.; Munirathinam, G. The Dynamic Face of Cadmium-Induced Carcinogenesis: Mechanisms, Emerging Trends, and Future Directions. *Curr. Res. Toxicol.* **2024**, *6*, 100166, doi:10.1016/j.crtox.2024.100166.
51. Hamid, Y.; Tang, L.; Sohail, M.I.; Cao, X.; Hussain, B.; Aziz, M.Z.; Usman, M.; He, Z.; Yang, X. An Explanation of Soil Amendments to Reduce Cadmium Phytoavailability and Transfer to Food Chain. *Sci. Total Environ.* **2019**, *660*, 80–96, doi:10.1016/j.scitotenv.2018.12.419.
52. Gu, J.; Zou, G.; Su, S.; Li, S.; Liu, W.; Zhao, H.; Liu, L.; Jin, L.; Tian, Y.; Zhang, X.; et al. Effects of pH on Available Cadmium in Calcareous Soils and Culture Substrates. *Eurasian Soil Sci.* **2022**, *55*, 1714–1719, doi:10.1134/S1064229322601391.
53. Blake, L.; Goulding, K.W.T. Effects of Atmospheric Deposition, Soil pH and Acidification on Heavy Metal Contents in Soils and Vegetation of Semi-Natural Ecosystems at Rothamsted Experimental Station, UK. *Plant Soil* **2002**, *240*, 235–251, doi:10.1023/A:1015731530498.
54. Zulfiqar, U.; Ayub, A.; Hussain, S.; Waraich, E.A.; El-Esawi, M.A.; Ishfaq, M.; Ahmad, M.; Ali, N.; Maqsood, M.F. Cadmium Toxicity in Plants: Recent Progress on Morpho-Physiological Effects and Remediation Strategies. *J. Soil Sci. Plant Nutr.* **2022**, *22*, 212–269, doi:10.1007/s42729-021-00645-3.
55. Kumar, V.; Rout, C.; Singh, J.; Saharan, Y.; Goyat, R.; Umar, A.; Akbar, S.; Baskoutas, S. A Review on the Clean-up Technologies for Heavy Metal Ions Contaminated Soil Samples. *Heliyon* **2023**, *9*, e15472, doi:10.1016/j.heliyon.2023.e15472.
56. Lwin, C.S.; Seo, B.-H.; Kim, H.-U.; Owens, G.; Kim, K.-R. Application of Soil Amendments to Contaminated Soils for Heavy Metal Immobilization and Improved Soil Quality—a Critical Review. *Soil Sci. Plant Nutr.* **2018**, *64*, 156–167, doi:10.1080/00380768.2018.1440938.
57. Zhu, H.; Chen, C.; Xu, C.; Zhu, Q.; Huang, D. Effects of Soil Acidification and Liming on the Phytoavailability of Cadmium in Paddy Soils of Central Subtropical China. *Environ. Pollut.* **2016**, *219*, 99–106, doi:10.1016/j.envpol.2016.10.043.
58. He, L.-L.; Huang, D.-Y.; Zhang, Q.; Zhu, H.-H.; Xu, C.; Li, B.; Zhu, Q.-H. Meta-Analysis of the Effects of Liming on Soil pH and Cadmium Accumulation in Crops. *Ecotoxicol. Environ. Saf.* **2021**, *223*, 112621, doi:10.1016/j.ecoenv.2021.112621.
59. Kumpiene, J.; Lagerkvist, A.; Maurice, C. Stabilization of As, Cr, Cu, Pb and Zn in Soil Using Amendments – a Review. *Waste Manage.* **2008**, *28*, 215–225, doi:10.1016/j.wasman.2006.12.012.
60. Palansooriya, K.N.; Shaheen, S.M.; Chen, S.S.; Tsang, D.C.W.; Hashimoto, Y.; Hou, D.; Bolan, N.S.; Rinklebe, J.; Ok, Y.S. Soil Amendments for Immobilization of Potentially Toxic Elements in Contaminated Soils: A Critical Review. *Environ. Int.* **2020**, *134*, 105046, doi:10.1016/j.envint.2019.105046.
61. Li, Q.; Wang, Y.; Li, Y.; Li, L.; Tang, M.; Hu, W.; Chen, L.; Ai, S. Speciation of Heavy Metals in Soils and Their Immobilization at Micro-Scale Interfaces among Diverse Soil Components. *Sci. Total Environ.* **2022**, *825*, 153862, doi:10.1016/j.scitotenv.2022.153862.
62. Yan, A.; Wang, Y.; Tan, S.N.; Mohd Yusof, M.L.; Ghosh, S.; Chen, Z. Phytoremediation: A Promising Approach for Revegetation of Heavy Metal-Polluted Land. *Front. Plant Sci.* **2020**, *11*, 359, doi:10.3389/fpls.2020.00359.
63. Nedjimi, B. Phytoremediation: A Sustainable Environmental Technology for Heavy Metals Decontamination. *SN Appl. Sci.* **2021**, *3*, 286, doi:10.1007/s42452-021-04301-4.
64. Bhat, S.A.; Bashir, O.; Ul Haq, S.A.; Amin, T.; Rafiq, A.; Ali, M.; Américo-Pinheiro, J.H.P.; Sher, F. Phytoremediation of Heavy Metals in Soil and Water: An Eco-Friendly, Sustainable and Multidisciplinary Approach. *Chemosphere* **2022**, *303*, 134788, doi:10.1016/j.chemosphere.2022.134788.

65. McGrath, S.P.; Zhao, F.J.; Lombi, E. Plant and Rhizosphere Processes Involved in Phytoremediation of Metal-Contaminated Soils. *Plant Soil* **2001**, *232*, 207–214, doi:10.1023/A:1010358708525.
66. Suman, J.; Uhlik, O.; Viktorova, J.; Macek, T. Phytoextraction of Heavy Metals: A Promising Tool for Clean-up of Polluted Environment? *Front. Plant Sci.* **2018**, *9*, 1476, doi:10.3389/fpls.2018.01476.
67. Ali, H.; Khan, E.; Sajad, M.A. Phytoremediation of Heavy Metals – Concepts and Applications. *Chemosphere* **2013**, *91*, 869–881, doi:10.1016/j.chemosphere.2013.01.075.
68. Newman, L.A.; Reynolds, C.M. Phytodegradation of Organic Compounds. *Curr. Opin. Biotechnol.* **2004**, *15*, 225–230, doi:10.1016/j.copbio.2004.04.006.
69. Limmer, M.; Burken, J. Phytovolatilization of Organic Contaminants. *Environ. Sci. Technol.* **2016**, *50*, 6632–6643, doi:10.1021/acs.est.5b04113.
70. Chandra, R.; Kumar, V. Phytoextraction of Heavy Metals by Potential Native Plants and Their Microscopic Observation of Root Growing on Stabilised Distillery Sludge as a Prospective Tool for in Situ Phytoremediation of Industrial Waste. *Environ. Sci. Pollut. Res.* **2017**, *24*, 2605–2619, doi:10.1007/s11356-016-8022-1.
71. Zhao, F.J.; Lombi, E.; McGrath, S.P. Assessing the Potential for Zinc and Cadmium Phytoremediation with the Hyperaccumulator Thlaspi Caerulescens. *Plant Soil* **2003**, *249*, 37–43, doi:10.1023/A:1022530217289.
72. Yang, X.E.; Long, X.X.; Ye, H.B.; He, Z.L.; Calvert, D.V.; Stoffella, P.J. Cadmium Tolerance and Hyperaccumulation in a New Zn-Hyperaccumulating Plant Species (Sedum Alfredii Hance). *Plant Soil* **2004**, *259*, 181–189, doi:10.1023/B:PLSO.0000020956.24027.f2.
73. Yanai, J.; Zhao, F.-J.; McGrath, S.P.; Kosaki, T. Effect of Soil Characteristics on Cd Uptake by the Hyperaccumulator Thlaspi Caerulescens. *Environ. Pollut.* **2006**, *139*, 167–175, doi:10.1016/j.envpol.2005.03.013.
74. Martos, S.; Gallego, B.; Sáez, L.; López-Alvarado, J.; Cabot, C.; Poschenrieder, C. Characterization of Zinc and Cadmium Hyperaccumulation in Three Noccaea (Brassicaceae) Populations from Non-Metalliferous Sites in the Eastern Pyrenees. *Front. Plant Sci.* **2016**, *7*, 128, doi:10.3389/fpls.2016.00128.
75. Liu, M.; Feng, Y.; Wang, M.; Sun, X.; Qi, C.Y.; Yang, X.; Zhang, D. Sedum Alfredii Hance: A Cadmium and Zinc Hyperaccumulating Plant. *Ecotoxicol. Environ. Saf.* **2025**, *290*, 117588, doi:10.1016/j.ecoenv.2024.117588.
76. Muszyńska, E.; Hanus-Fajerska, E. Why Are Heavy Metal Hyperaccumulating Plants so Amazing? *BioTechnologia* **2016**, *96*, 265–271, doi:10.5114/bta.2015.57730.
77. Xiang, L.; Harindintwali, J.D.; Wang, F.; Redmile-Gordon, M.; Chang, S.X.; Fu, Y.; He, C.; Muhoza, B.; Brahushi, F.; Bolan, N.; et al. Integrating Biochar, Bacteria, and Plants for Sustainable Remediation of Soils Contaminated with Organic Pollutants. *Environ. Sci. Technol.* **2022**, *56*, 16546–16566, doi:10.1021/acs.est.2c02976.
78. Cao, J.; Tan, Y.; Zhang, C. Combined Approaches for the Remediation of Cadmium- and Arsenic-Contaminated Soil: Phytoremediation and Stabilization Strategies. *Appl. Sci.* **2024**, *14*, 7144, doi:10.3390/app14167144.
79. Sharma, J.K.; Kumar, N.; Singh, N.P.; Santal, A.R. Phytoremediation Technologies and Their Mechanism for Removal of Heavy Metal from Contaminated Soil: An Approach for a Sustainable Environment. *Front. Plant Sci.* **2023**, *14*, 1076876, doi:10.3389/fpls.2023.1076876.
80. Sadgrove, N.; Padilla-González, G.; Phumthum, M. Fundamental Chemistry of Essential Oils and Volatile Organic Compounds, Methods of Analysis and Authentication. *Plants* **2022**, *11*, 789, doi:10.3390/plants11060789.
81. Hanif, M.A.; Nisar, S.; Khan, G.S.; Mushtaq, Z.; Zubair, M. Essential Oils. In: *Essential Oil Research*; Malik, S., Ed.; Springer International Publishing: Cham, 2019; pp. 3–17. ISBN 978-3-030-16545-1.
82. Dhifi, W.; Bellili, S.; Jazi, S.; Bahloul, N.; Mnif, W. Essential Oils' Chemical Characterization and Investigation of Some Biological Activities: A Critical Review. *Medicines* **2016**, *3*, 25, doi:10.3390/medicines3040025.
83. Borugă, O.; Jianu, C.; Mişcă, C.; Goleţ, I.; Gruia, A.T.; Horhat, F.G. *Thymus vulgaris* Essential Oil: Chemical Composition and Antimicrobial Activity. *J. Med. Life* **2014**, *7 Spec No. 3*, 56–60.
84. Ali, S.; Ekbbal, R.; Salar, S.; Yasheshwar; Ali, S.A.; Jaiswal, A.K.; Singh, M.; Yadav, D.K.; Kumar, S.; Gaurav: Quality Standards and Pharmacological Interventions of Natural Oils: Current Scenario and Future Perspectives. *ACS Omega* **2023**, *8*, 39945–39963, doi:10.1021/acsomega.3c05241.
85. Baccati, C.; Gibernau, M.; Paoli, M.; Ollitrault, P.; Tomi, F.; Luro, F. Chemical Variability of Peel and Leaf Essential Oils in the Citrus Subgenus Papeda (Swingle) and Few Relatives. *Plants* **2021**, *10*, 1117, doi:10.3390/plants10061117.
86. Prashar, A.; Locke, I.C.; Evans, C.S. Cytotoxicity of Lavender Oil and Its Major Components to Human Skin Cells. *Cell Prolif.* **2004**, *37*, 221–229, doi:10.1111/j.1365-2184.2004.00307.x.
87. Alma, M.H.; Ertaş, M.; Nitz, S.; Kollmannsberger, H. Chemical Composition and Content of Essential Oil from the Bud of Cultivated Turkish Clove (*Syzygium aromaticum* L.). *BioResources* **2007**, *2*, 265–269, doi:10.15376/biores.2.2.265-269.

88. Kamatou, G.P.P.; Viljoen, A.M. A Review of the Application and Pharmacological Properties of α-Bisabolol and α-Bisabolol-Rich Oils. *J. Am. Oil Chem. Soc.* **2010**, *87*, 1–7, doi:10.1007/s11746-009-1483-3.
89. Chaieb, K.; Hajlaoui, H.; Zmantar, T.; Kahla-Nakbi, A.B.; Rouabhia, M.; Mahdouani, K.; Bakhrouf, A. The Chemical Composition and Biological Activity of Clove Essential Oil, *Eugenia caryophyllata* (*Syzigium aromaticum* L. Myrtaceae): A Short Review. *Phytother. Res.* **2007**, *21*, 501–506, doi:10.1002/ptr.2124.
90. Abdelmohsen, U.R.; Elmaidomy, A.H. Exploring the Therapeutic Potential of Essential Oils: A Review of Composition and Influencing Factors. *Front. Nat. Prod.* **2025**, *4*, 1490511, doi:10.3389/fntpr.2025.1490511.
91. Youdim, K.A.; Deans, S.G.; Finlayson, H.J. The Antioxidant Properties of Thyme (*Thymus Zygis* L.) Essential Oil: An Inhibitor of Lipid Peroxidation and a Free Radical Scavenger. *J. Essent. Oil Res.* **2002**, *14*, 210–215, doi:10.1080/10412905.2002.9699825.
92. Hyldgaard, M.; Mygind, T.; Meyer, R.L. Essential Oils in Food Preservation: Mode of Action, Synergies, and Interactions with Food Matrix Components. *Front. Microbiol.* **2012**, *3*, 12, doi:10.3389/fmicb.2012.00012.
93. Ninkovic, V.; Markovic, D.; Rensing, M. Plant Volatiles as Cues and Signals in Plant Communication. *Plant Cell Environ.* **2021**, *44*, 1030–1043, doi:10.1111/pce.13910.
94. Bai, L.; Wang, W.; Hua, J.; Guo, Z.; Luo, S. Defensive Functions of Volatile Organic Compounds and Essential Oils from Northern White-Cedar in China. *BMC Plant Biol.* **2020**, *20*, 500, doi:10.1186/s12870-020-02716-6.
95. Machado, C.A.; Oliveira, F.O.; de Andrade, M.A.; Hodel, K.V.S.; Lepikson, H.; Machado, B.A.S. Steam Distillation for Essential Oil Extraction: An Evaluation of Technological Advances Based on an Analysis of Patent Documents. *Sustainability* **2022**, *14*, 7119, doi:10.3390/su14127119.
96. Li, G.; Xiang, S.; Pan, Y.; Long, X.; Cheng, Y.; Han, L.; Zhao, X. Effects of Cold-Pressing and Hydrodistillation on the Active Non-Volatile Components in Lemon Essential Oil and the Effects of the Resulting Oils on Aging-Related Oxidative Stress in Mice. *Front. Nutr.* **2021**, *8*, 689094, doi:10.3389/fnut.2021.689094.
97. Chemat, F.; Rombaut, N.; Sicaire, A.-G.; Meullemiestre, A.; Fabiano-Tixier, A.-S.; Abert-Vian, M. Ultrasound Assisted Extraction of Food and Natural Products. Mechanisms, Techniques, Combinations, Protocols and Applications. A Review. *Ultrason. Sonochem.* **2017**, *34*, 540–560, doi:10.1016/j.ultsonch.2016.06.035.
98. Zhou, W.; Li, J.; Wang, X.; Liu, L.; Li, Y.; Song, R.; Zhang, M.; Li, X. Research Progress on Extraction, Separation, and Purification Methods of Plant Essential Oils. *Separations* **2023**, *10*, 596, doi:10.3390/separations10120596.
99. Zabka, M.; Pavela, R.; Prokinova, E. Antifungal Activity and Chemical Composition of Twenty Essential Oils against Significant Indoor and Outdoor Toxigenic and Aeroallergenic Fungi. *Chemosphere* **2014**, *112*, 443–448, doi:10.1016/j.chemosphere.2014.05.014.
100. Swamy, M.K.; Akhtar, M.S.; Sinniah, U.R. Antimicrobial Properties of Plant Essential Oils against Human Pathogens and Their Mode of Action: An Updated Review. *Evid. Based Complement. Altern. Med.* **2016**, *2016*, 3012462, doi:10.1155/2016/3012462.
101. Nazzaro, F.; Fratianni, F.; Coppola, R.; Feo, V.D. Essential Oils and Antifungal Activity. *Pharmaceuticals* **2017**, *10*, 86, doi:10.3390/ph10040086.
102. Puškárová, A.; Bučková, M.; Kraková, L.; Pangallo, D.; Kozics, K. The Antibacterial and Antifungal Activity of Six Essential Oils and Their Cyto/Genotoxicity to Human HEL 12469 Cells. *Sci. Rep.* **2017**, *7*, 8211, doi:10.1038/s41598-017-08673-9.
103. Hou, T.; Sana, S.S.; Li, H.; Xing, Y.; Nanda, A.; Netala, V.R.; Zhang, Z. Essential Oils and Its Antibacterial, Antifungal and Antioxidant Activity Applications: A Review. *Food Biosci.* **2022**, *47*, 101716, doi:10.1016/j.fbio.2022.101716.
104. El-Tarabily, K.A.; El-Saadony, M.T.; Alagawany, M.; Arif, M.; Batiha, G.E.; Khafaga, A.F.; Elwan, H.A.M.; Elnesr, S.S.; E. Abd El-Hack, M. Using Essential Oils to Overcome Bacterial Biofilm Formation and Their Antimicrobial Resistance. *Saudi J. Biol. Sci.* **2021**, *28*, 5145–5156, doi:10.1016/j.sjbs.2021.05.033.
105. Di Pasqua, R.; Betts, G.; Hoskins, N.; Edwards, M.; Ercolini, D.; Mauriello, G. Membrane Toxicity of Antimicrobial Compounds from Essential Oils. *J. Agric. Food Chem.* **2007**, *55*, 4863–4870, doi:10.1021/jf0636465.
106. Lv, F.; Liang, H.; Yuan, Q.; Li, C. In Vitro Antimicrobial Effects and Mechanism of Action of Selected Plant Essential Oil Combinations against Four Food-Related Microorganisms. *Food Res. Int.* **2011**, *44*, 3057–3064, doi:10.1016/j.foodres.2011.07.030.
107. Bajpai, V.K.; Sharma, A.; Baek, K.-H. Antibacterial Mode of Action of *Cudrania tricuspidata* Fruit Essential Oil, Affecting Membrane Permeability and Surface Characteristics of Food-Borne Pathogens. *Food Control* **2013**, *32*, 582–590, doi:10.1016/j.foodcont.2013.01.032.

108. Bakkali, F.; Averbeck, S.; Averbeck, D.; Idaomar, M. Biological Effects of Essential Oils – A Review. *Food Chem. Toxicol.* **2008**, *46*, 446–475, doi:10.1016/j.fct.2007.09.106.
109. Huang, Y.; Ebrahimi, H.; Berselli, E.; Foti, M.C.; Amorati, R. Essential Oils as Antioxidants: Mechanistic Insights from Radical Scavenging to Redox Signaling. *Antioxidants* **2025**, *15*, 37, doi:10.3390/antiox15010037.
110. Ali, B.; Al-Wabel, N.A.; Shams, S.; Ahamad, A.; Khan, S.A.; Anwar, F. Essential Oils Used in Aromatherapy: A Systemic Review. *Asian Pac. J. Trop. Biomed.* **2015**, *5*, 601–611, doi:10.1016/j.apjtb.2015.05.007.
111. Horváth, G.; Ács, K. Essential Oils in the Treatment of Respiratory Tract Diseases Highlighting Their Role in Bacterial Infections and Their Anti-Inflammatory Action: A Review. *Flavour Fragr. J.* **2015**, *30*, 331–341, doi:10.1002/ffj.3252.
112. Durczyńska, Z.; Żukowska, G. Properties and Applications of Essential Oils: A Review. *J. Ecol. Eng.* **2024**, *25*, 333–340, doi:10.12911/22998993/177404.
113. Pandey, A.K.; Kumar, P.; Singh, P.; Tripathi, N.N.; Bajpai, V.K. Essential Oils: Sources of Antimicrobials and Food Preservatives. *Front. Microbiol.* **2017**, *7*, 2161, doi:10.3389/fmicb.2016.02161.
114. Cunha, C.; Ribeiro, H.M.; Rodrigues, M.; Araujo, A.R.T.S. Essential Oils Used in Dermocosmetics: Review about Its Biological Activities. *J. Cosmet. Dermatol.* **2022**, *21*, 513–529, doi:10.1111/jocd.14652.
115. Campolina, G.A.; Cardoso, M.D.G.; Caetano, A.R.S.; Nelson, D.L.; Ramos, E.M. Essential Oil and Plant Extracts as Preservatives and Natural Antioxidants Applied to Meat and Meat Products: A Review. *Food Technol. Biotechnol.* **2023**, *61*, 212–225, doi:10.17113/ftb.61.02.23.7883.
116. Ge, T.; Gao, W.; Liang, C.; Han, C.; Wang, Y.; Xu, Q.; Wang, Q. 4-Ethylphenol, a Volatile Organic Compound Produced by Disease-Resistant Soybean, Is a Potential Botanical Agrochemical against Oomycetes. *Front. Plant Sci.* **2021**, *12*, 717258, doi:10.3389/fpls.2021.717258.
117. Kundu, A.; Dutta, A.; Mandal, A.; Negi, L.; Malik, M.; Puramchatwad, R.; Antil, J.; Singh, A.; Rao, U.; Saha, S.; et al. A Comprehensive in Vitro and in Silico Analysis of Nematicidal Action of Essential Oils. *Front. Plant Sci.* **2021**, *11*, 614143, doi:10.3389/fpls.2020.614143.
118. Valcárcel, F.; Olmeda, A.S.; González, M.G.; Andrés, M.F.; Navarro-Rocha, J.; González-Coloma, A. Acaricidal and Insect Antifeedant Effects of Essential Oils from Selected Aromatic Plants and Their Main Components. *Front. Agron.* **2021**, *3*, 662802, doi:10.3389/fagro.2021.662802.
119. Deka, B.; Babu, A.; Baruah, C.; Sarkar, S. Plant Extracts as Potential Acaricides for the Management of Red Spider Mite, *Oligonychus coffeae* Nietner (Acarina: Tetranychidae), in the Tea Ecosystem: An Eco-Friendly Strategy. *Front. Agron.* **2022**, *4*, 685568, doi:10.3389/fagro.2022.685568.
120. Lahlali, R.; El Hamss, H.; Mediouni-Ben Jemâa, J.; Barka, E.A. Editorial: The Use of Plant Extracts and Essential Oils as Biopesticides. *Front. Agron.* **2022**, *4*, 921965, doi:10.3389/fagro.2022.921965.
121. Møller, M.T.; Birch, H.; Sjøholm, K.K.; Hammershøj, R.; Jenner, K.; Mayer, P. Biodegradation of an Essential Oil UVCB – Whole Substance Testing and Constituent Specific Analytics Yield Biodegradation Kinetics of Mixture Constituents. *Chemosphere* **2021**, *278*, 130409, doi:10.1016/j.chemosphere.2021.130409.
122. Reyes-Ávila, A.; Garrido Frenich, A.; Romero-González, R. Degradation of Limonene and trans-Cinnamaldehyde in Soil, and Detection of Their Metabolites by UHPLC and GC-HRMS. *Environ. Sci. Pollut. Res.* **2024**, *31*, 33058–33068, doi:10.1007/s11356-024-33334-6.
123. Matos, W.B.; Santos, A.C.C.; Lima, A.P.S.; Santana, E.D.R.; Silva, J.E.; Blank, A.F.; Araújo, A.P.A.; Bacci, L. Potential Source of Ecofriendly Insecticides: Essential Oil Induces Avoidance and Causes Lower Impairment on the Activity of a Stingless Bee than Organosynthetic Insecticides, in Laboratory. *Ecotoxicol. Environ. Saf.* **2021**, *209*, 111764, doi:10.1016/j.ecoenv.2020.111764.
124. Caren, J.; Zhu, Y.-C.; Read, Q.D.; Du, Y. Risk Assessment of Effects of Essential Oils on Honey Bees (*Apis mellifera* L.). *Insects* **2025**, *16*, 303, doi:10.3390/insects16030303.
125. Dyer, M.C.; Requintina, M.D.; Berger, K.A.; Puggioni, G.; Mather, T.N. Evaluating the Effects of Minimal Risk Natural Products for Control of the Tick, *Ixodes scapularis* (Acari: Ixodidae). *J. Med. Entomol.* **2020**, doi:10.1093/jme/tjaa188.
126. O'Sullivan, J.; Van Acker, R.; Grohs, R.; Riddle, R. Improved Herbicide Efficacy for Organically Grown Vegetables. *Org. Agric.* **2015**, *5*, 315–322, doi:10.1007/s13165-015-0107-5.
127. Arici, Ş.E.; Özkaya, R. Evaluation of Biofungicides in the Control against Powdery Mildew Disease [*Leveillula taurica* (Lev.) Arm.] in Pepper. *Kahramanmaraş Sütçü İmam Üniv. Tarım Ve Doğa Derg.* **2022**, *25*, 274–281, doi:10.18016/ksutarimdoga.vi.910742.
128. Pavela, R.; Benelli, G. Essential Oils as Ecofriendly Biopesticides? Challenges and Constraints. *Trends Plant Sci.* **2016**, *21*, 1000–1007, doi:10.1016/j.tplants.2016.10.005.
129. Dunan, L.; Malanga, T.; Benhamou, S.; Papaiconomou, N.; Desneux, N.; Lavoir, A.-V.; Michel, T. Effects of Essential Oil-Based Formulation on Biopesticide Activity. *Ind. Crops Prod.* **2023**, *202*, 117006, doi:10.1016/j.indcrop.2023.117006.

130. Tohidi, B.; Rahimmalek, M.; Trindade, H. Review on Essential Oil, Extracts Composition, Molecular and Phytochemical Properties of *Thymus* Species in Iran. *Ind. Crops Prod.* **2019**, *134*, 89–99, doi:10.1016/j.indcrop.2019.02.038.
131. Roselló, J.; Llorens-Molina, J.A.; Larran, S.; Sempere-Ferre, F.; Santamarina, M.P. Biofilm Containing the *Thymus serpyllum* Essential Oil for Rice and Cherry Tomato Conservation. *Front. Plant Sci.* **2024**, *15*, 1362569, doi:10.3389/fpls.2024.1362569.
132. Al-Ramamneh, E.A.-D.M. Plant Growth Strategies of *Thymus vulgaris* L. in Response to Population Density. *Ind. Crops Prod.* **2009**, *30*, 389–394, doi:10.1016/j.indcrop.2009.07.008.
133. Thompson, J.D.; Chalchat, J.-C.; Michet, A.; Linhart, Y.B.; Ehlers, B. Qualitative and Quantitative Variation in Monoterpene Co-Occurrence and Composition in the Essential Oil of *Thymus vulgaris* Chemotypes. *J. Chem. Ecol.* **2003**, *29*, 859–880, doi:10.1023/A:1022927615442.
134. Torras, J.; Grau, M.D.; López, J.F.; de las Heras, F.X.C. Analysis of Essential Oils from Chemotypes of *Thymus vulgaris* in Catalonia. *J. Sci. Food Agric.* **2007**, *87*, 2327–2333, doi:10.1002/jsfa.2995.
135. Hoffman-Pennesi, D.; Wu, C. The Effect of Thymol and Thyme Oil Feed Supplementation on Growth Performance, Serum Antioxidant Levels, and Cecal Salmonella Population in Broilers. *J. Appl. Poult. Res.* **2010**, *19*, 432–443, doi:10.3382/japr.2009-00141.
136. Vale-Silva, L.; Gonçalves, M.; Cavaleiro, C.; Salgueiro, L.; Pinto, E. Antifungal Activity of the Essential Oil of *Thymus viciosoi* against *Candida, Cryptococcus, Aspergillus* and Dermatophyte Species. *Planta Med.* **2010**, *76*, 882–888, doi:10.1055/s-0029-1240799.
137. Ivanovic, J.; Misic, D.; Zizovic, I.; Ristic, M. In Vitro Control of Multiplication of Some Food-Associated Bacteria by Thyme, Rosemary and Sage Isolates. *Food Control* **2012**, *25*, 110–116, doi:10.1016/j.foodcont.2011.10.019.
138. de Carvalho, R.J.; De Souza, G.T.; Honório, V.G.; De Sousa, J.P.; Da Conceição, M.L.; Maganani, M.; de Souza, E.L. Comparative Inhibitory Effects of *Thymus vulgaris* L. Essential Oil against *Staphylococcus aureus, Listeria monocytogenes* and Mesophilic Starter Co-Culture in Cheese-Mimicking Models. *Food Microbiol.* **2015**, *52*, 59–65, doi:10.1016/j.fm.2015.07.003.
139. Dandlen, S.A.; Lima, A.S.; Mendes, M.D.; Miguel, M.G.; Faleiro, M.L.; Sousa, M.J.; Pedro, L.G.; Barroso, J.G.; Figueiredo, A.C. Antioxidant Activity of Six Portuguese Thyme Species Essential Oils. *Flavour Fragr. J.* **2010**, *25*, 150–155, doi:10.1002/ffj.1972.
140. Sertel, S.; Eichhorn, T.; Plinkert, P.K.; Efferth, T. Cytotoxicity of *Thymus vulgaris* Essential Oil towards Human Oral Cavity Squamous Cell Carcinoma. *Anticancer Res.* **2011**, *31*, 81–87.
141. Çetinus, E.; Temiz, T.; Ergül, M.; Altun, A.; Çetinus, Ş.; Kaya, T. Thyme Essential Oil Inhibits Proliferation of DLD-1 Colorectal Cancer Cells through Antioxidant Effect. *Cumhur. Med. J.* **2013**, *35*, 14–24, doi:10.7197/1305-0028.1757.
142. Zeng, Q.; Che, Y.; Zhang, Y.; Chen, M.; Guo, Q.; Zhang, W. Thymol Isolated from *Thymus vulgaris* L. Inhibits Colorectal Cancer Cell Growth and Metastasis by Suppressing the Wnt/β-Catenin Pathway. *Drug Des. Dev. Ther.* **2020**, *14*, 2535–2547, doi:10.2147/DDDT.S254218.
143. Kemmerich, B.; Eberhardt, R.; Stammer, H. Efficacy and Tolerability of a Fluid Extract Combination of Thyme Herb and Ivy Leaves and Matched Placebo in Adults Suffering from Acute Bronchitis with Productive Cough. *Arzneim. Forsch.* **2011**, *56*, 652–660, doi:10.1055/s-0031-1296767.
144. Kowalczyk, A.; Przychodna, M.; Sopata, S.; Bodalska, A.; Fecka, I. Thymol and Thyme Essential Oil – New Insights into Selected Therapeutic Applications. *Molecules* **2020**, *25*, 4125, doi:10.3390/molecules25184125.
145. Park, J.-H.; Jeon, Y.-J.; Lee, C.-H.; Chung, N.; Lee, H.-S. Insecticidal Toxicities of Carvacrol and Thymol Derived from *Thymus vulgaris* L. against *Pochazia shantungensis* Chou & Lu., Newly Recorded Pest. *Sci. Rep.* **2017**, *7*, 40902, doi:10.1038/srep40902.
146. Wu, L.; Huo, X.; Zhou, X.; Zhao, D.; He, W.; Liu, S.; Liu, H.; Feng, T.; Wang, C. Acaricidal Activity and Synergistic Effect of Thyme Oil Constituents against Carmine Spider Mite (*Tetranychus cinnabarinus* (Boisduval)). *Molecules* **2017**, *22*, 1873, doi:10.3390/molecules22111873.
147. Barros, F.A.P.; Radünz, M.; Scariot, M.A.; Camargo, T.M.; Nunes, C.F.P.; de Souza, R.R.; Gilson, I.K.; Hackbart, H.C.S.; Radünz, L.L.; Oliveira, J.V.; et al. Efficacy of Encapsulated and Non-Encapsulated Thyme Essential Oil (*Thymus vulgaris* L.) in the Control of *Sitophilus zeamais* and Its Effects on the Quality of Corn Grains throughout Storage. *Crop Prot.* **2022**, *153*, 105885, doi:10.1016/j.cropro.2021.105885.
148. Ansari, M.N.; Rehman, N.U.; Karim, A.; Imam, F.; Hamad, A.M. Protective Effect of *Thymus serrulatus* Essential Oil on Cadmium-Induced Nephrotoxicity in Rats, through Suppression of Oxidative Stress and Downregulation of NF-κB, iNOS, and Smad2 mRNA Expression. *Molecules* **2021**, *26*, 1252, doi:10.3390/molecules26051252.
149. Rahmani, F.; Nabi, S.; Idliki, R.B.; Alimirzaei, M.; Barkhordar, S.M.A.; Shafaei, N.; Zareian, M.; Karimi, E.; Oskoueian, E. Thyme Oil Nanoemulsion Enhanced Cellular Antioxidant and Suppressed Inflammation in Mice Challenged by Cadmium-Induced Oxidative Stress. *Waste Biomass Valorization* **2022**, *13*, 3139–3146, doi:10.1007/s12649-022-01738-5.

150. Ünyayar, S.; Çelik, A.; Çekiç, F.Ö.; Gözel, A. Cadmium-Induced Genotoxicity, Cytotoxicity and Lipid Peroxidation in *Allium sativum* and *Vicia faba*. *Mutagenesis* **2006**, *21*, 77–81, doi:10.1093/mutage/gel001.
151. Souguir, D.; Ferjani, E.; Ledoigt, G.; Goupil, P. Sequential Effects of Cadmium on Genotoxicity and Lipoperoxidation in *Vicia faba* Roots. *Ecotoxicology* **2011**, *20*, 329–336, doi:10.1007/s10646-010-0582-0.
152. Żabka, A.; Winnicki, K.; Polit, J.T.; Wróblewski, M.; Maszewski, J. Cadmium (II)-Induced Oxidative Stress Results in Replication Stress and Epigenetic Modifications in Root Meristem Cell Nuclei of *Vicia faba*. *Cells* **2021**, *10*, 640–659, doi:10.3390/cells10030640.
153. Harpaz, S.; Glatman, L.; Drabkin, V.; Gelman, A. Effects of Herbal Essential Oils Used to Extend the Shelf Life of Freshwater-Reared Asian Sea Bass Fish (*Lates calcarifer*). *J. Food Prot.* **2003**, *66*, 410–417, doi:10.4315/0362-028X-66.3.410.
154. Soković, M.D.; Vukojević, J.; Marin, P.D.; Brkić, D.D.; Vajs, V.; Van Griensven, L.J.L.D. Chemical Composition of Essential Oilsof *Thymus* and *Mentha* Speciesand Their Antifungal Activities. *Molecules* **2009**, *14*, 238–249, doi:10.3390/molecules14010238.
155. Lorenzo, J.M.; Mousavi Khaneghah, A.; Gavahian, M.; Marszałek, K.; Eş, I.; Munekata, P.E.S.; Ferreira, I.C.F.R.; Barba, F.J. Understanding the Potential Benefits of Thyme and Its Derived Products for Food Industry and Consumer Health: From Extraction of Value-Added Compounds to the Evaluation of Bioaccessibility, Bioavailability, Anti-Inflammatory, and Antimicrobial Activities. *Crit. Rev. Food Sci. Nutr.* **2019**, *59*, 2879–2895, doi:10.1080/10408398.2018.1477730.
156. Martiniaková, S.; Ácsová, A.; Hojerová, J.; Krepsová, Z.; Kreps, F. Ceylon Cinnamon and Clove Essential Oils as Promising Free Radical Scavengers for Skin Care Products. *Acta Chim. Slovaca* **2022**, *15*, 1–11, doi:10.2478/acs-2022-0001.
157. Donsì, F.; Ferrari, G. Essential Oil Nanoemulsions as Antimicrobial Agents in Food. *J. Biotechnol.* **2016**, *233*, 106–120, doi:10.1016/j.jbiotec.2016.07.005.
158. Pavoni, L.; Perinelli, D.R.; Bonacucina, G.; Cespi, M.; Palmieri, G.F. An Overview of Micro- and Nanoemulsions as Vehicles for Essential Oils: Formulation, Preparation and Stability. *Nanomaterials* **2020**, *10*, 13, doi:10.3390/nano10010135.
159. Verdeguer, M.; Sánchez-Moreiras, A.M.; Araniti, F. Phytotoxic Effects and Mechanism of Action of Essential Oils and Terpenoids. *Plants* **2020**, *9*, 1571, doi:10.3390/plants9111571.
160. Grzanka, M.; Sobiech, L.; Stuper-Szablewska, K.; Danielewicz, J.; Skrzypczak, G. Effect of Selected Essential Oils on the Efficacy of Volunteer Oilseed Rape Control and Phytotoxicity in Maize Plants. *Chil. J. Agric. Res.* **2022**, *82*, 88–96, doi:10.4067/S0718-58392022000100088.

7. Dorobek naukowy

7.1. Spis publikacji niewchodzących w skład rozprawy doktorskiej

1. Żabka, A.; **Gocek-Szczurtek, N**.; Wróblewski, M.; Polit, J.T. Identification of Fibrillarin and Cajal Bodies under DNA Replication Stress Conditions in Root Meristem Cells of *Allium cepa*. *Int. J. Mol. Sci.* **2025**, *26*, 11321, doi:10.3390/ijms262311321.
2. Wróblewski, M.; **Gocek, N.**; Żabka, A.; Polit, J.T. Mitotic Disruption and Cytoskeletal Alterations Induced by *Acorus calamus* Essential Oil: Implications for Bioherbicidal Potential. *Int. J. Mol. Sci.* **2025**, *26*, 8933, doi:10.3390/ijms26188933.
3. Wróblewski, M.; Krajewski, K.; **Gocek, N**.; Żabka, A.; Polit, J.T. *Acorus calamus* L. Essential Oil Induces Oxidative Stress and DNA Replication Disruptions in Root Meristem Cells of Two Fabaceae and Two Brassicaceae Species. *Int. J. Mol. Sci.* **2025**, *26*, 4715, doi:10.3390/ijms26104715.
4. Wróblewski, M.; Piotrowska-Niczyporuk, A.; Ciereszko, I.; **Gocek, N**.; Żabka, A.; Szczeblewski, P.; Sobiech, Ł.; Saja-Garbarz, D.; Polit, J.T. Phytotoxicity and Bioherbicidal Potential of Sweet Flag (*Acorus calamus* L.) Essential Oil on Fabaceae and Brassicaceae Species. *Sci. Hortic*. **2025**, *347*, 114180, doi:10.1016/j.scienta.2025.114180.
5. Żabka, A.; **Gocek, N**.; Polit, J.T.; Maszewski, J. Oxidative Replication Stress Induced by Long-Term Exposure to Hydroxyurea in Root Meristem Cells of *Vicia faba*. *Plant Cell Rep.* **2024**, *43*, 87, doi:10.1007/s00299-024-03187-x.
6. Żabka, A.; **Gocek, N**.; Krajewski, K.; Szczeblewski, P.; Laskowski, T.; Polit, J. Changes in Epigenetic Patterns Related to DNA Replication in *Vicia faba* Root Meristem Cells under Cadmium-Induced Stress Conditions. *Cells* **2021**, *10*, 3409, doi:10.3390/cells10123409.

Sumaryczny współczynnik wpływu (*Impact Factor*, IF) publikacji niewchodzących w skład rozprawy doktorskiej: **34,8**

Łączna liczba punktów MNiSW dla publikacji niewchodzących w skład rozprawy doktorskiej: **940 pkt.**

Łączny dorobek publikacyjny:

- Sumaryczny współczynnik wpływu (IF): **52,3**
- Łączna liczba punktów MNiSW: **1460 pkt**.

7.2. Nagrody i wyróżnienia

- Nagroda za najlepszy plakat w sesji „*Ecology and Environmental Biology*”, International Doctoral Students' Conference in Life Sciences – BioOpen 2025
- Tytuł „Nauczyciel Roku” (Instytut Biologii Eksperymentalnej), rok akademicki 2023/2024
- Nagroda Rektora dla doktorantów za semestr zimowy 2023/2024, Uniwersytet Łódzki
- Nagroda Rektora dla doktorantów za semestr letni 2022/2023, Uniwersytet Łódzki
- List gratulacyjny JM Rektora, Uniwersytet Łódzki, 2021
- Stypendium Rektora dla najlepszych studentów, Uniwersytet Łódzki, 2017–2021

7.3. Doniesienia konferencyjne

7.3.1. Prezentacje plakatowe

- “Effect of thyme oil against oxidative stress, DNA damage and cell cycle disorders induced by cadmium in meristematic cells of *Vicia faba*”, poster prezentowany na International Doctoral Students' Conference in Life Sciences – BioOpen 2025, 15-16 maja 2025, Łódź.
- „Evaluation of the protective potential of thyme oil towards embryonic root merystem cells of *Vicia faba* var. *minor* exposed to cadmium toxicity”, poster prezentowany na X Międzynarodowym Sympozjum na temat rozwoju korzeni organizowanym przez Vlaams Instituut voor Biotechnologie (VIB), 15-18 maja 2023 r. Gandawa (Belgia).
- „The potential of plant secondary metabolites as sustainable pesticides: assessing the impact of emulsified sweet flag essential oil on root development of faba bean and rapeseed”, poster prezentowany na X Międzynarodowym Sympozjum na temat rozwoju korzeni organizowanym przez Vlaams Instituut voor Biotechnologie (VIB), 15-18 maja 2023 r., Gandawa (Belgia).
- „Ocena selektywnego działania olejku eterycznego z tataraku zwyczajnego na kiełkowanie bobowatych i kapustowatych”, poster prezentowany na Krajowa Konferencja Doktorantów BioOpen; 14 kwietnia 2023, Łódź.
- „Modyfikacje epigenetyczne towarzyszące stresowi oksydacyjno-replikacyjnemu generowanemu przez metale ciężkie w komórkach roślinnych oraz potencjał protekcyjny olejku tymiankowego”, poster prezentowany na Krajowej Konferencji Doktorantów BioOpen, 14 kwietnia 2023, Łódź.

7.4. Działalność naukowa

7.4.1. Granty badawcze i projekty

- Uzyskanie finansowania w ramach projektu PROM 2023 UŁ (NAWA) na udział w 10. Międzynarodowym Sympozjum na temat rozwoju korzeni, organizowanym przez Vlaams Instituut voor Biotechnologie (VIB) (15-18 maja 2023 r. w Gandawie – Belgia).
- Przygotowanie i złożenie wniosków projektowych w ramach konkursu IDUB (Inicjatywa Doskonałości – Uczelnia Badawcza), lata 2022 i 2024 (projekty nie uzyskały finansowania)

7.4.2. Szkolenia

- Szkolenie specjalistyczne „Western blot – technika, którą można zoptymalizować", organizowane przez Agrisera, 6 kwietnia 2022 r.
- Pięciodniowe szkolenie specjalistyczne z zakresu analizy mechanizmów antyoksydacyjnych w roślinach, Uniwersytet w Białymstoku, Wydział Biologii, Katedra Biologii i Ekologii Roślin, 10–14 lutego 2025 r.

7.5. Działalność organizacyjna

7.5.1. Działalność na rzecz Uniwersytetu Łódzkiego

- Pełnienie funkcji członka Komisji Dyscyplinarnej dla Doktorantów, kadencja 2021–2024
- Pełnienie funkcji członka Komitetu Organizacyjnego konferencji BioOpen 2023, Łódź, 2023.

7.5.2. Działalność na rzecz promocji nauki, Wydziału oraz Uniwersytetu

- Współorganizacja warsztatów w ramach akcji Uniwersytet Zawsze Otwarty w okresie 2023–2025 r. (współautorka programów zajęć oraz prowadząca warsztaty; udział w koordynacji wybranych działań dydaktycznych)
    - *Centrum dowodzenia komórki - jądro komórkowe i mitochondria*
    - *Skazani na siebie – organizmy, które stały się organellami*
    - *Księga szyfrów – materiał genetyczny*
    - *Tkanki roślinne – różnorodność i porozumienie podstawa sprawnego funkcjonowania organizmu*
    - *Atrybuty komórek roślinnych – ściana, wakuole i plastydy*
    - *Zaprojektuj swoją przygodę z mikroskopią fluorescencyjną*
- Współorganizacja warsztatów w ramach Instytutu Kreatywnej Biologii w okresie 2023–2025 r. (współautorka zajęć oraz prowadząca warsztaty; funkcja koordynatora Instytutu Kreatywnej Biologii w Katedrze Cytofizjologii w 2024 r.)

- *Różnorodność komórek roślinnych w obiektywie*
- *Tajemnice mikroświata komórek roślinnych*

- Współorganizacja wydziałowego charytatywnego kiermaszu roślin „Weź roślinkę, nakarm psinkę… i kotka też” w okresie 2022–2024 r.
- Współorganizacja wydarzenia „Fascynujący Dzień Roślin” (*Fascination of Plants Day*) w 2022 r.
  - *Wycieczka w makro- i mikroświat roślin – podróż z przewodnikiem*
- Współorganizacja Nocy Biologów w okresie 2021–2026 r. (aktywne współtworzenie i prowadzenie zajęć popularyzatorskich)
  - *Roślinne wiadomości: zobacz to, czego nie widać gołym okiem*
  - *Barwy Biosfery: komórkowy krajobraz roślin*
  - *Woda – życiodajny rozpuszczalnik dla barw przyrody - popłyńmy z nim poprzez komórki i tkanki roślin*
  - *Jak komórki roślin mogą zareagować na globalne zmiany środowiska*
  - *Naturalna mikroapteka podstawą piramidy zdrowego trybu życia*
- Współorganizacja II Dnia Otwartego Wydziału Chemii oraz Wydziału Biologii i Ochrony Środowiska, 5 kwietnia 2024 r.
- Współorganizacja III Dnia Otwartego Wydziału Chemii oraz Wydziału Biologii i Ochrony Środowiska, 14 marca 2025 r.
- Udział w spocie nakręconym we współpracy z KOLEO promującym wybór kolei jako ekologicznego środka transportu – data publikacji 13 maja 2024 r.
- Udział w wydarzeniu „Salon Maturzystów”, promującym ofertę edukacyjną Uniwersytetu Łódzkiego (16-17.09.2024).

8. Załączniki

1. Praca 1 (Załącznik nr 1)
2. Praca 2 (Załącznik nr 2)
3. Praca 3 (Załącznik nr 3)
4. Praca 4 (Załącznik nr 4)
5. Praca 5 (Załącznik nr 5)
6. Oświadczenia współautorów (Załącznik nr 6 A-J)

❖

Kopie prac wchodzących w skład rozprawy doktorskiej

❖

Praca 1 (Załącznik nr 1)

❖ **Gocek-Szczurtek, N.***; Żabka, A.; Wróblewski, M.; Kukula-Koch, W.; Szczeblewski, P.; Polit, J.T.
Thyme Oil Mitigates Cadmium-Induced Oxidative and Genotoxic Stress in *Vicia faba* Root Meristem Cells under *in vitro* Conditions.
Sci Rep **2025**, 15, 38689, doi:10.1038/s41598-025-22588-w.

* – autor korespondujący

- Współczynnik wpływu (IF): **3,9**
- Łączna liczba punktów MNiSW: **140 pkt**.

---

scientific reports

Check for updates

OPEN

Thyme oil mitigates cadmium-induced oxidative and genotoxic stress in *Vicia faba* root meristem cells under *in vitro* conditions

Natalia Gocek-Szczurtek[1]✉, Aneta Żabka[1], Mateusz Wróblewski[1], Wirginia Kukula-Koch[2], Paweł Szczeblewski[3] & Justyna Teresa Polit[1]

Cadmium is considered one of the most toxic and dangerous environmental agents among heavy metals. It induces oxidative stress state, which is a source of disruption to a wide range of key cellular processes in plants. The increasing problem of heavy metal accumulation in the environment necessitates the search for strategies that enhance plant resistance to the toxic effects of these elements. Therefore, the purpose of this study was to evaluate the protective potential of thyme oil (TO) against 175 µM cadmium chloride ($CdCl_2$)-induced toxicity in meristematic cells of *Vicia faba* var. *minor* primary roots under in vitro conditions. To assess the impact of TO, we analyzed reactive oxygen species (ROS) production, as cadmium-induced oxidative stress can trigger cellular damage. Hydrogen peroxide (H_2O_2) was detected using 3,3′-diaminobenzidine (DAB) staining, while superoxide anion ($O_2^{\bullet-}$) was visualized via Nitro Blue Tetrazolium (NBT) reduction. Since excessive ROS can lead to DNA damage, impair replication, and alter the proportion of interphase cells, we performed immunofluorescence labeling to examine replicating cells using a DNA synthesis marker (IdU). Additionally, we quantified disruptions in DNA replication and assessed the level of DNA damage using γ-phosphorylation of histone H2A.X at serine 139, a marker of DNA double-strand breaks (DSBs). Our results demonstrated that TO significantly mitigated cadmium-induced oxidative and genotoxic stress. Notably, TO treatment reduced the percentage of γ-H2A.X-positive cells by approximately 25% compared to cadmium-only treatment. Moreover, a 41,5% decrease in in the intensity of NBT staining (indicative of superoxide accumulation) and a 72,45% reduction in DAB staining intensity (reflecting hydrogen peroxide levels) were observed. These findings indicate that TO application may serve as a promising strategy for protecting plant tissues exposed to cadmium contamination in the future.

Keywords ROS, γ-H2A.X, Cell cycle, Replication, Cadmium, Essential oil

The rapid development of industry is a direct cause of the deterioration of soil functional qualities and the intensification of chemical pollution, particularly by trace elements that pose a serious threat to the natural environment. Industrial pollutant emissions, both in the form of dry and wet atmospheric precipitation, along with the irrational use of fertilizers and plant protection products, exacerbate the problem of heavy metals contamination in the environment[1]. Additionally, soil acidification caused by sulfur and nitrogen deposition increases heavy metals availability to crops[2]. The primary consequence of heavy metal accumulation in crop tissues is a reduction in their nutritional value. Among these chemical elements, cadmium (Cd) is particularly dangerous due to its geochemical properties. It exhibits high mobility in soils and is readily absorbed by plants through the root system and leaves, with uptake directly proportional to its environmental concentration[3].

The consequence of heavy metal toxicity is the initiation of oxidative and replicative stress in the plant organism[4]. Oxidative stress results from the excessive production and accumulation of molecules known as "reactive oxygen species" (ROS). The primary causes of this type of stress include an imbalance between ROS production and detoxification, which results from disruption in optimal cellular physiology, as well as the *de*

[1]Department of Cytophysiology, Faculty of Biology and Environmental Protection, University of Lodz, Lodz 90-236, Poland. [2]Department of Pharmacognosy with Garden of Medicinal Plants, Medical University of Lublin, 1 Chodzki Str., Lublin 20-093, Poland. [3]Department of Pharmaceutical Technology and Biochemistry and BioTechMed Centre, Faculty of Chemistry, Gdansk University of Technology, Gabriela Narutowicza Str. 11/12, Gdansk 80-233, Poland. ✉email: natalia.gocek.szczurtek@biol.uni.lodz.pl

novo biosynthesis of ROS, which plays a crucial role in stress signaling and response mechanisms necessary for defense and adaptation of the organism[5]. Excessive ROS levels shift the balance toward oxidation reactions harmful to cells, leading to damage to proteins, lipids and DNA[6]. Uncontrolled oxidative stress in the cell results in lipid peroxidation, depolarization and damage to cell membrane integrity, as well as the failure of organelles (such as mitochondria and plastids), ion leakage, and disruption of the structure and function of the genetic apparatus[4,6,7].

For the proper proliferation of plant cells, in addition to the efficient functioning of cytoplasmic structures, organelles, and the processes occurring within them, the preservation of an intact genetic material and the maintenance of uninterrupted DNA biosynthesis during the S phase of the cell cycle—dependent on the proper operation of replication forks—are also essential. These factors ensure the integrity of chromatin in the resulting daughter cells. Overaccumulation of ROS disrupts chromatin structure, leading to replication stress[8], as ROS can react directly with nitrogenous bases and deoxyribose, triggering oxidative modifications. These chemical changes can weaken DNA structure, leading to single- or double-strand breaks (SSB/DSB)[9]. DSBs are considered among the most dangerous types of DNA damage, as their formation activates numerous factors, including phosphorylation of the histone H2A.X variant at serine 139 (Ser139 γH2A.X)[10]. This histone variant, like other histones, plays a role in stabilizing genetic material[11]. In higher eukaryotes, γH2A.X is also the main component of the DNA damage detection and repair system. Its phosphorylation at serine 139 serves as an early signal for detecting double-stranded breaks and is a crucial step in initiating DNA repair[10,12]. Furthermore, γH2A.X foci are believed to facilitate the recruitment of repair proteins to the site of DNA damage by specifically attracting them[13,14]. In addition to its key role in repair protein recruitment, γH2A.X also participates in the activation of checkpoint proteins[15], which arrest cell cycle progression in response to stress factors. Insufficient checkpoint control in threat detection during S phase leads to abnormalities in the progression of the cell cycle. In plants, the proper sequence of successive cell cycle phases is also monitored by the Principal Control Points, PCP1 in the G1 phase and PCP2 in the G2 phase[16,17]. Under stress conditions, including those induced by exposure to heavy metals, cells may become arrested at these checkpoints, thereby limiting both replicative and mitotic activity[8,16,17].

Compounds derived from plant secondary metabolism, particularly fragrant essential oils, may prove to be a promising solution for protecting plants from the harmful effects of heavy metals in the future. A distinctive feature of essential oils is their highly diverse chemical composition, as they consist of mixtures containing up to several hundred volatile compounds, including alcohols, aldehydes, ketones, esters, amines, amides, phenols, terpenes and phenylpropane derivatives[18]. In addition to their activity against pathogenic microorganisms, essential oils also possess antioxidant properties enabling them to act as effective bioprotectors of animal tissues against toxic heavy metals, including, among others, Cd[19,20]. In animal organisms, Cd induces irreversible kidney tubular dysfunction and acute renal failure. This damage is caused by severe oxidative stress resulting from the disruption of the natural antioxidant defense system. Essential oil derived from *Thymus serrulatus* (TO) significantly attenuates Cd-induced nephrotoxicity due to its synergistic antioxidant, anti-inflammatory and antiapoptotic effects[19]. However, the available literature provides only limited information regarding the mechanisms of plant tissue protection, and comparable analyses in this area remain scarce. Our research, conducted in response to the growing needs of sustainable agriculture and changing regulations on plant protection products in the EU, aims to lay the foundations for the development of application solutions that may be crucial for maintaining high crop productivity, ensuring the highest quality crops, preserving wild species, preventing the irreversible loss of endangered species in their natural habitats, and using plants for efficient phytoremediation technology. In light of the limitations of conventional agricultural methods, testing natural bioprotectors, such as essential oils, is not only justified but becomes absolutely necessary. Increasing the contribution of plant protection products based on essential oils in agricultural practice may bring a variety of positive consequences: these compounds are characterized by low persistence in the natural environment, which reduces the risk of pollution, and at the same time they exhibit significantly lower toxicity to non-target organisms, such as mammals or aquatic organisms[21]. Therefore, the aim of this study was to evaluate the protective potential of TO against cadmium-induced damage in the meristematic cells of primary roots of *Vicia faba* var. *minor*.

The species *Vicia faba* var. *minor*, characterized by a distinct interphase chromatin and mitotic chromosome structure, was selected as a model for cytological studies. The aim of this study was to evaluate the protective potential of thyme oil against cadmium chloride ($CdCl_2$)-induced damage in the meristematic cells of primary roots. For this purpose, *V. faba* seedlings were incubated for 24 h in $CdCl_2$ (at a concentration of 175 µm), thyme oil (TO; at a concentration of 0.03%) in emulsified form, and in a combination of $CdCl_2$ and TO. The concentration of TO was selected based on preliminary studies. The $CdCl_2$ concentration (175 µM) applied in our study was determined from our previous research[22,23], in which a concentration of 150 µM was used. These studies demonstrated the effect of cadmium on cell cycle progression and revealed diverse changes in epigenetic modifications in meristematic cells. To accentuate the stress response, making it more pronounced and thus more easily detectable, and at the same time to evaluate the potential protective effect of thyme oil, we applied a slightly higher concentration (175 µM).

Seedlings incubated for 24 h in water and in the emulsifier solution used for TO emulsification served as control material. The plants were examined for: (1) production of ROS: hydrogen peroxide (H_2O_2) and superoxide anion ($O_2^{\bullet-}$) which were selected for analysis based on their key roles in oxidative stress and cell signaling, continuity with our previous studies using similar markers, and the availability of reliable histochemical methods enabling precise cellular localization, (2) percentage of interphase cells (G1, S and G2 phase), (3) immunofluorescence labeling of replicating cells, and (4) level of DSBs.

Materials and methods

Thyme oil composition by GC-MS

Commercially available thyme oil (TO; Etja, Poland) was used for the analyses.

Prior to the compositional studies on the gas chromatograph coupled with a mass spectrometer, the oil was diluted with dichloromethane in a ratio of 1 part of the oil in 100 parts of dichloromethane. The solution was injected on a Shimadzu GC-2010 Plus chromatograph (Kyoto, Japan) coupled with a mass spectrometer QP 2010 Ultra. The following method of the gas chromatograph was followed: initial oven temperature of 50˚C, holding time duration of 2 min, increment of temperature of 5˚C per minute up to 250˚C followed by a 15-minute-long hold. The injection temperature was set as 280˚C, the injection volume at 1 µL, the helium flow rate at 1 mL/min and the column was ZB-5MS with silica film of 0.25 mm thickness (Phenomenex, Torrance, CA, USA). Split injection mode of 1:20 was applied for the injections. The mass spectrometer was operated in an EI mode at 70 eV ionization energy, with ion trap temperature of 220˚C, the injection and interface temperature of 250˚C with the scan rate of 0.2 s per scan, within the range of 40–500 amu. The identification of metabolites was based on the spectral library (NIST 2011 and Mass Finder 2.1) and the literature data. The retention indices were calculated based on the co-injected of the homologous n-alkanes mixture (C6-C30) in the same conditions.

Plant material and seedlings culture

Seeds of cultivated field bean (*Vicia faba* L. var. *minor*) (W. Legutko The Seed Breeding Company in Jutrosin) were sown on moist blotting paper and germinated in the dark at 20 ± 21 °C. Four-day-old seedlings with primary roots 2–3 cm in length were used in the study. The seedlings selected by size were divided into experimental series: 1- control, incubated in water, 2- control, incubated in emulsifier solution used to emulsify the essential oil. 3- test, incubated in cadmium chloride ($CdCl_2$) solution at concentration of 175 µm, 4- test, incubated in emulsified thyme oil (TO; Etja, Poland) solution at a concentration of 0.03% and 5- test, incubated in cadmium chloride solution supplemented with emulsified form of TO (Table 1). The concentration of cadmium chloride was chosen based on literature data and preliminary studies conducted. The concentration of commercially available thyme oil was selected based on preliminary studies. In order to properly distribute TO in water, it was emulsified in a combination of C14-18 and unsaturated C16-18 - mono- and di-ethoxylated glycerides and ethoxylated *Brassica napus* oil. The above-mentioned emulsifier was mixed with TO in a ratio of 1:4 (v/v) and vigorously shaken with a vortex for 15 min. The emulsifier was provided by the Department of Agronomy of the University of Life Sciences in Poznań. Plants from each experimental series were grown in tightly sealed tall (3 cm) 25 cm diameter Petri dishes. In each dish, 10 plants were incubated for 24 h. The experiments were conducted in 3 repeats. Primary root meristems were used for analysis.

Detection of H_2O_2 using DAB

Hydrogen peroxide (H_2O_2) production was detected using 3,3-diaminobenzidine tetrachloride (DAB-HCl; Sigma-Aldrich, Poznań, Poland) according to the methodology of[24], with minor modifications. Seedlings were incubated for 3 h in 1 mg mL-1 DAB-HCl in TRIS buffer (10 mM Tris, 10 mM EDTA-2Na, 100 mM NaCl; pH 7.5) dissolved in water. The histochemical reaction was halted with distilled water. After staining, roots were fixed for 20 min in 4% paraformaldehyde dissolved in phosphate-buffered saline (PBS), washed three times with PBS and macerated for 15 min with 2.5% citric acid-buffered pectinase solution (pH 5.0; 37 °C). Root apical meristems were crushed on slides and then kept in a mixture of glycerol and PBS (9:1; v/v). The presence of H_2O_2 was visualized as brown aggregates of polymerized DAB on a Nikon Eclipse E- 600 microscope. The color images were grayscale converted and expressed in arbitrary units (a.u.) as a mean pixel value (p.v.), covering the range from 0 (dark) to 255 (white). The total number of cells analyzed was about 100.

Detection of $O_2^{\bullet-}$ using the NBT staining method

Superoxide anion radical ($O_2^{\bullet-}$) was visualized by reducing nitro blue tetrazolium (NBT; Sigma-Aldrich) to highly insoluble, colored formazan precipitates[25]. Extracellular $O_2^{\bullet-}$ production was analyzed using the NBT staining technique, as earlier described by[26]. Seedlings were immersed for 10 min in a solution of 3 mM NBT (Sigma-Aldrich) in 10 mM Tris-HCl buffer (pH 7.4) at 20 °C. The procedure's remaining steps were similar to those for the DAB assay.

Experimental group	Treatment description	$CdCl_2$ concentration	Thyme Oil (TO) concentration	Emulsifier	Incubation time
Control	Water	—	—	—	24 h
Emulsifier	Emulsifier (without TO or Cd)	—	—	Present (same volume as in TO-treated groups)	24 h
TO	Emulsified thyme oil	—	0.03% (v/v)	Present in 4:1 ratio (emulsifier: TO, v/v)	24 h
$CdCl_2$	Cadmium chloride	175 µM	—	—	24 h
$CdCl_2$ + TO	Cadmium chloride + emulsified thyme oil	175 µM	0.03% (v/v)	Present in 4:1 ratio (emulsifier: TO, v/v)	24 h

Table 1. Summary of applied treatments: chemical concentrations and incubation periods.

Feulgen staining and cytophotometry

Apical parts of *V. faba* primary roots from seedlings were fixed for 1 h in a mixture of cold absolute ethanol and glacial acetic acid (3:1, v/v), then washed several times with ethanol, rehydrated, hydrolyzed for 1 h in 4 M HCl and stained with Schiff's reagent (pararosaniline; Sigma- Aldrich) following standard methods[27].

After rinsing in SO_2-water, apical segments of 1.5 mm were sectioned off, rinsed with distilled water, placed in a drop of 45% acetic acid and crushed on microscope slides. After freezing with dry ice, the coverslips were removed, and the dehydrated slides were embedded in Canada balsam before analysis. Nuclear DNA content was assessed by means of cytophotometry (computer-assisted Cytophotometer v1.2, Forel, Lodz, Poland). The extinction of cell nuclei stained with Feulgen was measured at 565 nm and calibrated in arbitrary units (a.u.), with reference values of 2 C and 4 C recorded from cells in mid telophase and prophase, respectively. About 10,000 cells collected from 10 roots were analyzed in each experimental series.

Identification of replicating nuclei using IdU (5-iodo-2′-deoxyuridine)

V. faba seedlings were pulsed for 30 min with a 30 µM solution of 5-iodo-2'-deoxyuridine (IdU) at 20 °C in the dark. Excised meristems of 1.5 mm length were then rinsed with distilled water and fixed for 10 min in freshly prepared 4% paraformaldehyde at 4 °C. After fixation, the root tips were thoroughly washed for 10 min with ice-cold Tris buffer [10 mM Tris (hydroxy-methyl)-aminomethane, 10 mM EDTA-2Na, 100 mM NaCI, pH 7.2]. The excised root tips were then squeezed in a drop of Triss buffer between two microscope slides to collect nuclear samples (according to Żabka et al., 2021), which were dropped onto Super Frost Plus slides (Menzel-Gläser) and air-dried. The slides were then treated for 1.5 h in 1.5 M HCl at 25 °C for partial denaturation of nuclear DNA. After washing with Tris buffer containing 0.5% Triton X-100, blocking buffer (8% BSA, 0.1% Triton-X100 in Tris buffer) was added. Following a 50-minute incubation at 20 °C slides were washed with Tris buffer containing 0.5% Triton X-100, mouse anti-IdU monoclonal antibodies (Sigma-Aldrich) diluted in Tris buffer containing 0.5% Triton X-100 and 1% BSA (1:100) were added. After overnight incubation in a humidified atmosphere at 4 °C, slides were washed in Tris buffer (10 min, three times) and incubated for 1.5 h with Alexa Fluor®488-conjugated anti-rabbit IgG antibodies diluted in Tris buffer (1:200) (25 °C; wet dark chamber) and washed twice (10 min each) in Tris buffer. Slides were embedded in PBS/glycerol mixture (9:1) containing 2.5% 1,4-diazabicyclo[2.2.2]octane (DABCO). Observations and analyses of IdU-treated cells were made using Nikon Eclipse E600W fluorescence microscope equipped with U2 filter (UVB light; λ = 340–380 nm) for DAPI and B2 filter (blue light; λ = 465–496 nm) for Alexa Fluor® 488. All images were recorded at the same time of integration using a DS-Fil CCD camera (Nikon). Quantitative analyses of fluorescence intensity were made after converting color images into greyscale and expressed in arbitrary units as mean pixel value (p.v.) spanning the range from 0 (dark) to 255 (white).

Immunocytochemical detection of γ-phosphorylated H2A.X histones

Root meristems from *V. faba* seedlings were fixed for 10 min in 4% paraformaldehyde buffered PBS (Phosphate-Buffered Saline) at 4 °C; cell nuclei were then isolated, dropped onto glass slides and air-dried (procedure according to Żabka et al.[22]). After thorough rinsing with PBS, the apical parts of the roots were crushed on Super Frost Plus slides, dried and pretreated for 50 min with blocking buffer containing 5% BSA and 0.3% Triton X-100 (Sigma-Aldrich, Poznań, Poland) diluted in PBS in a wet chamber at 20 °C.

The slides were then incubated with a rabbit polyclonal antibody raised against human **γ**-H2A.X histones (anti-**γ**-H2A.X antibody; Sigma- Aldrich) at a dilution of 1:750 in PBS containing 1% BSA and 0.3% Triton X-100.

Incubations were conducted in a humidified atmosphere at 4 °C for 16 h. After rinsing with PBS, the slides were incubated for 1.5 h with Alexa Fluor®488-conjugated goat anti-rabbit secondary antibodies (1:500; Cell Signaling, Warsaw, Poland) at 20 °C. Slides were stained with DAPI, then washed with PBS, air-dried and embedded in a PBS/glycerol mixture (9:1) containing 2.5% 1,4-diazabicyclo[2.2.2]octane (DABCO). Observations and analyses of anti-histone H2A.X treated cells were made using Nikon Eclipse E600W fluorescence microscope equipped with U2 filter (UVB light; λ = 340–380 nm) for DAPI and B2 filter (blue light; λ = 465–496 nm) for Alexa Fluor® 488. All images were recorded at the same time of integration using a DS-Fil CCD camera (Nikon).

Statistical analysis

Data analysis was performed with GraphPad Prism software version 10 (GraphPad Software, Boston, MA, USA). Group distinctions were assessed through One-Way ANOVA, followed by Tukey's post-hoc test. Statistical significance was denoted by asterisks (****$p < 0.0001$, ***$p < 0.001$, **$p < 0.01$, *$p < 0.05$) and was defined as $p < 0.05$.

Results

GC-MS profiling of thyme oil

The implementation of the proposed method for analyzing thyme oil resulted in the identification of 21 clearly separated metabolites—components from the groups of monoterpenes, sesquiterpenes, oxygenated terpenes, alcohols, and phenols. The fingerprint of the analyzed oil is shown in Fig. 1, and Table 1 lists all metabolites along with their percentage content in the oil. Throughout the study, the retention indexes of each identified compound were determined. All compounds listed in Table 2 accounted for approximately 89% of the total composition. The most abundant substances in the extracts were thymol (28.39%), *p*-cymene (23.86%), followed by linalool (8.49%), caryophyllene (4.04%), limonene (3.15%), carvacrol (3.04%), *α*-pinene (2.91%), *γ*-terpinene (2.55%), *α*-terpineol (2.36%), eucalyptol (1.92%), *β*-pinene (1.89%), and 3-octanol (1.73%). The remaining metabolites

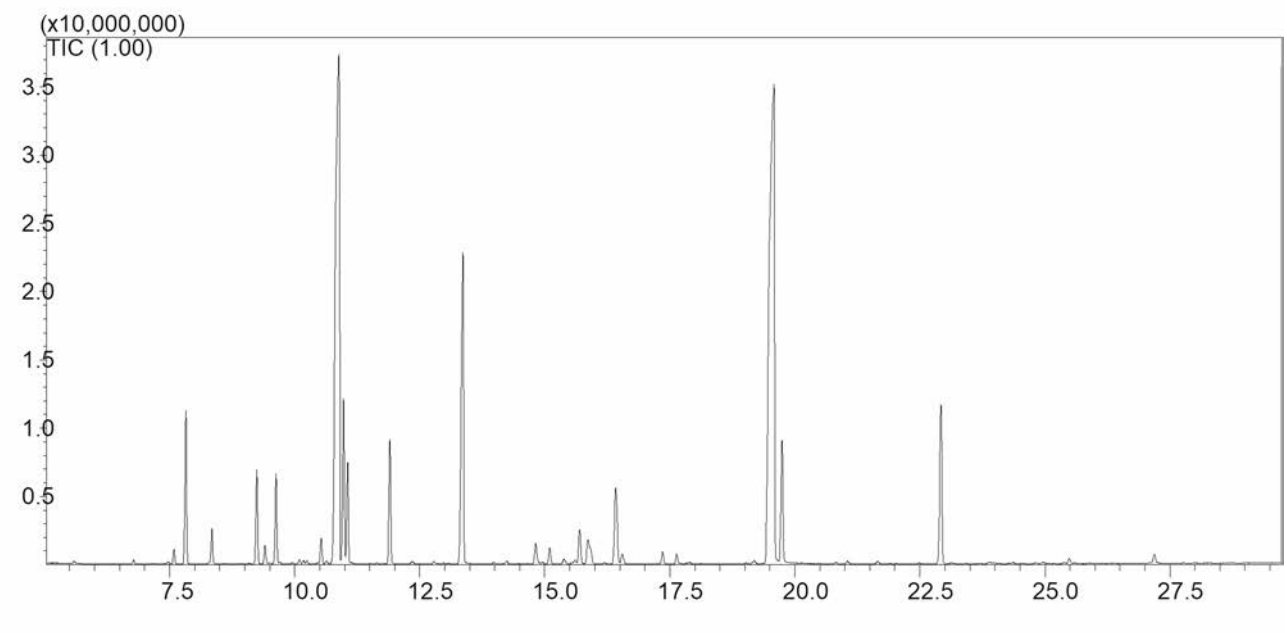

Fig. 1. The total ion chromatogram of the thyme oil (TO) sample.

Compound	Retention time [min]	Retention index	Percentage content
α-Pinene	7.8	935	2.91
Camphene	8.3	956	0.69
β-Pinene	9.24	979	1.89
β-Myrcene	9.4	993	0.39
3-Octanol	9.62	1002	1.73
α-Terpinene	10.5	1013	0.54
p-cymene	10.8	1019	23.86
Limonene	10.98	1032	3.15
Eucalyptol	11.06	1035	1.92
γ-Terpinene	11.9	1054	2.55
Linalool	13.36	1103	8.49
2-Bornanone	14.8	1131	0.56
Menthone	15.097	1149	0.38
Borneol	15.7	1171	0.87
Menthol	15.8	1186	1.06
α-Terpineol	16.4	1201	2.36
γ-Terpineol	16.5	1209	0.31
Isothymol	17.6	1250	0.26
Thymol	19.5	1370	28.39
Carvacrol	19.7	1394	3.04
Caryophyllene	22.9	1658	4.04
		Total percentage content:	**89.39**

Table 2. The volatile composition of thyme oil (TO).

occurred in amounts of 1% or less. These results are consistent with previously published literature data on the composition of thyme essential oil[28,29].

Hydrogen peroxide (H_2O_2) and superoxide anion radical ($O_2^{\bullet-}$) production

In the root meristem cells of *V. faba*, oxidative stress levels were assessed by detecting hydrogen peroxide (H_2O_2) and superoxide anion radical ($O_2^{\bullet-}$) using microcolorimetric analysis (Figs. 2 and 3).

The presence of H_2O_2 was detected using diaminobenzidine (DAB) polymerization, which, in the presence of enzymatic or non-enzymatic oxidizing agents, leads to the formation of insoluble brown-colored precipitates.

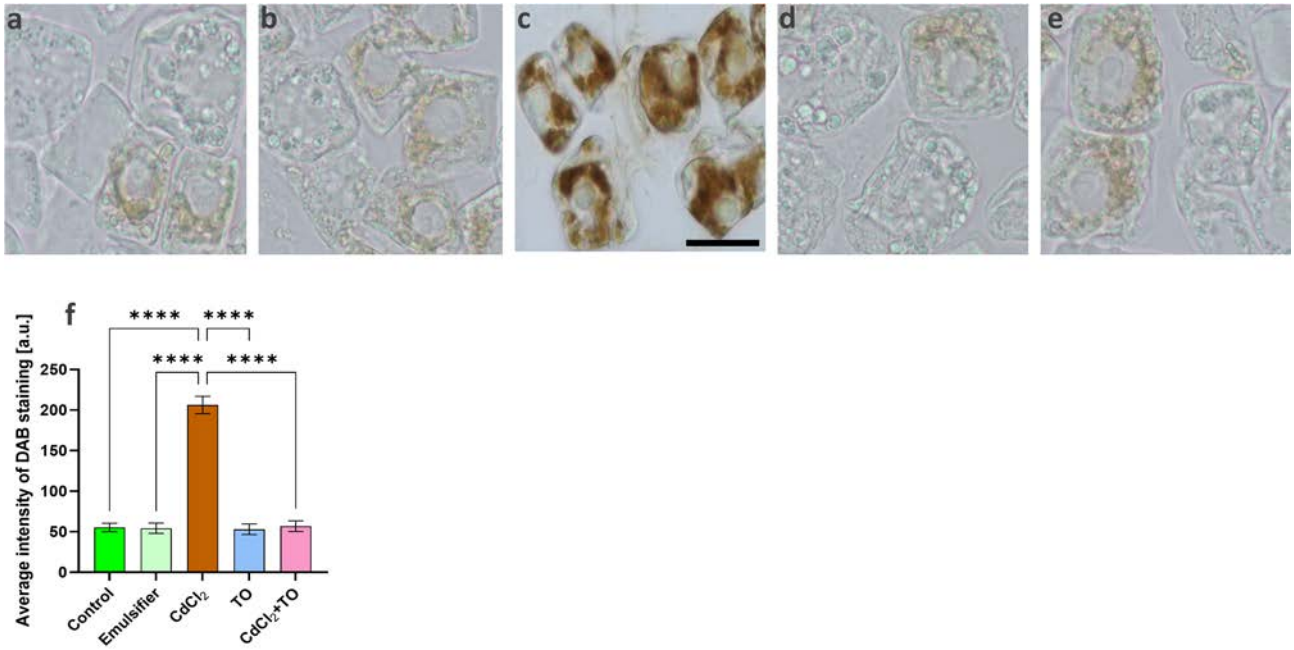

Fig. 2. Localization of H_2O_2 in *V. faba* control meristems (**a**) and after 24-hour incubation of root meristems with the emulfisier (**b**), $CdCl_2$ (**c**), TO (**d**), and a combination of $CdCl_2$ and TO (**e**). Scale bar = 20 µm. (**f**) The microcolorimetric analysis of DAB staining intensity, (arbitrary units [a.u.] ± SD for three biological replicates). ****$p < 0.0001$, (One-Way ANOVA with Tukey's test for multiple comparisons).

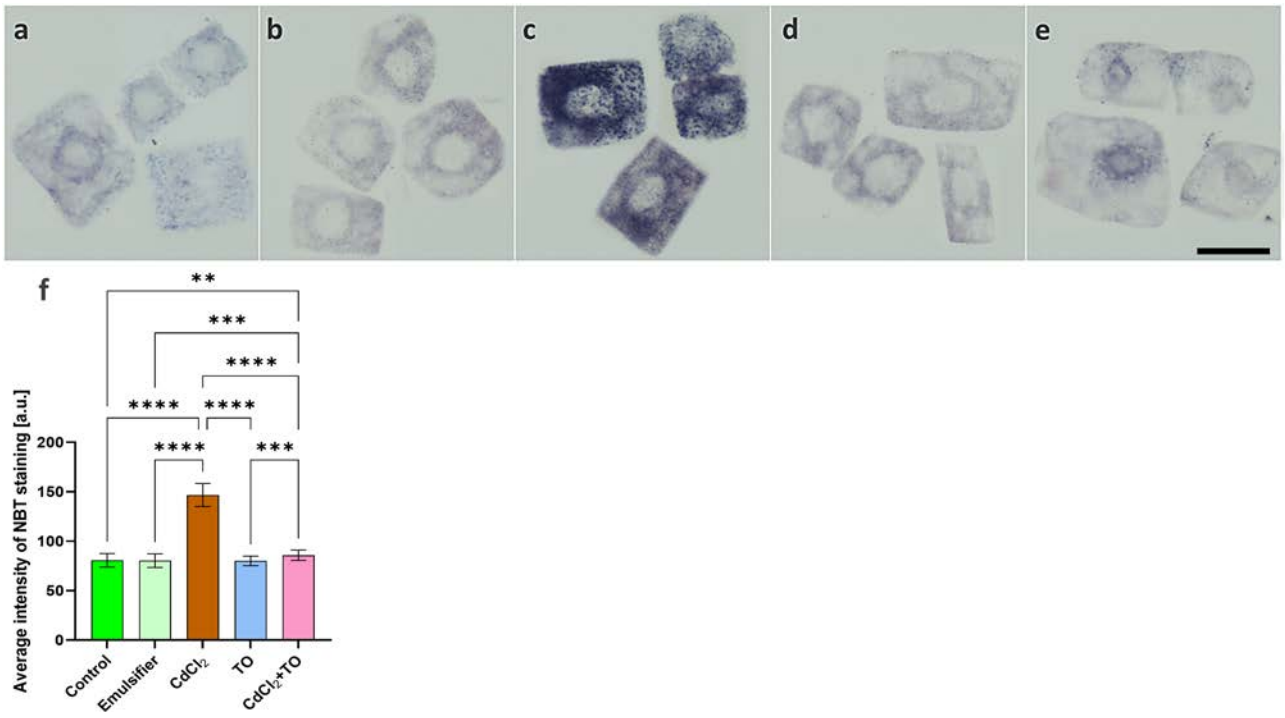

Fig. 3. Localization of $O_2^{\bullet-}$ detected by NBT staining in root meristem cells of *V. faba*. Control (**a**), emulsifier treatment (**b**), dark blue insoluble formazan deposits observed after $CdCl_2$ treatment (**c**), TO treatment (**d**), and combined $CdCl_2$ and TO treatment (**e**). Scale bar = 20 µm. (**f**) The microcolorimetric analysis of NBT staining intensity, (arbitrary units [a.u.] ± SD for three biological replicates). ****$p < 0.0001$, ***$p < 0.001$, **$p < 0.01$, (One-Way ANOVA with Tukey's test for multiple comparisons).

The intensity of these precipitates is proportional to the local concentration of H_2O_2 (Fig. 2f). Compared to the control (Fig. 2a) and emulsifier-treated plants (Fig. 2b), $CdCl_2$-treated cells exhibited characteristic brownish deposits dispersed in the cytoplasm (Fig. 2c). In seedlings treated with TO alone, hydrogen peroxide levels remained similar to those in the control (Fig. 2d). However, when seedlings were incubated with a combination of TO and $CdCl_2$ (Fig. 2e), a significantly lower intracellular H_2O_2 content was observed in meristem cells compared to those treated with $CdCl_2$ alone (Fig. 2c).

The level of the second type of the ROS analyzed, superoxide anion radical ($O_2^{\bullet-}$), was assessed using nitro blue tetrazolium (NBT) reduction (Fig. 3f). The characteristic blue-violet formazan staining, indicative of $O_2^{\bullet-}$ presence, appeared in control cells (Fig. 3a), as well as in cells treated with the emulsifier (Fig. 3b), TO (Fig. 3d), and the combination of $CdCl_2$ and TO (Fig. 3e). However, $CdCl_2$-treated root apical meristem (RAM) cells (Fig. 3c) exhibited a markedly higher accumulation of formazan deposits, with the most intense NBT staining observed in this group.

Distribution pattern of nuclear DNA content in root meristem cells

Cytophotometric measurements of nuclear DNA content in control plants revealed the highest percentage of cells in the S phase (2–4 C), while lower but approximately equal percentages of cells were observed in the G1 and G2 phases. A similar distribution of cells across interphase stages, comparable to that in water-incubated plants (Fig. 4a), was also observed in seedlings treated with the emulsifier (Fig. 4b) and the emulsified form of TO (Fig. 4d). Following $CdCl_2$ treatment, a reduction in the number of replicating cells was observed, as indicated by a deepened valley between the peaks characteristic of the G1 and G2 phases in the histogram. Meanwhile, the number of cells in G1 and G2 phases increased, compared to the control (compare Fig. 4c and a). The combined application of $CdCl_2$ and TO led to a slight decrease in the number of replicating cells and an increase in the number of cells in the G2 phase, while the proportion of cells in the G1 phase remained similar to the control (Fig. 4e).

Incorporation of IdU (5-iodo-2′-deoxyuridine) into nuclear DNA

Fluorescence-based evaluation of replication activity using the DNA synthesis marker IdU (5-iodo-2'-deoxyuridine) allowed us to assess the effects of the tested factors on genetic material duplication. Differences in 1. nuclear size, 2. luminescence intensity and 3. fluorescence foci distribution enabled us to determine the status of the DNA biosynthesis process (Fig. 5d). The proportion of early-, mid-, and late-S-phase cells was assessed based on the fluorescence staining pattern of cell nuclei: weak (granular, characteristic of early euchromatin replication; Fig. 5a), strong (granular, almost homogeneous indicative of mid-stage of euchromatin replication; Fig. 5b) and clustered (specific for late-replicated heterochromatin; Fig. 5c). Labeling index analyses confirmed a significant decrease in the number of all replicating cells following $CdCl_2$ treatment compared to control cells and those treated with the emulsifier or the emulsified form of TO. A slight reduction in replicating cells was also observed in meristems incubated in a medium containing both $CdCl_2$ and TO (Fig. 5e). Furthermore, an analysis of the percentage of early- (Fig. 5a'), mid- (Fig. 5b'), and late-S-phase cell nuclei (Fig. 5c') revealed that $CdCl_2$ exposure led to an accumulation of cells in the early replication stages - an effect not observed when the $CdCl_2$-containing medium was supplemented with TO (Fig. 5a').

Fluorescence intensity, which reflects the level of replicative activity in cell nuclei, varied depending on the experimental conditions (Fig. 6d). In the control groups, i.e., seedlings incubated in water (Fig. 6a) and those treated with the emulsifier, fluorescence intensity remained similar. However, exposure of the plants to $CdCl_2$ resulted in a significant decrease compared to the control groups (Fig. 6b). Analysis of the labeling intensity in replicating cells revealed an increase in fluorescence in seedlings treated only with the emulsified form of TO, while a slight decrease was observed after simultaneous treatment of seedlings with TO and $CdCl_2$ compared to the control groups (Fig. 6c).

Immunocytochemical detection of γ-phosphorylated H2A.X

The level of histone H2A.X phosphorylation in *V. faba* cells was analyzed using an immunocytochemical detection method. Immunofluorescent labeling appeared as small foci, scattered throughout the nuclear chromatin area (Fig. 7a-c). Comparable low labeling index values were observed in the control group (Figs. 7a, a' and d) and in roots incubated with the emulsifier or the emulsified form of TO (Fig. 7d). In contrast, exposure to $CdCl_2$ caused a significant increase in histone H2A.X phosphorylation, reaching 28.78%, compared to 1.55% in the control (Figs. 7b, b' and d). Interestingly, simultaneous application of TO and $CdCl_2$ (Figs. 7c, c' and d) resulted in a noticeable reduction in phosphorylation levels, with a labeling index of 3.73%, compared to roots treated with $CdCl_2$ alone.

Disscusion

Optimal environmental conditions, such as the availability of water, mineral salts, and nutrients, enable organisms to function efficiently. The absence or excess of any essential elements, as well as the presence of harmful substances, induces stress conditions. The complex machinery that governs the life and functioning of plant cells is not immune to external factors that can significantly disrupt its processes. Among these factors are heavy metals[30], including cadmium (Cd), which is ranked among the most toxic. Cadmium ions (Cd^{2+}) are readily absorbed by plant roots and transported throughout the organism, where they inhibit growth, cause chlorosis, alter chloroplast ultrastructure, and impair photosynthesis[4]. One of the consequences of heavy metal toxicity is the excessive production of reactive oxygen species (ROS), leading to oxidative stress. Thyme oil (TO), extracted from *Thymus vulgaris*, is rich in antioxidant compounds such as thymol, carvacrol, p-cymene and γ-terpinene which is in accordance to this study. These compounds may contribute to both scavenging free

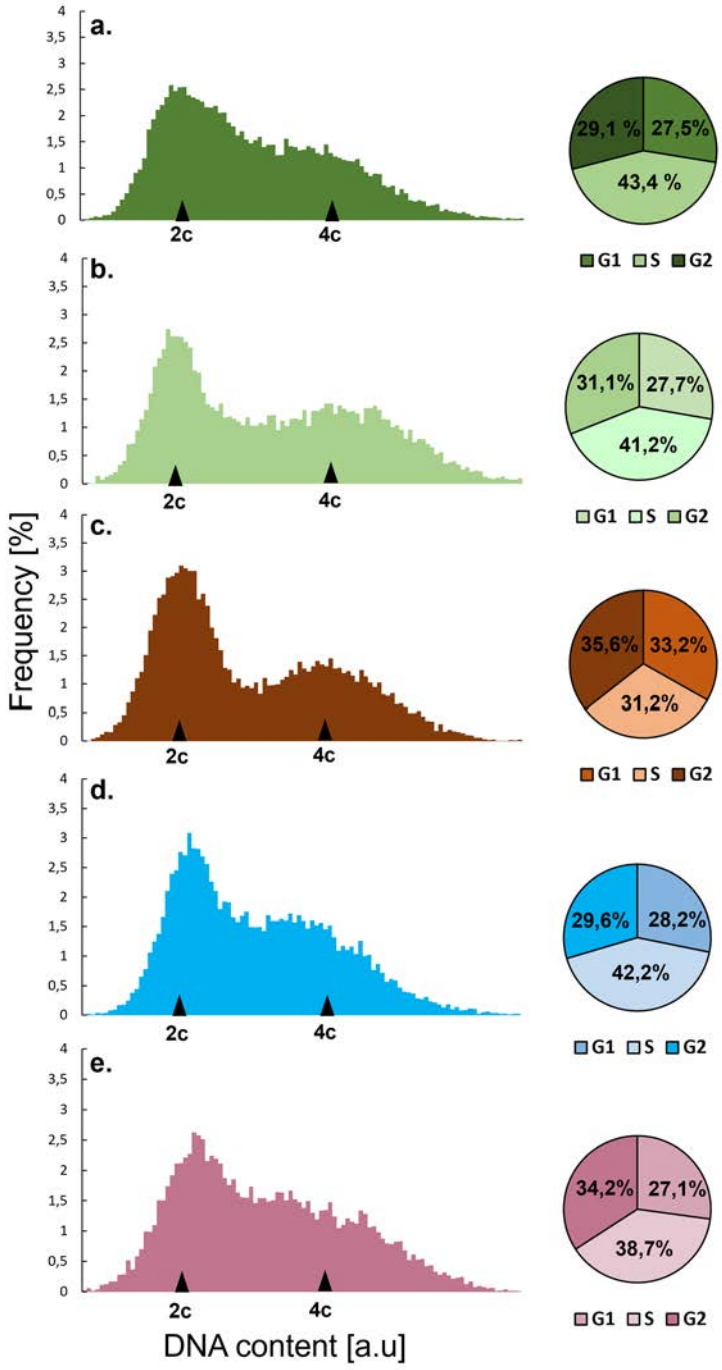

Fig. 4. Histograms of frequency distribution of nuclear DNA content (arbitrary units, [a.u.]) in *V. faba* control meristems (**a**) and after 24-hour incubation of root meristems with the emulfisier (**b**), $CdCl_2$ (**c**), TO (**d**) and the combination of $CdCl_2$ and TO (**e**). Each population consisted of more than 5,000 cell nuclei.The pie charts on the right side of each histogram represent the show estimated frequencies (%) of G1, S, and G2 phase cells in the respective experimental series.

radicals - thereby regulating intracellular ROS levels - and inducing protective mechanisms, such as enhancing antioxidant pathways[31].

The main component of the analyzed complex of secondary metabolites in thyme oil was thymol. Previous studies[31] demonstrate its significant role in inhibiting oxidation in vitro and in cell models. Thymol increased the levels of antioxidant enzymes in cells, boosting enzyme activity. This action led to higher levels of superoxide dismutase (SOD), glutathione peroxidase (GPx), glutathione-S-transferase (GST), and catalase (CAT). Additionally, non-enzymatic reactions were observed as part of its mechanisms, such as increased production of

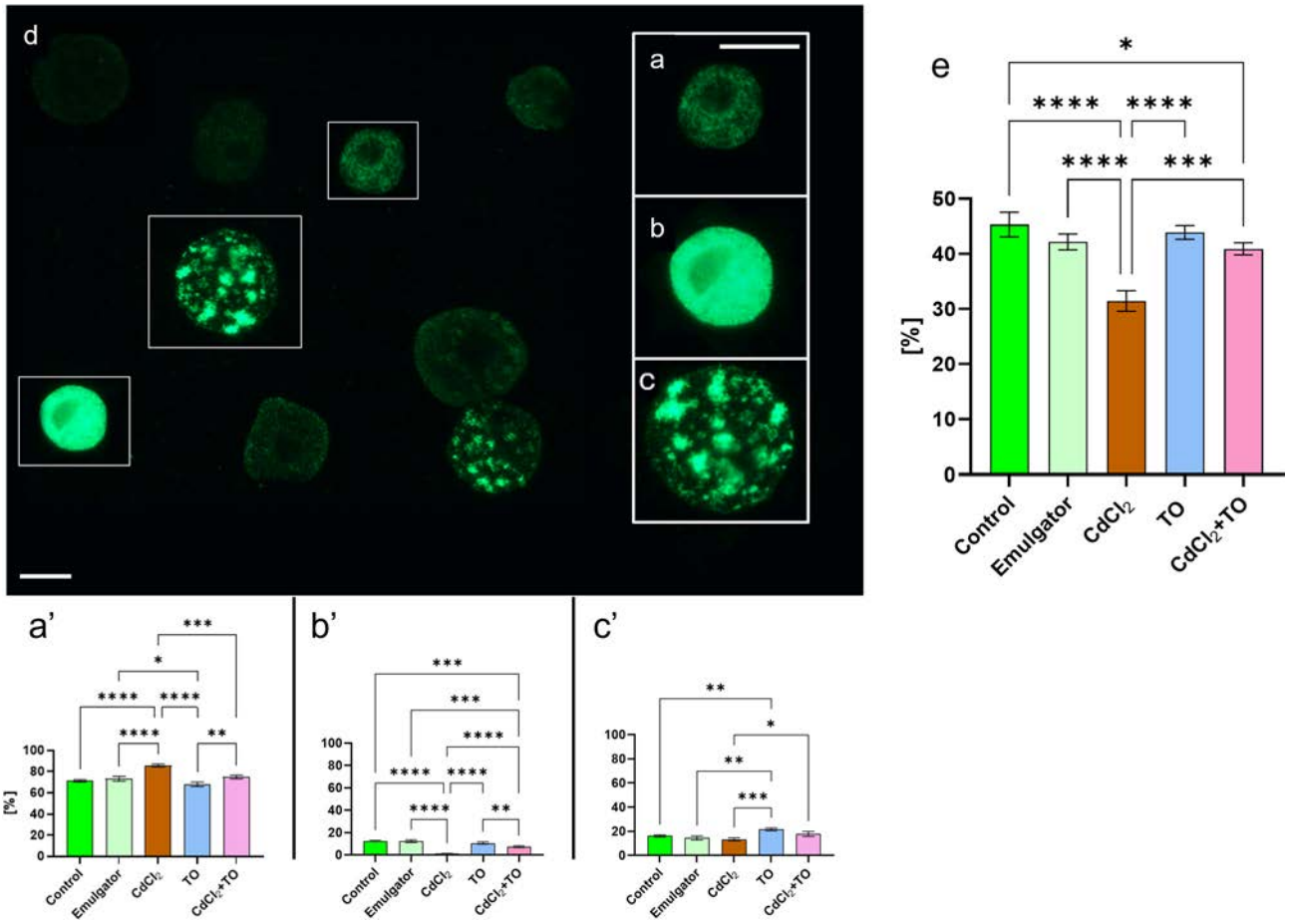

Fig. 5. DNA replication in *V. faba* root cell populations confirmed by IdU incorporation. Control cell population (**d**) (boxes indicate cell nuclei shown at higher magnification), early S phase (**a**), mid- S phase (**b**), late-S phase (**c**); Scale bar = 10 µm.(**e**) Mean percentage (± SD for three biological replicates) of IdU-labeled cells (labeling index). Fractions [(%) ± SD for three biological replicates] of early (a'), mid- (b') and late-S phase cells (c'), calculated by combining microfluorimetric quantification of DNA content in DAPI-stained cell nuclei with visual analysis of IdU fluorescence patterns. ****p < 0.0001, ***p < 0.001, **p < 0.01, *p < 0.05 (One-Way ANOVA with Tukey's test for multiple comparisons).

vitamin C, vitamin E, or reduced glutathione (GSH), supported by protection against lipid oxidation, which is crucial for maintaining cell membrane integrity. The aforementioned properties were proved in different assays that included mice and rat models of myocardial infarction, diabetes, obesity, inflammation or nephrotoxicity. According to the studies the active doses were within a range of 7.5–40 mg/kg body weight.

p-Cymene – the second most abundant ingredient found in thyme oil — belongs to compounds with proven antiradical properties. This monoterpene has been studied for its beneficial effects in mitigating the effects of oxidation processes[32]. Among its major mechanisms of action are the reduction of lipid peroxidation, a decrease in nitrile content measured in mice hippocampus, scavenging of reactive oxygen species, and enhancement of antioxidant enzyme activities such as SOD and CAT, starting from doses of 50 mg/kg body weight in animal studies.

Also caryophyllene showed strong antioxidant properties that can alleviate the properties of cadmium investigated in this study, that are similar to the properties of p-cymene and thymol[33]. These effects for caryophyllene were observed in animal studies already at the concentration of 10 mg/kg proving a stronger potential in anti-inflammatory action than in the case of p-cymene.

Given these properties, the potential use of TO as a protective agent for both plant and animal tissues, appears to be a promising direction. While research suggests that TO may mitigate cadmium-induced oxidative stress and inflammation in animal cells[34], literature data on analogous protective mechanisms for plant tissues is sparse and requires further exploration.

At the cellular level, Cd^{2+} ions bind to thiol and carbonyl groups of proteins, leading to enzyme inactivating and contributing to excessive ROS production in plant cells[35]. Our histochemical analyses, based on nitro blue tetrazolium (NBT) reduction in meristematic cells of *V. faba* primary roots, demonstrated that a 24-hour exposure of young seedlings to $CdCl_2$ significantly increased the production of superoxide anion radicals ($O_2^{\bullet-}$). Furthermore, our results indicate that TO inhibits $O_2^{\bullet-}$ overproduction due to its antioxidant properties.

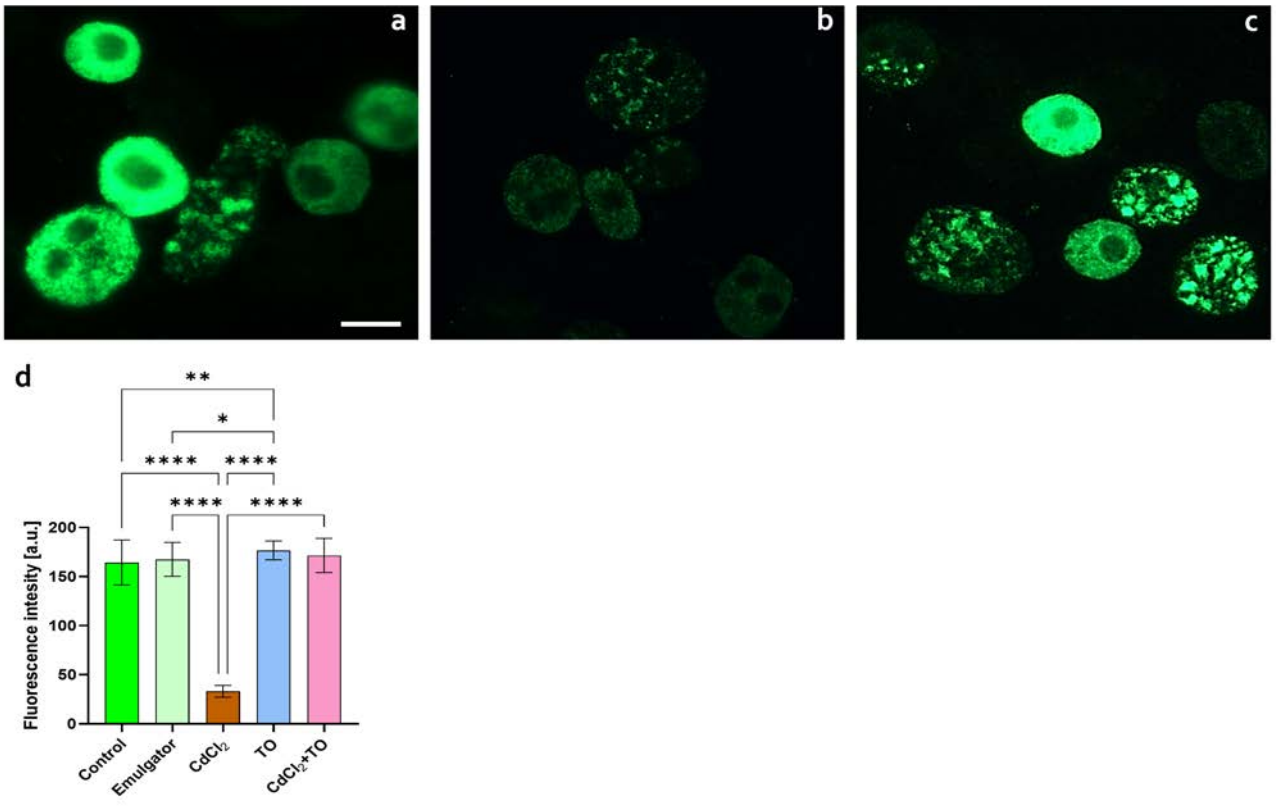

Fig. 6. DNA replication in *V. faba* RAM cell populations as evidenced by IdU incorporation. Control (**a**) $CdCl_2$ treatment (**b**) $CdCl_2$ and TO combined treatment (**c**). Scale bar = 10 µm. (d) Mean, (± SD for three biological replicates) IdU labeling intensity, (fluorescence intensity), expressed as a percentage of the maximum possible brightness, (pixel value = 255), evaluated for selected mid-S-phase nuclei, (determined microfluorimetrically following DAPI staining). $^{****}p < 0.0001$, $^{**}p < 0.01$, $^{*}p < 0.05$, (One-Way ANOVA with Tukey's test for multiple comparisons).

However, oxidative stress induced by $CdCl_2$ is not limited to superoxide anion radical overproduction, but it also leads to excessive hydrogen peroxide (H_2O_2) formation, as demonstrated by DAB staining. The microcolorimetric approach was chosen to quantify ROS levels specifically in meristematic cells, avoiding signal averaging from different root tissues that could obscure cell-type-specific differences. This method preserves the morphological and structural context of the sample, allowing precise visualization of reaction products (NBT, DAB) in individual cells and increasing the biological relevance of the data compared to whole-organ homogenate analyses. Superoxide anion radicals ($O_2^{\bullet -}$) are generated through the one-electron reduction of molecular oxygen, for instance, during electron transport in mitochondria. These radicals are subsequently converted into H_2O_2 by superoxide dismutases (SOD)[36]. The conversion of $O_2^{\bullet -}$ into H_2O_2, followed by the detoxification of H_2O_2, constitutes a crucial component of the plant defense system against oxidative stress induced by both abiotic and biotic factors. The efficiency of these mechanisms directly affects plant survival and adaptation under redox stress conditions. Under extremely harmful conditions, in which the antioxidant mechanisms of plant organisms become insufficient, there is a necessity to search for chemical compounds capable of supporting their functioning in ROS neutralization processes. Our findings show that supplementing the culture medium with TO resulted in a significant reduction in both formazan and reduced DAB deposits compared to root cells treated with $CdCl_2$ alone. This indicates the antioxidant potential of TO and its ability to mitigate $CdCl_2$-induced oxidative stress. Similar results were reported in studies on rice seedlings exposed to ammonium stress[37], where thymol was found to significantly reduce oxidative damage by inhibiting ROS accumulation and limiting lipid peroxidation. Likewise, study on tobacco (*Nicotiana tabacum*) tolerance to salinity[38] demonstrated that thymol - one of the primary components of TO – alleviated oxidative stress through the dynamic regulation of the antioxidant system. These findings support our observations regarding the protective properties of TO in the context of redox stress.

The protective mechanism of TO is not only limited to the activation of the antioxidant system; The reduction of Cd accumulation in cells also plays an important role, as demonstrated by our studies, which constitute an integral part of a forthcoming publication. Studies by Ye et al.[39] also showed that thymol, the main component of TO, significantly reduced the amount of free Cd^{2+} in roots, suggesting potential inhibition of its intake or increased capture and sequestration in a less toxic form. It was also found that thymol can stimulate the synthesis of glutathione, which participates in the chelation and detoxification of Cd^{2+} ions. The mechanisms described

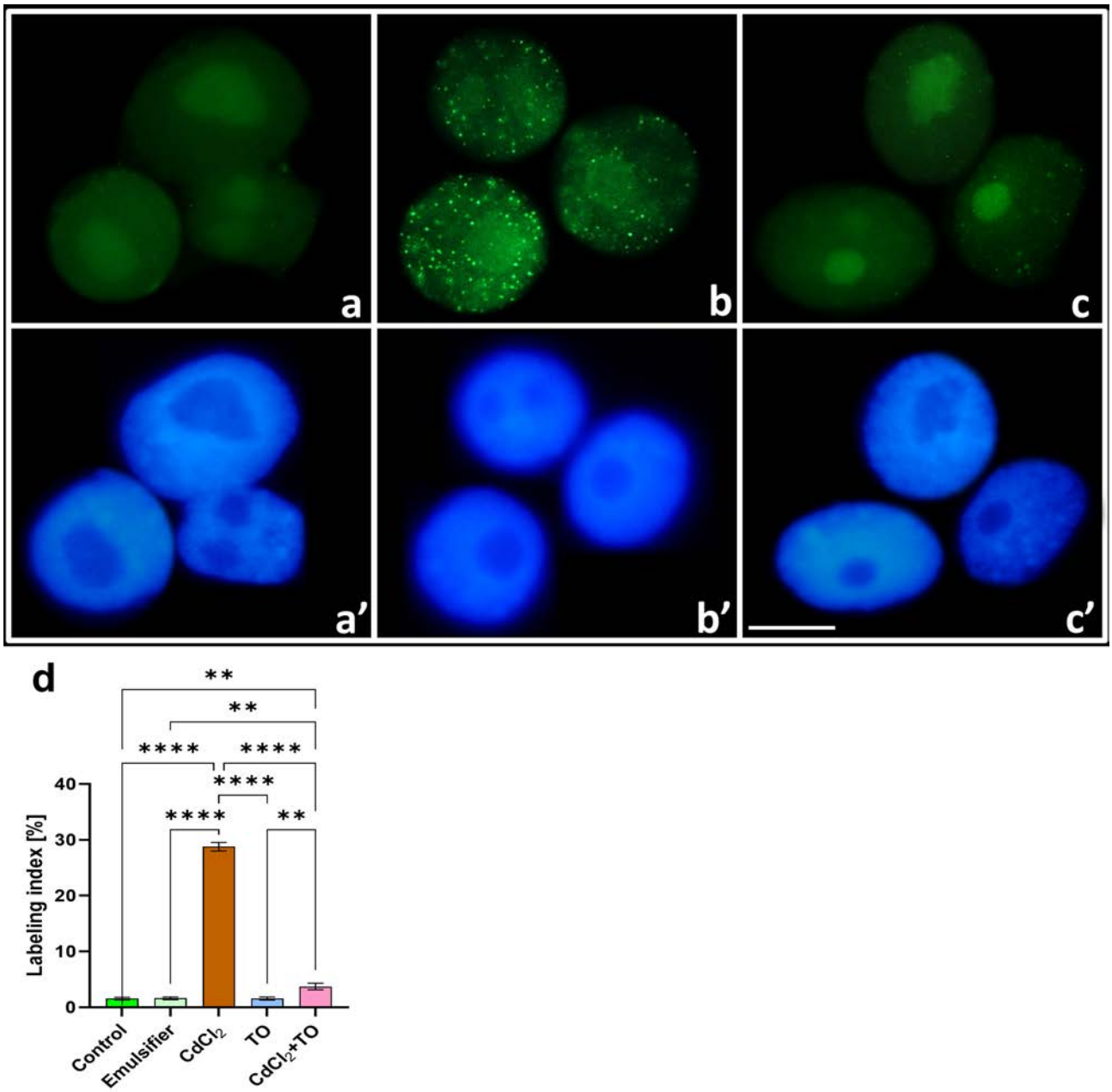

Fig. 7. Immunofluorescence detection of γ-phosphorylated H2A.X in *V. faba* control meristems (**a**) and after 24-hour incubation of root meristems with $CdCl_2$ (**b**), or after treatment with a combination of $CdCl_2$ and TO (**c**), along with corresponding images of cell nuclei stained with DAPI (**a'-c'**). Scale bar = 10 µm. (**d**) Labeling indices, (% ±SD for three biological replicates) estimated from immunofluorescence detection of γ-phosphorylated H2A.X foci in root meristem cell populations of *V. faba* in control seedlings and in seedlings exposed to 24 h of emulsifier, $CdCl_2$, TO, and $CdCl_2$ and TO combined. $^{****}p < 0.0001$, $^{**}p < 0.01$, (One-Way ANOVA with Tukey's test for multiple comparisons).

may therefore indicate a synergistic effect of TO – both by reducing the availability and transport of Cd into cells and by activating antioxidant and chelating defense systems. It is worth noting that in our unpublished studies, as well as in the study by Ye et al.[39], despite a reduction in cadmium accumulation, its content in root meristematic cells remained substantial. In our study, this persistence of elevated cadmium levels is evidenced by the observed alterations in the cellular oxidative state, the progression of the cell cycle, and the integrity of genetic material.

The plant cell cycle is a strictly controlled process that is sensitive to stress factors, including heavy metals, which can disrupt its normal course by generating oxidative stress. Cytophotometric measurements of nuclear DNA content in our study, demonstrated that $CdCl_2$ treatment resulted in a decrease in the number of replicating cells, accompanied by an increase in the proportion of cells in the G1 and G2 phases compared to control plants.

However, supplementation with TO in $CdCl_2$-treated cells led to only a minor decrease in replicating cells and a slight increase in the G2-phase cell population, while the abundance of G1-phase cells remained comparable to the control. The study conducted by [40] shows that heavy metals cause cell cycle disruption by inducing the expression of cyclin-dependent kinases (CDKs) inhibitors from the SIAMESE-RELATED (SMR) family, as well as activating the DNA damage response (DDR), which can lead to either cell cycle arrest or apoptosis. Increasing evidence suggests that this mechanism is largely mediated by ROS, generated in response to heavy metal ion exposure. The interplay between redox stress and cell cycle regulation in plants is highly complex and multifaceted. ROS can directly influence cell cycle progression by modulating transcription factors - proteins that bind to DNA and regulate gene expression[41]. Additionally, ROS may alter the activity of these transcription factors by modifying either their structure or the DNA sequences to which they bind[42]. Such modifications can lead to changes in the expression of cell cycle regulators, including CDKs and cyclins. Given the well-documented antioxidant properties of TO, it is highly plausible that by mitigating oxidative stress induced by cadmium toxicity, TO influences the expression of CDK inhibitors, thereby reducing the proportion of cells arrested at cycle checkpoints.

Precise DNA replication is crucial for the accurate transfer of genetic information to daughter cells, and its disruption—for example, as a result of heavy metal exposure—can trigger regulatory mechanisms that lead to a temporary pause in the cell cycle. Our studies on RAM cells of *V. faba* exposed to $CdCl_2$, using the DNA synthesis marker IdU, clearly illustrate the function of the checkpoint between the G1 and S phases. IdU incorporation showed that cadmium ions caused a reduction in the number of cells undergoing DNA synthesis. Moreover, a significant proportion of cells was accumulated in the initial stages of S phase, indicating that replication was proceeding at a slower pace. Additionally, we observed a marked reduction in the intensity of nuclear labeling, which also suggests a slowdown in DNA replication. In contrast, the application of TO significantly alleviated the inhibitory effect of cadmium on the replication process, as both the labeling index of replicating cells and the fluorescence intensity of the applied marker were significantly higher in the presence of TO compared to cells treated with $CdCl_2$ alone. Furthermore, plants treated only with the emulsified form of TO exhibited increased labeling intensity of replicating cells compared to those incubated in water. The overproduction of ROS induced by $CdCl_2$, which we demonstrated in our study, allows us to consider redox stress as a source of replication disturbances. Our results are consistent with other studies indicating that oxidative stress generates replication stress by disrupting nucleotide pool balance and causing DNA damage[8], which can (1) block the movement of replication forks (RFs)[43], leading to their stalling, breakage, or collapse[44], and (2) impair the progression of DNA polymerases[45]. ROS can also slow down replication by affecting the regulation of replication protein activity[46]. TO, on the other hand, is well known for its antioxidant properties, which contribute to its protective effect against various toxic substances. Scientific studies report that TO can (1) slow down oxidation processes by reducing ROS production and/or (2) promote the degradation of peroxides into stable substances, thereby preventing the intensification of oxidative damage[28]. Moreover, it is worth noting that even under control conditions, free radicals are continuously generate in cells as a byproduct of basic metabolic processes, which can lead to damage to biological membranes, enzymes and DNA[47]. A study by Chen et al.[48] demonstrated that the oil extracted from thyme, can prevent free radical-induced damage to blood cells, further supporting the hypothesis that TO significantly reduces ROS levels and their destructive effects. Thus, in light of our results and existing scientific reports, it seems likely that TO, due to its antioxidant properties, exerts a protective effect by reducing oxidative stress in cells, which may minimize or completely prevent ROS-induced damage to both DNA structure and the machinery responsible for genetic material replication.

In the presented study, the expression of H2A.X phosphorylation at serine 139, a marker of double-strand DNA breaks (DSBs), was analyzed to detect the genotoxic effects of cadmium ions. The results revealed a significantly higher presence of the phosphorylated histone γH2A.X variant in $CdCl_2$-treated cells, indicating an increased frequency of double-strand breaks due to its toxic effects. Our findings align with previous studies on *V. faba* root meristems exposed to DNA replication inhibitors such as aphidicolin and hydroxyurea[49], as well as studies on *A. cepa* root meristem cells exposed to β-lapachone[50]. Analogous results demonstrating a significant increase in γH2A.X foci, were also obtained in *V. faba* RAM cells exposed to $CdCl_2$ at a slightly lower concentration than used in our analyses[22]. Additionally, our study shows that TO inhibits the formation of the phosphorylated histone variant in $CdCl_2$-treated cells, effectively preventing the occurrence of double-strand breaks caused by cadmium toxicity. A similar protective effect of TO, but in animal organisms, appears to be confirmed by the study of Hassan et. al.[51], which demonstrated its protective and antimutagenic effects against the cytotoxicity of zinc oxide nanoparticles in rats. Using a comet assay on bone marrow and spleen cells, they revealed that simultaneous exposure to TO and ZnO nanoparticles significantly reduced the percentage of DNA within the comet tail, compared to cells treated with ZnO alone.

Based on the presented results, it appears that cellular responses to Cd toxicity involve a series of interrelated biochemical reactions that, through the generation of ROS and replication stress induced by DNA damage, ultimately activate signaling factors involved in cell cycle control pathways and DNA repair systems. On the other hand, TO, which exhibits strong antioxidant activity, seems to counteract the damaging effects of cadmium ions at every stage of this mechanism. The application of TO alone to RAM cells does not cause any harmful effects on the analyzed cellular processes, suggesting its potential biocompatibility and safety in the context of the metabolic and structural functions of plant cells.

Our studies provides valuable insights into the protective role of TO in mitigating cadmium-induced cellular damage in plant meristematic tissues. We demonstrated that TO, by significantly mitigating cadmium-induced oxidative stress, also alleviates replication stress. As a result, the proportion of cells in the successive phases of the cell cycle within the meristem is maintained at levels comparable to the control, due to a marked reduction in DNA damage and the preservation of proper replication dynamics. While the experimental model used here offers a well-controlled system for assessing cellular responses and is primarily a model for basic research, it

represents an important initial step toward broader application. Expanding this approach to include other plant species or more complex environmental conditions could help confirm the generalizability of these findings and the protective potential of thyme oil itself. Further investigations into the molecular mechanisms of TO action, including transcriptomic or proteomic analyses, epigenetic modifications, mechanisms related to cell cycle regulation, and the functioning of antioxidant systems, would significantly enhance our understanding of its mode of action in cells and its protective role. After analyzing these unknowns, the next logical step would be experimental application in open-field systems to evaluate the effects of thyme oil or its formulations on plants at different developmental stages. Simultaneously, we believe that the results obtained may serve as a foundation for developing strategies to mitigate metal-induced stress in agricultural crops. Natural substances such as thyme oil, due to their low toxicity, biodegradability, and efficacy, are promising candidates as alternatives to synthetic agrochemicals. Preparations based on essential oils can be applied, for example, as foliar sprays, soil watering, or microcapsules that enable controlled release of active compounds[52,53].

Data availability

The datasets generated during and analysed during the current study are available from the corresponding author on reasonable request.

Received: 20 March 2025; Accepted: 29 September 2025
Published online: 05 November 2025

References

1. Briffa, J., Sinagra, E. & Blundell, R. Heavy metal pollution in the environment and their toxicological effects on humans. *Heliyon* **6**, e04691. https://doi.org/10.1016/j.heliyon.2020.e04691(2020).
2. Yadav, D. S., Jaiswal, B., Gautam, M. & Agrawal, M. Soil acidification and its impact on plants. *Plant Responses To Soil Pollution* (eds Singh, P. et al.) 1–26 (Springer Singapore, 2020).
3. Hamid, Y. et al. Organic soil additives for the remediation of cadmium contaminated soils and their impact on the soil-plant system: A review. *Sci. Total Environ.* **707**, 136121 (2020).
4. Haider, F. U. et al. Cadmium toxicity in plants: impacts and remediation strategies. *Ecotoxicol. Environ. Saf.* **211**, 111887 (2021).
5. Demidchik, V. Mechanisms of oxidative stress in plants: from classical chemistry to cell biology. *Environ. Exp. Bot.* **109**, 212–228 (2015).
6. He, S., Yang, X., He, Z. & Baligar, V. C. Morphological and physiological responses of plants to cadmium toxicity: A review. *Pedosphere* **27**, 421–438 (2017).
7. Wakeel, A., Xu, M. & Gan, Y. Chromium-Induced reactive oxygen species accumulation by altering the enzymatic antioxidant system and associated cytotoxic, genotoxic, ultrastructural, and photosynthetic changes in plants. *Int. J. Mol. Sci.* **21**, 728 (2020).
8. Wilhelm, T. et al. Slow replication fork velocity of homologous recombination-defective cells results from endogenous oxidative stress. *PLoS Genet.* **12**(5), e1006007 (2016).
9. Bui, A. D., Sharma, R., Henkel, R. & Agarwal, A. Reactive oxygen species impact on sperm DNA and its role in male infertility. *Andrologia* **50**, e13012 (2018).
10. Stiff, T. et al. ATM and DNA-PK function redundantly to phosphorylate H2AX after exposure to ionizing radiation. *Cancer Res.* **64**, 2390–2396 (2004).
11. Varvara, P. V. et al. gamma-H2AX: A potential biomarker in breast cancer. *Tumor Biol.* **41**, 101042831987853 (2019).
12. Johnson, D. P., Chandrasekharan, M. B., Dutreix, M. & Bhaskara, S. Targeting DNA repair and chromatin crosstalk in cancer therapy. *Cancers* **13**, 381 (2021).
13. Kouzarides, T. Chromatin modifications and their function. *Cell* **128**, 693–705 (2007).
14. Taverna, S. D., Li, H., Ruthenburg, A. J., Allis, C. D. & Patel, D. J. How chromatin-binding modules interpret histone modifications: lessons from professional pocket pickers. *Nat. Struct. Mol. Biol.* **14**, 1025–1040 (2007).
15. Kobayashi, J., Antoccia, A., Tauchi, H., Matsuura, S. & Komatsu, K. NBS1 and its functional role in the DNA damage response. *DNA Repair.* **3**, 855–861 (2004).
16. Fowler, M. R., Eyre, S., Scott, N. W., Slater, A. & Elliott, M. C. The plant cell cycle in context. *Mol. Biotechnol.* **10**, 123–153 (1998).
17. Polit, J. T. Protein phosphorylation in *Vicia faba* root meristem cells during the first steps of leaving principal control points after sucrose application. *Plant. Cell. Rep.* **28**, 165–173 (2009).
18. Dhifi, W., Bellili, S., Jazi, S., Bahloul, N. & Mnif, W. Essential oils' chemical characterization and investigation of some biological activities: A critical review. *Medicines* **3**, 25 (2016).
19. Ansari, M. N., Rehman, N. U., Karim, A., Imam, F. & Hamad, A. M. Protective effect of *Thymus serrulatus* essential oil on cadmium-induced nephrotoxicity in rats, through suppression of oxidative stress and downregulation of NF-κB, iNOS, and Smad2 mRNA expression. *Molecules* **26**, 1252 (2021).
20. Ibrahim, S. & Abo-Kora, Y. Evaluation of the protective effect of *Cinnamomum zeylanicum* on cadmium testicular toxicity and Nrf2 gene expression in albino rats. *Int. J. Pharmacol. Toxicol.* **5**, 5–10 (2017).
21. Alonso-Gato, M., Astray, G., Mejuto, J. C. & Simal-Gandara J. Essential oils as antimicrobials crop protection. *Antibiotics* **10**, 34 (2021).
22. Żabka, A., Winnicki, K., Polit, J. T., Wróblewski, M. & Maszewski, J. Cadmium (II)-Induced oxidative stress results in replication stress and epigenetic modifications in root meristem cell nuclei of *Vicia faba*. *Cells* **10**, 640 (2021).
23. Żabka, A. et al. Changes in epigenetic patterns related to DNA replication in *Vicia faba* root meristem cells under cadmium-induced stress conditions. *Cells* **10**, 3409 (2021).
24. Thordal-Christensen, H., Zhang, Z., Wei, Y. & Collinge, D. B. Subcellular localization of H_2O_2 in plants. H_2O_2 accumulation in papillae and hypersensitive response during the barley—powdery mildew interaction. *Plant. J.* **11**, 1187–1194 (1997).
25. Bielski, B. H. J., Shiue, G. G. & Bajuk, S. Reduction of nitro blue tetrazolium by CO^{2-} and O^{2-} radicals. *J. Phys. Chem.* **84**, 830–833 (1980).
26. Soltys, D. et al. Cyanamide mode of action during inhibition of onion (*Allium cepa* L.) root growth involves disturbances in cell division and cytoskeleton formation. *Planta* **234**, 609–621 (2011).
27. Feulgen, R. & Rossenbeck, H. Mikroskopisch-chemischer Nachweis einer Nucleinsäure vom typus der Thymonucleinsäure und die- Darauf beruhende elektive Färbung von Zellkernen in Mikroskopischen Präparaten. *Hoppe-Seyler´s Z. Für Physiol. Chem.* **135**, 203–248 (1924).
28. Abdel-Wahhab, M. A. et al. Elimination of oxidative stress and genotoxicity of biosynthesized titanium dioxide nanoparticles in rats via supplementation with Whey protein-coated thyme essential oil. *Environ. Sci. Pollut Res.* **28**, 57640–57656 (2021).
29. Hudaib, M., Speroni, E., Di Pietra, A. M. & Cavrini, V. GC/MS evaluation of thyme (*Thymus vulgaris* L.) oil composition and variations during the vegetative cycle. *J. Pharm. Biomed. Anal.* **29**, 691–700 (2002).

30. Chibuike, G. U. & Obiora, S. C. Heavy metal polluted soils: effect on plants and bioremediation methods. *Appl. Environ. Soil Sci.* 1–12 (2014).
31. Nagoor Meeran, M. F., Javed, H., Taee, A., Azimullah, H. & Ojha, S. K. Pharmacological properties and molecular mechanisms of thymol: prospects for its therapeutic potential and pharmaceutical development. *Front. Pharmacol.* **8**, 380 (2017).
32. de Oliveira, T. M. et al. Evaluation of *p* -cymene, a natural antioxidant. *Pharm. Biol.* **53**, 423–428 (2015).
33. Gullì, M., Percaccio, E., Di Giacomo, S. & Di Sotto, A. Novel insights into the immunomodulatory effects of caryophyllane sesquiterpenes: A systematic review of preclinical studies. *Appl. Sci.* **12**, 2292 (2022).
34. Rahmani, F. et al. Thyme oil nanoemulsion enhanced cellular antioxidant and suppressed inflammation in mice challenged by Cadmium-Induced oxidative stress. *Waste Biomass Valorization* **13**, 3139–3146 (2022).
35. Srivastava, R. K., Pandey, P., Rajpoot, R., Rani, A. & Dubey, R. S. Cadmium and lead interactive effects on oxidative stress and antioxidative responses in rice seedlings. *Protoplasma* **251**, 1047–1065 (2014).
36. Cadenas, E. & Davies, K. J. A. Mitochondrial free radical generation, oxidative stress, and aging. *Free Radic Biol. Med.* **29**, 222–230 (2000).
37. Guo, K. et al. Thymol ameliorates ammonium toxicity via repressing polyamine oxidase-derived hydrogen peroxide and modulating ammonium transporters in rice root. *Food Prod. Process. Nutr.* **3**, 7 (2021).
38. Xu, L. et al. Thymol improves salinity tolerance of tobacco by increasing the sodium ion efflux and enhancing the content of nitric oxide and glutathione. *BMC Plant. Biol.* **22**, 31 (2022).
39. Ye, X. et al. Thymol mitigates cadmium stress by regulating glutathione levels and reactive oxygen species homeostasis in tobacco seedlings. *Molecules* **21**, 1339 (2016).
40. Hendrix, S. et al. Suppressor of gamma response 1 modulates the DNA damage response and oxidative stress response in leaves of cadmium-exposed *Arabidopsis thaliana*. *Front. Plant. Sci.* **11**, 366 (2020).
41. Vinck, M. et al. Principles of large-scale neural interactions. *Neuron* **111**, 987–1002 (2023).
42. Ramakrishnan, M. et al. Redox status of the plant cell determines epigenetic modifications under abiotic stress conditions and during developmental processes. *J. Adv. Res.* **42**, 99–116 (2022).
43. Budzowska, M. & Kanaar, R. Mechanisms of dealing with DNA damage-induced replication problems. *Cell. Biochem. Biophys.* **53**, 17–31 (2009).
44. Gelot, C., Magdalou, I. & Lopez, B. Replication stress in mammalian cells and its consequences for mitosis. *Genes* **6**, 267–298 (2015).
45. Wallace, S. S. Biological consequences of free radical-damaged DNA bases. *Free Radic Biol. Med.* **33**, 1–14 (2002).
46. Girard, P. M. et al. Inhibition of S-phase progression triggered by UVA-induced ROS does not require a functional DNA damage checkpoint response in mammalian cells. *DNA Repair.* **7**, 1500–1516 (2008).
47. Akbari, B., Baghaei-Yazdi, N. & Bahmaie, M. Mahdavi Abhari, F. The role of plant-derived natural antioxidants in reduction of oxidative stress. *BioFactors* **48**, 611–633 (2022).
48. Chen, X. et al. Antioxidant activities of essential oils and their major components in scavenging free radicals, inhibiting lipid oxidation and reducing cellular oxidative stress. *Molecules* **28**, 4559 (2023).
49. Rybaczek, D., Bodys, A. & Maszewski, J. H2AX foci in late S/G2- and M-phase cells after hydroxyurea- and aphidicolin-induced DNA replication stress in *Vicia*. *Histochem. Cell. Biol.* **128**, 227–241 (2007).
50. Żabka, A., Trzaskoma, P. & Maszewski, J. Dissimilar effects of β-lapachone- and hydroxyurea-induced DNA replication stress in root meristem cells of *Allium cepa*. *Plant. Physiol. Biochem.* **73**, 282–293 (2013).
51. Hassan, M. E. et al. Nanoencapsulation of thyme essential oil: a new avenue to enhance its protective role against oxidative stress and cytotoxicity of zinc oxide nanoparticles in rats. *Environ. Sci. Pollut Res.* **28**, 52046–52063 (2021).
52. Kesraoui, S., Andrés, M., Berrocal-Lobo, M., Soudani, S. & Gonzalez-Coloma, A. Direct and indirect effects of essential oils for sustainable crop protection. *Plants* **11**, 2144 (2022).
53. Ayllón-Gutiérrez, R., Díaz-Rubio, L., Montaño-Soto, M. & Haro-Vázquez, M. D. P. Córdova-Guerrero, I. Applications of plant essential oils in pest control and their encapsulation for controlled release: A review. *Agriculture* **14**, 1766 (2024).

Acknowledgements

This work was supported through the budget of the Doctoral School of Exact and Natural Sciences of the Univeristy of Lodz.

Author contributions

N.G.-S. is the author of the conception and design of the study. N.G.-S. coordinated the study, collected, interpreted and statistically analyzed the data. A.Ż. contributed to experimental work. M.W. contributed to statistical analyses. P.S. investigated the composition of thyme oil using the GC-MS.W.K.-K. investigated the composition of thyme oil using the GC-MS. J.T.P. participated in conception of the study, contributed to experimental work. The manuscript was written by N.G. and revised by A.Ż., J.T.P. All authors read and approved the final version of the manuscript. Credit authorship contribution statement: N.G.-S.: Conceptualization, Methodology, Investigation, Validation, Writing – Original Draft, Visualization, Project administration, Statistical analyses, Funding acquisition. A.Ż.: Methodology, Writing – Review and Editing. M.W.: Statistical analyses. W.K.-K.: Investigation. P.S.: Investigation. J.T.P.: Conceptualization, Methodology, Supervision, Validation, Writing – Review and Editing.

Declarations

Competing interests

The authors declare no competing interests.

Declaration of competing interest

The authors declare no competing financial interests or personal relationships that could have appeared to influence the work reported in this paper.

Additional information

Correspondence and requests for materials should be addressed to N.G.-S.

❖

Praca 2 (Załącznik nr 2)

❖ Żabka, A.*; **Gocek, N.**; Polit, J.T.; Maszewski, J.
Epigenetic Modifications Evidenced by Isolation of Proteins on Nascent DNA and Immunofluorescence in Hydroxyurea-Treated Root Meristem Cells of *Vicia faba*. *Planta* **2023**, 258, 95, doi:10.1007/s00425-023-04249-2.

* – autor korespondujący

- Współczynnik wpływu (IF): **3,8**
- Punkty MNiSW: **100 pkt**.

Planta (2023) 258:95
https://doi.org/10.1007/s00425-023-04249-2

ORIGINAL ARTICLE

Epigenetic modifications evidenced by isolation of proteins on nascent DNA and immunofluorescence in hydroxyurea-treated root meristem cells of *Vicia faba*

Aneta Żabka[1] · Natalia Gocek[1] · Justyna Teresa Polit[1] · Janusz Maszewski[1]

Received: 15 May 2023 / Accepted: 21 September 2023 / Published online: 9 October 2023

Abstract

Main conclusion **By implementation of the iPOND technique for plant material, changes in posttranslational modifications of histones were identified in hydroxyurea-treated root meristem cells of *Vicia*.**

Abstract Replication stress (RS) disrupts or inhibits replication forks and by altering epigenetic information of the newly formed chromatin can affect gene regulation and/or spatial organisation of DNA. Experiments on *Vicia faba* root meristem cells exposed to short-term treatment with 3 mM hydroxyurea (HU, an inhibitor of DNA replication) were aimed to understand epigenetic changes related to RS. To achieve this, the following histone modifications were studied using isolation of proteins on nascent DNA (iPOND) technique (for the first time on plant material) combined with immunofluorescence labeling: (i) acetylation of histone H3 at lysine 56 (H3K56Ac), (ii) acetylation of histone H4 at Lys 5 (H4K5Ac), and (iii) phosphorylation of histone H3 at threonine 45 (H3T45Ph). Certainly, the implementation of the iPOND method for plants may prove to be a key step for a more in-depth understanding of the cell's response to RS at the chromatin level.

Keywords DNA replication · Epigenetic modifications · Hydroxyurea · Isolation of proteins on nascent DNA (iPOND) · Replication stress · *Vicia faba*

Introduction

More than animals, plants depend on the local environment, suggesting that they have evolved a vast number of distinctive and efficient biochemical mechanisms to control DNA replication, cell divisions, and differentiation, all these processes being targeted precisely for successful progression of their specific developmental traits. To prevent the influence of adverse factors or threatening conditions, plants have advanced an intricate and complex molecular system that can recognize stress and elicit appropriate response activities (Bej and Basak 2017). Accordingly, they trigger various signal transduction pathways, switch on stress-inducible genes, cell cycle checkpoints and induce adequate changes at the biochemical, physiological and morphological levels. In consequence, they stimulate DNA damage repair machineries, temporal metabolic dormancy, or an animal-like programmed cell death (AL-PCD) processes (Hirayama and Shinozaki 2010; Viggiano and de Pinto 2017; Żabka et al. 2017).

Due to the sessile lifestyle, plants are continuously exposed to various environmental stresses (biotic and abiotic), some of which can cause DNA damage. Accordingly, they must integrate developmental processes and environmental signals (including poor resource availability, unfavorable water, soil, and light conditions), and to coordinate cell division, cell differentiation and organ growth (Nikitaki

Communicated by Anastasios Melis.

✉ Aneta Żabka
aneta.zabka@biol.uni.lodz.pl

Natalia Gocek
natalia.gocek@biol.uni.lodz.pl

Justyna Teresa Polit
justyna.polit@biol.uni.lodz.pl

Janusz Maszewski
janusz.maszewski@biol.uni.lodz.pl

[1] Faculty of Biology and Environmental Protection Department of Cytophysiology, University of Lodz, 90-236 Lodz, Poland

et al. 2018; Gentric et al. 2021; Szurman-Zubrzycka et al. 2023).

Plants, in common with all eukaryotes, organize their DNA into multiple units termed replicons, each containing a single replication origin (ORI). As a result, there are thousands of sites scattered across the genome in which DNA biosynthesis initiates (Bryant and Aves 2011; Leonard and Méchali 2013). The principal feature of this process is that replicons function in groups and the timing of their sequential activation during S-phase, at least in part, depends on the chromatin structure in which ORIs reside. Early replication of chromosomal domains, enriched in ORIs and origin recognition complexes (ORCs; multi-subunit DNA-binding protein complexes) are generally observed in transcriptionally operative gene-rich domains with active epigenetic marks. On the contrary, late replicating domains are observed in origin-poor heterochromatin regions that have low gene density, generally associated with repressive epigenetic states and numerous transposon elements (Fragkos et al. 2015). Consequently: (1) a precise temporal pattern of DNA replication occurs at a limited number of discrete foci localized within the nucleus, (2) not all ORIs fire at the same time, and (3), synchronously firing ORIs are not homogenously distributed throughout the genome. All this results in the appearance of well-conserved early and late replication pattern during S-phase progression, which can be visualized at the fluorescence microscopy level (Casas-Delucchi and Cardoso 2011).

Similar to all other organisms, plant DNA molecules need to strike a balance: on the one hand, they have to be rigid enough to protect the genetic information and to maintain chromosomal integrity, and on the other, they must be available and accessible to the cell cycle regulated activities and molecular interactions indispensable for differentiation-associated processes (Inzé and De Veylder 2006). Accordingly, the process of replication must be tightly regulated by means of precise synchronization of cellular pathways engaged to ensure sufficient energy and material supply and, in case of potential emergency, to arrange functional repair of the genome. Dysfunction of these mechanisms may contribute to the development of replication stress (RS) (Nisa et al. 2019).

Our current study on *Vicia faba* root meristem cells aimed to investigate and update our understanding of DNA replication-associated epigenetic changes appearing after short-term exposure to 3 mM hydroxyurea (HU; a classical inhibitor of DNA replication; Koç et al. 2004). To achieve this, histone H3 and H4 modifications investigated by iPOND (isolation of proteins on nascent DNA) technique combined with immunocytochemical labeling included: (i) histone H3 acetylation at lysine 56 (H3K56Ac), involved in S-phase transition (Li et al. 2008), DNA damage response (Driscoll et al. 2007; Masumoto et al. 2005; Wurtele et al. 2012), and transcription (Xu et al. 2005; Rufiange et al. 2007); (ii) histone H4 acetylation on Lys 5 (H4K5Ac), showing a strong correlation with DNA replication (Jasencakova et al. 2000); (iii) histone H3 phosphorylation on threonine 45 (H3T45Ph), which is involved in DNA replication and apoptosis (Hurd et al. 2009; Baker et al. 2010).

For the first time, by implementation and adaptation of the iPOND method, which allows the 'tracking' of protein association and deposition in active and stalled or damaged replication forks (RFs; Sirbu et al. 2011; Olcina et al. 2016), it was possible to determine and to compare changes in post-translational modifications of histones in the untreated (control) and HU-treated plant root meristem cells exposed to the DNA replication stress. To date, site-specific analysis of active and arrested replicons has only been performed on animal cells (e.g. Sirbu et al. 2011).

Materials and methods

Plant materials

Sterile seeds of faba bean (*Vicia faba* subsp. *minor* L.) were sown on dishes lined with moist filter paper and germinated in the dark at 20 °C. After 96 h, young seedlings with primary roots ranging from 1.5 to 2 cm were placed in Petri dishes containing distilled water (control) and 3 mM hydroxyurea solution (HU). Incubations were performed for 2 h in the dark. Primary root were chosen for practical reasons (large number of cells, short time of RAM isolation and low volume of incubation solutions).

Feulgen staining

After incubation in water and HU, severed roots were cut off, fixed in ice-cold Carnoy's solution (absolute ethanol and glacial acetic acid; 3:1, v/v) for 1 h, washed with ethanol, and then hydrolysed in 4 M HCl for 2 h. The pararosaniline (Schiff's reagent) staining procedure was performed according to the standard method (e.g. Żabka et al. 2010). After rinsing in SO_2-water (3 times) and distilled water, root meristems were cut off, placed in 45% acetic acid, crushed on slides, dried and embedded in Canada balsam.

EdU labeling

Control and HU-treated seedlings were incubated with 10 µM 5-ethinyl-2'-deoxyuridine (EdU, Thermo Fisher Scientific, Warsaw, Poland) for 20 min, in the dark. Excised root tips were fixed in PBS-buffered 4% paraformaldehyde (4 °C; pH 7.4) for 45 min and macerated for 15 min in citrate-buffered 2.5% pectinase (Sigma-Aldrich), pH 5.0. Meristems were crushed on slides (Polysine™, Menzel-Gläser,

Germany), dried, and after washing with PBS buffer, replication of nuclear DNA was visualized using the Click-iT DNA Alexa Fluor® 555 Imaging Kit (Thermo Fisher Scientific), according to the included instructions. Cell nuclei were stained for 15 min using 15 µM 4',6-diamidino-2-phenylindole (DAPI; Sigma-Aldrich). Dried slides were embedded in a mixture of PBS/glycerol/DABCO (2.3% diazabicyclo(2.2.2)octane).

iPOND technique

Isolation of proteins on nascent DNA (iPOND) technique was performed according to Sirbu et al. (2011, 2013), with some modifications for plant material. About 1000 dissected root meristems of *V. faba* (corresponding approximately to 1.0×10^8 cells) were labeled with EdU (10 min), transferred to 10 µM thymidine solution (Sigma-Aldrich) for 10 min, and finally exposed to H_2O (control series) or 3 mM HU. After 2 h, roots were fixed with 1% formaldehyde (Sigma-Aldrich) in PBS and incubated for 20 min at room temperature (RT). Formaldehyde cross-linking was inhibited by addition of 1.25 M glycine (Sigma-Aldrich). After washing with PBS (3 times), root meristems were trimmed to the length of 1 mm (jointly producing about 1.0×10^8 cells per series). Then, root tips were placed in a citric acid-buffered digestion solution (pH 5.0) containing 2.5% pectinase, 2.5% cellulase and 2.5% pectolyase (Sigma-Aldrich), and incubated at 37 °C for 60 min. After the digestion solution was removed, root tips were washed with PBS, and incubated for 30 min (RT) in permeabilization buffer (0.25% Triton X-100 in PBS). After centrifugation for 5 min at 900 g (4 °C), the supernatant was carefully decanted. Cells were washed 2 times with 0.5% BSA in PBS, centrifuged for 5 min at 900 g, (4 °C). The obtained pellet was placed into a click reaction cocktail (on ice, under dark conditions) consisting of: 1 × PBS (4.35 ml), 10 µM biotin-azide (0.05 ml; Invitrogen), 10 mM sodium ascorbate (0.5; Sigma-Aldrich), and 2 mM $CuSO_4$ (0.1 ml). Incubation with the cocktail was performed by gentle rotation at RT for 1–2 h. After centrifugation for 5 min at 900 g (4 °C), the supernatant was removed. Cells were washed with cold 0.5% BSA dissolved in PBS, centrifuged for 5 min at 900 g (4 °C), washed with PBS and decanted. Lysis buffer (1% SDS in 50 mM Tris, pH 8.0) was supplemented by aprotinin (Sigma-Aldrich) and leupeptin (Sigma-Aldrich) at a concentration of 1 µg/ml (each) before use. After resuspending the samples in lysis buffer, cells were sonicated (13–16 W, 20 s constant pulse, 40 s cell lysate pause; total pulse time: 4–5 min per sample). Then, samples were centrifuged for 10 min at 16 000 g, at RT. The resulting lysate was diluted 1:1 (v/v) with cold PBS containing 1 µg/ml of aprotinin and 1 µg/ml of leupeptin. 15 µl of lysate was placed on ice and kept as an input sample. The remaining lysate was used for streptavidin capture of biotin-labeled nascent DNA. Each experimental sample was incubated with streptavidin agarose beads at a concentration of 100 µl of bead suspension per 1×10^8 cells. First, the bead suspension was centrifuged at 1800 g for 1 min at RT, washed 2 times with lysis buffer containing aprotinin and leupeptin, and the supernatant was aspirated after each wash. Finally, the beads were washed again in PBS containing aprotinin and leupeptin (1:1 beads:PBS), the supernatant was aspirated and the beads were resuspended in PBS containing protease inhibitors. An equal volume of biotin beads was added to each sample and mixed for 16–20 h (4 °C). On the following day, streptavidin-agarose beads with captured DNA and associated proteins were centrifuged for 3 min at 1800 g, at RT. Most of the supernatant was withdrawn very slowly and carefully. 1 ml of cold lysis buffer (no additives) was added, spun at RT for 5 min, centrifuged for 1 min at 1800 g (RT), and the supernatant was drawn away. The beads were washed 1 time with 1 ml of 1 M NaCl, rotated at RT for 5 min, centrifuged for 1 min at 1800 g (RT), carefully aspirated and the supernatant discarded. Cold lysis buffer (no additives) was added to wash the beads, rotated at RT for 5 min, centrifuged for 1 min at 1800 g, at RT, carefully aspirated and the supernatant discarded. After the last wash, the entire supernatant was aspirated. To elute proteins bound to nascent DNA, 2 × SDS Laemmli sample buffer (2 × SB; 0.4 g SDS, 2 ml 100% glycerol, 1.25 ml 1 M Tris pH 6.8, and 0.01 g bromophenol blue in 8 ml H_2O) was added to the packed beads in a 1:1 ratio. Before using 2 × SB, 1 M DTT was added to a final concentration of 0.2 M. The sample with eluted protein as well as the previously prepared input sample were incubated for 25 min at 95 °C. All samples were then centrifuged for 1 min at 1800 g, at RT. The resulting supernatant was the 2 × eluted capture ready to use for immunoblotting procedure. Both the input sample and the purified iPOND capture sample were tested simultaneously.

DNA fragmentation assay by agarose gel electrophoresis

To examine DNA fragmentation size after sonication, 90 µl of H_2O and 4 µl of 5 M NaCl were added to 5 µl of lysate (control and after treatment with HU) and incubated overnight at 64 °C. Subsequently, samples were treated with 1 µl RNase A (20 mg/ml) for 30 min at 37 °C followed by Proteinase K (Sigma-Aldrich) treatment for 2 h at 45 °C (20 µl of 0.5 M EDTA, 40 µl of Tris pH 6.7 and 10 µl of Proteinase K). According to the procedure used earlier (Żabka et al. 2020), samples containing 10 µl of DNA and 2 µl of gel loading buffer (0.25% bromophenol blue, 30% glycerol in 1 × TAE composed of 40 mM Tris–HCl, 1 mM EDTA, 40 mM acetic acid, pH 8.0) were applied to 1.5% agarose gel in 1 × TAE buffer with ethidium bromide (1 mg/ml) and separated by electrophoresis at 75 V for 3 h at RT.

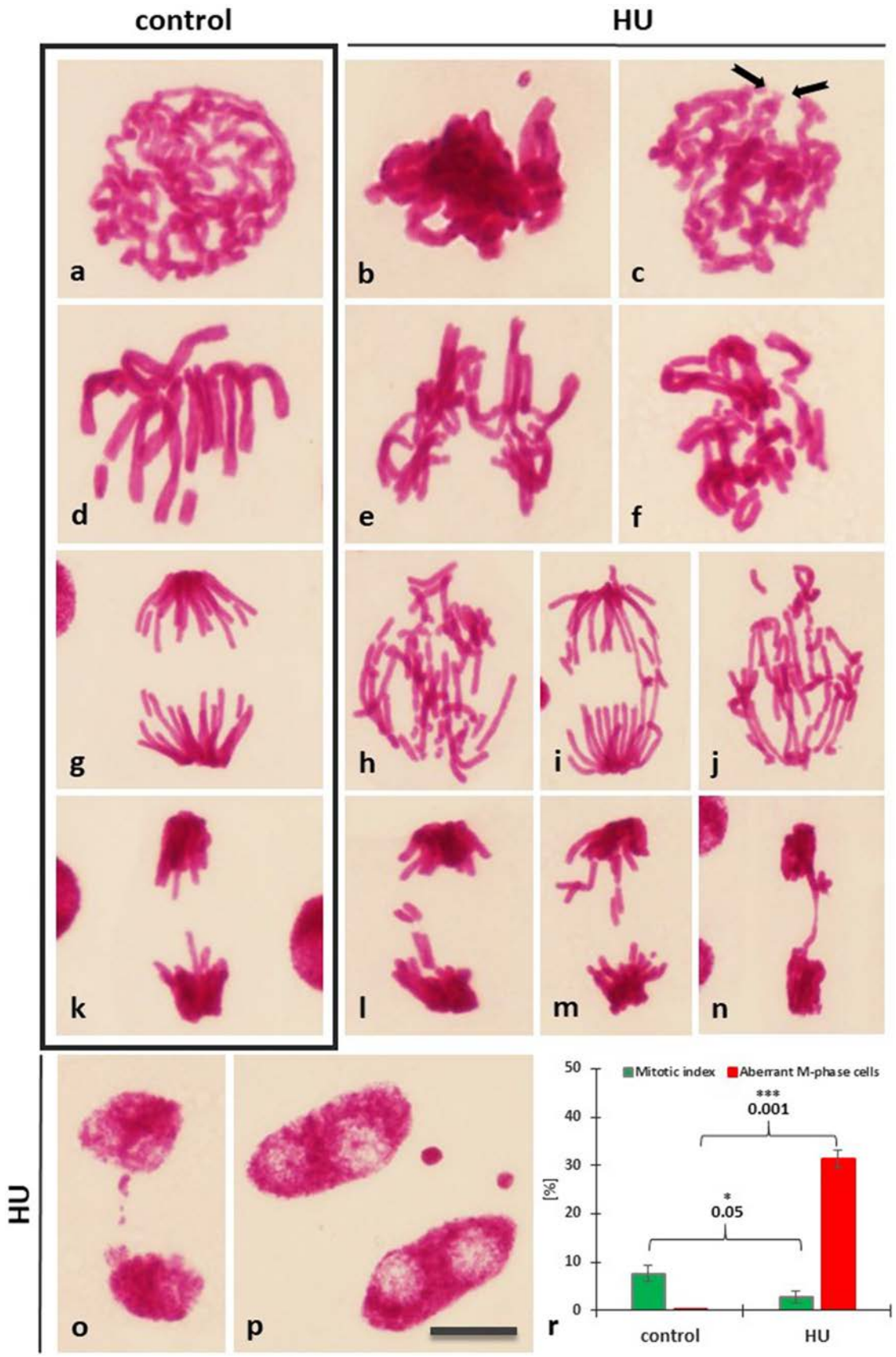
control
HU
a
b
c
d
e
f
g
h
i
j
k
l
m
n
HU
o
p
r
Mitotic index
Aberrant M-phase cells
***
0.001
*
0.05
[%]
50
40
30
20
10
0
control
HU

◂**Fig. 1** Feulgen DNA staining of *V. faba* cell nuclei from the control root meristems in **a** prophase, **d** metaphase, **g** anaphase, **k** telophase, and following 2-h treatment with 3 mM HU: (**b**, **c**) prophase, (**e**, **f**) metaphase, (**h–j**) anaphase, (**ln**) telophase. **o**, **p** Post-telophase cell nuclei with micronuclei formed after treatment with HU. Scale bar 10 µm. (*r*) Mitotic indices (% ± S.D.; green diagrams) and percentage of aberrant M-phase cells (% ± S.D.; red diagrams) in root meristem cells from *V. faba* seedlings after 2-h incubation with HU. Statistically significant change in MI values is marked by asterisks: * indicates $p < 0.05$ and *** indicates $p < 0.001$

UV-fluorescent DNA fragments were photographed using a Gel UV Slider (Phoretix 1D image store system; Phoretix, England) in the Laboratory of Microscopic Imaging and Specialized Biological Techniques at the Faculty of Biology and Environmental Protection (University of Lodz).

Immunoblotting procedure

All proteins were analysed by Western blotting as described previously (Żabka et al. 2010). Proteins from input and capture samples were fractionated on 4–12% Bis Tris/2-(4-morpholino)-ethanesulfonic acid SDS-NuPAGE Novex gel and blotted onto polyvinylidene fluoride membrane (0.2-µm pore size). Post-translational histone modifications and histone H3 were detected using rabbit antibodies: anti-histone H3K56Ac (monoclonal), rabbit anti-histone H4K5Ac (polyclonal), rabbit anti-histone H3T45Ph (polyclonal), and rabbit anti-histone H3 antibodies (polyclonal) diluted to 1:500 using the Chromogenic Western Blot Immunodetection Kit (Invitrogen). Secondary goat anti-rabbit IgG antibody conjugated with alkaline phosphatase were used to detect primary antibodies. Band intensities of histone modifications were quantified by densitometry.

Immunofluorescence detections of acetylation of histone H4 on lysine 5 (H4K5Ac), acetylation of histone H3 on lysine 56 (H3K56Ac), and phosphorylation of histone H3 on threonine 45 (H3T45Ph).

Root meristems were fixed in 4% PBS-buffered paraformaldehyde for 20 min (20 °C). Cell nuclei were isolated, dropped onto slides (procedure according to Żabka et al. 2021a), and after drying, incubated in PBS-buffered 8% BSA and 4% Triton X-100 (Sigma-Aldrich) for 50 min (20 °C). Slides were then incubated with:

1. rabbit polyclonal anti-histone H4K5Ac antibodies (Sigma-Aldrich, dilution of 1:200);
2. rabbit monoclonal anti-histone H3K56Ac antibodies (Abcam, dilution of 1:200);
3. rabbit polyclonal anti-histone H3T45Ph antibodies (Abcam, dilution of 1:100).

The antibodies were dissolved in PBS containing 1% BSA. Incubations were conducted in the dark for 18 h at 4 °C. After washing with PBS, slides were incubated for 1.5 h (20 °C) with Alexa Fluor® 488-conjugated goat anti-rabbit secondary antibodies (1:400; Cell Signaling) counterstained with propidium iodide (PI; 0.3 mg mL-1; control series) or DAPI (HU series) and embedded in a mixture of PBS/glycerol (9:1) with 2.3% DABCO.

AgNOR staining

AgNOR impregnation of the control cells was performed using procedure described by Żabka et al. (2021b). The seedlings were squeezed between two microscope slides to isolate chromosomes. The obtained suspension was dropped onto microscope slides, dried, and fixed with freshly prepared 3:1 methanol–acetic acid mixture (3:1, v/v). Slides were immersed in 2 × SSC at 60 °C for 45 min, rinsed in water, and dried. The freshly prepared staining solution consisting of 0.05% formic acid and 0.5 g of $AgNO_3$ was dropped onto microscope slides (100 mL^{-1} per slide). After covering with a coverslip, slides were put in a wet chamber (80 °C for 3 min), washed with distilled water, dried, and mounted (Canada balsam).

Observations and analyses

Fluorescence intensity analyses, the line plots and Interactive 3D Surface Plots were performed with the ImageJ software. Observations were made using E-600 epifluorescence microscope (Nikon) equipped with phase-contrast optics, U2 filter (UVB light; λ = 340–380 nm) for DAPI, G2 filter (green light; λ = 540/25 nm) for PI-stained cell nuclei, and B2 filter (blue light; λ = 465–496 nm) for Alexa Fluor® 488. Nuclear DNA fluorescence and quantitative analyses were made after converting colour images into greyscale images and expressed in arbitrary units as mean pixel value (pv) spanning the range from 0 (dark) to 255 (white). All data were expressed as the mean values ± standard deviation of the mean (± SD). Student's *t*-tests for paired data were used to compare individual variables. All immunofluorescence analyses were repeated (at least three times).

Identification of individual cells in G1, S, G2 phases (for histone modifications) and in early-, mid-, and late-S phase cells (for EdU) was done, respectively, by microfluorimetric measurements of DNA content (following nuclear staining with DAPI or propidium iodide) and by evaluating of the type of nuclear labelling. Microfluorimetric analyses were carried out with the computerized cytometry (Cytofotometer v1.2 system) and calibrated in arbitrary units (a.u.).

Results

Replication stress (RS) generates chromosomal aberrations

Microscopic analyses of Feulgen stained *V. faba* root meristems treated for 2 h with 3 mM HU revealed a portion of mitotic cells with changes in chromosomal morphology (Fig. 1). Compared to the control seedlings displaying almost exclusively normal mitotic figures (Fig. 1a, d, g, k), 2 h treatment of HU revealed clustered chromosomes in prophase (Fig. 1b), only subtle breaks in the continuity of condensing chromatids (Fig. 1c) and a fraction of cells with chromosomes misaligned from the equatorial metaphase plate (Fig. 1e, f). Other structural aberrations, such as acentric chromosome fragments and chromosomal bridges, were observed in ana- (Fig. 1h–j) and telophase (Fig. 1l–n). Moreover, incubation with HU gave rise to extra-nuclear micronuclei containing lagging chromosomes or broken chromosome fragments that failed to incorporate into the nucleus after cell division (Fig. 1o–p). After 2 h HU treatment, bean root meristems revealed a threefold decrease in the relative number of mitotic cells, and the number of cells with aberrant chromatin morphology reached about 31% (Fig. 1r). Many of the chromosomal changes in *V. faba* resembled the PCC-like cells of *Allium cepa* created after prolonged treatment with low levels (0.75 mM) of HU (Żabka et al. 2012).

HU-induced changes in DNA replication

The effect of a 2-h treatment with 3 mM HU on DNA replication was demonstrated by combining microfluorimetric quantification of DNA content in DAPI-stained cell nuclei (Fig. 2e) with EdU labeling analysis (Fig. 2a–d). Relative numbers of early-, mid-, and late-S phase cells were evaluated as the proportions of cell nuclei with weak (spotted), strong (almost homogeneous) and punctate (specific for heterochromatin) fluorescence staining patterns, respectively. The obtained data showed that the highest percentage of the control cells (about 50%) were in early-S-phase, and the lowest, in the late-S-phase (about 12%; Fig. 2f). HU drastically reduced all subpopulations of S-phase cells (to about 0.5%; Fig. 2f).

Analysis of histone modifications using iPOND

Changes in the post-translational protein modifications at the RFs damaged by HU treatment compared with the RFs from the untreated *V. faba* root meristem cells were made using the iPOND method. The experiments included the impact of replication stress on: (i) histone H3 acetylation on lysine 56 (H3K56Ac), (ii) histone H4 acetylation on lysine 5 (H4K5Ac), (iii) histone H3 phosphorylation on threonine 45 (H3T45Ph), and (iv) histone H3, as a control.

Firstly, to mark newly replicated DNA, roots were incubated for 10 min with EdU, a thymidine analogue. After a brief (10 min) treatment with thymidine, part of the seedlings were incubated for 2 h in 3 mM HU and another part (control) with water (Fig. 3). After cross-linking of proteins and DNA using formaldehyde, meristems were cut off, cell walls were macerated, and a click reaction was performed to combine biotin with EdU. After cell lysis and DNA fragmentation (sonication), proteins close to biotin and EdU-labeled DNA were purified using streptavidin-coated agarose beads.

Both the input samples and the purified iPOND samples were tested using Western blot technique (Fig. 4a). Due to the selective effect of the iPOND procedure, all input samples (with the exception of the H3 histones obtained from HU-treated root cells) resulted in stronger bands (differences statistically significant). Immunoblotting analysis of iPOND-captured proteins combined with quantitative densitometric analyses showed that the amounts of H4K5Ac histones in HU-treated cells was increased, compared with the control series (Fig. 4a, b). In contrast to the above series, no significant differences were found in the quantities of iPOND-captured H3K56Ac, and H3T45Ph (Fig. 4b).

Densitometric plots of iPOND/Western blot bands showed that the levels of H3K56Ac and H3T45Ph in the control and H3K56Ac in the HU-treated samples were twofold lower compared to histone H3. Slightly higher values than those for total H3 were observed after HU treatment for H4K5Ac and H3T45Ph modifications (Fig. 4c).

In order to evaluate the extent of DNA fragmentation, the agarose gel electrophoresis was used (Fig. 4d). In both the control and HU-treated samples, the highest density of chromatin fragments ranged between 2000 and 4000 bp (Fig. 4d).

Acetylation of histone H3 on lysine 56 (H3K56Ac)

HU-induced changes in histone 3 lysine-56 acetylation (H3K56Ac) were estimated by quantitation of the average number of intranuclear immunofluorescence foci, evidenced in G1, S and G2 phase cells (having 2, 2-4C and 4C DNA contents, respectively; Fig. 5a–f) by the Interactive 3D Surface Plot analysis (Fig. 5a'–f'). Both in the control and HU-treated root meristems, H3K56Ac foci were spread throughout the nuclear chromatin region (Fig. 5a–f) and localized at the border of the nucleolus and perinuclear chromatin (Fig. 5b, c). Incubation with HU brought about an increase in the average number of H3K56Ac histone foci at all stages of the cell cycle with the largest (nearly twofold) rise in the G1 and G2 phases of interphase (Fig. 5g).

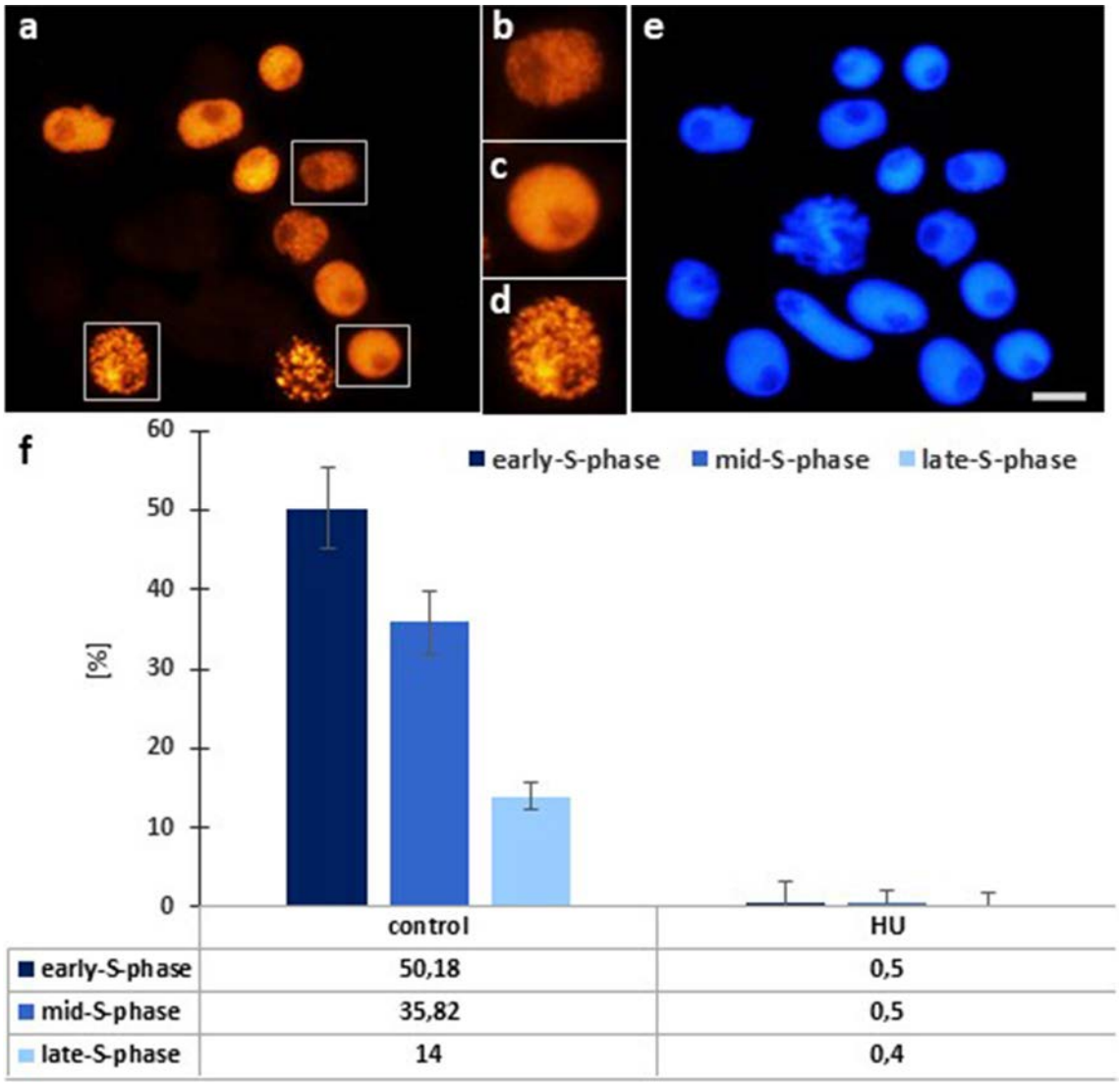

	control	HU
early-S-phase	50,18	0,5
mid-S-phase	35,82	0,5
late-S-phase	14	0,4

Fig. 2 DNA replication in *V. faba* root cell populations evidenced by EdU incorporation. **a** Control cell population (boxes indicate cell nuclei shown at higher magnification), **b** early S-phase, **c** middle S-phase, **d** late S-phase; **e** cell population stained with DAPI corresponds with the population of EDU stained cells in Fig. 2a. Scale bar = 20 µm. **f** Fractions [(%) ± SD] of early-, mid-, and late-S-phase cells, calculated by combining microfluorimetric quantitation of DNA contents in DAPI-stained cell nuclei and visual analysis of EdU fluorescence patterns

Acetylation of histone H4 on lysine 5 (H4K5Ac)

As compared to the previously described punctate (focal) distribution of chromatin regions enriched in lysine 56-acetylated H3 histones (H3K56Ac, characteristic of all types of nuclei both in the control and HU-treated root meristem cells in *V. faba*), immunofluorescence analysis of H4K5Ac revealed a considerably greater number of nuclear labeling patterns. The investigations performed throughout the whole cell cycle included quantitative estimation of: (1) cell nuclei with more or less homogeneous immunofluorescence staining, typical of euchromatin (Fig. 6a, b, a'–b'), (2) cell nuclei with large fluorescent areas of heterochromatin (Fig. 6c, d, c', d'), and (3) cell nuclei with intensely stained nucleoli, mainly associated with weaker or stronger labeling of euchromatin (Fig. 6e, f, e', f'). The performed analyses revealed that the relationships between the discerned nuclear areas enriched in H4K5Ac and different cell cycle stages are modified by HU-induced stress conditions, which is manifested by considerable changes in the proportions of cell nuclei with dominant immunofluorescence of euchromatin, heterochromatin, and/or nucleolar domains (Fig. 7a–c). Compared to the control population, a marked decrease in the intensity of H4K5Ac fluorescence in HU-treated root meristems was observed both in euchromatic-type nuclei (comprising mostly decondensed chromatin; Fig. 7a) and

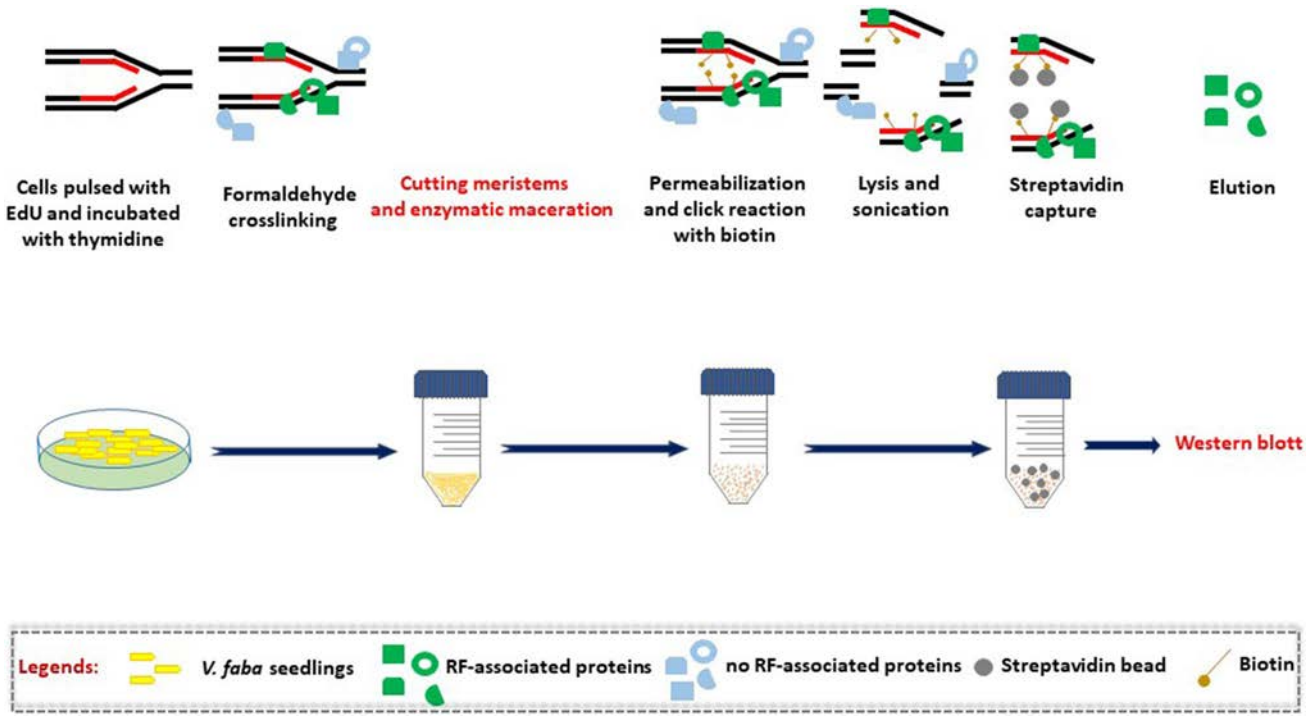

Fig. 3 Graphical representation of the iPOND technique principles

in the heterochromatic-type nuclei (comprising numerous clusters of condensed chromatin; Fig. 7b). Furthermore, at both G1 phase (in the control and HU-treated root meristems) and early S phase (in HU-treated plants), no cell nuclei were found with strongly stained condensed heterochromatin regions (Fig. 7b).

In most cases, intense fluorescence of nucleoli was associated with more or less stained euchromatin background (Fig. 6e); moreover, the nucleoli were often surrounded by a circle of fluorescing dots (Fig. 6f). In contrast to eu- and heterochromatic-type nuclei described above, the population of cells with heavily stained nucleoli increased considerably in HU-treated *V. faba* root apical meristem (RAM) cells (starting from early S- up to G2 phase of the cell cycle; Fig. 7c). The fluorescence spots visible in prometaphase and anaphase (in the control, Fig. 8a, b)) and metaphase (after treatment with HU; Fig. 8c) correspond probably to brown chromosomal nucleolus-organizing regions (NORs) identified using silver staining procedure (AgNOR; Fig. 8d, e).

Phosphorylation of histone H3 on threoninie 45 (H3T45Ph)

Control and HU-treated root meristem cells labeled using anti-H3T45Ph immunofluorescence procedure displayed various nuclear and nucleolar staining patterns (Figs. 9, 10). Frequently, strong fluorescent labeling of nucleoli was accompanied by more or less intense fluorescence of the nuclear region (Figs. 9a–d, a'–d'), whereas weekly stained nucleoli were surrounded by a garland of immunofluorescent dots (Fig. 9e, e').

Fluorescence intensity (FI) analysis of the whole nuclear areas in the G1, S, and G2 phase cells (Fig. 10), combined with line scans of fluorescence intensity (plots) through the nucleolar region revealed significantly higher levels of fluorescence in the nuclei of HU-treated meristematic cells (about 20% increase; Fig. 10a–c, a'–c') than in the chromatin regions in the control cell nuclei (Fig. 10d–f, d'–f'). Both in the control and HU-treated root meristems, the FI values scored for the G2-phase cells were found significantly lower than that for the G1 and S phase cells.

Discussion

The process of DNA replication requires both the dissociation of histones, separation of DNA strands and an integrated way of reassembling chromatin on the two DNA duplexes. Since both DNA replication and cellular response to replication stress (RS) occur in the context of chromatin, histone dynamics as well as functioning of proteins involved in the induction and progression of nuclear replication play a key roles in modulating replication forks (RFs) progression (Hsu et al. 2014; Zeman and Cimprich 2014). Prolonged disruption and/or inhibition of replication carries a high risk of altering newly formed chromatin in ways that can modify

epigenetic information, affect the spatial organization of DNA and deregulate gene expression (Khurana and Oberdoerffer 2015).

Investigating the process of DNA replication, chromatin folding and maturation and, in particular, the response to RS is a major challenging task in the context of plant material. Our previous research on RS has focused around prolonged treatment of *Allium cepa* root meristems with low (0.75 mM) concentrations of HU or 5-aminouracil (5-AU), causing either premature chromosome condensation (PCC) or an abnormal organization of nuclear structures forming interphase and mitotic (IM) domains of chromatin at opposite poles of the IM cell nucleus (Żabka et al. 2010, 2012, 2015, 2020). We have shown that long-term incubation with 0.75 mM HU results in the raised levels of cyclin B-like proteins (Żabka et al. 2010) and increased production of reactive oxygen species (ROS), leading to DNA damage (manifested by γ-phosphorylation of histone H2AX and chromosomal aberrations; Żabka et al. 2012). We also provided evidence that there is an association between the opposite poles of IM cell nuclei and the polarized accumulation sites of auxin efflux carriers (PIN2 proteins) and IAA (auxins; Żabka et al. 2015). Furthermore, we have shown that continuous treatment of onion cells with 5-AU is linked with accelerated dynamics of the DNA replication machinery and significantly increased levels of transcription and translation (Żabka et al. 2020).

Since, more recently, our research has focused on RS and epigenetic modifications after cadmium treatment (Żabka et al. 2021a, b), we, therefore, began to search for a more sensitive method that would allow the analysis of post-translational histone modifications in active and inhibited or damaged RFs. Our attention and interest was drawn to a technique called iPOND (isolation of proteins on nascent DNA), first published in 2011 by Sirbu et al. (2011), which provides a high-resolution spatial–temporal analysis of proteins in RFs. This method, developed for animal cells, is used: (1) to identify proteins associated with active replisomes, (2) to monitor changes in chromatin located at different distances from RFs and, (3) to detect protein recruitment or post-translational modifications of proteins in damaged forks (Sirbu et al. 2011, 2012, 2013). The iPOND technique makes it possible to obtain proteins bound directly or indirectly to the nascent DNA. In this procedure, the nascent DNA is labeled with 5-ethynyl-2′-deoxyuridine (EdU; a nucleoside analogue of thymidine), which, via an alkyne group, enables copper-catalysed cycloaddition (click chemistry) to the biotin azide, ultimately yielding a stable covalent bond. This facilitates the purification of EdU-labeled DNA–protein complexes, using streptavidin-coated beads. After a final elution, the resulting proteins and their modifications can be analyzed by Western blot or mass spectrometry (Sirbu et al. 2011; Olcina et al. 2016; Sirbu et al. 2013).

While the complex role of chromatin in the DNA replication process has been studied for many years (Bellush and Whitehouse 2017), it is now thought that the key aspects of the RS response are also linked to chromatin. Our current research, conducted on *V. faba* root meristem cells, has focused on understanding issues related to changes in epigenetic patterns following short-term exposure to HU-induced RS. To achieve this, three histone modifications were investigated using the iPOND technique combined with immunocytochemical labeling: (i) acetylation of histone H3 at lysine 56 (H3K56Ac), (ii) acetylation of histone H4 at Lys 5 (H4K5Ac), (iii) phosphorylation of histone H3 at threonine 45 (H3T45Ph).

Adaptation of the iPOND technique to plant material required overcoming of several difficulties. The first and most important step was the selection of the material and the acquisition of sufficient quantities of cells. According to Sirbu et al. (2013), each research sample necessitates approximately 1×10^8 of human cells for efficient capture of replicon proteins. The large number of cells needed for iPOND procedure is dictated by the sensitivity of the immunoblotting detection method. Taking into account a large nuclear DNA content (26.7 pg/2C nucleus) and a great number of cells per root meristem (about $12\,115 \pm 1295$), we considered *V. faba* as an excellent material for the iPOND procedure. Another important modification was the enzymatic digestion of the cell walls. HU (3 mM) was used as a replication stress factor to arrest active replisomes and DNA synthesis (tested using EdU) and to facilitate the analysis of histone modifications with transiently or permanently arrested RFs.

Various post-translational modifications of histones, such as acetylation, methylation and phosphorylation, regulate many cellular processes, including gene transcription, DNA replication and repair (Goldberg et al. 2007; Han et al. 2007a, b; Li et al. 2007). Newly formed histone H3/H4 molecules undergo acetylation prior to their incorporation into chromatin. Acetylation of histone H3 on lysine 56 (H3K56Ac) is unique in that it is recognized as a marker of newly synthesized H3 molecules and occurs mainly during S-phase, suggesting that this modification is involved in DNA replication (Hans and Dimitrov 2001; Bej and Basak 2017; Mursalimov et al. 2019). Since H3K56Ac is also a key modification that occurs in response to DNA damage (Wang et al. 2008; Fu et al. 2013; Gates et al. 2017; Mursalimov et al. 2019) and its level increases during S-phase (Mursalimov et al. 2019), we monitored histone H3 acetylation on lysine 56 during the cell cycle progression. Using the iPOND method, a strong H3K56Ac band in both control and HU-treated cells was observed, clearly demonstrating the validity of the applied technique, but we did not find increased levels of H3K56 acetylation on newly deposited histones after HU treatment. In contrast, immunocytochemical studies showed

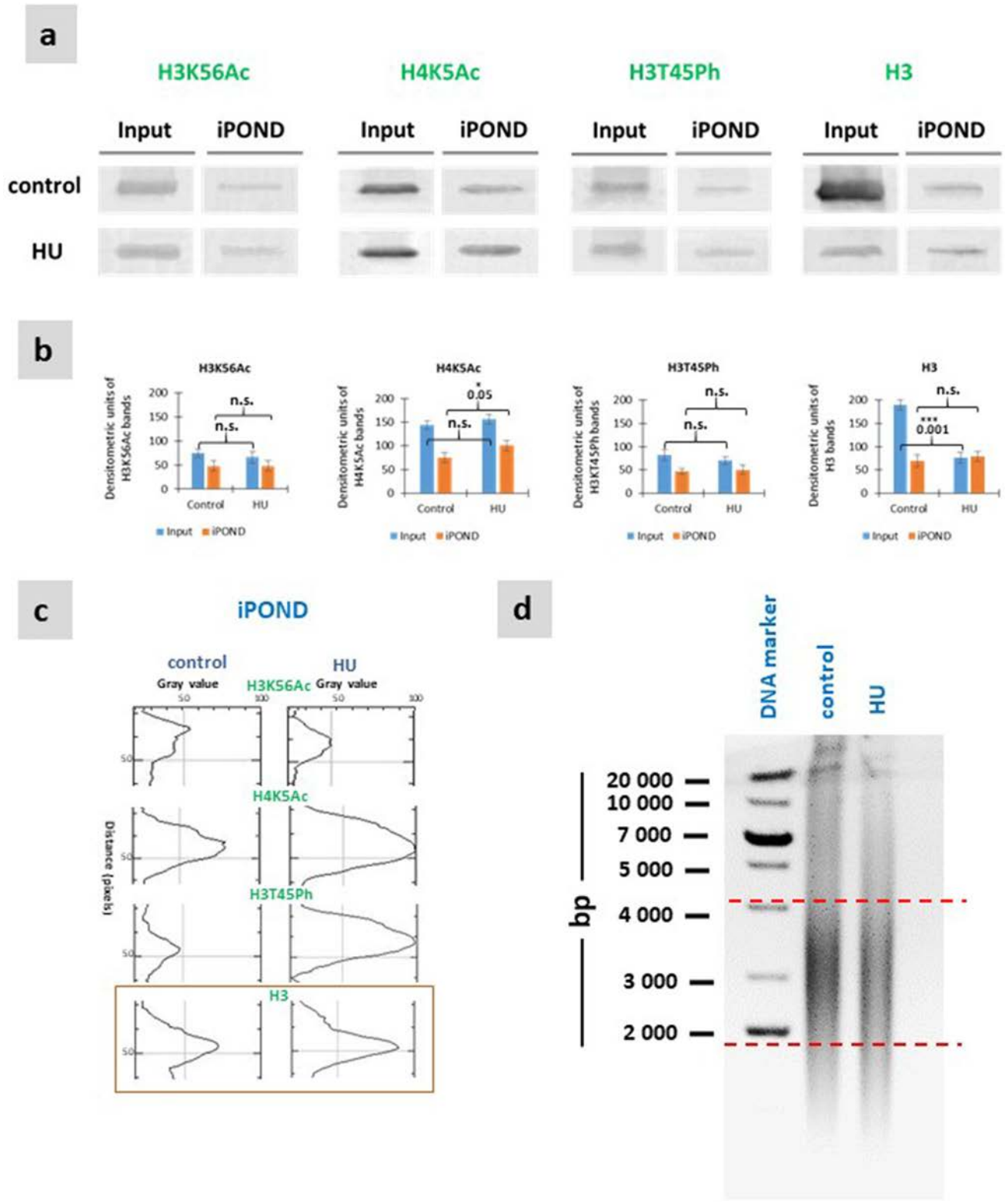

that, compared to untreated material, HU-treated cells displayed a significant increase in the mean number of intranuclear foci, which is consistent with our previous studies using $CdCl_2$-induced replication stress (Żabka et al. 2021a). Thus, the results obtained with these methods appear to be good indicators of DNA damage and support the theory of Masumoto et al. (Masumoto et al. 2005) that cells with DNA strand breaks maintain high levels of H3K56 acetylation and

◂**Fig. 4** Immunoblot analysis and densitometry graphs showing post-translational histone modifications. **a** Input and EdU-associated proteins (iPOND) were analysed by Western blot using antibodies against H3K56Ac, H4K5Ac, H3T45Ph, and H3. **b** Densitometry plots showing the intensity of the bands (for the SDS-PAGE gel). **c** Densitometric plots of iPOND/Western blot bands for control and HU showing the ratio of histone modifications H3K56Ac, H4K5Ac, H3T45Ph to total histone H3. **d** DNA fragmentation detected with agarose gel electrophoresis of DNA extracted *V. faba* root meristem cells: lane 1—mass marker, lane 2—control, and lane 3—HU treatment for 2 h. Statistically significant changes (±SD) in the intensity of the bands (for the SDS-PAGE gel) (±SD) were assessed with Student's t–test. The lack of significance is indicated by "n.s." (not significant)

that the maintenance of this modification depends on DNA damage checkpoint proteins, creating favorable chromatin environment for DNA repair.

During replication, both 'old' and 'new' nucleosomes are deposited on each of the two DNA strands (Serra-Cardona and Zhang 2018). De novo synthesized histone H4 carries acetyl marks on lysines 5 and 12 (Grover et al. 2018). Using iPOND technique, we showed that acetylation of histone H4 on lysine 5 (H4K5ac), which is more associated with DNA replication than transcription (Jasencakova et al. 2000; Żabka et al. 2021a), was significantly increased in HU-treated plants, suggesting a strong connection with cell cycle arrest during S phase. It can be inferred that H4K5ac may be a key epigenetic modification in the regulation of cell cycle arrest (Wang et al. 2008) and may have an important regulatory role in DNA replication (Żabka et al. 2021b).

Our immunofluorescence experiments indicate that the distribution of histone H4K5Ac in untreated cell nuclei is highly dependent on both the cell cycle phase and the intranuclear localization within territories occupied by euchromatin, heterochromatin or nucleoli. It was shown that the 2 h HU treatment drastically reduced the distribution of H4K5Ac in the euchromatin region in all phases of the cell cycle (especially in G1-phase) and that there was no or negligible labeling of H4K5Ac in the heterochromatin region in G1-phase and early S-phase. Histone H4K5 acetylation plays an important regulatory role in both DNA replication and transcription (Jasencakova et al. 2001). Each of these processes requires transient unwinding of DNA strands, making them extremely susceptible to ROS-induced damage (Chan et al. 2012). In fact, irrespectively of the character of the inhibitory effect exerted by HU (either primary, via inhibition of RNR, or secondary, via excess of generated ROS) suppression of DNA metabolism may result in erosion of epigenetic markers observed at all stages of interphase. Such an effect would be similar to the decrease in histone H4K5 acetylation observed in *V. faba* RAM cells after treatment with cadmium (Żabka et al. 2021a). In contrast, the process of H4K5 acetylation in the nucleolar regions is less susceptible to HU, which, according to other authors (Sogo et al. 1984; Conconi et al. 1989, 1992; Dammann et al. 1993) can be explained by the fact that transcriptionally active rDNA genes are devoid of nucleosomes. In addition, both studies in barley (Idei et al. 1996) and our earlier experiments in bean (Żabka et al. 2021b) showed that the fluorescent spots visible in mitotic chromosomes topologically corresponded to NORs, as visualized using silver staining procedure (AgNOR). The specific pattern of H4K5 acetylation in NORs observed in *V. faba* root meristems, which does not correlate with either replication or transcriptional activity, seems explainable on the assumption of Jeppesen (et al. 1997). According to this concept, epigenetic markers established by histone acetylation may represent a mechanism for the propagation of 'cellular memory', whereby genes in chromatin regions active prior to mitotic division are marked by histone acetylation and, as a consequence, have the potential to be preferentially reactivated in the G1 phase of the new cell cycle. Acetylated H4 histones may then act as 'markers' for proteins required during the subsequent interphase to initiate early transcription and metabolic reactivation.

Phosphorylation of histone H3 on threonine 45 (H3T45Ph), like acetylation of histone H3 on lysine 56, is an important modification that occurs during DNA replication and is required for chromatin reassembly (Hyland et al. 2005; Baker et al. 2010). In the yeast *Saccharomyces cerevisiae*, this phosphorylation regulates many nuclear functions, including DNA damage repair, transcription, mitosis, apoptosis and sporulation (Ito et al. 2007; Hurd et al. 2009; Żabka et al. 2021a). Using the iPOND technique in *V. faba* root meristem cells, no increased levels of H3T45Ph phosphorylation have been found on newly deposited histones after HU treatment. In contrast, immunocytochemical studies showed that the 2 h incubation with HU resulted in a slight but significant increase in H3T45Ph fluorescence; a similar result was obtained for *S. cerevisiae* (Baker et al. 2010). This results may be consistent with the theory of Lee et al. (2015) that phosphorylation of H3T45 by protein kinase B (AKT) facilitates transcriptional activation of DNA damage-induced genes.

Despite extensive knowledge of RS and its negative effects in animals, the molecular aspects of RS induction in the plant cell world are still poorly understood. The iPOND method is an excellent proteomic tool to facilitate the identification and quantification of mechanisms involved in DNA replication, chromatin maturation and the response to RS (Cortez et al. 2017). This technique offers a wide range of possibilities, related to the determination of protein dynamics and posttranslational modifications in active, arrested and collapsed RFs (Żabka et al. 2010; Sirbu et al. 2011, 2012). Adoption of this method allows to identify chromatin-associated proteins and factors involved in RS. Certainly, the iPOND method may prove to be a key first step for a more

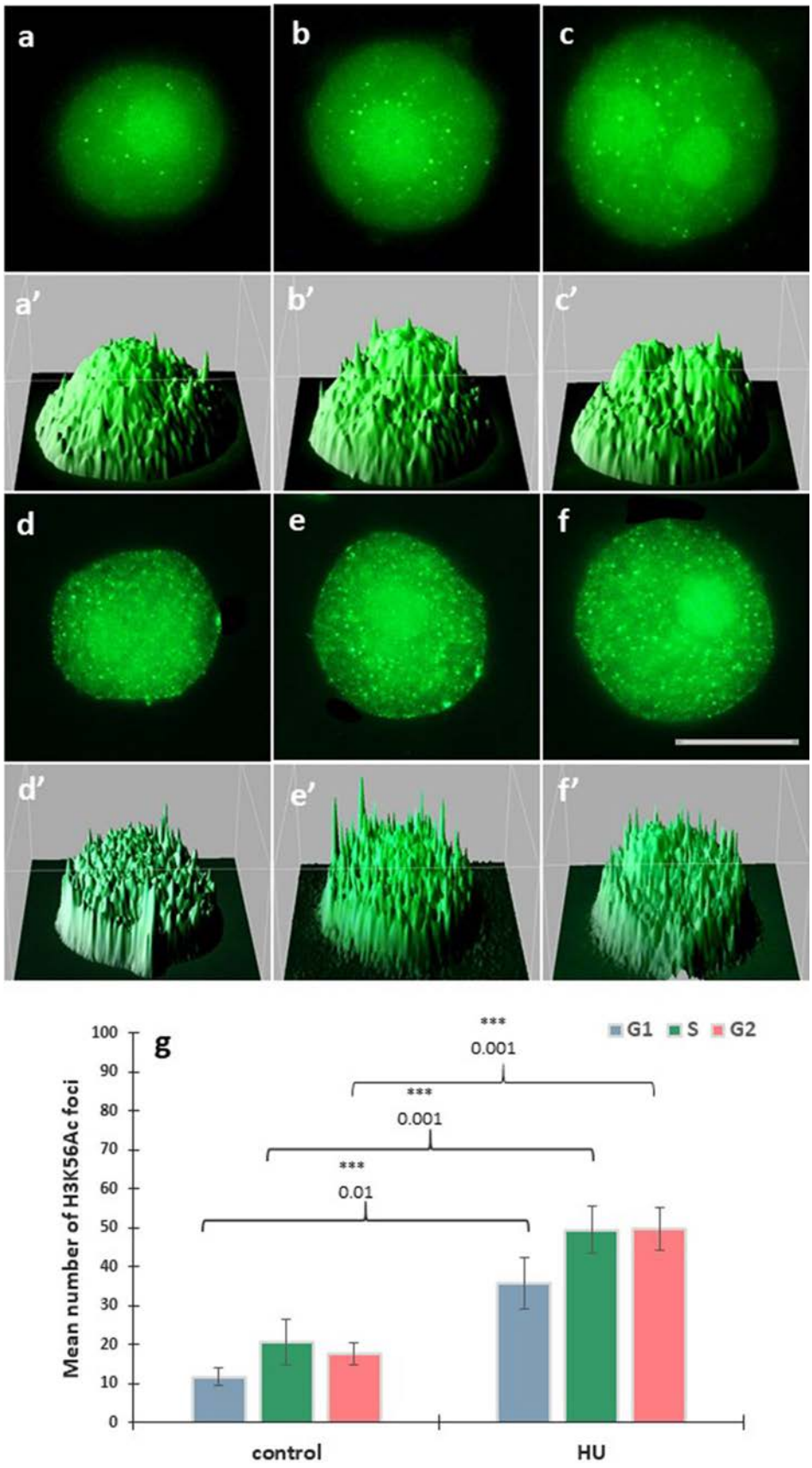

Fig. 5 Immunofluorescence detection of H3K56Ac in cell nuclei from the control (**a–c**) and HU-treated root meristems (**d–f**) in the G1 (**a**, **d**), S (**b**, **e**), and G2 phases (**c**, **f**); scale bar = 10 µm. Below of each micrograph, corresponding interactive 3D surface plots (**a'–f'**). Mean number of H3K56Ac foci in G1, S, G2 phase nuclei in the control and HU-treated root meristem cells (**g**). Statistically significant changes in the intensity of H3K5Ac fluorescence (± SD) were assessed with Student's *t*-test

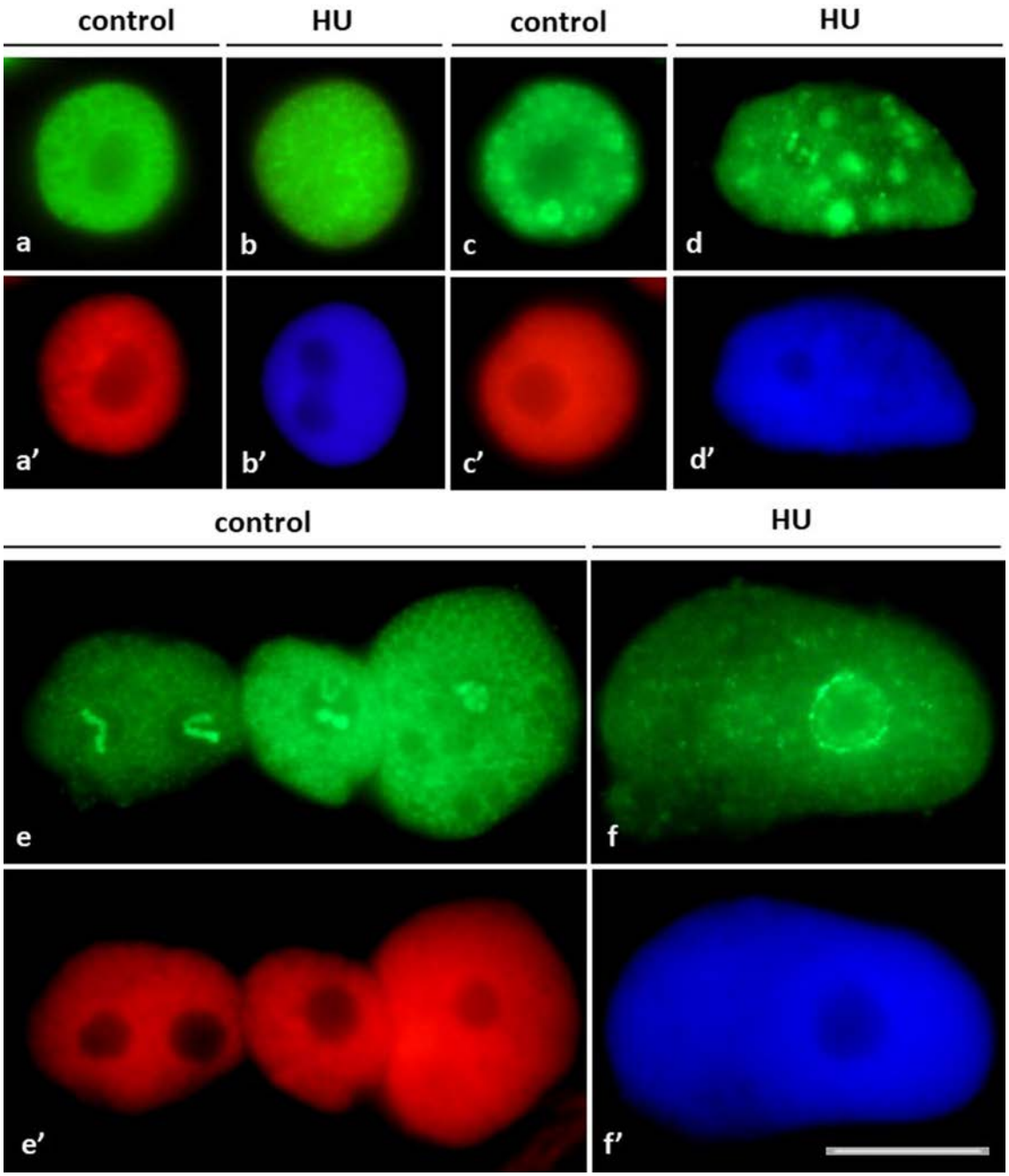

Fig. 6 Intranuclear distribution of H4K5Ac immunofluorescence. **a**, **b** Cell nuclei with immunostained euchromatin areas: **a** control, **b** HU-treated cells and corresponding images of cell nuclei stained with propidium iodide (**a**') and DAPI (**b**'). **c**, **d** Cell nuclei with immunostained heterochromatin areas: **c** control, **d** HU-treated cells and corresponding images of cell nuclei stained with propidium iodide (**c**') and DAPI (**d**'). **e**–**f** Cell nuclei with nucleolar staining: **e** control, **f** HU-treated cells and corresponding images of cell nuclei stained with propidium iodide (**e**') and DAPI (**f**'). Scale bar = 10 µm

in-depth understanding of the mechanism of DNA replication and cell's response to RS in plants, and may bring new data on how histone modifications, coincide with the key aspects of the RS response.

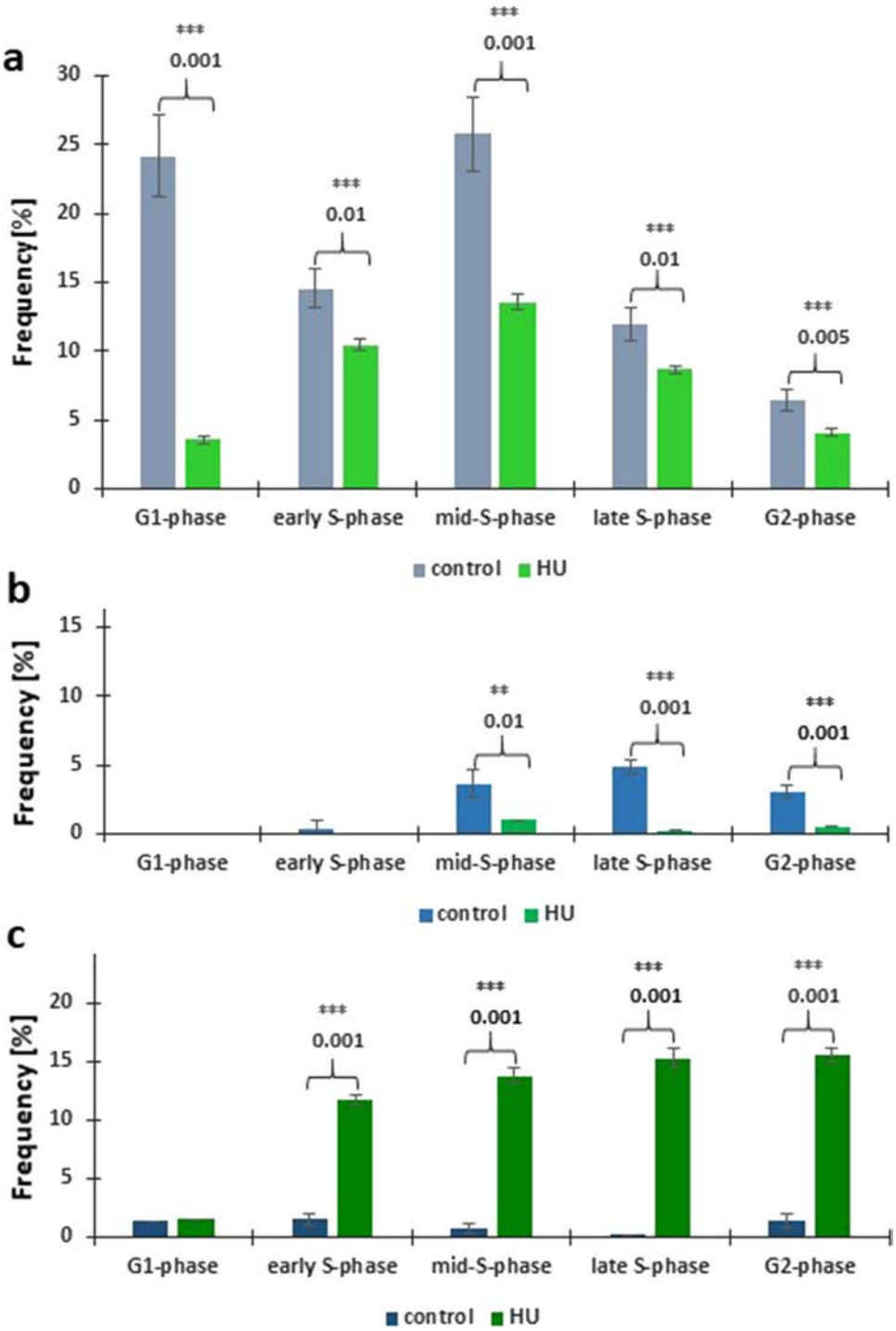

Fig. 7 **a–c** Frequencies (% ± SD) of nuclei with H4K5Ac immunolabeling localized in: **a** euchromatic, **b** heterochromatic, **c** and nucleolar regions, discriminated with respect to successive stages of the cell cycle in root meristems. Statistically significant changes in the intensity of H4K5Ac fluorescence (± SD) were assessed with Student's *t*-test

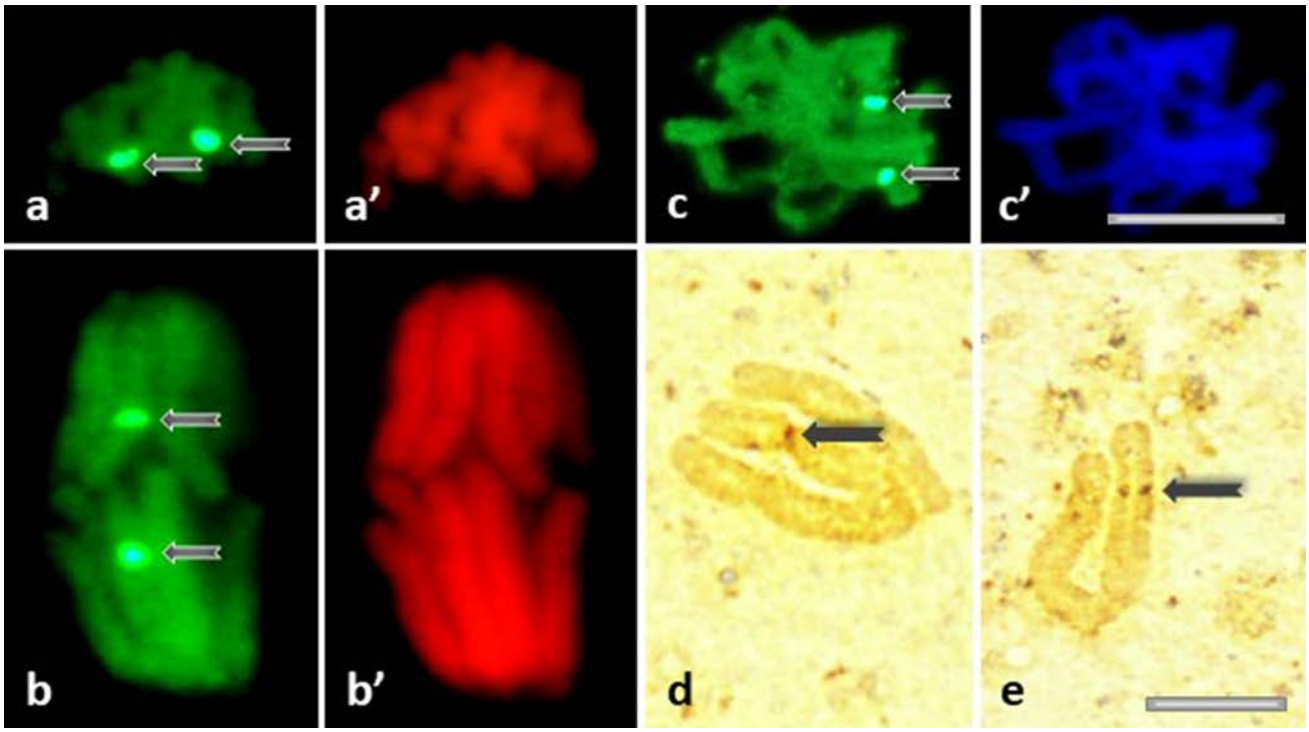

Fig. 8 **a–c** H4K5Ac immunofluorescence labeling of the chromosomal areas corresponding to the nucleolus-organizing regions (NORs) in the control root meristems during: prometaphase (**a**), anaphase (**b**), and in the HU-treated cells during metaphase (**c**). The corresponding images of cell nuclei stained with propidium iodide (**a'**, **b'**) and DAPI (**c'**). **d**, **e** AgNOR staining of the control chromosomes: NOR-carrying isolated metaphase chromosomes. Arrows show NORs regions. Scale bar = 10 µm

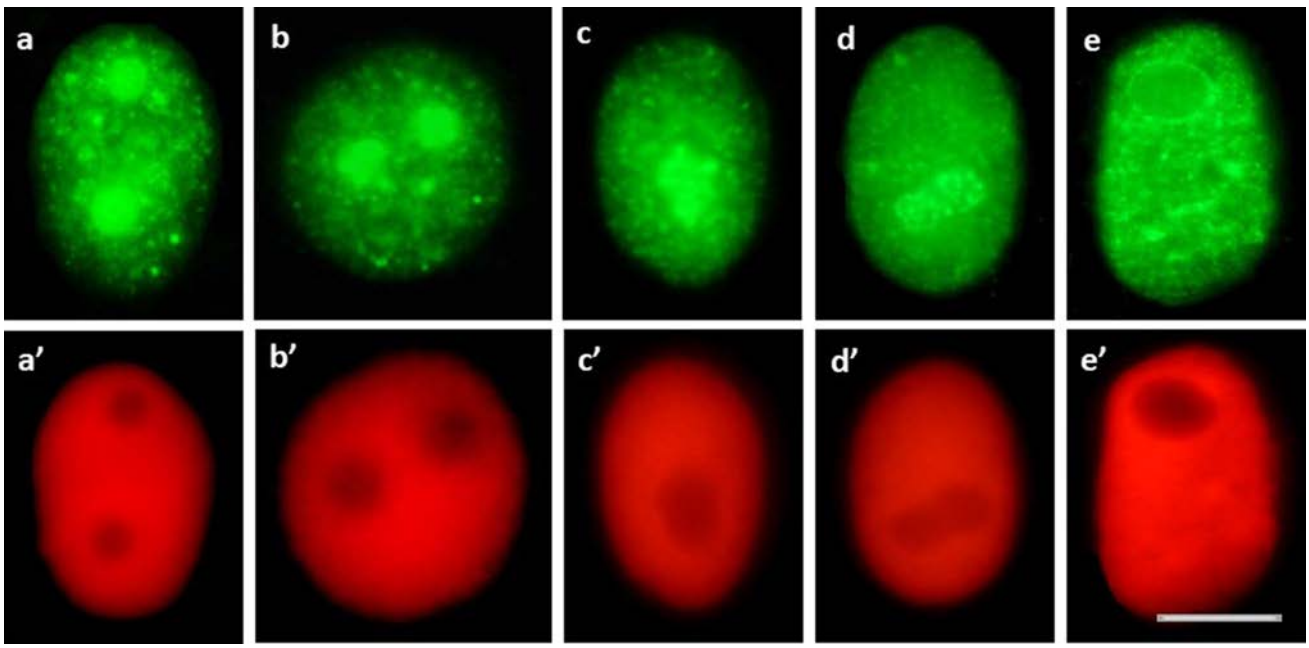

Fig. 9 Different immunofluorescence patterns observed in root meristem cell nuclei using antibodies against H4T45Ph (**a–e**) and corresponding images of cell nuclei stained with propidium iodide (**a'**–**e'**). The control cells revealed predominant nucleolar staining of H4T45Ph (**a**–**d**) and specific labeling around the nucleoli (**e**). Scale bar = 10 µm

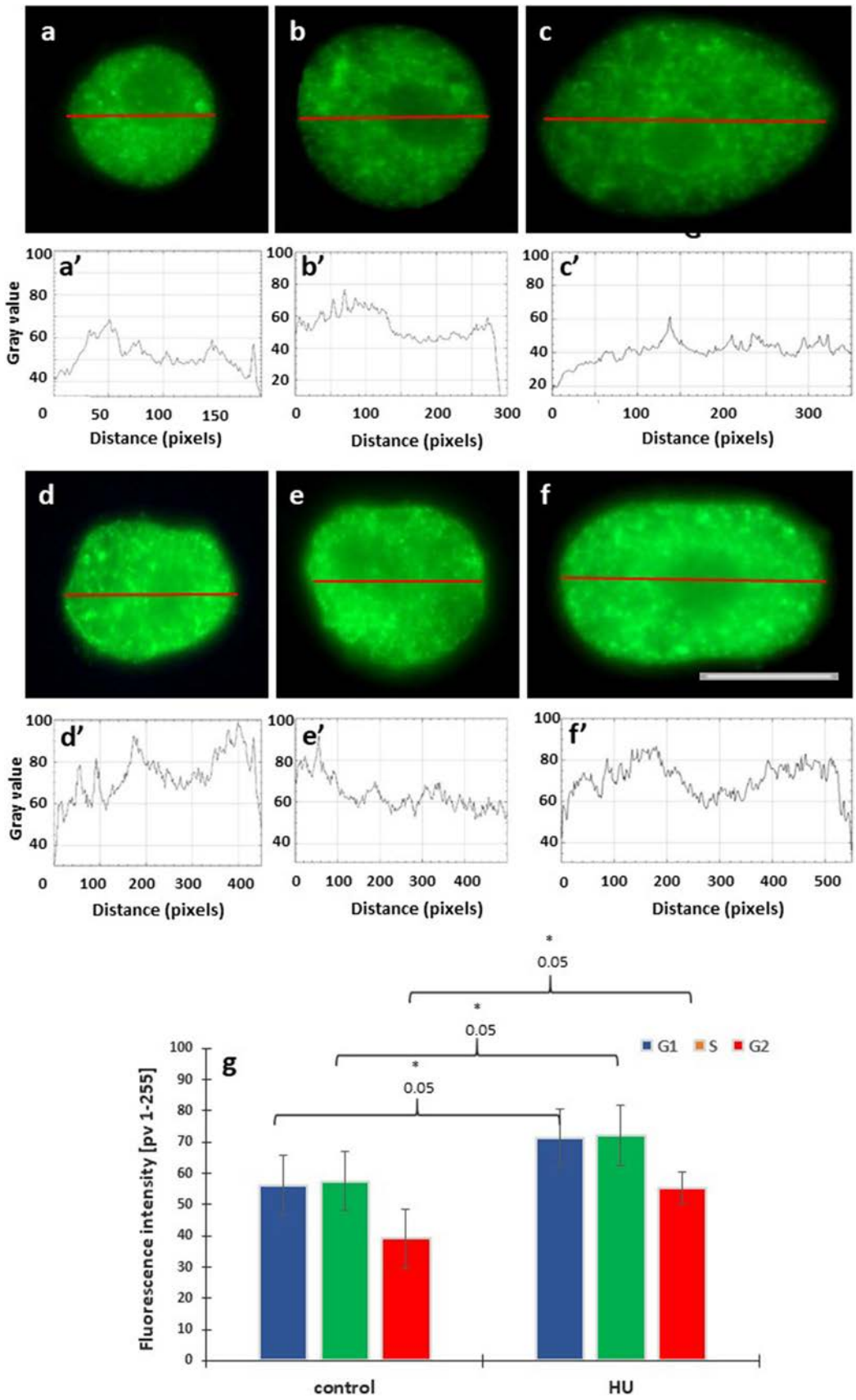
a
b
c
a'
b'
c'
Gray value
Distance (pixels)
d
e
f
d'
e'
f'
Gray value
Distance (pixels)
g
0.05
0.05
0.05
G1
S
G2
Fluorescence intensity [pv 1-255]
control
HU

◂**Fig. 10** Immunofluorescence detection of H3T45Ph in cell nuclei from the control (**a**–**c**) and HU-treated seedlings of *V. faba* (**d**–**f**), in the G1 (**a**, **d**), S (**b**, **e**) and G2 phases (**c**, **f**); scale bar = 10 µm. Densitometric plots showing changes in fluorescence of the nuclear and nucleolus regions in the control (**a**'–**c**') and HU-treated cells (**d**'–**f**'). Mean H3T45Ph fluorescence intensity of G1, S, G2 phase nuclei in the control and HU-treated meristem cells (**g**). Statistically significant changes in the intensity of H3K5Ac fluorescence (± SD) were assessed with Student's *t*-test

Author contribution statement AŻ planned and carried out the experiments and prepared the first draft of the article. NG and JTP equally contributed to acquisition of the results and performed the statistical analyses. JM participated in the design of the study and prepared the final version of the manuscript. All authors have read and agreed to the published version of the manuscript.

Funding This work was supported by a grant 2019/03/X/NZ3/00477 from the National Science Centre.

Data availability The datasets generated and/or analysed during the current study are available from the corresponding author on reasonable request.

Declarations

Conflict of interest The authors declare no conflict of interest.

References

Baker SP, Phillips J, Anderson S, Qiu Q, Shabanowitz J, Smith MM, Yates JR, Hunt DF, Grant PA (2010) Histone H3 Thr 45 phosphorylation is a replication-associated post-translational modification in *S. cerevisiae*. Nat Cell Biol 12:294–298

Bej S, Basak J (2017) Abiotic stress induced epigenetic modifications in plants: how much do we know? In: Rajewsky N, Jurga S, Barciszewski J (eds) Plant epigenetics. Springer, Cham, pp 493–512

Bellush JM, Whitehouse I (2017) DNA replication through a chromatin environment. Philos Trans R Soc Lond B Biol Sci 372:1731

Bryant JA, Aves SJ (2011) Initiation of DNA replication: functional and evolutionary aspects. Ann Bot 107:1119–1126

Casas-Delucchi CS, Cardoso MC (2011) Epigenetic control of DNA replication dynamics in mammals. Nucleus 2:370–382

Chan K, Sterling JF, Roberts SA, Bhagwat AS, Resnick MA, Gordenin DA (2012) Base damage within single-strand DNA underlies in vivo hypermutability induced by a ubiquitous environmental agent. PLoS Genet 8:e1003149

Conconi A, Widmer RM, Koller T, Sogo JM (1989) Two different chromatin structures coexist in ribosomal RNA genes throughout the cell cycle. Cell 57:753–761

Conconi A, Sogo JM, Ryan CA (1992) Ribosomal gene clusters are uniquely proportioned between open and closed chromatin structures in both tomato leaf cells and exponentially growing suspension cultures. Proc Natl Acad Sci USA 89:5256–5260

Cortez D (2017) Proteomic analyses of the eukaryotic replication machinery. Methods Enzymol 591:33–53

Dammann R, Lucchini R, Koller T, Sogo JM (1993) Chromatin structures and transcription of rDNA in yeast *Saccharomyces cerevisiae*. Nucleic Acids Res 21:2331–2323

Driscoll R, Hudson A, Jackson SP (2007) Yeast Rtt109 promotes genome stability by acetylating histone H3 on lysine 56. Science 315:649–652

Fragkos M, Ganier O, Coulombe P, Méchali M (2015) DNA replication origin activation in space and time. Nat Rev Mol Cell Biol 16:360–374

Fu H, Maunakea AK, Martin MM, Huang L, Zhang Y, Ryan M, Kim RG, Lin CM, Zhao K, Aladjem MI (2013) Methylation of histone H3 on lysine 79 associates with a group of replication origins and helps limit DNA replication once per cell cycle. PLoS Genet 9:e1003542

Gates LA, Shi J, Rohira AD, Feng Q, Zhu B, Bedford MT, Sagum CA, Jung SY, Qin J, Tsai MJ, Tsai SY, Li W, Foulds CE, O'Malley BW (2017) Acetylation on histone H3 lysine 9 mediates a switch from transcription initiation to elongation. J Biol Chem 292:14456–14472

Gentric N, Genschik P, Noir S (2021) Connections between the cell cycle and the DNA damage response in plants. Int J Mol Sci 22:9558

Goldberg AD, Allis CD, Bernstein E (2007) Epigenetics: a landscape takes shape. Cell 128:635–638

Grover P, Asa JS, Campos EI (2018) H3–H4 histone chaperone pathways. Ann Rev Genet 52:109–130

Han J, Zhou H, Horazdovsky B, Zhang K, Xu R-M, Zhang Z (2007a) Rtt109 acetylates histone H3 lysine 56 and functions in DNA replication. Science 315:653–655

Han J, Zhou H, Li Z, Xu R-M, Zhang Z (2007b) Acetylation of lysine 56 of histone H3 catalyzed by RTT109 and regulated by ASF1 is required for replisome integrity. J Biol Chem 282:28587–28596

Hans F, Dimitrov S (2001) Histone H3 phosphorylation and cell division. Oncogene 20:3021–3027

Hirayama T, Shinozaki K (2010) Research on plant abiotic stress responses in the post-genome era: past, present and future. Plant J 61:1041–1052

Hsu C-L, Chong SY, Lin C-Y, Kao C-F (2014) Histone dynamics during DNA replication stress. J Biomed Sci 28:48

Hurd PJ, Bannister AJ, Halls K, Dawson MA, Vermeulen M, Olsen JV, Ismail H, Somers J, Mann M, Owen-Hughes T, Gout I, Kouzarides T (2009) Phosphorylation of histone H3 Thr-45 is linked to apoptosis. J Biol Chem 284:16575–16583

Hyland EM, Cosgrove MS, Molina H, Wang D, Pandey A, Cottee RJ, Boeke JD (2005) Insights into the role of histone H3 and histone H4 core modifiable residues in saccharomyces cerevisiae. Mol Cell Biol 25:10060–10070

Idei S, Kondo K, Turner BM, Fukui K (1996) Tomographic distribution of acetylated histone H4 in plant chromosomes, nuclei and nucleoli. Chromosoma 105:293–302

Inzé D, De Veylder L (2006) Cell cycle regulation in plant development. Ann Rev Genet 40:77–105

Ito T (2007) Role of histone modification in chromatin dynamics. J Biochem 141:609–614

Jasencakova Z, Meister A, Schubert I (2001) Chromatin organization and its relation to replicationand histone acetylation during the cell cycle in barley. Chromosoma 110:83–92

Jasencakova Z, Meister A, Walter J, Turner BM, Schubert I (2000) Histone acetylation of euchromatin and heterochromatin is correlated with replication rather than with transcription. Plant Cell 12:2087–2100

Jeppesen P (1997) Histone acetylation: a possible mechanism for the inheritance of cell memory at mitosis. BioEssays 19:67–74

Khurana S, Oberdoerffer P (2015) Replication stress: a lifetime of epigenetic change. Genes (basel) 6:858–877

Koç A, Wheeler LJ, Mathews CK, Merrill GF (2004) Hydroxyurea arrests DNA replication by a mechanism that preserves basal dNTP pools. J Biol Chem 279:223–230

Lee J-H, Kang B-H, Jang H, Kim TW, Choi J, Kwak S, Han JP, Cho E-J, Youn H-D (2015) AKT phosphorylates H3-threonine 45 to facilitate termination of gene transcription in response to DNA damage. Nucl Acids Res 43:4505–4516

Leonard AC, Méchali M (2013) DNA replication origins. Cold Spring Harb Perspect Biol 5:a010116

Li B, Carey M, Workman JL (2007) The role of chromatin during transcription. Cell 128:707–719

Li Q, Zhou H, Wurtele H, Davies B, Horazdovsky B, Verreault A, Zhang Z (2008) Acetylation of histone H3 lysine 56 regulates replication-coupled nucleosome assembly. Cell 134:244–255

Masumoto H, Hawke D, Kobayashi R, Verreault A (2005) A role for cell-cycle-regulated histone H3 lysine 56 acetylation in the DNA damage response. Nature 436:294–298

Mursalimov S, Deineko E, Houben A, Demidov D (2019) Histone modifications during tobacco male meiosis. Biol Plant 63:681–689

Nikitaki Z, Holá M, Donà M, Pavlopoulou A, Michalopoulos I, Angelis KJ, Georgakilas AG, Macovei A, Balestrazzi A (2018) Integrating plant and animal biology for the search of novel DNA damage biomarkers. Mutat Res Rev Mutat Res 775:21–38

Nisa M-U, Huang Y, Benhamed M, Raynaud C (2019) The plant DNA damage response: signaling pathways leading to growth inhibition and putative role in response to stress conditions. Front Plant Sci 10:653

Olcina MM, Giaccia AJ, Hammong GM (2016) Isolation of proteins on nascent DNA in hypoxia and reoxygenation conditions. Adv Exp Med Biol 899:27–40

Rufiange A, Jacques PE, Bhat W, Robert F, Nourani A (2007) Genome-wide replication-independent histone H3 exchange occurs predominantly at promoters and implicates H3 K56 acetylation and Asf1. Mol Cell 27:393–405

Serra-Cardona A, Zhang Z (2018) Replication-coupled nucleosome assembly in the passage of epigenetic information and cell identity. Trends Biochem Sci 43:136–148

Sirbu BM, Couch FB, Feigerle JT, Bhaskara S, Hiebert SW, Cortez D (2011) Analysis of protein dynamics at active, stalled, and collapsed replication forks. Genes Dev 25:1320–1327

Sirbu BM, Couch FB, Cortez D (2012) Monitoring the spatiotemporal dynamics of proteins at replication forks and in assembled chromatin using isolation of proteins on nascent DNA (iPOND). Nat Protoc 7:594–605

Sirbu BM, McDonald WH, Dungrawala H, Badu-Nkansah A, Kavanaugh GM, Chen Y, Tabb DL, Cortez D (2013) Identification of proteins at active, stalled, and collapsed replication forks using isolation of proteins on nascent DNA (iPOND) coupled with mass spectrometry. J Biol Chem 288:31458–33167

Sogo JM, Ness PJ, Widmer RM, Parish RW, Koller T (1984) Psoralen-crosslinking of DNA as a probe for the structure of active nucleolar chromatin. J Mol Biol 178:897–928

Szurman-Zubrzycka M, Jędrzejek P, Szarejko I (2023) How do plants cope with DNA damage? A concise review on the DDR pathway in plants. Int J Mol Sci 24:2404

Viggiano L, de Pinto MC (2017) Dynamic DNA methylation patterns in stress response. In: Rajewsky N et al (eds) Plant Epigenetics, RNA Technologies. Springer International Publishing, pp 281–302

Wang Z, Zang C, Rosenfeld JA, Schones DE, Barski A, Cuddapah S, Cui K, Roh T-Y, Peng W, Zhang MQ, Zhao K (2008) Combinatorial patterns of histone acetylations and methylations in the human genome. Nat Genet 40:897–903

Wurtele H, Kaiser GS, Bacal J, St-Hilaire E, Lee E-H, Tsao S, Dorn J, Maddox P, Lisby M, Pasero P, Verreault A (2012) Histone H3 lysine 56 acetylation and the response to DNA replication fork damage. Mol Cell Biol 32:154–172

Xu F, Zhang K, Grunstein M (2005) Acetylation in histone H3 globular domain regulates gene expression in yeast. Cell 121:375–385

Żabka A, Polit JT, Maszewski J (2010) Inter- and intrachromosomal asynchrony of cell division cycle events in root meristem cells of *Allium cepa*: possible connection with gradient of cyclin B-like proteins. Plant Cell Rep 29:845–856

Żabka A, Polit JT, Maszewski J (2012) DNA replication stress induces deregulation of the cell cycle events in root meristems of *Allium cepa*. Ann Bot 110:1581–1591

Żabka A, Trzaskoma P, Winnicki K, Polit JT, Chmielnicka A, Maszewski J (2015) The biphasic interphase-mitotic polarity of cell nuclei induced under DNA replication stress seems to be correlated with Pin2 localization in root meristems of *Allium cepa*. J Plant Physiol 174:62–70

Żabka A, Winnicki K, Polit JT, Maszewski J (2017) Sanguinarine-induced oxidative stress and apoptosis-like programmed cell death (AL-PCD) in root meristem cells of *Allium cepa*. Plant Physiol Biochem 112:193–206

Żabka A, Winnicki K, Polit JT, Bernasińska-Słomczewska J, Maszewski J (2020) 5-Aminouracil and other inhibitors of DNA replication induce biphasic interphase–mitotic cells in apical root meristems of *Allium cepa*. Plant Cell Rep 39:1013–1028

Żabka A, Gocek N, Winnicki K, Szczeblewski P, Laskowski T, Polit J (2021a) Changes in epigenetic patterns related to DNA replication in *Vicia faba* root meristem cells under cadmium-induced stress condition. Cells 10:3409

Żabka A, Winnicki K, Polit JT, Wróblewski M, Maszewski J (2021b) Cadmium (II)-induced oxidative stress results in replication stress and epigenetic modifications in root meristem cell nuclei of *Vicia faba*. Cells 10:640

Zeman MK, Cimprich KA (2014) Causes and consequences of replication stress. Nat Cell Biol 16:2–9

❖

Praca 3 (Załącznik nr 3)

❖ **Gocek-Szczurtek, N.**; Żabka, A.; Wróblewski, M.; Polit, J.T.*
Stabilization of the MAPK–Epigenetic Signaling Axis Underlies the Protective Effect of Thyme Oil against Cadmium Stress in Root Meristem Cells of *Vicia faba*. *Int. J. Mol. Sci.* **2025**, 27, 208, doi:10.3390/ijms27010208

* – autor korespondujący

- Współczynnik wpływu (IF): **4,9**
- Punkty MNiSW: **140 pkt**.

International Journal of
Molecular Sciences

MDPI

Article

Stabilization of the MAPK–Epigenetic Signaling Axis Underlies the Protective Effect of Thyme Oil Against Cadmium Stress in Root Meristem Cells of *Vicia faba*

Natalia Gocek-Szczurtek [1,2], Aneta Żabka [1], Mateusz Wróblewski [1,2] and Justyna T. Polit [1,*]

[1] Department of Cytophysiology, Faculty of Biology and Environmental Protection, University of Lodz, 90-236 Lodz, Poland; natalia.gocek.szczurtek@biol.uni.lodz.pl (N.G.-S.); aneta.zabka@biol.uni.lodz.pl (A.Ż.); mateusz.wroblewski@biol.uni.lodz.pl (M.W.)
[2] Doctoral School of Exact and Natural Sciences, University of Lodz, 90-237 Lodz, Poland
* Correspondence: justyna.polit@biol.uni.lodz.pl

Abstract

Cadmium (Cd) induces oxidative stress and disrupts nuclear organization and chromatin-associated metabolic processes in plant cells. Therefore, identifying natural, biodegradable, non-bioaccumulative compounds that enhance plant tolerance to heavy metals is crucial. We hypothesized that Cd exposure (175 µM $CdCl_2$, 24 h) activates mitogen-activated protein kinases (MAPKs), triggering defined epigenetic modifications that lead to transcriptional repression, and that thyme oil (TO; 0.03% (v/v), emulsified) mitigates these effects by stabilizing chromatin organization. We analyzed nuclear MAPK (p44/42) activation, global DNA methylation (5-methylcytosine; 5-mC), and selected histone modifications as key components of early stress signaling and epigenetic regulation. We found that Cd exposure doubled global 5-mC levels and caused pronounced alterations in histone marks, including decreases in H3K4Me2 (~34%), H3T45Ph (~48%), and H4K5Ac, accompanied by strong increases in H3K9Ac (~57%) and H3K56Ac (~148%). These changes were associated with chromatin condensation and reduced transcriptional activity. In contrast, co-treatment with TO maintained MAPK activity and epigenetic parameters close to control levels, preventing chromatin compaction and transcriptional repression. Together, these findings indicate that TO stabilizes the nuclear signaling–epigenetic interface under Cd stress and represents a promising bioprotective strategy. This work provides the first demonstration that TO modulates both MAPK activation and Cd-induced histone modifications in plants.

Keywords: histone modification; DNA methylation; MAPK; transcription; cadmium; essential oil

Academic Editor: De-Guo Han

Received: 12 November 2025
Revised: 21 December 2025
Accepted: 22 December 2025
Published: 24 December 2025

1. Introduction

Heavy metal pollution represents a major environmental and agricultural concern due to its toxicity to living organisms [1]. While some heavy metals, such as copper, zinc, and molybdenum, serve essential physiological roles as micronutrients [2], others—like cadmium, lead, and mercury—have no biological function and are toxic even at low concentrations, readily accumulating in plant and animal tissues [3]. Although naturally occurring in the Earth's crust, the excessive environmental accumulation of heavy metals results primarily from anthropogenic activities, including industrial development, traffic, and the intensive use of fertilizers and agrochemicals. Among these metals, cadmium

(Cd) is of particular concern due to its widespread occurrence and well-documented toxicity [4,5].

Cd is a highly mobile heavy metal in plants that readily accumulates in tissues and exerts pronounced phytotoxic effects. Its toxicity results from direct interference with key cellular structures and fundamental physiological processes, including disruption of water balance, ion transport, membrane integrity, protein synthesis and stability, as well as DNA integrity [6,7]. At the same time, Cd acts as a potent stress signal, inducing the production of multiple signaling molecules such as reactive oxygen species (ROS) [8–10], nitric oxide (NO), phytohormones, cyclic nucleotides, calcium ions and sugars. To cope with this complex spectrum of damage- and signal-derived cues, plant cells integrate environmental information with core metabolic pathways and activate coordinated protective responses aimed at maintaining cellular homeostasis and genome integrity [11–19].

A central element of this signaling network is the mitogen-activated protein kinase (MAPK) cascade, composed of sequentially acting MAPKKK → MAPKK → MAPK modules that enable efficient signal amplification [20]. Plant MAPKs are evolutionarily conserved enzymes, among which MPK3 and MPK6 (p44/42), homologues of animal extracellular signal-regulated kinases (ERK1/ERK2), are the most extensively characterized in stress responses [20,21]. Once activated, MAPKs phosphorylate a wide range of target proteins, modulating their activity, stability and subcellular localization [22]. When cytoplasmic responses are insufficient to ensure long-term adaptation, MAPK-mediated signaling extends to the nucleus, where phosphorylation of transcription factors links stress perception at the plasma membrane with transcriptional reprogramming. This results in the induction of defense-related genes [23–25] that can collectively enhance plant tolerance to heavy metal stress.

Increasing evidence indicates that MAPK pathways extend beyond transcription factor activation and are closely linked with chromatin-level regulation, including DNA methylation and post-translational histone modifications [26–28]. DNA methylation is generally associated with transcriptional silencing, particularly when occurring in promoter regions [29–33], while a dynamic balance between methylation and demethylation maintains epigenome stability and enables flexible gene regulation under stress [34,35]. In parallel, reversible histone modifications, including acetylation, methylation, and phosphorylation, alter DNA–histone interactions and modulate chromatin structure and gene function in a context-dependent manner, with their functional versatility arising from the diversity of modification sites and the number of attached groups [36–47]. The combinatorial interplay of histone marks, together with DNA methylation, forms a dynamic regulatory layer that fine-tunes transcription and enables plants to rapidly adjust gene expression in response to stress [48]. Although cadmium exposure induces significant epigenetic alterations, the mechanisms by which MAPK signaling links oxidative stress to chromatin remodeling in plants remain poorly understood.

In parallel with efforts to understand stress signaling mechanisms, increasing attention has been directed toward identifying natural compounds capable of enhancing plant tolerance to environmental stress [6,49]. Among such candidates, thyme oil (TO), widely used in traditional medicine, cosmetics, and the food industry, has attracted considerable interest due to its well-documented biological properties [50–53]. TO is rich in phenolic monoterpenes, primarily thymol and carvacrol, which exhibit strong antioxidant and anti-inflammatory activities [54,55]. In vitro studies have demonstrated that TO enhances the activity of key antioxidant enzymes, such as catalase and superoxide dismutase, thereby increasing overall cellular antioxidant capacity [56]. In addition, its broad-spectrum antimicrobial activity (antiviral, antibacterial, and antifungal) [57], together with the synergistic action of multiple components, makes TO an attractive natural protective agent. Previous

studies indicates that TO can mitigate cadmium toxicity in animal models [54,58,59]; however, its potential as a bioprotective agent in plants exposed to heavy metals remains poorly explored, with only a limited number of studies addressing this aspect [60].

Building on these observations, our recent work demonstrated that TO, applied as a 0.03% (v/v) emulsion, significantly alleviates Cd-induced oxidative stress and genotoxic effect in root meristem cells of *V. faba* [55]. Given that cadmium exposure is known to disrupt chromatin organization and induce epigenetic alterations that may affect transcriptional activity, there is a strong rationale to investigate whether the protective effects of TO extend to the level of nuclear signaling and epigenetic regulation. To address this issue, we used primary roots of *Vicia faba* var. *minor*, a well-established model species in chromatin, cytogenetic, and epigenetic research. Its clearly defined meristematic zones, distinct nuclear morphology, and large chromosomes allow precise microscopic assessment of chromatin condensation, histone modifications, and nuclear signaling events. We incubated seedlings for 24 h in a solution of $CdCl_2$ (175 μM), emulsified TO (0.03%), or a combination of both treatments. Compared with control seedlings incubated in water or in the emulsifier solution used to prepare the oil emulsion, we analyzed nuclear MAPK activity, followed by assessment of global DNA methylation as a classical marker of chromatin remodeling and evaluation of changes in the epigenetic patterns of selected histone marks (H3K4Me2, H3T45Ph, H4K5Ac, H3K9Ac, H3K56Ac), representing distinct regulatory mechanisms involved in the cellular stress response. Finally, we evaluated transcriptional activity.

Our study was designed to test two hypotheses: (1) Cd exposure activates nuclear MAPKs and induces specific epigenetic modifications that result in reduced transcriptional activity; and (2) TO mitigates Cd-induced effects by limiting epigenetic alterations and maintaining chromatin stability. Overall, this study provides the first evidence linking the protective effects of TO with modulation of nuclear MAPK signaling and epigenetic regulation in plants exposed to heavy metal stress.

2. Results

2.1. Immunodetection of Dually Phosphorylated MAPKs

To determine the localization and activity level of mitogen-activated protein kinases (MAPKs) in *V. faba* meristem cells, an immunocytochemical approach was employed using commercial anti-phospho-p44/42 monoclonal antibodies. In members of the Fabaceae family, these antibodies recognize several MAPK isoforms containing TEY (Thr-Glu-Tyr) and TDY (Thr-Asp-Tyr) motifs within their activation loops [61], most notably MPK3 and MPK6. These kinases are well-characterized stress-responsive MAPKs and functional homologs of mammalian ERK1/2 and act as central nodes within MAPK cascades, integrating signals from multiple stress-signaling pathways, which makes them particularly reliable markers of cascade activation [62,63].

Immunofluorescence signals were detected as distinct nuclear foci. Quantitative analysis was based on three parameters: (1) the number of foci per nucleus (Figure 1F), (2) the foci area (Figure 1G), and (3) fluorescence intensity (FI) (Figure 1H). The number of foci reflects the frequency of distinct, clearly separated chromatin-associated MAPK signaling microdomains. Foci area indicates the spatial extent of these domains, potentially corresponding to the size of chromatin region influenced by kinases. FI reflects the local accumulation of active MAPKs and relative activation levels within individual domains. Together, these parameters capture the complexity of nuclear MAPK signaling.

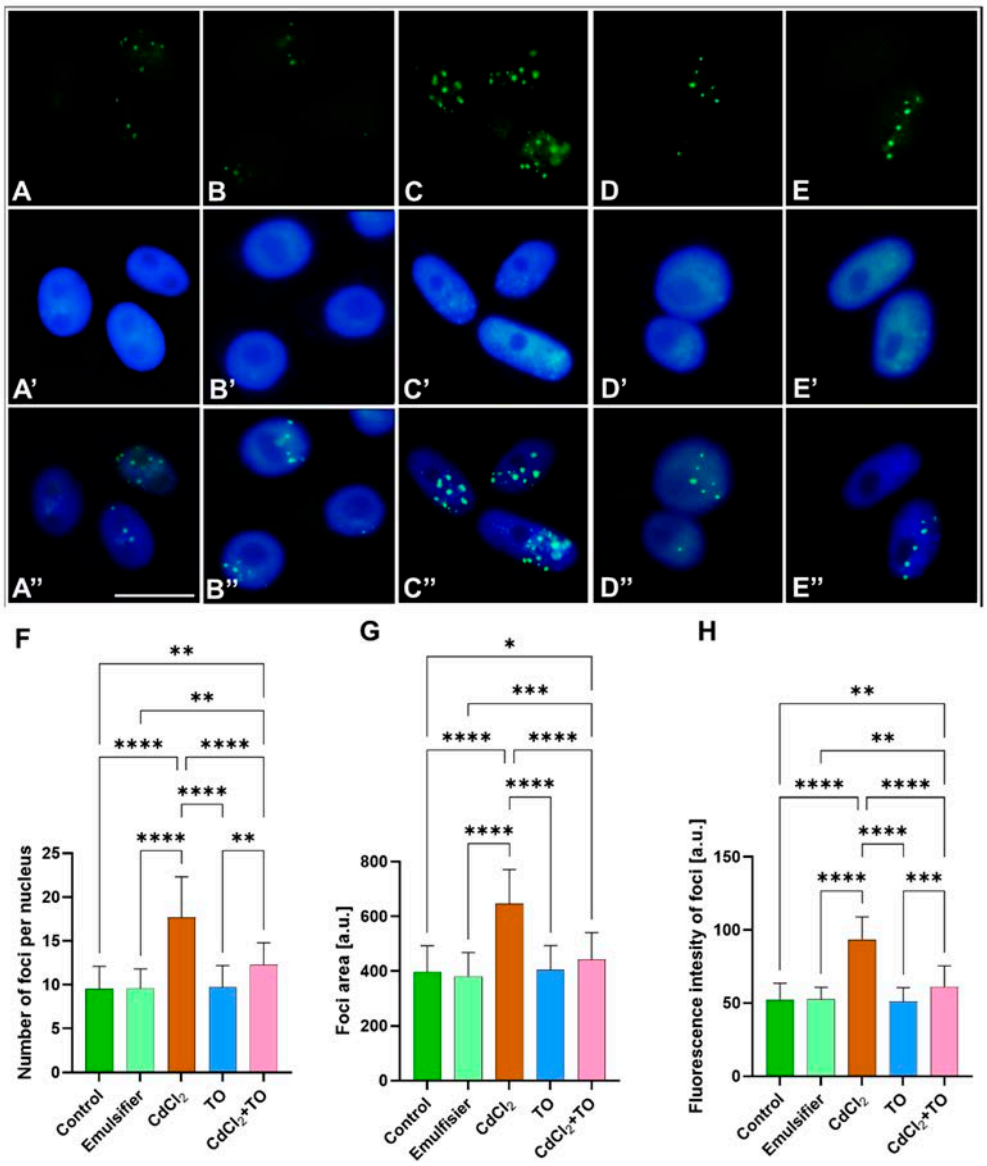

Figure 1. Immunofluorescence detection of dually phosphorylated MAPKs in primary root meristems cells of *V. faba* after 24 h of incubation with water—Control (**A**), emulsifier (**B**), $CdCl_2$ (**C**), TO (**D**) and a combination of $CdCl_2$ and TO (**E**). Corresponding images of cell nuclei stained with DAPI (**A′**–**E′**), and merged images of immunofluorescent signals with DAPI staining (**A″**–**E″**). Scale bar = 10 µm. Mean (± SD; n = 6 biological replicates) number of MAPK foci per nucleus; approximately 100 nuclei were analyzed per treatment (**F**). Mean (± SD; n = 6 biological replicates) area of MAPK foci; approximately 35 nuclei were analyzed per treatment (**G**). Mean (± SD; n = 6 biological replicates) fluorescence intensity of MAPK foci, expressed as pixel intensity (0–255); approximately 55 foci were analyzed per treatment (**H**). Statistical significance: **** $p < 0.0001$, *** $p < 0.001$, ** $p < 0.01$, * $p < 0.05$ (one-way ANOVA followed by Tukey's multiple comparison test).

Control roots (Figure 1A), as well as those treated with the emulsifier (Figure 1B) or emulsified form of TO (Figure 1D), exhibited similarly low numbers of nuclear foci, averaging approximately 10 per nucleus (Figure 1F), which is consistent with basal MAPK activity. In contrast, $CdCl_2$ treatment (Figure 1C) caused a significant, nearly twofold increase in foci number, indicating an expansion of functional MAPK microdomains. Co-treatment with $CdCl_2$ and TO (Figure 1E) significantly reduced the number of foci relative to $CdCl_2$ alone, suggesting partial normalization of nuclear MAPK domain frequency.

The mean foci area in control cells (Figure 1A), as well as in those exposed to the emulsifier (Figure 1B) and emulsified TO (Figure 1D), remained comparable (Figure 1G).

$CdCl_2$ exposure increased foci area by approximately 50% (Figure 1C), which is potentially consistent with an expansion of chromatin regions associated with active MAPKs or increased kinase density. In the combined $CdCl_2$ and TO treatment (Figure 1E), foci area was only slightly higher than in controls, indicating partial preservation of domain size.

A similar pattern was observed for fluorescence intensity. Control, emulsifier-treated (Figure 1A,B) and TO-treated nuclei (Figure 1D) showed low FI values—around 50 a.u. per focus (Figure 1H). Exposure to $CdCl_2$ (Figure 1C) induced a marked, nearly twofold increase in signal intensity, which may reflect enhanced local MAPK activity accumulation. In roots treated with combination of $CdCl_2$ and TO (Figure 1E), FI increased only modestly relative to controls, suggesting intermediate MAPK activity per domain under these conditions.

2.2. Immunodetection of 5-Methylcytosine (5-mC)

Immunofluorescence labeling with specific antibodies enabled the visualization of DNA methylation levels (5-methylcytosine; 5-mC) across the nuclear chromatin of *V. faba* root meristem cells. Fluorescence intensity, which reflects the degree of DNA methylation and is generally associated with transcriptionally silent chromatin, varied depending on the experimental treatment (Figure 2A–F). In control roots, i.e., those incubated in water (Figure 2A) or in the emulsifier solution used for oil preparation (Figure 2B), fluorescence intensity remained similarly low, indicating relatively low levels of DNA methylation. In contrast, exposure to $CdCl_2$ led to a pronounced, approximately twofold increase in signal intensity (Figure 2F). Treatment with TO alone produced fluorescence levels comparable to the control (Figure 2D). However, simultaneous exposure to TO and $CdCl_2$ (Figure 2E) resulted in only a slight elevation in fluorescence intensity—and consequently in DNA methylation—relative to the control roots.

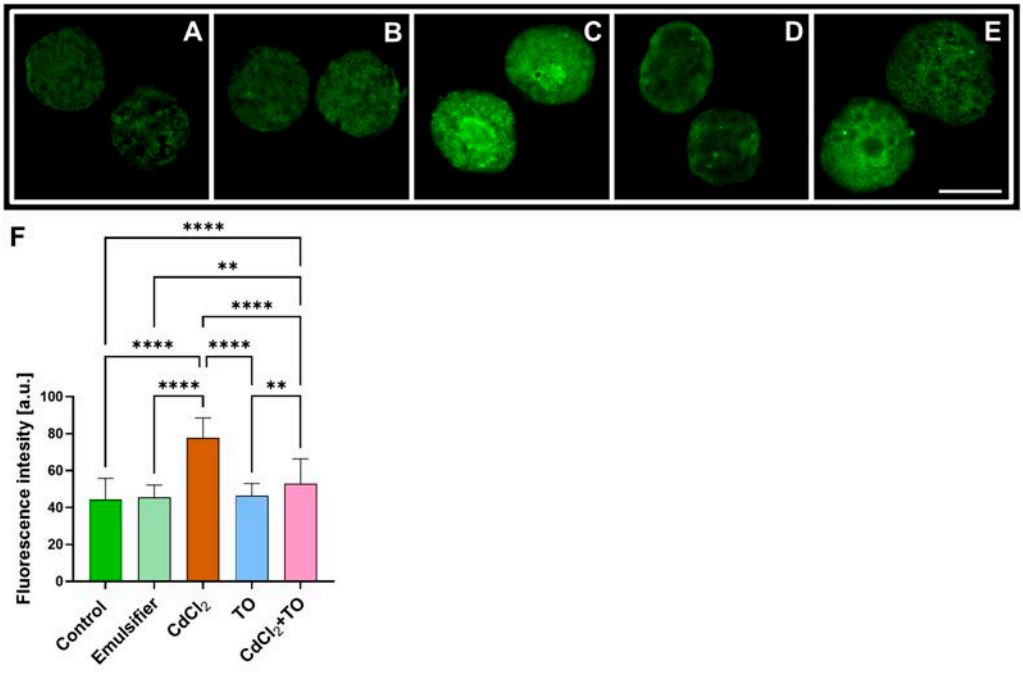

Figure 2. Immunofluorescence detection of 5-mC in nuclei of primary root meristem cells of *V. faba* after 24 h of incubation with water—Control (**A**), emulsifier (**B**), $CdCl_2$ (**C**), TO (**D**), and a combination of $CdCl_2$ and TO (**E**). Scale bar = 10 µm. Mean (± SD; $n = 6$ biological replicates) fluorescence intensity of 5-mC labeling; approximately 58 nuclei were analyzed per treatment (**F**). Statistical significance: **** $p < 0.0001$, ** $p < 0.01$ (one-way ANOVA followed by Tukey's multiple comparison test).

2.3. Dimethylation of Histone H3 on Lysine 4 (H3K4Me2)

After a 24 h incubation of primary *V. faba* roots in water (Figure 3A), an emulsifier solution (Figure 3B), $CdCl_2$ (Figure 3C), TO (Figure 3D), or a combination of $CdCl_2$ and TO (Figure 3E), root apical meristem cells were labeled with anti-H3K4Me2 antibodies, and fluorescence intensity (FI) across the entire nuclear area was quantified, as this modification produces a more diffuse and homogenous nuclear signal that does not form discrete foci suitable for count- or area-based analysis.

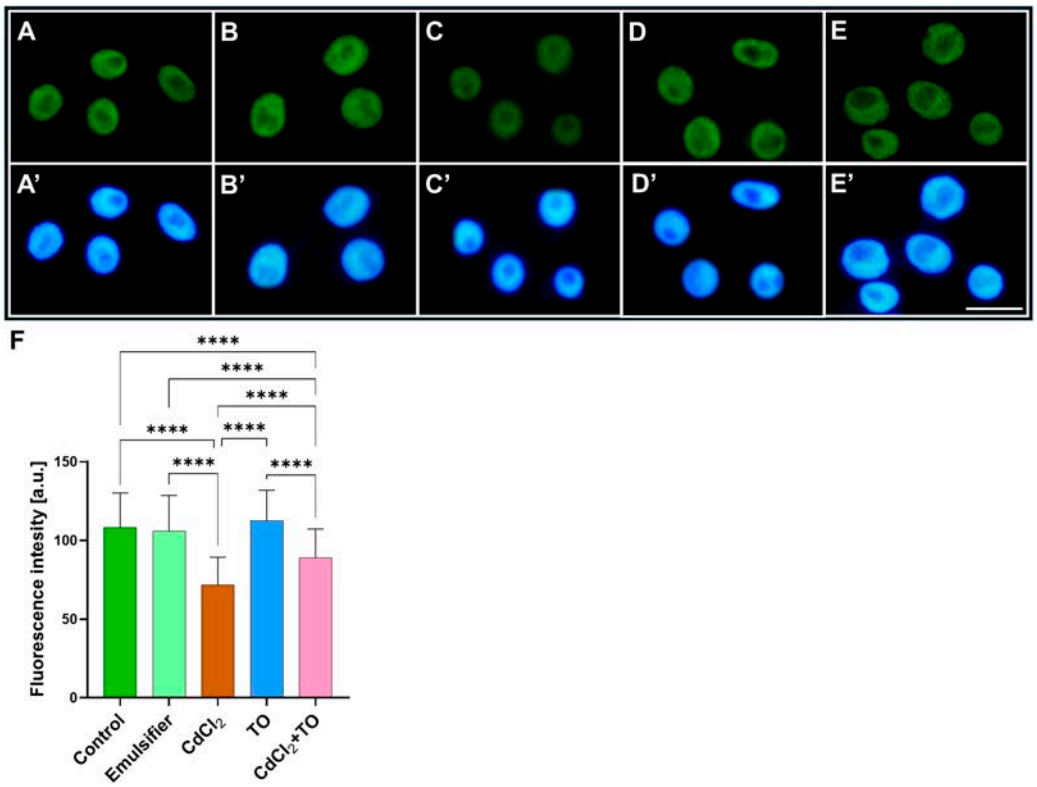

Figure 3. Immunofluorescence detection of H3K4Me2 in nuclei of primary root meristem cells of *V. faba* after 24 h incubation with water—Control (**A**), emulsifier (**B**), $CdCl_2$ (**C**), TO (**D**), and a combination of $CdCl_2$ and TO (**E**), along with corresponding images of cell nuclei stained with DAPI (**A'**–**E'**). Scale bar = 10 µm. Mean (± SD; $n = 6$ biological replicates) fluorescence intensity of H3K4Me2 labeling; approximately 120 nuclei were analyzed per treatment (**F**). Statistical significance: **** $p < 0.0001$ (one-way ANOVA followed by Tukey's multiple comparison test).

Compared with the control (Figure 3A) and emulsifier-treated roots (Figure 3B), exposure to $CdCl_2$ (Figure 3C) resulted in an approximately 33% reduction in H3K4Me2 fluorescence intensity (Figure 3F), which may indicate a decrease in chromatin regions associated with this mark and a potential link to reduced transcriptional activity. A 24 h incubation of seedlings in TO solution alone did not cause significant changes relative to the control (Figure 3D,F), suggesting maintenance of baseline H3K4Me2-associated chromatin states. However, simultaneous treatment of plants with TO and $CdCl_2$ led to a noticeable increase in fluorescence intensity compared with $CdCl_2$ alone, although the signal remained below control levels (Figure 3E,F), which may reflect partial restoration of H3K4Me2 levels.

2.4. Phosphorylation of Histone H3 on Threonine 45 (H3T45Ph)

Analysis of the relatively homogeneous fluorescence signal intensity obtained using specific antibodies against histone 3 phosphorylated at threonine 45 (H3T45Ph) revealed clear differences among the experimental series (Figure 4). Exposure to $CdCl_2$ resulted in a marked decrease in H3T45Ph fluorescence intensity in interphase nuclei (Figure 4C),

compared with roots incubated in water (Figure 4A), the emulsifier solution (Figure 4B), or the emulsified form of TO (Figure 4D). Such a reduction in H3T45Ph signal may indicate restricted nucleosome unwrapping dynamics, which can affect local DNA accessibility. After 24 h of simultaneous incubation of seedlings with $CdCl_2$ and TO, a decrease in fluorescence intensity was also observed (Figure 4E), although the reduction was substantially smaller than in roots exposed to $CdCl_2$ alone.

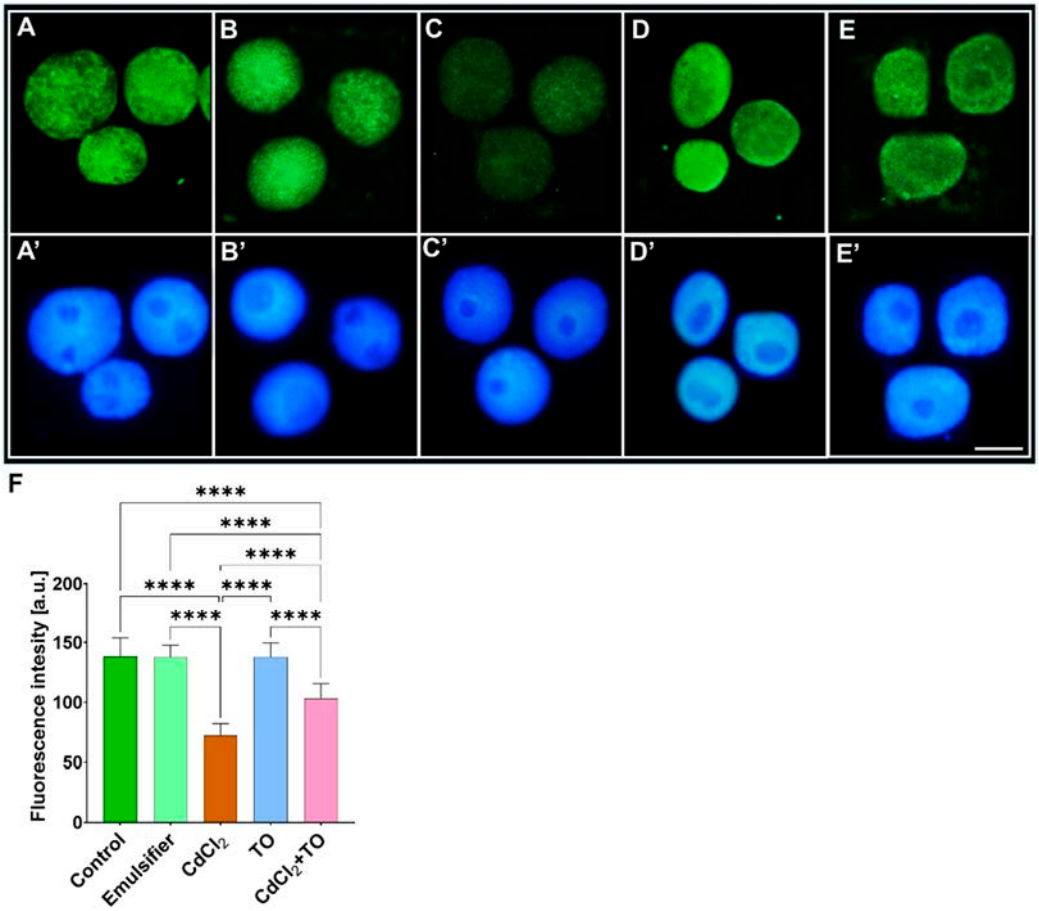

Figure 4. Immunofluorescence detection of H3T45Ph in nuclei of primary root meristem cells of *V. faba* after 24 h incubation with water—Control (**A**), emulsifier (**B**), $CdCl_2$ (**C**), TO (**D**), and a combination of $CdCl_2$ and TO (**E**), along with corresponding images of cell nuclei stained with DAPI (**A′**–**E′**). Scale bar = 10 µm. Mean (± SD; n = 6 biological replicates) fluorescence intensity of H3T45Ph labeling; approximately 50 nuclei were analyzed per treatment (**F**). Statistical significance: **** $p < 0.0001$ (one-way ANOVA followed by Tukey's multiple comparison test).

2.5. Acetylation of Histone H4 on Lysine 5 (H4K5Ac)

Immunodetection of histone H4 acetylation at lysine 5 (H4K5Ac) in interphase nuclei of *V. faba* root meristems revealed five distinct labeling patterns (Figure 5A–E), which were therefore analyzed separately. These included: 1. nuclei exhibiting homogeneous, strong labeling (Figure 5C); 2. nuclei with weaker labeling throughout the euchromatin region (Figure 5A,B,D); 3. nuclei displaying strong fluorescence within the nucleolus (Figure 5A); 4. nuclei showing fluorescence concentrated at the nucleolar periphery (Figure 5B); and 5. nuclei characterized by clustered fluorescence foci located in heterochromatin regions (Figure 5E). The frequency of these patterns varied among experimental treatment. Quantitative analysis therefore focused on determining the average percentage of interphase nuclei exhibiting each labeling type. It is worth noting that pronounced nuclear labeling is

generally associated with increased chromatin accessibility, whereas weaker signals may reflect its partial silencing or condensation.

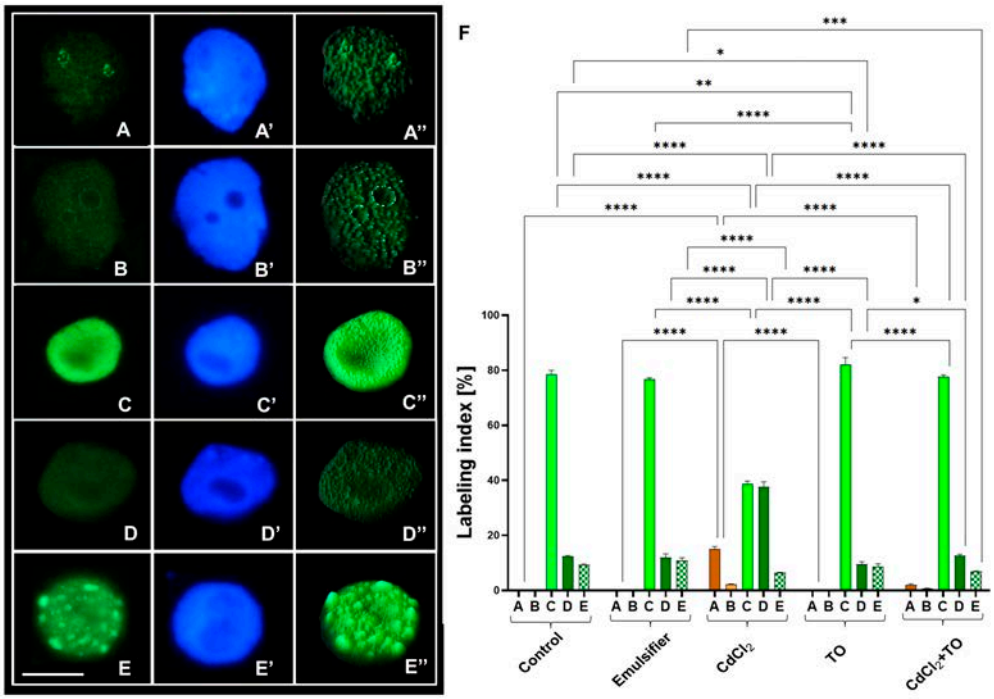

Figure 5. Representative immunofluorescence patterns of H4K5Ac labeling observed in nuclei of primary root meristem cells of *V. faba* after 24 h of treatment. Distinct labeling patterns were identified across all experimental variants and include: localization within the nucleolus (**A**), around nucleolar chromatin (**B**), strong euchromatic labeling (**C**), weak euchromatic labeling (**D**), and preferential heterochromatic labeling (**E**). Corresponding DAPI-stained nuclei (**A′**–**E′**), and interactive 3D surface plots (**A″**–**E″**) are shown. The frequencies (% ± SD; $n = 3$ biological replicates) of nuclei exhibiting each labeling pattern in control (water), emulsifier, $CdCl_2$, TO, and a $CdCl_2$ + TO treatments are quantified in panel (**F**). Scale bar = 10 µm. Statistical significance: **** $p < 0.0001$, *** $p < 0.001$, ** $p < 0.01$, * $p < 0.05$ (one-way ANOVA followed by Tukey's multiple comparison test).

Labeling restricted to the nucleolus or its borders (Figure 5A,B) occurred exclusively in $CdCl_2$ treated cells and, to a much lesser extent, in those incubated with the $CdCl_2$ and TO mixture. This pattern was absent in control root meristem cells and in those incubated with emulsified TO (Figure 5F). Homogeneous, intense labeling across the chromatin (Figure 5C) represented the predominant pattern in roots treated for 24 h with water, the emulsifier solution, emulsified TO, and the $CdCl_2$ + TO mixture. In contrast, seedlings exposed to $CdCl_2$ alone showed a pronounced decrease in this labeling index (37.56%) relative to the control (73%). Conversely, the labeling type characterized by markedly weaker fluorescence (Figure 5D) accounted for approximately 35.5% of interphase nuclei in $CdCl_2$-treated roots, whereas its frequency in the control, TO-treated, and $CdCl_2$ + TO series did not exceed 13%. The final pattern, localized by heterochromatin region (Figure 5E), occurred at similar frequencies in control and TO-treated roots. Its incidence decreased following $CdCl_2$ exposure. Supplementation with TO did not significantly modify the proportion of nuclei displaying this pattern relative to Cd-treated seedlings.

2.6. Acetylation of Histone H3 on Lysine 9 (H3K9Ac)

Changes in histone H3 lysine 9 acetylation (H3K9Ac) under the experimental treatments were evaluated by measuring fluorescence intensity (FI) across entire nuclei, which was appropriate given the homogeneous labeling pattern obtained using immunocyto-

chemical detection. Analyses of root meristem cells from the control groups, i.e., seedlings incubated in water (Figure 6A) or in the emulsifier solution (Figure 6B), revealed comparably low fluorescence levels. In contrast, exposure to $CdCl_2$ (Figure 6C), increased fluorescence intensity by approximately one-third relative to the control (Figure 6F), which may reflect a chromatin configuration that enhances accessibility to promoters of stress-responsive genes. Incubation of roots in emulsified TO (Figure 6D) did not alter histone acetylation levels compared with the control. Likewise, seedlings simultaneously treated with $CdCl_2$ and TO (Figure 6E) exhibited acetylation levels similar to those of the control.

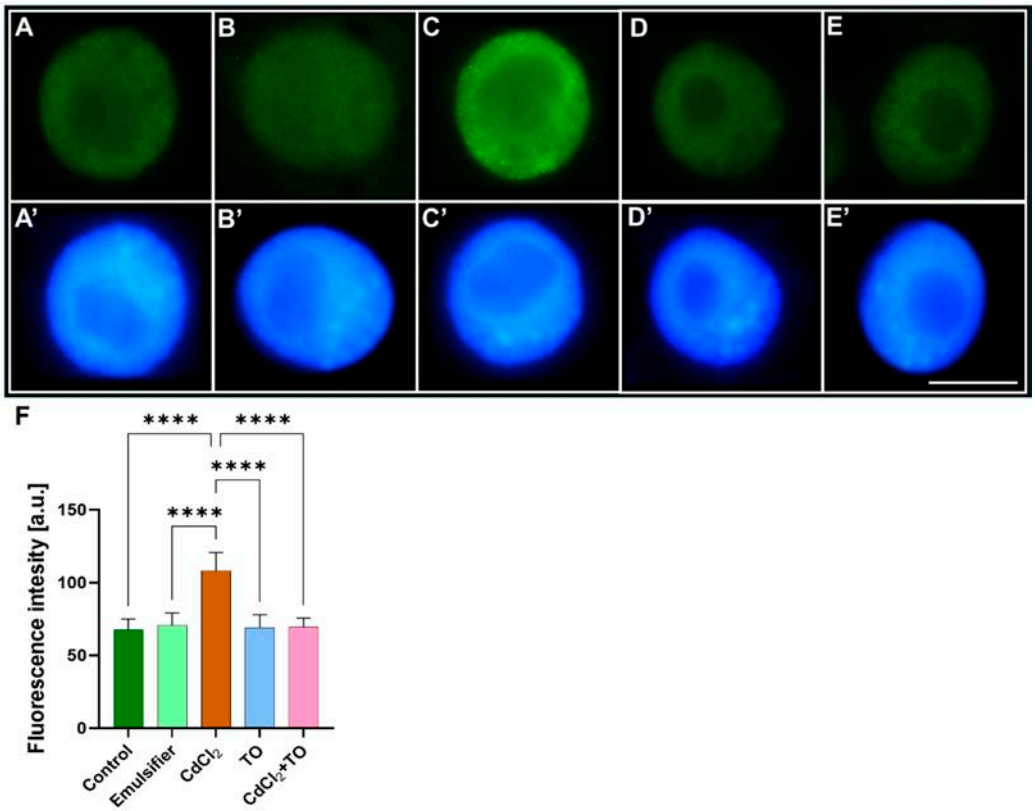

Figure 6. Immunofluorescence detection of H3K9Ac in nuclei of primary root meristem cells of *V. faba* after 24 h of incubation with water—Control (**A**), emulsifier (**B**), $CdCl_2$ (**C**), TO (**D**), and a combination of $CdCl_2$ and TO (**E**), along with corresponding images of cell nuclei stained with DAPI (**A'**–**E'**). Scale bar = 10 µm. Median (±CI; n = 6 biological replicates) intensity of H3K9Ac labeling; approximately 158 nuclei were analyzed in Control, 119 in emulsifier, 140 in $CdCl_2$, 149 in TO, and 158 in $CdCl_2$ + TO treatment groups (**F**). Statistical significance: **** $p < 0.0001$ (Kruskal–Wallis test with post hoc Dunn's multiple comparison test).

2.7. Acetylation of Histone H3 on Lysine 56 (H3K56Ac)

To assess the effects of the examined treatments on histone H3 lysine 56 acetylation (H3K56Ac) in *V. faba* root meristem cells, immunocytochemical labeling was performed. Microscopic image analysis enabled quantitative evaluation of the average number of fluorescent foci in G_1-, S-, and G_2-phase nuclei under the applied experimental conditions (Figure 7A–E). Due to the small size and dense distribution of the fluorescent signals, their area and intensity were not analyzed, as such measurements were technically challenging and yielded unreliable results.

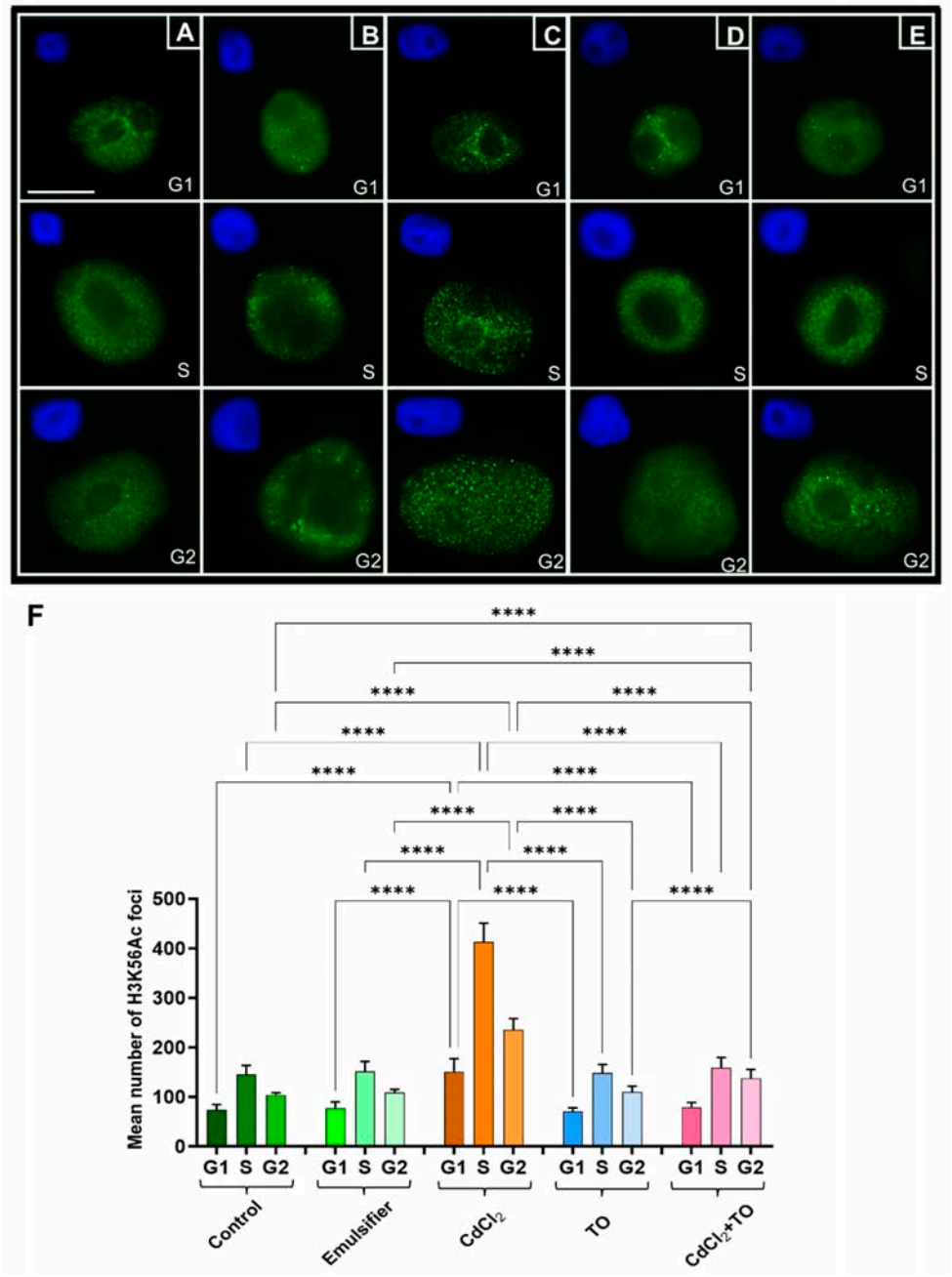

Figure 7. Immunofluorescence detection of H3K56Ac in G1-, S-, and G2-phase nuclei of primary root meristem cells of *V. faba* after 24 h incubation with water—Control (**A**), emulsifier (**B**), $CdCl_2$ (**C**), TO (**D**), and a combination of $CdCl_2$ and TO (**E**). Scale bar = 10 µm. Corresponding images of cell nuclei stained with DAPI, embedded in the upper left corners of each image. Quantitative analysis of the mean number of intracellular H3K56Ac foci in G1-, S-, and G2-phase nuclei for each treatment is presented in panel (**F**). Data are shown as mean (±SD; n = 6 biological replicates); approximately 90 nuclei were analyzed per treatment. Statistical significance: **** $p < 0.0001$ (one-way ANOVA followed by Tukey's multiple comparison test).

In the control groups, seedlings incubated in water (Figure 7A) or in the emulsifier solution (Figure 7B), the average number of H3K56Ac foci per nucleus was approximately 73, 145, and 104, and 78, 151, and 109 for G_1, S, and G_2 phases, respectively. Within each group, significant differences in foci number were observed between cell cycle phases, consistent with the dynamic incorporation of H3K56Ac into newly synthesized histones and its association with chromatin states permissive to DNA strand separation during replication. Exposure to $CdCl_2$ (Figure 7C) led to a marked increase in H3K56 acetylation

at all interphase stages. The number of foci approximately doubled in G_1, nearly tripled in S, and increased more than twofold in G_2 compared with controls (Figure 7F), reflecting enhanced chromatin relaxation potentially facilitating recruitment of DNA repair complexes. In TO-treated cells (Figure 7D), foci numbers in all phases remained comparable to controls. Simultaneous exposure to $CdCl_2$ and TO (Figure 7E) significantly reduced H3K56 acetylation relative to $CdCl_2$ alone. In G_1 and S phases, foci numbers returned to control-like levels, whereas in G_2, they remained lower than in $CdCl_2$-treated seedlings but were still significantly higher than in the control group.

2.8. Changes in Transcription Dynamics

To evaluate transcriptional activity in the root meristem cells of *V. faba*, incorporation of the alkyne-modified uridine analog 5-ethynyluridine (EU) was used. This approach allows detection of newly synthesized RNA through a copper-catalyzed cycloaddition reaction, eliminating the need for immunocytochemical labeling. Quantitative analysis was performed by measuring average fluorescence intensity within nucleoplasmic and nucleolar regions.

The strongest EU-derived fluorescence signals were detected in the nucleoli (Figure 8F), reflecting intense ribosomal RNA synthesis. Compared with cells incubated in water (Figure 8A) or emulsifier solution (Figure 8B), $CdCl_2$ treatment caused a pronounced reduction in fluorescence intensity in both the nucleoplasm and nucleoli (Figure 8C,F), indicating decreased RNA synthesis under these conditions. Treatment with TO alone (Figure 8D,F) maintained transcriptional activity at levels comparable to controls. Notably, co-treatment with TO and $CdCl_2$ (Figure 8E,F) substantially restored fluorescence intensity, reaching levels similar to controls and significantly higher than in $CdCl_2$-only treated roots.

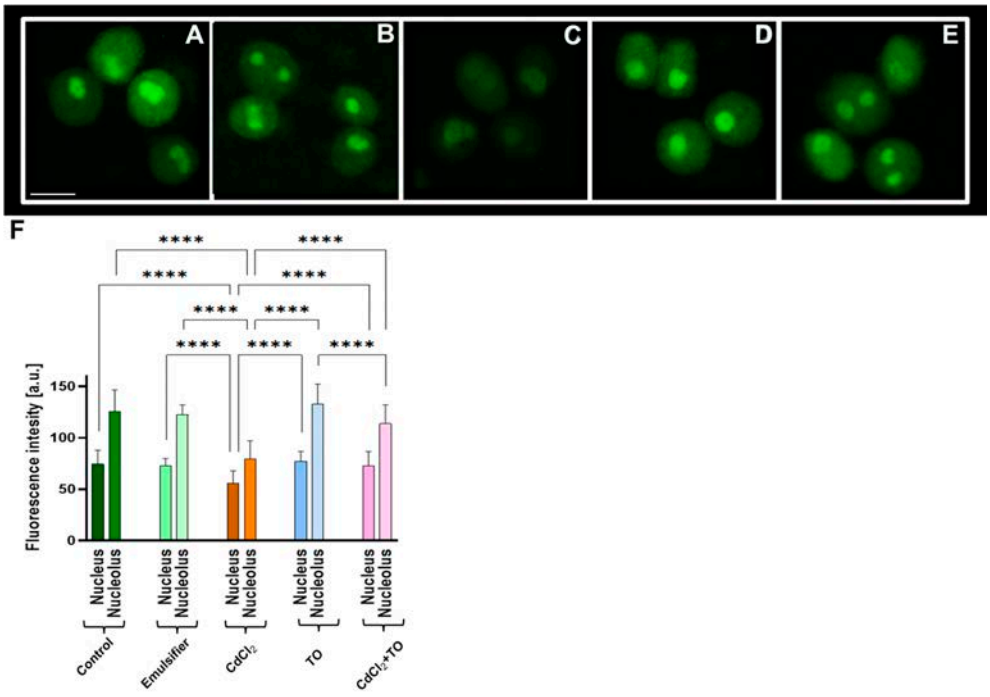

Figure 8. Detection of RNA synthesis using EU incorporation followed by Click-iT® RNA Alexa Fluor® 488 imaging in primary root meristem cells of *V. faba* after 24 h of incubation with water—Control (**A**), emulsifier (**B**), $CdCl_2$ (**C**), TO (**D**), and a combination of $CdCl_2$ and TO (**E**). Scale bar = 10 µm. Median (±CI; n = 6 biological replicates) EU labeling intensity (fluorescence intensity), expressed as a percentage of the maximum possible brightness (pixel value = 255); approximately 250 nuclei were analyzed per treatment (**F**). Statistical significance: **** $p < 0.0001$ (Kruskal–Wallis test with post hoc Dunn's multiple comparison test).

3. Discussion

Plants, due to their sessile lifestyle, have evolved sophisticated mechanisms for detecting environmental threats, including the presence of toxic heavy metals such as cadmium. These mechanisms are based on complex signaling networks that initiate defense and repair responses, as well as metabolic adjustments aimed at maintaining cellular homeostasis [62–66]. However, prolonged or high-intensity stress exposure can overwhelm these protective systems, leading to cellular dysfunctions that ultimately impair plant growth and development [67].

Consistent with such stress-induced cellular dysfunctions, exposure of *V. faba* seedlings to cadmium (175 μM $CdCl_2$) resulted in a marked increase in genotoxicity, reflected by an increase in the proportion of cells exhibiting DNA damage (identified by γ-H2A.X labeling characteristic of DNA double-strand breaks) from approximately 1% to nearly 30% [55]. This effect was associated with enhanced oxidative stress, manifested by a fourfold increase in hydrogen peroxide (H_2O_2) levels and a twofold increase in superoxide anion ($O_2\bullet^-$) content compared with control conditions [55].

Considering the need to identify natural and safe compounds capable of protecting plant cells against cadmium toxicity, particularly in the context of crop protection and yield stability, we further demonstrated that emulsified thyme oil (TO; 0.03%), rich in monoterpenes (thymol, *p*-cymene, carvacrol, limonene, and α-pinene), when applied simultaneously with cadmium, maintained ROS levels close to those of the control. As a result, TO effectively blocked the initiation of oxidative damage cascades, stabilized genome integrity, and reduced the proportion of cells exhibiting DNA double-strand breaks to approximately 5% [55].

Nevertheless, both heavy metals and ROS generated in their presence are potent activators of MAPK signaling cascades, which transmit stress-related information to the nucleus and initiate chromatin remodeling processes and stress-responsive gene regulation [26–28,68–72]. Since the mechanisms linking MAPK signaling with oxidative stress and chromatin regulation in plant cells remain insufficiently understood, in the present study we analyzed MAPK (p44/42) activation, global DNA methylation, histone modifications, and transcriptional activity. Together, all these analyses provide new insight into the relationship between MAPK signaling and epigenetic regulation under cadmium stress and demonstrate the ability of TO to modulate the plant cellular response pathway to cadmium stress.

3.1. Thyme Essential Oil Mitigates Cadmium-Induced Nuclear MAPK Activation

Cadmium exposure, along with increasing ROS levels in *V. faba* root meristem cells, leads to pronounced activation of nuclear MAPKs (MPK3/MPK6, homologs of ERK1/2 in animal cells). Immunocytochemical analyses revealed increases in the number, size, and intensity of MAPK-positive foci within chromatin, which is consistent with previous reports of cadmium-induced MAPK activation in *Medicago sativa* roots [13] and in *Oryza sativa* [73]. These results indicate that the applied Cd concentration activates a MAPK-dependent signaling pathway targeting the nucleus, thereby facilitating the initiation of defense mechanisms, including an epigenetic response. Such responses, mediated through chromatin reorganization, serve to protect DNA from endonuclease-mediated degradation [74] and enable adaptive transcriptional reprogramming [22,28].

A significant and, to our knowledge, previously unreported finding of this study is that TO prevents cadmium-induced activation of nuclear MAPKs in plant cells. While comparable plant studies are limited, similar effects of TO have been reported in animal models. Carvacrol, a major component of TO, inhibits p38 MAPK activity and reduces pro-inflammatory cytokine levels in the lungs of cadmium-exposed rats [75], and both

thymol and carvacrol were shown to suppress c-Jun N-terminal kinase (JNK) activation [76]. Considering our findings that TO reduces ROS levels under cadmium stress [55], together with our unpublished data confirming a robust activation of antioxidant defenses by TO, it is reasonable to propose that the protective effect of TO arises primarily from its ability to attenuate oxidative stress, thereby limiting nuclear MAPK phosphorylation. Therefore, MAPK activity remains close to control levels, correlating with normal seedling growth despite cadmium exposure. Thus, TO effectively alleviates cadmium toxicity by restraining MAPK-dependent nuclear stress signaling. Nonetheless, a direct inhibitory effect of specific TO components on MAPKs, analogous to that observed in animal cells, cannot be excluded.

3.2. Thyme Essential Oil Attenuates Cadmium-Induced DNA Hypermethylation

DNA methylation is a crucial regulatory mechanism in plants, controlling development, cell differentiation, and stress responses [77–79], while also maintaining genome stability by silencing transposable elements [80]. Methylation of promoter regions typically leads to chromatin condensation and transcriptional repression by restricting transcription factor access [29,81]. In the present study, immunofluorescence-based analysis of 5-mC revealed a pronounced increase in DNA methylation across nuclear chromatin in *V. faba* root meristem cells following $CdCl_2$ exposure. This hypermethylation coincided with enhanced nuclear MAPK activity, pointing to a functional link between stress-induced signaling and epigenetic regulation of the cellular response. Comparable cadmium-induced increases in global DNA methylation have been reported in soybean (*Glycine max*) and radish (*Raphanus sativus*), supporting the view that genome hypermethylation represents a conserved adaptive response to heavy metal stress in plants [82,83]. Importantly, co-treatment with Cd and TO effectively prevented the Cd-induced rise in 5-mC levels, which remained close to those observed in control cells. Given the established role of oxidative stress as an upstream driver of stress signaling and epigenetic remodeling, this effect is consistent with the ability of TO to attenuate ROS accumulation and limit the activation of downstream nuclear responses. In this context, the stabilization of DNA methylation patterns likely reflects a reduced propagation of stress signals toward chromatin remodeling pathways. This interpretation is further supported by our ongoing, unpublished analyses indicating enhanced antioxidant system activity in TO-treated seedlings under cadmium stress.

Although direct evidence for the impact of TO on DNA methylation in plants remains limited, studies in animal systems provide supportive parallels. Bozkurt et al. [84] demonstrated that *Thymus* spp. extracts reduce the expression of DNA methyltransferase 1 (DNMT1) in human cancer cells. Given that DNMT1 is functionally analogous to the plant maintenance methyltransferase 1 (MET1), responsible for preserving CG-context methylation [85], and that these enzymes share a high degree of homology within their catalytic domains [86], it is plausible that bioactive components of TO may also act at the enzymatic level in plant cells, modulating the DNA methylation machinery itself. Together, these observations suggest that TO-mediated modulation of DNA methylation represents an additional complementary layer of its protective action against cadmium-induced stress, beyond the upstream effects on ROS signaling pathway.

3.3. Thyme Essential Oil Modulates Cadmium-Induced Histone Modifications

Epigenetic DNA modifications act in concert with histone modifications to regulate chromatin accessibility for replication, repair, and transcription [87,88]. Abiotic stresses trigger dynamic changes in histone marks [89–92], allowing chromatin reorganization and gene expression reprogramming in response to DNA perturbations [93]. The direction and magnitude of these modifications, however, depend on species, tissue type, stressor, and metabolic context [91,94–97]. Our results indicate that cadmium strongly alters histone

methylation, acetylation, and phosphorylation patterns in *V. faba* root meristem cells, underscoring the central role of epigenetic regulation in response to heavy metal stress.

A well-conserved mark is methylation of lysine 4 on histone H3 (H3K4), which can exist in mono-, di-, and trimethylated forms [98]. While H3K4Me1 is mostly within coding regions, H3K4Me2 and H3K4Me3 are enriched at promoters near transcription start sites, a pattern conserved across yeast [99], animals [100], and plants [101,102]. Although H3K4 methylation generally marks active chromatin, the functional role of H3K4Me2 remains debated [100–103]. In plants, H3K4Me2 is often associated with transcriptional repression [104–106], whereas in mammals, it protects active promoters from de novo DNA methylation by preventing DNMT3L binding, a cofactor of DNMT3A/B methyltransferases that preferentially interacts with unmethylated H3K4 [107,108]. Importantly, H3K4Me2 function is context-dependent, and our observations, based on correlative immunocytochemistry, reflect global patterns rather than gene-specific effects. The cadmium-induced decrease in H3K4Me2 in *V. faba* root meristem cells aligns with increased global DNA methylation and reduced transcriptional activity. This suggests that cadmium may compromise epigenetic regulation at active promoters in a way that is reminiscent of the protective function of H3K4Me2 in animal systems. Comparable decreases in H3K4Me2/3 have been reported in tea (*Camellia sinensis*) cells under drought stress [109], whereas increases in H3K4Me2 were reported in maize (*Zea mays*) following drought and salt stress [110]. Together, these observations provide insight into how cadmium disrupts histone-mediated chromatin regulation and set the stage for examining how TO may counteract such epigenetic perturbations.

Phosphorylation of histone H3 at threonine 45 (H3T45Ph), which participates in nucleosome unwrapping, can significantly influence local DNA accessibility to transcriptional, repair, and replication complexes [111]. The T45 residue of H3, together with neighboring Y41 and R42, is located near the DNA entry/exit site of the nucleosome and forms part of the so-called "H3 latch," stabilizing DNA-histone interactions [112]. Phosphorylation of H3T45 changes the electrostatic charge of this residue, weakens its interaction with DNA, and facilitates the unwrapping of DNA ends, thereby promoting local chromatin relaxation. Although this modification remains poorly characterized in plants, studies in budding yeast (*Saccharomyces cerevisiae*) [113,114] and in HeLa cells [115] demonstrate its involvement in chromatin remodeling during DNA replication and the DNA damage response. Our results show that H3T45Ph levels were significantly reduced in *V. faba* meristem cells following cadmium exposure, consistent with the observed increase in DNA methylation and the overall reduction in transcriptional activity.

A similar conclusion arises from the analysis of histone H4 acetylation at lysine 5 (H4K5Ac). Under physiological conditions, H4K5Ac is abundant in interphase cells, present in both euchromatic and heterochromatic domains, and generally associated with chromatin relaxation required for transcription and replication [90]. Our immunocytochemical analyses revealed a significant decrease in H4K5Ac labeling intensity following cadmium exposure. This reduction correlates with diminished replication activity, the presence of DNA damage indicated by γH2AX immunostaining [55], and the overall reduction in transcriptional activity observed in this study. Together, these results support the conclusion that cadmium triggers a broad chromatin-silencing response. Similar decreases in H4K5Ac under abiotic stress have been reported in kenaf (*Hibiscus cannabinus*) subjected to NaCl and polyethylene glycol (PEG) treatments [116].

H4K5 acetylation is also linked to gene "priming," a preparatory marking of loci for rapid transcriptional activation in response to environmental cues [117]. This mechanism, observed in plant responses to abiotic stresses, may explain the strong H4K5Ac signal detected in a subset of nucleoli-associated nuclei, despite the overall reduction in this

modification in cadmium-treated cells. The nucleolus, responsible for rDNA transcription and ribosome biogenesis, is particularly sensitive to stress and responds through chromatin reorganization and transcriptional changes [118,119]. In this context, local enrichment of H4K5Ac within nucleolar regions may reflect an adaptive mechanism to sustain rDNA transcription and ribosome production under cadmium-induced oxidative stress and disrupted cellular homeostasis. The nucleolar labeling pattern may also indicate selective activation of genomic regions critical for the stress response. Considering the concurrent increase in global DNA methylation and the decrease in the potentially activating histone mark H3K4Me2, the presence of local H4K5Ac signals likely represents an effort to maintain expression of genes essential for cell survival. This interpretation is supported by Yue et al. [120], who showed that heat-stressed *Zea mays* cells exhibit nucleolar reorganization accompanied by increased histone acetylation within the 45S rDNA region, correlating with elevated pre-rRNA synthesis. Similarly, in pak choi (*Brassica rapa* subsp. *chinensis*) exposed to cadmium, enhanced H4K5Ac levels within the 45S rDNA promoter were associated with activation of rRNA transcription [121].

Although $CdCl_2$-induced stress generally decreases histone modifications associated with chromatin relaxation (H3K4Me2, H3T45Ph, H4K5Ac), we observed a concurrent increase in specific marks that accompany transcriptional activity under environmental stress. One such modification is the well-documented acetylation of histone H3 at lysine 9 (H3K9Ac), which in plants is enriched within promoter regions of genes activated by abiotic stressors [122]. In the context of heavy metal-induced oxidative stress, H3K9Ac may contribute to transcriptional reprogramming, enabling the rapid and selective induction of defense-related genes [123], including those encoding antioxidant proteins or detoxification enzymes (e.g., phytochelatin synthases), despite the overall transcriptional repression observed at the whole-nucleus level. This interpretation aligns with the findings of Wang et al. [124], who reported increased H3K9Ac accompanied by reduced histone methylation in plants exposed to heat stress, suggesting an epigenetic mechanism that supports dynamic transcriptional shift under changing environmental conditions. Similar observations were made in *Arabidopsis thaliana*, where elevated H3K9Ac levels in the promoters of stress-inducible genes such as *AtMYB29* and *AtGST1* correlated with their enhanced transcription [125]. Salt stress likewise promotes H3K9 acetylation: in *Oryza sativa*, severe salinity induced a pronounced increase in H3K9Ac, particularly in seedling leaves, with enrichment localized to promoters of salt-responsive genes [126]. Together with the previously discussed decreases in H3K4Me2, H3T45Ph, and H4K5Ac, these observations highlight a complex, locus-specific epigenetic response, in which certain stress-responsive genes remain transcriptionally active despite global chromatin condensation triggered by cadmium exposure.

The second histone modification that markedly increased following $CdCl_2$ treatment was the acetylation of lysine 56 on histone H3 (H3K56Ac), a well-established marker of the cellular response to DNA damage. While this mechanism is well characterized in yeast [127], its role in plants remains less understood [128]. H3K56Ac facilitates chromatin relaxation, supports DNA strand separation, and promotes recruitment of DNA repair complexes [127]. It is also associated with newly synthesized histone H3 incorporated during DNA replication [129]. In this study, cadmium exposure strongly induced H3K56Ac, particularly in S-phase cells. This increase should be considered part of the broader cellular response to compromised genomic integrity, consistent with previous reports of cadmium's genotoxic effects [55,90]. The functional importance of this modification for cell survival under stress is further supported by studies in *S. cerevisiae*, where mutation of lysine 56, preventing its acetylation, drastically reduces cell viability and renders cells hypersensitive to DNA damage and replication stress [130]. Collectively, these findings emphasize the

essential role of H3K56 acetylation in maintaining genome stability and supporting adaptive stress responses, including in plant systems.

Many of the observed epigenetic changes—such as increased DNA methylation and reduced levels of H3K4Me2, H3T45Ph, and H4K5Ac—appear to represent elements of a coordinated response to cadmium stress, consistent with oxidative stress-driven signaling pathways, including ROS-dependent MAPK activation [69,131,132]. At the same time, these changes cannot be interpreted exclusively as regulated adaptive responses. Cadmium is a well-known inhibitor of thiol-containing proteins [133,134], and numerous epigenetic enzymes, including histone acetyltransferases, methyltransferases, and kinases, contain cysteine residues within their catalytic domains [135,136]. Therefore, the cadmium-induced reduction in activating histone marks, accompanied by transcriptional repression, may reflect not only stress signaling-mediated chromatin remodeling but also direct toxic interference with enzymatic activity, resulting in a partial "freezing" of epigenetic states. Under prolonged heavy metal stress, both adaptive and damage-related mechanisms are likely to coexist and interact.

Importantly, the heterogeneous nature of the observed modifications indicates that cadmium does not simple induce uniform chromatin silencing. Instead, it appears to promote selective reorganization of chromatin accessibility, in which general transcriptional programs are suppressed while stress-responsive loci may remain permissive or even activated. Although this selective regulation cannot be conclusively demonstrated without locus-specific analyses, the observed pattern is consistent with a stress-adaptive redistribution of transcriptional activity. Against this background, a key finding of the present study is that concurrent application of thyme essential oil effectively counteracts cadmium-induced epigenetic alterations. TO consistently modulated histone modifications in the opposite direction to cadmium exposure: it restored marks associated with chromatin relaxation (H3K4Me2, H3T45Ph, and H4K5Ac) toward control levels and limited the excessive accumulation of stress-associated modifications (H3K9Ac, H3K56Ac). Although TO did not always fully normalize all parameters, the overall epigenetic profile clearly antagonized the effects of $CdCl_2$. To our knowledge, this study provides the first evidence that a plant essential oil can mitigate heavy metal toxicity by simultaneously modulating nuclear MAPK activity and multiple histone modifications, thereby stabilizing chromatin architecture and supporting transcriptional balance. The protective action of TO at the epigenomic level should be considered in a broader mechanistic context. Previous work demonstrated that TO reduces cadmium-induced ROS overproduction [55] and prevents excessive activation of nuclear MAPKs. Together with the present findings, this supports a model in which TO acts primarily at early stages of the stress response by limiting oxidative stress, which represents a major upstream trigger of MAPK signaling and downstream epigenetic remodeling (Figure 9). Similar protective mechanism have been described for *Rosmarinus officinalis* essential oil, which enhanced salt stress tolerance in durum wheat (*Triticum durum*) through ROS detoxification and stimulation of antioxidant defenses [137]. Collectively, these observations support the emerging view that plant essential oils can function as natural modulators of stress signaling and chromatin dynamics.

Finally, it cannot be excluded that cadmium-induced epigenetic responses in root meristem cells are also influenced by additional stress-related signals not directly linked to oxidative stress. Cadmium may impair the mobilization of endogenous reserves during early seedling development, including nitrogen pools, potentially activating alternative signaling pathways [138,139]. MAPK cascades are known to integrate diverse abiotic and metabolic cues [62,64], including nitrogen availability. For instance, RAF-like kinases at the MAPKKK level have been shown to respond to nitrogen status in green algae, illustrating how MAPK pathways can coordinate stress signaling with metabolic regulation [140].

Moreover, nitrogen deficiency has been reported to influence both MAPK activity and epigenetic modification dynamics in plants [141]. While these interactions remain speculative in the context of the present study, they point to additional regulatory layers that may shape chromatin responses under complex stress conditions and warrant targeted investigation in future work.

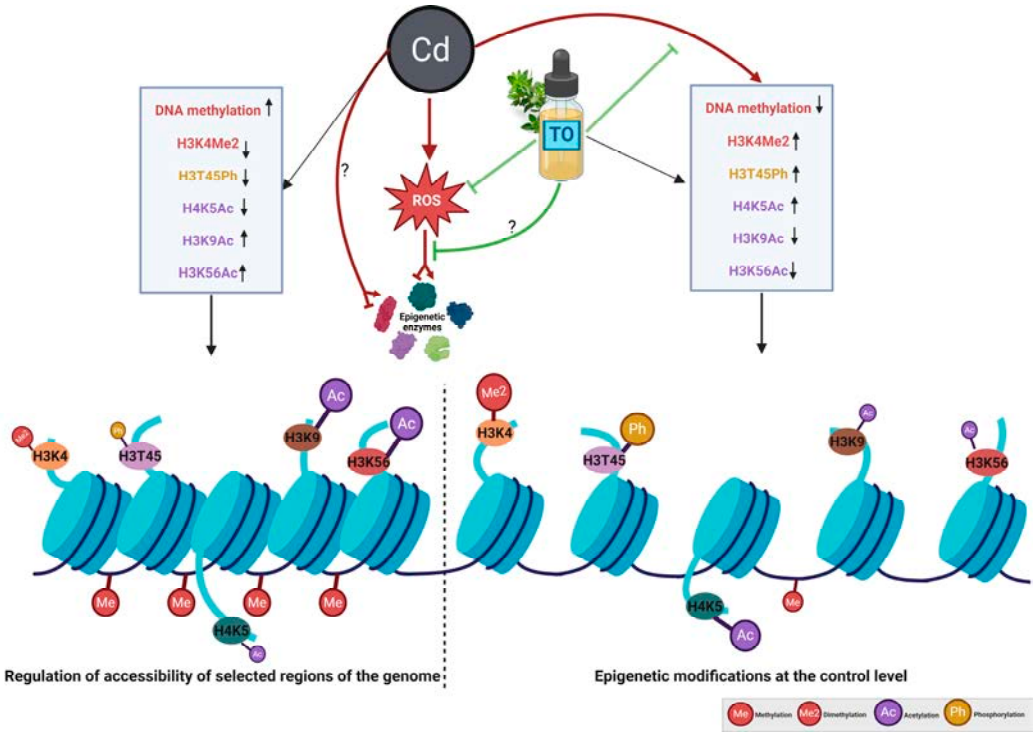

Figure 9. Schematic representation of the proposed mechanism illustrating the potential effects of cadmium (Cd) and thyme oil (TO) on epigenetic modifications. Arrows with sharp tips indicate activation or increase in enzymatic activity; arrows with flat tips indicate inhibition or reduction; arrows with both tips indicate that a factor can simultaneously activate some enzymes and inhibit others depending on the specific epigenetic mark. Cd exposure may induce oxidative stress (ROS), potentially affecting epigenetic enzyme activity and leading to changes in DNA methylation and histone modifications (↓H3K4Me2, ↓H3T45Ph, ↓H4K5Ac, ↑H3K9Ac, ↑H3K56Ac; arrows indicate increase [↑] or decrease [↓]). TO may counteract these effects by reducing oxidative stress, thereby restoring the histone modification profile (↓DNA methylation, ↑H3K4Me2, ↑H3T45Ph, ↑H4K5Ac, ↓H3K9Ac, ↓H3K56Ac). The bottom panel illustrates chromatin structural changes, highlighting potential regulation of genome accessibility under Cd alone or Cd combined with TO. This model is proposed and requires further functional studies for full confirmation. Created with BioRender.com.

3.4. Thyme Essential Oil Preserves Transcription Under Cadmium Stress

The epigenetic alterations described above provide a mechanistic framework for the transcriptional changes observed under cadmium stress, through their impact on chromatin accessibility [142–144].

Using EU incorporation and fluorescence microscopy, we observed a pronounced reduction in RNA synthesis in cadmium-treated cells, affecting both the nucleoplasm and the nucleolus. This finding is consistent with previous reports demonstrating that cadmium exposure leads to widespread transcriptional disturbances, typically characterized by global repression of gene expression. For example, Kovalchuk et al. [145] showed that chronic exposure of plants to 50 µM Cd altered the expression of 403 genes, with 65 upregulated and 338 downregulated. Similarly, in barley (*Hordeum vulgare*), cadmium treatment (80 µM) markedly reduced transcript levels in both roots and shoots [146]. Such transcrip-

tional suppression is a common feature of stress responses, in which energy-demanding growth-related programs are attenuated while resources are redirected toward defense and survival. At the same time, transcriptional regulation under stress is not uniform. Epigenetic modifications that repress and activate transcription can coexist within the same nucleus, reflecting the selective nature of stress responses [147]. While DNA methylation and loss of activating histone marks may silence genes involved in growth and development, stress-responsive loci can remain transcriptionally active or even be induced, for instance through histone acetylation such as H3K9Ac [148]. This model is supported by transcriptomic meta-analyses in rice, which revealed repression of photosynthesis-related pathways alongside activation of phytohormone- and stress-related genes under diverse stress conditions [149].

Importantly, our results show that TO effectively counteracts cadmium-induced transcriptional repression, restoring RNA synthesis to levels close to those observed in control cells. To our knowledge, this study provides the first evidence that plant essential oil can preserve transcriptional activity under heavy metal stress by simultaneously modulating MAPK signaling and epigenetic states thereby stabilizing chromatin organization. Although direct studies on the effect of TO on global transcription in plants are lacking, supportive data from animal systems indicate its broader regulatory potential. For instance, Firmino et al. [150] demonstrated that dietary supplementation with carvacrol- and thymol-containing blends significantly altered gene expression profiles in gilthead seabream (*Sparus aurata*), affecting 534 transcripts (393 upregulated and 141 downregulated). In *V. faba* the protective effect of TO on transcription likely represents a downstream consequence of its action at earlier stages of the stress response. By limiting oxidative stress and excessive MAPK activation, TO attenuates cadmium-induced epigenetic perturbations, preserves nucleolar integrity, and ultimately maintains transcriptional activity near physiological levels. Together, these findings place transcriptional preservation as the functional outcome of TO-mediated stabilization of the MAPK–epigenetic–chromatin axis under cadmium stress.

4. Materials and Methods

4.1. Plant Material

Sterile seeds of cultivated field bean (*Vicia faba* var. *minor*) (W. Legutko The Seed Breeding Company in Jutrosin, Poland) were sown in trays on moist blotting paper and germinated in darkness at 20 °C. After 72 h, seedlings with primary roots approximately 2–3 cm long were selected for uniform size, divided into experimental series and incubated for 24 h in the following media: 1—distilled water (control), 2—emulsifier solution used to prepare the essential oil emulsion, 3—cadmium chloride ($CdCl_2$) solution at a concentration of 175 µM, 4—emulsified thyme oil (TO; Etja, Elbląg, Poland; composition previously analyzed by GC-MS [55]) solution at a concentration of 0.03% and 5—$CdCl_2$ solution supplemented with emulsified TO. The $CdCl_2$ concentration was selected based on available literature data and preliminary experiments testing a concentration range of 100–200 µM [55,90,151–153]. The concentration of commercially accessible TO was determined based on preliminary tests within the 0.01–0.06% range and previously published studies [55]. For proper dispersion of TO in water, it was emulsified using a mixture of mono- and di-ethoxylated C14-18 and unsaturated C16-18 glycerides, together with ethoxylated *Brassica napus* oil. The emulsification process involved mixing the emulsifier with TO at a 1:4 (v/v) ratio (resulting in a final emulsifier concentration of 0.0075% v/v), followed by vigorous shaking with a vortex mixer for 15 min. The emulsifier was provided by the Department of Agronomy, University of Life Sciences in Poznań. The experiments were conducted on three independently prepared cultures. In each of them, five experimental series were prepared on separate Petri dishes (3 cm high, 25 cm in diameter), each containing

10 seedlings. Two seedlings were collected from each dish for each analysis. As a result, n = 6 biological replicates (root meristems) were obtained for each condition, except for the H4K5Ac analysis which was performed on 3 biological replicates (3 root meristems).

4.2. Immunocytochemical Detection of Dually Phosphorylated MAPKs

For immunocytochemical detection of dually phosphorylated mitogen-activated protein kinases (MAPKs), excised 1.5 mm long *V. faba* root tips were fixed for 45 min at 4 °C in 4% paraformaldehyde buffered with PBS, washed with PBS and then incubated for 45 min in citrate-buffered 2.5% pectinase (pH 5.0; 40 °C). After rinsing with PBS, root meristems were crushed on Super Frost Plus slides (Menzel-Gläser Thermo Fisher Scientific, Waltham, MA, USA) in a drop of distilled water. Following freezing on dry ice, coverslips were removed, the slides were washed with distilled water, and air dried. The preparations were then treated for 50 min with blocking buffer (8% BSA (Sigma-Aldrich, St. Louis, MO, USA) and 0.1% Triton X-100 (Sigma-Aldrich), PBS; 20 °C), followed by incubation with primary monoclonal anti-phospho-p44/42 MAPK antibodies, which cross-reacts with plant homologs MPK3 and MPK6 [61] (1:200, Cell Signaling Technology, Danvers, MA, USA) diluted in the antibody dilution buffer (1% w/v BSA, 0.3% v/v Triton X-100, PBS). After overnight incubation (4 °C), the slides were washed with PBS and incubated for 90 min with secondary Alexa Fluor 488-conjugated anti-rabbit IgG antibodies (1:1000, Sigma-Aldrich; 20 °C) diluted in the same antibody buffer. DNA was counterstained for 15 min with 5 µM DAPI (Sigma-Aldrich), followed by washing in PBS. Finally slides were mounted in a PBS/glycerol mixture (9:1) containing 2.5% 1,4-diazabicyclo [2.2.2]octane (DABCO).

4.3. Immunocytochemical Staining for DNA Methylation

Apical parts of *V. faba* primary roots were fixed for 10 min in freshly prepared 4% paraformaldehyde buffered with PBS (4 °C). After fixation, the root tips were washed with cold Tris buffer (10 mM Tris (hydroxy-methyl)-aminomethane, 10 mM EDTA-2Na, 100 mM NaCI; pH 7.2). Cell nuclei were then isolated, dropped onto Super Frost Plus slides (Menzel-Gläser) and air-dried (according to Żabka et al. [153]. Slides were treated with 4 M HCl for 90 min (20 °C) to partially denature the nuclear DNA, washed with Tris buffer containing 0.5% Triton X-100 (pH 7.4), and incubated with primary monoclonal anti-5-methylcytosine (5-mC, Sigma-Aldrich) antibodies dissolved in the antibody dilution buffer (1% w/v BSA, 0.3% v/v Triton X-100, PBS). Following an 16 h incubation (4 °C), slides were washed with Tris buffer and incubated for 90 min with the secondary goat anti-rabbit Alexa Fluor®488-conjugated antibodies (1:500; Cell Signaling, Warsaw, Poland) dissolved in the antibody dilution buffer (1% w/v BSA, 0.3% v/v Triton X-100, PBS; 20 °C), washed in Tris buffer, and embedded in PBS mixture/glycerol (9:1) with 2.3% DABCO.

4.4. Immunocytochemical Detection of Histone Methylation, Acetylation and Phosphorylation

Excised root tips of *V. faba* were fixed for 10 min in freshly prepared PBS-buffered 4% paraformaldehyde (4 °C) and washed with cold PBS. The excised root tips were then squeezed in a drop of cold PBS buffer between two microscope slides to collect nuclear samples, which were dropped onto Super Frost Plus slides (Menzel-Gläser) and air-dried. The slides were then pre-treated for 90 min with blocking buffer (8% BSA and 0.1% Triton X-100, PBS; 20 °C), rinsed 3 times with PBS buffer and incubated overnight in a humid atmosphere (4 °C) with primary antibodies against one of the following histone modifications: H3K4Me2 (rabbit polyclonal, 1:200), H3K56Ac (rabbit monoclonal, 1:200), H3T45Ph (rabbit polyclonal, 1:100), H3K9Ac (rabbit monoclonal, 1:200), or H4K5Ac (rabbit monoclonal, 1:200) (all from Cell Signaling). After washing with PBS, the slides were incubated for 90 min with the secondary Alexa Fluor 488-conjugated anti-rabbit IgG (1:1000, Sigma-Aldrich; 20 °C) and counterstained for 15 min with 5 µM DAPI (Sigma-Aldrich; 20 °C).

Slides washed with PBS were air dried and embedded in PBS mixture/glycerol (9:1) with 2.3% DABCO.

4.5. 5-Ethynyl Uridine (EU) Labeling and Visualization of Nascent RNA

V. faba seedlings were pulsed for 60 min with a 1 mM solution of 5-ethynyl uridine (5-EU; Thermo Fisher Scientific, Waltham, MA, USA) in the dark (20 °C). Then, excised meristems of 1.5 mm length were fixed for 45 min in PBS-buffered 4% paraformaldehyde (4 °C; pH 7.4), washed with PBS and incubated for 45 min with the citrate-buffered 2.5% pectinase (pH 5.0; 40 °C). After maceration, root meristems were washed with cold PBS, squashed onto Super Frost Plus slides (Menzel-Gläser), frozen with dry ice, washed with PBS and air dried. The slides were then permeabilized for 15 min with PBS containing 0.5% Triton X-100. Nascent RNA was visualized using Click-iT® RNA Alexa Fluor® 488 Imaging Kit with the reaction cocktail (Thermo Fisher Scientific). Following 60 min incubation (20 °C), slides were washed in Click-iT® reaction rinse buffer and PBS. DNA was stained for 15 min with 5 µM DAPI (Sigma-Aldrich), and then the slides were washed in PBS. Specimens were mounted in PBS mixture/glycerol (9:1) with 2.3% DABCO.

4.6. Microscopic Measurements, Observations, and Analyses

Observations were performed with a Nikon Eclipse E600W fluorescence microscope (Nikon, Tokyo, Japan) featuring phase-contrast optics, a U2 filter (UVB light; λ = 340–380 nm) for DAPI and a B2 filter (blue light; λ = 465–496 nm) for Alexa Fluor® 488. All images in each experimental series of a given experiment, using the specific antibodies, were captured at identical integration times with a DS-Fi1 CCD camera (Nikon, Tokyo, Japan). Under these conditions, negative control samples—incubated only with the secondary antibody conjugated to Alexa Fluor® 488, without the primary antibody—did not produce a detectable signal, appearing completely dark in the images. During the analysis of nuclei exhibiting epigenetic modifications, the cell cycle phase of each nucleus (G1, S, or G2) was estimated by measuring nuclear DNA content using microfluorimetric analysis after DAPI staining. Quantitative analyses and fluorescence intensity (FI) measurements were performed in ImageJ software ver. 1.54p after conversion of the color images to grayscale and were expressed in arbitrary units [a.u.] as the mean pixel value (p.v.) covering the range from 0 (dark) to 255 (white) according to the methods described [154,155]. Standard background subtraction was applied by subtracting the average signal from areas lacking specific fluorescence.

4.7. Statistical Analysis

Data were analyzed using GraphPad Prism version 10 software (GraphPad Software, Boston, MA, USA). Before selecting the appropriate statistical test, data normality was assessed using the Shapiro–Wilk test. For datasets meeting the assumptions of normality, one-way analysis of variance (ANOVA) was performed, followed by Tukey's post hoc test to evaluate differences between groups. For datasets not meeting normality assumptions, the non-parametric Kruskal–Wallis test with appropriate post hoc analysis was applied. In data presentation, variables with a normal distribution are reported as mean ± standard deviation (SD), whereas variables not meeting normality assumptions are presented as median with confidence interval (CI). In all analyses, the significance level was set at $p < 0.05$. Statistical significance in figures is indicated with asterisks (**** $p < 0.0001$, *** $p < 0.001$, ** $p < 0.01$, * $p < 0.05$).

5. Conclusions

Our study shows that DNA methylation and histone modifications form an integral part of the epigenetic response to cadmium stress. The observed changes contribute to

chromatin reorganization, which may simultaneously reduce basal transcriptional activity and permit the activation of stress-responsive genes (Figure 10). In this manner, epigenetic remodeling likely acts as a functional link between early stress signaling and downstream transcriptional outcomes.

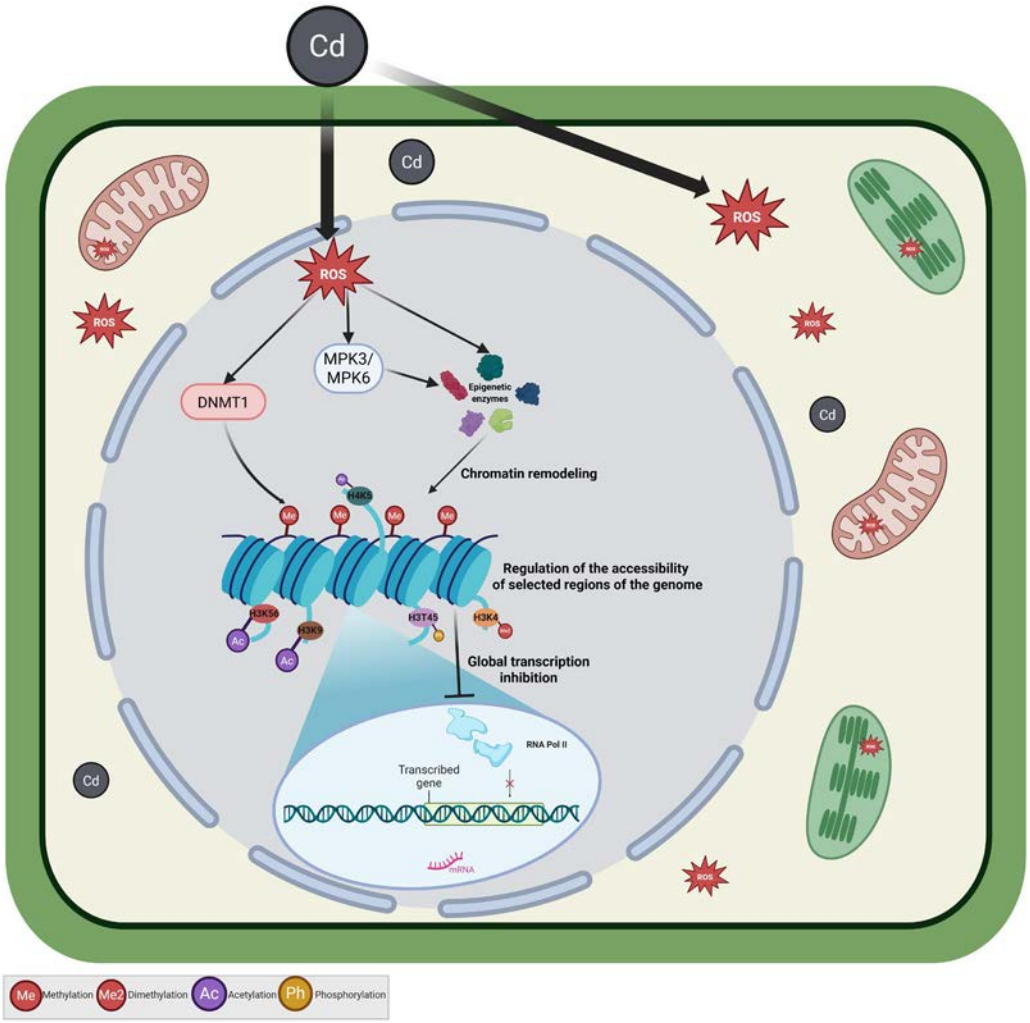

Figure 10. Proposed mechanism of cadmium (Cd) effects on the epigenetic regulation of gene expression. Arrows indicate the direction of processes or signaling pathways; arrows with pointed tips denote activation or enhancement, whereas arrows with blunt (flat) tips denote inhibition or suppression. Cd penetrates the cell, leading to the overproduction of reactive oxygen species (ROS). Elevated ROS levels activate signaling pathways involving MPK3/MPK6 kinases, which influence the activity of epigenetic enzymes. This triggers chromatin remodeling and changes in histone modifications, including methylation (H3K4), acetylation (H4K5, H3K9, H3K56), and phosphorylation (H3T45). Consequently, chromatin accessibility is reduced, and global gene transcription is inhibited. Created with BioRender.com.

The results also suggest potential mechanisms by which TO may mitigate cadmium-induced stress through modulation of epigenetic plasticity and transcriptional regulation. Our findings are consistent with the notion that TO acts during early stages of the cellular response, limiting the activation of detrimental signaling pathways and preventing alterations in chromatin structure (Figure 11).

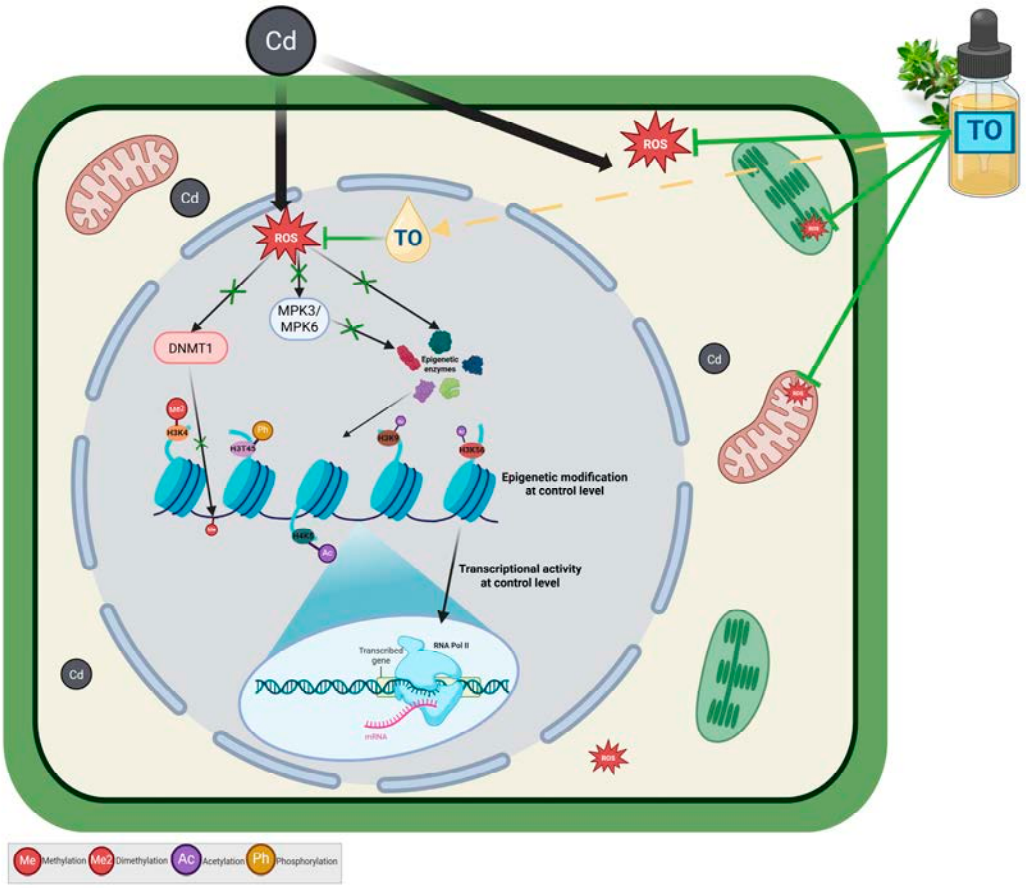

Figure 11. Proposed protective mechanism of thyme oil (TO) on cadmium (Cd)-induced epigenetic changes. Arrows indicate the direction of processes or signaling pathways; arrows with pointed tips denote activation or enhancement, whereas arrows with blunt (flat) tips denote inhibition or suppression. Exposure to Cd leads to the formation of reactive oxygen species (ROS), which disrupt the activity of epigenetic enzymes and MPK3/MPK6 kinases resulting in abnormal histone modifications (e.g., ↑H3K4Me2, ↓H3T45Ph, ↓H4K5Ac, ↑H3K9Ac, ↑H3K56Ac) and inhibition of global transcription. Treatment with TO reduces oxidative stress, restoring normal activity of epigenetic enzymes and maintaining balanced histone modifications. Consequently, chromatin structure is preserved and gene transcriptional activity remains at control levels. Created with BioRender.com.

Together, these observations expand current knowledge on epigenetic regulation under heavy metal stress and indicate that natural bioactive substances may contribute to strategies aimed at enhancing plant resilience in contaminated environments.

The presented data also support a broader perspective in which natural products such as TO, characterized by low toxicity, biodegradability, and high biological activity, may represent promising alternatives to synthetic agrochemicals. Essential oil-based formulations can be applied as foliar sprays, soil additives, or controlled-release systems such as microcapsules [156,157], in line with the principles of sustainable agriculture and the growing need to maintain crop performance under increasing heavy-metal pollution.

It should be emphasized that the present study was conducted exclusively on meristematic cells of *V. faba* exposed to a single cadmium concentration and a 24 h treatment with a defined TO dose. While this experimental design ensures clear and interpretable results, it also underscores the necessity for further investigation prior to practical application. Future studies should include a broader range of plant species, cadmium concentrations, and TO doses, as well as extended exposure periods, to better characterize dose- and time-dependent responses. From a molecular perspective, analysis of genes associated with oxidative stress responses and cell cycle regulation represents an important next step.

Ultimately, comprehensive transcriptomic approaches combined with targeted validation of selected marker genes will enable more precise integration of physiological, biochemical, and epigenetic responses to cadmium toxicity and the protective action of TO.

Author Contributions: Conceptualization, N.G.-S. and J.T.P.; methodology, N.G.-S., A.Ż. and J.T.P.; validation, N.G.-S. and J.T.P.; formal analysis, N.G.-S.; investigation, N.G.-S. resources, N.G.-S. and A.Ż.; data curation, N.G.-S.; writing—original draft preparation, N.G.-S.; writing—review and editing, A.Ż. and J.T.P.; visualization, N.G.-S. and M.W., supervision, J.T.P.; project administration, N.G.-S. funding acquisition, N.G.-S. All authors have read and agreed to the published version of the manuscript.

Funding: This work was supported through the budget of the Doctoral School of Exact and Natural Sciences of the University of Lodz.

Institutional Review Board Statement: Not applicable.

Informed Consent Statement: Not applicable.

Data Availability Statement: The raw data supporting the conclusions of this article will be made available by the authors on request.

Conflicts of Interest: The authors declare no conflicts of interest.

Abbreviations

The following abbreviations are used in this manuscript:

Cd	Cadmium
TO	Thyme oil
ROS	Reactive oxygen species
MAPK	Mitogen-activated protein kinases
ERK	Extracellular signal-regulated kinase
5-mC	5-methylcytosine
MET1	Methyltransferase 1
DNMT1	DNA (cytosine-5)-methyltransferase 1
CMT3	Chromomethylase 3
DRM2	Domains rearranged methylase 2
RdDM	RNA-directed DNA methylation
ROS1	Repressor of silencing 1
DME	Transcriptional activator Demeter
DML2	Demeter-like protein 2
DML3	Demeter-like protein 3
SUMO	Small ubiquitin-like modifier
HATs	Histone acetyltransferases
HDACs	Histone deacetylases
HMTs	Histone methyltransferases

References

1. Hussain, B.; Lin, Q.; Hamid, Y.; Sanaullah, M.; Di, L.; Hashmi, M.L.U.R.; Khan, M.B.; He, Z.; Yang, X. Foliage Application of Selenium and Silicon Nanoparticles Alleviates Cd and Pb Toxicity in Rice (*Oryza sativa* L.). *Sci. Total Environ.* **2020**, *712*, 136497. [CrossRef]
2. Merchant, S.S. The Elements of Plant Micronutrients. *Plant Physiol.* **2010**, *154*, 512–515. [CrossRef]
3. Rana, M.N.; Tangpong, J.; Rahman, M.M. Toxicodynamics of Lead, Cadmium, Mercury and Arsenic- Induced Kidney Toxicity and Treatment Strategy: A Mini Review. *Toxicol. Rep.* **2018**, *5*, 704–713. [CrossRef]
4. Zhang, X.Y.; Lin, F.F.; Wong, M.T.F.; Feng, X.L.; Wang, K. Identification of Soil Heavy Metal Sources from Anthropogenic Activities and Pollution Assessment of Fuyang County, China. *Environ. Monit. Assess.* **2009**, *154*, 439–449. [CrossRef]

5. Yi, Y.; Liu, H.; Chen, G.; Wu, X.; Zeng, F. Cadmium Accumulation in Plants: Insights from Phylogenetic Variation into the Evolution and Functions of Membrane Transporters. *Sustainability* **2023**, *15*, 12158. [CrossRef]
6. Abbas, T.; Rizwan, M.; Ali, S.; Adrees, M.; Zia-ur-Rehman, M.; Qayyum, M.F.; Ok, Y.S.; Murtaza, G. Effect of Biochar on Alleviation of Cadmium Toxicity in Wheat (*Triticum aestivum* L.) Grown on Cd-Contaminated Saline Soil. *Environ. Sci. Pollut. Res.* **2018**, *25*, 25668–25680. [CrossRef] [PubMed]
7. Younis, U.; Malik, S.A.; Rizwan, M.; Qayyum, M.F.; Ok, Y.S.; Shah, M.H.R.; Rehman, R.A.; Ahmad, N. Biochar Enhances the Cadmium Tolerance in Spinach (*Spinacia oleracea*) through Modification of Cd Uptake and Physiological and Biochemical Attributes. *Environ. Sci. Pollut. Res.* **2016**, *23*, 21385–21394. [CrossRef] [PubMed]
8. Heyno, E.; Klose, C.; Krieger-Liszkay, A. Origin of Cadmium-induced Reactive Oxygen Species Production: Mitochondrial Electron Transfer versus Plasma Membrane NADPH Oxidase. *New Phytol.* **2008**, *179*, 687–699. [CrossRef] [PubMed]
9. Li, C.; Tang, Y.; Gu, F.; Wang, X.; Yang, W.; Han, Y.; Ruan, Y. Phytochemical Analysis Reveals an Antioxidant Defense Response in *Lonicera japonica* to Cadmium-Induced Oxidative Stress. *Sci. Rep.* **2022**, *12*, 6840. [CrossRef]
10. Cuypers, A.; Vanbuel, I.; Iven, V.; Kunnen, K.; Vandionant, S.; Huybrechts, M.; Hendrix, S. Cadmium-Induced Oxidative Stress Responses and Acclimation in Plants Require Fine-Tuning of Redox Biology at Subcellular Level. *Free Radic. Biol. Med.* **2023**, *199*, 81–96. [CrossRef]
11. Winter, H.; Huber, S.C. Regulation of Sucrose Metabolism in Higher Plants: Localization and Regulation of Activity of Key Enzymes. *Crit. Rev. Biochem. Mol. Biol.* **2000**, *35*, 253–289. [CrossRef]
12. Richard, C.; Lescot, M.; Inzé, D.; De Veylder, L. Effect of Auxin, Cytokinin, and Sucrose on Cell Cycle Gene Expression in *Arabidopsis thaliana* cell Suspension Cultures. *Plant Cell Tissue Organ. Cult.* **2002**, *69*, 167–176. [CrossRef]
13. Jonak, C.; Nakagami, H.; Hirt, H. Heavy Metal Stress. Activation of Distinct Mitogen-Activated Protein Kinase Pathways by Copper and Cadmium. *Plant Physiol.* **2004**, *136*, 3276–3283. [CrossRef]
14. Chen, L.; Xu, B.; Liu, L.; Luo, Y.; Zhou, H.; Chen, W.; Shen, T.; Han, X.; Kontos, C.D.; Huang, S. Cadmium Induction of Reactive Oxygen Species Activates the mTOR Pathway, Leading to Neuronal Cell Death. *Free Radic. Biol. Med.* **2011**, *50*, 624–632. [CrossRef]
15. Gupta, D.K.; Pena, L.B.; Romero-Puertas, M.C.; Hernández, A.; Inouhe, M.; Sandalio, L.M. NADPH Oxidases Differentially Regulate ROS Metabolism and Nutrient Uptake under Cadmium Toxicity. *Plant Cell Environ.* **2017**, *40*, 509–526. [CrossRef]
16. Jamsheer, K.M.; Jindal, S.; Laxmi, A. Evolution of TOR–SnRK Dynamics in Green Plants and Its Integration with Phytohormone Signaling Networks. *J. Exp. Bot.* **2019**, *70*, 2239–2259. [CrossRef]
17. Hernández-Cruz, E.Y.; Arancibia-Hernández, Y.L.; Loyola-Mondragón, D.Y.; Pedraza-Chaverri, J. Oxidative Stress and Its Role in Cd-Induced Epigenetic Modifications: Use of Antioxidants as a Possible Preventive Strategy. *Oxygen* **2022**, *2*, 177–210. [CrossRef]
18. Li, S.; Han, X.; Lu, Z.; Qiu, W.; Yu, M.; Li, H.; He, Z.; Zhuo, R. MAPK Cascades and Transcriptional Factors: Regulation of Heavy Metal Tolerance in Plants. *Int. J. Mol. Sci.* **2022**, *23*, 4463. [CrossRef] [PubMed]
19. Luo, P.; Wu, J.; Li, T.-T.; Shi, P.; Ma, Q.; Di, D.-W. An Overview of the Mechanisms through Which Plants Regulate ROS Homeostasis under Cadmium Stress. *Antioxidants* **2024**, *13*, 1174. [CrossRef] [PubMed]
20. Kalapos, B.; Hlavová, M.; Nádai, T.V.; Galiba, G.; Bišová, K.; Dóczi, R. Early Evolution of the Mitogen-Activated Protein Kinase Family in the Plant Kingdom. *Sci. Rep.* **2019**, *9*, 4094. [CrossRef]
21. Moustafa, K.; Vos, D.L.-D.; Leprince, A.-S.; Savouré, A.; Laurière, C. Analysis of the *Arabidopsis* Mitogen-Activated Protein Kinase Families: Organ Specificity and Transcriptional Regulation upon Water Stresses. *Sch. Res. Exch.* **2008**, 143656. [CrossRef]
22. Bigeard, J.; Hirt, H. Nuclear Signaling of Plant MAPKs. *Front. Plant Sci.* **2018**, *9*, 469. [CrossRef] [PubMed]
23. Clayton, A.L.; Rose, S.; Barratt, M.J.; Mahadevan, L.C. Phosphoacetylation of Histone H3 on c-*Fos*- and c-*Jun*-Associated Nucleosomes upon Gene Activation. *EMBO J.* **2000**, *19*, 3714–3726. [CrossRef]
24. Li, B.; Jiang, S.; Yu, X.; Cheng, C.; Chen, S.; Cheng, Y.; Yuan, J.S.; Jiang, D.; He, P.; Shan, L. Phosphorylation of Trihelix Transcriptional Repressor ASR3 by MAP KINASE4 Negatively Regulates *Arabidopsis* Immunity. *Plant Cell* **2015**, *27*, 839–856. [CrossRef]
25. Roux, M.E.; Rasmussen, M.W.; Palma, K.; Lolle, S.; Regué, À.M.; Bethke, G.; Glazebrook, J.; Zhang, W.; Sieburth, L.; Larsen, M.R.; et al. The mRNA Decay Factor PAT 1 Functions in a Pathway Including MAP Kinase 4 and Immune Receptor SUMM 2. *EMBO J.* **2015**, *34*, 593–608. [CrossRef]
26. Lee, J.; Eschen-Lippold, L.; Lassowskat, I.; Böttcher, C.; Scheel, D. Cellular Reprogramming through Mitogen-Activated Protein Kinases. *Front. Plant Sci.* **2015**, *6*, 940. [CrossRef]
27. Sheikh, A.H.; Eschen-Lippold, L.; Pecher, P.; Hoehenwarter, W.; Sinha, A.K.; Scheel, D.; Lee, J. Regulation of WRKY46 Transcription Factor Function by Mitogen-Activated Protein Kinases in *Arabidopsis thaliana*. *Front. Plant Sci.* **2016**, *7*, 61. [CrossRef] [PubMed]
28. Latrasse, D.; Jégu, T.; Li, H.; De Zelicourt, A.; Raynaud, C.; Legras, S.; Gust, A.; Samajova, O.; Veluchamy, A.; Rayapuram, N.; et al. MAPK-Triggered Chromatin Reprogramming by Histone Deacetylase in Plant Innate Immunity. *Genome Biol.* **2017**, *18*, 131. [CrossRef]
29. Luan, A.; Chen, C.; Xie, T.; He, J.; He, Y. Methylation Analysis of CpG Islands in Pineapple SERK1 Promoter. *Genes* **2020**, *11*, 425. [CrossRef] [PubMed]

30. Lister, R.; O'Malley, R.C.; Tonti-Filippini, J.; Gregory, B.D.; Berry, C.C.; Millar, A.H.; Ecker, J.R. Highly Integrated Single-Base Resolution Maps of the Epigenome in *Arabidopsis*. *Cell* **2008**, *133*, 523–536. [CrossRef]
31. Leichter, S.M.; Du, J.; Zhong, X. Structure and Mechanism of Plant DNA Methyltransferases. In *DNA Methyltransferases—Role and Function*; Jeltsch, A., Jurkowska, R.Z., Eds.; Advances in Experimental Medicine and Biology; Springer International Publishing: Cham, Switzerland, 2022; Volume 1389, pp. 137–157, ISBN 978-3-031-11453-3.
32. Zhang, H.; Lang, Z.; Zhu, J.-K. Dynamics and Function of DNA Methylation in Plants. *Nat. Rev. Mol. Cell Biol.* **2018**, *19*, 489–506. [CrossRef]
33. Stroud, H.; Do, T.; Du, J.; Zhong, X.; Feng, S.; Johnson, L.; Patel, D.J.; Jacobsen, S.E. Non-CG Methylation Patterns Shape the Epigenetic Landscape in *Arabidopsis*. *Nat. Struct. Mol. Biol.* **2014**, *21*, 64–72. [CrossRef]
34. Kumar, S.; Mohapatra, T. Dynamics of DNA Methylation and Its Functions in Plant Growth and Development. *Front. Plant Sci.* **2021**, *12*, 596236. [CrossRef] [PubMed]
35. Sun, M.; Yang, Z.; Liu, L.; Duan, L. DNA Methylation in Plant Responses and Adaption to Abiotic Stresses. *Int. J. Mol. Sci.* **2022**, *23*, 6910. [CrossRef]
36. Chang, Y.; Zhu, C.; Jiang, J.; Zhang, H.; Zhu, J.; Duan, C. Epigenetic Regulation in Plant Abiotic Stress Responses. *J. Integr. Plant Biol.* **2020**, *62*, 563–580. [CrossRef]
37. Stankovic-Valentin, N.; Melchior, F. Control of SUMO and Ubiquitin by ROS: Signaling and Disease Implications. *Mol. Asp. Med.* **2018**, *63*, 3–17. [CrossRef]
38. Ueda, M.; Seki, M. Histone Modifications Form Epigenetic Regulatory Networks to Regulate Abiotic Stress Response. *Plant Physiol.* **2020**, *182*, 15–26. [CrossRef]
39. Berr, A.; Shafiq, S.; Shen, W.-H. Histone Modifications in Transcriptional Activation during Plant Development. *Biochim. Biophys. Acta (BBA)—Gene Regul. Mech.* **2011**, *1809*, 567–576. [CrossRef] [PubMed]
40. Eberharter, A.; Becker, P.B. Histone Acetylation: A Switch between Repressive and Permissive Chromatin: Second in Review Series on Chromatin Dynamics. *EMBO Rep.* **2002**, *3*, 224–229. [CrossRef] [PubMed]
41. Li, S.; Lin, Y.-C.J.; Wang, P.; Zhang, B.; Li, M.; Chen, S.; Shi, R.; Tunlaya-Anukit, S.; Liu, X.; Wang, Z.; et al. The AREB1 Transcription Factor Influences Histone Acetylation to Regulate Drought Responses and Tolerance in *Populus trichocarpa*. *Plant Cell* **2019**, *31*, 663–686. [CrossRef]
42. Tanaka, M.; Kikuchi, A.; Kamada, H. The *Arabidopsis* Histone Deacetylases HDA6 and HDA19 Contribute to the Repression of Embryonic Properties after Germination. *Plant Physiol.* **2008**, *146*, 149–161. [CrossRef]
43. Rossetto, D.; Avvakumov, N.; Côté, J. Histone Phosphorylation: A Chromatin Modification Involved in Diverse Nuclear Events. *Epigenetics* **2012**, *7*, 1098–1108. [CrossRef] [PubMed]
44. Cheung, P.; Allis, C.D.; Sassone-Corsi, P. Signaling to Chromatin through Histone Modifications. *Cell* **2000**, *103*, 263–271. [CrossRef]
45. Hu, H.; Du, J. Structure and Mechanism of Histone Methylation Dynamics in *Arabidopsis*. *Curr. Opin. Plant Biol.* **2022**, *67*, 102211. [CrossRef] [PubMed]
46. Liu, C.; Lu, F.; Cui, X.; Cao, X. Histone Methylation in Higher Plants. *Annu. Rev. Plant Biol.* **2010**, *61*, 395–420. [CrossRef]
47. Bannister, A.J.; Kouzarides, T. Regulation of Chromatin by Histone Modifications. *Cell Res.* **2011**, *21*, 381–395. [CrossRef]
48. Jenuwein, T.; Allis, C.D. Translating the Histone Code. *Science* **2001**, *293*, 1074–1080. [CrossRef] [PubMed]
49. Hermans, C.; Chen, J.; Coppens, F.; Inzé, D.; Verbruggen, N. Low Magnesium Status in Plants Enhances Tolerance to Cadmium Exposure. *New Phytol.* **2011**, *192*, 428–436. [CrossRef]
50. Soković, M.D.; Vukojević, J.; Marin, P.D.; Brkić, D.D.; Vajs, V.; Van Griensven, L.J.L.D. Chemical Composition of Essential Oils of *Thymus* and *Mentha* Species and Their Antifungal Activities. *Molecules* **2009**, *14*, 238–249. [CrossRef]
51. Lorenzo, J.M.; Mousavi Khaneghah, A.; Gavahian, M.; Marszałek, K.; Eş, I.; Munekata, P.E.S.; Ferreira, I.C.F.R.; Barba, F.J. Understanding the Potential Benefits of Thyme and Its Derived Products for Food Industry and Consumer Health: From Extraction of Value-Added Compounds to the Evaluation of Bioaccessibility, Bioavailability, Anti-Inflammatory, and Antimicrobial Activities. *Crit. Rev. Food Sci. Nutr.* **2019**, *59*, 2879–2895. [CrossRef]
52. Martiniaková, S.; Ácsová, A.; Hojerová, J.; Krepsová, Z.; Kreps, F. Ceylon Cinnamon and Clove Essential Oils as Promising Free Radical Scavengers for Skin Care Products. *Acta Chim. Slovaca* **2022**, *15*, 1–11. [CrossRef]
53. Harpaz, S.; Glatman, L.; Drabkin, V.; Gelman, A. Effects of Herbal Essential Oils Used To Extend the Shelf Life of Freshwater-Reared Asian Sea Bass Fish (*Lates calcarifer*). *J. Food Prot.* **2003**, *66*, 410–417. [CrossRef]
54. Rahmani, F.; Nabi, S.; Idliki, R.B.; Alimirzaei, M.; Barkhordar, S.M.A.; Shafaei, N.; Zareian, M.; Karimi, E.; Oskoueian, E. Thyme Oil Nanoemulsion Enhanced Cellular Antioxidant and Suppressed Inflammation in Mice Challenged by Cadmium-Induced Oxidative Stress. *Waste Biomass Valor.* **2022**, *13*, 3139–3146. [CrossRef]
55. Gocek-Szczurtek, N.; Żabka, A.; Wróblewski, M.; Kukula-Koch, W.; Szczeblewski, P.; Polit, J.T. Thyme Oil Mitigates Cadmium-Induced Oxidative and Genotoxic Stress in *Vicia faba* Root Meristem Cells under in vitro Conditions. *Sci. Rep.* **2025**, *15*, 38689. [CrossRef] [PubMed]

56. Pandur, E.; Micalizzi, G.; Mondello, L.; Horváth, A.; Sipos, K.; Horváth, G. Antioxidant and Anti-Inflammatory Effects of Thyme (*Thymus vulgaris* L.) Essential Oils Prepared at Different Plant Phenophases on *Pseudomonas aeruginosa* LPS-Activated THP-1 Macrophages. *Antioxidants* **2022**, *11*, 1330. [CrossRef] [PubMed]
57. Kowalczyk, A.; Przychodna, M.; Sopata, S.; Bodalska, A.; Fecka, I. Thymol and Thyme Essential Oil—New Insights into Selected Therapeutic Applications. *Molecules* **2020**, *25*, 4125. [CrossRef]
58. Ansari, M.N.; Rehman, N.U.; Karim, A.; Imam, F.; Hamad, A.M. Protective Effect of *Thymus serrulatus* Essential Oil on Cadmium-Induced Nephrotoxicity in Rats, through Suppression of Oxidative Stress and Downregulation of NF-κB, iNOS, and Smad2 mRNA Expression. *Molecules* **2021**, *26*, 1252. [CrossRef]
59. Mohammed, A.A.; Ali, A.A.A.A.; Abdullah, S.A.G. Protective Role of Thyme Oil (*Thymus vulgaris*) Against Cadmium Chloride-Induced Renal Damage in Common Carp (*Cyprinus carpio*). *J. Basrah Res. (Sci.)* **2024**, *50*, 298–317. [CrossRef]
60. Maresca, V.; Badalamenti, N.; Ilardi, V.; Bruno, M.; Bontempo, P.; Basile, A. Chemical Composition of *Thymus leucotrichus* var. *creticus* Essential Oil and Its Protective Effects on Both Damage and Oxidative Stress in *Leptodictyum riparium* Hedw. Induced by Cadmium. *Plants* **2022**, *11*, 3529. [CrossRef] [PubMed]
61. Winnicki, K.; Żabka, A.; Bernasińska, J.; Matczak, K.; Maszewski, J. Immunolocalization of Dually Phosphorylated MAPKs in Dividing Root Meristem Cells of *Vicia faba*, *Pisum sativum*, *Lupinus luteus* and *Lycopersicon esculentum*. *Plant Cell Rep.* **2015**, *34*, 905–917. [CrossRef]
62. Sinha, A.K.; Jaggi, M.; Raghuram, B.; Tuteja, N. Mitogen-Activated Protein Kinase Signaling in Plants under Abiotic Stress. *Plant Signal. Behav.* **2011**, *6*, 196–203. [CrossRef] [PubMed]
63. Hann, C.T.; Ramage, S.F.; Negi, H.; Bequette, C.J.; Vasquez, P.A.; Stratmann, J.W. Dephosphorylation of the MAP Kinases MPK6 and MPK3 Fine-Tunes Responses to Wounding and Herbivory in *Arabidopsis*. *Plant Sci.* **2024**, *339*, 111962. [CrossRef] [PubMed]
64. Taj, G.; Agarwal, P.; Grant, M.; Kumar, A. MAPK Machinery in Plants: Recognition and Response to Different Stresses through Multiple Signal Transduction Pathways. *Plant Signal. Behav.* **2010**, *5*, 1370–1378. [CrossRef] [PubMed]
65. Saijo, Y.; Loo, E.P. Plant Immunity in Signal Integration between Biotic and Abiotic Stress Responses. *New Phytol.* **2020**, *225*, 87–104. [CrossRef] [PubMed]
66. Porter, T.K.; Heinz, M.N.; Lundberg, D.J.; Brooks, A.M.; Lew, T.T.S.; Silmore, K.S.; Koman, V.B.; Ang, M.C.-Y.; Khong, D.T.; Singh, G.P.; et al. A Theory of Mechanical Stress-Induced H_2O_2 Signaling Waveforms in Planta. *J. Math. Biol.* **2023**, *86*, 11. [CrossRef]
67. Petrov, V.; Hille, J.; Mueller-Roeber, B.; Gechev, T.S. ROS-Mediated Abiotic Stress-Induced Programmed Cell Death in Plants. *Front. Plant Sci.* **2015**, *6*, 69. [CrossRef]
68. Anjum, S.A.; Tanveer, M.; Hussain, S.; Bao, M.; Wang, L.; Khan, I.; Ullah, E.; Tung, S.A.; Samad, R.A.; Shahzad, B. Cadmium Toxicity in Maize (*Zea mays* L.): Consequences on Antioxidative Systems, Reactive Oxygen Species and Cadmium Accumulation. *Environ. Sci. Pollut. Res.* **2015**, *22*, 17022–17030. [CrossRef] [PubMed]
69. Liu, X.-M.; Kim, K.E.; Kim, K.-C.; Nguyen, X.C.; Han, H.J.; Jung, M.S.; Kim, H.S.; Kim, S.H.; Park, H.C.; Yun, D.-J.; et al. Cadmium Activates *Arabidopsis* MPK3 and MPK6 via Accumulation of Reactive Oxygen Species. *Phytochemistry* **2010**, *71*, 614–618. [CrossRef]
70. Mondal, S. Heavy Metal Stress–Induced Activation of Mitogen-Activated Protein Kinase Signalling Cascade in Plants. *Plant Mol. Biol. Rep.* **2022**, *41*, 15–26. [CrossRef]
71. Li, H.; Yan, S.; Zhao, L.; Tan, J.; Zhang, Q.; Gao, F.; Wang, P.; Hou, H.; Li, L. Histone Acetylation Associated Up-Regulation of the Cell Wall Related Genes Is Involved in Salt Stress Induced Maize Root Swelling. *BMC Plant Biol.* **2014**, *14*, 105. [CrossRef]
72. Chinnusamy, V.; Zhu, J.-K. Epigenetic Regulation of Stress Responses in Plants. *Curr. Opin. Plant Biol.* **2009**, *12*, 133–139. [CrossRef] [PubMed]
73. Yeh, C.-M.; Hsiao, L.-J.; Huang, H.-J. Cadmium Activates a Mitogen-Activated Protein Kinase Gene and MBP Kinases in Rice. *Plant Cell Physiol.* **2004**, *45*, 1306–1312. [CrossRef]
74. Genchi, G.; Sinicropi, M.S.; Lauria, G.; Carocci, A.; Catalano, A. The Effects of Cadmium Toxicity. *Int. J. Environ. Res. Public Health* **2020**, *17*, 3782. [CrossRef]
75. Yesildag, K.; Gur, C.; Ileriturk, M.; Kandemir, F.M. Evaluation of Oxidative Stress, Inflammation, Apoptosis, Oxidative DNA Damage and Metalloproteinases in the Lungs of Rats Treated with Cadmium and Carvacrol. *Mol. Biol. Rep.* **2022**, *49*, 1201–1211. [CrossRef]
76. Gholijani, N.; Gharagozloo, M.; Farjadian, S.; Amirghofran, Z. Modulatory Effects of Thymol and Carvacrol on Inflammatory Transcription Factors in Lipopolysaccharide-Treated Macrophages. *J. Immunotoxicol.* **2016**, *13*, 157–164. [CrossRef]
77. Shafiq, S.; Khan, A.R. Plant Epigenetics and Crop Improvement. In *PlantOmics: The Omics of Plant Science*; Barh, D., Khan, M.S., Davies, E., Eds.; Springer: New Delhi, India, 2015; pp. 157–179, ISBN 978-81-322-2171-5.
78. Zhang, M.; Kimatu, J.N.; Xu, K.; Liu, B. DNA Cytosine Methylation in Plant Development. *J. Genet. Genom.* **2010**, *37*, 1–12. [CrossRef]
79. Miryeganeh, M. Plants' Epigenetic Mechanisms and Abiotic Stress. *Genes* **2021**, *12*, 1106. [CrossRef] [PubMed]
80. Sriraman, A.; Debnath, T.K.; Xhemalce, B.; Miller, K.M. Making It or Breaking It: DNA Methylation and Genome Integrity. *Essays Biochem.* **2020**, *64*, 687–703. [CrossRef]

81. Kim, S.; Park, J.-S.; Lee, J.; Lee, K.K.; Park, O.-S.; Choi, H.-S.; Seo, P.J.; Cho, H.-T.; Frost, J.M.; Fischer, R.L.; et al. The DME Demethylase Regulates Sporophyte Gene Expression, Cell Proliferation, Differentiation, and Meristem Resurrection. *Proc. Natl. Acad. Sci. USA* **2021**, *118*, e2026806118, Correction in *Proc. Natl. Acad. Sci. USA* **2023**, *120*, e2311112120. https://doi.org/10.1073/pnas.2311112120. [CrossRef]
82. Sun, D.-D.; Sun, J.-W.; Huang, L.-Y.; Chen, N.; Wang, Q.-W. Effects of Cadmium Stress on DNA Methylation in Soybean. *Biotechnol. Biotechnol. Equip.* **2021**, *35*, 1696–1705. [CrossRef]
83. Tang, M.; Xu, L.; Wang, Y.; Dong, J.; Zhang, X.; Wang, K.; Ying, J.; Li, C.; Liu, L. Melatonin-Induced DNA Demethylation of Metal Transporters and Antioxidant Genes Alleviates Lead Stress in Radish Plants. *Hortic. Res.* **2021**, *8*, 124. [CrossRef]
84. Bozkurt, E.; Atmaca, H.; Kisim, A.; Uzunoglu, S.; Uslu, R.; Karaca, B. Effects of *Thymus serpyllum* Extract on Cell Proliferation, Apoptosis and Epigenetic Events in Human Breast Cancer Cells. *Nutr. Cancer* **2012**, *64*, 1245–1250. [CrossRef]
85. Tirot, L.; Jullien, P.E.; Ingouff, M. Evolution of CG Methylation Maintenance Machinery in Plants. *Epigenomes* **2021**, *5*, 19. [CrossRef]
86. Finnegan, E.J.; Kovac, K.A. Plant DNA methyltransferases. *Plant Mol. Biol.* **2000**, *43*, 189–201. [CrossRef] [PubMed]
87. Karakaidos, P.; Karagiannis, D.; Rampias, T. Resolving DNA Damage: Epigenetic Regulation of DNA Repair. *Molecules* **2020**, *25*, 2496. [CrossRef]
88. Zhang, Y.; Zhang, Q.; Zhang, Y.; Han, J. The Role of Histone Modification in DNA Replication-Coupled Nucleosome Assembly and Cancer. *Int. J. Mol. Sci.* **2023**, *24*, 4939. [CrossRef]
89. Fasani, E.; Giannelli, G.; Varotto, S.; Visioli, G.; Bellin, D.; Furini, A.; DalCorso, G. Epigenetic Control of Plant Response to Heavy Metals. *Plants* **2023**, *12*, 3195. [CrossRef]
90. Żabka, A.; Gocek, N.; Winnicki, K.; Szczeblewski, P.; Laskowski, T.; Polit, J.T. Changes in Epigenetic Patterns Related to DNA Replication in *Vicia faba* Root Meristem Cells under Cadmium-Induced Stress Conditions. *Cells* **2021**, *10*, 3409. [CrossRef]
91. Kim, J.-M.; To, T.K.; Ishida, J.; Morosawa, T.; Kawashima, M.; Matsui, A.; Toyoda, T.; Kimura, H.; Shinozaki, K.; Seki, M. Alterations of Lysine Modifications on the Histone H3 N-Tail under Drought Stress Conditions in *Arabidopsis thaliana*. *Plant Cell Physiol.* **2008**, *49*, 1580–1588. [CrossRef] [PubMed]
92. Hou, H.; Zhao, L.; Zheng, X.; Gautam, M.; Yue, M.; Hou, J.; Chen, Z.; Wang, P.; Li, L. Dynamic Changes in Histone Modification Are Associated with Upregulation of Hsf and rRNA Genes during Heat Stress in Maize Seedlings. *Protoplasma* **2019**, *256*, 1245–1256. [CrossRef] [PubMed]
93. Dabin, J.; Fortuny, A.; Polo, S.E. Epigenome Maintenance in Response to DNA Damage. *Mol. Cell* **2016**, *62*, 712–727. [CrossRef]
94. Chen, L.-T.; Wu, K. Role of Histone Deacetylases HDA6 and HDA19 in ABA and Abiotic Stress Response. *Plant Signal. Behav.* **2010**, *5*, 1318–1320. [CrossRef] [PubMed]
95. Hu, Y.; Zhang, L.; He, S.; Huang, M.; Tan, J.; Zhao, L.; Yan, S.; Li, H.; Zhou, K.; Liang, Y.; et al. Cold Stress Selectively Unsilences Tandem Repeats in Heterochromatin Associated with Accumulation of H3K9ac. *Plant Cell Environ.* **2012**, *35*, 2130–2142. [CrossRef]
96. Kim, J.-M.; To, T.K.; Ishida, J.; Matsui, A.; Kimura, H.; Seki, M. Transition of Chromatin Status During the Process of Recovery from Drought Stress in *Arabidopsis thaliana*. *Plant Cell Physiol.* **2012**, *53*, 847–856. [CrossRef]
97. Bhadouriya, S.L.; Mehrotra, S.; Basantani, M.K.; Loake, G.J.; Mehrotra, R. Role of Chromatin Architecture in Plant Stress Responses: An Update. *Front. Plant Sci.* **2021**, *11*, 603380. [CrossRef]
98. Xiao, M.; Wang, J.; Xu, F. Methylation Hallmarks on the Histone Tail as a Linker of Osmotic Stress and Gene Transcription. *Front. Plant Sci.* **2022**, *13*, 967607. [CrossRef]
99. Pokholok, D.K.; Harbison, C.T.; Levine, S.; Cole, M.; Hannett, N.M.; Lee, T.I.; Bell, G.W.; Walker, K.; Rolfe, P.A.; Herbolsheimer, E.; et al. Genome-Wide Map of Nucleosome Acetylation and Methylation in Yeast. *Cell* **2005**, *122*, 517–527. [CrossRef] [PubMed]
100. Barski, A.; Cuddapah, S.; Cui, K.; Roh, T.-Y.; Schones, D.E.; Wang, Z.; Wei, G.; Chepelev, I.; Zhao, K. High-Resolution Profiling of Histone Methylations in the Human Genome. *Cell* **2007**, *129*, 823–837. [CrossRef]
101. Oya, S.; Takahashi, M.; Takashima, K.; Kakutani, T.; Inagaki, S. Transcription-Coupled and Epigenome-Encoded Mechanisms Direct H3K4 Methylation. *Nat. Commun.* **2022**, *13*, 4521. [CrossRef]
102. Zhang, X.; Bernatavichute, Y.V.; Cokus, S.; Pellegrini, M.; Jacobsen, S.E. Genome-Wide Analysis of Mono-, Di- and Trimethylation of Histone H3 Lysine 4 in *Arabidopsis thaliana*. *Genome Biol.* **2009**, *10*, R62. [CrossRef] [PubMed]
103. Howe, F.S.; Fischl, H.; Murray, S.C.; Mellor, J. Is H3K4me3 Instructive for Transcription Activation? *BioEssays* **2017**, *39*, 1–12. [CrossRef]
104. Kim, T.; Xu, Z.; Clauder-Münster, S.; Steinmetz, L.M.; Buratowski, S. Set3 HDAC Mediates Effects of Overlapping Noncoding Transcription on Gene Induction Kinetics. *Cell* **2012**, *150*, 1158–1169. [CrossRef]
105. Ishihara, H.; Sugimoto, K.; Tarr, P.T.; Temman, H.; Kadokura, S.; Inui, Y.; Sakamoto, T.; Sasaki, T.; Aida, M.; Suzuki, T.; et al. Primed Histone Demethylation Regulates Shoot Regenerative Competency. *Nat. Commun.* **2019**, *10*, 1786. [CrossRef] [PubMed]
106. Liu, Y.; Liu, K.; Yin, L.; Yu, Y.; Qi, J.; Shen, W.-H.; Zhu, J.; Zhang, Y.; Dong, A. H3K4me2 Functions as a Repressive Epigenetic Mark in Plants. *Epigenetics Chromatin* **2019**, *12*, 40. [CrossRef] [PubMed]

107. Meissner, A.; Mikkelsen, T.S.; Gu, H.; Wernig, M.; Hanna, J.; Sivachenko, A.; Zhang, X.; Bernstein, B.E.; Nusbaum, C.; Jaffe, D.B.; et al. Genome-Scale DNA Methylation Maps of Pluripotent and Differentiated Cells. *Nature* **2008**, *454*, 766–770. [CrossRef]
108. Li, Y.; Chen, X.; Lu, C. The Interplay between DNA and Histone Methylation: Molecular Mechanisms and Disease Implications. *EMBO Rep.* **2021**, *22*, e51803. [CrossRef] [PubMed]
109. Chen, Q.; Guo, L.; Yuan, Y.; Hu, S.; Guo, F.; Zhao, H.; Yun, Z.; Wang, Y.; Wang, M.; Ni, D.; et al. Ectopic Overexpression of Histone H3K4 Methyltransferase CsSDG36 from Tea Plant Decreases Hyperosmotic Stress Tolerance in *Arabidopsis thaliana*. *Int. J. Mol. Sci.* **2021**, *22*, 5064. [CrossRef] [PubMed]
110. Kamal, K.Y.; Khodaeiaminjan, M.; Yahya, G.; El-Tantawy, A.A.; El-Moneim, D.A.; El-Esawi, M.A.; Abd-Elaziz, M.A.A.; Nassrallah, A.A. Modulation of Cell Cycle Progression and Chromatin Dynamic as Tolerance Mechanisms to Salinity and Drought Stress in Maize. *Physiol. Plant.* **2021**, *172*, 684–695. [CrossRef]
111. Brehove, M.; Wang, T.; North, J.; Luo, Y.; Dreher, S.J.; Shimko, J.C.; Ottesen, J.J.; Luger, K.; Poirier, M.G. Histone Core Phosphorylation Regulates DNA Accessibility. *J. Biol. Chem.* **2015**, *290*, 22612–22621. [CrossRef]
112. Armeev, G.A.; Kniazeva, A.S.; Komarova, G.A.; Kirpichnikov, M.P.; Shaytan, A.K. Histone Dynamics Mediate DNA Unwrapping and Sliding in Nucleosomes. *Nat. Commun.* **2021**, *12*, 2387. [CrossRef]
113. Baker, S.P.; Phillips, J.; Anderson, S.; Qiu, Q.; Shabanowitz, J.; Smith, M.M.; Yates, J.R.; Hunt, D.F.; Grant, P.A. Histone H3 Thr 45 Phosphorylation Is a Replication-Associated Post-Translational Modification in *S. cerevisiae*. *Nat. Cell Biol.* **2010**, *12*, 294–298. [CrossRef]
114. Hurd, P.J.; Bannister, A.J.; Halls, K.; Dawson, M.A.; Vermeulen, M.; Olsen, J.V.; Ismail, H.; Somers, J.; Mann, M.; Owen-Hughes, T.; et al. Phosphorylation of Histone H3 Thr-45 Is Linked to Apoptosis. *J. Biol. Chem.* **2009**, *284*, 16575–16583. [CrossRef] [PubMed]
115. Lee, J.-H.; Kang, B.-H.; Jang, H.; Kim, T.W.; Choi, J.; Kwak, S.; Han, J.; Cho, E.-J.; Youn, H.-D. AKT Phosphorylates H3-Threonine 45 to Facilitate Termination of Gene Transcription in Response to DNA Damage. *Nucleic Acids Res.* **2015**, *43*, 4505–4516. [CrossRef] [PubMed]
116. Wei, F.; Tang, D.; Li, Z.; Kashif, M.H.; Khan, A.; Lu, H.; Jia, R.; Chen, P. Molecular Cloning and Subcellular Localization of Six HDACs and Their Roles in Response to Salt and Drought Stress in Kenaf (*Hibiscus cannabinus* L.). *Biol. Res.* **2019**, *52*, 20. [CrossRef] [PubMed]
117. Park, C.; Rehrauer, H.; Mansuy, I.M. Genome-Wide Analysis of H4K5 Acetylation Associated with Fear Memory in Mice. *BMC Genom.* **2013**, *14*, 539. [CrossRef] [PubMed]
118. Lewinska, A.; Wnuk, M.; Grzelak, A.; Bartosz, G. Nucleolus as an Oxidative Stress Sensor in the Yeast *Saccharomyces cerevisiae*. *Redox Rep.* **2010**, *15*, 87–96. [CrossRef]
119. Sapio, R.T.; Burns, C.J.; Pestov, D.G. Effects of Hydrogen Peroxide Stress on the Nucleolar Redox Environment and Pre-rRNA Maturation. *Front. Mol. Biosci.* **2021**, *8*, 678488. [CrossRef]
120. Yue, M.; Gautam, M.; Chen, Z.; Hou, J.; Zheng, X.; Hou, H.; Li, L. Histone Acetylation of 45S rDNA Correlates with Disrupted Nucleolar Organization during Heat Stress Response in *Zea mays* L. *Physiol. Plant.* **2021**, *172*, 2079–2089. [CrossRef]
121. Xiang, Y.; Zhang, M.; Hu, Y.; Wang, L.; Xiao, X.; Yin, F.; Cao, X.; Sui, M.; Yao, Y. Epigenetic Modifications of 45S rDNA Associates with the Disruption of Nucleolar Organisation during Cd Stress Response in Pakchoi. *Ecotoxicol. Environ. Saf.* **2024**, *270*, 115859. [CrossRef]
122. Song, J.; Henry, H.; Tian, L. Drought-inducible Changes in the Histone Modification H3K9ac Are Associated with Drought-responsive Gene Expression in *Brachypodium Distachyon*. *Plant Biol. J.* **2020**, *22*, 433–440. [CrossRef]
123. Gallo-Franco, J.J.; Sosa, C.C.; Ghneim-Herrera, T.; Quimbaya, M. Epigenetic Control of Plant Response to Heavy Metal Stress: A New View on Aluminum Tolerance. *Front. Plant Sci.* **2020**, *11*, 602625. [CrossRef]
124. Wang, P.; Zhao, L.; Hou, H.; Zhang, H.; Huang, Y.; Wang, Y.; Li, H.; Gao, F.; Yan, S.; Li, L. Epigenetic Changes Are Associated with Programmed Cell Death Induced by Heat Stress in Seedling Leaves of *Zea mays*. *Plant Cell Physiol.* **2015**, *56*, 965–976. [CrossRef]
125. Zheng, Y.; Ding, Y.; Sun, X.; Xie, S.; Wang, D.; Liu, X.; Su, L.; Wei, W.; Pan, L.; Zhou, D.-X. Histone Deacetylase HDA9 Negatively Regulates Salt and Drought Stress Responsiveness in *Arabidopsis*. *J. Exp. Bot.* **2016**, *67*, 1703–1713. [CrossRef]
126. Chang, Y.; Liu, J.; Guo, M.; Ouyang, W.; Yan, J.; Xiong, L.; Li, X. Drought-Responsive Dynamics of H3K9ac-Marked 3D Chromatin Interactions Are Integrated by OsbZIP23-Associated Super-Enhancer-like Promoter Regions in Rice. *Genome Biol.* **2024**, *25*, 262. [CrossRef]
127. Masumoto, H.; Hawke, D.; Kobayashi, R.; Verreault, A. A Role for Cell-Cycle-Regulated Histone H3 Lysine 56 Acetylation in the DNA Damage Response. *Nature* **2005**, *436*, 294–298. [CrossRef]
128. Das, C.; Lucia, M.S.; Hansen, K.C.; Tyler, J.K. CBP/P300-Mediated Acetylation of Histone H3 on Lysine 56. *Nature* **2009**, *459*, 113–117; Erratum in *Nature* **2009**, *460*, 1164. https://doi.org/10.1038/nature08360. [CrossRef] [PubMed]
129. Duan, S.; Nodelman, I.M.; Zhou, H.; Tsukiyama, T.; Bowman, G.D.; Zhang, Z. H3K56 Acetylation Regulates Chromatin Maturation Following DNA Replication. *Nat. Commun.* **2025**, *16*, 134. [CrossRef] [PubMed]

130. Ge, Z.; Nair, D.; Guan, X.; Rastogi, N.; Freitas, M.A.; Parthun, M.R. Sites of Acetylation on Newly Synthesized Histone H4 Are Required for Chromatin Assembly and DNA Damage Response Signaling. *Mol. Cell. Biol.* **2013**, *33*, 3286–3298. [CrossRef] [PubMed]
131. Opdenakker, K.; Remans, T.; Vangronsveld, J.; Cuypers, A. Mitogen-Activated Protein (MAP) Kinases in Plant Metal Stress: Regulation and Responses in Comparison to Other Biotic and Abiotic Stresses. *Int. J. Mol. Sci.* **2012**, *13*, 7828–7853. [CrossRef]
132. Liu, Y.; He, C. A Review of Redox Signaling and the Control of MAP Kinase Pathway in Plants. *Redox Biol.* **2017**, *11*, 192–204. [CrossRef]
133. Wu, X.; Yalowich, J.C.; Hasinoff, B.B. Cadmium Is a Catalytic Inhibitor of DNA Topoisomerase II. *J. Inorg. Biochem.* **2011**, *105*, 833–838. [CrossRef]
134. Balali-Mood, M.; Naseri, K.; Tahergorabi, Z.; Khazdair, M.R.; Sadeghi, M. Toxic Mechanisms of Five Heavy Metals: Mercury, Lead, Chromium, Cadmium, and Arsenic. *Front. Pharmacol.* **2021**, *12*, 643972. [CrossRef]
135. Ng, D.W.-K.; Wang, T.; Chandrasekharan, M.B.; Aramayo, R.; Kertbundit, S.; Hall, T.C. Plant SET Domain-Containing Proteins: Structure, Function and Regulation. *Biochim. Et. Biophys. Acta—Gene Struct. Expr.* **2007**, *1769*, 316–329. [CrossRef]
136. Kerchner, K.M.; Mou, T.-C.; Sun, Y.; Rusnac, D.-V.; Sprang, S.R.; Briknarová, K. The Structure of the Cysteine-Rich Region from Human Histone-Lysine N-Methyltransferase EHMT2 (G9a). *J. Struct. Biol. X* **2021**, *5*, 100050. [CrossRef]
137. Ben Saad, R.; Ben Romdhane, W.; Wiszniewska, A.; Baazaoui, N.; Bouteraa, M.T.; Chouaibi, Y.; Alfaifi, M.Y.; Kačániová, M.; Čmiková, N.; Ben Hsouna, A.; et al. *Rosmarinus officinalis* L. Essential Oil Enhances Salt Stress Tolerance of Durum Wheat Seedlings through ROS Detoxification and Stimulation of Antioxidant Defense. *Protoplasma* **2024**, *261*, 1207–1220. [CrossRef] [PubMed]
138. Jaouani, K.; Karmous, I.; Ostrowski, M.; Ferjani, E.E.; Jakubowska, A.; Chaoui, A. Cadmium Effects on Embryo Growth of Pea Seeds during Germination: Investigation of the Mechanisms of Interference of the Heavy Metal with Protein Mobilization-Related Factors. *J. Plant Physiol.* **2018**, *226*, 64–76. [CrossRef] [PubMed]
139. Sfaxi-Bousbih, A.; Chaoui, A.; Ferjani, E.E. Cadmium Impairs Mineral and Carbohydrate Mobilization during the Germination of Bean Seeds. *Ecotoxicol. Environ. Saf.* **2010**, *73*, 1123–1129. [CrossRef]
140. Gomez-Osuna, A.; Calatrava, V.; Galvan, A.; Fernandez, E.; Llamas, A. Identification of the MAPK Cascade and Its Relationship with Nitrogen Metabolism in the Green Alga *Chlamydomonas reinhardtii*. *Int. J. Mol. Sci.* **2020**, *21*, 3417. [CrossRef]
141. Wen, Y.; Li, X.; Guo, C.; Ma, C.; Duan, W.; Lu, W.; Xiao, K. Characterization and Expression Analysis of Mitogen-Activated Protein Kinase Cascade Genes in Wheat Subjected to Phosphorus and Nitrogen Deprivation, High Salinity, and Drought. *J. Plant Biochem. Biotechnol.* **2015**, *24*, 184–196. [CrossRef]
142. Wang, X.; Tan, N.W.K.; Chung, F.Y.; Yamaguchi, N.; Gan, E.-S.; Ito, T. Transcriptional Regulators of Plant Adaptation to Heat Stress. *Int. J. Mol. Sci.* **2023**, *24*, 13297. [CrossRef]
143. Pucholt, P.; Sjödin, P.; Weih, M.; Rönnberg-Wästljung, A.C.; Berlin, S. Genome-Wide Transcriptional and Physiological Responses to Drought Stress in Leaves and Roots of Two Willow Genotypes. *BMC Plant Biol.* **2015**, *15*, 244; Erratum in *BMC Plant Biol.* **2015**, *15*, 285. https://doi.org/10.1186/s12870-015-0665-4. [CrossRef] [PubMed]
144. Song, L.; Huang, S.C.; Wise, A.; Castanon, R.; Nery, J.R.; Chen, H.; Watanabe, M.; Thomas, J.; Bar-Joseph, Z.; Ecker, J.R. A Transcription Factor Hierarchy Defines an Environmental Stress Response Network. *Science* **2016**, *354*, aag1550. [CrossRef] [PubMed]
145. Kovalchuk, I.; Titov, V.; Hohn, B.; Kovalchuk, O. Transcriptome Profiling Reveals Similarities and Differences in Plant Responses to Cadmium and Lead. *Mutat. Res. Fundam. Mol. Mech. Mutagen.* **2005**, *570*, 149–161. [CrossRef]
146. Kintlová, M.; Vrána, J.; Hobza, R.; Blavet, N.; Hudzieczek, V. Transcriptome Response to Cadmium Exposure in Barley (*Hordeum vulgare* L.). *Front. Plant Sci.* **2021**, *12*, 629089. [CrossRef]
147. Duncan, R.F.; Hershey, J.W.B. Translational Repression by Chemical Inducers of the Stress Response Occurs by Different Pathways. *Arch. Biochem. Biophys.* **1987**, *256*, 651–661. [CrossRef]
148. Hinnebusch, A.G. The eIF-2α Kinases: Regulators of Protein Synthesis in Starvation and Stress. *Semin. Cell Biol.* **1994**, *5*, 417–426. [CrossRef]
149. Cohen, S.P.; Leach, J.E. Abiotic and Biotic Stresses Induce a Core Transcriptome Response in Rice. *Sci. Rep.* **2019**, *9*, 6273. [CrossRef]
150. Firmino, J.P.; Fernández-Alacid, L.; Vallejos-Vidal, E.; Salomón, R.; Sanahuja, I.; Tort, L.; Ibarz, A.; Reyes-López, F.E.; Gisbert, E. Carvacrol, Thymol, and Garlic Essential Oil Promote Skin Innate Immunity in Gilthead Seabream (*Sparus aurata*) Through the Multifactorial Modulation of the Secretory Pathway and Enhancement of Mucus Protective Capacity. *Front. Immunol.* **2021**, *12*, 633621. [CrossRef]
151. Ünyayar, S.; Çelik, A.; Çekiç, F.Ö.; Gözel, A. Cadmium-Induced Genotoxicity, Cytotoxicity and Lipid Peroxidation in *Allium sativum* and *Vicia faba*. *Mutagenesis* **2006**, *21*, 77–81. [CrossRef] [PubMed]
152. Souguir, D.; Ferjani, E.; Ledoigt, G.; Goupil, P. Sequential Effects of Cadmium on Genotoxicity and Lipoperoxidation in *Vicia faba* Roots. *Ecotoxicology* **2011**, *20*, 329–336. [CrossRef] [PubMed]

153. Żabka, A.; Winnicki, K.; Polit, J.T.; Wróblewski, M.; Maszewski, J. Cadmium (II)-Induced Oxidative Stress Results in Replication Stress and Epigenetic Modifications in Root Meristem Cell Nuclei of *Vicia faba*. *Cells* **2021**, *10*, 640. [CrossRef] [PubMed]
154. Żabka, A.; Polit, J.T.; Maszewski, J. Inter- and Intrachromosomal Asynchrony of Cell Division Cycle Events in Root Meristem Cells of *Allium cepa*: Possible Connection with Gradient of Cyclin B-like Proteins. *Plant Cell Rep.* **2010**, *29*, 845–856. [CrossRef]
155. Żabka, A.; Polit, J.T.; Maszewski, J. DNA Replication Stress Induces Deregulation of the Cell Cycle Events in Root Meristems of *Allium cepa*. *Ann. Bot.* **2012**, *110*, 1581–1591. [CrossRef]
156. Kesraoui, S.; Andrés, M.; Berrocal-Lobo, M.; Soudani, S.; Gonzalez-Coloma, A. Direct and Indirect Effects of Essential Oils for Sustainable Crop Protection. *Plants* **2022**, *11*, 2144. [CrossRef] [PubMed]
157. Ayllón-Gutiérrez, R.; Díaz-Rubio, L.; Montaño-Soto, M.; Haro-Vázquez, M.D.P.; Córdova-Guerrero, I. Applications of Plant Essential Oils in Pest Control and Their Encapsulation for Controlled Release: A Review. *Agriculture* **2024**, *14*, 1766. [CrossRef]

❖

Praca 4 (Załącznik nr 4)

❖ **Gocek-Szczurtek, N**.; Wróblewski, M.; Żabka, A.; Polit, J.T.*
Thyme Oil Alleviates Cadmium Induced Disturbances in Mitotic Activity, Cytoskeletal Organization and H3T3/H3S10 Phosphorylation in *Vicia faba*. *Int. J. Mol. Sci.* **2026**, 27, 2798, doi:10.3390/ijms27062798

* – autor korespondujący

- Współczynnik wpływu (IF): **4,9**
- Punkty MNiSW: **140 pkt**.

International Journal of
Molecular Sciences

MDPI

Article

Thyme Oil Alleviates Cadmium-Induced Disturbances in Mitotic Activity, Cytoskeletal Organization and H3T3/H3S10 Phosphorylation in *Vicia faba*

Natalia Gocek-Szczurtek [1,2], Mateusz Wróblewski [1], Aneta Żabka [1] and Justyna T. Polit [1,*]

[1] Department of Cytophysiology, Faculty of Biology and Environmental Protection, University of Lodz, 90-236 Lodz, Poland; natalia.gocek.szczurtek@biol.uni.lodz.pl (N.G.-S.); mateusz.wroblewski@biol.uni.lodz.pl (M.W.); aneta.zabka@biol.uni.lodz.pl (A.Ż.)
[2] Doctoral School of Exact and Natural Sciences, University of Lodz, 90-237 Lodz, Poland
* Correspondence: justyna.polit@biol.uni.lodz.pl

Abstract

Cadmium (Cd) contamination, through induction of oxidative stress, severely impairs plant growth. Using primary roots of *Vicia faba*, we investigated how a 24 h incubation in $CdCl_2$ solution (175 µM) affects mitotic progression in meristems and assessed whether thyme essential oil (TO; 0.03%, *v*/*v*), as a natural antioxidant, can protect proliferating cells during simultaneous Cd exposure. Cd strongly inhibited root growth, reduced mitotic index tenfold (to 0.6%), induced chromatin condensation, decreased CDKA protein levels and CycB transcripts and proteins, caused pronounced microtubule bundling and alterations in their arrangement, disorganization of actin filaments, and disturbances in histone H3 phosphorylation (H3T3Ph, H3S10Ph). TO led to a partial recovery of mitotic index (to ~50% of the control), normalization of chromosome condensation, maintenance of cell-cycle regulators at near-control levels, preservation of proper cytoskeletal organization, and restoration of the correct H3 phosphorylation pattern. This enabled cells to progress from metaphase to anaphase and maintain phase proportions close to the control, resulting in normal root growth. These findings indicate that TO protects the mitotic cellular environment against Cd-induced disturbances. To the best of our knowledge, this is the first evidence that TO safeguards the plant mitotic apparatus under Cd stress, highlighting its potential as a natural bioprotective agent supporting plant growth.

Keywords: mitosis; CDK; cyclin; microtubules; epigenetics; cadmium; essential oil

Academic Editor: Karel Doležal

Received: 21 February 2026
Revised: 16 March 2026
Accepted: 17 March 2026
Published: 19 March 2026

1. Introduction

Cadmium (Cd) is a major environmental pollutant that, even at low concentrations, disrupts plant physiology and poses risks to human and animal health [1,2]. Cd exposure induces multiple cellular disturbances, including oxidative stress, membrane damage, and genome instability [3–5]. A key mechanism of its toxicity involves interference with essential ions and proteins: Cd competes with Ca^{2+}, Zn^{2+}, Mg^{2+}, and Fe^{2+} and binds to protein thiol groups, leading to enzyme inactivation and metabolic dysregulation [6,7]. Rapidly proliferating cells, such as plant meristematic cells, are particularly sensitive to these effects because their proper function requires strict control of genome stability and cell cycle progression [3,8,9]. Due to its direct contact with contaminated substrates, the root apical meristem represents a useful model for studying cadmium-induced alterations in mitosis.

The plant cell cycle is regulated by two principal control points (PCP1 and PCP2) located in G1 and G2 phases that respond to environmental signals [10–12], and its progression is controlled by cyclin-dependent kinases (CDKs) and their cyclin partners (Cyc), whose activity is further modulated by regulatory proteins, including cyclin-dependent kinase inhibitors (CKIs), that can arrest S- and M-phase CDK complexes under stress conditions [13–17]. Mitotic entry is driven by CycA- and CycB-dependent activation of CDKA (the plant homolog of Cdc2/CDK1) and plant-specific CDKB kinases, which together constitute the plant M-phase promoting factor (MPF) activity [18]. MPF activity is negatively regulated by WEE1-dependent inhibitory phosphorylation and activated by CDK-activating kinases (CAKs), together with removal of the inhibitory phosphate by a CDC25-like protein [19–21]. The active CDK–Cyc complex initiates mitosis via phosphorylation of downstream substrates, whereas mitotic exit requires degradation of mitotic cyclins mediated by the anaphase-promoting complex/cyclosome (APC/C) with the involvement of CCS52 [22,23].

The proper progression of plant cell division depends on the dynamic cytoskeleton composed of microtubules and actin filaments [24]. Microtubules, formed by α- and β-tubulin heterodimers, exhibit dynamic instability, enabling rapid reorganization during the cell cycle [25]. During interphase, cortical microtubules reorganize into the preprophase band (PPB), marking the future division site before disappearing prior to metaphase [26,27]. Concurrently, actin filaments form an "actin cage" that stabilizes the mitotic spindle and maintains its position [24]. In prophase and prometaphase, a bipolar spindle assembles despite the absence of centrosomes [28]. Spindle microtubules attach to chromosome centromeres via kinetochores, ensuring accurate chromosome segregation [29–31]. Improper attachment activates the spindle assembly checkpoint (SAC), which arrests the metaphase-anaphase transition by inhibiting APC/C [32]. Microtubule nucleation involves the γ-TuRC complex associated with the nuclear envelope and recruited to existing microtubules via augmin, whereas microtubule dynamics are regulated by microtubule-associated proteins (MAPs) [33–36]. In metaphase, chromosomes align at the equatorial plate through kinesin-driven activity [36,37], followed by separase-mediated cohesin cleavage and poleward chromatid separation during anaphase [36,38]. In telophase and cytokinesis, microtubules form the phragmoplast, stabilized by MAP65-3 and supported by actin filaments, guiding vesicles with cell wall components to complete cell plate formation [39–41]. Coordinated microtubule and actin dynamics thus ensure accurate division and daughter cell integrity [42].

During mitotic entry, epigenetic histone modifications drive chromatin condensation and centromere formation for kinetochore assembly [43,44]. These modifications also modulate sister chromatid cohesion by influencing cohesin binding and integrate environmental and cellular signals that shape chromatin states during the cell cycle [45,46]. Among the best-characterized mitotic marks are phosphorylations of histone H3 at threonine 3 (H3T3Ph) and serine 10 (H3S10Ph), which correlate with chromosome condensation [47]. H3T3 phosphorylation, catalyzed by Haspin kinase and distributed along plant chromosomes, promotes recruitment of chromosomal passenger complex (CPC) components involved in correcting kinetochore–microtubule attachments [48–50]. A core CPC component, Aurora B kinase, mediates H3S10 phosphorylation. In *Arabidopsis thaliana*, Aurora kinases (AtAUR1–3) phosphorylate H3S10 in pericentromeric regions, supporting cohesion maintenance and proper chromatid segregation [51,52]. The dynamics of these modifications are controlled by the balance between kinase and phosphatase activities, particularly protein phosphatases PP1 and PP2A, which regulate the phosphorylation status of mitotic proteins, chromatin and kinetochore components, thereby influencing the stability of kinetochore–microtubule attachments and the proper progression of mitosis [53].

Dysregulation of cell division control leads to genome instability, developmental defects, and reduced adaptive capacity in plants, and these disturbances are further intensified by environmental stresses associated with ecosystem degradation [23]. In the context of increasing heavy metal contamination driven by industrialization, intensive agriculture, and urbanization [54], identifying compounds that help maintain cellular homeostasis and the stability of cell division processes has become particularly important. Essential oils have attracted attention as biologically active mixtures of volatile plant metabolites. Among them, thyme essential oil (TO), rich in phenolic monoterpenes such as thymol and carvacrol, exhibits strong antioxidant properties and can modulate endogenous plant defense systems involved in redox regulation [55–57].

Although the protective effects of TO under cadmium stress have been reported in animal models [58], its impact on proliferating plant cells remains poorly understood. Our previous studies on root meristems of *Vicia faba* var. *minor* demonstrated that TO mitigates cadmium-induced oxidative stress in interphase cells, reduces replication stress and DNA damage, and stabilizes epigenetic modifications of histones and DNA, thereby supporting transcriptional activity [59,60].

The aim of the present study was to evaluate the protective potential of TO on mitotic cells exposed to cadmium chloride ($CdCl_2$). The same experimental model as in our previous studies was employed, namely the root meristems of *V. faba*, a species widely used in plant mitosis research due to its low chromosome number ($2n = 12$), large chromosome size, and distinct morphology, features that allow precise assessment of cell division processes. Seedlings were subjected to a 24 h incubation in $CdCl_2$ solution, in the emulsified form of TO, and in a combination of both substances. Seedlings incubated for 24 h in water or in the emulsifier (mixture of C14-18 and unsaturated C16-18—mono- and di-ethoxylated glycerides and ethoxylated *Brassica napus* oil) solution used to prepare the oil served as control material.

Based on literature reports indicating that cadmium interferes with cell-cycle regulation and mitotic progression in plant cells [3,61–64], we hypothesized that cadmium may disrupt the activation of mitosis by interfering with the function of the plant MPF complex, which is responsible for its initiation, and may further impair the progression of mitosis by affecting the cytoskeletal structures and mitotic chromosomes, as well as their mutual interactions. In this context, TO may exert a protective effect by safeguarding these fundamental processes in dividing cells from the toxic impact of cadmium, potentially through mechanisms related to its previously reported antioxidant properties. To test this hypothesis, we assessed primary root growth, the mitotic and phase indices, levels of CDKA and CycB, the organization of microtubules and actin filaments, as well as epigenetic modifications of histone H3 (H3T3Ph and H3S10Ph). This approach provides mechanistic insight into the effects of cadmium on plant cells and allows evaluation of the protective potential of TO under heavy metal-induced stress.

2. Results

Prior to the main study, a preliminary screening of Cd (100–200 µM) and TO (0.01–0.06% v/v) concentrations, including their combinations, was conducted based on the mitotic index in root meristem cells (Table S1, Supplementary Materials). For the main study, 175 µM Cd was selected as a concentration that strongly (but not extremely) inhibited the mitotic index, and 0.03% TO was chosen as the lowest dose consistently eliciting a protective effect without markedly affecting cell division when applied alone.

2.1. Primary Root Growth

Primary root growth is driven by the apically located meristematic tissue. Therefore, to evaluate the effects of the tested compounds on seedling growth after 24 h of incubation, the increase in root length was analyzed (Figure 1A,B). Under control conditions, including incubation of seedlings in distilled water as well as in the emulsifier solution used for TO emulsification, embryonic roots elongated by approximately 8 mm. In the presence of cadmium ($CdCl_2$), root elongation was reduced by about 50% and reached an average of 4 mm. Application of TO alone did not cause statistically significant changes in root length increment compared to the control. In contrast, simultaneous application of TO and $CdCl_2$ resulted in a root length increase comparable to that observed in the control variant, despite the presence of the heavy metal.

Figure 1. Seedlings of *V. faba* (**A**) and increments in primary root length (**B**) after 24 h of incubation in water—Control, emulsifier, $CdCl_2$, thyme essential oil (TO), and the combination of $CdCl_2$ and TO. Scale bar = 10 mm. Data are presented as mean ± SEM (n = 17; each replicate representing an individual seedling). Statistical significance: *** $p < 0.001$; ** $p < 0.01$ (one-way ANOVA followed by Tukey's multiple comparison test).

2.2. Chromatin Structure and Mitotic Activity

Differences in the intensity of primary root growth observed among the experimental variants prompted an analysis of meristematic cell activity (Figures 2 and 3). In control and emulsifier-treated meristems, interphase nuclei stained with the Feulgen method displayed a typical reticulate nuclear structure with visible chromocenters (Figure 2A–C). Within the uniformly stained chromatin, more highly condensed regions were distinguishable, forming characteristic chromocenters corresponding to heterochromatin-rich pericentromeric and telomeric regions. Chromatin organized in this manner underwent normal condensation into mitotic chromosomes, and the resulting mitotic figures exhibited typical chromosome morphology (Figure 2C). Under these conditions, the mitotic index reached approximately 6%. Among dividing cells, prophase predominated (about 50%), followed by metaphase (up to 25%). Anaphases and telophases accounted for over 10% and about 15% of all mitotic figures, respectively (Figure 3A,B).

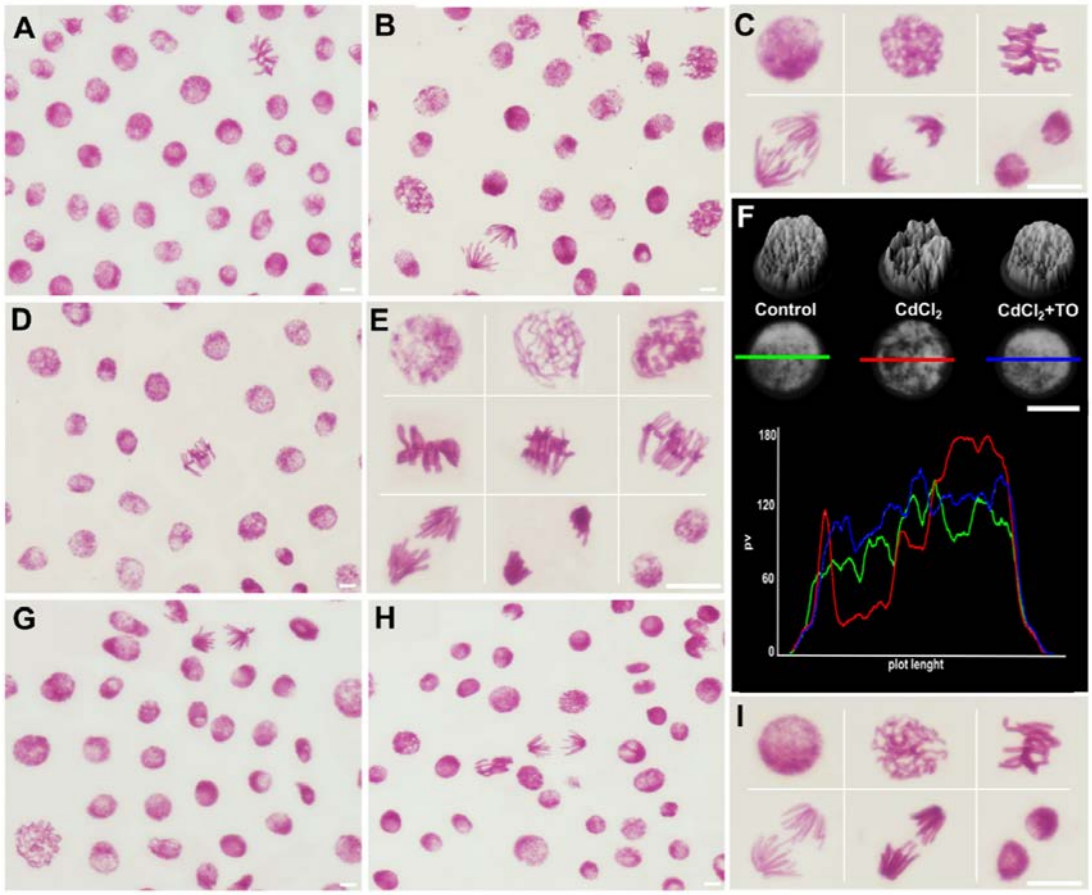

Figure 2. Feulgen DNA staining illustrating overall view of cell population in primary root meristems of *V. faba* after 24 h of incubation in water—Control (**A**), emulsifier (**B**,**C**), $CdCl_2$ (**D**,**E**), thyme essential oil (TO) (**G**), and the combination of $CdCl_2$ and TO (**H**,**I**). Higher-magnification images showing representative interphase nuclei and successive mitotic stages: control or emulsifier (**C**), $CdCl_2$ (**E**), and TO or $CdCl_2$ + TO (**I**). Identical mitotic figures for control and emulsifier, as well as for TO and $CdCl_2$ + TO, are shown once due to the lack of detectable structural differences. (**F**) Densitometric plots illustrating relative chromatin condensation (expressed as pixel values (pv) from 1 to 255) in nuclei from control (green line), $CdCl_2$-treated (red line), and $CdCl_2$ + TO-treated (blue line) meristems. Plot length = 18 μm. Scale bar = 10 μm.

In primary root meristems exposed to cadmium, interphase nuclei exhibited a pronounced change in chromatin structure (Figure 2D,E), as confirmed by both 3D surface profiles and densitometric analysis of Feulgen-stained nuclei (Figure 2F). Chromatin appeared less uniform and displayed a network-like, lacy pattern, with DNA-rich regions interspersed with unstained or lightly stained gaps (sharply defined valleys and high peaks in the 3D images; Figure 2F). Chromocenters, clearly visible and not obscured by the surrounding chromatin, were particularly distinct and exhibited increased compaction (Figure 2D–F). The interphase chromatin subsequently condensed into mitotic chromosomes, which in early prophase retained this lacy organization, became strongly and irregularly condensed in late prophase, and appeared short and highly condensed in metaphase, with telomeric regions showing a tendency to adhere. Chromatid separation during anaphase was impeded, particularly in early anaphase, due to sticky telomeric ends. These defects resulted in strongly condensed telophase and post-mitotic nuclei, whose chromatin structure resembled that of cells entering mitosis (Figure 2E). Mitotic activity was markedly reduced, not exceeding 0.6%. Among dividing cells, over 65% were in prophase, approximately 25% in metaphase, and cells in later stages (anaphase and telophase) collectively accounted for less than 10% (Figure 3A,B).

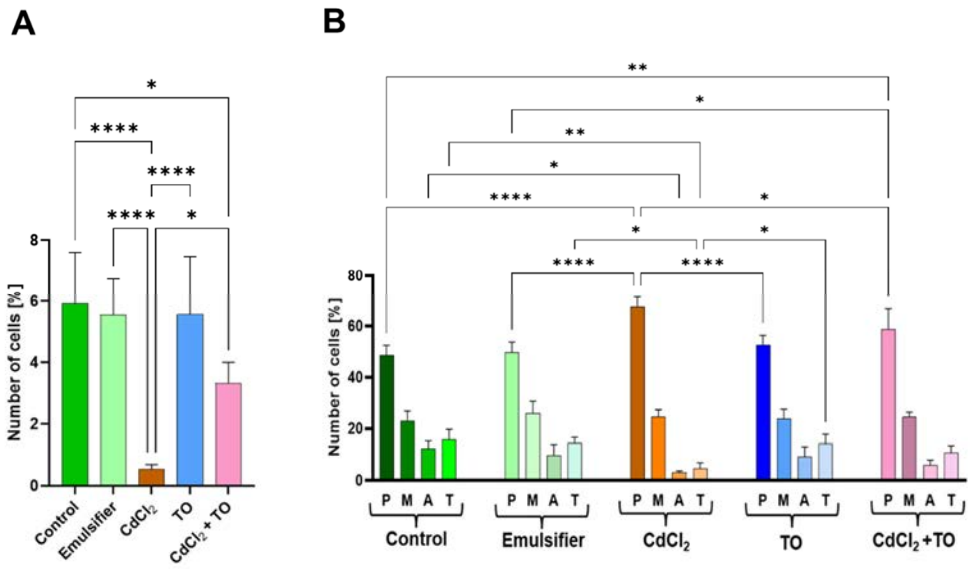

Figure 3. Mitotic index (% ± SD) (**A**) and mitotic phase indices (% ± SD) (**B**) in primary root meristem cells of *V. faba* after 24 h of incubation in water—Control, emulsifier, $CdCl_2$, thyme essential oil (TO), and a combination of $CdCl_2$ and TO. Abbreviations: P—prophase; M—metaphase; A—anaphase; T—telophase. Mean values of the mitotic index were calculated based on five root meristems, with 500 cells analyzed per meristem. Statistical significance: **** $p < 0.0001$, ** $p < 0.01$, and * $p < 0.05$ (one-way ANOVA followed by Tukey's multiple comparison test).

The emulsified form of TO did not induce noticeable changes in the structure of interphase nuclei or mitotic chromosomes compared with the control (Figure 2G), nor did it significantly affect the mitotic index or the proportions of cells in different mitotic phases (Figure 3A,B). Simultaneous treatment with TO and cadmium mitigated severe structural alterations: interphase nuclei and their densitometric profiles showed only a slight shift toward increased condensation, remaining clearly similar to the control (Figure 2H,I,F). Mitotic chromosome condensation and mitotic figure abnormalities were also markedly reduced (Figure 2I). This was accompanied by partial preservation of mitotic activity, exceeding 3%, and smaller deviations in the distribution of cells across mitotic phases compared with the control (Figure 3A,B).

2.3. Dynamics of CDKA Kinase and CycB

The observed decrease in mitotic activity in primary root meristems of *V. faba* under cadmium exposure prompted an analysis of principal mitotic regulators, including CDKA, which remains relatively constant throughout the cell cycle, and its regulatory partner, CycB, characterized by periodic synthesis and degradation [65].

The level of CDKA kinase was assessed directly in meristematic cells using immunodetection (Figure 4A–E,A′–E′,A″–E″), with quantitative fluorescence intensity analysis (Figure 4F). These results were further validated by Western blotting (Figure 4G), combined with densitometric analysis of band intensities using GelAnalyzer 23.1.1 software (Figure 4H). Both immunofluorescence and Western blot analyses indicated comparable CDKA levels in control seedlings (Figure 4A) and those treated with the emulsifier (Figure 4B), with relative fluorescence intensity of approximately 160 a.u. (Figure 4F) and relative band intensities of 59 and 53 a.u., respectively (Figure 4G,H). Cadmium exposure resulted in a slight decrease in CDKA signal, reflected in both fluorescence intensity (128 a.u.; Figure 4C,F) and band intensity (46 a.u.; Figure 4G,H), indicating a modest reduction of this protein in meristematic cells. Treatment with emulsified TO alone did not significantly alter CDKA levels compared to the control, as confirmed by both immunofluorescence images (Figure 4D,F) and Western blot analysis (54 a.u.; Figure 4G,H). Notably,

the presence of TO during cadmium exposure partially prevented this slight decrease, with fluorescence intensity measured at 138 a.u. and band intensity at 52 a.u. (Figure 4E–H).

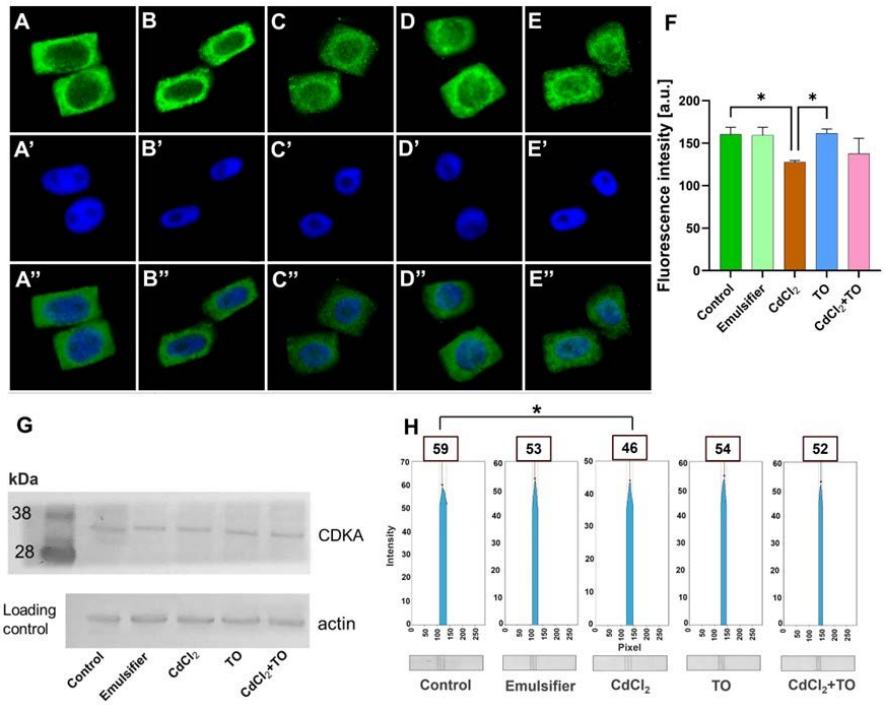

Figure 4. Immunofluorescence detection of CDKA in primary root meristem cells of *V. faba* after 24 h of incubation in water—Control (**A**), emulsifier (**B**), $CdCl_2$ (**C**), thyme essential oil TO (**D**) and a combination of $CdCl_2$ and TO (**E**). Corresponding images of cell nuclei stained with DAPI (**A′**–**E′**), and merged images (**A″**–**E″**). Scale bar = 10 µm. Median (±CI; $n = 5$ biological replicates; each representing an individual seedling) intensity of CDKA labeling; approximately 100 cells were analyzed per treatment (**F**). Statistical significance: * $p < 0.05$ (Kruskal–Wallis test with post hoc Dunn's multiple comparison test). Western blot analysis of CDKA in protein extracts obtained from the apical region of primary roots after 24 h incubation under the same treatment conditions (**G**). The blot shown is representative of independent biological replicates showing comparable patterns. Actin was used as a loading control (38–49 kDa). Microdensitometric analysis of CDKA band intensity was performed using GelAnalyzer software to compare relative protein abundance across treatments (**H**). The densitometric profiles shown illustrate the distribution of signal intensity within representative bands. Quantitative comparisons between treatments were performed using densitometric values obtained from independent biological replicates ($n = 3$; each representing an independent incubation experiment). Statistical significance: * $p < 0.05$ (one-way ANOVA followed by Tukey's multiple comparison test).

The level of CycB in meristematic cells was determined by Western blotting, complemented by densitometric analysis of band intensities using GelAnalyzer software (Figure 5A,B). These results were independently verified by qPCR (Figure 5C), enabling quantitative assessment of transcript levels of the *CycB* gene. Both Western blot and qPCR analyses showed comparable CycB protein abundance and transcript levels in control seedlings and those treated with the emulsifier alone (Figure 5A–C). Cadmium exposure led to a clear reduction in CycB protein level, accompanied by decreased transcript abundance, indicating an inhibitory effect of Cd on both protein accumulation and gene expression. Interestingly, despite maintaining mitotic activity comparable to the control in root meristems, treatment with emulsified TO alone also resulted in a marked reduction in CycB protein level and transcript level relative to the control. In contrast, the combined $CdCl_2$ + TO treatment maintained CycB protein levels close to control values and was associated with elevated transcript levels, as confirmed by qPCR (Figure 5A–C).

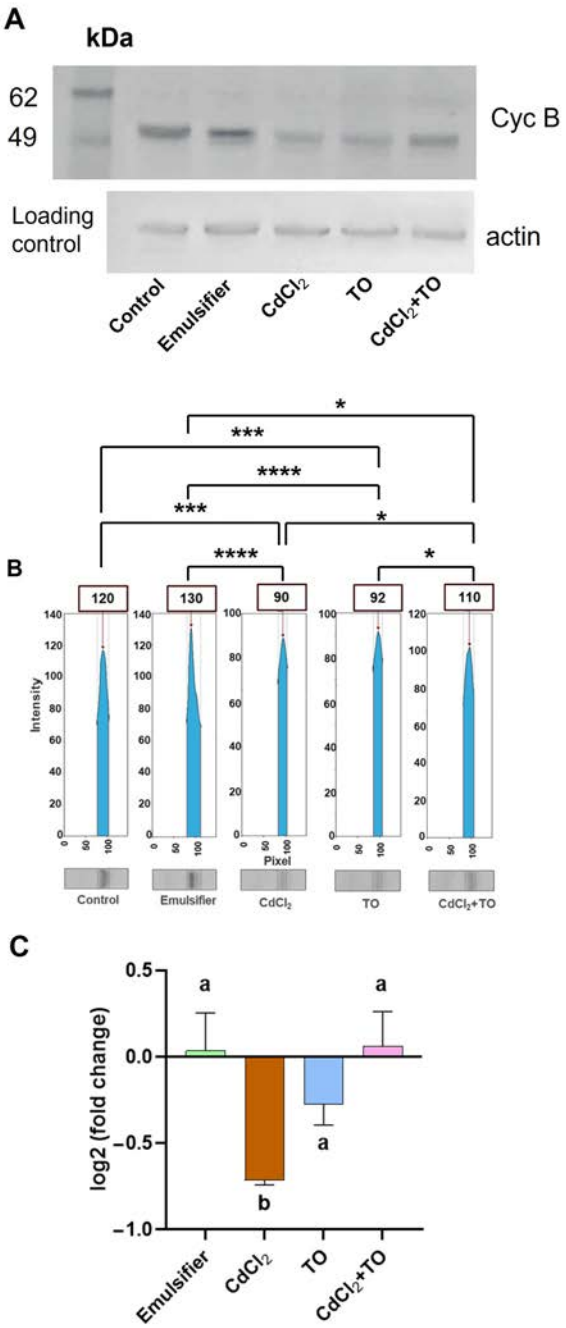

Figure 5. Western blot analysis of CycB in protein extracts obtained from the apical region of *V. faba* primary roots after 24 h of incubation with water—Control, emulsifier, $CdCl_2$, thyme essential oil (TO) and a combination of $CdCl_2$ and TO (**A**). The blot shown is representative of independent biological replicates showing comparable patterns. Actin was used as a loading control (38–49 kDa). Microdensitometric analysis of CycB band intensity was performed using GelAnalyzer software to compare relative protein abundance across treatments (**B**). The densitometric profiles shown illustrate the distribution of signal intensity within representative bands. Quantitative comparisons between treatments were performed using densitometric values obtained from independent biological replicates (n = 3; each representing an independent incubation experiment). Statistical significance: **** $p < 0.0001$, *** $p < 0.001$, * $p < 0.05$ (one-way ANOVA followed by Tukey's multiple comparison test). Gene expression of *CycB* in the apical region of primary roots was assessed by qPCR and is presented as $\log_2$ (fold change) relative to the control (**C**). Values are shown as the mean (±SD, n = 3 biological replicates; each representing an independent incubation experiment). Statistical significance is indicated by different letters (a, b); means sharing at least one common letter are not significantly different at $p < 0.05$ (one-way ANOVA followed by Tukey's multiple comparison test).

2.4. Immunocytochemical Analysis of Cytoskeletal Organization

The pronounced decline in mitotic activity in Cd-exposed cells, accompanied by reduced CycB transcript and protein levels—a major regulator of cell cycle progression—prompted further analysis of microtubule organization, as these structures are responsible for the formation of dynamically reorganized karyokinetic and cytokinetic spindles. Since microtubules are formed by polymerization of α/β-tubulin heterodimers, β-tubulin distribution was examined by immunocytochemistry using fluorescence microscopy.

In both control root meristem cells (Figure 6A–G,A′–G′,A″–G″) and cells treated with the emulsifier (Figure 7A–G,A′–G′,A″–G″), microtubule organization at successive stages of the cell cycle appeared normal. During interphase, cortical microtubules formed a regular network of fine, parallel fibers surrounding the cell (Figures 6A–A″ and 7A–A″). In cells preparing for division, these arrays are reorganized into a distinct and continuous preprophase band composed of parallel microtubules encircling the nucleus at the equatorial plane and marking the future division site (Figures 6B–B″ and 7B–B″). In prophase and prometaphase, further reorganization of the preprophase band gave rise to a dense microtubule array concentrated around the disassembling nuclear envelope (Figures 6C–C″ and 7C–C″). At metaphase, prominent kinetochore microtubules formed a typical bipolar spindle (Figures 6D–D″ and 7D–D″). During early anaphase, kinetochore microtubules responsible for chromatid segregation were accompanied by polar microtubule bundles (Figures 6E–E″ and 7E–E″). These bundles became particularly conspicuous in late anaphase, contributing to the formation of the midzone required for subsequent cell plate assembly (Figures 6F–F″ and 7F–F″). In late telophase, following the disassembly of the karyokinetic spindle, a well-developed phragmoplast was observed within this region (Figures 6G–G″ and 7G–G″).

In cells exposed to cadmium, pronounced disturbances in microtubule organization and their reorganization into mitotic spindle structures were observed (Figure 8A–G,A′–G′,A″–G″). Already at interphase, cortical microtubules failed to form the regular, parallel arrays characteristic of control cells. Instead, short and frequently thickened rod-like microtubules, typical of cadmium stress, predominated and were chaotically distributed throughout the cytoplasm (Figure 8A–A″). Cd also markedly affected the organization of the preprophase band, which was often incomplete or discontinuous and showed a loss of the typical parallel microtubule alignment (Figure 8B–B″). In prophase, microtubules derived from preprophase band reorganization did not establish a well-ordered fibrous array concentrated around the nuclear envelope; rather, they appeared as a dispersed mass of short, entangled structures (Figure 8C–C″). At metaphase, the mitotic spindle was clearly deformed, and kinetochore microtubule bundles were shorter and less abundant than in control cells (Figure 8D–D″). During early anaphase, kinetochore fibers that normally formed distinct bundles toward the spindle poles displayed a dispersed pattern, while polar microtubules in the central spindle region were poorly organized, irregularly arranged, and frequently fragmented (Figure 8E–E″). In telophase, marked disturbances were observed in the organization of polar microtubules preceding phragmoplast formation. Instead of the uniform, parallel bundles typical of control cells, microtubules formed heterogeneous structures differing in thickness and apparent polymerization status (Figure 8F–F″). In late telophase, the phragmoplast showed pronounced deviations from normal architecture: rather than evenly distributed, dense, and parallel microtubules of comparable length, short, intensely fluorescent, thickened bundles were observed, often lacking coherent orientation and embedded within regions of weak and irregular fluorescence signal (Figure 8G–G″).

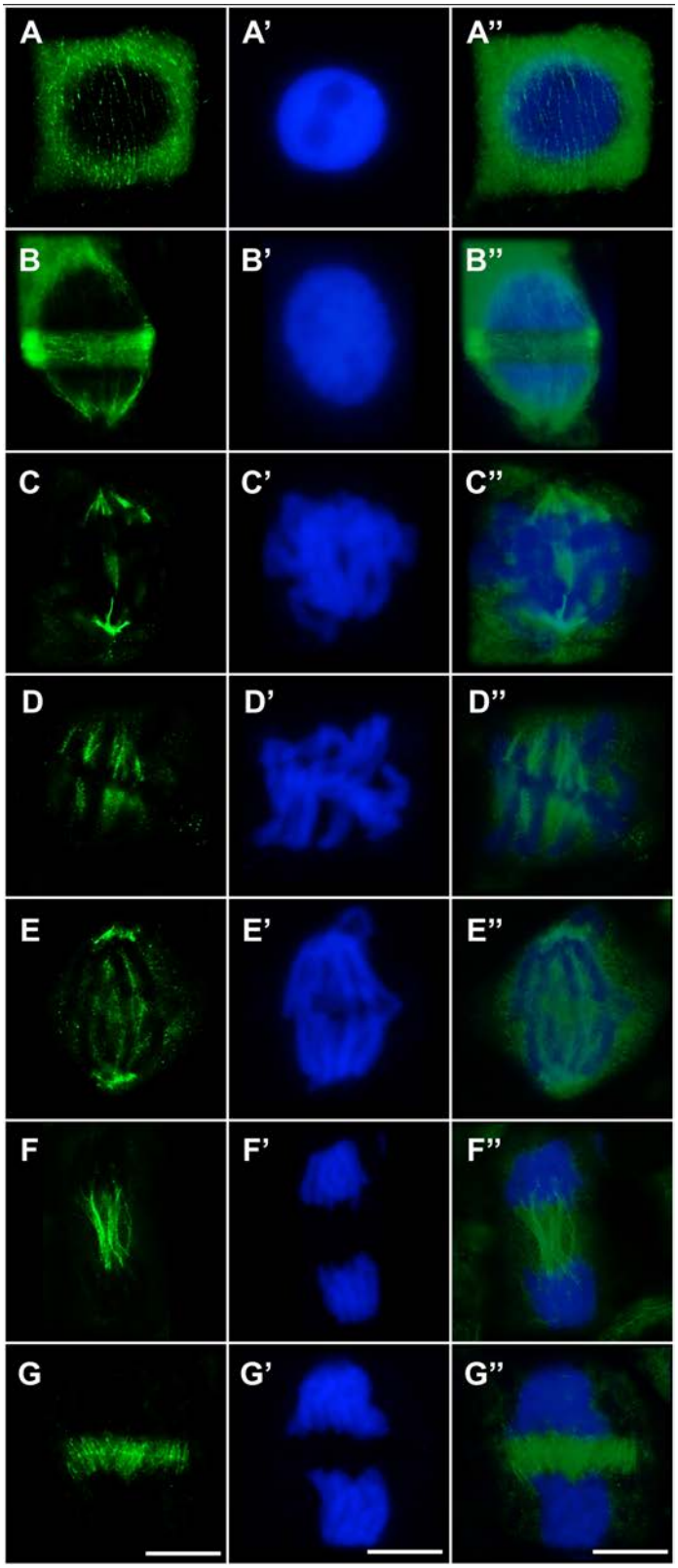

Figure 6. Immunocytochemical detection of β-tubulin (**A**–**G**) in primary root meristem cells of *V. faba* after 24 h of incubation in water—Control. Corresponding images of cell nuclei stained with DAPI (**A′**–**G′**) and merged images (**A″**–**G″**). Scale bar = 10 μm.

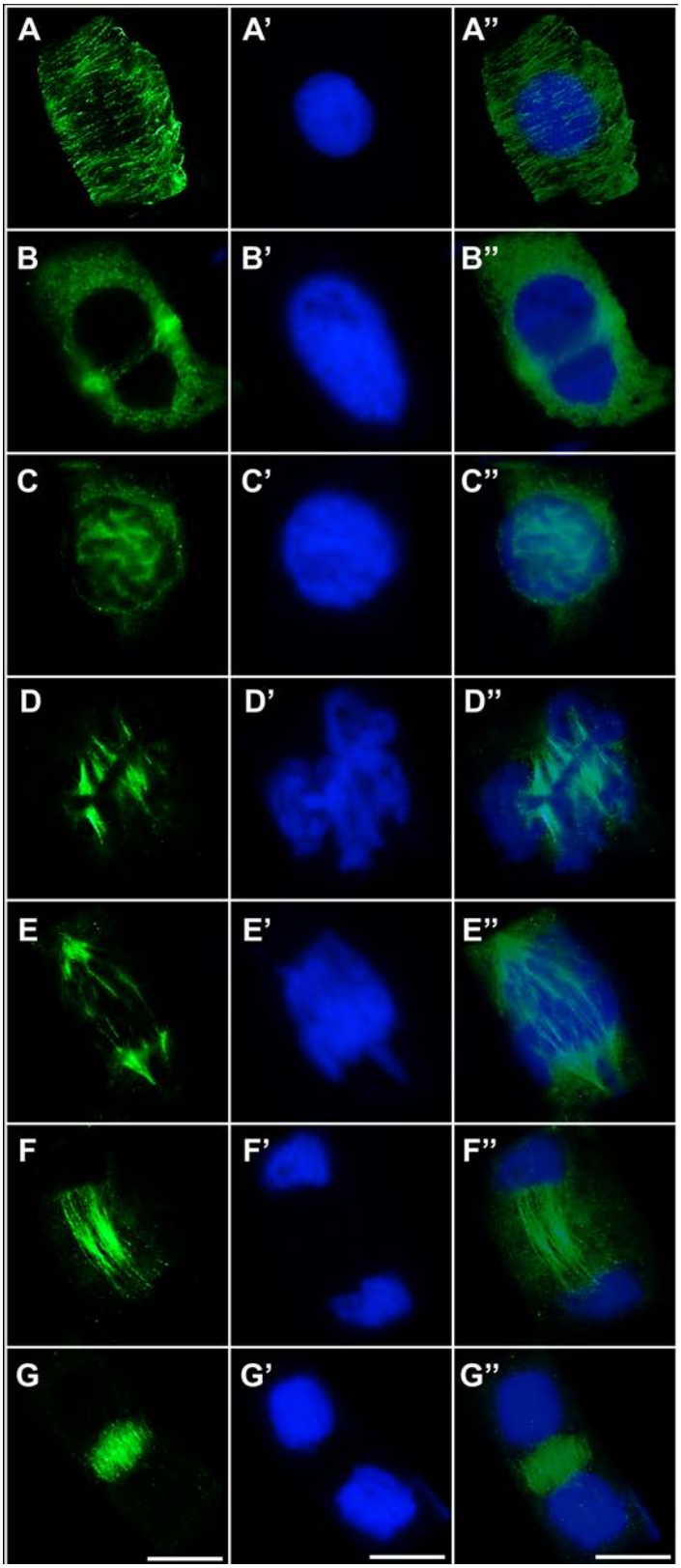

Figure 7. Immunocytochemical detection of β-tubulin (**A**–**G**) in primary root meristem cells of *V. faba* after 24 h of incubation in emulsifier. Corresponding images of cell nuclei stained with DAPI (**A′**–**G′**) and merged images (**A″**–**G″**). Scale bar = 10 µm.

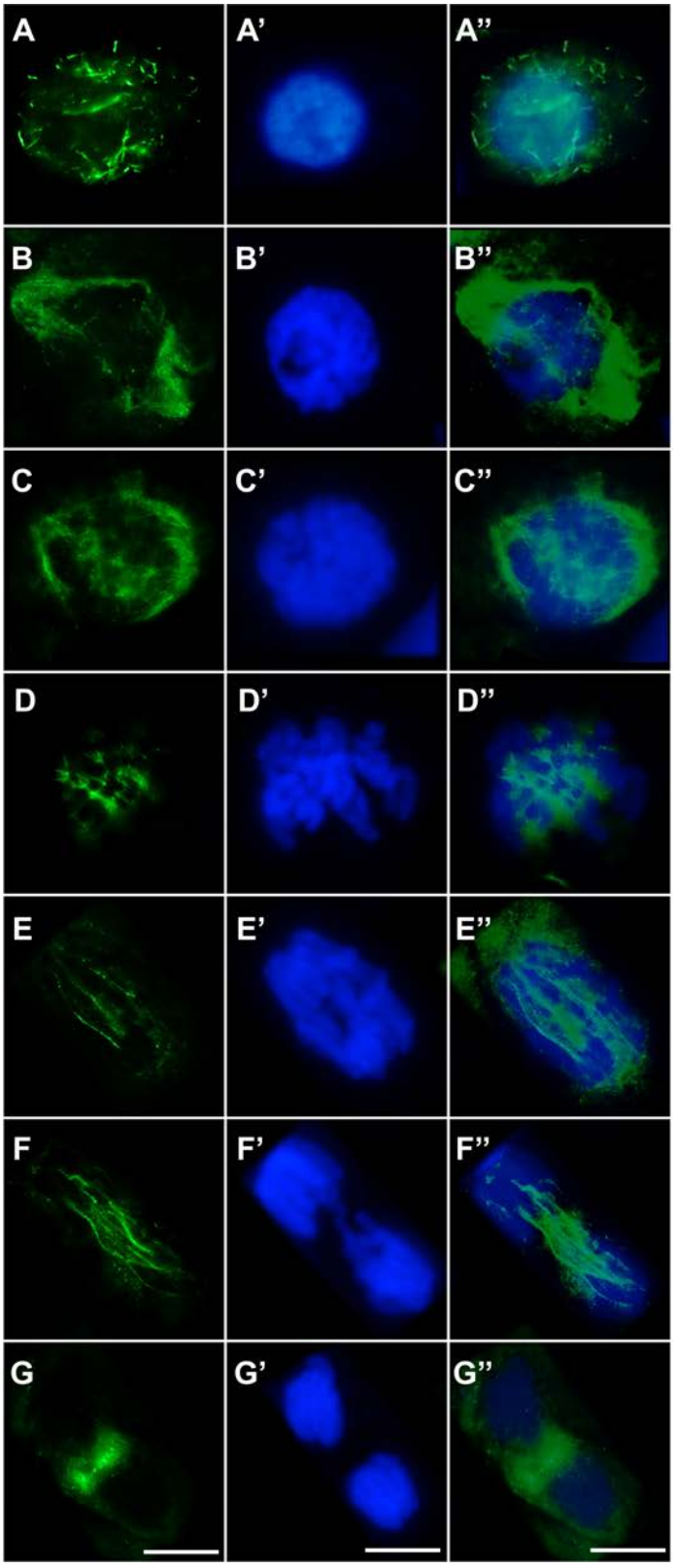

Figure 8. Immunocytochemical detection of β-tubulin (**A**–**G**) in primary root meristem cells of *V. faba* after 24 h of incubation in $CdCl_2$. Corresponding images of cell nuclei stained with DAPI (**A′**–**G′**) and merged images (**A″**–**G″**). Scale bar = 10 µm.

In cells exposed to the emulsified form of TO, microtubule organization did not deviate from the pattern observed in control cells (Figure 9A–G,A′–G′,A″–G″). Both cortical microtubules and preprophase band microtubules in interphase (Figure 9A–A″,B–B″), as well

as elements of the mitotic spindle in prophase (Figure 9C–C″), metaphase (Figure 9D–D″), early and late anaphase (Figure 9E–E″,F–F″), and telophase (Figure 9G–G″), exhibited a well-ordered structure typical for each cell cycle stage.

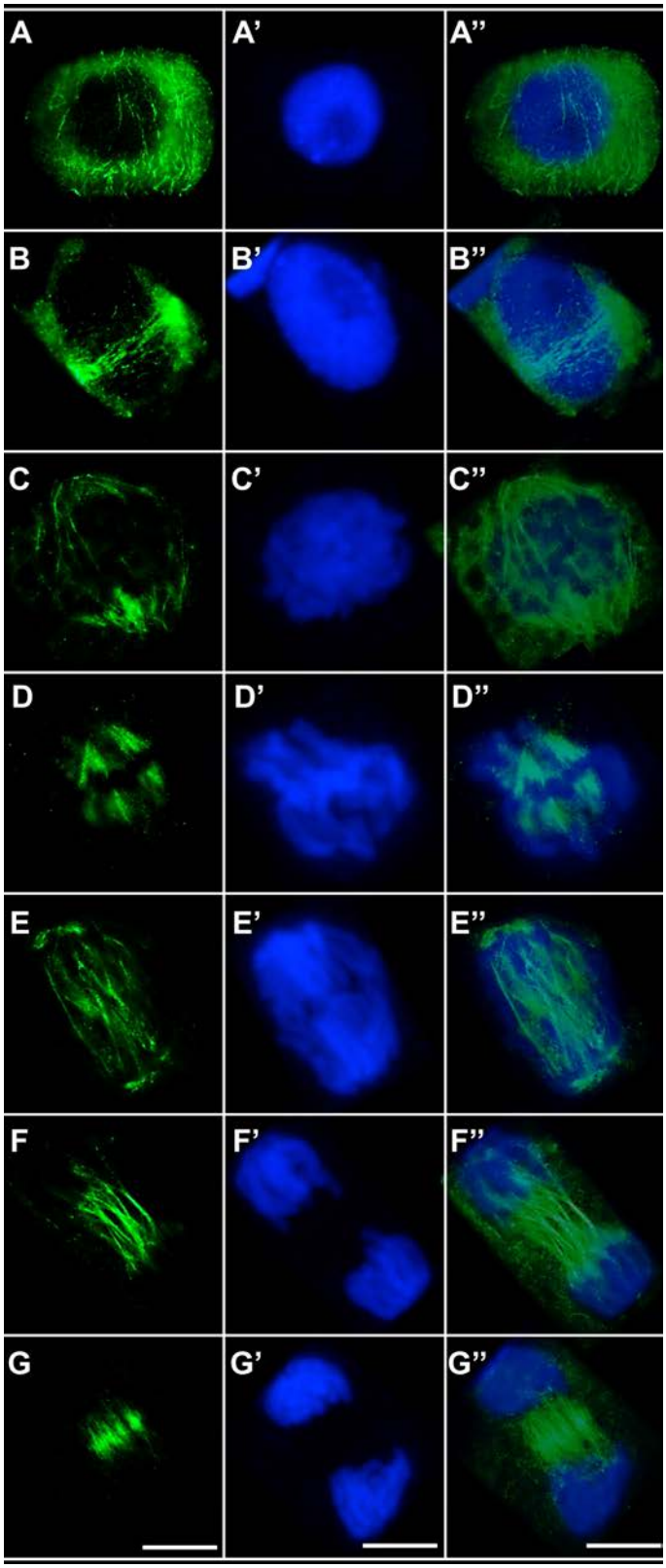

Figure 9. Immunocytochemical detection of β-tubulin (**A**–**G**) in root meristem cells of *V. faba* after 24 h of incubation in thyme essential oil—TO. Corresponding images of cell nuclei stained with DAPI (**A′**–**G′**) and merged images (**A″**–**G″**). Scale bar = 10 µm.

A similar pattern was observed in cells treated simultaneously with $CdCl_2$ and TO (Figure 10A–G,A′–G′,A″–G″). Cortical microtubules maintained a regular arrangement of long, parallel fibers; the mitotic spindle displayed normal bipolar symmetry with properly organized kinetochore and polar microtubule bundles, and the phragmoplast formed a regular structure composed of short, parallel-aligned microtubules.

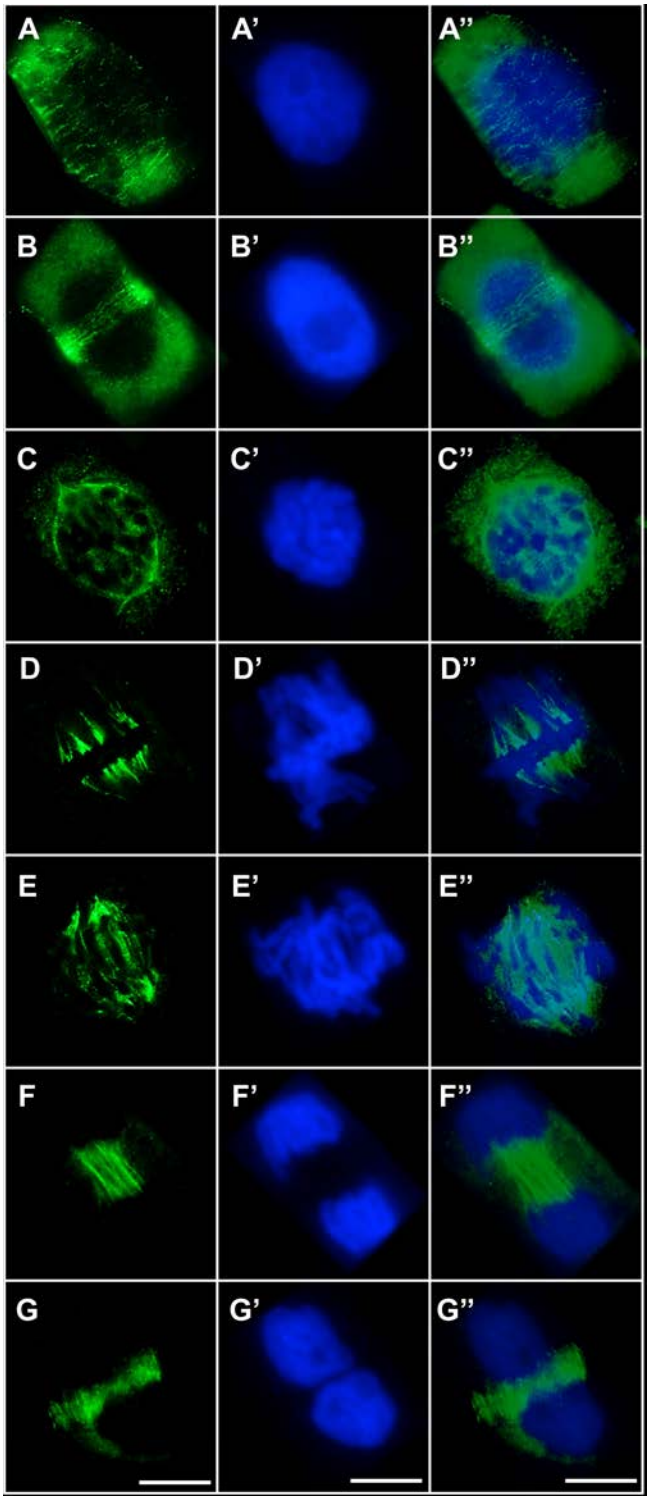

Figure 10. Immunocytochemical detection of β-tubulin (**A**–**G**) in primary root meristem cells of *V. faba* after 24 h of incubation in combination of $CdCl_2$ and thyme essential oil—TO. Corresponding images of cell nuclei stained with DAPI (**A′**–**G′**) and merged images (**A″**–**G″**). Scale bar = 10 μm.

In light of the observed disturbances in microtubule structure and organization in Cd-exposed cells, we also analyzed the remodeling of actin filaments, which constitute an essential component of the cytoskeleton in dividing cells. Actin filaments, supporting microtubule function, undergo dynamic rearrangements, forming both locally organized, dense bundles and thin, elongated filaments that contribute to a more extensive network.

In control meristem cells and those treated with the emulsifier, both filament forms were present: compact, intensely fluorescent bundles of short filaments (Figure 11A,C), as well as a fine, diffuse network composed of long filaments extending along the longitudinal axis of the cells (Figure 11B,D). Following 24 h of $CdCl_2$ exposure, the overall filament arrangement remained comparable to the control, but both the short bundles and the longer filaments exhibited noticeable thickening and increased fluorescence intensity, suggesting additional lateral filament interactions (Figure 11E,F). In cells treated with the emulsified form of TO, the organization, packing, thickness, and orientation of filaments resembled those observed in control cells (Figure 11G,H). In the case of simultaneous exposure to $CdCl_2$ and TO, only moderate thickening of short actin bundles was observed, while the longer filaments retained a control-like appearance, with no obvious increase in fluorescence intensity or disruption of the filament network (Figure 11I,J).

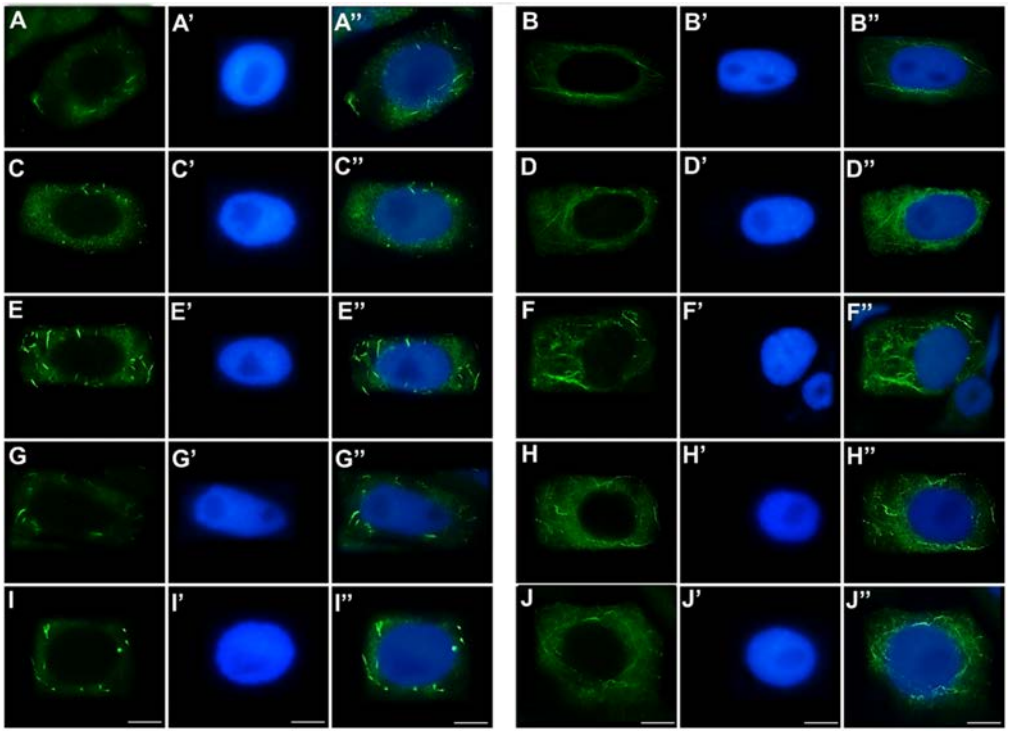

Figure 11. Immunocytochemical detection of actin in primary root meristem cells of *V. faba* after 24 h of incubation in water—Control (**A**,**B**), emulsifier (**C**,**D**), $CdCl_2$ (**E**,**F**), thyme essential oil—TO (**G**,**H**), and a combination of $CdCl_2$ and TO (**I**,**J**). Corresponding images of cell nuclei stained with DAPI (**A′**–**J′**) and merged images (**A″**–**J″**). Scale bar = 10 µm.

2.5. Immunocytochemical Analysis of Mitotic Epigenetic Modifications of Histone H3

Given that both chromatin condensation into mitotic chromosomes and the proper function of the cytoskeleton required for chromatid segregation and cell division depend on the recruitment of specific mitotic regulators—which in turn are influenced by dynamic epigenetic modifications—we analyzed selected, commonly studied histone H3 modifications. Specifically, phosphorylation of threonine 3 (H3T3Ph; Figure 12) and serine 10 (H3S10Ph; Figure 13) was examined using immunocytochemical methods.

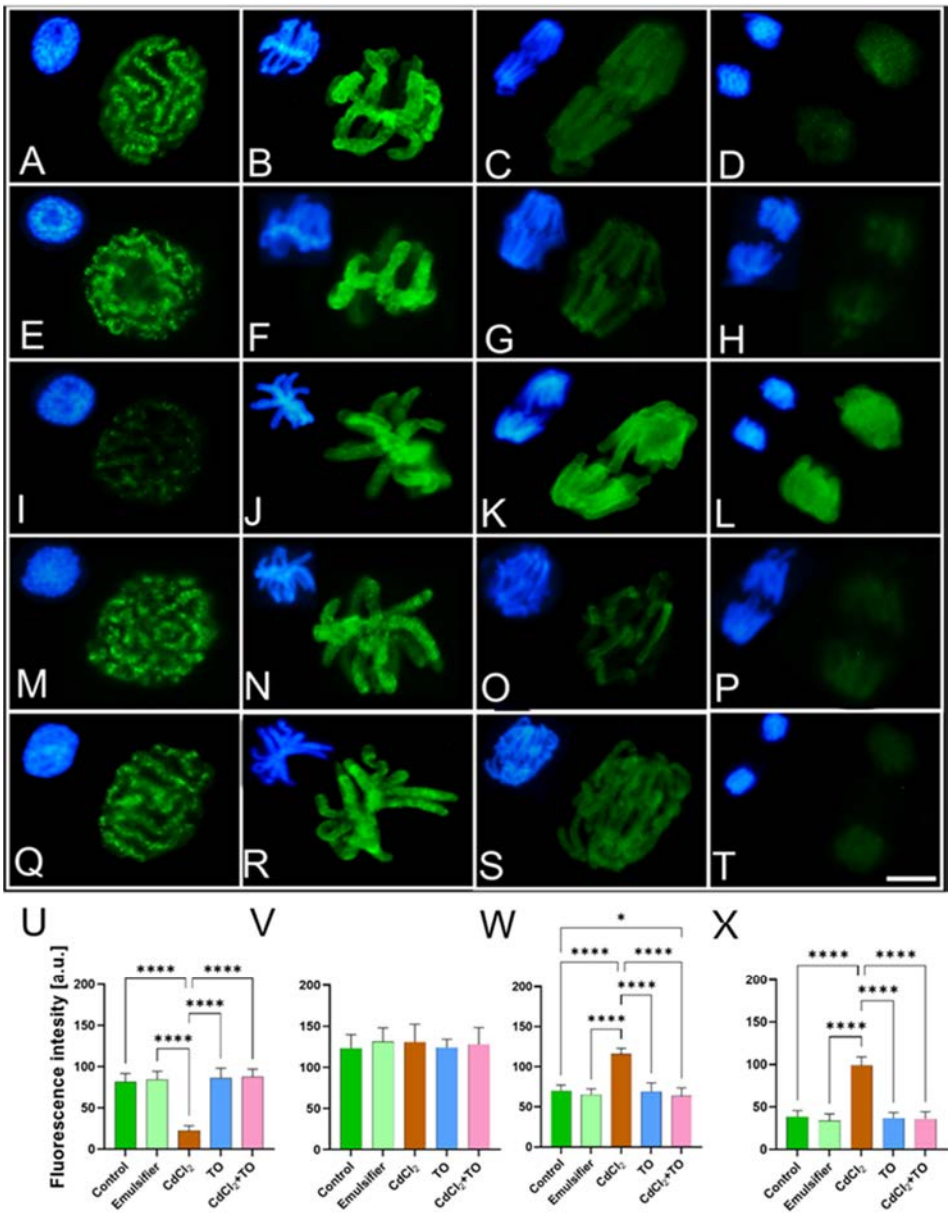

Figure 12. Immunofluorescence detection of H3T3Ph in mitotic figures of the primary root meristem cells of *V. faba* after 24 h of incubation in water—Control (**A**–**D**) emulsifier (**E**–**H**), $CdCl_2$ (**I**–**L**), thyme essential oil (TO) (**M**–**P**), and a combination of $CdCl_2$ and TO (**Q**–**T**). Scale bar = 10 µm. Corresponding images of cell nuclei stained with DAPI, embedded in the upper left corners of each image. Mean (± SD; n = 3 biological replicates; each representing an individual seedling) intensity of H3T3Ph labeling in prophase (**U**), metaphase (**V**), anaphase (**W**) and telophase (**X**); approximately 30 nuclei were analyzed per treatment. Statistical significance: **** $p < 0.0001$, * $p < 0.05$ (one-way ANOVA followed by Tukey's multiple comparison test).

In the analysis of H3T3Ph, meristem cells from control seedlings and those treated with the emulsifier exhibited a strong immunopositive signal during prophase, appearing as numerous distinct foci of variable size distributed along the arms of condensing chromosomes (Figure 12A,E,U). During metaphase, the entire chromosomes displayed intense mosaic fluorescence, with the strongest labeling localized in the pericentromeric regions (Figure 12B,F,V). Following sister chromatid separation in anaphase, the H3T3Ph signal was markedly reduced, and chromosomes in telophase were devoid of specific labeling (Figure 12C,D,G,H,W,X).

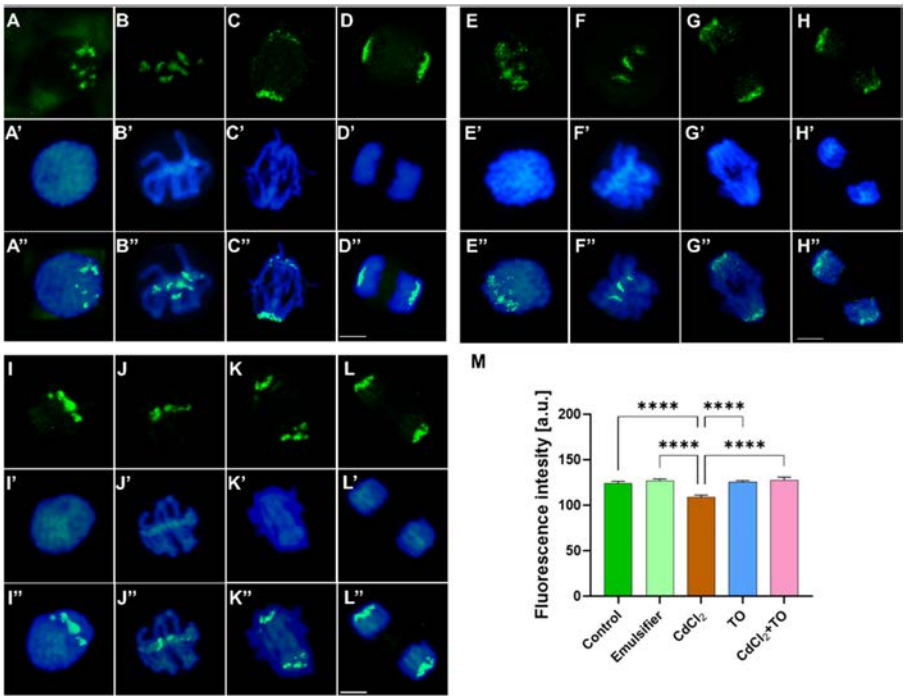

Figure 13. Immunofluorescence detection of H3S10Ph in mitotic figures of the primary root meristem cells of *V. faba* after 24 h of incubation in water—Control (**A**–**D**), $CdCl_2$ (**E**–**H**), and a combination of $CdCl_2$ and thyme essential oil—TO (**I**–**L**). Corresponding images of cell nuclei stained with DAPI (**A′**–**L′**) and merged images (**A″**–**L″**). Images for the emulsifier and TO were omitted since they showed no differences compared with the control. Scale bar = 10 µm. Mean (± SD; $n = 5$ biological replicates; each representing an individual seedling) intensity of H3S10Ph labeling in mitotic figures; approximately 50 nuclei were analyzed per treatment (**M**). Statistical significance: **** $p < 0.0001$ (one-way ANOVA followed by Tukey's multiple comparison test).

Cells exposed to $CdCl_2$ showed clear alterations in the pattern of this epigenetic modification (Figure 12I–L,U–W,X). Compared with control, the H3T3Ph signal in prophase, while retaining its focal pattern along condensing chromosomes, was noticeably weaker (Figure 12I,U). In metaphase, the intensity and labeling pattern were not significantly different from those observed in control conditions (Figure 12J,V). However, in subsequent mitotic stages (anaphase and telophase), the H3T3Ph signal did not undergo the typical attenuation but remained at a relatively high level, similar to that in metaphase (Figure 12K,L,W,X), indicating a disruption of the normal phase-dependent dynamics of histone H3 phosphorylation at threonine 3.

In cells treated with emulsified TO, both the labeling pattern and fluorescence intensity of H3T3Ph were comparable to those observed in control cells (Figure 12M–P,U–W,X), suggesting preserved physiological dynamics of this modification across mitotic stages. In cells simultaneously exposed to $CdCl_2$ and TO, the first two stages of mitosis exhibited a H3T3Ph signal pattern and intensity similar to the control (Figure 12Q,R,U,V). The main difference was the prolonged presence of a very weak signal extending into anaphase, during which H3T3Ph phosphorylation remained detectable along the arms of separating sister chromatids (Figure 12S,W). By telophase, the labeling pattern normalized and resembled that of control cells (Figure 12T,X).

In the analysis of H3S10Ph, meristem cells from control seedlings (Figure 13A–D) and those treated with the emulsifier exhibited an identical labeling pattern. The H3S10Ph signal appeared already in early prophase as intensely fluorescent clusters localized in the strongly condensed pericentromeric regions of chromosomes, concentrated near one pole of the nucleus (Figure 13A–A″). This arrangement reflects pronounced chromosome polarization,

consistent with Rabl's model, which proposes an ordered, non-random organization of chromosomes in the interphase nucleus. During metaphase, the H3S10Ph signal was clearly visible in the pericentromeric regions of chromosomes aligned at the metaphase plate (Figure 13B–B″). During anaphase, the labeled regions migrated with the centromeres of separating sister chromatids toward opposite poles of the cell (Figure 13C–C″). In telophase, the H3S10Ph signal remained confined to narrow, brightly fluorescent regions corresponding to the centromeres of single-chromatid daughter chromosomes that had reached the cell poles (Figure 13D–D″).

In cells incubated with $CdCl_2$, the overall localization of the H3S10Ph signal did not markedly differ from that observed in control cells (Figure 13E–H,E′–H′,E″–H″), remaining concentrated in the pericentromeric regions throughout mitosis. However, subtle changes in signal morphology and dispersion were evident. In prophase, fluorescent foci appeared more dispersed and finely granular ("sandy") compared with the distinct clustered structures seen in control cells (Figure 13E–E″). During metaphase, the foci were less numerous (Figure 13F–F″). In anaphase and telophase, a weak H3S10Ph signal persisted not only in the pericentromeric regions but also along the chromosome arms (Figure 13G–G″,H–H″), which was not observed in control cells. Quantitative fluorescence analysis revealed a reduction in H3S10Ph signal intensity in $CdCl_2$-treated meristems compared with the other experimental variants (Figure 13M), indicating that cadmium affects histone H3 phosphorylation at serine 10, despite maintaining the relative localization of the signal. In cells treated with TO and in cells simultaneously exposed to $CdCl_2$ and TO (Figure 13I–L,I′–L′,I″–L″), the H3S10Ph labeling pattern closely resembled that of control cells in terms of signal localization, dynamic changes throughout mitotic stages, and fluorescence intensity (Figure 13M).

3. Discussion

Mitosis is a tightly regulated, multi-level process that requires precise coordination of cell cycle regulators (CDK–Cyc complexes), establishment of mitosis-specific histone modifications, preparation of chromatin for condensation, and dynamic reorganization of the microtubule–actin cytoskeleton [66–68]. Disruption of any of these components can result in delays, abnormal progression, or complete inhibition of mitosis. Cadmium, described both in our previous studies [59,60] and in the broader literature as a potent genotoxic and pro-oxidative agent, significantly interferes with key mechanisms regulating cell cycle progression [69,70]. The present data further suggest that TO, known for its antioxidant properties [59,71], has the potential to mitigate cadmium-induced mitotic disturbances.

3.1. Cadmium Effects on Meristematic Cell Division and Root Growth in V. faba Seedlings

The meristematic tissue responsible for primary root growth is particularly sensitive to abiotic stresses, including cadmium toxicity [72]. In the present study, cadmium exposure reduced root elongation by approximately 50% and decreased the mitotic index nearly tenfold, confirming strong inhibition of organ growth through impaired cell proliferation [61,73,74]. Reduced mitotic activity may result from cell cycle arrest during interphase, inhibition of mitotic entry, or disturbances in mitotic progression, as suggested by the accumulation of prophase cells and the reduced proportion of anaphase and telophase figures.

Studies on *Zea mays* meristematic tissue have shown that cadmium accumulation prolongs the cell cycle, partly by inhibiting the G1-to-S phase transition [9]. A similar mechanism was indicated by our previous observations in *V. faba*, where cadmium reduced the number of replicating cells and caused their accumulation in early S phase, suggesting

slowed DNA replication [59]. As a strong inducer of oxidative stress, cadmium can also cause DNA damage, that activates the DNA damage response (DDR), which delays cell cycle progression until lesions are repaired [75,76]. Our studies in *V. faba* confirmed the genotoxic effects of cadmium [59], indicating that replication stress likely contributed to the reduced mitotic activity observed here.

Cadmium-treated roots also exhibited increased chromatin condensation in interphase nuclei, visible as compact and irregular regions of genetic material, as observed in the present study. These structural changes may result from cadmium-induced epigenetic modifications, including DNA methylation and histone modifications, associated with chromatin compaction and transcriptional repression, as demonstrated in our parallel study [60]. These alterations may prolong interphase and further reduce the proportion of dividing cells. However, disturbances in the regulation of the G2/M transition in cells that have completed interphase cannot be excluded. Therefore, the activity of key regulators of this transition, CDKA and CycB, was analyzed.

3.2. Cadmium Disrupts Cell Cycle Regulators: CDKA and CycB

Cell cycle progression depends on the activity of CDK–Cyc complexes, in which relatively stable CDKs are regulated by periodic cyclin accumulation, enabling entry into mitosis [22]. Disturbances in the levels of these components can arrest the cell cycle [77] and may occur under environmental stress, DNA damage, or exposure to toxic agents [78–82].

Exposure to $CdCl_2$ caused a slight but distinct reduction in the conserved CDKA protein level. Literature data indicate that cadmium effects on cell cycle regulators are dose-dependent. Moderate concentrations can increase the expression of genes such as *CDKA1* or the cell cycle inhibitor *WEE1* [8], or may not cause significant changes in *CDKA* levels, as reported in *Glycine max* cultures [83]. In contrast, severe toxic stress suppresses the expression of cell cycle-related genes [8]. The relatively high concentration used in this study (175 µM $CdCl_2$) therefore likely reflects stress conditions sufficient to disrupt even relatively stable components of the cell-cycle regulatory machinery. The modest magnitude of this change may reflect homeostatic control of CDKA levels, although it does not eliminate its sensitivity to stress. Similar trends have been reported in *A. thaliana* meristems exposed to salt stress, where NaCl-induced reductions in *CDC2aAt* and *CDC2bAt* expression correlated with decreased mitotic activity [84]. Although salt and cadmium stress differ in their primary triggers, both induce secondary oxidative stress, leading to ROS overproduction, redox imbalance, DNA damage, and activation of cell cycle checkpoints [59,75,84,85]. Under such conditions, reduced CDKA activity can contribute to cell cycle arrest and prevent entry into mitosis in cells with damaged genomes (Figure 14). Cadmium stress may also induce broader epigenetic and transcriptional reprogramming [60,86,87]. In this context, the observed decrease in CDKA could partly reflect general repression of proliferation-associated genes under severe stress rather than specific targeting of this regulator. In contrast to the moderate reduction in CDKA, a pronounced decrease in CycB protein levels and transcript abundance was observed after 24 h exposure to 175 µM $CdCl_2$. Similar repression of B-type cyclins under cadmium stress has been reported in *A. thaliana* root cells [86,88], *Z. mays* meristems and leaves [9], and *G. max* suspension cultures [83]. These findings suggest that inhibition of B-type cyclin expression represents a key mechanism limiting mitotic activity and preventing cells that have completed interphase from entering mitosis (Figure 14).

3.3. Cadmium-Induced Alterations in Cytoskeleton: Actin Filaments and Microtubules

Cadmium, even at low concentrations (0.25 µM), is known to disrupt cytoskeletal organization, affecting both microtubules and actin filaments and thereby impairing cell

cycle progression and root growth [61,73,89–91]. In the present study, exposure of *V. faba* seedlings to 175 µM $CdCl_2$ caused pronounced disturbances in the microtubule-actin cytoskeleton of root meristems. In interphase cells, the cortical microtubule network lost its regular orientation and appeared as short, rod-like structures. Similar alterations have been reported in the green alga *Spirogyra decimina* [92] and in higher plant cells, where microtubules also fragmented into segments of variable lengths [63,90,93]. Disruption of cortical microtubules impaired preprophase band formation and the subsequent assembly of a functional mitotic spindle, potentially contributing to delays in early mitotic stages and to the increased proportion of prophase cells observed in this study. Comparable effects have been reported in cadmium-treated root cells of *Salix matsudana*, where spindle fibers formed condensed arrays in metaphase and aggregated during anaphase and telophase [93] as we also observed. Microtubule aggregation, which reduces their dynamic behavior, likely contributed to the lower frequency of anaphase and telophase cells, prolonging mitosis and limiting primary root growth. Similar effects on spindle stability and mitotic stage distribution have been reported under cadmium stress [61].

Microtubule aggregation and difficulties in their reorganization may reflect adaptive cellular responses to oxidative stress and disturbed redox homeostasis under cadmium exposure [75]. These responses may involve ROS-induced post-translational modifications of tubulin, such as acetylation and detyrosination, which have been shown to increase microtubule mechanical resistance but reduce their dynamic remodeling [94]. Similar stress-induced stabilization has been reported in sponge cells (*Clathrina clathrus*) [95] and in *G. max* root cells exposed to cadmium [90]. However, excessive stabilization ultimately impairs microtubule function [94].

The regulation of microtubule organization also involves microtubule-associated proteins (MAPs) [36], including MAP65-1, which bundles parallel microtubules [96–98]. Literature data indicate that it can mediate atypical tubulin polymers under ROS disturbances [99] and preferentially binds stabilized filaments, enhancing local microtubule density [100]. MAP65 activity is controlled by CDKA–CycB dependent phosphorylation: when phosphorylated, it detaches from microtubules, increasing their dynamics [97]. Under cadmium stress, the reduced CDKA and CycB levels observed in our study may therefore affect MAP65 phosphorylation status and potentially favor its association with microtubules. Together with tubulin acetylation and detyrosination, which are reported on in [94], this may contribute to increased bundling and altered organization of microtubules observed in our immunocytochemical analyses.

Cadmium is also known to disrupt Ca^{2+} homeostasis through interactions with membrane channels and calcium-binding proteins. Literature reports indicate that both ROS-mediated pathways and the direct action of $CdCl_2$ increase cytosolic Ca^{2+} levels [101,102], and that disturbances in calcium balance can affect microtubule organization and stability [103]. Elevated cytosolic Ca^{2+} promotes depolymerization at microtubule ends, thereby destabilizing these structures [104]. Calcium imbalance may influence not only microtubules but also actin filaments. In our study, cadmium markedly altered the organization of actin filaments in *V. faba* meristematic cells. Thickening of both short bundles and long filaments, reflected by increased fluorescence intensity, suggests enhanced filament aggregation and the formation of less ordered actin structures. Similar effects may result from direct interactions between Cd^{2+} ions and actin, leading to aggregate formation [105]. However, an indirect mechanism related to disturbed calcium signaling cannot be excluded. According to literature reports, elevated cytosolic Ca^{2+} activates signaling cascades that regulate numerous actin-binding proteins involved in controlling filament organization, including processes such as severing, stabilization, or inhibition of elongation [106]. The filament bundling and local stabilization observed in our study may therefore reflect the

combined effects of direct Cd^{2+} action and indirect consequences of oxidative stress and disrupted calcium signaling.

The cytoskeletal response to cadmium stress therefore appears to be multilayered and the result of the interplay of several regulatory mechanisms. Changes in tubulin post-translational modifications, modulation of microtubule-associated protein activity, and disturbances in calcium and redox signaling together form an integrated response network in which filament stabilization may represent an adaptive reaction to unfavorable conditions. However, such stabilization, while increasing the mechanical resistance of cytoskeletal structures, may also be associated with reduced flexibility of their organization, as observed in *V. faba* primary root meristems (Figure 14). Such alterations in microtubule organization could therefore contribute to difficulties in chromatid separation and proper segregation of genetic material into daughter nuclei. Future studies using transmission electron microscopy (TEM) will enable detailed ultrastructural analyses of microtubule organization and provide a quantitative framework to complement the qualitative observations presented in this study.

3.4. Cadmium-Induced Changes in Mitosis-Related H3 Phosphorylation (H3T3 and H3S10) Patterns

Enhanced chromosome condensation and the presence of "sticky" telomeric regions of sister chromatids—particularly evident in metaphase and promoting their adhesion in anaphase—may result from cadmium–induced mutations in genes encoding non–histone chromatin–associated proteins, as well as from direct interactions of cadmium with histones. Such effects can disrupt chromosome condensation and segregation, manifesting as chromosomal stickiness [107,108]. However, the chromosome abnormalities and spindle defects observed in our study—such as microtubule aggregation and the increased proportion of cells arrested in prophase and metaphase—may also reflect disturbed regulation of mitosis-specific epigenetic histone modifications. In particular, histone H3 phosphorylation forms a functional cascade in which phosphorylation at threonine 3 (H3T3Ph) precedes and facilitates phosphorylation at serine 10 (H3S10Ph). Phosphorylation of H3T3, essential for proper chromosome condensation and spindle assembly checkpoint function, is catalyzed by the AtHaspin kinase identified in *A. thaliana* [109]. This modification acts as a recruitment signal for the chromosomal passenger complex (CPC), a mitosis-specific complex responsible for correcting improper kinetochore–microtubule attachments, ensuring accurate chromosome segregation, and contributing to spindle disassembly. In plants, the CPC includes Aurora B kinases of the AtAUR family (identified in *A. thaliana*), together with homologs of other CPC components known from animal cells [50,110]. Recruitment of the CPC to chromosomes leads to local activation of Aurora B kinases, which in plants phosphorylate H3S10 mainly in pericentromeric regions, a modification associated with maintenance of sister chromatid cohesion and their faithful segregation [51,52].

According to literature, H3T3Ph and H3S10Ph levels are tightly regulated not only by kinases but also by the protein phosphatases PP1 and PP2A [111,112]. Temporal suppression of these enzymes is essential for mitotic entry, while timely reactivation ensures proper progression through mitosis, coordinating mitotic kinases (Haspin and Aurora B), chromatin condensation, microtubule organization, and the metaphase-to-anaphase transition [113–115]. PP1 dephosphorylates H3T3, controlling CPC recruitment and Aurra kinase activity, which ultimately affects H3S10 phosphorylation and sister chromatid segregation [116,117]. PP2A regulates phosphorylated centromeric and kinetochore proteins, indirectly modulating CPC and Aurora function in pericentromeric regions [118]. In our study, the H3T3Ph signal, which normally declined during anaphase in control cells, remained elevated in $CdCl_2$-treated cells throughout anaphase and telophase. This suggests that cadmium may inhibit PP1/PP2A activity, sustaining Haspin activation and preventing

full H3T3 dephosphorylation [119]. Similar mitotic defects, including sticky chromatid ends, have been reported following PP1/2A inhibition with okadaic acid in *V. faba* [114]. Moreover, high Cd concentrations reduce PP1/PP2A gene expression in plants [120,121], and in animal models, cadmium via ROS overproduction also inhibits PP2A [122]. Insufficient phosphatase activity may thus sustain H3T3Ph impair CPC/Aurora recruitment, limit H3S10 phosphorylation, and delay metaphase-to-anaphase progression, as observed in our experiments. Reduced H3S10Ph could also result from altered chromatin architecture limiting the accessibility of the S10 residue or from impaired activation of Aurora kinases by CDK–Cyc complexes [123], consistent with our observations of decreased CycB and modestly reduced CDKA. Literature further indicates that ROS can mislocalize Aurora B along chromosome arms without changing its total levels [124,125]. In line with this, we observed subtle spreading of the H3S10Ph along chromosome arms, suggesting a shift in Aurora B localization away from centromeres and related mitotic dysfunction (Figure 14).

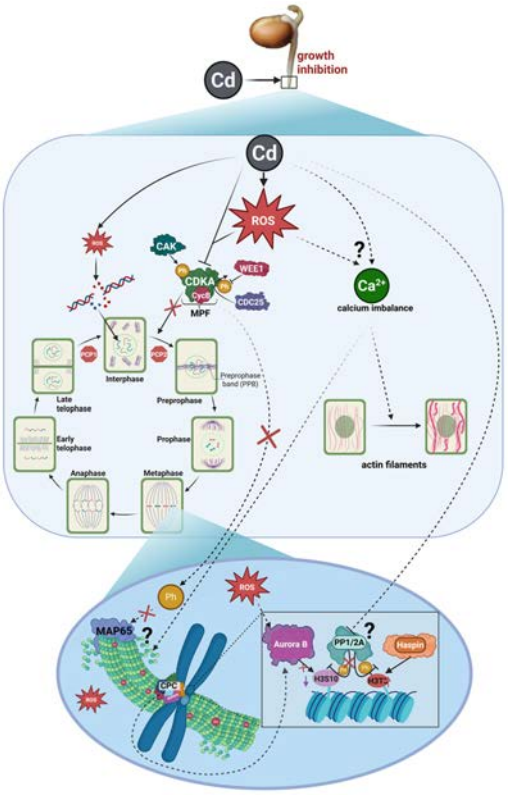

Figure 14. Proposed mechanism of cadmium (Cd) effects on mitotic progression. Arrows indicate the direction of processes or signaling pathways; arrows with pointed tips denote activation or enhancement, whereas arrows with blunt (flat) tips denote inhibition or suppression. Solid arrows indicate relationships directly supported by experimental data obtained in our study. Dashed arrows and question marks indicate proposed mechanisms inferred from prior literature and not directly tested here. Cross symbols (X) indicate inhibition or suppression of the indicated processes or interactions. Cd enters the cell and induces overproduction of reactive oxygen species (ROS). Elevated ROS levels are proposed to disrupt calcium metabolism and affect the formation or activity of CDK–Cyc complexes, resulting in cell cycle arrest at the G2/M transition and reduced mitotic entry. Reduced levels/activity of the M-phase Promoting Factor (MPF) may impair inhibitory phosphorylation of MAP65. Consequently, MAP65 may contribute to increased microtubule stabilization, which could affect proper spindle organization. Additionally, Cd-induced stress may interfere with protein phosphatases PP1 and PP2A, thereby potentially altering the regulation of mitotic kinases such as Aurora B and Haspin. Disruption of histone H3 phosphorylation dynamics may in turn affect chromatin organization. Collectively, these proposed alterations could contribute to reduced mitotic index and impaired root growth. Created in BioRender. Gocek-Szczurtek N. (2026). https://BioRender.com/on5o09l.

3.5. Thyme Oil Mitigates Cadmium-Induced Disruptions in Mitosis and Its Regulatory Mechanisms

A promising strategy to enhance plant tolerance to cadmium, is the use of natural compounds with protective properties. Since cadmium is a strong inducer of oxidative stress [75,126] and TO has well-documented antioxidant activity [127–129], TO was tested here as a potential protective agent. Applied alone at 0.03% (*v*/*v*), TO had no effect on primary root growth, mitotic progression, or mitosis-related structural changes in *V. faba*. The apparent disparity between the reduced CycB transcript and protein levels and the unchanged mitotic activity in the TO-treated series can likely be explained by the regulatory characteristics of the G2/M transition. Although TO alone caused a decrease in CycB abundance, the magnitude of this reduction may have remained within the tolerance range of the mitotic regulatory system and therefore did not translate into a measurable decrease in the mitotic index. This interpretation is consistent with the hysteresis behavior of the G2/M transition, in which mitotic entry depends on threshold activation of CDK–Cyc complexes rather than on linear changes in cyclin abundance [130]. Importantly, the decrease in CycB levels was not accompanied by changes in CDKA protein abundance. This observation is consistent with the established regulatory framework of the plant cell cycle, where CDK proteins are typically maintained at relatively stable levels, whereas cyclins represent the more dynamically regulated component controlling CDK activity [131–133]. The modest CycB reduction may result from redox-dependent regulation of cell-cycle genes. ROS act not only as damaging agents but also as signaling molecules controlling proliferation-related transcription [134]. TO's antioxidant activity, including enhanced SOD, CAT, and APX activities reported in the literature [55] and supported by our unpublished data, lowers ROS levels and may attenuate redox-dependent signaling pathways that normally stimulate the expression of periodically activated cell-cycle genes such as CycB. As a result, CycB levels may be slightly reduced without impairing overall mitotic regulation, keeping mitotic parameters comparable to those observed in the control. While this study integrates cytological observations with selected G2/M markers (CDKA and CycB), further refinement could include additional cell-cycle regulators or direct measurements of CDK activity to better define how Cd and TO modulate the mitotic regulatory network.

TO applied during seedling exposure to $CdCl_2$ revealed a clear protective effect against cadmium toxicity in plant cells. Disturbances observed under $CdCl_2$ treatment alone were largely reduced or absent in the combined treatment. At the macroscopic level, root growth remained close to the control, and the dynamics of cell division, although not fully restored to control values, were maintained at a relatively high level. The protective action of TO was reflected in the preservation of normal interphase chromatin structure and mitotic chromosome organization, as well as in the maintenance of proper actin filaments and microtubule architecture within the cytoskeleton. This was accompanied by sustained functionality of CDKA–CycB regulatory complexes and by the correct progression of mitosis-related histone H3 phosphorylation (Figure 15).

The collected results indicate that TO exerts a protective effect at a higher organizational level, integrating multiple aspects of cellular organization and cell cycle regulation. This effect may be linked to modulation of redox homeostasis, which could act as a coordinating hub integrating chromatin remodeling, cytoskeletal organization, mitotic enzyme activity, and the execution of epigenetic modifications. This interpretation is consistent with previously reported antioxidant properties of TO, attributed primarily to its main components, thymol, p-cymene, and carvacrol, which have been shown to limit ROS accumulation in various experimental systems [59,135–137].

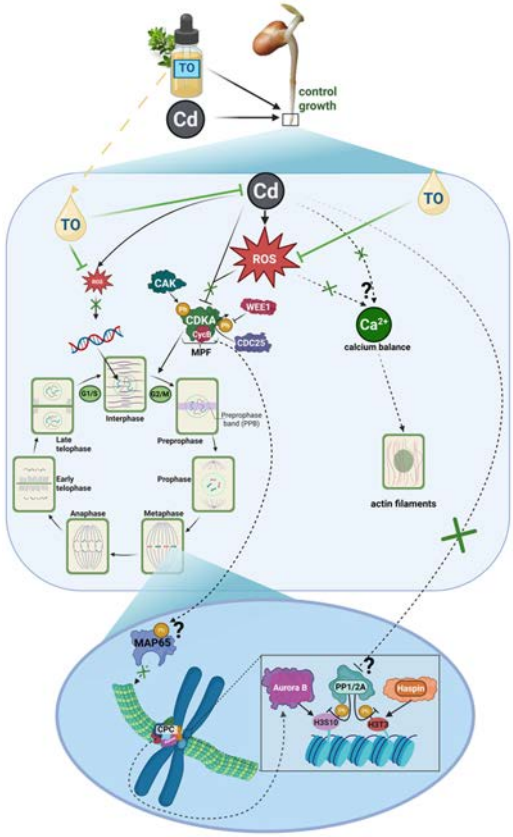

Figure 15. Proposed protective mechanism of thyme oil (TO) against cadmium (Cd)-induced mitotic disturbances. Arrows indicate the direction of processes or signaling pathways; arrows with pointed tips denote activation or enhancement, whereas arrows with blunt (flat) tips denote inhibition or suppression. Solid arrows indicate relationships directly supported by experimental data obtained in our study. Dashed arrows and question marks indicate proposed mechanisms inferred from prior literature and not directly tested here. Cross symbols (X) indicate inhibition or suppression of the indicated processes or interactions. TO treatment is proposed to mitigate Cd-induced oxidative stress, thereby helping to restore calcium homeostasis and proper regulation of CDK–Cyc complexes. This may facilitate proper M-phase Promoting Factor (MPF) activity, enabling inhibitory phosphorylation of MAP65 and preventing excessive microtubule stabilization. TO may also support PP1/PP2A activity, contributing to balanced regulation of mitotic kinases such as Aurora B and Haspin, and thereby maintaining appropriate histone H3 phosphorylation dynamics and chromatin organization. Collectively, the proposed TO-induced changes could increase the mitotic index and promote restoration of root growth in plants exposed to cadmium toxicity. Created in BioRender. Gocek-Szczurtek N. (2026) https://BioRender.com/7jv86za.

This notion is supported by the study of Dentato et al. [138], who demonstrated that basil extracts, containing among other compounds carvacrol, promoted germination and growth of *Raphanus sativus* seedlings exposed to Cd by enhancing antioxidant enzyme activity, reducing ROS levels, and consequently limiting DNA damage. Consistent observations were reported in our previous publication, in which experiments were conducted in parallel with those presented here and were based on the same experimental system and identical conditions. In that work, Cd-induced ROS overproduction and its significant reduction in the presence of TO were directly demonstrated. Moreover, TO reduced replication stress and DNA damage in *V. faba* interphase cells by limiting oxidative stress [59] and by enhancing the activity of enzymatic and non-enzymatic antioxidant defense systems (unpublished data). Furthermore, TO prevented excessive oxidative stress and stabilized epigenetic modifications and chromatin organization in interphase, supporting transcription, in line with our parallel experiments [60]. In the presence of TO, cadmium-exposed cells did not

accumulate excessively in interphase but progressed through it more evenly and entered mitosis, contributing to the maintenance of a substantial proportion of mitotic cells in the meristems, as observed in the present study. However, the population of dividing cells did not reach control levels and remained approximately 50% lower than in the untreated control. This phenomenon can be interpreted in terms of CDKA–CycB hysteresis, according to which the minimal level of CycB and CDKA activity required for entry into mitosis is higher than that needed to maintain mitotic progression. Thus, cells that have already obtained a "mitotic license" may tolerate moderate decreases in CDKA activity and continue dividing, whereas cells that have not yet reached the G2/M decision point do not initiate mitosis under suboptimal complex activity [130,138,139]. In light of our results, although *CycB* transcription in the $CdCl_2$ + TO treatment reached or slightly exceeded control levels, the amount of CycB protein, despite being higher than in cells exposed only to cadmium, may still have been insufficient to trigger mitotic entry. This may particularly concern cells that had just completed interphase in a TO-protected yet still cadmium-containing environment and were approaching the G2/M decision point. Consequently, likely only a subset of the population could reach the CDKA–CycB activity threshold required for mitotic entry, especially since CDKA levels (detected by immunofluorescence) did not fully reach those observed in control cells.

With regard to the cells that nevertheless proceeded to division, an antioxidant mechanism of TO action also appears plausible. Based on literature reports, it can be proposed that in a cellular environment protected by TO, compensatory cytoskeletal stabilization mechanisms, such as increased tubulin acetylation or enhanced interactions with MAPs [90,94,97], are not strongly induced. Consequently, as observed in our study, the cytoskeleton does not undergo excessive rigidification or bundling and retains the dynamic properties required for the formation of the karyokinetic and cytokinetic spindle. This supports proper metaphase-to-anaphase transition and maintains proportions of cells at individual mitotic stages comparable to those in the control (Figure 15). Similar restorative effects of antioxidants on ROS-disrupted cytoskeletal organization have also been reported in other experimental models [140,141].

Previous studies conducted in the same experimental system demonstrated that TO reduces ROS levels [59]. This effect, potentially linked to the activation of antioxidant defense mechanisms, may favor the maintenance of PP1/PP2A activity, which, according to literature reports, can be impaired by cadmium-induced oxidative stress [122]. Preservation of these phosphatases supports proper H3T3 phosphorylation dynamics, essential for correct chromosome condensation, interaction with the spindle apparatus, and sister chromatid separation. This interpretation is consistent with literature reports showing that normalization of PP1/PP2A activity restores appropriate histone H3 phosphorylation profiles [142]. Further support for this interpretation comes from studies on other natural antioxidants. For example, literature data indicate that resveratrol protects phosphatases from oxidative inactivation and restores proper protein phosphorylation dynamics in cadmium-exposed neurons [143]. A similar relationship may apply to Aurora B kinase, whose localization and activity are reported to be sensitive to redox disturbances [124,125]. In our study, the restoration of distinct pericentromeric labeling and the disappearance of dispersed signals in the presence of TO suggest that reduced oxidative stress favored the recovery of proper Aurora B localization and the H3S10 phosphorylation pattern characteristic of normal mitosis. In this context, TO may be viewed as a factor supporting mitotic homeostasis by enabling the reversibility of epigenetic changes induced by cadmium-triggered oxidative stress (Figure 15).

Considering the complexity of the cellular response to cadmium stress, the reduction of ROS levels alone likely does not explain the full spectrum of TO's protective action. Literature data indicate that TO, as well as related essential oils rich in phenolic compounds and sesquiterpenes, can reduce cadmium toxicity and bioavailability in tissues. Ye et al. [144] demonstrated that thymol mitigates cadmium stress in *Nicotiana tabacum* seedlings by modulating glutathione (GSH) and phytochelatin levels, thereby promoting Cd sequestration into bound forms and its redistribution away from the cytoplasm. Similarly, Rahmani et al. [145] and Askari et al. [146] showed in animal models that thyme and clove oils containing caryophyllene markedly reduce Cd accumulation in tissues, accompanied by enhanced antioxidant activity and reduced oxidative stress. A common conclusion from these studies is that induction of endogenous Cd chelation (involving GSH and metallothioneins/phytochelatins) decreases the pool of biologically active Cd within the cell, thereby lowering its cytoplasmic bioavailability. Limiting the availability of free cadmium reduces its capacity to induce oxidative stress, while strengthened antioxidant defenses helps mitigate the effects of the remaining active fraction. Literature reports further indicate that both the reduced oxidative stress and decreased Cd bioavailability may indirectly limit secondary disturbances in calcium homeostasis arising from ROS- and Ca^{2+}-dependent signaling pathways [147–149]. Stabilization of these cellular processes may support proper cell cycle progression. Consequently, the activity of cyclin-dependent kinase complexes, such as CDKA–CycB, may remain more appropriately regulated [150], potentially enabling correct phosphorylation of microtubule-associated proteins, including MAP65, and supporting proper cytoskeletal organization during mitosis [147–149].

In light of the obtained results, TO appears to mitigate the negative effects of Cd exposure in meristematic cells by supporting the preservation of principal elements of proper mitotic progression. This may allow maintenance of reduced yet still effective mitotic activity, reflected in the retention of root growth potential. Although the detailed molecular mechanisms require further investigation, the results indicate a protective role of TO in sustaining cell division under cadmium-induced stress (Figure 15).

4. Materials and Methods

4.1. Plant Material

Selected based on the appropriate size and color, sterile seeds of *Vicia faba* var. *minor* L. (W. Legutko The Seed Breeding Company in Jutrosin, Poland) were sown in trays lined with moist blotting paper and germinated at a temperature of 20 ± 1 °C in the dark. Four-day-old seedlings with primary roots approximately 2.5 cm long were placed in Petri dishes containing distilled water (control), the emulsifier solution used for essential oil emulsification prepared and handled in the same manner as the TO-containing solution, 175 µM cadmium chloride solution ($CdCl_2$), 0.03% (v/v) emulsified thyme essential oil (TO; Etja, Elbląg, Poland), and $CdCl_2$ supplemented with emulsified TO. The composition of the TO was previously characterized by GC-MS [59] and corresponds to a thymol-rich chemotype of *Thymus vulgaris*, with thymol (28.39%), *p*-cymene (23.86%), linalool (8.49%), caryophyllene (4.04%), carvacrol (3.04%), limonene (3.15%), α-pinene (2.91%), γ-terpinene (2.55%), and α-terpineol (2.36%) as the main constituents. All experiments presented in our previous publications, referenced in the Discussion [59,60], in the present study, and in unpublished work assessing the efficiency of antioxidant systems in meristems were performed using the same batch of oil as analyzed in the first work [59] to ensure compositional consistency. The applied $CdCl_2$ concentration was determined through a combination of literature analysis and preliminary optimization experiments evaluating doses between 100 and 200 µM [59,60,74,87,151,152]. The final concentration of TO was chosen based on preliminary screening tests (0.01–0.06% v/v) and supported by earlier

reports [59,60]. The results of these preliminary tests, conducted during the optimization phase of the experimental system, evaluating different Cd and TO concentrations, as well as their combined effects, are summarized in Table S1 (Supplementary Materials). Due to the lipophilic nature of the essential oil, an emulsified form was used to obtain a stable and homogeneous dispersion in the aqueous medium and to ensure uniform contact with the biological material. Treatments with non-emulsified oil were excluded from further analyses due to a lack of reproducibility. To distribute TO sufficiently in water, it was emulsified in a mixture of C14-18 and unsaturated C16-18—mono- and di-ethoxylated glycerides and ethoxylated *Brassica napus* oil. The emulsifier mentioned above was mixed with TO in a ratio of 1:4 (v/v) (resulting in a final emulsifier concentration of 0.0075% v/v) and vortexed vigorously for 15 min; the emulsifier-only control underwent the same mixing and vortexing procedure. The emulsifier was donated by the Department of Agronomy at Poznań University of Life Sciences. Incubations were performed for 24 h in airtight, tall Petri dishes in the dark. The 24 h incubation period was chosen because it corresponds approximately to the duration of a complete mitotic cycle in root meristematic cells, allowing the detection of cadmium-induced alterations across successive phases of the cell cycle. Primary root meristems were used for analysis. The plant material used in the studies originated from independent germination batches and incubations performed on different days. Seedlings derived from these independent experimental runs were randomly assigned to the respective treatment conditions and served as biological replicates. The number of primary roots examined in each treatment depended on the type of analysis and is given in the relevant methodological subsections, together with detailed information on the number of analyzed cells or nuclei.

4.2. Root Length Measurement

Seedlings were measured using ImageJ software ver. 1.54p before and after 24 h incubation of root meristems with water (control), the emulsifier, $CdCl_2$, TO, and the combination of $CdCl_2$ and TO from the root tip to the hypocotyl. Root length increments were calculated by subtracting the length of the root before treatment from the length of the root after treatment. Overall, 17 seedlings were used for measurements in each experimental series.

4.3. Feulgen Staining for Mitotic and Mitotic Phase Indices

Apical parts of primary roots of *V. faba* seedlings were fixed in a mixture of cold absolute ethanol and glacial acetic acid (3:1, v/v) for 1 h. After rinsing several times with ethanol, the dissected root meristems were rehydrated and hydrolyzed in 4 M HCl for 1 h. Then, after rinsing with distilled water, the roots were placed in Schiff's reagent (acidified pararosaniline solution; Sigma-Aldrich, St. Louis, MI, USA) for 1 h. After staining, the roots were first rinsed in SO_2-water and then in distilled water. The cut, apical segments of the roots were then placed in a drop of 45% acetic acid and crushed on microscope slides. The slides were then frozen on dry ice, the coverslips were removed, and the slides were rinsed in 70% ethanol, then left to dry and embedded in Canada balsam. For each experimental series, 5 seedlings were used, and 500 nuclei were analyzed per root, resulting in 2500 Feulgen DNA-stained cells analyzed per series. The mitotic index (IM) value was calculated as the ratio of dividing cells to all meristematic cells × 100%. Phase index (IF) values were calculated as the ratio of the number of cells in a specific phase of mitosis to all mitotic cells × 100%. Photographic documentation was performed using an Eclipse E-600 microscope and a DS-Fi1 digital camera (Nikon, Tokyo, Japan).

4.4. Immunocytochemical Staining of Microtubules (β-Tubulin) and Actin Filaments

Root apical fragments (3 mm) were fixed in 4% (*w*/*v*) paraformaldehyde buffered with MTSB (50 mM PIPES, 5 mM EGTA, 5 mM MgSO4, pH 7.0) for 45 min, and then rinsed twice in PBS and transferred to the citrate-buffered mixture containing 2.5% (*w*/*v*) pectinase, 2.5% (*w*/*v*) cellulase and 2.5% (*w*/*v*) pectolyase (Sigma-Aldrich); pH 5.0; 40 °C) for 45 min. After rinsing with cold PBS (4 °C), root meristems were crushed on Super Frost Plus slides (Menzel-Gläser, Thermo Fisher Scientific, Waltham, MA, USA) in a drop of cold PBS. After freezing with dry ice, coverslips were removed, slides were washed with distilled water, and air-dried. Macerated cells were permeabilized with 0.5% (*v*/*v*) Triton X-100 for 15 min, then treated with blocking buffer (8% BSA and 0.1% Triton X-100, PBS; 20 °C) for 50 min. Slides were then rinsed with PBS and incubated overnight in a humid atmosphere (4 °C) with mouse monoclonal anti-β-tubulin antibodies (1:750, Sigma-Aldrich) and monoclonal actin antibodies (Sigma-Aldrich). All antibodies were dissolved in the antibody dilution buffer (1% *w*/*v* BSA, 0.3% *v*/*v* Triton X-100, PBS). The slides were then washed in PBS and incubated with the secondary Alexa Fluor 488-conjugated anti-rabbit IgG (1:500, Sigma-Aldrich) dissolved in the antibody dilution buffer (1% *w*/*v* BSA, 0.3% *v*/*v* Triton X-100, PBS) at 25 °C for 90 min. Nuclear DNA was stained with 5 µM DAPI (Sigma-Aldrich) for 15 min, and then the slides were washed in PBS. The specimens were mounted in PBS/glycerol mixture (9:1) containing 2.5% 1,4-diazabicyclo[2.2.2]octane (DABCO). For each experimental series, 3 root apical fragments were used.

4.5. Immunocytochemical Detection of CDKA Kinase and Phosphorylated H3 Histones (Thr3 and Ser10)

Root meristems from *V. faba* cuttings were fixed in PBS-buffered 4% (*w*/*v*) paraformaldehyde for 45 min, washed with PBS, and placed in the citrate-buffered mixture containing 2.5% (*w*/*v*) pectinase, 2.5% (*w*/*v*) cellulase, and 2.5% (*w*/*v*) pectolyase (Sigma-Aldrich) (pH 5.0; 40 °C) for 45 min. After washing with PBS and distilled water, root meristems were squashed onto slides, air dried, and pre-treated with PBS-buffered 8% BSA and 4% Triton X-100 (Sigma-Aldrich) for 50 min (20 °C). Then, slides were incubated with rabbit polyclonal anti-CDC2 antibody (1:500; Agrisera, Vännäs, Sweden), recognizing the conserved plant CDKA homolog; rabbit polyclonal anti-H3S10Ph antibody (1:500; Sigma-Aldrich); and rabbit polyclonal anti-H3T3Ph antibody (1:500; Sigma-Aldrich). All antibodies were dissolved in PBS containing 1% BSA (*w*/*v*) and 0.3% Triton X-100 (*v*/*v*). Incubations were carried out overnight in a humid atmosphere at 4 °C. Following rinsing with PBS, slides were incubated with secondary goat anti-rabbit conjugated to Alexa Fluor® 488 antibody (1:500; Cell Signaling Technology, Danvers, MA, USA) dissolved in PBS at 20 °C for 90 min. Slides were counterstained with 5 µM DAPI (Sigma-Aldrich) at 20 °C for 15 min., washed with PBS, and embedded in PBS/glycerol mixture (9:1) containing 2.5% 1,4-diazabicyclo[2.2.2]octane (DABCO). For immunocytochemical analyses, five seedlings per treatment were used for CDKA and H3S10Ph detection, and three seedlings per treatment for H3T3Ph detection. Within each root meristem, fluorescence intensity was measured in multiple nuclei: 20 nuclei per root for CDKA (100 nuclei per treatment), 10 nuclei per root for H3S10Ph (50 nuclei per treatment), and 10 nuclei per root for H3T3Ph (30 nuclei per treatment).

4.6. Western Blotting of Kinase CDKA and CycB

Proteins were extracted from apical parts of primary roots of *V. faba* with the use of Pierce™ Plant Total Protein Extraction Kit (Thermo Fisher Scientific, Waltham, MA, USA) supplemented with Protease Inhibitor Cocktail (Sigma-Aldrich). Protein concentration was spectrophotometrically measured using Pierce BCA Protein Assay Kit (Thermo Fisher Scientific). The extracts were fractionated on NuPAGE® Novex® 4–12% Bis-Tris gel (Thermo Fisher Scientific) and then blotted onto polyvinylidene fluoride (PVDF) membrane,

0.2-µm pore size (Thermo Fisher Scientific). Membrane blocking, antibody incubation, and chromogenic detection were performed using the WesternBreeze Chromogenic Kit, anti-rabbit (Thermo Fisher Scientific), according to the manufacturer's protocol. CDKA protein kinase was detected using polyclonal Anti-CDC2 antibodies (Agrisera, Vännäs, Sweden) diluted 1:3000, recognizing the conserved plant CDKA homolog. CycB was detected using polyclonal Anti-CycB antibodies (Agrisera) diluted 1:2500. Actin was detected using monoclonal actin antibodies (Sigma-Aldrich) diluted 1:4000. Membrane blocking, antibody incubation, and chromogenic detection were performed using WesternBreeze Chromogenic Kit, anti-rabbit (Thermo Fisher Scientific) according to the manufacturer's protocol. The chromogenic signal was developed for 60 min for CDKA and CycB and 30 min for Actin. PVDF membranes were imaged with the ProXima 2750 imaging system (Isogen Life Sciences, De Meern, The Netherlands). Quantitative microdensitometric evaluation of the membranes was carried out using GelAnalyzer version 23.1.1 (www.gelanalyzer.com, accessed on 1 March 2025; Istvan Lazar Jr., PhD, and Istvan Lazar Sr., PhD). Following image import, the software automatically identified lane baselines and protein bands. Band intensities were determined from lane profiles by integrating the selected peaks and correcting the values by subtracting the corresponding baseline.

For Western blot analyses, each biological replicate corresponded to an independent incubation experiment, from which apical regions of 5 primary roots were pooled to obtain sufficient protein for extraction. The blots presented in the figures are representative of 3 replicate experiments showing consistent patterns. Densitometric quantification was performed for each biological replicate (n = 3) using GelAnalyzer 23.1.1 (available at www.gelanalyzer.com (accessed on 1 March 2025) by Istvan Lazar Jr., PhD, and Istvan Lazar Sr., PhD, and the obtained values were used for statistical comparisons between treatments.

4.7. Gene Expression Analysis

To assess gene expression, five excised roots were snap-frozen in liquid nitrogen and ground into a fine powder using a mortar and pestle. A total of 200 mg of this powder was used for RNA extraction with the NucleoSpin RNA Plant and Fungi Mini Kit (Macherey-Nagel, Düren, Germany), following the manufacturer's instructions. RNA concentration and purity were measured using a BioDrop Duo spectrophotometer (BioDrop Ltd., Cambridge, UK), and all samples showed A260/A280 ratios below 2.0. The integrity of RNA was confirmed by running 1 µg of each sample on a 1% agarose gel prepared in 1X Tris-acetate-EDTA (TAE) buffer containing 1 mg·mL^{-1} ethidium bromide at 110 V for 1.5 h at room temperature. Distinct ribosomal RNA bands were observed, and no evidence of degradation was detected.

Prior to cDNA synthesis, genomic DNA was removed using RQ1 RNase-Free DNase (Promega, Madison, WI, USA) using 3 µg RNA for each sample. Reverse transcription was carried out using 2 µg of RNA with Oligo(dT)18 primers and SuperScript™ III Reverse Transcriptase (Thermo Fisher Scientific), according to the manufacturer's protocol. The obtained cDNA was diluted 100X with nuclease-free water and stored at −20 °C until further use.

Quantitative real-time PCR (qPCR) was performed with PowerTrack™ SYBR Green Master Mix (Thermo Fisher Scientific) using 1 ng of cDNA per 10 µL reaction in four technical replicates. Primer concentrations were adjusted to 300 nM, and the annealing/extension temperature was set to 61 °C on a RotorGene Q 5-plex HRM instrument (QIAGEN, Hilden, Germany). Melting curve analysis was conducted to confirm amplification specificity. Relative expression levels were calculated using the $2^{-\Delta\Delta Ct}$ method [153] and normalized to the reference gene cyclophilin (CYP2) [154]. Data are presented as $\log_2$(fold change),

corresponding to −ΔΔCt values. Primers targeting coding sequences (CDS) were designed using Primer3 (available online: https://primer3.ut.ee/, accessed on 1 March 2025) [155] and validated in silico against *V. faba* cv. 'Hedin/2' v1 CDS using BLAST (Galaxy platform, IPK Gatersleben, Germany; https://galaxy-web.ipk-gatersleben.de, accessed on 1 March 2025). The primer sequences were as follows:

4.7.1. *CycB*

Forward:5′-GGCTGCTGGTAGAAGTGTGT-3′
Reverse:5′-TGGCATTTATATCGGGCTGTGA-3′
Amplicon size: 176 bp

4.7.2. *CYP2* (Reference Gene)

Forward: 5′-TGCCGATGTCACTCCCAGAA-3′
Reverse: 5′-CAGCGAACTTGGAACCGTAGA-3′

For gene expression analyses, each biological replicate corresponded to an independent incubation experiment, from which five excised primary roots were pooled to obtain sufficient material for RNA extraction. Reverse transcription and qPCR analyses were performed independently for each biological replicate (n = 3). Each qPCR reaction was conducted in four technical replicates, and the mean Ct value obtained for a given biological replicate was used for further calculations of relative expression. Statistical comparisons between treatments were performed using the values obtained for the biological replicates.

4.8. Microscopic Measurements, Observations and Analyses

Observations were performed with a Nikon Eclipse E600W fluorescence microscope (Nikon, Tokyo, Japan) featuring phase-contrast optics, a U2 filter (UVB light; λ = 340–380 nm) for DAPI and a B2 filter (blue light; λ = 465–496 nm) for Alexa Fluor® 488. All images in each experimental series of a given experiment, using the specific antibodies, were captured at identical integration times with a DS-Fi1 CCD camera (Nikon, Tokyo, Japan). Under these conditions, negative control samples—incubated only with the secondary antibody conjugated to Alexa Fluor® 488, without the primary antibody—did not produce a detectable signal, appearing completely dark in the images. Quantitative analyses and fluorescence intensity (FI) measurements were performed in ImageJ software ver. 1.54p after conversion of the color images to grayscale and were expressed in arbitrary units [a.u.] as the mean pixel value (p.v.) covering the range from 0 (dark) to 255 (white) according to the methods described [156,157]. Standard background subtraction was applied by subtracting the average signal from areas lacking specific fluorescence. In microscopy-based analyses, independent biological replicates consisted of individual seedlings (primary roots) obtained from separate germination batches and independent incubations performed on different days. Depending on the analysis, three to five independent roots were analyzed per treatment. Within each biological replicate, fluorescence intensity was measured in multiple nuclei within the root meristem. Statistical analyses were performed using independent biological replicates (individual roots), while measurements from multiple nuclei within each root were treated as technical observations.

4.9. Statistical Analysis

Data were analyzed using GraphPad Prism version 10 software (GraphPad Software, Boston, MA, USA). Before selecting the appropriate statistical test, data normality was assessed using the Shapiro–Wilk test. For datasets meeting the assumptions of normality, one-way analysis of variance (ANOVA) was performed, followed by Tukey's post hoc test to evaluate differences between groups. For datasets not meeting normality assumptions, the non-parametric Kruskal–Wallis test with appropriate post hoc analysis was applied. In

data presentation, variables with a normal distribution are reported as mean ± standard deviation (SD), whereas variables not meeting normality assumptions are presented as median with confidence interval (CI). In all analyses, the significance level was set at $p < 0.05$. Statistical significance in figures is indicated with asterisks (**** $p < 0.0001$, *** $p < 0.001$, ** $p < 0.01$, * $p < 0.05$).

5. Conclusions

In light of the obtained results, TO demonstrates a clear protective potential toward meristematic cells of primary roots of *V. faba* subjected to the toxic effects of cadmium ($CdCl_2$) at a concentration of 175 µM during a 24 h incubation. TO, widely described in the literature as a compound with antioxidant properties, when applied at a concentration of 0.03% (*v*/*v*), reversed (to control or near-control levels) disturbances that can be associated with elevated ROS levels typically accompanying cadmium stress.

In the presence of TO, despite the continued presence of cadmium, the control level of the constitutively transcribed CDKA protein was maintained, and high levels of periodically cell-cycle-regulated CycB transcripts and protein were restored; both had been reduced in cells treated with cadmium alone. The maintenance of active CDKA–CycB complexes likely supported proper phosphorylation of microtubule-associated proteins (MAPs), which in turn may have limited excessive microtubule bundling and stabilization, allowing proper spindle organization during karyokinesis and cytokinesis. At the same time, the proper organization of actin filaments was re-established. Moreover, the restoration of the correct mitotic phosphorylation pattern of histone H3 (T3Ph and S10Ph) points to a preserved balance between the activities of the kinases (Haspin and Aurora B) and phosphatases (PP1/PP2A) responsible for these modifications. Such a state favored the reversal of excessive mitotic chromosome condensation, proper recruitment of the chromosomal passenger complex (CPC) in association with Aurora B kinase, and correct spindle microtubule attachment, successful metaphase-to-anaphase transition and accurate sister chromatid segregation, thereby re-establishing proportions of cells at individual mitotic stages similar to those observed in the control. As a result, the tenfold cadmium-induced decrease in the mitotic index was partially reversed, reaching approximately 50% of the control value. These changes were accompanied by primary root growth comparable to that of the control.

An interpretation referring to the antioxidant action of TO is consistent with earlier observations obtained in the same model, where TO alleviated symptoms of oxidative stress in interphase cells, reduced replication stress and the level of DNA damage, stabilized epigenetic modifications and interphase chromatin organization, and supported the maintenance of transcriptional activity while preventing interphase arrest. These effects could have additionally contributed to maintaining, as observed in the present study, a pool of cells capable of entering mitosis.

To the best of our knowledge, this study provides the first evidence that TO may exert a protective effect on the mitotic apparatus of plant meristematic cells exposed to cadmium stress. The obtained data indicate that TO may act as a natural factor supporting plant tolerance to heavy metal stress and could serve as a potential component of strategies aimed at protecting plant cells from the toxic effects of cadmium.

It should be noted, however, that the study was conducted using a single model species and a single exposure duration, which naturally limits the generalizability of the findings. At the same time, this approach allowed for a detailed, multi-level analysis of meristematic cell responses to cadmium stress and an evaluation of the protective effects of TO under controlled conditions. In future studies, it would be advisable to include varied exposure times and concentrations, as well as to extend the analyses to other plant species, which

would help better define the dynamics of cellular responses and the universality of the observed mechanisms. Additionally, complementing cytological methods with biochemical analyses, assessing the activity of antioxidant systems, glutathione metabolism, and phytochelatin synthesis, would enable a more comprehensive confirmation of the mechanisms proposed based on the observed cellular effects. In this context, the present work not only documents the protective effect of TO on meristematic cells exposed to cadmium stress but also provides a basis for more in-depth mechanistic studies on the use of biologically active natural compounds to modulate plant responses to environmental stress. From a broader perspective, natural products such as TO, characterized by relatively low toxicity and biodegradability, are increasingly explored as complements to synthetic agrochemicals. Essential oil-based formulations have been proposed for agricultural applications in forms such as foliar sprays, soil amendments, or controlled-release systems [158,159]. However, it should be emphasized that the present study was conducted under controlled laboratory conditions using root meristem cells, and verification of such applications will require further soil-based and field-scale investigations.

Supplementary Materials: The following supporting information can be downloaded at: https://www.mdpi.com/article/10.3390/ijms27062798/s1.

Author Contributions: Conceptualization, N.G.-S. and J.T.P.; methodology, N.G.-S., M.W. and J.T.P.; validation, N.G.-S. and J.T.P.; formal analysis, N.G.-S.; investigation, N.G.-S. and M.W. resources, N.G.-S. and A.Ż.; data curation, N.G.-S.; writing—original draft preparation, N.G.-S.; writing—review and editing, A.Ż. and J.T.P.; visualization, N.G.-S., supervision, J.T.P.; project administration, N.G.-S. funding acquisition, N.G.-S. All authors have read and agreed to the published version of the manuscript.

Funding: This work was supported through the budget of the Doctoral School of Exact and Natural Sciences of the University of Lodz.

Institutional Review Board Statement: Not applicable.

Informed Consent Statement: Not applicable.

Data Availability Statement: The original contributions presented in this study are included in the article/Supplementary Material. Further inquiries can be directed to the corresponding author.

Conflicts of Interest: The authors declare no conflicts of interest.

Abbreviations

The following abbreviations are used in this manuscript:

APC/C	Anaphase-promoting complex/cyclosome
CAK	CDK-activating kinase
Cd	Cadmium
Cdc2	Cell division control 2
CDC25	Cell division cycle 25 phosphatase
CDKs	Cyclin-dependent kinases
CKIs	Cyclin-dependent kinase inhibitors
CMTs	Cortical microtubules
CPC	Chromosomal passenger complex
Cyc	Cyclin
MPF	M-phase-promoting factor
PP1-2A, B, C	Protein Phosphatase 1-2A, B, C
PPB	Preprophase band
ROS	Reactive oxygen species
SAC	Spindle assembly checkpoint
TO	Thyme oil
γ-TuRC	γ-tubulin ring complex

References

1. Hu, Y.; He, R.; Mu, X.; Zhou, Y.; Li, X.; Wang, H.; Xing, W.; Liu, D. Cadmium Toxicity in Plants: From Transport to Tolerance Mechanisms. *Plant Signal. Behav.* **2025**, *20*, 2544316. [CrossRef]
2. Yang, Y.; Hassan, M.F.; Ali, W.; Zou, H.; Liu, Z.; Ma, Y. Effects of Cadmium Pollution on Human Health: A Narrative Review. *Atmosphere* **2025**, *16*, 225. [CrossRef]
3. Seth, C.S.; Misra, V.; Chauhan, L.K.S.; Singh, R.R. Genotoxicity of Cadmium on Root Meristem Cells of Allium Cepa: Cytogenetic and Comet Assay Approach. *Ecotoxicol. Environ. Saf.* **2008**, *71*, 711–716. [CrossRef]
4. Nagajyoti, P.C.; Lee, K.D.; Sreekanth, T.V.M. Heavy Metals, Occurrence and Toxicity for Plants: A Review. *Environ. Chem. Lett.* **2010**, *8*, 199–216. [CrossRef]
5. Younis, U.; Malik, S.A.; Rizwan, M.; Qayyum, M.F.; Ok, Y.S.; Shah, M.H.R.; Rehman, R.A.; Ahmad, N. Biochar Enhances the Cadmium Tolerance in Spinach (*Spinacia oleracea*) through Modification of Cd Uptake and Physiological and Biochemical Attributes. *Environ. Sci. Pollut. Res.* **2016**, *23*, 21385–21394. [CrossRef] [PubMed]
6. Moulis, J.-M. Cellular Mechanisms of Cadmium Toxicity Related to the Homeostasis of Essential Metals. *BioMetals* **2010**, *23*, 877–896. [CrossRef]
7. Rai, G.K.; Bhat, B.A.; Mushtaq, M.; Tariq, L.; Rai, P.K.; Basu, U.; Dar, A.A.; Islam, S.T.; Dar, T.U.H.; Bhat, J.A. Insights into Decontamination of Soils by Phytoremediation: A Detailed Account on Heavy Metal Toxicity and Mitigation Strategies. *Physiol. Plant.* **2021**, *173*, 287–304. [CrossRef]
8. Cui, W.; Wang, H.; Song, J.; Cao, X.; Rogers, H.J.; Francis, D.; Jia, C.; Sun, L.; Hou, M.; Yang, Y.; et al. Cell Cycle Arrest Mediated by Cd-Induced DNA Damage in Arabidopsis Root Tips. *Ecotoxicol. Environ. Saf.* **2017**, *145*, 569–574. [CrossRef] [PubMed]
9. Bertels, J.; Huybrechts, M.; Hendrix, S.; Bervoets, L.; Cuypers, A.; Beemster, G.T.S. Cadmium Inhibits Cell Cycle Progression and Specifically Accumulates in the Maize Leaf Meristem. *J. Exp. Bot.* **2020**, *71*, 6418–6428. [CrossRef] [PubMed]
10. Polit, J.T.; Maszewski, J.; Kaźmierczak, A. Effect of BAP and IAA on the Expression of G1 and G2 Control Points and G1-S and G2-M Transitions in Root Meristem Cells of *Vicia faba*. *Cell Biol. Int.* **2003**, *27*, 559–566. [CrossRef]
11. West, G.; Inzé, D.; Beemster, G.T.S. Cell Cycle Modulation in the Response of the Primary Root of Arabidopsis to Salt Stress. *Plant Physiol.* **2004**, *135*, 1050–1058. [CrossRef]
12. Polit, J.T. Protein Phosphorylation in Vicia Faba Root Meristem Cells during the First Steps of Leaving Principal Control Points after Sucrose Application. *Plant Cell Rep.* **2009**, *28*, 165–173. [CrossRef]
13. De Veylder, L.; Larkin, J.C.; Schnittger, A. Molecular Control and Function of Endoreplication in Development and Physiology. *Trends Plant Sci.* **2011**, *16*, 624–634. [CrossRef]
14. Wang, K.; Ndathe, R.W.; Kumar, N.; Zeringue, E.A.; Kato, N.; Larkin, J.C. The CDK Inhibitor SIAMESE Targets Both CDKA;1 and CDKB1 Complexes to Establish Endoreplication in Trichomes. *Plant Physiol.* **2020**, *184*, 165–175. [CrossRef] [PubMed]
15. Dubois, M.; Selden, K.; Bediée, A.; Rolland, G.; Baumberger, N.; Noir, S.; Bach, L.; Lamy, G.; Granier, C.; Genschik, P. SIAMESE-RELATED1 Is Regulated Posttranslationally and Participates in Repression of Leaf Growth under Moderate Drought. *Plant Physiol.* **2018**, *176*, 2834–2850. [CrossRef]
16. Braat, J.; Havaux, M. The SIAMESE Family of Cell-Cycle Inhibitors in the Response of Plants to Environmental Stresses. *Front. Plant Sci.* **2024**, *15*, 1362460. [CrossRef]
17. Kumar, N.; Larkin, J.C. Why Do Plants Need so Many Cyclin-Dependent Kinase Inhibitors? *Plant Signal. Behav.* **2017**, *12*, e1282021. [CrossRef]
18. Xing, X.; Tian, Z.; Yang, S.; Wang, X.; Xing, Z.; Wu, D.; Zheng, S.; Guo, Y. BvHP4b Gene in Red Beet Promotes Tuber Enlargement and Enhances Resistance to Pst DC3000. *BMC Genom.* **2025**, *26*, 731. [CrossRef]
19. Takatsuka, H.; Ohno, R.; Umeda, M. The Arabidopsis Cyclin-Dependent Kinase-Activating Kinase CDKF;1 Is a Major Regulator of Cell Proliferation and Cell Expansion but Is Dispensable for CDKA Activation. *Plant J.* **2009**, *59*, 475–487. [CrossRef] [PubMed]
20. Dissmeyer, N.; Weimer, A.K.; De Veylder, L.; Novak, B.; Schnittger, A. The Regulatory Network of Cell-Cycle Progression Is Fundamentally Different in Plants versus Yeast or Metazoans. *Plant Signal. Behav.* **2010**, *5*, 1613–1618. [CrossRef]
21. Spadafora, N.D.; Doonan, J.H.; Herbert, R.J.; Bitonti, M.B.; Wallace, E.; Rogers, H.J.; Francis, D. Arabidopsis T-DNA Insertional Lines for CDC25 Are Hypersensitive to Hydroxyurea but Not to Zeocin or Salt Stress. *Ann. Bot.* **2011**, *107*, 1183–1192. [CrossRef] [PubMed]
22. Inzé, D.; De Veylder, L. Cell Cycle Regulation in Plant Development. *Annu. Rev. Genet.* **2006**, *40*, 77–105. [CrossRef] [PubMed]
23. Qi, F.; Zhang, F. Cell Cycle Regulation in the Plant Response to Stress. *Front. Plant Sci.* **2020**, *10*, 1765. [CrossRef]
24. Li, S.; Sun, T.; Ren, H. The Functions of the Cytoskeleton and Associated Proteins during Mitosis and Cytokinesis in Plant Cells. *Front. Plant Sci.* **2015**, *6*, 282. [CrossRef]
25. Amoah-Darko, F.L., Jr.; White, D. Modeling Microtubule Dynamic Instability: Microtubule Growth, Shortening and Pause. *J. Theor. Biol.* **2022**, *553*, 111257. [CrossRef]
26. Rose, A.; Patel, S.; Meier, I. The Plant Nuclear Envelope. *Planta* **2004**, *218*, 327–336. [CrossRef]

27. Kirschner, G.K. Cell Division Visualized: Barley Reporter Lines for Chromosome and Microtubule Dynamics. *Plant J.* **2023**, *115*, 600–601. [CrossRef] [PubMed]
28. Zhang, H.; Dawe, R.K. Mechanisms of Plant Spindle Formation. *Chromosome Res.* **2011**, *19*, 335–344. [CrossRef]
29. Laband, K.; Le Borgne, R.; Edwards, F.; Stefanutti, M.; Canman, J.C.; Verbavatz, J.-M.; Dumont, J. Chromosome Segregation Occurs by Microtubule Pushing in Oocytes. *Nat. Commun.* **2017**, *8*, 1499. [CrossRef]
30. Cairo, G.; Lacefield, S. Establishing Correct Kinetochore-Microtubule Attachments in Mitosis and Meiosis. *Essays Biochem.* **2020**, *64*, 277–287. [CrossRef] [PubMed]
31. Navarro, A.P.; Cheeseman, I.M. Kinetochore Assembly throughout the Cell Cycle. *Semin. Cell Dev. Biol.* **2021**, *117*, 62–74. [CrossRef]
32. Motta, M.R.; Schnittger, A. A Microtubule Perspective on Plant Cell Division. *Curr. Biol.* **2021**, *31*, R547–R552. [CrossRef]
33. Seltzer, V.; Janski, N.; Canaday, J.; Herzog, E.; Erhardt, M.; Evrard, J.-L.; Schmit, A.-C. Arabidopsis GCP2 and GCP3 Are Part of a Soluble γ-Tubulin Complex and Have Nuclear Envelope Targeting Domains. *Plant J.* **2007**, *52*, 322–331. [CrossRef]
34. Oakley, B.R.; Paolillo, V.; Zheng, Y. γ-Tubulin Complexes in Microtubule Nucleation and Beyond. *Mol. Biol. Cell* **2015**, *26*, 2957–2962. [CrossRef] [PubMed]
35. Gabel, C.A.; Li, Z.; DeMarco, A.G.; Zhang, Z.; Yang, J.; Hall, M.C.; Barford, D.; Chang, L. Molecular Architecture of the Augmin Complex. *Nat. Commun.* **2022**, *13*, 5449. [CrossRef] [PubMed]
36. Liu, B.; Lee, Y.-R.J. Spindle Assembly and Mitosis in Plants. *Annu. Rev. Plant Biol.* **2022**, *73*, 227–254. [CrossRef] [PubMed]
37. Masoud, K.; Herzog, E.; Chabouté, M.-E.; Schmit, A.-C. Microtubule Nucleation and Establishment of the Mitotic Spindle in Vascular Plant Cells. *Plant J.* **2013**, *75*, 245–257. [CrossRef]
38. Moschou, P.N.; Gutierrez-Beltran, E.; Bozhkov, P.V.; Smertenko, A. Separase Promotes Microtubule Polymerization by Activating CENP-E-Related Kinesin Kin7. *Dev. Cell* **2016**, *37*, 350–361. [CrossRef]
39. Murata, T.; Sano, T.; Sasabe, M.; Nonaka, S.; Higashiyama, T.; Hasezawa, S.; Machida, Y.; Hasebe, M. Mechanism of Microtubule Array Expansion in the Cytokinetic Phragmoplast. *Nat. Commun.* **2013**, *4*, 1967. [CrossRef]
40. Ho, C.-M.K.; Lee, Y.-R.J.; Kiyama, L.D.; Dinesh-Kumar, S.P.; Liu, B. *Arabidopsis* Microtubule-Associated Protein MAP65-3 Cross-Links Antiparallel Microtubules toward Their plus Ends in the Phragmoplast via Its Distinct C-Terminal Microtubule Binding Domain. *Plant Cell* **2012**, *24*, 2071–2085. [CrossRef]
41. Maeda, K.; Sasabe, M.; Hanamata, S.; Machida, Y.; Hasezawa, S.; Higaki, T. Actin Filament Disruption Alters Phragmoplast Microtubule Dynamics during the Initial Phase of Plant Cytokinesis. *Plant Cell Physiol.* **2020**, *61*, 445–456. [CrossRef]
42. Petrášek, J.; Schwarzerová, K. Actin and Microtubule Cytoskeleton Interactions. *Curr. Opin. Plant Biol.* **2009**, *12*, 728–734. [CrossRef]
43. Wilkins, B.J.; Rall, N.A.; Ostwal, Y.; Kruitwagen, T.; Hiragami-Hamada, K.; Winkler, M.; Barral, Y.; Fischle, W.; Neumann, H. A Cascade of Histone Modifications Induces Chromatin Condensation in Mitosis. *Science* **2014**, *343*, 77–80. [CrossRef]
44. Wong, C.Y.Y.; Lee, B.C.H.; Yuen, K.W.Y. Epigenetic Regulation of Centromere Function. *Cell. Mol. Life Sci.* **2020**, *77*, 2899–2917. [CrossRef]
45. Eot-Houllier, G.; Fulcrand, G.; Watanabe, Y.; Magnaghi-Jaulin, L.; Jaulin, C. Histone Deacetylase 3 Is Required for Centromeric H3K4 Deacetylation and Sister Chromatid Cohesion. *Genes Dev.* **2008**, *22*, 2639–2644. [CrossRef]
46. Kim, J.-S.; Lim, J.Y.; Shin, H.; Kim, B.-G.; Yoo, S.-D.; Kim, W.T.; Huh, J.H. ROS1-Dependent DNA Demethylation Is Required for ABA-Inducible *NIC3* Expression. *Plant Physiol.* **2019**, *179*, 1810–1821. [CrossRef]
47. Li, Y.; Butenko, Y.; Grafi, G. Histone Deacetylation Is Required for Progression through Mitosis in Tobacco Cells. *Plant J.* **2005**, *41*, 346–352. [CrossRef]
48. Caperta, A.D.; Rosa, M.; Delgado, M.; Karimi, R.; Demidov, D.; Viegas, W.; Houben, A. Distribution Patterns of Phosphorylated Thr 3 and Thr 32 of Histone H3 in Plant Mitosis and Meiosis. *Cytogenet. Genome Res.* **2008**, *122*, 73–79. [CrossRef] [PubMed]
49. Haase, J.; Bonner, M.K.; Halas, H.; Kelly, A.E. Distinct Roles of the Chromosomal Passenger Complex in the Detection of and Response to Errors in Kinetochore-Microtubule Attachment. *Dev. Cell* **2017**, *42*, 640–654.e5. [CrossRef] [PubMed]
50. Tsunematsu, T.; Mouri, Y.; Shao, W.; Arakaki, R.; Ruppert, J.G.; Murano, K.; Ishimaru, N.; Guardavaccaro, D.; Pagano, M.; Kudo, Y. Sustained Chromosomal Passenger Complex Activity Preserves the Pluripotency of Human Embryonic Carcinoma Cells. *Sci. Signal.* **2025**, *18*, eadg4626. [CrossRef] [PubMed]
51. Kawabe, A.; Matsunaga, S.; Nakagawa, K.; Kurihara, D.; Yoneda, A.; Hasezawa, S.; Uchiyama, S.; Fukui, K. Characterization of Plant Aurora Kinases during Mitosis. *Plant Mol. Biol.* **2005**, *58*, 1–13. [CrossRef]
52. Zhang, X.; Li, X.; Marshall, J.B.; Zhong, C.X.; Dawe, R.K. Phosphoserines on Maize CENTROMERIC HISTONE H3 and Histone H3 Demarcate the Centromere and Pericentromere during Chromosome Segregation. *Plant Cell* **2005**, *17*, 572–583. [CrossRef] [PubMed]
53. Moura, M.; Conde, C. Phosphatases in Mitosis: Roles and Regulation. *Biomolecules* **2019**, *9*, 55. [CrossRef] [PubMed]
54. Dagdag, O.; Quadri, T.W.; Haldhar, R.; Kim, S.-C.; Daoudi, W.; Berdimurodov, E.; Akpan, E.D.; Ebenso, E.E. An Overview of Heavy Metal Pollution and Control. In *Heavy Metals in the Environment: Management Strategies for Global Pollution*; Verma, D.K.,

Verma, C., Mahish, P.K., Eds.; ACS Symposium Series; American Chemical Society: Washington, DC, USA, 2023; Volume 1456, pp. 3–24.
55. Pandur, E.; Micalizzi, G.; Mondello, L.; Horváth, A.; Sipos, K.; Horváth, G. Antioxidant and Anti-Inflammatory Effects of Thyme (*Thymus vulgaris* L.) Essential Oils Prepared at Different Plant Phenophases on Pseudomonas Aeruginosa LPS-Activated THP-1 Macrophages. *Antioxidants* **2022**, *11*, 1330. [CrossRef]
56. Sellamuthu, P.S.; Sivakumar, D.; Soundy, P.; Korsten, L. Essential Oil Vapours Suppress the Development of Anthracnose and Enhance Defence Related and Antioxidant Enzyme Activities in Avocado Fruit. *Postharvest Biol. Technol.* **2013**, *81*, 66–72. [CrossRef]
57. Saltos-Rezabala, L.A.; Silveira, P.R.D.; Tavares, D.G.; Moreira, S.I.; Magalhães, T.A.; Botelho, D.M.D.S.; Alves, E. Thyme Essential Oil Reduces Disease Severity and Induces Resistance against Alternaria Linariae in Tomato Plants. *Horticulturae* **2022**, *8*, 919. [CrossRef]
58. Ansari, M.N.; Rehman, N.U.; Karim, A.; Imam, F.; Hamad, A.M. Protective Effect of Thymus Serrulatus Essential Oil on Cadmium-Induced Nephrotoxicity in Rats, through Suppression of Oxidative Stress and Downregulation of NF-κB, iNOS, and Smad2 mRNA Expression. *Molecules* **2021**, *26*, 1252. [CrossRef]
59. Gocek-Szczurtek, N.; Żabka, A.; Wróblewski, M.; Kukula-Koch, W.; Szczeblewski, P.; Polit, J.T. Thyme Oil Mitigates Cadmium-Induced Oxidative and Genotoxic Stress in Vicia Faba Root Meristem Cells under in Vitro Conditions. *Sci. Rep.* **2025**, *15*, 38689. [CrossRef]
60. Gocek-Szczurtek, N.; Żabka, A.; Wróblewski, M.; Polit, J.T. Stabilization of the MAPK–Epigenetic Signaling Axis Underlies the Protective Effect of Thyme Oil against Cadmium Stress in Root Meristem Cells of *Vicia faba*. *Int. J. Mol. Sci.* **2025**, *27*, 208. [CrossRef]
61. Fusconi, A.; Gallo, C.; Camusso, W. Effects of Cadmium on Root Apical Meristems of *Pisum sativum* L.: Cell Viability, Cell Proliferation and Microtubule Pattern as Suitable Markers for Assessment of Stress Pollution. *Mutat. Res. Toxicol. Environ. Mutagen.* **2007**, *632*, 9–19. [CrossRef]
62. Zhang, S.; Zhang, H.; Qin, R.; Jiang, W.; Liu, D. Cadmium Induction of Lipid Peroxidation and Effects on Root Tip Cells and Antioxidant Enzyme Activities in *Vicia faba* L. *Ecotoxicology* **2009**, *18*, 814–823. [CrossRef] [PubMed]
63. Xu, P.; Liu, D.; Jiang, W. Cadmium Effects on the Organization of Microtubular Cytoskeleton in Interphase and Mitotic Cells of Allium Sativum. *Biol. Plant.* **2009**, *53*, 387–390. [CrossRef]
64. Huybrechts, M.; Cuypers, A.; Deckers, J.; Iven, V.; Vandionant, S.; Jozefczak, M.; Hendrix, S. Cadmium and Plant Development: An Agony from Seed to Seed. *Int. J. Mol. Sci.* **2019**, *20*, 3971. [CrossRef] [PubMed]
65. Sorrell, D.A.; Menges, M.; Healy, J.M.S.; Deveaux, Y.; Amano, C.; Su, Y.; Nakagami, H.; Shinmyo, A.; Doonan, J.H.; Sekine, M.; et al. Cell Cycle Regulation of Cyclin-Dependent Kinases in Tobacco Cultivar Bright Yellow-2 Cells. *Plant Physiol.* **2001**, *126*, 1214–1223. [CrossRef]
66. Fourest-Lieuvin, A.; Peris, L.; Gache, V.; Garcia-Saez, I.; Juillan-Binard, C.; Lantez, V.; Job, D. Microtubule Regulation in Mitosis: Tubulin Phosphorylation by the Cyclin-Dependent Kinase Cdk1. *Mol. Biol. Cell* **2006**, *17*, 1041–1050. [CrossRef]
67. Andonegui-Elguera, M.A.; Cáceres-Gutiérrez, R.E.; López-Saavedra, A.; Cisneros-Soberanis, F.; Justo-Garrido, M.; Díaz-Chávez, J.; Herrera, L.A. The Roles of Histone Post-Translational Modifications in the Formation and Function of a Mitotic Chromosome. *Int. J. Mol. Sci.* **2022**, *23*, 8704. [CrossRef] [PubMed]
68. Pellarin, I.; Dall'Acqua, A.; Favero, A.; Segatto, I.; Rossi, V.; Crestan, N.; Karimbayli, J.; Belletti, B.; Baldassarre, G. Cyclin-Dependent Protein Kinases and Cell Cycle Regulation in Biology and Disease. *Signal Transduct. Target. Ther.* **2025**, *10*, 11. [CrossRef]
69. Yang, P.-M.; Chiu, S.-J.; Lin, K.-A.; Lin, L.-Y. Effect of Cadmium on Cell Cycle Progression in Chinese Hamster Ovary Cells. *Chem. Biol. Interact.* **2004**, *149*, 125–136. [CrossRef]
70. Badawi, K.; El Sharazly, B.M.; Negm, O.; Khan, R.; Carter, W.G. Is Cadmium Genotoxicity Due to the Induction of Redox Stress and Inflammation? A Systematic Review. *Antioxidants* **2024**, *13*, 932. [CrossRef]
71. Amiri, H. Essential Oils Composition and Antioxidant Properties of Three *Thymus* Species. *Evid.-Based Complement. Altern. Med.* **2012**, *2012*, 728065. [CrossRef]
72. Feng, Y.; Li, H.; Zhang, X.; Li, X.; Zhang, J.; Shi, L.; Chen, X.; Nong, W.; Wang, C.; Shabala, S.; et al. Effects of Cadmium Stress on Root and Root Border Cells of Some Vegetable Species with Different Types of Root Meristem. *Life* **2022**, *12*, 1401. [CrossRef]
73. Pizzaia, D.; Nogueira, M.L.; Mondin, M.; Carvalho, M.E.A.; Piotto, F.A.; Rosario, M.F.; Azevedo, R.A. Cadmium Toxicity and Its Relationship with Disturbances in the Cytoskeleton, Cell Cycle and Chromosome Stability. *Ecotoxicology* **2019**, *28*, 1046–1055. [CrossRef]
74. Żabka, A.; Gocek, N.; Krajewski, K.; Szczeblewski, P.; Laskowski, T.; Polit, J. Changes in Epigenetic Patterns Related to DNA Replication in Vicia Faba Root Meristem Cells under Cadmium-Induced Stress Conditions. *Cells* **2021**, *10*, 3409. [CrossRef] [PubMed]

75. Hernández-Cruz, E.Y.; Arancibia-Hernández, Y.L.; Loyola-Mondragón, D.Y.; Pedraza-Chaverri, J. Oxidative Stress and Its Role in Cd-Induced Epigenetic Modifications: Use of Antioxidants as a Possible Preventive Strategy. *Oxygen* **2022**, *2*, 177–210. [CrossRef]
76. Vandionant, S.; Hendrix, S.; Alfano, R.; Plusquin, M.; Cuypers, A. Comparing Cadmium-Induced Effects on the Regulation of the DNA Damage Response and Cell Cycle Progression between Entire Rosettes and Individual Leaves of Arabidopsis Thaliana. *Plant Physiol. Biochem.* **2023**, *204*, 108105. [CrossRef] [PubMed]
77. Inagaki, S.; Umeda, M. Cell-Cycle Control and Plant Development. In *International Review of Cell and Molecular Biology*; Elsevier: Amsterdam, The Netherlands, 2011; Volume 291, pp. 227–261.
78. Hendrix, S.; Iven, V.; Eekhout, T.; Huybrechts, M.; Pecqueur, I.; Horemans, N.; Keunen, E.; De Veylder, L.; Vangronsveld, J.; Cuypers, A. Suppressor of Gamma Response 1 Modulates the DNA Damage Response and Oxidative Stress Response in Leaves of Cadmium-Exposed Arabidopsis Thaliana. *Front. Plant Sci.* **2020**, *11*, 366–378. [CrossRef]
79. Carneiro, A.K.; Montessoro, P.D.F.; Fusaro, A.F.; Araújo, B.G.; Hemerly, A.S. Plant CDKs—Driving the Cell Cycle through Climate Change. *Plants* **2021**, *10*, 1804. [CrossRef]
80. Considine, M.J.; Foyer, C.H. Stress Effects on the Reactive Oxygen Species-Dependent Regulation of Plant Growth and Development. *J. Exp. Bot.* **2021**, *72*, 5795–5806. [CrossRef]
81. Pedroza-Garcia, J.A.; Xiang, Y.; De Veylder, L. Cell Cycle Checkpoint Control in Response to DNA Damage by Environmental Stresses. *Plant J.* **2022**, *109*, 490–507. [CrossRef]
82. Davidova, S.; Milushev, V.; Satchanska, G. The Mechanisms of Cadmium Toxicity in Living Organisms. *Toxics* **2024**, *12*, 875. [CrossRef]
83. Sobkowiak, R.; Deckert, J. Cadmium-Induced Changes in Growth and Cell Cycle Gene Expression in Suspension-Culture Cells of Soybean. *Plant Physiol. Biochem.* **2003**, *41*, 767–772. [CrossRef]
84. Burssens, S.; Himanen, K.; Van De Cotte, B.; Beeckman, T.; Van Montagu, M.; Inzé, D.; Verbruggen, N. Expression of Cell Cycle Regulatory Genes and Morphological Alterations in Response to Salt Stress in Arabidopsis Thaliana. *Planta* **2000**, *211*, 632–640. [CrossRef]
85. Hasanuzzaman, M.; Raihan, M.R.H.; Masud, A.A.C.; Rahman, K.; Nowroz, F.; Rahman, M.; Nahar, K.; Fujita, M. Regulation of Reactive Oxygen Species and Antioxidant Defense in Plants under Salinity. *Int. J. Mol. Sci.* **2021**, *22*, 9326. [CrossRef] [PubMed]
86. Wang, B.; Li, Y.; Shao, C.; Tan, Y.; Cai, L. Cadmium and Its Epigenetic Effects. *Curr. Med. Chem.* **2012**, *19*, 2611–2620. [CrossRef]
87. Żabka, A.; Winnicki, K.; Polit, J.T.; Wróblewski, M.; Maszewski, J. Cadmium (II)-Induced Oxidative Stress Results in Replication Stress and Epigenetic Modifications in Root Meristem Cell Nuclei of *Vicia faba*. *Cells* **2021**, *10*, 640. [CrossRef] [PubMed]
88. Cao, X.; Wang, H.; Zhuang, D.; Zhu, H.; Du, Y.; Cheng, Z.; Cui, W.; Rogers, H.J.; Zhang, Q.; Jia, C.; et al. Roles of MSH2 and MSH6 in Cadmium-Induced G2/M Checkpoint Arrest in Arabidopsis Roots. *Chemosphere* **2018**, *201*, 586–594. [CrossRef]
89. Wan, L.; Zhang, H. Cadmium Toxicity: Effects on Cytoskeleton, Vesicular Trafficking and Cell Wall Construction. *Plant Signal. Behav.* **2012**, *7*, 345–348. [CrossRef] [PubMed]
90. Gzyl, J.; Chmielowska-Bąk, J.; Przymusiński, R.; Gwóźdź, E.A. Cadmium Affects Microtubule Organization and Post-Translational Modifications of Tubulin in Seedlings of Soybean (*Glycine max* L.). *Front. Plant Sci.* **2015**, *6*, 937. [CrossRef]
91. Yemets, A.; Horiunova, I.; Blume, Y. Cadmium, Nickel, Copper, and Zinc Influence on Microfilament Organization in *Arabidopsis* Root Cells. *Cell Biol. Int.* **2021**, *45*, 211–226. [CrossRef]
92. Přibyl, P.; Cepák, V.; Zachleder, V. Cytoskeletal Alterations in Interphase Cells of the Green Alga Spirogyra Decimina in Response to Heavy Metals Exposure: I. The Effect of Cadmium. *Protoplasma* **2005**, *226*, 231–240. [CrossRef]
93. Zou, J.; Wang, G.; Ji, J.; Wang, J.; Ouyang, J.; Li, B. Cadmium's Effect on the Organizationof Microtubular Cytoskeleton in Root Tips Cellsof Salix Matsudana Koidz. *Pol. J. Environ. Stud.* **2018**, *27*, 939–945. [CrossRef]
94. Li, L.; Yang, X.-J. Tubulin Acetylation: Responsible Enzymes, Biological Functions and Human Diseases. *Cell. Mol. Life Sci.* **2015**, *72*, 4237–4255. [CrossRef]
95. Ledda, F.D.; Ramoino, P.; Ravera, S.; Perino, E.; Bianchini, P.; Diaspro, A.; Gallus, L.; Pronzato, R.; Manconi, R. Tubulin Posttranslational Modifications Induced by Cadmium in the Sponge Clathrina Clathrus. *Aquat. Toxicol.* **2013**, *141*, 98–105. [CrossRef]
96. Mao, T.; Jin, L.; Li, H.; Liu, B.; Yuan, M. Two Microtubule-Associated Proteins of the Arabidopsis MAP65 Family Function Differently on Microtubules. *Plant Physiol.* **2005**, *138*, 654–662. [CrossRef]
97. Smertenko, A.P.; Chang, H.-Y.; Sonobe, S.; Fenyk, S.I.; Weingartner, M.; Bögre, L.; Hussey, P.J. Control of the AtMAP65-1 Interaction with Microtubules through the Cell Cycle. *J. Cell Sci.* **2006**, *119*, 3227–3237. [CrossRef]
98. Livanos, P.; Galatis, B.; Apostolakos, P. The Interplay between ROS and Tubulin Cytoskeleton in Plants. *Plant Signal. Behav.* **2014**, *9*, e28069. [CrossRef] [PubMed]
99. Livanos, P.; Galatis, B.; Quader, H.; Apostolakos, P. Disturbance of Reactive Oxygen Species Homeostasis Induces Atypical Tubulin Polymer Formation and Affects Mitosis in Root-Tip Cells of *Triticum turgidum* and *Arabidopsis thaliana*. *Cytoskeleton* **2012**, *69*, 1–21. [CrossRef] [PubMed]

100. Tulin, A.; McClerklin, S.; Huang, Y.; Dixit, R. Single-Molecule Analysis of the Microtubule Cross-Linking Protein MAP65-1 Reveals a Molecular Mechanism for Contact-Angle-Dependent Microtubule Bundling. *Biophys. J.* **2012**, *102*, 802–809. [CrossRef] [PubMed]
101. Mori, I.C.; Schroeder, J.I. Reactive Oxygen Species Activation of Plant Ca^{2+} Channels. A Signaling Mechanism in Polar Growth, Hormone Transduction, Stress Signaling, and Hypothetically Mechanotransduction. *Plant Physiol.* **2004**, *135*, 702–708. [CrossRef]
102. Ren, Q.; Xu, Z.; Xue, Y.; Yang, R.; Ma, X.; Sun, J.; Wang, J.; Lin, S.; Wang, W.; Yang, L.; et al. Mechanism of Calcium Signal Response to Cadmium Stress in Duckweed. *Plant Signal. Behav.* **2022**, *17*, 2119340. [CrossRef]
103. Hepler, P.K.; Hush, J.M. Behavior of Microtubules in Living Plant Cells. *Plant Physiol.* **1996**, *112*, 455–461. [CrossRef] [PubMed]
104. Perrino, B.; Chou, I. Role of Calmodulin in Cadmium-Induced Microtubule Disassembly. *Cell Biol. Int. Rep.* **1986**, *10*, 565–573. [CrossRef] [PubMed]
105. DalleDonne, I.; Milzani, A.; Colombo, R. Actin Assembly by Cadmium Ions. *Biochim. Biophys. Acta BBA—Mol. Cell Res.* **1997**, *1357*, 5–17. [CrossRef] [PubMed]
106. Qian, D.; Xiang, Y. Actin Cytoskeleton as Actor in Upstream and Downstream of Calcium Signaling in Plant Cells. *Int. J. Mol. Sci.* **2019**, *20*, 1403. [CrossRef]
107. Mittal, N.; Srivastava, A.K. Cd^{2+} + Cr^{6+} Causes Toxic Effects on Chromosomal Development of Microspore in Carthamus Tinctorius. *AIMS Genet.* **2019**, *6*, 001–010. [CrossRef]
108. Hajmoradi, F.; Kakaei, M. Genotoxic Effects of Heavy Metals on Mitotic Chromosomes of *Trigonella foenum-graecum* L. *J. Genet. Resour.* **2021**, *7*, 265–271. [CrossRef]
109. Ashtiyani, R.K.; Moghaddam, A.M.B.; Schubert, V.; Rutten, T.; Fuchs, J.; Demidov, D.; Blattner, F.R.; Houben, A. AtHaspin Phosphorylates Histone H3 at Threonine 3 during Mitosis and Contributes to Embryonic Patterning in Arabidopsis. *Plant J.* **2011**, *68*, 443–454. [CrossRef]
110. Komaki, S.; Takeuchi, H.; Hamamura, Y.; Heese, M.; Hashimoto, T.; Schnittger, A. Functional Analysis of the Plant Chromosomal Passenger Complex. *Plant Physiol.* **2020**, *183*, 1586–1599. [CrossRef]
111. Nasa, I.; Kettenbach, A.N. Coordination of Protein Kinase and Phosphoprotein Phosphatase Activities in Mitosis. *Front. Cell Dev. Biol.* **2018**, *6*, 30–43. [CrossRef]
112. Corno, A.; Cordeiro, M.H.; Allan, L.A.; Lim, Q.-W.; Harrington, E.; Smith, R.J.; Saurin, A.T. A Bifunctional Kinase–Phosphatase Module Balances Mitotic Checkpoint Strength and Kinetochore–Microtubule Attachment Stability. *EMBO J.* **2023**, *42*, e112630. [CrossRef]
113. Ayaydin, F.; Vissi, E.; Mészáros, T.; Miskolczi, P.; Kovács, I.; Fehér, A.; Dombrádi, V.; Erdödi, F.; Gergely, P.; Dudits, D. Inhibition of Serine/Threonine-Specific Protein Phosphatases Causes Premature Activation of cdc2MsF Kinase at G2/M Transition and Early Mitotic Microtubule Organisation in Alfalfa. *Plant J.* **2000**, *23*, 85–96. [CrossRef]
114. Polit, J.T.; Kaźmierczak, A. Okadaic Acid (1 μM) Accelerates S Phase and Mitosis but Inhibits Heterochromatin Replication and Metaphase–Anaphase Transition in *Vicia faba* Meristem Cells. *J. Exp. Bot.* **2007**, *58*, 2785–2797. [CrossRef] [PubMed]
115. Nilsson, J. Protein Phosphatases in the Regulation of Mitosis. *J. Cell Biol.* **2019**, *218*, 395–409. [CrossRef]
116. Qian, J.; Lesage, B.; Beullens, M.; Van Eynde, A.; Bollen, M. PP1/Repo-Man Dephosphorylates Mitotic Histone H3 at T3 and Regulates Chromosomal Aurora B Targeting. *Curr. Biol.* **2011**, *21*, 766–773. [CrossRef]
117. Hindriksen, S.; Lens, S.M.A.; Hadders, M.A. The Ins and Outs of Aurora B Inner Centromere Localization. *Front. Cell Dev. Biol.* **2017**, *5*, 112–132. [CrossRef]
118. Vallardi, G.; Allan, L.A.; Crozier, L.; Saurin, A.T. Division of Labour between PP2A-B56 Isoforms at the Centromere and Kinetochore. *eLife* **2019**, *8*, e42619. [CrossRef] [PubMed]
119. Choy, M.S.; Nguyen, H.T.; Kumar, G.S.; Peti, W.; Kettenbach, A.N.; Page, R. A Protein Phosphatase 1 Specific *Phos* Phatase *Ta* Rgeting *p* Eptide (PhosTAP) to Identify the PP1 Phosphatome. *Proc. Natl. Acad. Sci. USA* **2024**, *121*, e2415383121. [CrossRef]
120. Lima, A.I.G.; Da Cruz E Silva, E.; Figueira, E.M.P.A. Cd-Induced Signaling Pathways in Plants: Possible Regulation of PC Synthase by Protein Phosphatase 1. *Environ. Exp. Bot.* **2012**, *79*, 31–36. [CrossRef]
121. Chen, J.; Wang, X.; Zhang, W.; Zhang, S.; Zhao, F.-J. Protein Phosphatase 2A Alleviates Cadmium Toxicity by Modulating Ethylene Production in *Arabidopsis thaliana*. *Plant Cell Environ.* **2020**, *43*, 1008–1022. [CrossRef]
122. Chen, L.; Liu, L.; Huang, S. Cadmium Activates the Mitogen-Activated Protein Kinase (MAPK) Pathway via Induction of Reactive Oxygen Species and Inhibition of Protein Phosphatases 2A and 5. *Free Radic. Biol. Med.* **2008**, *45*, 1035–1044. [CrossRef] [PubMed]
123. Saurin, A.T. Kinase and Phosphatase Cross-Talk at the Kinetochore. *Front. Cell Dev. Biol.* **2018**, *6*, 62–84. [CrossRef]
124. Monaco, L.; Kolthur-Seetharam, U.; Loury, R.; Murcia, J.M.; De Murcia, G.; Sassone-Corsi, P. Inhibition of Aurora-B Kinase Activity by Poly(ADP-Ribosyl)Ation in Response to DNA Damage. *Proc. Natl. Acad. Sci. USA* **2005**, *102*, 14244–14248. [CrossRef]
125. Cho, M.-G.; Ahn, J.-H.; Choi, H.-S.; Lee, J.-H. DNA Double-Strand Breaks and Aurora B Mislocalization Induced by Exposure of Early Mitotic Cells to H_2O_2 Appear to Increase Chromatin Bridges and Resultant Cytokinesis Failure. *Free Radic. Biol. Med.* **2017**, *108*, 129–145. [CrossRef]

126. Cuypers, A.; Plusquin, M.; Remans, T.; Jozefczak, M.; Keunen, E.; Gielen, H.; Opdenakker, K.; Nair, A.R.; Munters, E.; Artois, T.J.; et al. Cadmium Stress: An Oxidative Challenge. *BioMetals* **2010**, *23*, 927–940. [CrossRef]
127. Youdim, K.A.; Deans, S.G.; Finlayson, H.J. The Antioxidant Properties of Thyme (*Thymus zygis* L.) Essential Oil: An Inhibitor of Lipid Peroxidation and a Free Radical Scavenger. *J. Essent. Oil Res.* **2002**, *14*, 210–215. [CrossRef]
128. Dawidowicz, A.L.; Olszowy, M. Does Antioxidant Properties of the Main Component of Essential Oil Reflect Its Antioxidant Properties? The Comparison of Antioxidant Properties of Essential Oils and Their Main Components. *Nat. Prod. Res.* **2014**, *28*, 1952–1963. [CrossRef] [PubMed]
129. Sallam, M.F.; Ahmed, H.M.S.; Diab, K.A.; El-Nekeety, A.A.; Abdel-Aziem, S.H.; Sharaf, H.A.; Abdel-Wahhab, M.A. Improvement of the Antioxidant Activity of Thyme Essential Oil against Biosynthesized Titanium Dioxide Nanoparticles-Induced Oxidative Stress, DNA Damage, and Disturbances in Gene Expression in Vivo. *J. Trace Elem. Med. Biol.* **2022**, *73*, 127024. [CrossRef] [PubMed]
130. Sha, W.; Moore, J.; Chen, K.; Lassaletta, A.D.; Yi, C.-S.; Tyson, J.J.; Sible, J.C. Hysteresis Drives Cell-Cycle Transitions in *Xenopus laevis* Egg Extracts. *Proc. Natl. Acad. Sci. USA* **2003**, *100*, 975–980. [CrossRef] [PubMed]
131. Arellano, M.; Moreno, S. Regulation of CDK/Cyclin Complexes during the Cell Cycle. *Int. J. Biochem. Cell Biol.* **1997**, *29*, 559–573. [CrossRef]
132. Vermeulen, K.; Van Bockstaele, D.R.; Berneman, Z.N. The Cell Cycle: A Review of Regulation, Deregulation and Therapeutic Targets in Cancer. *Cell Prolif.* **2003**, *36*, 131–149. [CrossRef]
133. Ding, L.; Cao, J.; Lin, W.; Chen, H.; Xiong, X.; Ao, H.; Yu, M.; Lin, J.; Cui, Q. The Roles of Cyclin-Dependent Kinases in Cell-Cycle Progression and Therapeutic Strategies in Human Breast Cancer. *Int. J. Mol. Sci.* **2020**, *21*, 1960. [CrossRef]
134. De Almeida, A.J.P.O.; De Oliveira, J.C.P.L.; Da Silva Pontes, L.V.; De Souza Júnior, J.F.; Gonçalves, T.A.F.; Dantas, S.H.; De Almeida Feitosa, M.S.; Silva, A.O.; De Medeiros, I.A. ROS: Basic Concepts, Sources, Cellular Signaling, and Its Implications in Aging Pathways. *Oxid. Med. Cell. Longev.* **2022**, *2022*, 1225578. [CrossRef] [PubMed]
135. Becer, E.; Mutlu Altundag, E.; Başer, K.H.C.; Vatansever, H.S. Cytotoxic Activity and Antioxidant Effects of *Origanum onites* Essential Oil and Its Two Major Contents, Carvacrol and *p*-Cymene on Human Colorectal (HCT116) and Hepatocelluler Carcinoma (HepG2) Cell Lines. *J. Essent. Oil Res.* **2022**, *34*, 514–523. [CrossRef]
136. Imran, M.; Aslam, M.; Alsagaby, S.A.; Saeed, F.; Ahmad, I.; Afzaal, M.; Arshad, M.U.; Abdelgawad, M.A.; El-Ghorab, A.H.; Khames, A.; et al. Therapeutic Application of Carvacrol: A Comprehensive Review. *Food Sci. Nutr.* **2022**, *10*, 3544–3561. [CrossRef] [PubMed]
137. Sun, C.; Chen, J.; Wang, L.; Li, J.; Shi, Z.; Yang, L.; Yu, X. Thymol Deploys Multiple Antioxidative Systems to Suppress ROS Accumulation in Chinese Cabbage Seedlings under Saline Stress. *Agronomy* **2024**, *14*, 1059. [CrossRef]
138. Dentato, M.; Polito, F.; Basile, A.; De Feo, V.; De Marino, E.; Postiglione, A.; Maresca, V. *Ocium basilicum* Essential Oil Biostimulant Activity and Protective Effects on Cadmium-Induced DNA Damage and Oxidative Stress in *Raphanus sativus* L. *Ind. Crops Prod.* **2025**, *235*, 121830. [CrossRef]
139. Serpico, A.F.; Pisauro, C.; Grieco, D. On the Assembly of the Mitotic Spindle, Bistability and Hysteresis. *Cell. Mol. Life Sci.* **2023**, *80*, 83–87. [CrossRef] [PubMed]
140. Piermarini, E.; Cartelli, D.; Pastore, A.; Tozzi, G.; Compagnucci, C.; Giorda, E.; D'Amico, J.; Petrini, S.; Bertini, E.; Cappelletti, G.; et al. Frataxin Silencing Alters Microtubule Stability in Motor Neurons: Implications for Friedreich's Ataxia. *Hum. Mol. Genet.* **2016**, *25*, 4288–4301. [CrossRef]
141. Diab, K.A.; Fahmy, M.A.; Hassan, Z.M.; Hassan, E.M.; Salama, A.B.; Omara, E.A. Genotoxicity of Carbon Tetrachloride and the Protective Role of Essential Oil of Salvia Officinalis L. in Mice Using Chromosomal Aberration, Micronuclei Formation, and Comet Assay. *Environ. Sci. Pollut. Res.* **2018**, *25*, 1621–1636. [CrossRef]
142. Nowak, S.J.; Pai, C.-Y.; Corces, V.G. Protein Phosphatase 2A Activity Affects Histone H3 Phosphorylation and Transcription in *Drosophila melanogaster*. *Mol. Cell. Biol.* **2003**, *23*, 6129–6138. [CrossRef]
143. Liu, C.; Zhang, R.; Sun, C.; Zhang, H.; Xu, C.; Liu, W.; Gao, W.; Huang, S.; Chen, L. Resveratrol Prevents Cadmium Activation of Erk1/2 and JNK Pathways from Neuronal Cell Death via Protein Phosphatases 2A and 5. *J. Neurochem.* **2015**, *135*, 466–478. [CrossRef]
144. Ye, X.; Ling, T.; Xue, Y.; Xu, C.; Zhou, W.; Hu, L.; Chen, J.; Shi, Z. Thymol Mitigates Cadmium Stress by Regulating Glutathione Levels and Reactive Oxygen Species Homeostasis in Tobacco Seedlings. *Molecules* **2016**, *21*, 1339. [CrossRef] [PubMed]
145. Rahmani, F.; Nabi, S.; Idliki, R.B.; Alimirzaei, M.; Barkhordar, S.M.A.; Shafaei, N.; Zareian, M.; Karimi, E.; Oskoueian, E. Thyme Oil Nanoemulsion Enhanced Cellular Antioxidant and Suppressed Inflammation in Mice Challenged by Cadmium-Induced Oxidative Stress. *Waste Biomass Valorization* **2022**, *13*, 3139–3146. [CrossRef]
146. Askari, E.; Fallah, A.A.; Habibian Dehkordi, S.; Bahadoran, S.; Mohebbi, A.; Mohamadi, S. Effect of Dietary Clove (*Syzygium aromaticum*) Essential Oil on Growth Performance, Oxidative Indices, Lipid Profile, and Cadmium Accumulation in Cd-Exposed Quails. *J. Environ. Health Sustain. Dev.* **2022**, *7*, 1755–1766. [CrossRef]

147. Choong, G.; Liu, Y.; Templeton, D.M. Interplay of Calcium and Cadmium in Mediating Cadmium Toxicity. *Chem. Biol. Interact.* **2014**, *211*, 54–65. [CrossRef] [PubMed]
148. Zeng, L.; Zhu, T.; Gao, Y.; Wang, Y.; Ning, C.; Björn, L.O.; Chen, D.; Li, S. Effects of Ca Addition on the Uptake, Translocation, and Distribution of Cd in Arabidopsis Thaliana. *Ecotoxicol. Environ. Saf.* **2017**, *139*, 228–237. [CrossRef]
149. Zhang, Y.; Wang, Z.; Liu, Y.; Zhang, T.; Liu, J.; You, Z.; Huang, P.; Zhang, Z.; Wang, C. Plasma Membrane-Associated Calcium Signaling Modulates Cadmium Transport. *New Phytol.* **2023**, *238*, 313–331. [CrossRef]
150. Guo, W.; Xing, Y.; Luo, X.; Li, F.; Ren, M.; Liang, Y. Reactive Oxygen Species: A Crosslink between Plant and Human Eukaryotic Cell Systems. *Int. J. Mol. Sci.* **2023**, *24*, 13052. [CrossRef]
151. Ünyayar, S.; Çelik, A.; Çekiç, F.Ö.; Gözel, A. Cadmium-Induced Genotoxicity, Cytotoxicity and Lipid Peroxidation in *Allium sativum* and *Vicia faba*. *Mutagenesis* **2006**, *21*, 77–81. [CrossRef]
152. Souguir, D.; Ferjani, E.; Ledoigt, G.; Goupil, P. Sequential Effects of Cadmium on Genotoxicity and Lipoperoxidation in Vicia Faba Roots. *Ecotoxicology* **2011**, *20*, 329–336. [CrossRef]
153. Livak, K.J.; Schmittgen, T.D. Analysis of Relative Gene Expression Data Using Real-Time Quantitative PCR and the $2^{-\Delta\Delta CT}$ Method. *Methods* **2001**, *25*, 402–408. [CrossRef]
154. Gutierrez, N.; Giménez, M.J.; Palomino, C.; Avila, C.M. Assessment of Candidate Reference Genes for Expression Studies in Vicia Faba L. by Real-Time Quantitative PCR. *Mol. Breed.* **2011**, *28*, 13–24. [CrossRef]
155. Untergasser, A.; Cutcutache, I.; Koressaar, T.; Ye, J.; Faircloth, B.C.; Remm, M.; Rozen, S.G. Primer3—New Capabilities and Interfaces. *Nucleic Acids Res.* **2012**, *40*, e115. [CrossRef]
156. Żabka, A.; Polit, J.T.; Maszewski, J. Inter- and Intrachromosomal Asynchrony of Cell Division Cycle Events in Root Meristem Cells of Allium Cepa: Possible Connection with Gradient of Cyclin B-like Proteins. *Plant Cell Rep.* **2010**, *29*, 845–856. [CrossRef] [PubMed]
157. Żabka, A.; Polit, J.T.; Maszewski, J. DNA Replication Stress Induces Deregulation of the Cell Cycle Events in Root Meristems of Allium Cepa. *Ann. Bot.* **2012**, *110*, 1581–1591. [CrossRef] [PubMed]
158. Kesraoui, S.; Andrés, M.; Berrocal-Lobo, M.; Soudani, S.; Gonzalez-Coloma, A. Direct and Indirect Effects of Essential Oils for Sustainable Crop Protection. *Plants* **2022**, *11*, 2144. [CrossRef] [PubMed]
159. Ayllón-Gutiérrez, R.; Díaz-Rubio, L.; Montaño-Soto, M.; Haro-Vázquez, M.D.P.; Córdova-Guerrero, I. Applications of Plant Essential Oils in Pest Control and Their Encapsulation for Controlled Release: A Review. *Agriculture* **2024**, *14*, 1766. [CrossRef]

Table S1. Preliminary screening of $CdCl_2$ and thyme essential oil (TO) concentrations used for selecting the experimental conditions in *Vicia faba* root meristem cells.

Treatment	Concentration	Mitotic index (% ± SD)	% of control	Interpretation
Control	**–**	**5.92 ± 1.67**	**100**	**Normal mitotic activity**
$CdCl_2$	100 μM	4.57 ± 1.1	77	Mild inhibition of mitosis
$CdCl_2$	150 μM	2.2 ± 0.7	38	Strong inhibition (used in previous studies [1,2])
$CdCl_2$	**175 μM**	**0.54 ± 0.2**	**9**	**Strong but sublethal mitotic inhibition - selected (used in previous studies [3,4])**
$CdCl_2$	200 μM	0.2 ± 0.05	3.4	Severe inhibition; poor meristem/cell condition
TO	0.01%	6.0 ± 1.1	101	No effect on mitosis
TO	**0.03%**	**5.6 ± 1.9**	**94**	**Comparable to control - selected**
TO	0.06%	5.1 ± 1.2	86	Mild inhibition of mitotic activity
$CdCl_2$ + TO	175 μM + 0.01%	1.97 ± 0.5	33	Partial recovery of mitotic activity
$CdCl_2$ + TO	**175 μM + 0.03%**	**3.3 ± 0.68**	**56**	**Strong mitigation of Cd-induced mitotic inhibition - selected**
$CdCl_2$ + TO	175 μM + 0.06%	2.89 ± 0.97	48.7	Mitigation of Cd-induced mitotic inhibition

References:

1. Żabka, A.; Winnicki, K.; Polit, J.T.; Wróblewski, M.; Maszewski, J. Cadmium (II)-Induced Oxidative Stress Results in Replication Stress and Epigenetic Modifications in Root Meristem Cell Nuclei of *Vicia faba*. *Cells* **2021**, *10*, 640, doi:10.3390/cells10030640.

2. Żabka, A.; Gocek, N.; Winnicki, K.; Szczeblewski, P.; Laskowski, T.; Polit, J.T. Changes in Epigenetic Patterns Related to DNA Replication in *Vicia faba* Root Meristem Cells under Cadmium-Induced Stress Conditions. *Cells* **2021**, *10*, 3409, doi:10.3390/cells10123409.

3. Gocek-Szczurtek, N.; Żabka, A.; Wróblewski, M.; Kukula-Koch, W.; Szczeblewski, P.; Polit, J.T. Thyme Oil Mitigates Cadmium-Induced Oxidative and Genotoxic Stress in *Vicia faba* Root Meristem Cells under in vitro Conditions. *Sci Rep* **2025**, *15*, 38689, doi:10.1038/s41598-025-22588-w.

4. Gocek-Szczurtek, N.; Żabka, A.; Wróblewski, M.; Polit, J.T. Stabilization of the MAPK–Epigenetic Signaling Axis Underlies the Protective Effect of Thyme Oil Against Cadmium Stress in Root Meristem Cells of *Vicia faba*. *IJMS* **2025**, *27*, 208, doi:10.3390/ijms27010208.

❖

Praca 5 (Załącznik nr 5)

❖ **Gocek-Szczurtek, N.***; Piotrowska-Niczyporuk, A.; Zambrzycka-Szelewa, E.; Ciereszko, I.; Żabka, A.; Wróblewski, M.; Polit, J.T.
Thyme Essential Oil Reduces Cadmium Uptake and Toxicity in *Vicia faba* Root Meristem Cells, Involving Stabilization of Cell Ultrastructure and Modulation of Redox Response and Thiol Metabolism.
manuskrypt wysłany do czasopisma *The Plant Journal*

* – autor korespondujący

- Współczynnik wpływu (IF) dla czasopisma, do którego wysłano pracę: **5,7**
- Punkty MNiSW czasopisma, do którego wysłano pracę: **140 pkt**.

---

the plant journal SEB SOCIETY FOR EXPERIMENTAL BIOLOGY

Original Article

Thyme Essential Oil Reduces Cadmium Uptake and Toxicity in Vicia faba Root Meristem Cells, Involving Stabilization of Cell Ultrastructure and Modulation of Redox Response and Thiol Metabolism

Submission ID 7f050075-2644-4a3d-98f3-b615dc465ac1

Submission Version Initial Submission

PDF Generation 28 Mar 2026 04:50:13 EST by Atypon ReX

Authors

Mrs. Natalia Gocek-Szczurtek
Corresponding Author
Submitting Author

Affiliations
- Department of Cytophysiology, Faculty of Biology and Environmental Protection, University of Lodz, 90-236 Lodz, Poland
- Doctoral School of Exact and Natural Sciences, University of Lodz, 90-237 Lodz, Poland

Prof. Alicja Piotrowska-Niczyporuk

Affiliations
- Department of Plant Biology and Ecology, Faculty of Biology, University of Bialystok, 15-245 Białystok, Poland

Dr. Elżbieta Zambrzycka-Szelewa

Affiliations
- Department of Analytical Chemistry, Faculty of Chemistry, University of Bialystok, 15-245 Białystok, Poland

Prof. Iwona Ciereszko

Affiliations
- Department of Plant Biology and Ecology, Faculty of Biology, University of Bialystok, 15-245 Białystok, Poland

Dr. Aneta Żabka

Affiliations

- Department of Cytophysiology, Faculty of Biology and Environmental Protection, University of Lodz, 90-236 Lodz, Poland

Mr. Mateusz Wróblewski

Affiliations

- Department of Cytophysiology, Faculty of Biology and Environmental Protection, University of Lodz, 90-236 Lodz, Poland

Prof. Justyna T. Polit

Affiliations

- Department of Cytophysiology, Faculty of Biology and Environmental Protection, University of Lodz, 90-236 Lodz, Poland

Files for peer review

All files submitted by the author for peer review are listed below. Files that could not be converted to PDF are indicated; reviewers are able to access them online.

Name	Type of File	Size	Page
Manuscript- The Plant Journal.docx	Main Document - MS Word	4.6 MB	Page 4

Thyme Essential Oil Reduces Cadmium Uptake and Toxicity in *Vicia faba* Root Meristem Cells, Involving Stabilization of Cell Ultrastructure and Modulation of Redox Response and Thiol Metabolism

Natalia Gocek-Szczurtek [1,2] *, Alicja Piotrowska-Niczyporuk [3], Elżbieta Zambrzycka-Szelewa [4], Iwona Ciereszko [3], Aneta Żabka [1], Mateusz Wróblewski [1], Justyna T. Polit [1]

[1] Department of Cytophysiology, Faculty of Biology and Environmental Protection, University of Lodz, 90-236 Lodz, Poland
[2] Doctoral School of Exact and Natural Sciences, University of Lodz, 90-237 Lodz, Poland
[3] Department of Plant Biology and Ecology, Faculty of Biology, University of Bialystok, 15-245 Białystok, Poland
[4] Department of Analytical Chemistry, Faculty of Chemistry, University of Bialystok, 15-245 Białystok, Poland

*Author to whom correspondence should be addressed.

Keywords: heavy metal; essential oil; redox homeostasis; ROS; antioxidant system; phytochelatins; *Vicia faba*; primary roots

Significance statement: Despite increasing interest in natural bioactive compounds, their role in modulating plant responses to heavy metal stress remains poorly resolved. Here, we demonstrate that thyme essential oil limits cadmium accumulation and enhances antioxidant capacity in root meristems, reducing oxidative damage and preserving cellular organization, thereby identifying essential oils as promising modulators of plant tolerance to heavy metal stress.

Contact information:

- Natalia Gocek-Szczurtek: email: natalia.gocek.szczurtek@biol.uni.lodz.pl; ORCID: 0000-0001-5484-2340
- Alicja Piotrowska – Niczyporuk: email: alicjap@uwb.edu.pl; ORCID: 0000-0001-5357-2115
- Elżbieta Zambrzycka-Szelewa: email: elazamb@uwb.edu.pl; ORCID: 0000-0002-1164-4747
- Iwona Ciereszko: email: icier@uwb.edu.pl; ORCID: 0000-0003-2694-7991
- Aneta Żabka: email: aneta.zabka@biol.uni.lodz.pl; ORCID: 0000-0001-6401-2068
- Mateusz Wróblewski: email: mateusz.wroblewski@biol.uni.lodz.pl; ORCID: 0000-0001-9656-4967
- Justyna T. Polit: email: justyna.polit@biol.uni.lodz.pl; ORCID: 0000-0002-9655-001X

Data availability statement: Data will be made available on request

Funding statement: This work was supported through the budget of the Doctoral School of Exact and Natural Sciences of the University of Lodz.

Conflict of interest disclosure: The authors declare no competing financial interests or personal relationships that could have appeared to influence the work reported in this paper.

Ethics approval statement: not applicable

Patient consent statement: not applicable

Permission to reproduce material from other sources: not applicable

Summary:

The role of essential oils as modulators of plant responses to heavy metal-induced stress remains insufficiently understood. In this study, using primary roots of *Vicia faba* L. var. *minor*, we investigated the effects of thyme essential oil (TO; 0.03 %) on meristematic cells exposed to $CdCl_2$ solution (175 µM; 24 h), analyzing changes at both biochemical and ultrastructural levels. Accumulation of cadmium in meristems disrupted redox homeostasis, triggering activation of antioxidant defense mechanisms and enhanced thiol metabolism. However, these responses proved insufficient to restore redox balance, resulting in sustained oxidative stress, as reflected by a fourfold increase in H_2O_2 levels, and leading to lipid peroxidation and DNA fragmentation. At the ultrastructural level, these changes correlated with pronounced disorganization of cellular structures and organelles. They could result from impaired barrier function of the cell wall, likely due to defects in its reinforcement, as indicated by Golgi-derived vesicles depleted of fibrous cell wall precursors, and from restricted synthesis of essential proteins, reflected by a reduced number of ribosomes in the cytoplasm. TO reduced Cd accumulation in meristematic tissues by 38%, which was accompanied by enhanced enzymatic and non-enzymatic antioxidant responses, prevention of excessive H_2O_2 accumulation (50% lower than in Cd-treated roots), limited lipid peroxidation, and preservation of DNA integrity. Simultaneously, ultrastructural organization of organelles improved, production of cell wall precursors in Golgi secretory vesicles was stimulated, and transport of ribosomal subunits to the cytoplasm, associated with the formation of nucleolar vacuoles, was increased. These processes were accompanied by intensified protein synthesis, reflected by increased ribosome deposition on the endoplasmic reticulum, highlighting TO's potential as a natural bioprotective agent supporting plant stress tolerance.

Introduction:

The disruption of natural geochemical processes by human activity has led to the accelerated mobilization of heavy metals, increased their bioavailability, and promoted their accumulation in the environmental (Violante *et al.*, 2010; Briffa *et al.*, 2020; Ju *et al.*, 2024; Gavrilaș *et al.*, 2025). Cadmium (Cd) is a particularly hazardous element due to the combination of several toxicological characteristics. As a non-essential metal with no known biological function, Cd readily enters living organisms by exploiting transport pathways for physiological ions such as Fe^{2+}, Zn^{2+}, and Ca^{2+} (Song *et al.*, 2017). Its uptake from soil by edible plants, especially cereals and legumes, makes the diet one of the main sources of human exposure (Wang *et al.*, 2023). Moreover, cadmium is highly persistent – it is not biodegradable, and its residence time in soils is measured in decades (Edo *et al.*, 2024). At the molecular level, Cd is not a redox-active metal; nevertheless, it effectively induces oxidative stress (Cuypers *et al.*, 2010). It disrupts cellular homeostasis by displacing essential metal ions from enzyme active sites (Bashir *et al.*, 2015; Genchi *et al.*, 2020), binding to thiol groups (Branca *et al.*, 2020a; Hernández-Cruz *et al.*, 2022), and destabilizing mitochondria and chloroplasts, which leads to secondary overproduction of reactive oxygen species (ROS) (Branca *et al.*, 2020b; Sperdouli *et al.*, 2022).

Moreover, oxidative stress and heavy metal toxicity remain in a bidirectional relationship based on a positive feedback loop. Lipid peroxidation induced by elevated ROS levels increases the permeability of biological membranes, disrupts ion transport selectivity, and facilitates the influx of heavy metal cations, including Cd, into the cell (Hirata *et al.*, 2023; Sood, 2025). Oxidation of thiol (–SH) groups in ion-binding proteins and chelating complexes leads to the release of previously sequestered elements, thereby enlarging the pool of reactive forms (Ruttkay-Nedecky *et al.*, 2013; Mansoor *et al.*, 2023). As a consequence, a self-amplifying system is established: increased metal accumulation enhances ROS production, while oxidative stress further elevates metal bioavailability. This phenomenon results in a range of ultrastructural and functional alterations in plant cells, including mitochondrial swelling, disorganization of mitochondrial cristae, impaired membrane integrity, and degradation of plastid structures. Cytoplasmic condensation and nuclear changes are also observed, including chromatin condensation and deformation of the nuclear envelope (Barceló *et al.*, 1988; Liu and Kottke, 2004; Gzyl *et al.*, 2009; Ge *et al.*, 2012; Ali *et al.*, 2014; Sun *et al.*, 2020). In parallel, ROS directly affect genetic material by inducing DNA base modifications, and oxidative adduct formation, as well as single- and double-strand DNA breaks (Gill and Tuteja, 2010; Srinivas *et al.*, 2019). These lesions may disrupt cell cycle progression and consequently inhibit cell proliferation and plant organ growth (Potters *et al.*, 2007; El Rasafi *et al.*, 2022).

In response to cadmium exposure, plants activate an integrated detoxification system (Clemens, 2006). The first step involves the binding of Cd^{2+} ions in the cytoplasm by thiol-rich compounds. Glutathione (GSH) and phytochelatins (PC), synthesized from glutathione, play a key role by forming stable Cd–PC complexes and thereby reducing the pool of free metal ions (Cobbett and Goldsbrough, 2002; Park *et al.*, 2012). These complexes are subsequently sequestered into vacuoles via membrane transporters (Mendoza-Cózatl *et al.*, 2010). Simultaneously, a portion of cadmium ions can be immobilized in the cell wall through binding to the carboxyl groups of pectins, which restricts their transport into the

symplast (Loix *et al.*, 2017). Since cadmium induces secondary oxidative stress, plants also enhance their antioxidant defense system. This response includes increased activity of enzymes such as superoxide dismutase (SOD), catalase (CAT), ascorbate peroxidase (APX), monodehydroascorbate reductase (MDHAR), and dehydroascorbate reductase (DHAR), as well as elevated levels of non-enzymatic antioxidants (Semane *et al.*, 2007; Yu *et al.*, 2013). The coordinated action of these mechanisms limits oxidative damage and determines the degree of plant tolerance to cadmium stress.

The scale of the threat associated with the presence of cadmium in the environment necessitates the development of strategies aimed at reducing its toxicity. Approaches applied in agricultural and environmental practice primarily focus on decreasing its bioavailability in soil, for example through immobilization treatments and the modification of soil chemical conditions to promote ionic competition (e.g., involving Ca^{2+}, Zn^{2+}, or Fe^{2+}) (McBride, 2002; Alloway, 2013; Bolan *et al.*, 2014; He *et al.*, 2019). Although these measures effectively reduce metal uptake by the root system, they do not completely prevent its entry into the plant (Chețan *et al.*, 2025). In this context, a complementary approach is gaining importance, targeting the mitigation of the secondary physiological effects of cadmium after its uptake, particularly in situations where complete elimination of exposure is not feasible. In this framework, essential oils represent a potential tool. In their native plants, essential oils primarily play defensive, signaling, and allelopathic roles; however, numerous studies indicate that the exogenous application of selected essential oils can modulate stress responses in other organisms (Pichersky and Gershenzon, 2002; Dudareva *et al.*, 2006; Lee *et al.*, 2017; Kaya *et al.*, 2024; Madkour *et al.*, 2025).

The fact that essential oils are mixtures of various volatile secondary metabolites means that their activity is not limited to a single molecular mechanism (Bunse *et al.*, 2022; De Sousa *et al.*, 2023). On the contrary, their biological effects are multi-level in nature, resulting both from the chemical diversity of their constituents and from potential synergistic interactions among them (Youdim *et al.*, 2002; Dawidowicz and Olszowy, 2014). A particularly interesting example is thyme essential oil (TO; derived from *Thymus vulgaris* L.), whose biological activity has been well documented in both plant and animal models (Kowalczyk *et al.*, 2020; Abdel-Wahhab *et al.*, 2021; Hassan *et al.*, 2021; Pandur *et al.*, 2022; Rahmani *et al.*, 2022; Mohammed *et al.*, 2024). It is characterized by a high content of phenolic monoterpenes, primarily thymol, with carvacrol also present, both of which, due to the presence of a phenolic hydroxyl group, are capable of donating a hydrogen atom to reactive oxygen species. This reaction leads to the formation of a relatively stable phenoxyl radical and interrupts the chain reaction of lipid peroxidation (Yanishlieva *et al.*, 1999; Hudaib *et al.*, 2002; Gocek-Szczurtek *et al.*, 2025a). The lipophilic nature of thymol also enables its interaction with biological membranes, which at appropriate concentrations may contribute to membrane stabilization and reduction of oxidative damage (Liolios *et al.*, 2009).

Our previous studies allowed us to formulate a coherent picture of cadmium action on the regulation of key nuclear processes, cell cycle progression, and the proliferative stability of meristematic cells. We demonstrated that exposure to Cd at a concentration of 175 μM leads to ROS overproduction, which is reflected in the reorganization of the epigenome, alterations in chromatin structure,

destabilization of DNA replication, disturbances in cell cycle progression, and impairment of mitotic divisions (Gocek-Szczurtek *et al.*, 2025a; Gocek-Szczurtek *et al*., 2025b; Gocek-Szczurtek *et al.*, 2026). Oxidative stress thus emerges as a central factor driving the cytological changes observed under cadmium exposure. At the same time, the obtained results indicate that TO at a concentration of 0.03% significantly reduces the extent of these disturbances, maintaining ROS levels close to the control, preserving the balance of nuclear processes, and supporting more normal dynamics of the cell cycle (Gocek-Szczurtek *et al.*, 2025a; Gocek-Szczurtek *et al.*, 2025b; Gocek-Szczurtek *et al.*, 2026). Collectively, our data suggest that its protective effect is associated with the modulation of redox balance as a primary regulatory hub under cadmium stress (**Figure 1**). A natural consequence of this sequence of studies has therefore been the transition from identifying the epigenetic and cytological effects of the tested factors to a direct and more in-depth analysis of the underlying antioxidant mechanisms.

In this study, we employed an established model system: the primary roots of *Vicia faba* L. var. *minor*. This species is an agriculturally important crop plant, and its sensitivity to metal stress makes it a useful model for investigating the mechanisms of cadmium toxicity in the context of food safety (Segers *et al.*, 2022). The combination of cytological sensitivity and agronomic relevance renders this model particularly suitable for analyzing both the molecular and physiological aspects of plant responses to cadmium stress, as well as potential mitigation strategies (Arya and Mukherjee, 2014). Seedlings were exposed for 24 hours to $CdCl_2$ solution, to emulsified thyme essential oil (TO), and to a combination of both factors. Control material consisted of plants incubated in distilled water and in the solution of the emulsifier used for the preparation of the oil emulsion. To confirm the degree of Cd accumulation in the plant material, its content was determined in seedlings from all experimental variants. Subsequently, to evaluate the potential protective properties of TO against Cd toxicity and to elucidate its mechanism of action in root cells, the effect of the tested factors on the level of the reactive oxygen species (ROS) hydrogen peroxide (H_2O_2) was analyzed. At the same time, the functioning of non-enzymatic and enzymatic components of the antioxidant system was assessed. In the analysis of non-enzymatic antioxidants, the contents of ascorbate, phytochelatins, glutathione, cysteine, γ-glutamylcysteine, and proline were determined, whereas the activity of enzymatic components was evaluated by measuring the activities of superoxide dismutase (SOD, EC 1.15.1.1), catalase (CAT, EC 1.11.1.6), ascorbate peroxidase (APX, EC 1.11.1.11), and glutathione reductase (GR, EC 1.8.1.7). Cellular damage was assessed based on the level of lipid peroxidation, expressed as malondialdehyde (MDA) content. Furthermore, DNA integrity in meristematic cells was analyzed using the TUNEL assay, and ultrastructural alterations were examined by transmission electron microscopy (TEM).

Based on the results obtained to date and the adopted experimental model, the following research hypotheses were formulated: (1) exposure of *V. faba* seedlings to $CdCl_2$ leads to Cd accumulation in root tissues, induction of oxidative stress, and partial and insufficient activation of adaptive mechanisms of the antioxidant system, accompanied by enhanced cellular damage manifested by increased lipid peroxidation, DNA fragmentation, and ultrastructural alterations; and (2) TO exerts a mitigating effect against Cd toxicity by partially reducing its accumulation in tissues and by modulating redox balance – including a reduction in ROS levels and activation of enzymatic and non-enzymatic

antioxidant mechanisms – which results in decreased damage to cellular membranes, preservation of DNA integrity, and stabilization of the ultrastructure of meristematic cells.

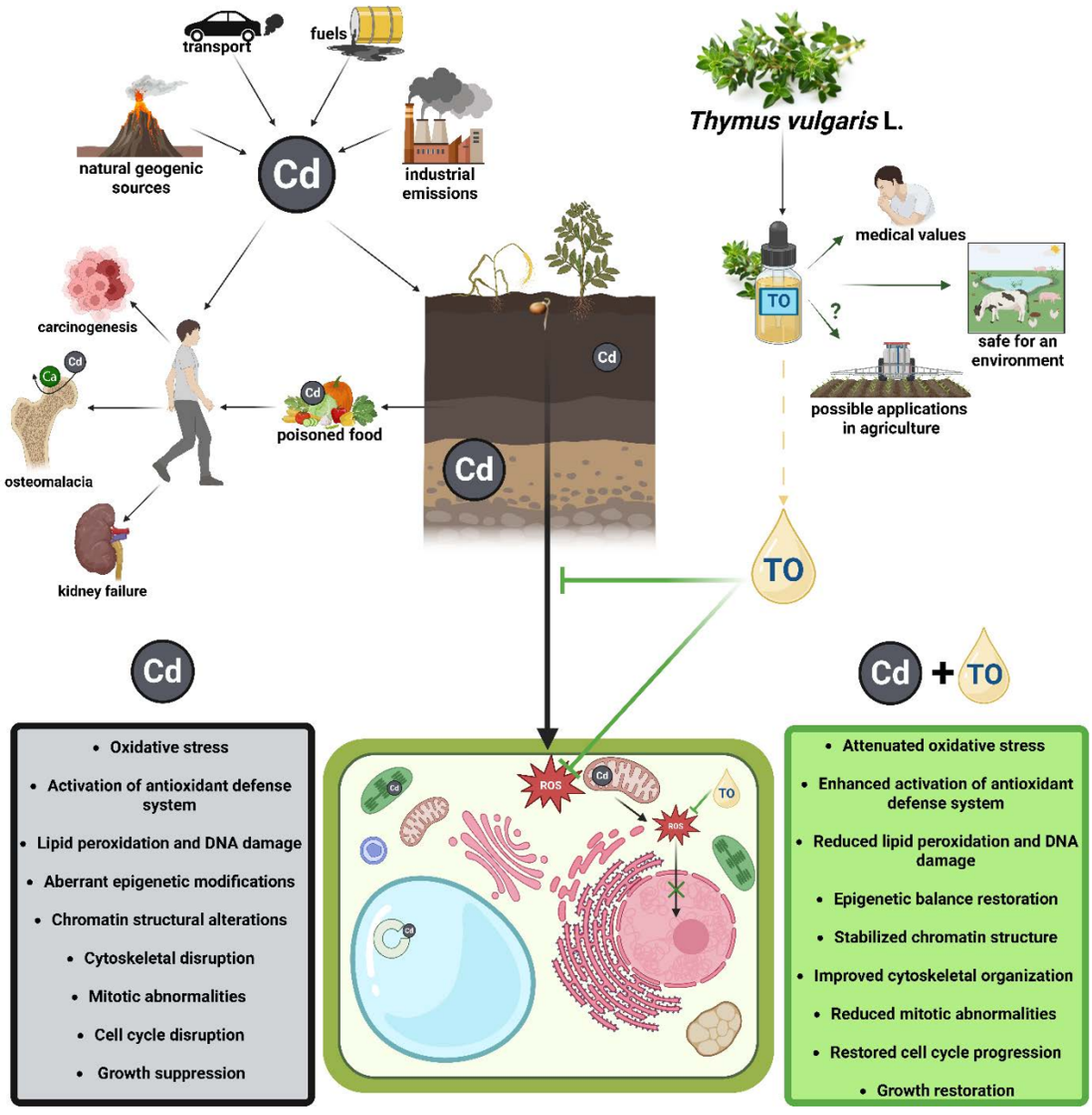

Figure 1. Conceptual framework illustrating sources of cadmium (Cd) contamination, its biological impact, and the proposed protective role of thyme essential oil (TO) in plant systems. Arrows indicate the direction of processes or signaling pathways. Sharp-ended arrows represent activation or stimulation, while blunt-ended arrows indicate inhibition or suppression. Created in BioRender. Gocek-Szczurtek, N. (2026) https://BioRender.com/jp6ugne

Results:

Cadmium Content

The total cadmium (Cd) content in primary root meristems was determined using FAAS (**Figure 2**). In control meristems, treated with the emulsifier solution and with emulsified thyme essential oil (TO), Cd levels were below the limit of quantification (< LOQ), indicating the absence of measurable accumulation of this element. Exposure to $CdCl_2$ resulted in the accumulation of 254.637 µg/g Cd in root meristems, whereas the simultaneous presence of TO reduced its level by 38% to 157.691 µg/g. This finding suggests that TO may limit Cd uptake or its further accumulation in meristematic tissues. Despite the marked reduction in Cd accumulation in the presence of TO, its level remained high and potentially detrimental to the integrity of plant cells.

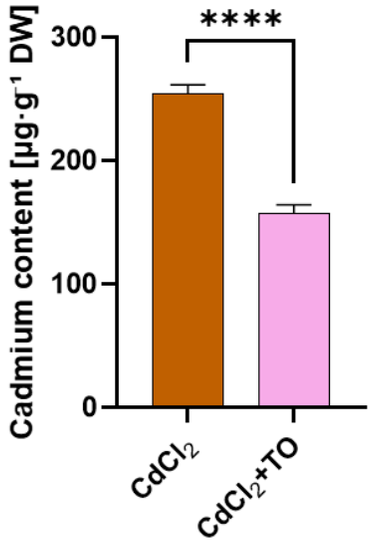

Figure 2. Cadmium (Cd) content in *V. faba* primary roots after 24-hour incubation with $CdCl_2$ and with a combination of $CdCl_2$ and TO. Data are presented as means ± SD from four biological replicates. Only variants with Cd concentrations above the limit of quantification (LOQ) are shown. Statistical significance: **** $p < 0.0001$ (one-way ANOVA followed by Tukey's multiple comparison test).

Hydrogen Peroxide (H_2O_2) Production and Superoxide Dismutase (SOD) and Catalase (CAT) Activity

Hydrogen peroxide (H_2O_2), at physiological concentrations, functions as a signaling molecule, whereas its excessive accumulation leads to oxidative stress in cells. An increase in its level may also result from the activity of superoxide dismutase (SOD), which constitutes the first line of enzymatic antioxidant defense by catalyzing the dismutation of the superoxide radical ($O_2^{\bullet -}$) into H_2O_2 and molecular oxygen. In turn, catalase (CAT), by decomposing H_2O_2 into water and oxygen, limits potential oxidative damage to cells.

The physiological level of H_2O_2 characteristic of control root meristems was maintained in roots incubated with the emulsifier (**Figure 3 A**), and these tissues exhibited comparable activities of both SOD (**Figure 3 B**) and CAT (**Figure 3 C**). Exposure of seedlings to $CdCl_2$ led to a pronounced disturbance of redox homeostasis, reflected by an approximately fourfold increase in H_2O_2 levels (**Figure 3 A**), accompanied by a significant rise in the activity of both antioxidant enzymes(**Figure 3 B, C**). In roots incubated in the presence of emulsified TO, the slight increase in H_2O_2 content was not statistically significant; however, SOD and CAT activities were moderately elevated (**Figure 3 A-C**),. In contrast, in roots treated simultaneously with TO and $CdCl_2$, H_2O_2 levels remained elevated relative to the control but were nearly twofold lower than in meristems exposed to $CdCl_2$ alone, indicating a clear reduction in ROS overproduction in the presence of the essential oil (**Figure 3 A**). Notably, these meristems displayed the highest activities of both SOD and CAT, exceeding control values as well as those observed in the $CdCl_2$-only treatment (**Figure 3 B, C**). These findings suggest that TO may enhance the cellular capacity for enzymatic ROS neutralization by intensifying the activity of both SOD and CAT.

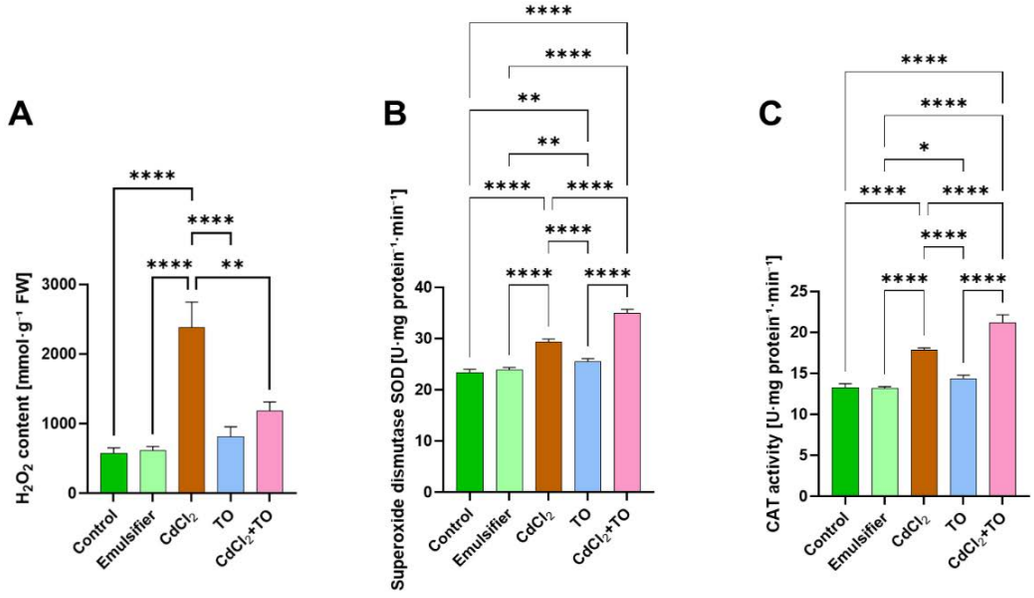

Figure 3. Hydrogen peroxide (H_2O_2) content (**A**), superoxide dismutase (SOD) (**B**) and catalase (CAT) (**C**) activity in *V. faba* primary roots after 24-hour incubation with water - Control, emulsifier, $CdCl_2$, TO, and a combination of $CdCl_2$ and TO. Data are presented as means ± SD from four biological replicates. Statistical significance: **** $p < 0.0001$, ** $p < 0.01$, * $p < 0.05$ (one-way ANOVA followed by Tukey's multiple comparison test).

Ascorbate Content and Ascorbate Peroxidase (APX) Activity

Ascorbate (AsA) and ascorbate peroxidase (APX) constitute central components of the ascorbate–glutathione cycle. APX catalyzes the reduction of H_2O_2 using AsA as an electron donor; therefore, changes in enzyme activity and AsA levels reflect the functional efficiency of this pathway under stress conditions. No significant differences were observed in either AsA content or APX activity between control root meristems and those treated with the emulsifier (**Figure 4 A, B**). Incubation of seedlings in the presence of $CdCl_2$ induced pronounced changes – AsA levels increased by approximately 50% (**Figure 4 A**), while APX activity rose by 35% relative to the control (**Figure 4 B**). Emulsified TO did not induce statistically significant changes in either parameter compared with the control; however, a slight, non-significant increase in AsA content was noted relative to the emulsifier-treated roots (**Figure 4 A, B**). The strongest response was recorded in roots treated with the $CdCl_2$ + TO mixture. In this variant, AsA content was twofold higher than in the control, whereas APX activity increased by nearly 75%. Both parameters also exceeded by approximately 30% the values observed in roots exposed to cadmium alone (**Figure 4 A, B**). These findings indicate an enhanced efficiency of the ascorbate cycle under the combined action of both factors.

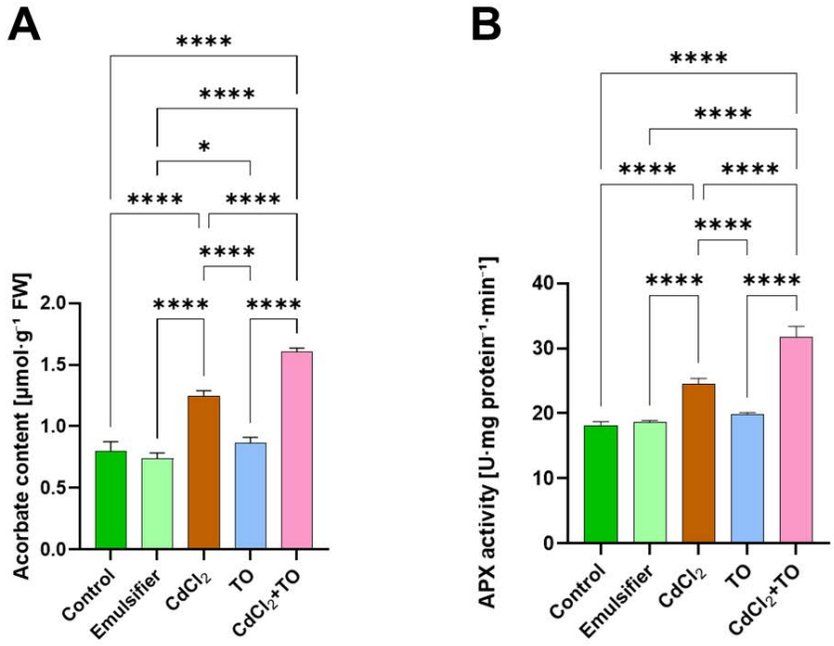

Figure 4. Ascorbate content (**A**) and ascorbate peroxidase (APX) activity (**B**) in *V. faba* primary roots after 24-hour incubation with water – Control, emulfisier, $CdCl_2$, TO, and a combination of $CdCl_2$ and TO. Data are presented as means ± SD from four biological replicates. Statistical significance: **** $p < 0.0001$, * $p < 0.05$ (one-way ANOVA followed by Tukey's multiple comparison test).

Glutathione Content and Glutathione Reductase (GR) Activity

Glutathione (GSH) acts in cells as a thiol-based redox buffer, participating in both the direct neutralization of ROS and in heavy metal chelation as well as phytochelatin synthesis. Changes in its level reflect cellular metabolic reprogramming under stress conditions. Glutathione reductase (GR) plays a key role in maintaining a high GSH/GSSG ratio by regenerating reduced GSH from its oxidized form (GSSG). Its activity determines the ability of cells to sustain redox potential over prolonged stress exposure.

GSH content in plants incubated in water and in those treated with the emulsifier was comparable (**Figure 5 A**), as was GR activity (**Figure 5 B**). Exposure of seedlings to $CdCl_2$ resulted in an almost 100% increase in the GSH pool and an over 30% increase in GR activity (**Figure 5 A, B**), indicating an elevated demand for reducing compounds, the need for GSH regeneration, and its involvement in metal detoxification processes. TO applied alone induced a moderate, approximately 40% increase in glutathione levels (**Figure 5 A**) and did not significantly affect GR activity in the analyzed meristems (**Figure 5 B**). The highest – nearly threefold higher compared with the control – GSH content was observed in roots treated simultaneously with $CdCl_2$ and TO (**Figure 5 A**). In this variant, the highest increase in GR activity was also recorded (approximately 45%), indicating an enhanced rate of the glutathione cycle (**Figure 5 B**).

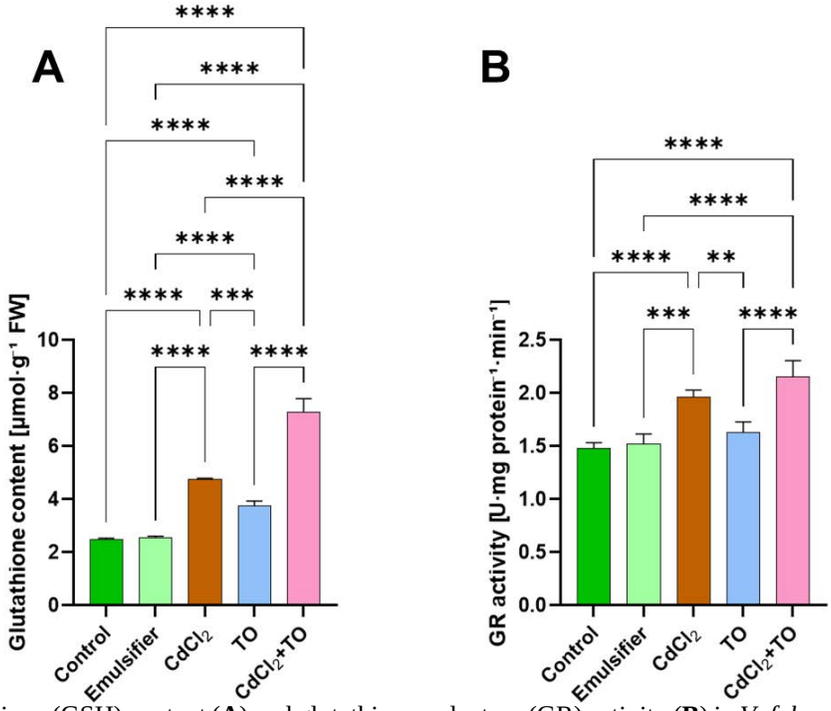

Figure 5. Glutathione (GSH) content (**A**) and glutathione reductase (GR) activity (**B**) in *V. faba* primary roots after 24-hour incubation with water - Control, emulfisier, $CdCl_2$, TO, and a combination of $CdCl_2$ and TO. Data are presented as means ± SD from four biological replicates. Statistical significance: **** $p < 0.0001$, *** $p < 0.001$, ** $p < 0.01$ (one-way ANOVA followed by Tukey's multiple comparison test).

Cysteine and Glutamylcysteine Content

Cysteine is the primary sulfur-containing amino acid involved in glutathione synthesis, whereas γ-glutamylcysteine is its direct precursor, formed in the first step of GSH biosynthesis catalyzed by γ-glutamylcysteine synthetase. Changes in the levels of both compounds may therefore reflect the intensity of the glutathione biosynthetic pathway and the potential redirection of sulfur metabolism under stress conditions.

Minor differences in cysteine and γ-glutamylcysteine contents in control and emulsifier-treated roots were not statistically significant (**Figure 6 A, B**). Exposure to $CdCl_2$ resulted in a marked (1.75-fold) increase in both cysteine levels and a twofold increase in γ-glutamylcysteine (**Figure 6 A, B**), suggesting enhanced substrate availability for the synthesis of glutathione and phytochelatins. Treatment with TO alone induced a moderate increase in cysteine content (by 25%; **Figure 6 A**) and a more pronounced, over threefold increase in γ-glutamylcysteine levels (**Figure 6 B**), which may indicate activation of the first step of GSH biosynthesis. The highest concentrations of both compounds were observed in seedlings treated simultaneously with $CdCl_2$ and TO – cysteine and γ-glutamylcysteine levels exceeded control values (twofold and nearly fivefold, respectively) and were also higher than those recorded after exposure to $CdCl_2$ alone (**Figure 6 A, B**).

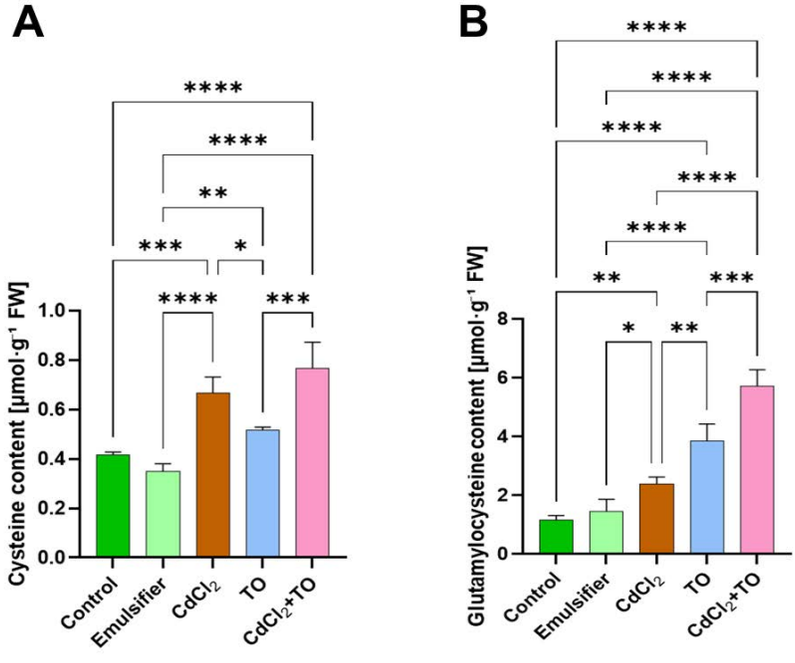

Figure 6. Cysteine (**A**) and γ-glutamylcysteine content **B**) in *V. faba* primary roots after 24-hour incubation with water - Control, emulfisier, $CdCl_2$, TO, and a combination of $CdCl_2$ and TO. Data are presented as means ± SD from four biological replicates. Statistical significance: **** $p < 0.0001$, *** $p < 0.001$, ** $p < 0.01$, * $p < 0.05$ (one-way ANOVA followed by Tukey's multiple comparison test).

Proline Content

Proline is a low-molecular-weight amino acid whose accumulation represents a characteristic component of plant responses to abiotic stress. Under conditions of disturbed homeostasis, it functions as an osmoprotectant, stabilizing protein structures. It also participates in the regulation of redox balance, as its biosynthesis involves the consumption of NADPH and the regeneration of $NADP^+$, thereby supporting the maintenance of cellular reducing power and limiting secondary ROS generation.

Proline content in root meristems of control and emulsifier-treated plants was comparable (**Figure 7**). Exposure of seedlings to $CdCl_2$ resulted in a marked 60% increase in proline accumulation relative to the control (**Figure 7**). TO applied alone induced a slight increase in proline levels of approximately 15% compared with the control (**Figure 7**). The highest proline accumulation was observed in roots treated simultaneously with $CdCl_2$ and TO, where its content was 2.6-fold higher than in the control and 1.6-fold higher than in plants exposed to cadmium alone (**Figure 7**). These results indicate enhanced activation of adaptive mechanisms associated with the maintenance of redox balance and cellular stability.

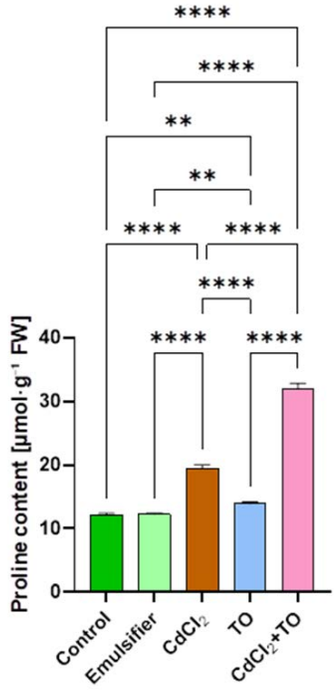

Figure 7. Proline content in *V. faba* primary roots after 24-hour incubation with water - Control, emulfisier, $CdCl_2$, TO, and a combination of $CdCl_2$ and TO. Data are presented as means ± SD from four biological replicates. Statistical significance: **** $p < 0.0001$, ** $p < 0.01$ (one-way ANOVA followed by Tukey's multiple comparison test).

Phytochelatin (PC) Content

Phytochelatins (PCs) are low-molecular-weight thiol peptides synthesized in plants in response to the presence of heavy metals such as cadmium. They are formed in an enzymatic reaction catalyzed by phytochelatin synthase using glutathione (GSH) as a substrate. Their general structure is based on repeating γ-Glu–Cys units terminated with a glycine residue, $(\gamma\text{-Glu–Cys})_n$–Gly, where the number of repeats (n) determines the length of the peptide chain. The designations PC2, PC3, PC4, and PC5 correspond to peptides containing 2, 3, 4, and 5 γ-Glu–Cys units, respectively. As the chain length increases, the number of thiol groups (-SH) increases as well, thereby enhancing the potential capacity for metal ion binding. Under cadmium stress, PC2 and PC3 typically predominate, representing the primary and most rapidly synthesized phytochelatin fractions. Longer forms (PC4 and PC5) arise through further chain elongation and are usually present in lower amounts, playing a supplementary role under stronger or prolonged metal stress conditions.

In root meristems of control plants and those incubated with the emulsifier or emulsified TO, phytochelatin levels remained below the detection threshold, confirming that their synthesis is primarily induced by the presence of heavy metals. Exposure of plants to $CdCl_2$ resulted in a significant increase in all analyzed PC fractions (PC2–PC5) compared with the control. The quantitative structure revealed a clear predominance of PC2, followed by PC3, with markedly lower levels of PC4 and PC5 (**Figure 8**), suggesting that under the applied $CdCl_2$ concentration, the detoxification response is mainly based on shorter phytochelatin forms. In root meristems treated simultaneously with $CdCl_2$ and TO, an increase in phytochelatin content was also observed relative to the control, and the distribution pattern of their fractions was similar to that recorded under cadmium treatment alone. However, their levels were approximately 30% lower than in cells exposed exclusively to $CdCl_2$. Significant differences between the treatments in which these peptides were detected were recorded only for the PC2 and PC3 fractions (**Figure 8**).

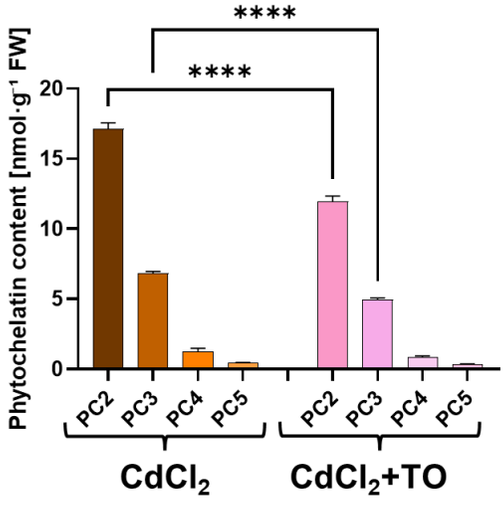

Figure 8. Phytochelatin oligomers content (PC2–PC5) in *V. faba* primary roots after 24-hour incubation with $CdCl_2$ and with a combination of $CdCl_2$ and TO. Only series with detectable phytochelatins are shown. Data are presented as means ± SD from four biological replicates. Statistical significance: **** $p < 0.0001$ (one-way ANOVA followed by Tukey's multiple comparison test).

Lipid Peroxidation

Malondialdehyde (MDA) is one of the main products of lipid peroxidation and serves as an indicator of oxidative damage to cellular membranes. Its level reflects the extent of oxidative stress and lipid degradation in plant cells.

In root meristems of control plants and those treated with the emulsifier, MDA content was comparable (**Figure 9**), indicating the absence of significant oxidative stress and the stability of cellular membranes under emulsifier treatment. Incubation of plants with $CdCl_2$ resulted in a fourfold increase in MDA levels (**Figure 9**), reflecting enhanced lipid peroxidation in response to metal-induced stress. The slight increase in MDA observed in meristems treated with TO alone was not statistically significant compared with the control (**Figure 9**). In roots treated simultaneously with $CdCl_2$ and TO, MDA levels were twofold higher than in the control but significantly lower than in seedlings exposed to $CdCl_2$ alone (**Figure 9**). These results suggest that the presence of TO mitigates lipid peroxidation and alleviates oxidative stress, thereby reducing membrane damage induced by excess H_2O_2 and other ROS.

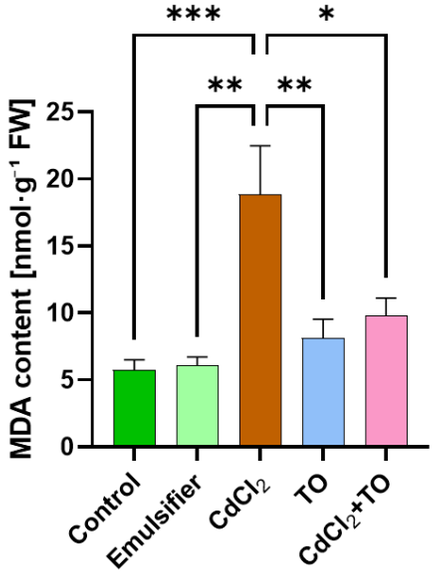

Figure 9. Level of lipid peroxidation in *V. faba* primary roots after 24-hour incubation with water - Control, emulfisier, $CdCl_2$, TO, and a combination of $CdCl_2$ and TO. Data are presented as means ± SD from four biological replicates. Statistical significance: *** $p < 0.001$, ** $p < 0.01$, * $p < 0.05$ (one-way ANOVA followed by Tukey's multiple comparison test).

Assessment of DNA Fragmentation by TUNEL Assay

The observed increase in ROS levels in the meristems, changes in antioxidant system activity, and particularly the enhancement of lipid peroxidation prompted an assessment of whether disturbances in redox homeostasis translate into damage to genetic material. For this purpose, the TUNEL assay was applied to detect DNA fragmentation by identifying free 3'-OH ends generated as a result of single-strand (SSB) and double-strand (DSB) DNA breaks (**Figure 10 A**).

In control meristems (**Figure 10 B**) and in those treated with the emulsifier (**Figure 10 C**), no clear fluorescent signal was detected; non-fluorescent nuclei were observed. Only approximately 2% of cells exhibited very weak fluorescence at the detection threshold (**Figure 10 G**), indicating that the emulsifier had no significant effect on DNA integrity. In root meristems exposed to $CdCl_2$, a distinct fluorescent signal was observed in the nuclei (**Figure 10 D**), indicating DNA fragmentation. Quantitative analysis showed that approximately 37% of cells exhibited signs of DNA damage (**Figure 10 G**). In meristems treated with emulsified TO (**Figure 10 E**) and in those exposed simultaneously to $CdCl_2$ and TO (**Figure 10 F**), the microscopic image was comparable to the control, and a slight increase in the number of cells showing fluorescence at the detection limit was not statistically significant (**Figure 10 G**). These results indicate a significant reduction in DNA fragmentation in the presence of TO compared with cadmium treatment alone.

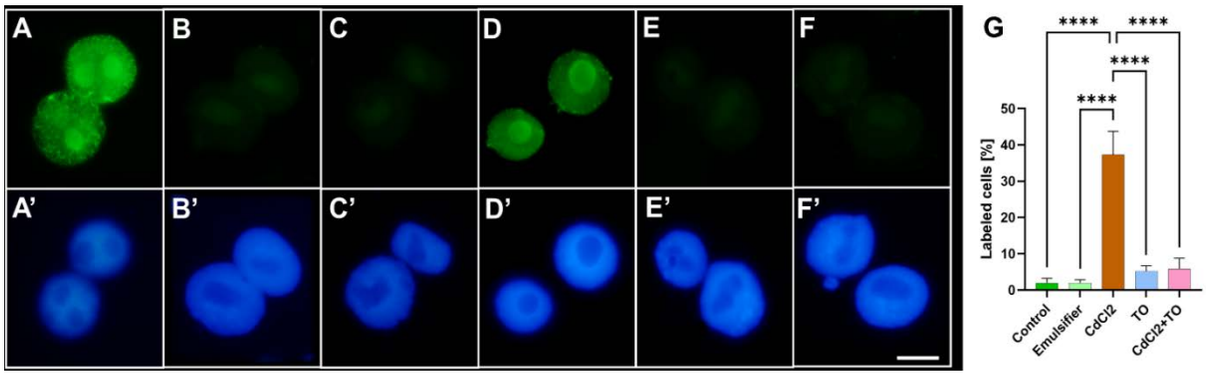

Figure 10. Detection of DNA breaks using the TUNEL assay in nuclei of root meristem cells of *V. faba* (**A–F**) after 24-hour incubation with water - Control (**B**), emulfisier (**C**), $CdCl_2$ **(D)**, TO (**E**), and a combination of $CdCl_2$ and TO (**F**). Positive control (DNase I treatment) is shown in (**A**). Corresponding DNA staining with DAPI is shown in (**A'–F'**). Scale bar: 10 µm. Frequencies of TUNEL-positive nuclei in root meristem cells are shown in (**G**). Data are presented as mean indices ± SD from five biological replicates. Statistical significance: **** $p < 0.0001$ (one-way ANOVA followed by Tukey's multiple comparison test).

Ultrastructural Analyses

In control cells, as well as in cells treated with the emulsifier alone, the cell wall exhibited a typical ultrastructural organization (**Figure 11 A–C**). A distinct electron-dense middle lamella and a slightly more electron-lucent primary cell wall were clearly visible, both showing a uniform and well-ordered fibrillar arrangement. Electron-dense plasmodesmata containing strands of endoplasmic reticulum were present within the wall (**Figure 11 A–B**). The slightly undulated wall contour locally formed protrusions corresponding to sites of cell wall component deposition, where secretory vesicles fused with the plasma membrane and released their contents into the apoplast (**Figure 11 B, C**). Along the entire wall surface, the plasma membrane remained closely appressed to the inner wall layer. Fibrous precursors of cell wall components were transported by secretory vesicles derived from well-developed and active Golgi apparatus (**Figure 11 D**). Mitochondria contained loosely arranged cristae and a clearly visible intermembrane space (**Figure 11 C, F, G**), while plastids contained several small or larger starch grains, single plastoglobules, and a homogeneous stroma with a few short invaginations of the inner membrane (**Figure 11 E, F**). Numerous ribosomes were present in both types of organelles. Vacuoles surrounded by regular membranes showed an electron-lucent content, and small myelin bodies were occasionally observed. The nucleus, enclosed by a double nuclear envelope with distinct nuclear pores, contained both dispersed electron-lucent and compact electron-dense chromatin arranged in a mosaic pattern (**Figure 11 H, I**). The nucleolus displayed a dense fibrillar component surrounding fibrillar centers and a densely packed granular component, indicating active ribosome biogenesis (**Figure 11 J**). Numerous ribosomes were also present freely in the cytoplasm and associated with the membranes of the endoplasmic reticulum forming a network of channels (**Figure 11 A–I**).

The overall ultrastructural organization of cells treated with TO was largely comparable to that observed in control cells. The cell wall retained a similar architecture; however, the middle lamella appeared slightly looser and less distinctly separated, resulting in a less clearly defined boundary with the primary cell wall and giving both layers a more homogeneous appearance (**Figure 11 K–M**). The most noticeable changes concerned the endoplasmic reticulum, which, particularly in regions adjacent to the cell wall, formed a highly developed network of electron-lucent channels with markedly dilated cisternae often terminating in characteristic vesicular expansions (**Figure 11 M, N**). Other organelles and cellular structures showed no obvious differences compared with control cells.

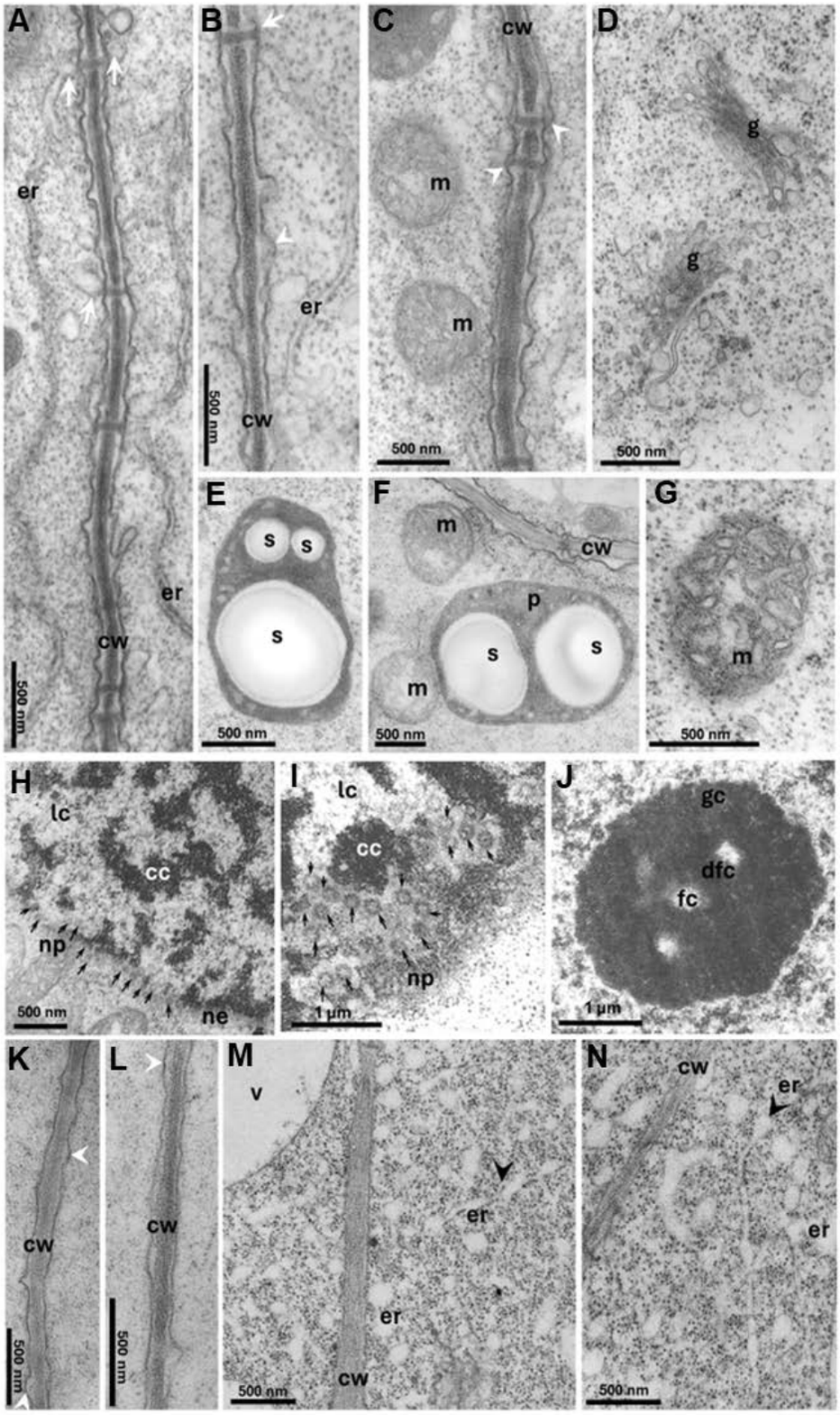

Figure 11. **Ultrastructure of root meristem cells of *V. faba* after 24 h of incubation in water – Control (A–J) and thyme essential oil – TO (K–N);** cw – cell wall, er – endoplasmic reticulum, g – Golgi apparatus, m – mitochondria, p – plastid, s – starch, cc – condensed chromatin, lc – loose chromatin, ne – nuclear envelope, np – nuclear pores, dfc – dense fibrillar component, fc – fibrillar center, gc – granular component, v – vacuole. White arrows indicate strands of endoplasmic reticulum passing through plasmodesmata in the cell wall. White arrowheads indicate protrusions corresponding to sites of cell wall component deposition. Black arrows indicate nuclear pores, while black arrowheads indicate vesicles and the lumen of endoplasmic reticulum channels.

In cells exposed to cadmium, the ultrastructure of the cell wall underwent pronounced alterations and displayed a heterogeneous appearance (**Figure 12 A–F**). Both wall layers showed uneven and disordered distribution of components (**Figure 12 A–E**), and in some regions the typical fibrillar structure was markedly blurred (**Figure 12 F**). The electron-dense middle lamella locally formed relatively compact, dark but narrow bands (**Figure 12 A, D**), often discontinuous (**Figure 12 B**), whereas in other regions it appeared wider, diffuse, and lacked a clear boundary with the primary cell wall (**Figure 12 F**). Darker plasmodesmata with a clearly reduced number of endoplasmic reticulum channels, as well as locally electron-dense deposits in their vicinity, were observed within the cell wall (**Figure 12 A, C, D**). The cell wall margin was distinctly undulated, with electron-lucent protrusions, and the plasma membrane was locally poorly defined (**Figure 12 E, F**). Golgi dictyosomes were clearly narrowed, and the associated secretory vesicles were sparse and mostly electron-lucent, occasionally containing single fibrillar precursors of cell wall components (**Figure 12 F, G**). Mitochondria exhibited a strongly reduced cristae network, with extensive electron-lucent regions of the matrix in their central part (**Figure 12 H, K, P**). Plastids were generally poor in starch grains or most often lacked them entirely (**Figure 12 I–K**). Their interior contained plastoglobules and more developed, elongated invaginations of the inner membrane (**Figure 12 J, L**). The membranes surrounding organelles were locally poorly defined and lacked sharply outlined edges, and the number of ribosomes within them was markedly reduced. Vacuoles were more numerous and larger, and their membranes were locally irregular with numerous invaginations. Their interior contained membranous structures and frequently amorphous or slightly fibrillar material (**Figure 12 M, N**). Numerous myelin bodies and autophagosome-like structures, appearing as irregular concentric membranes enclosing fragments of cytoplasm, were visible in the cytoplasm (**Figure 12 O**). The cytoplasm was relatively loose and clearly poor in ribosomes, and the endoplasmic reticulum network, with faintly visible membranes, was poorly developed (**Figure 12 K**). Cell nuclei, characterized by a clear predominance of broad regions of strongly condensed chromatin, were surrounded by a poorly defined double envelope with numerous pores showing an electron-dense but indistinct structure (**Figure 12 P, R**). Small nucleolar vacuoles were present in the nucleoli; the fibrillar component was strongly reduced or absent, whereas the granular component remained relatively densely packed (**Figure 12 S**).

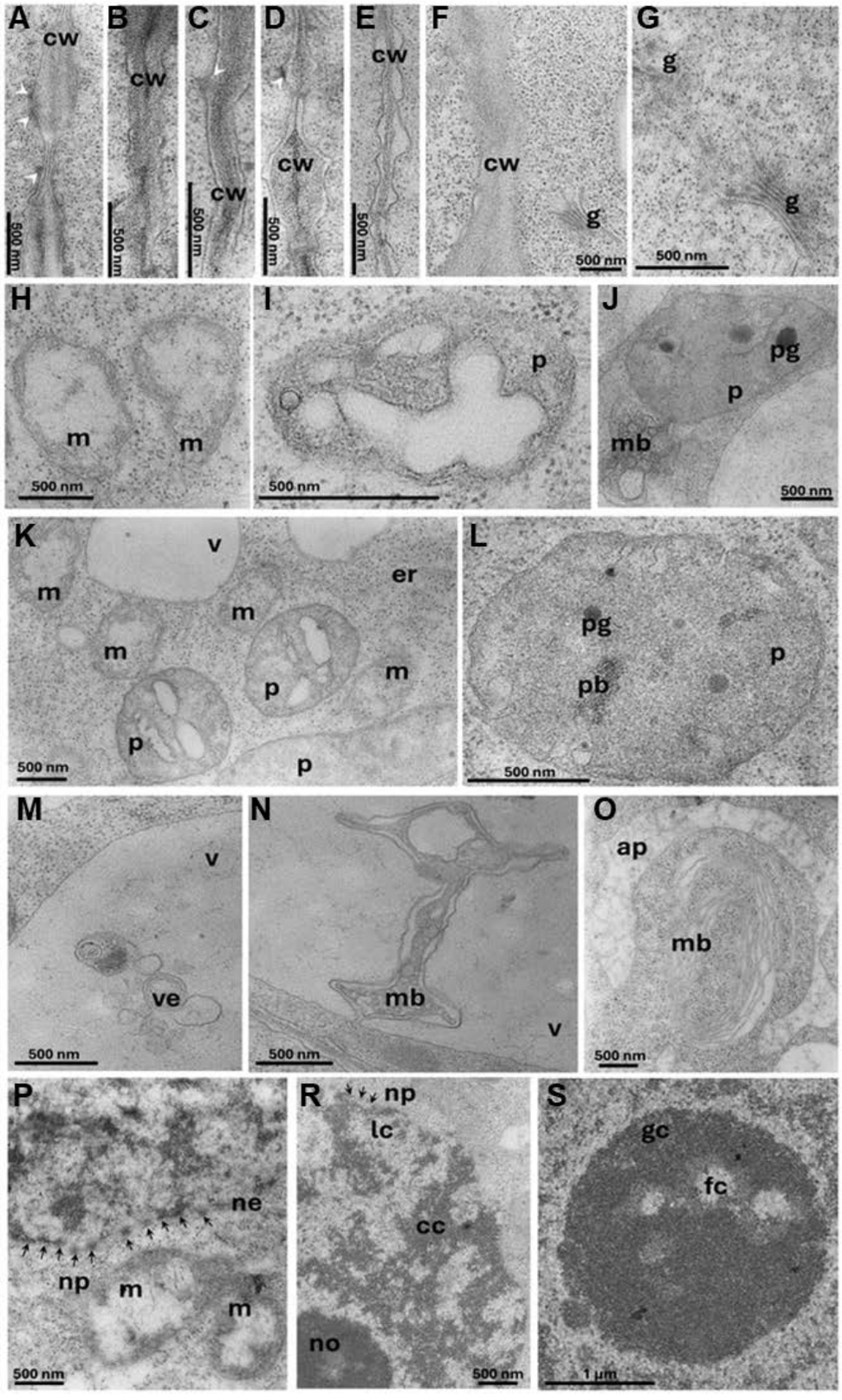

Figure 12. Ultrastructure of root meristem cells of *V. faba* after 24 h of incubation in $CdCl_2$ (A–S); cw – cell wall, er – endoplasmic reticulum, g – Golgi apparatus, v – vacuole, m – mitochondria, p – plastid, pb – prolamellar body, pg – plastoglobule, mb – myelin body, ve – vesicle, ap – autophagosome, , cc – condensed chromatin, lc – loose chromatin, ne – nuclear envelope, np – nuclear pores, no – nucleolus, fc – fibrillar center, gc – granular component. White arrowheads indicate electron-dense deposits within the cell wall and in the vicinity of plasmodesmata. Black arrows indicate nuclear pores.

In cells exposed to the cadmium–TO mixture, the cell wall appeared more compact, resembling the control cells to a greater extent, although it still exhibited cadmium-induced alterations, albeit less pronounced. The relatively broad middle lamella and the remaining regions of the cell wall contained densely packed fibrillar material arranged in a more ordered, parallel manner. Undulations at the cell wall edges were less frequent, and protrusions were filled with fibrillar material rather than electron-lucent. Distinct plasmodesmata were present, and the plasma membrane remained closely appressed to the wall in most regions (**Figure 13 A, B**). Well-developed Golgi apparatuses contained numerous large secretory vesicles filled with clearly visible fibrillar precursors of cell wall components (**Figure 13 C**). Mitochondria exhibited loosely arranged cristae, and some contained small electron-lucent regions in the central matrix, within which a delicate network of fibrils was visible (**Figure 13 C, D, G, H**). Plastids, despite a slightly more developed membrane network, also contained starch grains of varying size and occasional plastoglobules. Their double envelopes were mostly well defined (**Figure 13 E, F, I**). Vacuoles were relatively small and numerous, containing minor amounts of fibrillar material. Myelin bodies were occasionally observed in cytoplasm. The cytoplasm was relatively dense and rich in ribosomes, and the endoplasmic reticulum formed a well-developed network of narrow, electron-gray, content-filled channels without excessive cisternal dilations or pronounced accumulation near the cell wall; these channels were densely studded with ribosomes (**Figure 13 C, D**). Cell nuclei, despite containing regions of strongly condensed chromatin, exhibited a mosaic-like arrangement similar to control cells (**Figure 13 M, N**). The nuclear envelope was clearly defined, with a well-visible intermembrane space of electron density comparable to the endoplasmic reticulum channels (**Figure 13 M**), and contained numerous sharply outlined nuclear pores (**Figure 13 J**). Nucleoli contained numerous, often large, nucleolar vacuoles (**Figure 13 L, N**). The fibrillar component was present but limited and not always clearly visible, whereas the granular component remained relatively dense, (**Figure 13 K, L, N**).

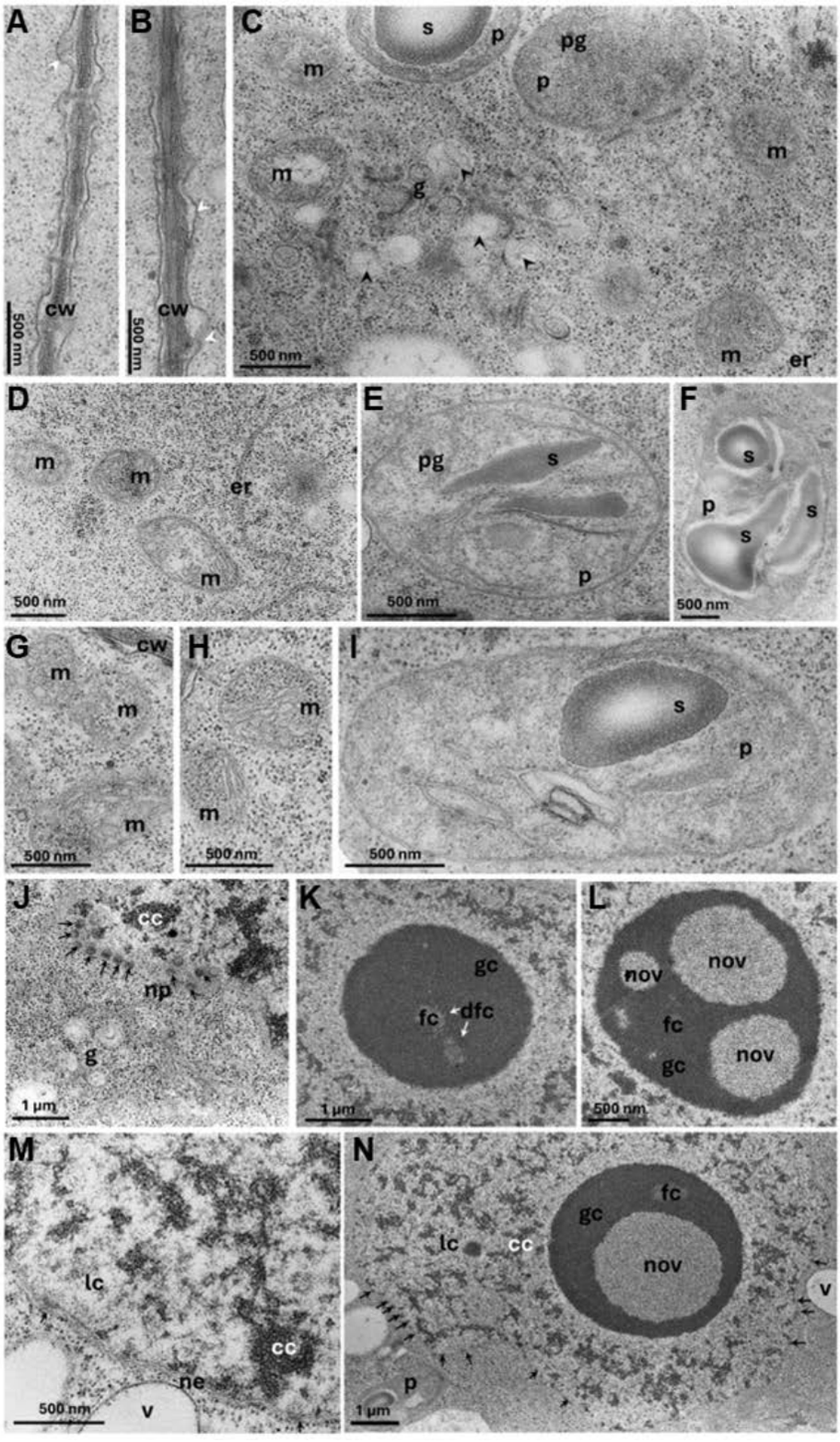

Figure 13. Ultrastructure of root meristem cells of *V. faba* after 24 h of incubation in the combination of $CdCl_2$ and thyme essential oil – TO (A–N); cw – cell wall, er – endoplasmic reticulum, g – Golgi apparatus, v – vacuole, m – mitochondria, p – plastid, s – starch, pg – plastoglobule, cc – condensed chromatin, lc – loose chromatin, ne – nuclear envelope, np – nuclear pores, fc – fibrillar center, gc – granular component, dfc – dense fibrillar component, nov – nucleolar vacuole. White arrowheads indicate protrusions corresponding to sites of cell wall component deposition. Black arrows indicate nuclear pores. White arrows indicate the dense fibrillar component within the nucleolus.

Discussion:

Plant responses to cadmium stress are inherently multi-layered, encompassing coordinated processes of metal transport and distribution, perturbations in redox homeostasis, and activation of both detoxification and adaptive mechanisms (Hu *et al.*, 2025). Once inside the cell, cadmium induces a range of functional and structural disruptions (Cuypers *et al.*, 2023), the severity of which closely correlates with the level of metal accumulation in plant tissues (Luo *et al.*, 2024). This aspect is particularly critical in the root meristems of seedlings, which represent the primary interface between young plants and their environment.

Within the stress-inducing system examined here, thyme essential oil (TO) constitutes an additional, biologically active component. TO is a complex mixture of volatile secondary metabolites, predominantly phenolic monoterpenes (Gocek-Szczurtek *et al.*, 2025a). The chemical heterogeneity of this mixture prevents the attribution of its biological activity to any single constituent. Rather, the overall effect of TO results from the integrated action of its components, encompassing both potential synergistic interactions and complementary molecular mechanisms (Youdim *et al.*, 2002). Due to their functional groups capable of interacting with biomolecules and their variable lipophilicity, these compounds can influence multiple aspects of cellular function - from modulating the physicochemical properties of membranes and stabilizing or scavenging reactive oxygen species (ROS), to affecting redox signaling and the expression of stress-responsive genes (Yanishlieva *et al.*, 1999; Ferreira *et al.*, 2016; Sun *et al.*, 2024). Our previous work further demonstrates that TO contributes to a more stable regulation of nuclear processes and cell cycle dynamics in cadmium-exposed plants (Gocek-Szczurtek *et al.*, 2025a; Gocek-Szczurtek *et al.* 2025b; Gocek-Szczurtek *et al.*, 2026). Consequently, incorporating essential oil into the experimental system necessitates interpreting plant responses not only through the lens of classical heavy metal stress but also in terms of potential modulation of antioxidant defenses and detoxification mechanisms by an additional, biologically active factor.

Mechanistic Insights into the Modulation of Cadmium Accumulation

In the experimental system employed, based on hydroponic culture, strict control of nutrient solution composition enables the analysis of changes in Cd content while eliminating factors characteristic of soil environments, such as metal sorption to organic matter or complexation by mineral fractions (Kubier *et al.*, 2019). Under such conditions, Cd accumulation in roots reflects the combined effects of physicochemical processes in the solution, the properties of cellular membranes and membrane transporters, as well as intra-tissue defense mechanisms regulating metal tolerance (Noor *et al.*, 2024). Our analyses demonstrated that simultaneous exposure of seedlings to Cd and TO resulted in an approximately 38% reduction in cadmium accumulation compared with plants treated with Cd alone, suggesting that TO may modulate processes responsible for metal uptake and/or accumulation in plant tissues. However, before attributing this effect solely to biological mechanisms, the potential influence of the physicochemical properties of the solution itself must be considered.

Due to the lipophilic nature of essential oils, their direct mixing with water typically leads to the formation of unstable systems in which the oil phase separates from the aqueous phase (Dhifi *et al.*,

2016; Liao *et al.*, 2021). Therefore, emulsifiers are commonly used to obtain homogeneous and stable dispersions (Donsì and Ferrari, 2016; Pavoni *et al.*, 2020; Verdeguer *et al.*, 2020). In our hydroponic system, TO was stabilized using a non-ionic ethoxylated surfactant, facilitating the formation of a dilute oil-in-water (O/W) colloidal system. Such structures are characterized by the presence of oil droplets surrounded by a surfactant layer and an expanded interfacial area, the properties of which differ from those of the bulk aqueous phase (Kumar *et al.*, 2019). At the preliminary stage, an additional experimental series was included, involving simultaneous exposure of plants to Cd and the emulsifier alone. In this group, growth parameters and the mitotic index were assessed. No significant differences were observed compared with plants treated with Cd alone (data not shown); therefore, this series was not included in further analyses. The absence of significant differences between Cd-treated plants and those exposed to Cd together with the emulsifier alone indicates that the observed reduction in cadmium accumulation in the presence of TO cannot be attributed to the surfactant itself.

It is important to emphasize that a solution containing only the emulsifier and one containing both surfactant and an oil phase are not physicochemically equivalent (Yakoubi *et al.*, 2021). A non-ionic ethoxylated emulsifier in water forms micellar structures (Born *et al.*, 2026), whereas the addition of an oil phase leads to the formation of stabilized oil droplets, thereby altering the architecture of the solution and the nature of interfacial microenvironments (Silva *et al.*, 2015). Although Cd^{2+}, as a hydrophilic ion, remains in the aqueous phase, reorganization of the colloidal system may modify its local activity and diffusion conditions in the rhizosphere. This, in turn, may limit metal influx into the apoplast and its subsequent transport into the symplast, despite an unchanged total cadmium concentration in the solution (Berkelaar and Hale, 2003; Degryse *et al.*, 2006; Krzesłowska, 2011). Thus, the reduction in cadmium accumulation may be associated both with modifications of the physicochemical properties of the medium in the presence of TO and - more importantly, as discussed below - with the direct action of its bioactive constituents. Support for a biological, rather than purely physicochemical, basis of the observed effect is provided by reports of reduced Cd accumulation following treatment with other compounds known to support antioxidant systems, such as organic acids (e.g., malic or tartaric acid) (Shabbir *et al.*, 2025). These compounds are hydrophilic, do not form separate phases in solution, and lack the physicochemical properties typical of lipid-based substances that could alter surface tension or micellar structure. This suggests that the reduction in Cd uptake may result from an active metabolic response of plants, involving regulation of transporters, thiol metabolism, and redox homeostasis.

Thymol, the major constituent of TO, together with carvacrol, are highly lipophilic compounds that readily insert into lipid bilayers, leading to modifications of their physical properties, including fluidity, lipid packing, and permeability (Sánchez *et al.*, 2004). These phenolic monoterpenes localize within the hydrophobic core of the membrane, in close proximity to fatty acid chains, i.e., in a region particularly susceptible to the initiation and propagation of lipid peroxidation chain reactions (Ferreira *et al.*, 2016). Their direct presence within the bilayer may therefore contribute to the local stabilization of membrane organization. Indeed, liposomal model studies have demonstrated that these compounds effectively inhibit phospholipid peroxidation by acting as chain-breaking antioxidants (Aeschbach *et al.*, 1994). Accordingly, the decrease in malondialdehyde (MDA) levels observed in our experiments under combined $CdCl_2$ and TO treatment may, at least in part, reflect a direct, localized protective effect within

the lipid bilayer itself, rather than solely a consequence of an overall reduction in oxidative stress. At the same time, alterations in the lipid environment of the membrane may have important functional consequences. Evidence suggests that thymol can modulate ion channel activity by altering membrane physical properties. For instance, Szentandrássy *et al.* (2003) demonstrated a concentration-dependent inhibition of Ca^{2+} conductance in mammalian muscle cells. In plant cells, Cd^{2+} enters primarily via non-selective divalent cation transporters and Ca^{2+}-permeable channels (Huang *et al.*, 2020). Thus, thymol-induced stabilization and reorganization of the lipid environment may indirectly modulate the activity of membrane proteins involved in divalent cation transport, potentially reducing the efficiency of Cd^{2+} influx into the cell.

The observed decrease in MDA levels under combined Cd and TO treatment should, however, be interpreted as the result of both local and systemic effects. Simultaneous exposure of plants to these factors led to the enhancement of both enzymatic and non-enzymatic defense mechanisms, accompanied by an overall reduction in oxidative stress, which further limited the initiation of lipid peroxidation. This aspect is particularly relevant in the context of the bidirectional relationship between oxidative stress and heavy metal toxicity. Elevated ROS levels increase membrane permeability, disrupt selectivity, and promote deregulation of ion transport systems, thereby potentially enhancing Cd^{2+} influx into cells (Pei *et al.*, 2000; Perfus-Barbeoch *et al.*, 2002; Zheng *et al.*, 2025). A reduction in H_2O_2 levels and reinforcement of antioxidant defenses following TO supplementation may have disrupted this feedback loop: improved redox balance limited membrane damage and prevented excessive increases in permeability, thereby reducing stress-induced metal influx. Taken together, these findings strongly suggest that TO acts via a dual mechanism: (1) directly, through the insertion of thymol and carvacrol into the lipid bilayer and consequent structural stabilization, and (2) indirectly, through a global reduction in ROS levels and enhancement of antioxidant capacity, preventing oxidative alterations in membrane permeability and transporter function. Such an integrated mode of action, targeting both membrane structure and redox regulation, provides a coherent explanation for the observed reduction in MDA levels as well as the decreased Cd accumulation in roots, and is consistent with the cellular ultrastructure revealed by transmission electron microscopy (TEM). In cells exposed to both Cd and TO, the plasma membrane, nuclear envelope, and organelle membranes remained largely continuous and well-defined, in contrast to the locally blurred or microdamaged membranes observed under Cd treatment alone. This preservation of membrane integrity enabled the maintenance of proper organization of the plasmalemma, nuclear envelope, mitochondrial cristae, and plastid structure, thereby sustaining organelle functionality and efficient metabolism despite the presence of the stress factor.

Although mechanisms related to metal bioavailability in the solution and its transport across the plasma membrane are most likely the dominant factors underlying the observed reduction in cadmium accumulation in roots following the application of emulsified TO, the contribution of cell wall–associated processes as a supporting mechanism cannot be excluded. The cell wall plays a significant role in Cd accumulation, particularly in the roots of plants exhibiting tolerance to this heavy metal (Parrotta, 2015; Yu *et al.*, 2020). The principal cell wall polysaccharides, pectins, hemicelluloses, and cellulose, determine its physical properties, including porosity and permeability, thereby influencing ion movement within the apoplastic space (Cheng *et al.*, 2025). The presence of numerous negatively

charged functional groups, primarily carboxyl groups in pectins, confers the ability to electrostatically bind divalent cations, including Cd^{2+} (Yu *et al.*, 2020). Consequently, the cell wall may function as an ion-buffering compartment, limiting the flux of metal ions reaching the plasma membrane and reducing their availability to membrane transporters.

An additional regulatory component may involve cadmium-induced callose deposition (Gzyl *et al.*, 2015; Srivastava *et al.*, 2018). The accumulation of β-1,3-glucan at plasmodesmata reduces their diameter and permeability, thereby restricting symplastic transport between cells (O'Lexy *et al.*, 2018; Wu *et al.*, 2018). Although callose itself does not exhibit strong sorptive capacity for Cd^{2+}, its increased deposition may act as a physical barrier (Amsbury *et al.*, 2018), hindering both the uptake and subsequent distribution of the metal within young roots**.** Our ultrastructural analyses revealed pronounced alterations in cell wall architecture under cadmium exposure, manifested as irregular organization of fibrillar components. However, no clear cadmium deposits, distinctly constricted plasmodesmata, or unequivocal callose accumulations were observed. Instead, cells exposed to Cd exhibited a markedly reduced network of endoplasmic reticulum channels traversing and surrounding plasmodesmata, along with localized electron-dense regions in the cell wall at the sites of their emergence. These features may indicate reduced plasmodesmatal permeability, although they do not allow for definitive conclusions regarding complete blockage.

Support for the interpretation that, in the presence of TO, stabilization and remodeling of the cell wall may contribute to limiting Cd distribution within the root is provided by the findings of Li *et al.* (2025), who demonstrated that thymol reduces the activity of cell wall–degrading enzymes. This results in increased levels of cellulose and protopectins, along with reduced solubilization of pectins, thereby promoting the maintenance of mechanical integrity and functional properties of the wall and potentially reinforcing the apoplastic barrier. Consistent with this, our ultrastructural observations of cells treated with both Cd and TO revealed thicker and more regularly organized cell walls, with densely packed fibrillar material in the middle lamella and distinct fibrillar structures forming protrusions along the wall margins. In addition, we observed intensified production of cell wall precursors, evident as prominent secretory vesicles within the Golgi apparatus, likely associated with wall reinforcement processes; such features were not detected in cells exposed to cadmium alone. Nevertheless, this mechanism alone does not appear sufficient to fully account for the observed decrease in total Cd content in the tissue, but rather likely represents a complementary component acting in concert with processes that limit metal influx into the root.

Redox Imbalance and Compensatory Activation of Antioxidant Defenses under Cadmium Stress

In plant cells, the maintenance of redox homeostasis relies on a dynamic balance between the generation of reactive oxygen species (ROS) and their neutralization by an integrated system of enzymatic and non-enzymatic antioxidants (Burton and Jauniaux, 2011). Under cadmium stress, this balance is disrupted (**Figure 14**). Although Cd does not directly participate in Fenton reactions, it indirectly enhances ROS production by interfering with electron transport chains in chloroplasts and mitochondria, displacing essential cations from enzyme active sites, and destabilizing cellular membranes (Bi *et al.*, 2009; Rodríguez-Serrano *et al.*, 2009; Cuypers *et al.*, 2010; Keunen *et al.*, 2011). These effects were reflected

in our ultrastructural analyses as pronounced alterations in the organization of mitochondria and plastids. Impaired mitochondrial performance likely led to reduced efficiency of cellular respiration and disturbances in cellular energy balance, thereby promoting the mobilization of carbon reserves stored in plastids (Busi *et al.*, 2011). The near-complete depletion of starch content, accompanied by the reorganization of internal membrane systems within plastids, may therefore reflect a metabolic reprogramming of meristematic cells in response to oxidative stress (Zechmann, 2019). Stress signals perceived at the cytoplasmic level in meristematic cells also extended to the nucleus, where they induced increased chromatin condensation, thereby protecting genetic material and markedly reducing transcriptional activity. This was evident as a reduction in the dense fibrillar component surrounding the fibrillar centers of the nucleolus. A decrease in transcriptional activity was also confirmed in our previous analyses using a fluorescence-based assay with 5-ethynyl uridine (EU) *(*Gocek-Szczurtek *et al.*, 2025b).

The first functional line of defense against oxidative stress involves the conversion of superoxide anion ($O_2^{\bullet-}$) into hydrogen peroxide (H_2O_2), catalyzed by superoxide dismutase (SOD). Under stress conditions, including heavy metal exposure, increased SOD activity is frequently accompanied by elevated H_2O_2 levels, reflecting a redistribution of oxidative pressure from superoxide radicals toward the regulation of hydrogen peroxide (Alscher, 2002; Mittler, 2002; Kumar *et al.*, 2008; Zhang *et al.*, 2010; Pandey and Singh, 2012). This mechanism does not imply the elimination of oxidative stress, but rather its reorganization within the redox network. In this context, the activation of SOD observed in $CdCl_2$-treated seedlings, accompanied by H_2O_2 accumulation, is consistent with the classical model of an early enzymatic response to superoxide overproduction. This observation aligns with our previous findings demonstrating elevated superoxide levels in cadmium-exposed tissues (Gocek-Szczurtek *et al.*, 2025a), suggesting that SOD induction represents a secondary response to an initial disturbance of redox balance. Functionally, this indicates that the initial step of ROS detoxification - the conversion of $O_2^{\bullet-}$ to H_2O_2 - was efficiently activated; however, the resulting hydrogen peroxide required further coordinated detoxification involving downstream components of the antioxidant system.

At this stage, the interplay between catalase (CAT) and ascorbate peroxidase (APX) becomes critical. CAT is responsible for the rapid, high-capacity decomposition of H_2O_2 under conditions of its elevated concentration, whereas APX operates in close association with the ascorbate–glutathione cycle (Pukacka and Ratajczak, 2006; Corpas *et al.*, 2024). The concurrent increase in the activity of both enzymes in response to $CdCl_2$ observed in our study is consistent with reports indicating that cadmium stress induces activation of both the catalase pathway and the ascorbate-dependent H_2O_2-scavenging system in plant species such as maize (*Zea mays* L.) (Kumar *et al.*, 2008) and pea (*Pisum sativum* L.) (Dixit *et al.*, 2001).

The elevated activities of CAT and APX suggest that cells engage parallel pathways for H_2O_2 removal in an attempt to limit its accumulation. Activation of the ascorbate-dependent pathway simultaneously implies an increased demand for ascorbate as an electron donor in the APX-catalyzed reduction of H_2O_2 (Karyotou and Donaldson, 2005). Accordingly, the increase in ascorbate levels observed in our experiments can be interpreted as a compensatory response aimed at maintaining the efficiency of this

enzymatic detoxification system. Our results are in agreement with observations in barley (*Hordeum vulgare* L.) seedlings exposed to a range of cadmium concentrations (10–300 μM), where a concurrent increase in APX activity and ascorbate (AsA) pool size was reported (Jócsák *et al.*, 2020). Since ascorbate oxidation during APX-mediated reactions necessitates the involvement of glutathione (GSH) in its regeneration, the observed increase in glutathione reductase (GR) activity and elevated GSH levels in $CdCl_2$-treated seedlings can be regarded as an essential extension of this response (Foyer and Kunert, 2024; Noctor, 2025). By catalyzing the reduction of oxidized glutathione (GSSG) using NADPH, GR ensures the maintenance of a high GSH/GSSG ratio and thereby the stability of the cellular redox environment (Pannala *et al.*, 2013). Taken together, these findings indicate that the activation of CAT and APX did not occur in isolation, but rather formed part of a broader reorganization of the redox system, in which enzymatic and non-enzymatic components are functionally interconnected (**Figure 14**).

In the analyzed system, a pronounced increase in cysteine and γ-glutamylcysteine levels was also observed, both of which are key precursors of glutathione. Their accumulation suggests activation of sulfur metabolism to enhance GSH biosynthesis, representing a strategic cellular adjustment to sustained oxidative pressure (Harada *et al.*, 2002; Nacca *et al.*, 2021). Under cadmium stress, however, the expansion of the glutathione pool is not only relevant for maintaining cellular redox homeostasis but also plays a crucial role in detoxification, as GSH serves as a direct substrate for phytochelatin (PC) synthesis (Grill *et al.*, 1989; Blum *et al.*, 2007). Consistent with this mechanism, our analyses demonstrated that $CdCl_2$ exposure induced the formation of phytochelatins PC2, PC3, PC4, and PC5. Previous studies have shown that the degree of PC polymerization correlates with the intensity of metal stress and the level of intracellular metal accumulation (Gupta and Goldsbrough, 1990; Najmanova *et al.*, 2012). Similar co-occurrence of increased GSH levels and enhanced phytochelatin synthesis under cadmium exposure has been widely reported across plant species (Gupta *et al.*, 2002; Maier *et al.*, 2003; Xiao *et al.*, 2020). Taken together, these results indicate that $CdCl_2$ exposure triggered a coordinated response involving both enhanced GSH biosynthesis through activation of sulfur metabolism and the induction of phytochelatin production. Complementing these enzymatic and thiol-based mechanisms, an accumulation of proline was also observed. It is highly likely that the increased proline levels detected in our study represent an adaptive response to cadmium stress. The accumulation of this amino acid is commonly reported under metal stress conditions and is associated with its role in stabilizing proteins and membranes, as well as mitigating oxidative damage (Szabados and Savouré, 2010; Behtash *et al.*, 2024). Moreover, proline metabolism has been suggested to indirectly support cellular redox balance by influencing the $NAD(P)H/NAD(P)^+$ ratio (Giberti *et al.*, 2014; Zdunek-Zastocka *et al.*, 2021). Therefore, the cellular response can be considered integrative in nature, encompassing both the stabilization of redox homeostasis and the direct chelation and sequestration of cadmium ions (**Figure 14**). Despite the activation of these protective mechanisms at both structural and molecular levels, they were not sufficient to fully prevent stress-induced damage, as evidenced by the ultrastructural alterations of cellular organelles observed in TEM images.

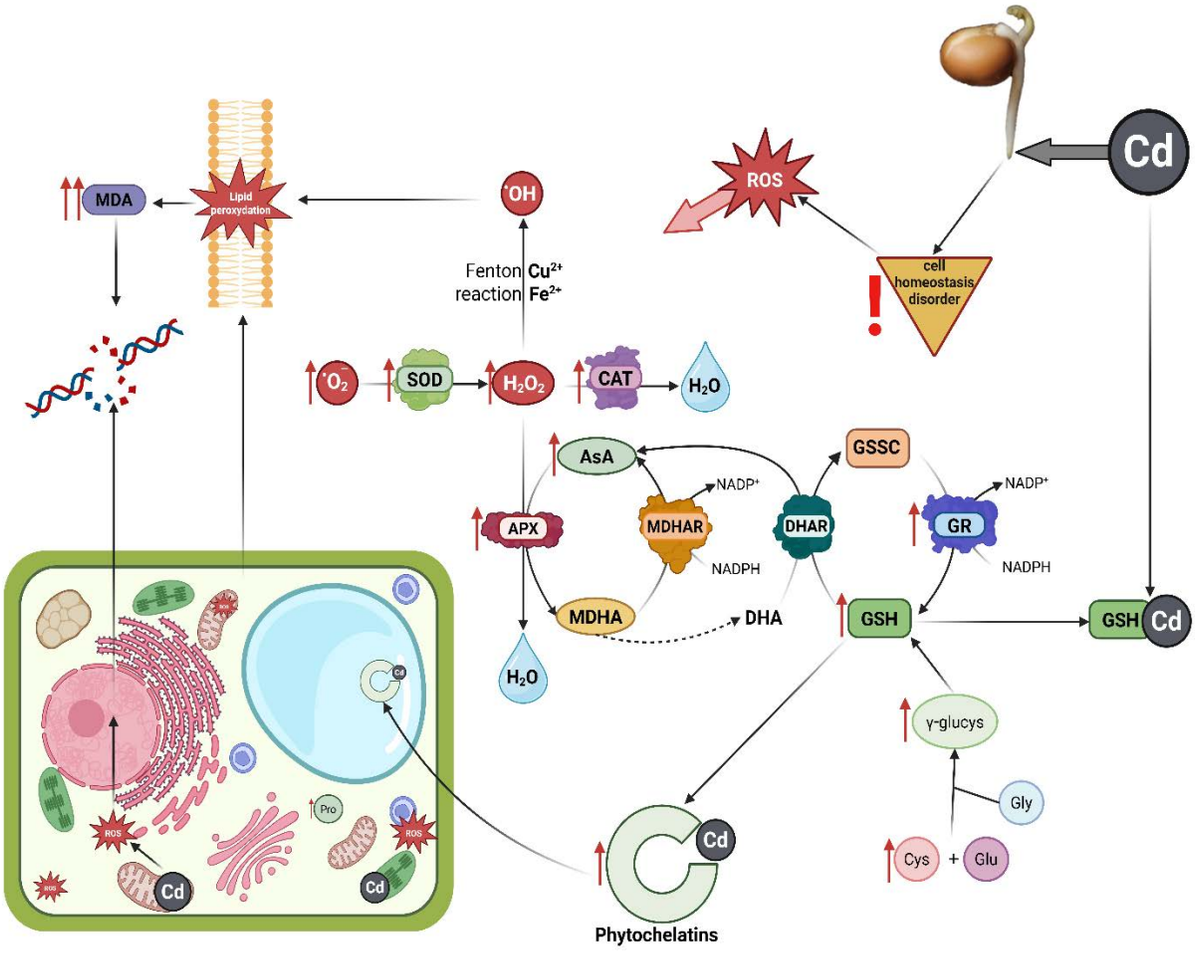

Figure 14. Proposed mechanism of cadmium (Cd) effects on redox imbalance and compensatory activation of antioxidant defenses in plant cells. Schematic representation based on our experimental results and literature data. Cd exposure leads to excessive production of reactive oxygen species (ROS). The resulting oxidative stress causes lipid peroxidation and DNA damage. In response, a coordinated antioxidant defense system is activated, including enzymatic components and non-enzymatic antioxidants as well as detoxification mechanisms based on phytochelatin synthesis, which bind Cd ions and facilitate their sequestration in vacuoles. Arrows indicate the direction of processes or signaling pathways, while upward arrows denote an increase in the level or activity of a given component. Created in BioRender. Gocek-Szczurtek, N. (2026) https://BioRender.com/5adh682

Redox Fine-Tuning by Thyme Essential Oil under Basal Conditions

In contrast to cadmium exposure, treatment with TO alone did not lead to an increase in H_2O_2 levels nor - according to our previous findings - to changes in superoxide ($O_2^{\bullet -}$) levels relative to the control (Gocek-Szczurtek *et al.*, 2025a). The absence of ROS overproduction, together with the preservation of normal organelle ultrastructure, indicates that TO at the applied concentration did not exert pro-oxidative effects and did not trigger secondary oxidative stress leading to damage of cellular membranes, mitochondrial cristae, or plastid and nuclear structures. This is particularly relevant in the context of its potential protective role. At the same time, the observed moderate activation of SOD and CAT, in the absence of significant changes in APX and GR activities, suggests a partial engagement of the enzymatic antioxidant system, restricted primarily to the early stage of H_2O_2 control. The lack of full activation of the ascorbate–glutathione axis may indicate that the redox signal did not exceed the threshold required

to trigger the entire AsA–GSH cycle (Hasanuzzaman *et al.*, 2020). A slight increase in the ascorbate pool can be interpreted in this context as maintaining basal redox buffering capacity rather than reflecting an increased demand for APX-dependent H_2O_2 detoxification (Nakano and Asada, 1981). Such a pattern of responses is often described as a form of mild stimulation of defense pathways or as a metabolic "priming" effect (**Figure 15**), whereby cellular readiness to respond to subsequent stress is enhanced without imposing an actual oxidative burden (Jisha and Puthur, 2016; Nasrallah *et al.*, 2022; Fejes *et al.*, 2025). At the ultrastructural level, this priming-like state may be reflected in the well-developed network of endoplasmic reticulum bearing numerous ribosomes, with terminal regions of cisternae exhibiting distinct dilations. This structural organization may indicate enhanced protein biosynthesis and trafficking, potentially associated with maintaining redox homeostasis and supporting cell wall remodeling processes.

A particularly noteworthy pattern emerges with regard to thiol metabolism, which appears to be one of the key processes modulated by TO. The observed increase in cysteine levels, together with pronounced accumulation of γ-glutamylcysteine and glutathione, may indicate a metabolic shift toward GSH synthesis rather than enhanced recycling of its oxidized form. The lack of changes in GR activity supports the notion that the expanded glutathione pool primarily results from activation of the biosynthetic pathway and potential stimulation of sulfur metabolism, rather than from a compensatory response to GSH oxidation (Ding *et al.*, 2020). This profile of changes thus suggests an enhancement of the redox buffering capacity rather than a response to actual oxidative overload (**Figure 15**). In this context, the slight increase in proline levels can be interpreted as part of a subtle reorganization of cellular metabolism, contributing to the stabilization of protein structures and maintenance of redox homeostasis. This interpretation aligns with reports on the effects of natural compounds that act as modulators rather than stress inducers (Shafiq *et al.*, 2018; Salemi *et al.*, 2019). These observations are consistent with a growing body of literature indicating that both complete thyme essential oil compositions and their dominant phenolic constituents can modulate the activity of antioxidant enzymes - such as SOD, CAT, and GR - and influence glutathione levels, without causing a marked overproduction of ROS. Similar effects have been reported in plant models as well as in selected animal models (Ghafarifarsani *et al.*, 2022; Sallam *et al.*, 2021; Sellamuthu *et al.*, 2013; Sönmez *et al.*, 2015; Sun *et al.*, 2024), suggesting a relatively universal biochemical effect of phenolic monoterpenes on mechanisms regulating redox homeostasis.

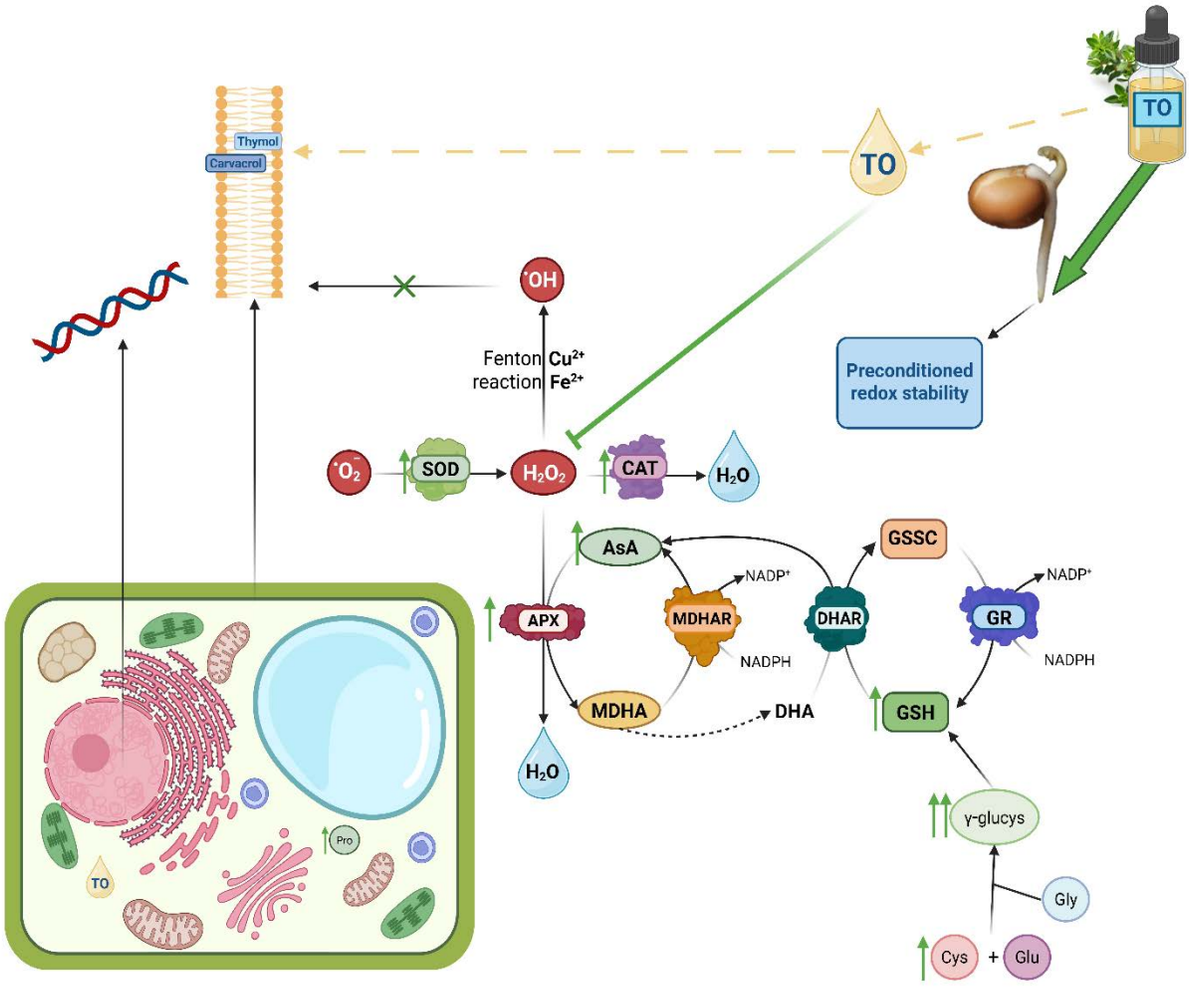

Figure 15. Proposed mechanism of thyme essential oil (TO) effects on redox fine-tuning under basal conditions in plant cells. Schematic representation based on our experimental results and literature data. TO treatment leads to a slight activation of antioxidant defense systems, including enzymatic components and non-enzymatic antioxidants, exceeding the control level without disturbing redox homeostasis. At the same time, reactive oxygen species (ROS) levels remain comparable to the control, and no lipid peroxidation or DNA damage is induced. Arrows indicate the direction of processes or signaling pathways; upward arrows denote an increase, whereas downward arrows indicate a decrease in the level or activity of a given component. Sharp-ended arrows represent activation or stimulation, while blunt-ended arrows indicate inhibition or suppression. Dashed arrows indicate a proposed mechanism based on available data and literature. Created in BioRender. Gocek-Szczurtek, N. (2026) https://BioRender.com/xav0pe5

Redox Reprogramming under Combined Cadmium and Thyme Oil Exposure

The most complex pattern of redox response emerged under the combined exposure of seedlings to Cd and TO (**Figure 16**). In this system, activation of the enzymatic components of the antioxidant machinery was particularly pronounced. However, unlike the scenario observed under cadmium treatment alone, this activation was not accompanied by sustained accumulation of H_2O_2 or $O_2^{\bullet -}$ (Gocek-Szczurtek *et al.*, 2025a). This suggests that in the presence of TO, the increases in SOD, CAT, APX, and GR activities were not merely compensatory but effectively contributed to limiting ROS levels. It can therefore be inferred that a better synchronization occurred between ROS generation and their subsequent metabolism, indicating a more efficient coordination of the overall redox system (Rodrigues De Queiroz *et al.*, 2023). The concurrent elevation of cysteine, γ-glutamylcysteine, glutathione, and ascorbate pools further supports this interpretation. Enhanced availability of reduced metabolites likely

increased the cell's capacity to buffer redox potential and stabilized the function of enzymatic H_2O_2 detoxification pathways (Noctor and Foyer, 1998). In this context, the simultaneous activation of GR and the increase in GSH levels may reflect maintenance of a more favorable GSH/GSSG ratio and a more efficient reductive turnover within the ascorbate–glutathione cycle (Ding *et al.*, 2016). The reinforced antioxidant capacity of the cells likely arises from the sufficient availability of antioxidant enzymes and detoxification proteins and is reflected in ultrastructural observations. The presence of numerous and large nucleolar vacuoles indicates enhanced transport of ribosomal subunits into the cytoplasm. Their increased accumulation along electron-dense channels of the endoplasmic reticulum and within the nuclear envelope suggests intensified translation, supporting elevated synthesis of proteins essential under stress conditions (Stępiński, 2014)**.**

Literature reports indicate that thymol, the dominant component of TO, can mitigate cadmium toxicity through modulation of redox responses and regulation of glutathione metabolism in plant models (Ye *et al.*, 2016; Hong *et al.*, 2026). Similar protective effects have also been reported for carvacrol and *Thymus* essential oils in animal models (Ansari *et al.*, 2021; Ghafarifarsani *et al.*, 2022; Kandemir *et al.*, 2021; Rahmani *et al.*, 2022). It is important to note, however, that most available studies focus on individual constituents, whereas analyses of whole thyme essential oil compositions are far less common, particularly in plant systems. Evidence suggesting that the complete mixture may exert stronger antioxidant activity than its isolated components (Youdim *et al.*, 2002) supports the interpretation of the observed effect as a result of synergistic, multi-component modulation of the redox system, rather than the action of a single compound.

An important element of the cellular response to heavy metal exposure is the activation of the phytochelatin pathway. In the Cd-containing medium supplemented with TO, the presence of all oligomers (PC2–PC5) indicates that despite reduced metal accumulation, cells remained exposed to biologically active Cd^{2+} and retained the capacity for its chelation. Concurrently, the lower phytochelatin concentrations, approximately 30–34% lower than those observed in Cd-only treated plants, corresponded proportionally to the ~38% reduction in tissue Cd content. This suggests that the intensity of PC synthesis reflected the actual cadmium load, in line with the well-documented correlation between Cd levels and PC accumulation (Keltjens and Van Beusichem, 1998; Wu *et al.*, 2016). It should be emphasized that despite the reduced metal accumulation, tissue Cd content remained within a range considered biologically significant and potentially toxic (Dguimi *et al.*, 2008). This indicates that cells were still operating under substantial cadmium pressure, and the observed reduction in ROS cannot be explained solely by decreased metal uptake. Taken together, these results indicate that TO acts at multiple levels in the presence of cadmium: it partially limits metal accumulation while simultaneously reorganizing the activity of both enzymatic and non-enzymatic components of the antioxidant system under sustained metal stress (**Figure 16**). The protective action of TO consequently results in marked improvement of cellular and organelle ultrastructure. In line with these observations, comparable protective effects of essential oils under cadmium stress have been reported in other plant systems, including lettuce (*Lactuca sativa)* treated with *Ocimum basilicum* essential oil and durum wheat (*Triticum turgidum* L. var. *durum)* exposed to *Lobularia maritima* essential oil, where attenuation of

oxidative stress, activation of antioxidant responses, and, in some cases, reduced Cd accumulation were observed (Landi *et al.*, 2025; Ben Saad *et al.*, 2026).

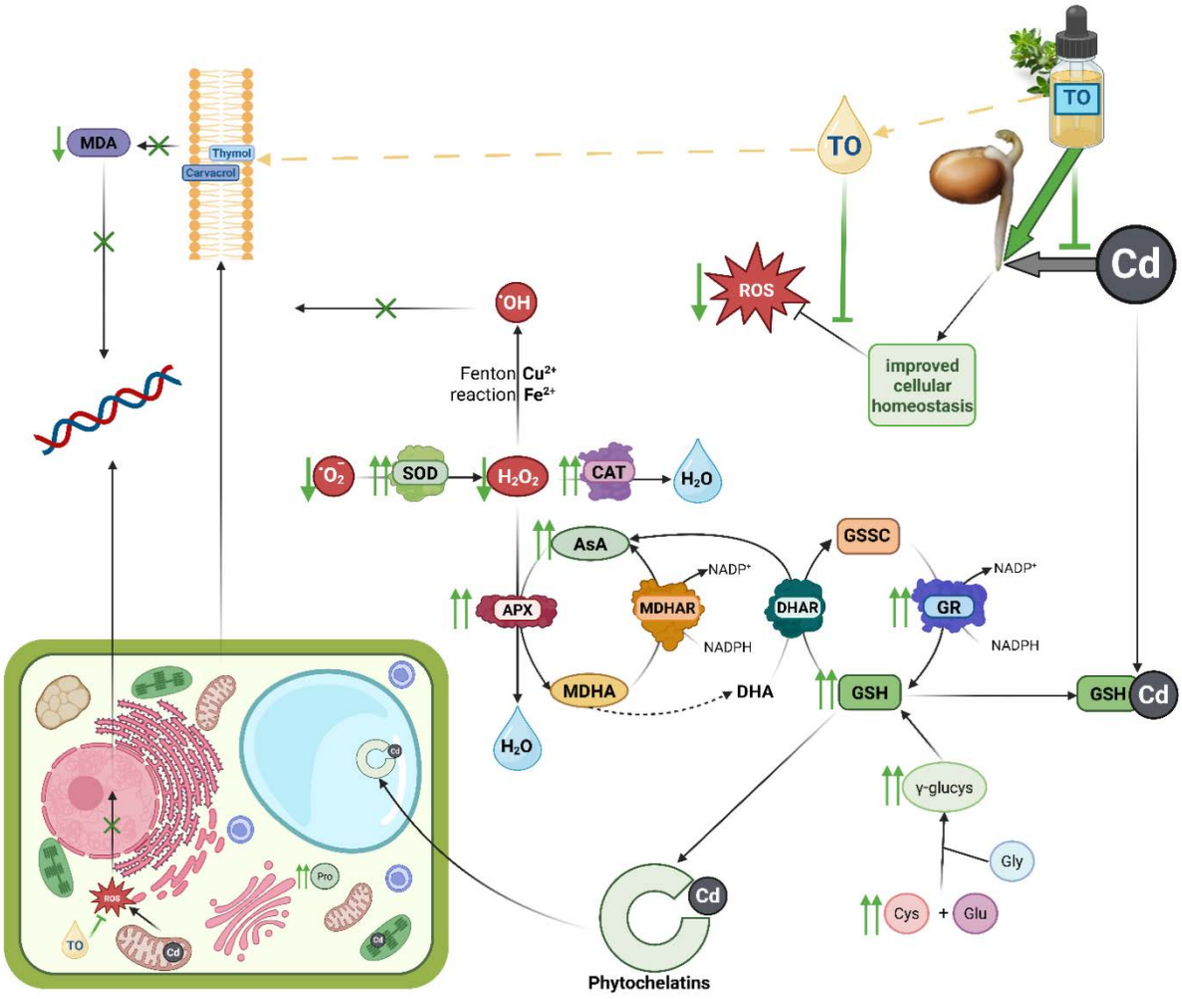

Figure 16. Proposed mechanism of combined cadmium (Cd) and thyme essential oil (TO) effects on redox balance and antioxidant responses in plant cells. Schematic representation based on our experimental results and literature data. Cd exposure leads to excessive production of reactive oxygen species (ROS). In the presence of TO, ROS levels are reduced compared to Cd treatment alone, reflecting mitigation of Cd-induced oxidative stress. This effect is associated with enhanced activation of antioxidant defense systems, including enzymatic components and non-enzymatic antioxidants, as well as detoxification mechanisms based on phytochelatin synthesis, facilitating Cd binding and its sequestration in vacuoles. Consequently, TO alleviates Cd-induced cellular damage and contributes to the restoration of redox balance and cellular homeostasis. Arrows indicate the direction of processes or signaling pathways; upward arrows denote an increase, whereas downward arrows indicate a decrease in the level or activity of a given component. Sharp-ended arrows represent activation or stimulation, while blunt-ended arrows indicate inhibition or suppression. Dashed arrows indicate a proposed mechanism based on available data and literature. Created in BioRender. Gocek-Szczurtek, N. (2026) https://BioRender.com/kgoej11

From Lipid Peroxidation to DNA Damage: The Oxidative–Genotoxic Axis

A direct consequence of ROS overproduction is lipid peroxidation - a radical, chain reaction of oxidation of polyunsaturated fatty acids present in biological membranes (Valgimigli, 2023). Lipid degradation generates reactive aldehydes, including malondialdehyde (MDA), commonly used as a marker of oxidative damage to membrane structures (Esterbauer and Cheeseman, 1990; Ayala *et al.*, 2014).

Elevated MDA levels in plant tissues exposed to $CdCl_2$ indicate intensified lipid peroxidation and compromised membrane integrity under metal-induced stress. Similar increases in MDA content in response to cadmium have been reported in numerous plant species, including *Thlaspi caerulescens*, *Brassica juncea*, *Nicotiana tabacum* (Wang *et al.*, 2008), *Pistia stratiotes* L. (Y., Li *et al.*, 2013), and *Hibiscus cannabinus* L. (F., Li *et al.*, 2013). In most experimental models, MDA accumulation was accompanied by increased H_2O_2 levels and altered antioxidant enzyme activity, highlighting the close relationship between oxidative pressure and membrane destabilization. Our results align with this pattern and suggest that, despite activation of defense mechanisms, the response was largely compensatory and did not provide full protection of membrane structures.

It is important to note that reactive aldehydes produced during lipid peroxidation, including MDA, are not merely markers of membrane damage but also possess significant genotoxic potential (Marnett, 1999). These compounds can form adducts with DNA, destabilize the double helix, and promote mutation formation (Gentile *et al.*, 2017). Consequently, lipid peroxidation becomes a secondary source of genetic damage (**Figure 14**), amplifying the direct effects of ROS, such as oxidation of nitrogenous bases and induction of single- and double-strand DNA breaks (Srinivas *et al.*, 2019). In this context, the 37% of root cells exhibiting DNA fragmentation after $CdCl_2$ exposure (visualized by TUNEL assay) can be interpreted as the combined effect of two synergistic mechanisms: primary oxidative pressure and secondary action of reactive lipid degradation products. This interpretation is consistent with reports of cadmium genotoxicity in plant cells (Lin *et al.*, 2007; Gichner *et al.*, 2008).

The absence of changes in MDA levels and DNA fragmentation in seedlings treated with TO alone logically complements the previously discussed redox profile for this variant. Maintenance of control-level ROS together with moderate modulation of antioxidant enzyme activity indicates that the observed redox reorganization was regulatory rather than a response to oxidative damage. In other words, the lack of lipid peroxidation and genotoxicity markers confirms that, at the applied concentration, TO did not initiate the peroxidation–genotoxic cascade but instead contributed to mild modulation of redox homeostasis (**Figure 15**). This interpretation is consistent with reports indicating that phenolic constituents of essential oils can stabilize membrane structures and limit the initiation of lipid peroxidation (Aeschbach *et al.*, 1994; Ferreira *et al.*, 2016).

The most comprehensive profile of changes was observed in the combined $CdCl_2$ and TO treatment. Significantly lower MDA levels compared with Cd-only plants suggest that TO presence mitigated the intensity of lipid peroxidation, which can be associated with more effective ROS control and stabilization of cellular redox status (**Figure 16**). In numerous plant models of cadmium stress, enhanced antioxidant capacity and improved redox balance co-occurred with reduced lipid damage (Jia *et al.*, 2023; Shabbir *et al.*, 2025). Similar effects were also reported following application of phenolic essential oil components such as thymol (Ye *et al.*, 2016), as well as in animal models using oils from the genus *Thymus* (Ansari *et al.*, 2021). The reduction in lipid peroxidation was reflected in a marked decrease in TUNEL-positive cells (to approximately 6%), reaching values statistically indistinguishable from controls. This finding suggests that TO not only diminished direct oxidative pressure on DNA but also limited the secondary effects of reactive lipid degradation products, interrupting a potential oxidative–

genotoxic cascade. Literature indicates that exogenous application of compounds enhancing cellular antioxidant systems can reduce DNA damage, including double-strand breaks (Hassan *et al.*, 2021; Purcarea *et al.*, 2022), consistent with the observed decrease in the proportion of TUNEL-positive cells in our study. Collectively, the results indicate that under cadmium exposure, lipid peroxidation and DNA fragmentation are linked elements of a single oxidative–genotoxic axis. The presence of TO limits this axis at the redox regulation level, contributing to stabilization of cellular membranes and preservation of genome integrity.

Conclusions:

The toxic effects of cadmium (Cd) in root meristems of faba bean (*Vicia faba* var. *minor*) result from its accumulation within cells. The elevated Cd content may be associated with impaired barrier function of the cell wall, likely due to disturbances in its reinforcement. This is supported by alterations in Golgi-derived vesicles, which, under cadmium exposure, are depleted of fibrillar wall precursors. Cadmium entering the cells induces enhanced production of reactive oxygen species (ROS), disrupts their detoxification, and disturbs redox homeostasis, ultimately leading to lipid peroxidation and cascading damage to cellular membranes, organelles, and genetic material. Although Cd exposure triggers the activation of both enzymatic and non-enzymatic antioxidant systems, as well as thiol metabolism, these responses appear largely compensatory and insufficient to fully restore redox balance. The limited effectiveness of these defense mechanisms may additionally be linked to impaired protein biosynthesis, resulting from reduced rRNA transcriptional activity, as indicated by a decreased content of the dense fibrillar component in nucleoli and a reduced number of ribosomes in the cytoplasm.

The presence of thyme essential oil (TO) in cells exposed to cadmium exerts a multi-level protective effect. TO reduces cadmium accumulation in meristems and promotes cell wall reinforcement by sustaining enhanced production of wall precursors, visible as numerous fibers accumulating in large and abundant Golgi-derived secretory vesicles. In addition, TO improves the coordination of enzymatic and non-enzymatic antioxidant mechanisms, maintaining a balance between ROS production and detoxification, thereby stabilizing redox homeostasis. This enhanced antioxidant capacity is likely supported by increased availability of functional proteins, associated with intensive transport of ribosomal subunits into the cytoplasm, as evidenced by the formation of nucleolar vacuoles, and their connection with the endoplasmic reticulum network, indicative of active translation. Consequently, TO limits oxidative damage, stabilizes cellular membranes, preserves organelle integrity, and protects nuclear DNA. In summary, these findings indicate that TO enhances the adaptive capacity of root meristem cells to cadmium stress, acting as a multifaceted modulator that integrates reduced metal accumulation, improved redox regulation, and maintenance of cellular structure and architecture.

These results further highlight the potential of TO as a biologically active agent supporting plant defense responses against cadmium-induced abiotic stress. From a practical perspective, a plant-derived product such as TO could in the future serve as a complementary or alternative approach to conventional agrochemicals. However, as these findings were obtained under controlled laboratory conditions using a simplified experimental model, further studies under soil-based and field conditions are necessary to validate their practical applicability for the studied species and other plants exposed to environmentally relevant cadmium levels.

Material and methods:

Plant Material

Sterile seeds of *Vicia faba* L. var. *minor* (W. Legutko The Seed Breeding Company, Jutrosin, Poland) were germinated on moist blotting paper in trays and maintained in darkness at 20 °C. After 72 h, uniformly developed seedlings with primary roots approximately 2-3 cm in length were selected and subjected to a 24 h incubation in defined treatment solutions. The experimental design comprised the following variants: distilled water (control), emulsifier solution, 175 µM $CdCl_2$, 0.03% (v/v) emulsified thyme essential oil (TO; Etja, Elbląg, Poland), and 175 µM $CdCl_2$ supplemented with emulsified TO. The chemical composition of TO was previously characterized by GC–MS (Gocek-Szczurtek, *et al.*, 2025a) and corresponded to a thymol-rich chemotype of *Thymus vulgaris*, with major constituents listed in descending order of abundance, including thymol, *p*-cymene, linalool, caryophyllene, carvacrol, limonene, α-pinene, γ-terpinene, and α-terpineol. To ensure compositional consistency, the same batch of TO as that used in the initial characterization study (Gocek-Szczurtek *et al.*, 2025a) was applied throughout all experiments. The concentration of $CdCl_2$ was established based on preliminary range-finding tests and literature data (100–200 µM) (Ünyayar *et al.*, 2006; Souguir *et al.*, 2011; Żabka *et al.*, 2021; Żabka *et al.*, 2021; Gocek-Szczurtek *et al.*, 2025a; Gocek-Szczurtek *et al.*, 2025b), whereas the TO concentration was selected following preliminary experiments performed within the 0.01–0.06% range and supported by previously published studies (Gocek-Szczurtek *et al.*, 2025a; Gocek-Szczurtek 2025b; Gocek-Szczurtek *et al.*, 2026). To ensure homogeneous dispersion of the hydrophobic essential oil in water, TO was emulsified using a mixture of mono- and di-ethoxylated C14–18 and unsaturated C16–18 glycerides combined with ethoxylated *Brassica napus* oil. The emulsifier was mixed with TO at a 1:4 (v/v) ratio, resulting in a final emulsifier concentration of 0.0075% (v/v), and homogenized for 15 min using a vortex mixer. The emulsifier was supplied by the Department of Agronomy, Poznań University of Life Sciences. In preliminary experiments, an additional treatment consisting of $CdCl_2$ combined with the emulsifier alone (without TO) was included to exclude any potential protective effect of the surfactant itself. As this variant did not produce measurable biological differences compared with $CdCl_2$ treatment alone, it was not incorporated into subsequent detailed analyses. Further analyses were performed in three or four experimental repeats of each series.

Determination of Cadmium Content

Cadmium (Cd) accumulation in dried primary roots of *V. faba* (0.25 g) was determined after microwave-assisted digestion with concentrated HNO_3 (5 mL) and 30% H_2O_2 (1 mL) using an Ethos Lean system (Milestone, Sorisole, Italy). Digestion was performed under controlled conditions at 120–130 °C (850 W). The resulting mineralizates were diluted with deionized water prior to analysis. Cd concentration was quantified by flame atomic absorption spectrometry (FAAS; ICE 3500, Thermo Electron Corporation, UK) using an air–acetylene flame and deuterium background correction. Calibration was carried out with external standards prepared in 1 M HNO_3 over the range of 0.01–1.0 µg mL^{-1}. The limits of detection (LOD) and quantification (LOQ) were 0.012 and 0.04 µg mL^{-1}, respectively. Results were calculated taking dilution factors into account and expressed on a dry weight basis.

Determination of H_2O_2 and Lipid Peroxidation

Frozen root samples (100 mg, previously snap-frozen in liquid nitrogen), were homogenized using a bead mill. The homogenates were incubated in 5% (w/v) trichloroacetic acid (TCA) on ice for 10 min and subsequently centrifuged at 9000 × g for 15 min at 3 °C. The obtained supernatant was used for the determination of hydrogen peroxide (H_2O_2) and malondialdehyde (MDA) levels.

For H_2O_2 quantification, aliquots of the supernatant were combined (1:1, v/v) with a reaction solution containing 2.5 mM potassium phosphate buffer (pH 7.0) and 500 mM potassium iodide. Absorbance was measured at 390 nm, and H_2O_2 concentration was calculated according to established protocols (Velikova *et al.*, 2000; Talarek-Karwel *et al.*, 2020).

Lipid peroxidation was assessed by measuring MDA content using the thiobarbituric acid (TBA) assay. The supernatant was mixed with 0.5% (w/v) TBA prepared in 20% (w/v) TCA and heated at 95 °C for 20 min. After rapid cooling on ice, samples were centrifuged to remove precipitates, and absorbance was measured at 532 and 600 nm. The nonspecific absorption was subtracted from the absorbance measured at 532 nm. MDA concentration was calculated using an extinction coefficient of 155 mM^{-1} cm^{-1}, following previously described procedures (Heath and Packer, 1968; Cakmak and Horst, 1991; Talarek-Karwel *et al.*, 2020). All analyses were performed using 4 biological replicates.

Antioxidant Enzyme Activity Determination

The activity of ascorbate peroxidase (APX; EC 1.11.1.11) was assayed following the method of (Nakano and Asada, 1981) by detecting the absorbance rate at 290 nm using the extinction coefficient 2.8 mM^{-1} cm^{-1}. The designation was performed in 3 mL reaction mixture containing 50 mM potassium phosphate buffer (pH 7.0), 0.5 mM ascorbate, 1 mM H_2O_2, and 100 µL of enzyme extract in 3 min. 25 °C. Enzyme activity was expressed as µmol of ascorbate oxidized per minute per milligram of soluble protein.

Superoxide dismutase (SOD; EC 1.15.1.1) activity was determined according to (Beauchamp and Fridovich, 1971) by measuring the inhibition of nitroblue tetrazolium (NBT) photochemical reduction at 560 nm. The assay mixture (3 mL) consisted of 50 mM sodium carbonate buffer (pH 10.2), 24 µM NBT, 0.1 mM EDTA, 1 µM hydroxylamine, 0.03% (v/v) Triton X-100, and 70 µL of enzyme extract. One unit of SOD activity was defined as the amount of enzyme required to cause 50% inhibition of NBT reduction and was expressed per milligram of soluble protein.

Catalase (CAT; EC 1.11.1.6) activity was assessed following (Aebi, 1984) by monitoring the decrease in absorbance at 240 nm associated with H_2O_2 decomposition (ε = 39.4 M^{-1} cm^{-1}). The reaction mixture (3 mL) contained 50 mM potassium phosphate buffer (pH 7.0), 15 mM H_2O_2, and 100 µL of enzyme extract. Absorbance changes were recorded for 30 s at 25 °C. Enzyme activity was calculated as µmol of H_2O_2 decomposed per minute per milligram of soluble protein.

Glutathione reductase (GR; EC 1.8.1.7) activity was measured according (Schaedle and Bassham, 1977) by monitoring NADPH oxidation at 340 nm (ε = 6.2 mM^{-1} cm^{-1}). The 3 mL reaction mixture contained 50 mM potassium phosphate buffer (pH 7.6), 1 mM oxidized glutathione (GSSG), 0.5 mM EDTA, and

0.1 mM NADPH, with the reaction initiated by the addition of 100 µL enzyme extract. The decrease in absorbance at 25 °C was used to calculate GR activity, which was expressed per milligram of soluble protein. All enzyme assays were conducted using four biological replicates.

Determination of Ascorbate and Proline

The ascorbate (ASC) level was quantified following the procedure described by (Kampfenkel *et al.*, 1995). Plant tissue was homogenized for 5 min in 2 mL of 5% (w/v) trichloroacetic acid (TCA) using a bead mill and subsequently centrifuged at 9000 × *g* for 10 min. An aliquot of the resulting supernatant was combined with a reaction solution containing 10 mM dithiothreitol (DTT), 0.2 M phosphate buffer (pH 7.4), 0.5% (w/v) N-ethylmaleimide, 10% (w/v) TCA, 42% (v/v) H_3PO_4, 4% (w/v) 2,2′-bipyridyl, and 3% (w/v) $FeCl_3$. The mixture was incubated at 42 °C for 40 min. Absorbance was then recorded at 525 nm.

Proline (Pro) content was determined spectrophotometrically (according to (Bates *et al.*, 1973)) following homogenization of plant tissue in a bead mill. Plant tissue was homogenized in 2 ml potassium phosphate buffer (pH 7.5) and centrifuged at 9000 × g for 10 min. The obtained supernatant was reacted with acidic 2.5% (w/v) ninhydrin reagent and incubated under controlled conditions. After cooling, absorbance was measured at 546 nm. All measurements were performed for 4 biological replicates.

Determination of Cysteine, γ-Glutamylcysteine, Glutathione, and Phytochelatins

The analysis of phytochelatins (PCs) and their precursors content (cysteine, Cys; *γ*-glutamylcysteine, *γ*-Glu-Cys; glutathione, GSH), was performed according to (Le Faucheur *et al.*, 2006). Plant material was homogenized in a bead mill in extraction medium containing 0.1% (w/v) trifluoroacetic acid (TFA) and 6.3 mM diethylenetriaminepentaacetic acid (DTPA), followed by centrifugation to obtain clear supernatants. Thiol groups present in the extracts were derivatized with monobromobimane (mBBr) by incubation for 30 min at 45 °C in darkness.

HPLC analyses were carried out using an Agilent 1260 HPLC system (Agilent Technologies, Santa Clara, CA, USA) equipped with 1260 Infinity Agilent Quaternary pump G1311B, 1260 Infinity Fluorescence Detector G1321B, 1260 Infinity ALS G1329B Automated Sample Injector, 1290 Infinity Autosampler Thermostat G1330B, and a thermostatted column oven 1290 Infinity TCC G1316C. The system was controlled by Agilent OpenLab ChemStation software. Separation of thiol compounds was achieved on a Cosmosil C18-MS-II column (4.6 × 250 mm, 5 µm; maintained at 37 °C). Samples of 25 µL were injected and run in a gradient: 0–15 min, 12–25 % (v/v) MeOH; 15–29 min, 25–35 % (v/v) MeOH; 29–50 min, 35–50 % (v/v) MeOH. The column was then cleaned with 100 % (v/v) MeOH and reequilibrated in 12 % (v/v) MeOH. The excitation wavelength was 380 nm; the emission wavelength was 470 nm. The retention times of PC precursors (Cys, *γ*-Glu-Cys, and GSH) and PC oligomers were confirmed using their standards (AnaSpec, Fremont, CA, USA). The obtained chromatograms were analyzed using Agilent OpenLAB ChemStation Edition C.01.09 for LC systems (Agilent Technologies Inc., Santa Clara, CA, USA). Evaluation was performed for 4 biological replicates.

TUNEL-Based Assessment of Genomic Integrity

Primary root meristems were fixed in 4% (w/v) paraformaldehyde prepared in 0.01 M phosphate-buffered saline (PBS) for 40 min at 4 °C. Following fixation, tissues were washed twice with 0.01 M PBS and subjected to enzymatic digestion in 0.1 M citrate buffer containing 2.5% (w/v) pectinase, 2.5% (w/v) pectolyase, and 2.5% (w/v) cellulase (Sigma-Aldrich, St. Louis, MI, USA) for 30 min at 37 °C.

DNA fragmentation was detected using the Click-iT® TUNEL Alexa Fluor® 488 Imaging Assay kit (Thermo Fisher Scientific, Waltham, MA, USA) according to the manufacturer's protocol. Nuclei were counterstained with DAPI (15 µM; 4′,6-diamidino-2-phenylindole, Sigma-Aldrich) for 15 min and subsequently washed three times in 0.01 M PBS (10 min each). Samples were mounted on microscope slides in a medium composed of 0.01 M PBS, glycerol, and DABCO. Analyses were performed for 4 biological replicates.

Transmission Electron Microscopy

The apical parts of roots were fixed in 2% (v/v) glutaraldehyde prepared in 1% cacodylate buffer (pH 7.3) and fixed for 3 h at 4 °C. Following primary fixation, samples were post-fixed in 1% osmium tetroxide (OsO_4) in 1% cacodylate buffer (pH 7.3) for an additional 3 h. The material was subsequently dehydrated through a graded ethanol series and infiltrated with a resin mixture composed of Epon 812 and Spurr's resin prior to polymerization. Ultrathin sections were obtained using an ultramicrotome and contrasted with uranyl acetate and lead citrate following standard staining procedures (Reynolds, 1963; Polit, 2009). Prepared sections were observed and documented using a JEOL JEM 1010 transmission electron microscope.

Data statement: Data will be made available on request.

Acknowledgments: This work was supported through the budget of the Doctoral School of Exact and Natural Sciences of the University of Lodz.

We thank the Laboratory of Microscopic Imaging and Specialized Biological Techniques of the Faculty of Biology and Environmental Protection of the University of Lodz for providing access to the research facilities.

Credit authorship contribution statement:

Natalia Gocek-Szczurtek: Writing – original draft, Visualization, Validation, Project administration, Methodology, Investigation, Funding acquisition, Formal analysis, Conceptualization. **Alicja Piotrowska-Niczyporuk**: Validation, Methodology, Investigation. **Elżbieta Zambrzycka-Szelewa**: Methodology. **Iwona Ciereszko**: Writing – review & editing, Validation, Methodology. **Aneta Żabka**: Writing – Writing review & editing , Resources. **Mateusz Wróblewski**: Investigation. **Justyna T. Polit**: Writing review & editing, Validation, Supervision, Methodology, Conceptualization.

Conflict of interest disclosure: The authors declare no competing financial interests or personal relationships that could have appeared to influence the work reported in this paper.

References:

Abdel-Wahhab, M.A., El-Nekeety, A.A., Mohammed, H.E., Elshafey, O.I., Abdel-Aziem, S.H. and Hassan, N.S. (2021) Elimination of oxidative stress and genotoxicity of biosynthesized titanium dioxide nanoparticles in rats via supplementation with whey protein-coated thyme essential oil. *Environ. Sci. Pollut. Res.*, **28**, 57640–57656.

Aebi, H. (1984) Catalase in vitro. In: *Methods in Enzymology*, Vol. **105** (ed. by Packer, L.). Elsevier, pp. 121–126.

Aeschbach, R., Löliger, J., Scott, B.C., Murcia, A., Butler, J., Halliwell, B. and Aruoma, O.I. (1994) Antioxidant actions of thymol, carvacrol, 6-gingerol, zingerone and hydroxytyrosol. *Food Chem. Toxicol.*, **32**, 31–36.

Ali, B., Qian, P., Jin, R., Ali, S., Khan, M., Aziz, R., Tian, T. and Zhou, W. (2014) Physiological and ultra-structural changes in *Brassica napus* seedlings induced by cadmium stress. *Biol. Plant.*, **58**, 131–138.

Alloway, B.J. (ed.) (2013) Heavy metals in soils: trace metals and metalloids in soils and their bioavailability. Dordrecht: Springer.

Alscher, R.G. (2002) Role of superoxide dismutases (SODs) in controlling oxidative stress in plants. *J. Exp. Bot.*, **53**, 1331–1341.

Amsbury, S., Kirk, P. and Benitez-Alfonso, Y. (2018) Emerging models on the regulation of intercellular transport by plasmodesmata-associated callose. *J. Exp. Bot.*, **69**, 105–115.

Ansari, M.N., Rehman, N.U., Karim, A., Imam, F. and Hamad, A.M. (2021) Protective effect of *Thymus serrulatus* essential oil on cadmium-induced nephrotoxicity in rats, through suppression of oxidative stress and downregulation of NF-κB, iNOS, and Smad2 mRNA expression. *Molecules*, **26**, 1252.

Arya, S.K. and Mukherjee, A. (2014) Sensitivity of A*llium cepa* and *Vicia faba* towards cadmium toxicity. *J. Soil Sci. Plant Nutr.*, **14**, 447-458.

Ayala, A., Muñoz, M.F. and Argüelles, S. (2014) Lipid peroxidation: production, metabolism, and signaling mechanisms of malondialdehyde and 4-hydroxy-2-nonenal. *Oxid. Med. Cell. Longevity*, **2014**, 1–31.

Barceló, J., Vázquez, M.D. and Poschenrieder, C. (1988) Structural and ultrastructural disorders in cadmium-treated bush bean plants (*Phaseolus vulgaris* L.). *New Phytol.*, **108**, 37–49.

Bashir, H., Qureshi, M.I., Ibrahim, M.M. and Iqbal, M. (2015) Chloroplast and photosystems: impact of cadmium and iron deficiency. *Photosynthetica*, **53**, 321–335.

Bates, L.S., Waldren, R.P. and Teare, I.D. (1973) Rapid determination of free proline for water-stress studies. *Plant Soil*, **39**, 205–207.

Beauchamp, C. and Fridovich, I. (1971) Superoxide dismutase: improved assays and an assay applicable to acrylamide gels. *Anal. Biochem.*, **44**, 276–287.

Behtash, F., Amini, T., Mousavi, S.B., Seyed Hajizadeh, H. and Kaya, O. (2024) Efficiency of zinc in alleviating cadmium toxicity in hydroponically grown lettuce (*Lactuca sativa* L. cv. Ferdos). *BMC Plant Biol.*, **24**, 648–659.

Ben Saad, R., Ben Romdhane, W., Wiszniewska, A., et al. (2026) *Lobularia maritima* essential oil modulates heavy-metal transporter expression and mitigates cadmium stress in durum wheat. *Protoplasma*, **263**, 497–512.

Berkelaar, E. and Hale, B.A. (2003) Accumulation of cadmium by durum wheat roots: bases for citrate-mediated exceptions to the free ion model. *Environ. Toxicol. Chem.*, **22**, 1155–1161.

Bi, Y., Chen, W., Zhang, W., Zhou, Q., Yun, L. and Xing, D. (2009) Production of reactive oxygen species, impairment of photosynthetic function and dynamic changes in mitochondria are early events in cadmium-induced cell death in *Arabidopsis thaliana*. *Biol. Cell*, **101**, 629–643.

Blum, R., Beck, A., Korte, A., Stengel, A., Letzel, T., Lendzian, K. and Grill, E. (2007) Function of phytochelatin synthase in catabolism of glutathione-conjugates. *Plant J.*, **49**, 740–749.

Bolan, N., Kunhikrishnan, A., Thangarajan, R., Kumpiene, J., Park, J., Makino, T., Kirkham, M.B. and Scheckel, K. (2014) Remediation of heavy metal(loid)s contaminated soils – to mobilize or to immobilize? *J. Hazard. Mater.*, **266**, 141–166.

Born, D., Mussi Luz, A., Wanderley Tavares, F. and Manske, C. (2026) CMC and cloud point of nonionic ethoxylated surfactants: experimental data and molecular thermodynamics. *J. Chem. Eng. Data*, **71**, 555–565.

Branca, J. J. V., Fiorillo, C., Carrino, D., Paternostro, F., Taddei, N., Gulisano, M., Pacini, A. and Becatti, M. (2020) Cadmium-induced oxidative stress: focus on the central nervous system. *Antioxidants*, **9**, 492–512.

Branca, J. J. V., Pacini, A., Gulisano, M., Taddei, N., Fiorillo, C. and Becatti, M. (2020) Cadmium-induced cytotoxicity: effects on mitochondrial electron transport chain. *Front. Cell Dev. Biol.*, **8**, 604377.

Briffa, J., Sinagra, E. and Blundell, R. (2020) Heavy metal pollution in the environment and their toxicological effects on humans. *Heliyon*, **6**, e04691.

Bunse M., Daniels R., Gründemann C., Heilmann J., Kammerer D. R., Keusgen M., Lindequist U., Melzig M. F., Morlock G. E., Schulz H., Schweiggert R., Simon M., Stintzing F. C. and Wink M. (2022) Essential oils as multicomponent mixtures and their potential for human health and well-being. *Front. Pharmacol.*, **13**, 956541.

Burton, G.J. and Jauniaux, E. (2011) Oxidative stress. *Best Pract. Res. Clin. Obstet. Gynaecol.*, **25**, 287–299.

Busi, M.V., Gomez-Lobato, M.E., Rius, S.P., Turowski, V.R., Casati, P., Zabaleta, E.J., Gomez-Casati, D.F. and Araya, A. (2011) Effect of mitochondrial dysfunction on carbon metabolism and gene expression in flower tissues of *Arabidopsis thaliana*. *Mol. Plant*, **4**, 127–143.

Cakmak, I. and Horst, W.J. (1991) Effect of aluminium on lipid peroxidation, superoxide dismutase, catalase, and peroxidase activities in root tips of soybean (*Glycine max*). *Physiol. Plant.*, **83**, 463–468.

Cheng, Z., Wang, C., Tang, F., Zhou, Y., Zhu, C. and Ding, Y. (2025) The cell wall functions in plant heavy metal response. *Ecotoxicol. Environ. Saf.*, **299**, 118326.

Chețan, F., Moraru, P.I., Rusu, T., Șimon, A., Dinca, L. and Murariu, G. (2025) From contamination to mitigation: addressing cadmium pollution in agricultural soils. *Agriculture*, **15**, 2179.

Clemens, S. (2006) Toxic metal accumulation, responses to exposure and mechanisms of tolerance in plants. *Biochimie*, **88**, 1707–1719.

Cobbett, C. and Goldsbrough, P. (2002) Phytochelatins and metallothioneins : roles in heavy metal detoxification and homeostasis. *Annu. Rev. Plant Biol.*, **53**, 159–182.

Corpas, F.J., González-Gordo, S. and Palma, J.M. (2024) Ascorbate peroxidase in fruits and modulation of its activity by reactive species. *J. Exp. Bot.*, **75**, 2716–2732.

Cuypers, A., Plusquin, M., Remans, T., Jozefczak, M., Keunen, E., Gielen, H., Opdenakker, K., Ravindran Nair, A., Munters, E., Artois, T.J., Nawrot, T., Vangronsveld, J. and Smeets, K. (2010) Cadmium stress: an oxidative challenge. *BioMetals*, **23**, 927–940.

Cuypers, A., Vanbuel, I., Iven, V., Kunnen, K., Vandionant, S., Huybrechts, M. and Hendrix, S. (2023) Cadmium-induced oxidative stress responses and acclimation in plants require fine-tuning of redox biology at subcellular level. *Free Radical Biol. Med.*, **199**, 81–96.

Dawidowicz, A.L. and Olszowy, M. (2014) Does antioxidant properties of the main component of essential oil reflect its antioxidant properties? The comparison of antioxidant properties of essential oils and their main components. *Nat. Prod. Res.*, **28**, 1952–1963.

De Sousa, D.P., Damasceno, R.O.S., Amorati, R., Elshabrawy, H.A., De Castro, R.D., Bezerra, D.P., Nunes, V.R.V., Gomes, R.C. and Lima, T.C. (2023) Essential oils: chemistry and pharmacological activities. *Biomolecules*, **13**, 1144.

Degryse, F., Smolders, E. and Merckx, R. (2006) Labile Cd complexes increase Cd availability to plants. *Environ. Sci. Technol.*, **40**, 830–836.

Dguimi, H. M. , Debouba, M., Ghorbel, M.H. and Gouia, H. (2008) Tissue-specific cadmium accumulation and its effects on nitrogen metabolism in tobacco (*Nicotiana tabaccum*, bureley v. Fb9). *C. R., Biol.*, **332**, 58–68.

Dhifi, W., Bellili, S., Jazi, S., Bahloul, N. and Mnif, W. (2016) Essential oils' chemical characterization and investigation of some biological activities: a critical review. *Medicines*, **3**, 25–40.

Ding, H., Wang, B., Han, Y. and Li, S. (2020) The pivotal function of dehydroascorbate reductase in glutathione homeostasis in plants. *J. Exp. Bot.*, 71, 3405–3416.

Ding, S., Wang, L., Yang, Z., Lu, Q., Wen, X. and Lu, C. (2016) Decreased glutathione reductase2 leads to early leaf senescence in *Arabidopsis*. *J. Integr. Plant Biol.*, **58**, 29–47.

Dixit, V., Pandey, V. and Shyam, R. (2001) Differential antioxidative responses to cadmium in roots and leaves of pea (*Pisum sativum* L. cv. Azad). *J. Exp. Bot.*, **52**, 1101–1109.

Donsì, F. and Ferrari, G. (2016) Essential oil nanoemulsions as antimicrobial agents in food. *J. Biotechnol.*, **233**, 106–120.

Dudareva, N., Negre, F., Nagegowda, D.A. and Orlova, I. (2006) Plant volatiles: recent advances and future perspectives. *Crit. Rev. Plant Sci.*, **25**, 417–440.

Edo, G.I., Samuel, P.O., Oloni, G.O., et al. (2024) Environmental persistence, bioaccumulation, and ecotoxicology of heavy metals. *Chem. Ecol.*, **40**, 322–349.

El Rasafi, T., Oukarroum, A., Haddioui, A., et al. (2022) Cadmium stress in plants: a critical review of the effects, mechanisms, and tolerance strategies. *Crit. Rev. Environ. Sci. Technol.*, **52**, 675–726.

Esterbauer, H. and Cheeseman, K.H. (1990) Determination of aldehydic lipid peroxidation products: malondialdehyde and 4-hydroxynonenal. In: *Methods in Enzymology*, Vol. **186** (ed. by Packer, L.). Elsevier, pp. 407–421.

Fejes, G., Bodor, T., Szőllősi, R., Kondak, S., Kutasi, K., Fotopoulos, V. and Kolbert, Z. (2025) Nitric oxide as an integral element in priming-induced tolerance and plant stress memory. *J. Exp. Bot.*, 76, 3669–3685.

Ferreira, J.V.N., Capello, T.M., Siqueira, L.J.A., Lago, J.H.G. and Caseli, L. (2016) Mechanism of action of thymol on cell membranes investigated through lipid langmuir monolayers at the air–water interface and molecular simulation. *Langmuir*, **32**, 3234–3241.

Foyer, C.H. and Kunert, K. (2024) The ascorbate–glutathione cycle coming of age. *J. Exp. Bot.*, **75**, 2682–2699.

Gavrilaș, S., Burescu, F.-L., Chereji, B.-D. and Munteanu, F.-D. (2025) The impact of anthropogenic activities on the catchment's water quality parameters. *Water*, **17**, 1791.

Ge, W., Jiao, Y.Q., Sun, B.L., Qin, R., Jiang, W.S. and Liu, D.H. (2012) Cadmium-mediated oxidative stress and ultrastructural changes in root cells of poplar cultivars. *S. Afr. J. Bot.*, **83**, 98–108.

Genchi, G., Sinicropi, M.S., Lauria, G., Carocci, A. and Catalano, A. (2020) The effects of cadmium toxicity. *Int. J. Environ. Res. Public Health*, **17**, 3782.

Gentile, F., Arcaro, A., Pizzimenti, S., et al. (2017) DNA damage by lipid peroxidation products: implications in cancer, inflammation and autoimmunity. *AIMS Genet.*, **4**, 103–137.

Ghafarifarsani, H., Hoseinifar, S.H., Sheikhlar, A., Raissy, M., Chaharmahali, F.H., Maneepitaksanti, W., Faheem, M. and Van Doan, H. (2022) The effects of dietary thyme oil (Thymus vulgaris) essential oil on common carp (*Cyprinus carpio*): growth performance, digestive enzyme activity, antioxidant defense, tissue and mucus immune parameters, and resistance against *Aeromonas hydrophila*. *Aquacult. Nutr.*, 2022, 1–13.

Giberti, S., Funck, D. and Forlani, G. (2014) Δ1-pyrroline-5-carboxylate reductase from Arabidopsis thaliana: stimulation or inhibition by chloride ions and feedback regulation by proline depend on whether NADPH or NADH acts as co-substrate. *New Phytol.*, **202**, 911–919.

Gichner, T., Patková, Z., Száková, J., Žnidar, I. and Mukherjee, A. (2008) DNA damage in potato plants induced by cadmium, ethyl methanesulphonate and γ-rays. *Environ. Exp. Bot.*, **62**, 113–119.

Gill, S.S. and Tuteja, N. (2010) Reactive oxygen species and antioxidant machinery in abiotic stress tolerance in crop plants. *Plant Physiol. Biochem.*, **48**, 909–930.

Gocek-Szczurtek, N., Wróblewski, M., Żabka, A. and Polit, J.T. (2026) Thyme oil alleviates cadmium-induced disturbances in mitotic activity, cytoskeletal organization and H3T3/H3S10 phosphorylation in *Vicia faba*. *Int. J. Mol. Sci.*, **27**, 2798.

Gocek-Szczurtek, N., Żabka, A., Wróblewski, M., Kukula-Koch, W., Szczeblewski, P. and Polit, J.T. (2025) Thyme oil mitigates cadmium-induced oxidative and genotoxic stress in *Vicia faba* root meristem cells under in vitro conditions. *Sci. Rep.*, **15**, 38689.

Gocek-Szczurtek, N., Żabka, A., Wróblewski, M. and Polit, J.T. (2025) Stabilization of the MAPK–epigenetic signaling axis underlies the protective effect of thyme oil against cadmium stress in root meristem cells of *Vicia faba*. *Int. J. Mol. Sci.*, **27**, 208.

Grill, E., Löffler, S., Winnacker, E.-L. and Zenk, M.H. (1989) Phytochelatins, the heavy-metal-binding peptides of plants, are synthesized from glutathione by a specific γ-glutamylcysteine dipeptidyl transpeptidase (phytochelatin synthase). *Proc. Natl. Acad. Sci.*, **86**, 6838–6842.

Gupta, D., Tohoyama, H., Joho, M. and Inouhe, M. (2002) Possible roles of phytochelatins and glutathione metabolism in cadmium tolerance in chickpea roots. *J. Plant Res.*, **115**, 429–437.

Gupta, S.C. and Goldsbrough, P.B. (1990) Phytochelatin accumulation and stress tolerance in tomato cells exposed to cadmium. *Plant Cell Rep.*, 9, 466-469.

Gzyl, J., Chmielowska-Bąk, J., Przymusiński, R. and Gwóźdź, E.A. (2015) Cadmium affects microtubule organization and post-translational modifications of tubulin in seedlings of soybean (*Glycine max* L.). *Front. Plant Sci.*, **6**, 1–13.

Gzyl, J., Przymusiński, R. and Gwóźdź, E.A. (2009) Ultrastructure analysis of cadmium-tolerant and -sensitive cell lines of cucumber (*Cucumis sativus* L.). *Plant Cell Tissue Organ Cult. (PCTOC)*, **99**, 227–232.

Harada, E., Yamaguchi, Y., Koizumi, N. and Sano, H. (2002) Cadmium stress induces production of thiol compounds and transcripts for enzymes involved in sulfur assimilation pathways in *Arabidopsis*. *J. Plant Physiol.*, **159**, 445–448.

Hasanuzzaman, M., Bhuyan, M.H.M., Zulfiqar, F., Raza, A., Mohsin, S., Mahmud, J., Fujita, M. and Fotopoulos, V. (2020) Reactive oxygen species and antioxidant defense in plants under abiotic stress: revisiting the crucial role of a universal defense regulator. *Antioxidants*, **9**, 681–732.

Hassan, M.E., Hassan, R.R., Diab, K.A., El-Nekeety, A.A., Hassan, N.S. and Abdel-Wahhab, M.A. (2021) Nanoencapsulation of thyme essential oil: a new avenue to enhance its protective role against oxidative stress and cytotoxicity of zinc oxide nanoparticles in rats. *Environ. Sci. Pollut. Res.*, **28**, 52046–52063.

He, D., Cui, J., Gao, M., et al. (2019) Effects of soil amendments applied on cadmium availability, soil enzyme activity, and plant uptake in contaminated purple soil. *Sci. Total Environ.*, **654**, 1364–1371.

Heath, R.L. and Packer, L. (1968) Photoperoxidation in isolated chloroplasts. *Arch. Biochem. Biophys.*, **125**, 189–198.

Hernández-Cruz, E.Y., Arancibia-Hernández, Y.L., Loyola-Mondragón, D.Y. and Pedraza-Chaverri, J. (2022) Oxidative stress and its role in Cd-induced epigenetic modifications: use of antioxidants as a possible preventive strategy. *Oxygen*, **2**, 177–210.

Hirata, Y., Cai, R., Volchuk, A., Steinberg, B.E., Saito, Y., Matsuzawa, A., Grinstein, S. and Freeman, S.A. (2023) Lipid peroxidation increases membrane tension, Piezo1 gating, and cation permeability to execute ferroptosis. *Curr. Biol.*, **33**, 1282 –1294.e5.

Hong, Y., Zhang, W., Yang, L., Cao, Y., Sheng, H., Chen, J. and Yu, X. (2026) Thymol detoxifies and reduces cadmium accumulation in vegetables by activating multiple antioxidative systems and regulating cadmium transport. *Agronomy*, **16**, 475.

Hu, Y., He, R., Mu, X., Zhou, Y., Li, X., Wang, H., Xing, W. and Liu, D. (2025) Cadmium toxicity in plants: from transport to tolerance mechanisms. *Plant Signaling Behav.*, **20**, 2544316.

Huang, X., Duan, S., Wu, Q., Yu, M. and Shabala, S. (2020) Reducing cadmium accumulation in plants: structure–function relations and tissue-specific operation of transporters in the spotlight. *Plants*, **9**, 223–240.

Hudaib, M., Speroni, E., Di Pietra, A.M. and Cavrini, V. (2002) GC/MS evaluation of thyme (*Thymus vulgaris* L.) oil composition and variations during the vegetative cycle. *J. Pharm. Biomed. Anal.*, **29**, 691–700.

Jia, K., Zhan, Z., Wang, B., Wang, W., Wei, W., Li, D., Huang, W. and Xu, Z. (2023) Exogenous selenium enhances cadmium stress tolerance by improving physiological characteristics of cabbage (*Brassica oleracea* L. var. capitata) seedlings. *Horticulturae*, **9**, 1016.

Jisha, K.C. and Puthur, J.T. (2016) Seed priming with BABA (β-aminobutyric acid): a cost-effective method of abiotic stress tolerance in *Vigna radiata* (L.) Wilczek. *Protoplasma*, **253**, 277–289.

Jócsák, I., Malgwi, I., Rabnecz, G., Szegő, A., Varga-Visi, É., Végvári, G. and Pónya, Z. (2020) Effect of cadmium stress on certain physiological parameters, antioxidative enzyme activities and biophoton emission of leaves in barley (*Hordeum vulgare* L.) seedlings. PLOS One, **15**, e0240470.

Ju, Y., Luo, Z., Bi, J., Liu, C. and Liu, X. (2024) Transfer of heavy metals from soil to tea and the potential human health risk in a regional high geochemical background area in southwest China. *Sci. Total Environ.*, **908**, 168122.

Kampfenkel, K., Van Montagu, M. and Inzé, D. (1995) Extraction and determination of ascorbate and dehydroascorbate from plant tissue. *Anal. Biochem.*, **225**, 165–167.

Kandemir, F.M., Caglayan, C., Darendelioğlu, E., Küçükler, S., İzol, E. and Kandemir, Ö. (2021) Modulatory effects of carvacrol against cadmium-induced hepatotoxicity and nephrotoxicity by molecular targeting regulation. *Life Sci.*, **277**, 119610.

Karyotou, K. and Donaldson, R.P. (2005) Ascorbate peroxidase, a scavenger of hydrogen peroxide in glyoxysomal membranes. *Arch. Biochem. Biophys.*, **434**, 248–257.

Kaya, O., Bozkurt, A., Karakus, S., Daler, S. and Yilmaz, T. (2024) Essential oil compounds modulate nutritional quality and stress response in botrytis cinerea-infected grape (*Vitis vinifera* L. cv. 'Karaerik'). *Physiol. Mol. Plant Pathol.*, **133**, 102346.

Keltjens, W.G. and Van Beusichem, M.L. (1998) Phytochelatins as biomarkers for heavy metal stress in maize (*Zea mays* L.) and wheat (*Triticum aestivum* L.): combined effects of copper and cadmium. *Plant Soil*, **203**, 119–126.

Keunen, E., Remans, T., Bohler, S., Vangronsveld, J. and Cuypers, A. (2011) Metal-induced oxidative stress and plant mitochondria. *Int. J. Mol. Sci.*, **12**, 6894–6918.

Kowalczyk, A., Przychodna, M., Sopata, S., Bodalska, A. and Fecka, I. (2020) Thymol and thyme essential oil—new insights into selected therapeutic applications. *Molecules*, **25**, 4125.

Krzesłowska, M. (2011) The cell wall in plant cell response to trace metals: polysaccharide remodeling and its role in defense strategy. *Acta Physiol. Plant.*, **33**, 35–51.

Kubier, A., Wilkin, R.T. and Pichler, T. (2019) Cadmium in soils and groundwater: a review. *Appl. Geochem.*, **108**, 104388.

Kumar, M., Bishnoi, R.S., Shukla, A.K. and Jain, C.P. (2019) Techniques for formulation of nanoemulsion drug delivery system: a review. *Prev. Nutr. Food Sci.*, **24**, 225–234.

Kumar, P., Tewari, R.K. and Sharma, P.N. (2008) Cadmium enhances generation of hydrogen peroxide and amplifies activities of catalase, peroxidases and superoxide dismutase in maize. *J. Agron. Crop Sci.*, **194**, 72–80.

Landi, S., Polito, F., Esposito, S., Sorbo, S., Cianciullo, P., Postiglione, A., De Feo, V., Basile, A. and Maresca, V. (2025) Protective effect of *Ocimum basilicum* L. essential oil on *Lactuca sativa* L. treated with cadmium. *Plant Physiol. Biochem.*, **219**, 109437.

Le Faucheur, S., Schildknecht, F., Behra, R. and Sigg, L. (2006) Thiols in *Scenedesmus vacuolatus* upon exposure to metals and metalloids. *Aquat. Toxicol.*, **80**, 355–361.

Lee, M., Lim, S., Song, J.-A., Kim, M.-E. and Hur, M.-H. (2017) The effects of aromatherapy essential oil inhalation on stress, sleep quality and immunity in healthy adults: randomized controlled trial. *Eur. J. Integr. Med.*, **12**, 79–86.

Li, F., Qi, J., Zhang, G., Lin, L., Fang, P., Tao, A. and Xu, J. (2013) Effect of cadmium stress on the growth, antioxidative enzymes and lipid peroxidation in two kenaf (*Hibiscus cannabinus* L.) plant seedlings. *J. Integr. Agric.*, **12**, 610–620.

Li, X., Wang, X., Chen, J., Luo, D., Cao, S. and Ba, L. (2025) Thymol maintains peppers quality by regulating antioxidant capacity, cell wall metabolism and membrane lipid metabolism. *Food Chem.: X*, **25**, 102138.

Li, Y., Zhang, S., Jiang, W. and Liu, D. (2013) Cadmium accumulation, activities of antioxidant enzymes, and malondialdehyde (MDA) content in *Pistia stratiotes* L. *Environ. Sci. Pollut. Res.*, **20**, 1117–1123.

Liao, W., Dumas, E., Ghnimi, S., Elaissari, A. and Gharsallaoui, A. (2021) Effect of emulsifier and droplet size on the antibacterial properties of emulsions and emulsion-based films containing essential oil compounds. *J. Food Process. Preserv.*, **45**, e16072.

Lin, A., Zhang, X., Chen, M. and Cao, Q. (2007) Oxidative stress and DNA damages induced by cadmium accumulation. *J. Environ. Sci.*, **19**, 596–602.

Liolios, C.C., Gortzi, O., Lalas, S., Tsaknis, J. and Chinou, I. (2009) Liposomal incorporation of carvacrol and thymol isolated from the essential oil of *Origanum dictamnus* L. and in vitro antimicrobial activity. *Food Chem.*, **112**, 77–83.

Liu, D. and Kottke, I. (2004) Subcellular localization of cadmium in the root cells of *Allium cepa* by electron energy loss spectroscopy and cytochemistry. *J. Biosci.*, **29**, 329–335.

Loix, C., Huybrechts, M., Vangronsveld, J., Gielen, M., Keunen, E. and Cuypers, A. (2017) Reciprocal interactions between cadmium-induced cell wall responses and oxidative stress in plants. *Front. Plant Sci.*, **8**, 1867.

Luo, P., Wu, J., Li, T.-T., Shi, P., Ma, Q. and Di, D.-W. (2024) An overview of the mechanisms through which plants regulate ROS homeostasis under cadmium stress. *Antioxidants*, **13**, 1174.

Madkour, M., Hosny, M., Aboelazab, O., Fahmy, S., Rayan, G., Ali, A.H.H., Abdel Moati, Y.A., Elolimy, A.A. and Fathi, M. (2025) Dietary encapsulated essential oils improve growth performance and regulate stress-responsive genes in heat-stressed broilers. *J. Anim. Sci.*, **103**, skaf417.

Maier, E.A., Matthews, R.D., McDowell, J.A., Walden, R.R. and Ahner, B.A. (2003) Environmental cadmium levels increase phytochelatin and glutathione in lettuce grown in a chelator-buffered nutrient solution. *J. Environ. Qual.*, **32**, 1356–1364.

Mansoor, S., Ali, A., Kour, N., Bornhorst, J., AlHarbi, K., Rinklebe, J., Abd El Moneim, D., Ahmad, P. and Chung, Y.S. (2023) Heavy metal induced oxidative stress mitigation and ROS scavenging in plants. *Plants*, **12**, 3003.

Marnett, L.J. (1999) Lipid peroxidation—DNA damage by malondialdehyde. *Mutat. Res. Fundam. Mol. Mech. Mutagen.*, **424**, 83–95.

McBride, M.B. (2002) Cadmium uptake by crops estimated from soil total Cd and pH: *Soil sci.*, **167**, 62–67.

Mendoza-Cózatl, D.G., Zhai, Z., Jobe, T.O., et al. (2010) Tonoplast-localized Abc2 transporter mediates phytochelatin accumulation in vacuoles and confers cadmium tolerance. *J. Biol. Chem.*, **285**, 40416–40426.

Mittler, R. (2002) Oxidative stress, antioxidants and stress tolerance. *Trends Plant Sci.*, **7**, 405–410.

Mohammed, A.A., Al- Ali, A.A.A. and Abdullah, S.A.G. (2024) Protective role of thyme oil (*Thymus vulgaris*) against cadmium chloride-induced renal damage in common carp (*Cyprinus carpio*). *Basrah Res. Sci.*, **50**, 298–317.

Nacca, F., Cozzolino, C., Carillo, P., Woodrow, P., Fuggi, A. and Ciarmiello, L.F. (2021) An HPLC-automated derivatization for glutathione and related thiols analysis in *Brassica rapa* L. *Agronomy*, **11**, 1157.

Najmanova, J., Neumannova, E., Leonhardt, T., Zitka, O., Kizek, R., Macek, T., Mackova, M. and Kotrba, P. (2012) Cadmium-induced production of phytochelatins and speciation of intracellular cadmium in organs of *Linum usitatissimum* seedlings. *Ind. Crops Prod.*, **36**, 536–542.

Nakano, Y. and Asada, K. (1981) Hydrogen peroxide is scavenged by ascorbate-specific peroxidase in spinach chloroplasts. *Plant Cell Physiol.*, **22**, 867–880.

Nasrallah, A.K., Atia, M.A.M., Abd El-Maksoud, R.M., Kord, M.A. and Fouad, A.S. (2022) Salt priming as a smart approach to mitigate salt stress in faba bean (*Vicia faba* L.). *Plants*, **11**, 1610.

Noctor, G. (2025) Hydrogen peroxide, ascorbate, and glutathione: building the foyer–halliwell–asada pathway. *Planta*, **261**, 132.

Noctor, G. and Foyer, C.H. (1998) Ascorbate and glutathione: keeping active oxygen under control. *Annu. Rev. Plant Physiol. Plant Mol. Biol.*, **49**, 249–279.

Noor, I., Sohail, H., Akhtar, M.T., et al. (2024) From stress to resilience: unraveling the molecular mechanisms of cadmium toxicity, detoxification and tolerance in plants. *Sci. Total Environ.*, **954**, 176462.

O'Lexy, R., Kasai, K., Clark, N., Fujiwara, T., Sozzani, R. and Gallagher, K.L. (2018) Exposure to heavy metal stress triggers changes in plasmodesmatal permeability via deposition and breakdown of callose. *J. Exp. Bot.*, **69**, 3715–3728.

Pandey, N. and Singh, G.K. (2012) Studies on antioxidative enzymes induced by cadmium in pea plants (*Pisum sativum*). *J. Environ. Biol.*, **33**, 201–206.

Pandur, E., Micalizzi, G., Mondello, L., Horváth, A., Sipos, K. and Horváth, G. (2022) Antioxidant and anti-inflammatory effects of thyme (*Thymus vulgaris* L.) essential oils prepared at different plant phenophases on *Pseudomonas aeruginos*a LPS-activated THP-1 macrophages. *Antioxidants*, **11**, 1330.

Pannala, V.R., Bazil, J.N., Camara, A.K.S. and Dash, R.K. (2013) A biophysically based mathematical model for the catalytic mechanism of glutathione reductase. *Free Radical Biol. Med.*, **65**, 1385–1397.

Park, J., Song, W.-Y., Ko, D., Eom, Y., Hansen, T.H., Schiller, M., Lee, T.G., Martinoia, E. and Lee, Y. (2012) The phytochelatin transporters AtABCC1 and AtABCC2 mediate tolerance to cadmium and mercury. *Plant J.*, **69**, 278–288.

Parrotta, L. (2015) Target or barrier? The cell wall of early- and later-diverging plants vs cadmium toxicity: differences in the response mechanisms. *Front. Plant Sci.*, **6**, 1–16.

Pavoni, L., Perinelli, D.R., Bonacucina, G., Cespi, M. and Palmieri, G.F. (2020) An overview of micro- and nanoemulsions as vehicles for essential oils: formulation, preparation and stability. *Nanomaterials*, **10**, 135–158.

Pei, Z.-M., Murata, Y., Benning, G., Thomine, S., Klüsener, B., Allen, G.J., Grill, E. and Schroeder, J.I. (2000) Calcium channels activated by hydrogen peroxide mediate abscisic acid signalling in guard cells. *Nature*, **406**, 731–734.

Perfus-Barbeoch, L., Leonhardt, N., Vavasseur, A. and Forestier, C. (2002) Heavy metal toxicity: cadmium permeates through calcium channels and disturbs the plant water status. *Plant J.*, **32**, 539–548.

Pichersky, E. and Gershenzon, J. (2002) The formation and function of plant volatiles: perfumes for pollinator attraction and defense. *Curr. Opin. Plant Biol.*, **5**, 237–243.

Polit, J.T. (2009) Protein phosphorylation in *Vicia faba* root meristem cells during the first steps of leaving principal control points after sucrose application. *Plant Cell Rep.*, **28**, 165–173.

Potters, G., Pasternak, T.P., Guisez, Y., Palme, K.J. and Jansen, M.A.K. (2007) Stress-induced morphogenic responses: growing out of trouble? *Trends Plant Sci.*, **12**, 98–105.

Pukacka, S. and Ratajczak, E. (2006) Antioxidative response of ascorbate–glutathione pathway enzymes and metabolites to desiccation of recalcitrant *Acer saccharinum* seeds. *J. Plant Physiol.*, **163**, 1259–1266.

Purcarea, C., Laslo, V., Memete, A.R., Agud, E., Miere (Groza), F. and Vicas, S.I. (2022) Antigenotoxic and antimutagenic potentials of proline in *Allium cepa* exposed to the toxicity of cadmium. *Agriculture*, **12**, 1568.

Rahmani, F., Nabi, S., Idliki, R.B., Alimirzaei, M., Barkhordar, S.M.A., Shafaei, N., Zareian, M., Karimi, E. and Oskoueian, E. (2022) Thyme oil nanoemulsion enhanced cellular antioxidant and suppressed inflammation in mice challenged by cadmium-induced oxidative stress. *Waste Biomass Valorization*, **13**, 3139–3146.

Reynolds, E.S. (1963) The use of lead citrate at high pH as an electron-opaque stain in electron microscopy. *J. Cell Biol.*, **17**, 208–212.

Rodrigues De Queiroz, A., Hines, C., Brown, J., et al. (2023) The effects of exogenously applied antioxidants on plant growth and resilience. *Phytochem. Rev.*, **22**, 407–447.

Rodríguez-Serrano, M., Romero-Puertas, M.C., Pazmiño, D.M., Testillano, P.S., Risueño, M.C., Del Río, L.A. and Sandalio, L.M. (2009) Cellular response of pea plants to cadmium toxicity: cross talk between reactive oxygen species, nitric oxide, and calcium. *Plant Physiol.*, **150**, 229–243.

Ruttkay-Nedecky, B., Nejdl, L., Gumulec, J., Zitka, O., Masarik, M., Eckschlager, T., Stiborova, M., Adam, V. and Kizek, R. (2013) The role of metallothionein in oxidative stress. *Int. J. Mol. Sci.*, **14**, 6044–6066.

Salemi, F., Nasr Esfahani, M. and Tran, L.-S.P. (2019) Mechanistic insights into enhanced tolerance of early growth of alfalfa (*Medicago sativa* L.) under low water potential by seed-priming with ascorbic acid or polyethylene glycol solution. *Ind. Crops Prod.*, **137**, 436–445.

Sallam, N.M.A., Ali, E.F., Abo-Elyousr, K.A.M., Bereika, M.F.F. and Seleim, M.A.A. (2021) Thyme oil treatment controls bacterial wilt disease symptoms by inducing antioxidant enzyme activity in *Solanum tuberosum*. *J. Plant Pathol.*, **103**, 563–572.

Sánchez, M.E., Turina, A.D.V., García, D.A., Verónica Nolan, M. and Perillo, M.A. (2004) Surface activity of thymol: implications for an eventual pharmacological activity. *Colloids Surf., B*, **34**, 77–86.

Schaedle, M. and Bassham, J.A. (1977) Chloroplast glutathione reductase. *Plant Physiol.*, **59**, 1011–1012.

Segers, A., Dumoulin, L., Megido, R.C., et al. (2022) Varietal and environmental effects on the production of faba bean (vicia faba L.) seeds for the food industry by confrontation of agricultural and nutritional traits with resistance against bruchus spp. (coleoptera: chrysomelidae, bruchinae). *Agric. Ecosyst. Environ.*, **327**, 107831.

Sellamuthu, P.S., Sivakumar, D., Soundy, P. and Korsten, L. (2013) Essential oil vapours suppress the development of anthracnose and enhance defence related and antioxidant enzyme activities in avocado fruit. *Postharvest Biol. Technol.*, **81**, 66–72.

Semane, B., Cuypers, A., Smeets, K., Van Belleghem, F., Horemans, N., Schat, H. and Vangronsveld, J. (2007) Cadmium responses in *Arabidopsis thaliana*: glutathione metabolism and antioxidative defence system. *Physiol. Plant.*, **129**, 519–528.

Shabbir, A., Shah, A.A., Usman, S., Ahmed, S., Kaleem, M., Shafique, S. and Gatasheh, M.K. (2025) Efficacy of malic and tartaric acid in mitigation of cadmium stress in *Spinacia oleracea* L. via modulations in physiological and biochemical attributes. *Sci. Rep.*, **15**, 3366.

Shafiq, F., Raza, S.H., Bibi, A., Khan, I. and Iqbal, M. (2018) Influence of proline priming on antioxidative potential and ionic distribution and its relationship with salt tolerance of wheat. *Cereal Res. Commun.*, **46**, 287–300.

Silva, H.D., Cerqueira, M.A. and Vicente, A.A. (2015) Influence of surfactant and processing conditions in the stability of oil-in-water nanoemulsions. *J. Food Eng.*, **167**, 89–98.

Song, Y., Jin, L. and Wang, X. (2017) Cadmium absorption and transportation pathways in plants. *Int. J. Phytorem.*, **19**, 133–141.

Sönmez, A.Y., Bilen, S., Alak, G., Hisar, O., Yanık, T. and Biswas, G. (2015) Growth performance and antioxidant enzyme activities in rainbow trout (*Oncorhynchus mykiss*) juveniles fed diets supplemented with sage, mint and thyme oils. *Fish Physiol. Biochem.*, **41**, 165–175.

Sood, M. (2025) Reactive oxygen species (ROS): plant perspectives on oxidative signalling and biotic stress response. *Discov. Plants*, **2**, 187.

Souguir, D., Ferjani, E., Ledoigt, G. and Goupil, P. (2011) Sequential effects of cadmium on genotoxicity and lipoperoxidation in *Vicia faba* roots. *Ecotoxicology*, **20**, 329–336.

Sperdouli, I., Adamakis, I.-D., Dobrikova, A., Apostolova, E., Hanć, A. and Moustakas, M. (2022) Excess zinc supply reduces cadmium uptake and mitigates cadmium toxicity effects on chloroplast structure, oxidative stress, and photosystem II photochemical efficiency in *Salvia sclarea* plants. *Toxics*, **10**, 36–51.

Srinivas, U.S., Tan, B.W.Q., Vellayappan, B.A. and Jeyasekharan, A.D. (2019) ROS and the DNA damage response in cancer. *Redox Biol.*, **25**, 101084.

Srivastava, R.K., Rajpoot, R., Pandey, P., Rani, A. and Dubey, R.S. (2018) Cadmium alters mitochondrial membrane potential, inhibits electron transport chain activity and induces callose deposition in rice seedlings. *J. Plant Growth Regul.*, **37**, 335–344.

Stępiński, D. (2014) Functional ultrastructure of the plant nucleolus. *Protoplasma*, **251**, 1285–1306.

Sun, C., Chen, J., Wang, L., Li, J., Shi, Z., Yang, L. and Yu, X. (2024) Thymol deploys multiple antioxidative systems to suppress ROS accumulation in Chinese cabbage seedlings under saline stress. *Agronomy*, **14**, 1059.

Sun, H., Wang, X., Li, H., Bi, J., Yu, J., Liu, X., Zhou, H. and Rong, Z. (2020) Selenium modulates cadmium-induced ultrastructural and metabolic changes in cucumber seedlings. *RSC Adv.*, **10**, 17892–17905.

Szabados, L. and Savouré, A. (2010) Proline: a multifunctional amino acid. *Trends Plant Sci.*, **15**, 89–97.

Szentandrássy, N., Szentesi, P., Magyar, J., Nánási, P.P. and Csernoch, L. (2003) Effect of thymol on kinetic properties of Ca and K currents in rat skeletal muscle. *BMC Pharmacol.*, **3**, 9–16.

Talarek-Karwel, M., Bajguz, A. and Piotrowska-Niczyporuk, A. (2020) 24-epibrassinolide modulates primary metabolites, antioxidants, and phytochelatins in *Acutodesmus obliquus* exposed to lead stress. *J. Appl. Phycol.*, **32**, 263–276.

Ünyayar, S., Çelik, A., Çekiç, F.Ö. and Gözel, A. (2006) Cadmium-induced genotoxicity, cytotoxicity and lipid peroxidation in *Allium sativum* and *Vicia faba*. *Mutagenesis*, **21**, 77–81.

Valgimigli, L. (2023) Lipid peroxidation and antioxidant protection. *Biomolecules*, **13**, 1291.

Velikova, V., Yordanov, I. and Edreva, A. (2000) Oxidative stress and some antioxidant systems in acid rain-treated bean plants. *Plant Sci.*, **151**, 59–66.

Verdeguer, M., Sánchez-Moreiras, A.M. and Araniti, F. (2020) Phytotoxic effects and mechanism of action of essential oils and terpenoids. *Plants*, **9**, 1571.

Violante, A., Cozzolino, V., Perelomov, L., Caporale, A.G. and Pigna, M. (2010) Mobility and bioavailability of heavy metals and metalloids in soil environments. *J. Soil Sci. Plant Nutr.*, **10**, 1–25.

Wang, R., Sang, P., Guo, Y., Jin, P., Cheng, Y., Yu, H., Xie, Y., Yao, W. and Qian, H. (2023) Cadmium in food: source, distribution and removal. *Food Chem.*, **405**, 134666.

Wang, Z., Zhang, Y., Huang, Z. and Huang, L. (2008) Antioxidative response of metal-accumulator and non-accumulator plants under cadmium stress. *Plant Soil*, **310**, 137–149.

Wu, S.-W., Kumar, R., Iswanto, A.B.B. and Kim, J.-Y. (2018) Callose balancing at plasmodesmata. *J. Exp. Bot.*, 69, 5325–5339.

Wu, Y., Guo, Z., Zhang, W., Tan, Q., Zhang, L., Ge, X. and Chen, M. (2016) Quantitative relationship between cadmium uptake and the kinetics of phytochelatin induction by cadmium in a marine diatom. *Sci. Rep.*, **6**, 35935.

Xiao, Q., Wang, Y., Lü, Q., Wen, H., Han, B., Chen, S., Zheng, X. and Lin, R. (2020) Responses of glutathione and phytochelatins biosysthesis in a cadmium accumulator of *Perilla frutescens* (L.) Britt. under cadmium- contaminated conditions. *Ecotoxicol. Environ. Saf.*, **201**, 110805.

Yakoubi, S., Kobayashi, I., Uemura, K., Nakajima, M., Isoda, H., Ksouri, R., Saidani-Tounsi, M. and Neves, M.A. (2021) Essential-oil-loaded nanoemulsion lipidic-phase optimization and modeling by response surface methodology (RSM): enhancement of their antimicrobial potential and bioavailability in nanoscale food delivery system. *Foods*, **10**, 3149.

Yanishlieva, N.V., Marinova, E.M., Gordon, M.H. and Raneva, V.G. (1999) Antioxidant activity and mechanism of action of thymol and carvacrol in two lipid systems. *Food Chem.*, **64**, 59–66.

Ye, X., Ling, T., Xue, Y., Xu, C., Zhou, W., Hu, L., Chen, J. and Shi, Z. (2016) Thymol mitigates cadmium stress by regulating glutathione levels and reactive oxygen species homeostasis in tobacco seedlings. *Molecules*, **21**, 1339.

Youdim, K.A., Deans, S.G. and Finlayson, H.J. (2002) The antioxidant properties of thyme (*Thymus zygis* L.) essential oil: an inhibitor of lipid peroxidation and a free radical scavenger. *J. Essent. Oil Res.*, **14**, 210–215.

Yu, F., Liu, K., Li, M., Zhou, Z., Deng, H. and Chen, B. (2013) Effects of cadmium on enzymatic and non-enzymatic antioxidative defences of rice (*Oryza Sativa* L.). *Int. J. Phytorem.*, **15**, 513–521.

Yu, H., Wu, Y., Huang, H., Zhan, J., Wang, K. and Li, T. (2020) The predominant role of pectin in binding Cd in the root cell wall of a high Cd accumulating rice line (*Oryza sativa* L.). *Ecotoxicol. Environ. Saf.*, **206**, 111210.

Żabka, A., Gocek, N., Krajewski, K., Szczeblewski, P., Laskowski, T. and Polit, J. (2021) Changes in epigenetic patterns related to DNA replication in *Vicia faba* root meristem cells under cadmium-induced stress conditions. *Cells*, **10**, 3409.

Żabka, A., Winnicki, K., Polit, J.T., Wróblewski, M. and Maszewski, J. (2021) Cadmium (II)-induced oxidative stress results in replication stress and epigenetic modifications in root meristem cell nuclei of *Vicia faba*. *Cells*, **10**, 640–659.

Zdunek-Zastocka, E., Grabowska, A., Michniewska, B. and Orzechowski, S. (2021) Proline concentration and its metabolism are regulated in a leaf age dependent manner but not by abscisic acid in pea plants exposed to cadmium stress. *Cells*, **10**, 946–961.

Zechmann, B. (2019) Ultrastructure of plastids serves as reliable abiotic and biotic stress marker. *PLOS One*, **14**, e0214811.

Zhang, H., Zhang, F., Xia, Y., Wang, G. and Shen, Z. (2010) Excess copper induces production of hydrogen peroxide in the leaf of *Elsholtzia haichowensis* through apoplastic and symplastic CuZn-superoxide dismutase. *J. Hazard. Mater.*, **178**, 834–843.

Zheng, C., Chen, J.-P., Wang, X.-W. and Li, P. (2025) Reactive oxygen species in plants: metabolism, signaling, and oxidative modifications. *Antioxidants*, **14**, 617.

❖

Oświadczenia współautorów publikacji

Łódź, 25.03.2026

mgr Natalia Gocek-Szczurtek
Katedra Cytofizjologii
Wydział Biologii i Ochrony Środowiska
Uniwersytet Łódzki

Oświadczenie współautora publikacji

Oświadczam, że mój udział w publikacji:

1. Żabka, A.*; **Gocek, N.**; Polit, J.T.; Maszewski, J. Epigenetic Modifications Evidenced by Isolation of Proteins on Nascent DNA and Immunofluorescence in Hydroxyurea-Treated Root Meristem Cells of *Vicia faba*. *Planta* **2023**, *258*, 95, doi:10.1007/s00425-023-04249-2.

polegał na:

- współuczestnictwie w: uzyskaniu wyników badań oraz przeprowadzeniu i opracowaniu analiz statystycznych.

Oświadczam, że mój udział w poniżej wymienionych publikacjach:

1. **Gocek-Szczurtek, N***.; Żabka, A.; Wróblewski, M.; Kukula-Koch, W.; Szczeblewski, P.; Polit, J.T. Thyme Oil Mitigates Cadmium-Induced Oxidative and Genotoxic Stress in *Vicia faba* Root Meristem Cells under in vitro Conditions. *Sci. Rep.* **2025**, *15*, 38689, doi:10.1038/s41598-025-22588-w.

2. **Gocek-Szczurtek, N.**; Żabka, A.; Wróblewski, M.; Polit, J.T.* Stabilization of the MAPK-Epigenetic Signaling Axis Underlies the Protective Effect of Thyme Oil against Cadmium Stress in Root Meristem Cells of *Vicia faba*. *Int. J. Mol. Sci.* **2025**, *27*, 208, doi:10.3390/ijms27010208.

3. **Gocek-Szczurtek, N.**; Wróblewski, M.; Żabka, A.; Polit, J.T.* Thyme Oil Alleviates Cadmium Induced Disturbances in Mitotic Activity, Cytoskeletal Organization and H3T3/H3S10 Phosphorylation in *Vicia faba*. *Int. J. Mol. Sci* **2026**, 27, 2798, doi:10.3390/ijms27062798.

4. **Gocek-Szczurtek, N.***; Piotrowska-Niczyporuk, A.; Zambrzycka-Szelewa, E.; Ciereszko, I.; Żabka, A.; Wróblewski, M.; Polit, J.T. Thyme Essential Oil Reduces Cadmium Uptake and Toxicity in *Vicia faba* Root Meristem Cells, Involving Stabilization of Cell Ultrastructure and Modulation of Redox Response and Thiol Metabolism. - manuskrypt przygotowany do złożenia w czasopiśmie *The Plant Journal*

polegał na:

- pozyskaniu finansowania badań i administrowaniu projektem,
- współuczestnictwie w: opracowaniu koncepcji badań, planowaniu pracy eksperymentalnej, opracowaniu i dostosowaniu metodyki badawczej, walidacji uzyskanych wyników,
- przeprowadzeniu eksperymentów przy wsparciu pomocy technicznej i opiekunów poszczególnych zadań w macierzystej jednostce badawczej oraz w jednostkach zewnętrznych,
- zarzadzaniu danymi badawczymi,
- przygotowaniu manuskryptu,
- przygotowaniu szaty graficznej przy wsparciu w zakresie walorów estetycznych - układu, czytelności i spójności,
- współudziale w korekcie manuskryptu zgodnej z zaleceniami recenzentów.

* - autor korespondujący

Natalia Gocek-Szczurtek
Podpis

Łódź, 25.03.2026

dr hab. Justyna T. Polit, prof. UŁ
Katedra Cytofizjologii
Wydział Biologii i Ochrony Środowiska
Uniwersytet Łódzki

Oświadczenie współautora publikacji

Oświadczam, że mój udział w publikacji:

1. Żabka, A.*; Gocek, N.; **Polit, J.T.**; Maszewski, J. Epigenetic Modifications Evidenced by Isolation of Proteins on Nascent DNA and Immunofluorescence in Hydroxyurea-Treated Root Meristem Cells of *Vicia Faba*. *Planta* **2023**, *258*, 95, doi:10.1007/s00425-023-04249-2.

polegał na:

- współuczestnictwie w: uzyskaniu wyników badań oraz przeprowadzeniu i opracowaniu analiz statystycznych.

Oświadczam, że mój udział w poniżej wymienionych publikacjach:

1. Gocek-Szczurtek, N*.; Żabka, A.; Wróblewski, M.; Kukula-Koch, W.; Szczeblewski, P.; **Polit, J.T.** Thyme Oil Mitigates Cadmium-Induced Oxidative and Genotoxic Stress in *Vicia faba* Root Meristem Cells under in vitro Conditions. *Sci. Rep.* **2025**, *15*, 38689, doi:10.1038/s41598-025-22588-w.

2. Gocek-Szczurtek, N.; Żabka, A.; Wróblewski, M.; **Polit, J.T.*** Stabilization of the MAPK-Epigenetic Signaling Axis Underlies the Protective Effect of Thyme Oil against Cadmium Stress in Root Meristem Cells of *Vicia faba*. *Int. J. Mol. Sci.* **2025**, *27*, 208, doi:10.3390/ijms27010208.

3. Gocek-Szczurtek, N.; Wróblewski, M.; Żabka, A.; **Polit, J.T.*** Thyme Oil Alleviates Cadmium Induced Disturbances in Mitotic Activity, Cytoskeletal Organization and H3T3/H3S10 Phosphorylation in *Vicia faba*. *Int. J. Mol. Sci* 2026, 27, 2798, doi:10.3390/ijms27062798.

4. Gocek-Szczurtek, N.*; Piotrowska-Niczyporuk, A.; Zambrzycka-Szelewa, E.; Ciereszko, I.; Żabka, A.; Wróblewski, M.; **Polit, J.T.** Thyme Essential Oil Reduces Cadmium Uptake and Toxicity in *Vicia faba* Root Meristem Cells, Involving Stabilization of Cell Ultrastructure and Modulation of Redox Response and Thiol Metabolism. - manuskrypt przygotowany do złożenia w czasopiśmie *The Plant Journal*

polegał na:

- wsparciu merytorycznym w pozyskaniu finansowania badań,
- współuczestnictwie w: opracowaniu koncepcji badań, planowaniu pracy eksperymentalnej oraz opracowywaniu i dostosowywaniu metodyki badawczej,
- sprawowaniu nadzoru merytorycznego nad prowadzonymi badaniami,
- uczestnictwie w walidacji uzyskanych wyników,
- wprowadzaniu korekt do przygotowywanego manuskryptu oraz do jego poprawek zgodnych z zaleceniami recenzentów.

* - autor korespondujący

Justyna Polit
.....
Podpis

Łódź, 25.03.2026

dr Aneta Żabka
Katedra Cytofizjologii
Wydział Biologii i Ochrony Środowiska
Uniwersytet Łódzki

Oświadczenie współautora publikacji

Oświadczam, że mój udział w publikacji:

1. **Żabka, A.***; Gocek, N.; Polit, J.T.; Maszewski, J. Epigenetic Modifications Evidenced by Isolation of Proteins on Nascent DNA and Immunofluorescence in Hydroxyurea-Treated Root Meristem Cells of *Vicia faba*. *Planta* **2023**, *258*, 95, doi:10.1007/s00425-023-04249-2.

polegał na:

- współuczestnictwie w: opracowaniu koncepcji badań i projektowaniu oraz przeprowadzaniu eksperymentów, analizie wyników, przygotowaniu manuskryptu głównego oraz w opracowaniu figur, przygotowaniu i weryfikacji poprawionej wersji manuskryptu.

Oświadczam, że mój udział w poniżej wymienionych publikacjach:

1. Gocek-Szczurtek, N*.; **Żabka, A.**; Wróblewski, M.; Kukula-Koch, W.; Szczeblewski, P.; Polit, J.T. Thyme Oil Mitigates Cadmium-Induced Oxidative and Genotoxic Stress in *Vicia faba* Root Meristem Cells under in vitro Conditions. *Sci. Rep.* **2025**, *15*, 38689, doi:10.1038/s41598-025-22588-w.

2. Gocek-Szczurtek, N.; **Żabka, A.**; Wróblewski, M.; Polit, J.T.* Stabilization of the MAPK-Epigenetic Signaling Axis Underlies the Protective Effect of Thyme Oil against Cadmium Stress in Root Meristem Cells of *Vicia faba*. *Int. J. Mol. Sci.* **2025**, *27*, 208, doi:10.3390/ijms27010208.

3. Gocek-Szczurtek, N.; Wróblewski, M.; **Żabka, A.**; Polit, J.T.* Thyme Oil Alleviates Cadmium Induced Disturbances in Mitotic Activity, Cytoskeletal Organization and H3T3/H3S10 Phosphorylation in *Vicia faba*. *Int. J. Mol. Sci* **2026**, 27, 2798, doi:10.3390/ijms27062798.

4. Gocek-Szczurtek, N.*; Piotrowska-Niczyporuk, A.; Zambrzycka-Szelewa, E.; Ciereszko, I.; **Żabka, A.**; Wróblewski, M.; Polit, J.T. Thyme Essential Oil Reduces Cadmium Uptake and Toxicity in *Vicia faba* Root Meristem Cells, Involving Stabilization of Cell Ultrastructure and Modulation of Redox Response and Thiol Metabolism. - manuskrypt przygotowany do złożenia w czasopiśmie *The Plant Journal*

polegał na:

- współuczestnictwie w: opracowaniu koncepcji badań, planowaniu pracy eksperymentalnej oraz opracowywaniu i dostosowywaniu metodyki badawczej,
- uczestnictwie w walidacji uzyskanych wyników.

* - autor korespondujący

Aneta Żabka
.....
Podpis

Łódź, 25.03.2026

mgr Mateusz Wróblewski
Katedra Cytofizjologii
Wydział Biologii i Ochrony Środowiska
Uniwersytet Łódzki

Oświadczenie współautora publikacji

Oświadczam, że mój udział w poniżej wymienionych publikacjach:

1. Gocek-Szczurtek, N*.; Żabka, A.; **Wróblewski, M.**; Kukula-Koch, W.; Szczeblewski, P.; Polit, J.T. Thyme Oil Mitigates Cadmium-Induced Oxidative and Genotoxic Stress in *Vicia faba* Root Meristem Cells under in vitro Conditions. *Sci. Rep.* **2025**, *15*, 38689, doi:10.1038/s41598-025-22588-w.

2. Gocek-Szczurtek, N.; Żabka, A.; **Wróblewski, M.**; Polit, J.T.* Stabilization of the MAPK-Epigenetic Signaling Axis Underlies the Protective Effect of Thyme Oil against Cadmium Stress in Root Meristem Cells of *Vicia faba*. *Int. J. Mol. Sci.* **2025**, *27*, 208, doi:10.3390/ijms27010208.

3. Gocek-Szczurtek, N.; **Wróblewski, M.**; Żabka, A.; Polit, J.T.* Thyme Oil Alleviates Cadmium Induced Disturbances in Mitotic Activity, Cytoskeletal Organization and H3T3/H3S10 Phosphorylation in *Vicia faba*. *Int. J. Mol. Sci* **2026**, 27, 2798, doi:10.3390/ijms27062798.

4. Gocek-Szczurtek, N.*; Piotrowska-Niczyporuk, A.; Zambrzycka-Szelewa, E.; Ciereszko, I.; Żabka, A.; **Wróblewski, M.**; Polit, J.T. Thyme Essential Oil Reduces Cadmium Uptake and Toxicity in *Vicia faba* Root Meristem Cells, Involving Stabilization of Cell Ultrastructure and Modulation of Redox Response and Thiol Metabolism. - manuskrypt przygotowany do złożenia w czasopiśmie *The Plant Journal*

polegał na:

- współuczestnictwie w: pracach technicznych związanych z przygotowaniem prac eksperymentalnych, realizacji analiz z wykorzystaniem techniki qPCR oraz doradztwie w zakresie przeprowadzenia analiz statystycznych.

* - autor korespondujący

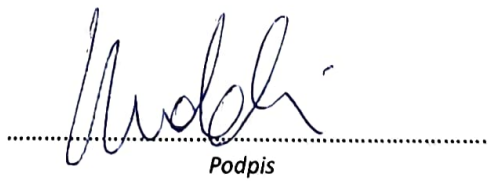

.....
Podpis

Lublin, 18.03.2026

prof. dr hab. Wirginia Kukuła-Koch
Katedra Farmakognozji i Botaniki Farmaceutycznej
Wydział Farmaceutyczny
Uniwersytet Medyczny w Lublinie

Oświadczenie współautora publikacji

Oświadczam, że mój udział w publikacji:

1. Gocek-Szczurtek, N*.; Żabka, A.; Wróblewski, M.; **Kukuła-Koch, W.**; Szczeblewski, P.; Polit, J.T. Thyme Oil Mitigates Cadmium-Induced Oxidative and Genotoxic Stress in *Vicia faba* Root Meristem Cells under in vitro Conditions. *Scientific Reports* **2025**, 15, 38689, doi:10.1038/s41598-025-22588-w

polegał na:

- współuczestnictwie w: przeprowadzeniu analiz składu chemicznego olejku tymiankowego z wykorzystaniem techniki GC-MS oraz interpretacji uzyskanych wyników, a także konsultacji korekt dotyczących tych badań w odpowiedzi na uwagi recenzentów.

* - autor korespondujący

Wirginia Anna Kukuła-Koch

Elektronicznie podpisany przez Wirginia Anna Kukuła-Koch
Data: 2026.03.23 16:57:43 +01'00'

.....

Podpis

Ministerstwo Finansów

Krajowa Administracja Skarbowa

SISC SYSTEM INFORMACYJNY SKARBOWO-CELNY

Raport weryfikacji

Wynik	**WAŻNY/PRAWIDŁOWY**
Wynik przetwarzania	**Zakończono**
Skrót pliku z podpisem	**5743d091830f845bbd05227cb186cc45e1599e86**
Nazwa pliku z podpisem	**udział W. Kukuła-Koch (2)_s.pdf**
Identyfikator weryfikacji	**88A59B154FC4781BC3A97A841DCA2B84EA8F88ED**

Lista podpisów

Status weryfikacji podpisu	**WAŻNY/PRAWIDŁOWY**
Data i czas wykonania podpisu	**2026-03-23 16:57:43 GMT+01:00**
Data i czas weryfikacji podpisu	**2026-03-23 17:01:20 GMT+01:00**
Format podpisu	**PKCS7**
Poziom podpisu	**BES (Podpis w postaci podstawowej)**
Certyfikat podpisującego	**kwalifikowany**

Ścieżka certyfikacji

Certyfikat podpisującego

Walidacja certyfikatu	**WAŻNY/PRAWIDŁOWY**
Status certyfikatu	**WAŻNY**
Wystawiony dla	**surname=Kukuła-Koch, givenName=Wirginia Anna, CN=Wirginia Anna Kukuła-Koch, O=Uniwersytet Medyczny w Lublinie, C=PL,**
Wystawiony przez	**CN=COPE SZAFIR - Kwalifikowany, O=Krajowa Izba Rozliczeniowa S.A., C=PL**
Ważny od	**2025-12-22 08:00:00 GMT+01:00**
Ważny do	**2027-12-22 08:00:00 GMT+01:00**
Data wystawienia CRL/OCSP	**2026-03-23 16:57:37 GMT+01:00**
Numer seryjny	**113ffc4ef360c723c5e287b182905e0b958dc115**

Certyfikat wystawcy

Walidacja certyfikatu	**WAŻNY/PRAWIDŁOWY**
Status certyfikatu	**WAŻNY**
Wystawiony dla	**CN=COPE SZAFIR - Kwalifikowany, O=Krajowa Izba Rozliczeniowa S.A., C=PL**
Wystawiony przez	**CN=Narodowe Centrum Certyfikacji, O=Narodowy Bank Polski, C=PL**
Ważny od	**2021-12-06 11:36:59 GMT+01:00**
Ważny do	**2032-12-07 00:59:59 GMT+01:00**
Numer seryjny	**062aac8d84b0ddcc**

Gdańsk, 18.03.2026

dr inż. Paweł Szczeblewski
Katedra Technologii Leków i Biochemii
Wydział Chemiczny
Politechnika Gdańska

Oświadczenie współautora publikacji

Oświadczam, że mój udział w publikacji:

1. Gocek-Szczurtek, N*.; Żabka, A.; Wróblewski, M.; Kukula-Koch, W.; **Szczeblewski, P.**; Polit, J.T. Thyme Oil Mitigates Cadmium-Induced Oxidative and Genotoxic Stress in *Vicia faba* Root Meristem Cells under in vitro Conditions. *Scientific Reports* **2025**, 15, 38689, doi:10.1038/s41598-025-22588-w

polegał na:

- współuczestnictwie w: przeprowadzeniu analiz składu chemicznego olejku tymiankowego z wykorzystaniem techniki GC-MS oraz interpretacji uzyskanych wyników.

* - autor korespondujący

Podpis

Białystok, 18.03.2026

dr hab. Alicja Piotrowska-Niczyporuk
Katedra Biologii i Ekologii Roślin
Wydział Biologii
Uniwersytet w Białymstoku

Oświadczenie współautora publikacji

Oświadczam, że mój udział w publikacji:

1. Gocek-Szczurtek, N.*; **Piotrowska-Niczyporuk, A.**; Zambrzycka-Szelewa, E.; Ciereszko, I.; Żabka, A.; Wróblewski, M.; Polit, J.T. Thyme Essential Oil Reduces Cadmium Uptake and Toxicity in *Vicia faba* Root Meristem Cells, Involving Stabilization of Cell Ultrastructure and Modulation of Redox Response and Thiol Metabolism. - manuskrypt przygotowany do złożenia w czasopiśmie *The Plant Journal*

polegał na:

- współuczestnictwie w: planowaniu części pracy eksperymentalnej (obejmującej analizę stresu oksydacyjnego, systemu antyoksydacyjnego oraz akumulacji fitochelatyn), opracowywaniu i dostosowywaniu metodyki badawczej, zapewnieniu materiałów oraz przeprowadzaniu doświadczeń w mojej jednostce badawczej, w której odbywał się pobyt doktorantki,
- uczestnictwie w walidacji uzyskanych wyników.

PODPIS ZAUFANY
Alicja
PIOTROWSKA-NICZYPORUK
23.03.2026 11:13:23 GMT+1
Dokument podpisany elektronicznie podpisem zaufanym

.....

Podpis

Ministerstwo Finansów

Krajowa Administracja Skarbowa

SISC SYSTEM INFORMACYJNY SKARBOWO-CELNY

Raport weryfikacji

Wynik	**WAŻNY/PRAWIDŁOWY**
Wynik przetwarzania	**Zakończono**
Szczegóły weryfikacji:	**Podpis elektroniczny nie został złożony za pomocą kwalifikowanego urządzenia do składania podpisu (QSCD)**
Skrót pliku z podpisem	**44b43b7115d8c3d1fcaf6e071fe59fc6592530d8**
Nazwa pliku z podpisem	**udział A.Piotrowska-Niczyporuk-2 (1).pdf**
Identyfikator weryfikacji	**798D49382C5693C2C63CC6B32D2BA4C3089D8599**

Lista podpisów

Status weryfikacji podpisu	**WAŻNY/PRAWIDŁOWY**
Data i czas wykonania podpisu	**2026-03-23 11:13:23 GMT+01:00**
Data i czas weryfikacji podpisu	**2026-03-23 11:35:42 GMT+01:00**
Format podpisu	**PAdES**
Poziom podpisu	**BES (Podpis w postaci podstawowej)**
Certyfikat podpisującego	**kwalifikowany**

Osoba podpisująca (profil zaufany ePUAP)

Imię i nazwisko	**: Alicja Piotrowska-Niczyporuk**

Ścieżka certyfikacji

Certyfikat podpisującego

Walidacja certyfikatu	**WAŻNY/PRAWIDŁOWY**
Status certyfikatu	**WAŻNY**
Wystawiony dla	**CN=Minister do spraw informatyzacji - pieczęć podpisu zaufanego, O=Ministerstwo Cyfryzacji, C=PL**
Wystawiony przez	**CN=Centrum Kwalifikowane EuroCert, O=EuroCert Sp. z o.o., C=PL,**
Ważny od	**2024-02-13 10:27:09 GMT+01:00**
Ważny do	**2027-02-12 10:27:09 GMT+01:00**
Data wystawienia CRL/OCSP	**2026-03-23 07:00:01 GMT+01:00**
Numer seryjny	**efd46f5b31b845d08071c5eed94d4eb9d37d**

Certyfikat wystawcy

Walidacja certyfikatu	**WAŻNY/PRAWIDŁOWY**
Status certyfikatu	**WAŻNY**
Wystawiony dla	**CN=Centrum Kwalifikowane EuroCert, O=EuroCert Sp. z o.o., C=PL,**
Wystawiony przez	**CN=Narodowe Centrum Certyfikacji, O=Narodowy Bank Polski, C=PL**
Ważny od	**2017-02-14 13:26:19 GMT+01:00**
Ważny do	**2028-02-15 00:59:59 GMT+01:00**
Numer seryjny	**1a5734b0d472d251e1d37cfe3d796ac117102490**

Białystok, 18.03.2026

dr Elżbieta Zambrzycka-Szelewa
Katedra Chemii Analitycznej i Nieorganicznej
Wydział Chemii
Uniwersytet w Białymstoku

Oświadczenie współautora publikacji

Oświadczam, że mój udział w publikacji:

1. Gocek-Szczurtek, N.*; Piotrowska-Niczyporuk, A.; **Zambrzycka-Szelewa, E.**; Ciereszko, I.; Żabka, A.; Wróblewski, M.; Polit, J.T. Thyme Essential Oil Reduces Cadmium Uptake and Toxicity in *Vicia faba* Root Meristem Cells, Involving Stabilization of Cell Ultrastructure and Modulation of Redox Response and Thiol Metabolism. - manuskrypt przygotowany do złożenia w czasopiśmie *The Plant Journal*

polegał na:

- współuczestnictwie w: oznaczaniu zawartości kadmu w tkankach roślinnych metodą atomowej spektrometrii absorpcyjnej z atomizacją w płomieniu (FAAS), opracowywaniu i walidacji uzyskanych wyników.

Elżbieta Zambrzycka-Szelewa
Podpis

Białystok, 18.03.2026

prof. dr hab. Iwona Ciereszko
Katedra Biologii i Ekologii Roślin
Wydział Biologii
Uniwersytet w Białymstoku

Oświadczenie współautora publikacji

Oświadczam, że mój udział w publikacji:

1. Gocek-Szczurtek, N.*; Piotrowska-Niczyporuk, A.; Zambrzycka-Szelewa, E.; **Ciereszko, I.**; Żabka, A.; Wróblewski, M.; Polit, J.T. Thyme Essential Oil Reduces Cadmium Uptake and Toxicity in *Vicia faba* Root Meristem Cells, Involving Stabilization of Cell Ultrastructure and Modulation of Redox Response and Thiol Metabolism. - manuskrypt przygotowany do złożenia w czasopiśmie *The Plant Journal*

polegał na:

- współuczestnictwie w: planowaniu części pracy eksperymentalnej (obejmującej analizę stresu oksydacyjnego i systemu antyoksydacyjnego),
- sprawowaniu opieki merytorycznej nad tym etapem realizacji badań, w mojej jednostce badawczej, w której odbywał się pobyt doktorantki,
- uczestnictwie w dyskusji dotyczącej uzyskanych wyników.

PODPIS ZAUFANY
IWONA
CIERESZKO
18.03.2026 14:29:09 GMT+1
Dokument podpisany elektronicznie
podpisem zaufanym

.....

Podpis

Ministerstwo Finansów

Krajowa Administracja Skarbowa

SISC SYSTEM INFORMACYJNY SKARBOWO-CELNY

Raport weryfikacji

Wynik	**WAŻNY/PRAWIDŁOWY**
Wynik przetwarzania	**Zakończono**
Szczegóły weryfikacji:	**Podpis elektroniczny nie został złożony za pomocą kwalifikowanego urządzenia do składania podpisu (QSCD)**
Skrót pliku z podpisem	**edecd93bdd8158a15f2e105897fdc127dee7e1cf**
Nazwa pliku z podpisem	**udział I.Ciereszko elektroniczy podpis zaufany.pdf**
Identyfikator weryfikacji	**5F0CA9E3BC6A689A860DB260A61FED1C36C8E94E**

Lista podpisów

Status weryfikacji podpisu	**WAŻNY/PRAWIDŁOWY**
Data i czas wykonania podpisu	**2026-03-18 14:29:09 GMT+01:00**
Data i czas weryfikacji podpisu	**2026-03-22 16:08:52 GMT+01:00**
Format podpisu	**PAdES**
Poziom podpisu	**BES (Podpis w postaci podstawowej)**
Certyfikat podpisującego	**kwalifikowany**

Osoba podpisująca (profil zaufany ePUAP)

Imię i nazwisko	**: IWONA CIERESZKO**

Ścieżka certyfikacji

Certyfikat podpisującego

Walidacja certyfikatu	**WAŻNY/PRAWIDŁOWY**
Status certyfikatu	**WAŻNY**
Wystawiony dla	**CN=Minister do spraw informatyzacji - pieczęć podpisu zaufanego, O=Ministerstwo Cyfryzacji, C=PL**
Wystawiony przez	**CN=Centrum Kwalifikowane EuroCert, O=EuroCert Sp. z o.o., C=PL,**
Ważny od	**2024-02-13 10:27:09 GMT+01:00**
Ważny do	**2027-02-12 10:27:09 GMT+01:00**
Data wystawienia CRL/OCSP	**2026-03-22 07:00:01 GMT+01:00**
Numer seryjny	**efd46f5b31b845d08071c5eed94d4eb9d37d**

Certyfikat wystawcy

Walidacja certyfikatu	**WAŻNY/PRAWIDŁOWY**
Status certyfikatu	**WAŻNY**
Wystawiony dla	**CN=Centrum Kwalifikowane EuroCert, O=EuroCert Sp. z o.o., C=PL,**
Wystawiony przez	**CN=Narodowe Centrum Certyfikacji, O=Narodowy Bank Polski, C=PL**
Ważny od	**2017-02-14 13:26:19 GMT+01:00**
Ważny do	**2028-02-15 00:59:59 GMT+01:00**
Numer seryjny	**1a5734b0d472d251e1d37cfe3d796ac117102490**

Łódź, 25.03.2026

prof. dr hab. Janusz Maszewski
Katedra Cytofizjologii
Wydział Biologii i Ochrony Środowiska
Uniwersytet Łódzki

Oświadczenie współautora publikacji

Oświadczam, że mój udział w publikacji:

1. Żabka, A.*; Gocek, N.; Polit, J.T.; **Maszewski, J**. Epigenetic Modifications Evidenced by Isolation of Proteins on Nascent DNA and Immunofluorescence in Hydroxyurea-Treated Root Meristem Cells of *Vicia faba*. *Planta* **2023**, *258*, 95, doi:10.1007/s00425-023-04249-2.

polegał na:

- współuczestnictwie w: opracowaniu projektu badania oraz przygotowaniu ostatecznej wersji manuskryptu.

* - autor korespondujący

.....
Podpis